~~C. Martin~~
V.S. Mummert

BISSETT-BERMAN
APOLLO GUIDANCE AND
NAVIGATION NOTES

Volume XI

(NASA-CR-145640) APOLLO GUIDANCE AND NAVIGATION NOTES, VOLUME 11 (Bissett-Berman Corp.) 536 p

N75-77179

Unclas
00/98 39939

JAN 1972
RECEIVED
NASA STI FACILITY
INPUT BRANCH

R. Wagner

The Bissett-Berman Corporation 2941 Nebraska Avenue, Santa Monica, California EXbrook 4-3270

Contract NAS 9-4435
1 July 1965

Volume XI

APOLLO GUIDANCE AND NAVIGATION NOTES

TABLE OF CONTENTS

Note No.	Title	
351	Mariner High Frequency Residuals	H. Epstein/ L. Lustick
352	Latitude, Longitude, Orbit Inclination and Inertial Heading at a Specified Radius or Time in the Error Analysis Program	C. H. Dale
353	Generation of Weighting Functions of the Orbit Parameters	M. Blasgen/ H. Epstein/ L. Lustick
354	Comparison of One-Dimension and Three-Dimension Troposphere Models	B. Murphy
355	Arbitrary Weighting of Data	H. Engel
356	Estimation of LEM/CSM Relative Position	H. Engel
357	Relative Efficiency of Unweighted Least Squares Orbit Parameter Estimators Where the Noise Samples are Exponentially Auto-Correlated	J. R. Holdsworth
358	Optimum Sampling Interval	H. Engel
359	Calculation of Information Matrices Based Upon Sextant Data Taken Between Stars and Earth or Moon Disks	C. H. Dale

Wagner

Volume XI - Bissett-Berman Apollo Guidance and Navigation Notes

Note No.	Title	Author(s)
360	The Integrated Trajectory Error Analysis Program	C. Siska/ M. Blasgen
361	Re-Entry — Equations of Motion	E. Cortina
362	Checkout of the Latitude, Longitude, Orbital Inclination, Flight Path Angle and Inertial Heading Routines of the Error Analysis Program	J. Childress/ L. Lustick
363	One-Dimensional Combined Troposphere-Ionosphere Models and Associated Tracking Errors	B. Murphy
364	Modifications to the Station Visibility Program	W. Buffington/ C. Siska
365	Time-Sigma Scaling in the Bissett-Berman Error Analysis Program	M. Blasgen
366	Optimum Powered Flight Tracking and Monitoring	G. F. Floyd
367	Changes and Corrections To Apollo Notes Nos. 329, 328, 320, and 295	H. Dale/ H. Engel/ L. Lustick
368	A Modification of the Error Analysis Program to Permit Angle Measurables from One Vehicle to Another, Both in Elliptic Orbits	C. H. Dale
369	Some Thoughts on "Powered Flight Ect." from a Work Load Point of View	C. H. Dale
370	A Peak Electron Density Model for Refractive Index Predictions in the Anomalous Quiet Ionosphere	H. R. Wright

Volume XI - Bissett-Berman Apollo Guidance and Navigation Notes

Note No.	Title	Author(s)
371	Effect of Lunar Ephemeris Errors on the Expected Orbit of a Satellite of the Moon	L. Bonin
372	Addition of Refraction Parameters to Orbit Error Analysis Program	L. Lustick
373	Checkout of the Ship Velocity Program	J. C. Childress, III
374	Checkout of the QE (Cov_0) QE^T Routine of the Orbit Error Analysis Program	J. C. Childress, III
375	Checkout of the Lunar Ephemeris Routine of the Error Analysis Program	J. C. Childress, III
376	Some Comments Concerning Equivalent Slab Thickness and Scale Height Interpretations in Relation to the Question of Thermal Equilibrium	H. R. Wright
377	Computational Procedure for Refractive Index Estimates Based on a Global Time Dependent Slab Model Ionosphere	H. R. Wright
378	Peak Ionization Level Height Anomalies	H. R. Wright
379	Ionospheric Phase Path Sensitivity to Chapman Parameter Variations	H. R. Wright

Volume XI - Bissett-Berman Apollo Guidance and Navigation Notes

Note No.	Title	Author(s)
380	Effect Of Clock Errors On The Ephemeris of a Lunar Satellite	L. Bonin
381	Optimal Weighting Functions II	J. R. Holdsworth
382	Constant, Linear Eccentricity	J. W. Childress, III
383	Effect of Changing Updated Parameters	H. Engel
384	Optimal Batching of Estimates	J. Holdsworth/ L. Lustick
385	Tracking and Monitoring During LEM Ascent	E. Cortina/ H. Dale
386	Equivalence of Data Processing Schemes	E. Pugh
387	Use Of Cholesky Decomposition To Invert Ill Conditioned Matrices	P. Gluckman
388	Global Time-Dependent Slab Model Ionosphere Program	J. B. Murphy
389	Multiple Station Version Of OEA Program	G. Hempstead/ L. Lustick
390	An Empirical Model Of The Quiet Equatorial Anomaly To Demonstrate Its World Wide Refractive Effects	H. R. Wright
391	Two-Way And Three-Way Data In The OEA Program	H. Engel
392	Effect Of Lunar Ephemeris Errors On The Expected Orbit Of A Satellite Approaching The Moon	L. Bonin
393	The Effects Of Doppler Radar Errors	H. Engel
394	Remarks On Covariance Matrices	H. Engel
395	Comparison Of Filters	E. Pugh
396	Effect of Model Errors	H. Engel
397	Check-Out Of Refraction Parameters	L. Lustick

APOLLO NOTE NO. 351
(Task I, Item II)

H. Epstein/
L. Lustick
1 July 1965

MARINER HIGH FREQUENCY RESIDUALS

PURPOSE

The purpose of this note is to present data on the high frequency noise components, (two-way doppler mode) consistent with the Mariner data supplied to Bissett-Berman by the Jet Propulsion Laboratory.

INTRODUCTION

Preliminary analysis of the Mariner residuals indicated the high frequency noise in the Mariner residuals did not appear to be stationary. In particular, the data prior to somewhere near Febraury 22 seemed to have a lower variance than that subsequent to that date. Conversation with JPL personnel indicated that they had observed similar results. This report is tailored to shed some light on the possible source of the increasing high frequency noise.

DATA ANALYZED

The data analyzed in this report is the two-way, one minute doppler data from the Goldstone station on the 21st and 28th of February 1965. These two particular days were chosen because analysis of the residuals indicated a significant difference in the standard deviations of the high frequency noise. Also, the preliminary analysis of the residuals had indicated that somewhere in the interval between the 21st and 28th the population of the residuals had changed. The data observation interval for these two days was about 450 minutes long.

METHOD OF ANALYSIS

Macroscopically the noise in the residuals must come from either noise sources in the measurable, or noise sources in the computed measurable. In order to pin point which of these two sources were responsible the predicts (computed measurable) were analyzed for high frequency noise.

The records were of sufficient length to make it difficult to fit the total record with polynomials. Hence, the following two methods of analysis were chosen:

1. The predict record for each of the days considered were broken into 5 subgroups and each subgroup was fit with a sixth and seventh degree polynomial, and the residuals and variance for each group was obtained.

2. The total predict record for each day was analyzed with the "variate difference method". In particular, successive differences (1-5) were obtained for each day's predicts and the variance and correlation function of these successive differences was then obtained. The variance of the high frequency noise in the original record can be obtained by dividing the variance in each difference by an appropriate factor. Beyond a certain difference the variance of the original process should be the same and this type of stability is taken to indicate the order of the difference required to analyze the data. Under the hypothesis of independent noise in each one minute predict, the following characteristics for the variate difference method are presented:

ith Difference	$\sigma_{\text{ith Difference}}/\sigma_{\text{Original Process}}$
1	$\sqrt{2}$
2	$\sqrt{6}$
3	$\sqrt{20}$
4	$\sqrt{70}$
5	$\sqrt{252}$

Table 1.

Ratio of Standard Deviation of ith Difference To The Standard Deviation of Original Process

R. Wagner

The following Table indicates the effect of the differencing operation on the correlation function:

ith diff / ρ (j)	1	2	3	4	5
1	- 1/2	- 2/3	-3/4	- 4/5	- 5/6
2		+ 1/6	+ 3/10	+ 2/5	+ 10/21
3			- 1/20	- 4/35	- 5/28
4				+ 1/70	+ 5/126
5					- 1/252

ρ = normalized correlation functions

j = lag considered

Table 2.

The Normalized Correlation Function As A Function Of the Difference

RESULTS

The results are presented in the following logical order:

1. The standard deviation obtained by analyzing the residuals on February 21st and 28th are presented in Table 3.

2. The standard deviation in the predicts for each group (about 90 points) and for each day are presented in Table 4.

3. The standard deviations and correlation function for the predicts as determined by the variate difference method are presented in Table 5.

The standard deviation in the residuals for each of the days considered is presented in Table 3 below:

Day	Iteration No.	No. of Points
2/21/65	2	466

Polynomial Degree	Standard Deviation (cycles/sec (one min. samples)
0	.007188
1	.0070405
2	.0062296

Day	Iteration No.	No. of Points
2/28/65	2	428

Polynomial Degree	Standard of Deviation
0	.010731
1	.010727
2	.010293

Table 3.

Standard Deviation of the One Minute Doppler Residual

The difference in the standard deviation on these two days is statistically significant since the standard deviation in the estimate of (σ) for this length record is only about 3% of the true standard deviation, whereas the percent change in the observed standard deviations is greater than 30%. Table 4 presents the standard deviations of the predicts as determined by fitting polynomials to subgroups of the predict records. Group No. 3 was discarded on each day since there were many missing points in this group and the polynomial did not fit well as evidenced by low frequency indicated in the correlation functions. Comparison of the average standard deviation for

the two days indicates no significant difference between the high frequency noise in the predicts for these two days.

2/21/65 Sta (11) 1 Min. Predicts Iteration 2

Group No.	No. of Pts.	σ_{6th}	σ_{7th}
1	92	.003663	.0035722
2	93	.003199	.0031437
3*	94	.015368	.015174
4	95	.002933	.0029772
5	93	.0030168	.0029772
Average		.00322	.00322

2/28/65 Sta (11) 1 Min. Predicts Iteration 2

Group No.	No. of Pts.	σ_{6th}	σ_{7th}
1	86	.003836	.0038295
2	86	.003839	.0038236
3*	86	.0053381	.0046419
4	85	.0034008	.0033613
5	85	.0032612	.0032385
Average		.00362	.00362

*not included in Average.

Table 4.

Standard Deviation in Predicts as Determined by Fitting Polynomials to Portions of the Data

If the third group was included the 21st predicts would have indicated that the noise in the predicts were worst on the 21st than on the 28th.

Table 5 shows the results obtained with the variate difference method. The last entry in this Table σ_o is the standard deviation of the original process as determined from the standard deviation in the difference.

Day 2/21/65	No. of Pts. 456	Poly Deg. 0	
$\rho(\tau)$	3rd Diff.	4th Diff.	5th Diff.
1	-.772431	-.819210	-.849902
2	+.346736	+.442234	.513842
3	-.094566	-.157269	-.216342
4	+.025232	+.038810	.060728
5	-.017740	-.019547	-.023281
6	+.052494	+.054591	+.053684
7	-.120963	-.113592	-.099780
σ	.0157544	.029726	.0567916
σ_o	.00352	.00354	.00355

Day 2/28/65	No of Pts. 401	Poly Deg. 0	
$\rho(\tau)$	3rd Diff.	4th Diff.	5th Diff.
1	-.742334	-.793791	-.821671
2	.295753	.393039	.481475
3	-.062093	-.127136	-.199907
4	+.012274	.031594	.061110
5	-.004763	-.008521	-.014701
6	+.018369	.011573	+.007965
7	-.040683	-.035715	-.031724
σ	.0163181	.030432	.0575018
σ_o	.00363	.00362	.00362

σ = standard deviation of difference
σ_o = standard deviation of original process

Table 5

Summary of Variate Difference Results
(2nd iteration, 1 Min. Predicts, Sta. 11)

Both the polynomial data and the variate difference data indicate that the high frequency noise in the predicts is about ($.0035 \frac{\text{cycles}}{\text{sec.}}$) with no significant difference between the days. Since the predicts presented to us were rounded to the nearest .01 cycle/sec., this number is in agreement with what one would expect from the roundoff quantization error.

CONCLUSIONS

1. The analysis of the residuals indicates a statistically significant difference between the high frequency noise on the 21st and 28th of February.

2. Analysis of the predicts for the 21st and 28th did not indicate any significant difference in the high frequency noise in the predicts.

3. For the two days analyzed, the increased high frequency noise on the 28th of February was, most probably, in the measurable itself.

FUTURE STUDIES

The analysis of raw measurable data will be undertaken in the near future.

The Bissett-Berman Corporation 2941 Nebraska Avenue, Santa Monica, California EXbrook 4-3270

APOLLO NOTE NO. 352

H. Dale
6 July 1965

LATITUDE, LONGITUDE, ORBIT INCLINATION AND INERTIAL HEADING AT A SPECIFIED RADIUS OR TIME IN THE ERROR ANALYSIS PROGRAM

(A Simplification of Apollo Note No. 345)

H. Engel has pointed out that a number of the calculations described in Apollo Note No. 345 already exist in the program. Thus, the following is a simplified set of equations yielding the desired results:

$$\text{Is } (\mu/.49 \times 10^{13}) > 1 \tag{1}$$

If true, then the attracting body must be the Earth; if false, then the attracting body is the Moon.

Whether QE or QR are called for, the state vector at the time, T, is given in the primed system. These numbers are x', y', z', $\dot{x}'$, $\dot{y}'$, $\dot{z}'$, all at T.

Now get the state vector in the tilda system:

$$\begin{vmatrix} \tilde{x} \\ \tilde{y} \\ \tilde{z} \end{vmatrix} = \mathbb{L}^T \begin{vmatrix} x' \\ y' \\ z' \end{vmatrix}, \qquad \begin{vmatrix} \tilde{\dot{x}} \\ \tilde{\dot{y}} \\ \tilde{\dot{z}} \end{vmatrix} = \mathbb{L}^T \begin{vmatrix} \dot{x}' \\ \dot{y}' \\ \dot{z}' \end{vmatrix} \tag{2}$$

Now if Equation (1) is true, then the momentum is:

$$\mathrm{MOM} = \overline{R} \times \dot{\overline{R}} = \begin{bmatrix} (\tilde{y}\dot{\tilde{z}} - \tilde{z}\dot{\tilde{y}}) \\ (\tilde{z}\dot{\tilde{x}} - \tilde{x}\dot{\tilde{z}}) \\ (\tilde{x}\dot{\tilde{y}} - \tilde{y}\dot{\tilde{x}}) \end{bmatrix} \tag{3}$$

$$\left|\mathrm{MOM}\right| = \left|\overline{R} \times \dot{\overline{R}}\right| = \left[(\tilde{y}\dot{\tilde{z}} - \tilde{z}\dot{\tilde{y}})^2 + (\tilde{z}\dot{\tilde{x}} - \tilde{x}\dot{\tilde{z}})^2 + (\tilde{x}\dot{\tilde{y}} - \tilde{y}\dot{\tilde{x}})^2\right]^{1/2} \tag{4}$$

$$\text{Inclination} = \cos^{-1}\left[\frac{\overline{\mathrm{MOM}} \cdot \hat{\tilde{z}}}{\left|\overline{\mathrm{MOM}}\right|}\right] = \cos^{-1}\left[\frac{\tilde{x}\dot{\tilde{y}} - \tilde{y}\dot{\tilde{x}}}{\left|\mathrm{MOM}\right|}\right], \tag{5}$$

$$0 \leq \text{inclination} \leq \pi$$

where $\hat{\tilde{z}}$ is a unit vector in the direction of $\tilde{z}$.

$$R = \left|\overline{R}\right| = (\tilde{x}^2 + \tilde{y}^2 + \tilde{z}^2)^{1/2} \tag{6}$$

$$\left.\begin{aligned} &\text{Flight Path Angle} = \sin^{-1}\left[\frac{\dot{\overline{R}} \cdot \overline{R}}{\left|\dot{\overline{R}}\right| R}\right] = \sin^{-1}\left[\frac{\tilde{x}\dot{\tilde{x}} + \tilde{y}\dot{\tilde{y}} + \tilde{z}\dot{\tilde{z}}}{(\dot{\tilde{x}}^2 + \dot{\tilde{y}}^2 + \dot{\tilde{z}}^2)^{1/2} R}\right], \\ &\qquad -\frac{\pi}{2} \leq \text{Elev. Angle} \leq \frac{\pi}{2} \end{aligned}\right\} \tag{7}$$

$$\text{Latitude} = \sin^{-1}\left[\frac{\overline{R} \cdot \hat{\tilde{z}}}{R}\right] = \sin^{-1}\left[\frac{\tilde{z}}{R}\right], \quad -\frac{\pi}{2} \leq \text{Latitude} \leq \frac{\pi}{2} \tag{8}$$

$$\text{Longitude} = -\omega_m T + \cos^{-1}\left[\frac{\tilde{x}}{(\tilde{x}^2 + \tilde{y}^2)^{1/2}}\right]$$

$$= -\omega_m T + \sin^{-1}\left[\frac{\tilde{y}}{(\tilde{x}^2 + \tilde{y}^2)^{1/2}}\right] \tag{9}$$

$$\bar{R} \cdot \dot{\bar{R}} = \tilde{x}\dot{\tilde{x}} + \tilde{y}\dot{\tilde{y}} + \tilde{z}\dot{\tilde{z}} \tag{10}$$

The vector projection of the velocity on a unit sphere at the point of $\bar{R}$ is $\dot{\bar{R}} - (\dot{\bar{R}} \cdot \bar{R})\,\bar{R} / |\bar{R}|^2$

$$\overline{\text{H VEL}} = \begin{bmatrix} \dot{\tilde{x}} \\ \dot{\tilde{y}} \\ \dot{\tilde{z}} \end{bmatrix} - \frac{(\bar{R} \cdot \dot{\bar{R}})}{R^2} \begin{bmatrix} \tilde{x} \\ \tilde{y} \\ \tilde{z} \end{bmatrix} = \begin{bmatrix} \left[\dot{\tilde{x}} - \frac{(\bar{R} \cdot \dot{\bar{R}})}{R^2}\tilde{x}\right] \\ \left[\dot{\tilde{y}} - \frac{(\bar{R} \cdot \dot{\bar{R}})}{R^2}\tilde{y}\right] \\ \left[\dot{\tilde{z}} - \frac{(\bar{R} \cdot \dot{\bar{R}})}{R^2}\tilde{z}\right] \end{bmatrix} \tag{11}$$

$$\left|\overline{\text{H VEL}}\right| = \left\{ [\quad]^2 + [\quad]^2 + [\quad]^2 \right\}^{1/2} \tag{12}$$

A unit vector normal to the radius and $\tilde{z}$ axis (in an easterly direction) is:

$$\overline{EAST} = \frac{\hat{\tilde{z}} \times \overline{R}}{|\overline{R}| \cos(\text{Latitude})} = \frac{1}{\cos(\text{Latitude})} \begin{bmatrix} \frac{-\tilde{y}}{R} \\ \frac{\tilde{x}}{R} \\ 0 \end{bmatrix} = \begin{bmatrix} \frac{-\tilde{y}}{(\tilde{x}^2 + \tilde{y}^2)^{1/2}} \\ \frac{\tilde{x}}{(\tilde{x}^2 + \tilde{y}^2)^{1/2}} \\ 0 \end{bmatrix} \quad (13)$$

Now:

$$\left.\begin{aligned} \sin(A_z) = \frac{\overline{HVEL} \cdot \overline{EAST}}{|HVEL|} = \frac{1}{|HVEL|} (\tilde{x}^2 + \tilde{y}^2)^{-1/2} \Bigg\{ & \left[\dot{\tilde{x}} - \frac{(\overline{R} \cdot \dot{\overline{R}})}{R^2} \tilde{x} \right] (-\tilde{y}) \\ & + \left[\dot{\tilde{y}} - \frac{(\overline{R} \cdot \dot{\overline{R}})}{R^2} \tilde{y} \right] (\tilde{x}) \Bigg\} \end{aligned}\right\} \quad (14)$$

$$\left.\begin{aligned} \cos(A_z) = \frac{|\overline{HVEL} \times \overline{EAST}|}{|HVEL|} = \frac{1}{|HVEL|} (\tilde{x}^2 + \tilde{y}^2)^{-1/2} \\ \left[(\tilde{x}^2 + \tilde{y}^2) \left(\dot{\tilde{z}} - \frac{(\overline{R} \cdot \dot{\overline{R}})}{R^2} \tilde{z} \right)^2 + \left\{ \tilde{x} \left(\dot{\tilde{x}} + \frac{(\overline{R} \cdot \dot{\overline{R}})}{R^2} \tilde{x} \right) \right.\right. \\ \left.\left. + \tilde{y} \left(\dot{y} + \frac{(\overline{R} \cdot \dot{\overline{R}})}{R^2} \tilde{y} \right) \right\}^2 \right]^{1/2} \end{aligned}\right\} \quad (15)$$

from which azimuth may be obtained. If, however, Equation (1) is false, then:

$$\begin{vmatrix} x \\ y \\ z \end{vmatrix} = K^T \begin{vmatrix} \tilde{x} \\ \tilde{y} \\ \tilde{z} \end{vmatrix} \; ; \; \begin{vmatrix} x \\ \dot{y} \\ \dot{z} \end{vmatrix} = K^T \begin{vmatrix} \dot{\tilde{x}} \\ \dot{\tilde{y}} \\ \dot{\tilde{z}} \end{vmatrix}$$

And by substituting x for $\tilde{x}$ through $\dot{z}$ for $\dot{\tilde{z}}$, Equations (3) through (13) may be solved with the one extra substitution of ω_{Earth} for ω_{Moon} in Equation (9).

APOLLO NOTE NO. 353
(Task II, Item II)

M. Blasgen/
H. Epstein/
L. Lustick
1 July 1965

GENERATION OF WEIGHTING FUNCTIONS OF THE ORBIT PARAMETERS

PURPOSE

The purpose of this note is to describe how the weighting function for the orbit parameters can be obtained and to illustrate the utility of these weighting functions for evaluating the effect of time varying error sources.

ANALYSIS

Let C = total information matrix.

Δa_j = column vector of the orbit parameters.

$$C\Delta a_j = \sum_i \frac{1}{\sigma_i^2} \begin{bmatrix} \sum_k \frac{\partial m_i}{\partial a_j}(t_k) \left[m_i(t_k) - m_{c_i}(t_k) \right] \\ 0 \\ 0 \\ 0 \\ \sum_k \frac{\partial m_i}{\partial a_n}(t_n) \left[m_i(t_k) - m_{c_i}(t_k) \right] \end{bmatrix}$$

$$+ C_{a\ priori}\ \Delta a_{j\,a\ priori}$$

Each measurable contributes to the prior in the orbit parameter Δa_j in the following way:

$$\Delta a_j^i = \frac{1}{\sigma_i^2} \left[C_{j1}^{-1} \;\; C_{j2}^{-1} \ldots . \; C_{jn}^{-1} \right] \begin{bmatrix} \sum_k \frac{\partial m_i}{\partial a_j}(t_k) \left[m_i(t_k) - m_{c_i}(t_k) \right] \\ \vdots \\ \sum_k \frac{\partial m_i}{\partial a_n}(t_k) \left[m_i(t_k) - m_{c_i}(t_k) \right] \end{bmatrix}$$

If we define $w_j^i(k)$ as the weighting functions for the jth orbit parameter and the ith measurable then:

$$\Delta a_j^i = \sum_k w_j^i(k) \, \mathcal{E}^i(k)$$

$$\text{where } w_j^i(k) = \frac{1}{\sigma_i^2} \left[C_{j1}^{-1}, \; C_{j2}^{-1} \ldots . \; C_{jn}^{-1} \right] \begin{bmatrix} \frac{\partial m_i}{\partial a_j}(t_k) \\ \vdots \\ \frac{\partial m_i}{\partial a_n}(t_k) \end{bmatrix}$$

$\mathcal{E}^i(k)$ = error in the ith measurable at time, t_k

If $\mathcal{E}^i(k)$ independent at every value of k, and the measurables i are not cross correlated, the following simplification obtains:

$$\Delta a_j^i = \frac{1}{\sigma_i^2} C^{-1} \begin{bmatrix} \sum_k \frac{\partial m_i}{\partial a_j}(t_k) \; \mathcal{E}^i(k) \\ \vdots \\ \sum_k \frac{\partial m_i}{\partial a_n}(t_k) \; \mathcal{E}^i(k) \end{bmatrix}$$

$$\overline{\Delta a_j^i \, \Delta a_j^{i\,T}} = C^{-1} \, C_i \, C^{-1}$$

$$\text{where } C_i = \frac{1}{\sigma_i^2} \begin{bmatrix} A_{\ell m} \end{bmatrix}$$

$$A_{\ell m} = \sum_k \frac{\partial m_i}{\partial a_\ell} \frac{\partial m_i}{\partial a_m}$$

The total error

$$\overline{\Delta a_j \, \Delta a_j^T} = C^{-1} \left[\sum_i C_i + C_{a \text{ priori}} \right] C^{-1} = C^{-1}$$

and this is the total error due to the white noise components. $C^{-1}C_iC^{-1}$, is the white noise contribution for each measurable.

For other time varying noise sources the contribution to the error in each orbit parameter for each measurable can be obtained from the weighting

functions as:

$$\Delta a^i_j = \sum_k w^i_j (k) \, \varepsilon^i (k)$$

where $\varepsilon^i(k)$ can be any time varying function.

Thus far, we have discussed how to obtain the weighting function at a particular time. The following analysis illustrates how to obtain the weighting function at any other time, T.

$$\left[\Delta a^i (T) \right] = Q(T) \, \Delta a^i_j (t = o)$$

$$= Q(T) \frac{1}{\sigma_i^2} C^{-1} \begin{bmatrix} \sum_k \frac{\partial m_i}{\partial a_j} (t_k) \left[m_i(t_k) - m_{c_i}(t_k) \right] \\ \vdots \\ \sum_k \frac{\partial m_i}{\partial a_n} (t_k) \left[m_i(t_k) - m_{c_i}(t_k) \right] \end{bmatrix}$$

let us define $\hat{C} = Q(T) \, C^{-1}$

then:

$$\Delta a^i (T) = \frac{1}{\sigma_i^2} \hat{C} \begin{bmatrix} \sum_k \frac{\partial m_i}{\partial a_j} (t_k) \left[m_i (t_k) - m_{c_i} (t_k) \right] \\ \vdots \\ \sum_k \frac{\partial m_i}{\partial a_n} (t_k) \left[m_i (t_k) - m_{c_i} (t_k) \right] \end{bmatrix}$$

or:

$$\Delta a_j^i(T) = \frac{1}{\sigma_i^2}\left[\hat{C}_{j1}\ \hat{C}_{j2} \ldots \hat{C}_{jn}\right] \begin{bmatrix} \sum_k \frac{\partial m_i}{\partial a_j}(t_k)\left[m_i(t_k) - m_{c_i}(t_k)\right] \\ \vdots \\ \sum_k \frac{\partial m_i}{\partial a_n}(t_k)\left[m_i(t_k) - m_{c_i}(t_k)\right] \end{bmatrix}$$

$$\Delta a_j^i(T) = \sum_k w_j^i(k)\ \varepsilon^i(k)$$

$$\text{where } w_j^i(k) = \frac{1}{\sigma_i^2}\left[\hat{C}_{ji}, \hat{C}_{j2} \ldots \hat{C}_{jn}\right] \begin{bmatrix} \frac{\partial m_i}{\partial a_j}(t_k) \\ \vdots \\ \frac{\partial m_i}{\partial a_n}(t_k) \end{bmatrix}$$

ILLUSTRATIONS OF WEIGHTING FUNCTION FOR TRANSLUNAR ORBIT

Conditions

Translunar Orbit

Tracking from three stations:

- Madrid - Master
- Ascension - Slave
- Antigua - Slave

Observation interval 16 min. - 3 hrs.

Measurable Range Rate

No a priori information

Error in measurable 3cm. /sec.

Data every second

Prediction of six orbit parameters no errors in the required nuisance parameters.

RESULTS

The weighting function for each of the orbit parameters were obtained both for the orbit parameters at time zero (translunar injection) and the orbit parameters at about the time of entrance to the LSOI.

The covariance matrices for both times are listed in Table 1 and 2 respectively. Graphs of the weighting functions are presented in the following order:

Figures 1 - 6 - $x, y, z, \dot{x}, \dot{y}, \dot{z}$ at time equal to zero station Madrid.

Figures 7 - 12 - $x, y, x, \dot{x}, \dot{y}, \dot{z}$ at time equal to zero station Ascension.

Figures 13 -18 - $x, y, z, \dot{x}, \dot{y}, \dot{z}$ at time equal to zero station Antigua.

Figures 19 - 24 - $x, y, z, \dot{x}, \dot{y}, \dot{z}$ at time equal to 2982 minutes station Madrid.

Figures 25 - 30 - $x, y, z, \dot{x}, \dot{y}, \dot{z}$ at time equal to 2982 minutes station Ascension.

Figures 31-36 - $x, y, z, \dot{x}, \dot{y}, \dot{z}$ at time equal to 2982 minutes station Antigua.

FUTURE STUDIES

1. Herm Epstein has done some work to be reported at a later date using the weighting functions to determine the time variations in bounded noise which will hurt us the most.

2. Taking the Fouier transform of the weighting function will give us the frequency response which, in some cases, can be an interesting way to look at the problem.

Table 1.

Covariance Matrix at Translunar Injection

0.275871E 03	0.456260E 03	0.432728E 02	-0.818349E 00	-0.956584E-01	0.108309E-00
0.456260E 03	0.769921E 03	0.614131E 02	-0.137063E 01	-0.155301E-00	0.210516E-00
0.432728E 02	0.614131E 02	0.238622E 02	-0.110812E-00	-0.181273E-01	0.190639E-01
-0.818349E 00	-0.137063E 01	-0.110812E-00	0.245726E-02	0.278780E-03	-0.342492E-03
-0.956584E-01	-0.155301E-00	-0.181273E-01	0.278780E-03	0.340181E-04	-0.341873E-04
0.108309E-00	0.210516E-00	0.190639E-01	-0.342492E-03	-0.341873E-04	0.198522E-03

Table 2.

Covariance Matrix at the LSOI

0.967071E 06	0.887288E 06	0.993627E 03	0.421790E 01	0.216498E 01	0.138664E-00
0.887288E 06	0.841526E 06	0.202674E 05	0.380803E 01	0.212080E 01	0.188782E-00
0.993627E 03	0.202674E 05	0.680760E 05	-0.342964E-01	0.100582E-00	0.188372E-00
0.421790E 01	0.380803E 01	-0.342964E-01	0.185369E-04	0.914003E-05	0.482059E-06
0.216498E 01	0.212080E 01	0.100582E-00	0.914003E-05	0.550590E-05	0.624215E-06
0.138664E-00	0.188782E-00	0.188372E-00	0.482059E-06	0.624215E-06	0.585491E-06

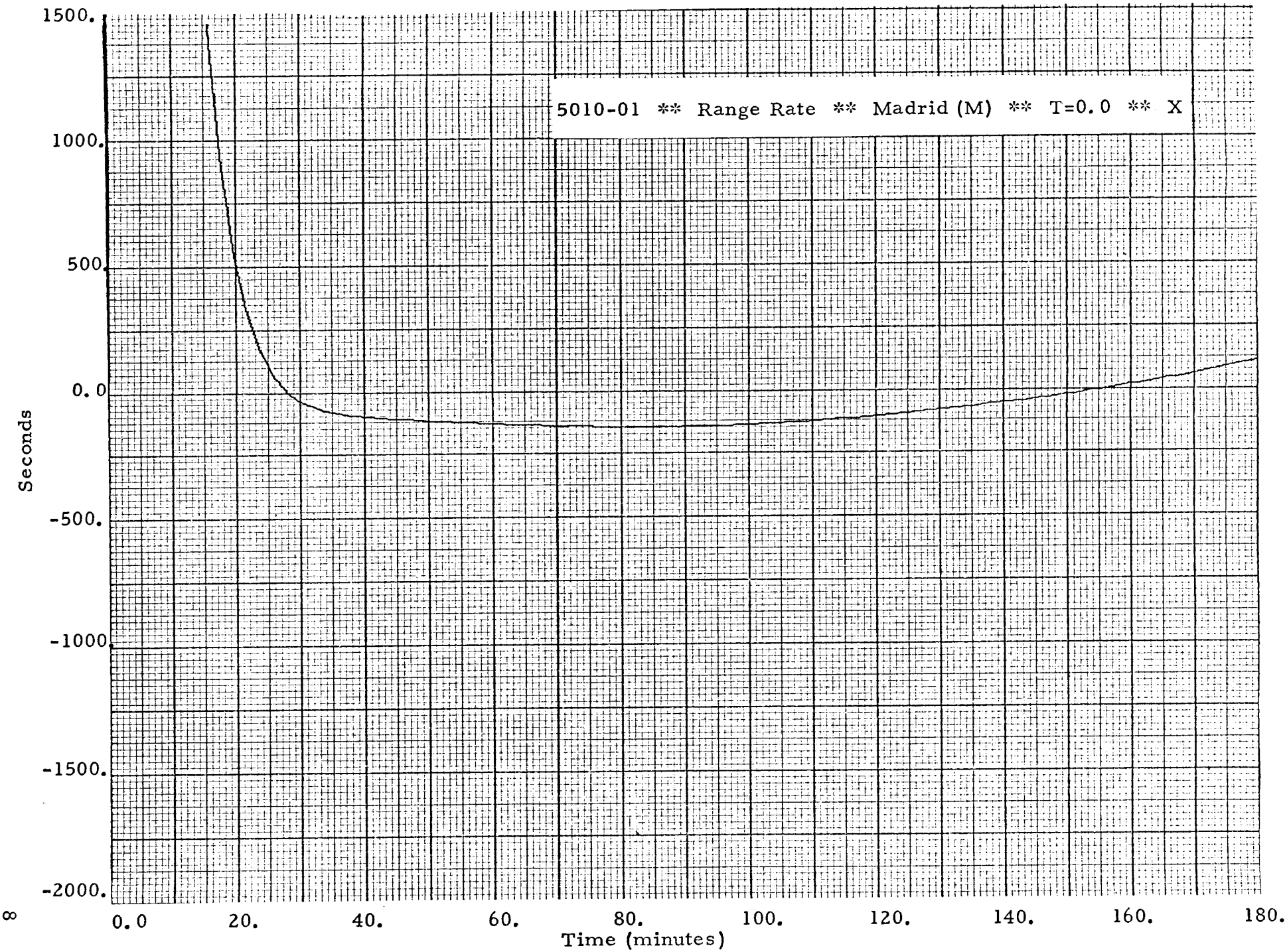
5010-01 ** Range Rate ** Madrid (M) ** T=0.0 ** X
1500.
1000.
500.
0.0
-500.
-1000.
-1500.
-2000.
Seconds
0.0
20.
40.
60.
80.
100.
120.
140.
160.
180.
Time (minutes)

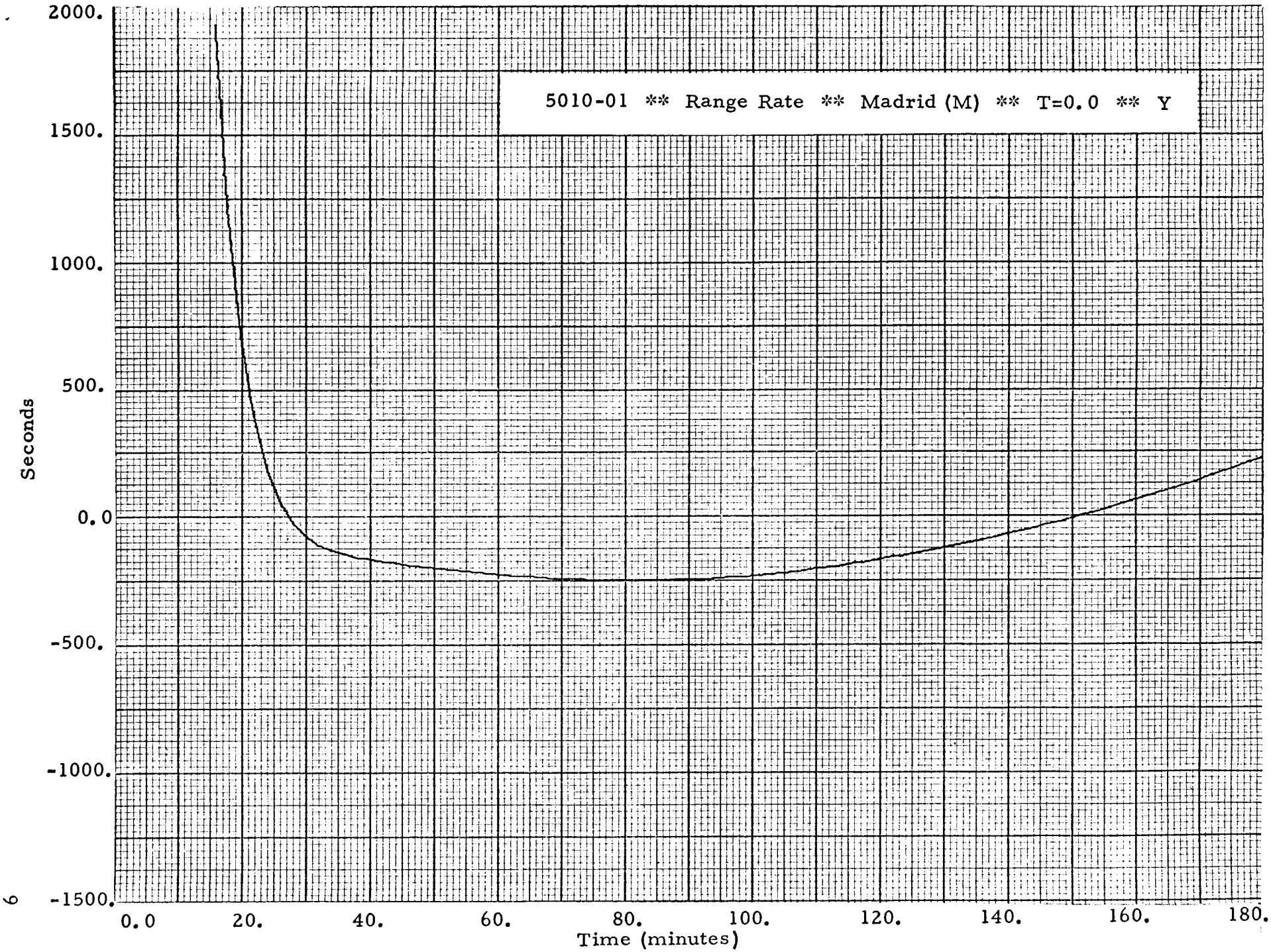
5010-01 ** Range Rate ** Madrid (M) ** T=0.0 ** Y
2000.
1500.
1000.
500.
0.0
-500.
-1000.
-1500.
Seconds
0.0
20.
40.
60.
80.
100.
120.
140.
160.
180.
Time (minutes)

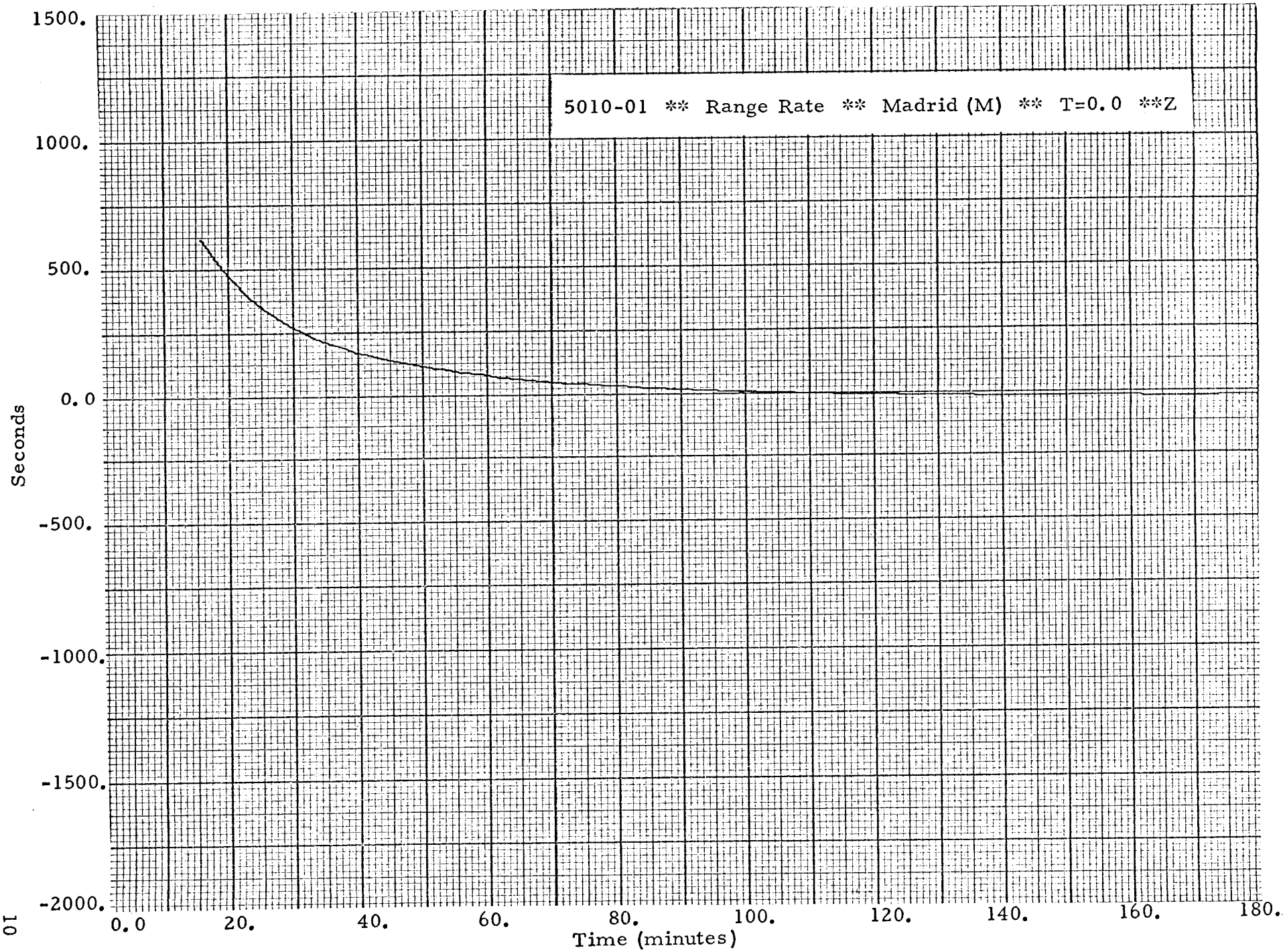
5010-01 ** Range Rate ** Madrid (M) ** T=0.0 **Z
1500.
1000.
500.
0.0
-500.
-1000.
-1500.
-2000.
Seconds
0.0
20.
40.
60.
80.
100.
120.
140.
160.
180.
Time (minutes)

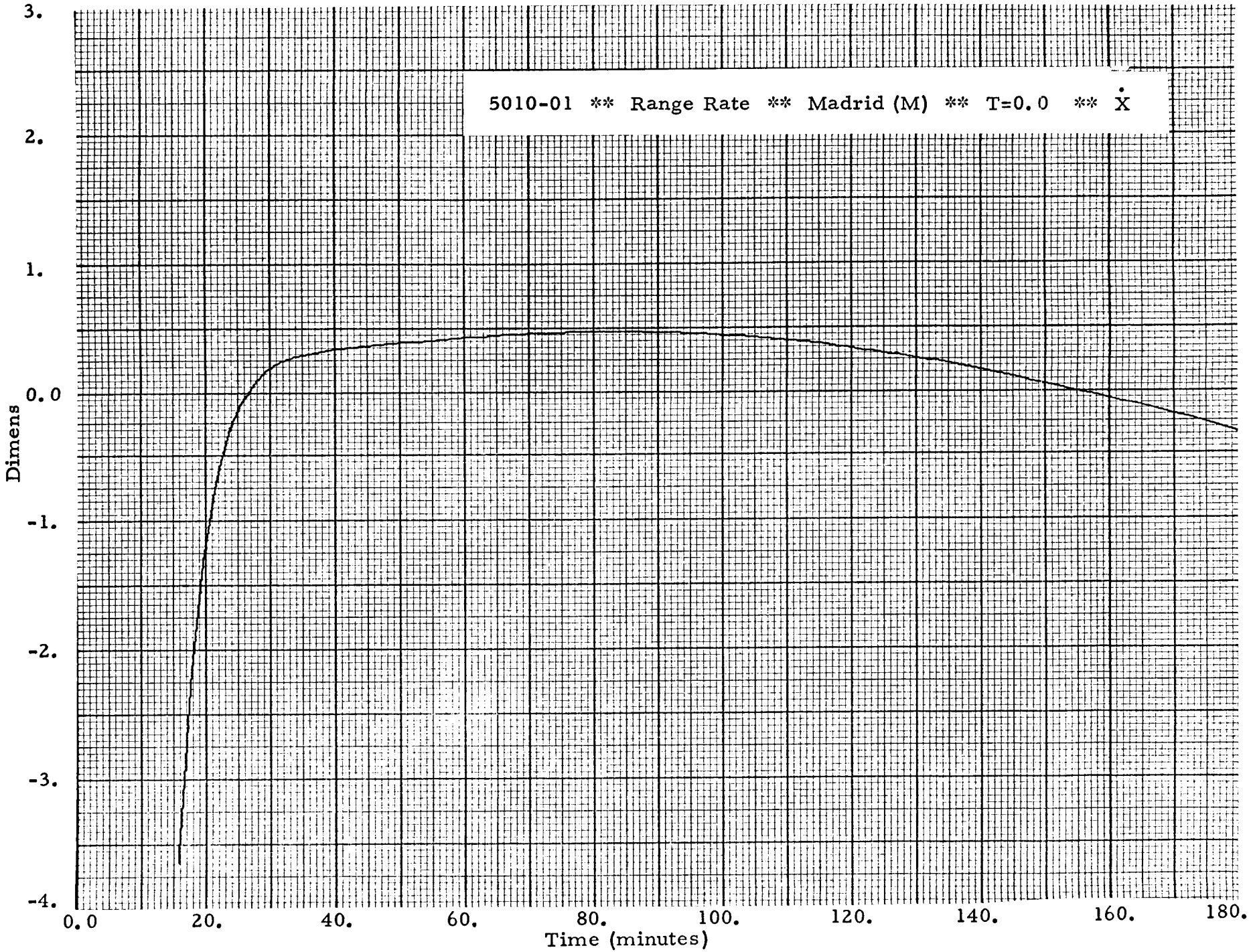
5010-01 ** Range Rate ** Madrid (M) ** T=0.0 ** $\dot{X}$
3.
2.
1.
0.0
-1.
-2.
-3.
-4.
Dimens
0.0
20.
40.
60.
80.
100.
120.
140.
160.
180.
Time (minutes)

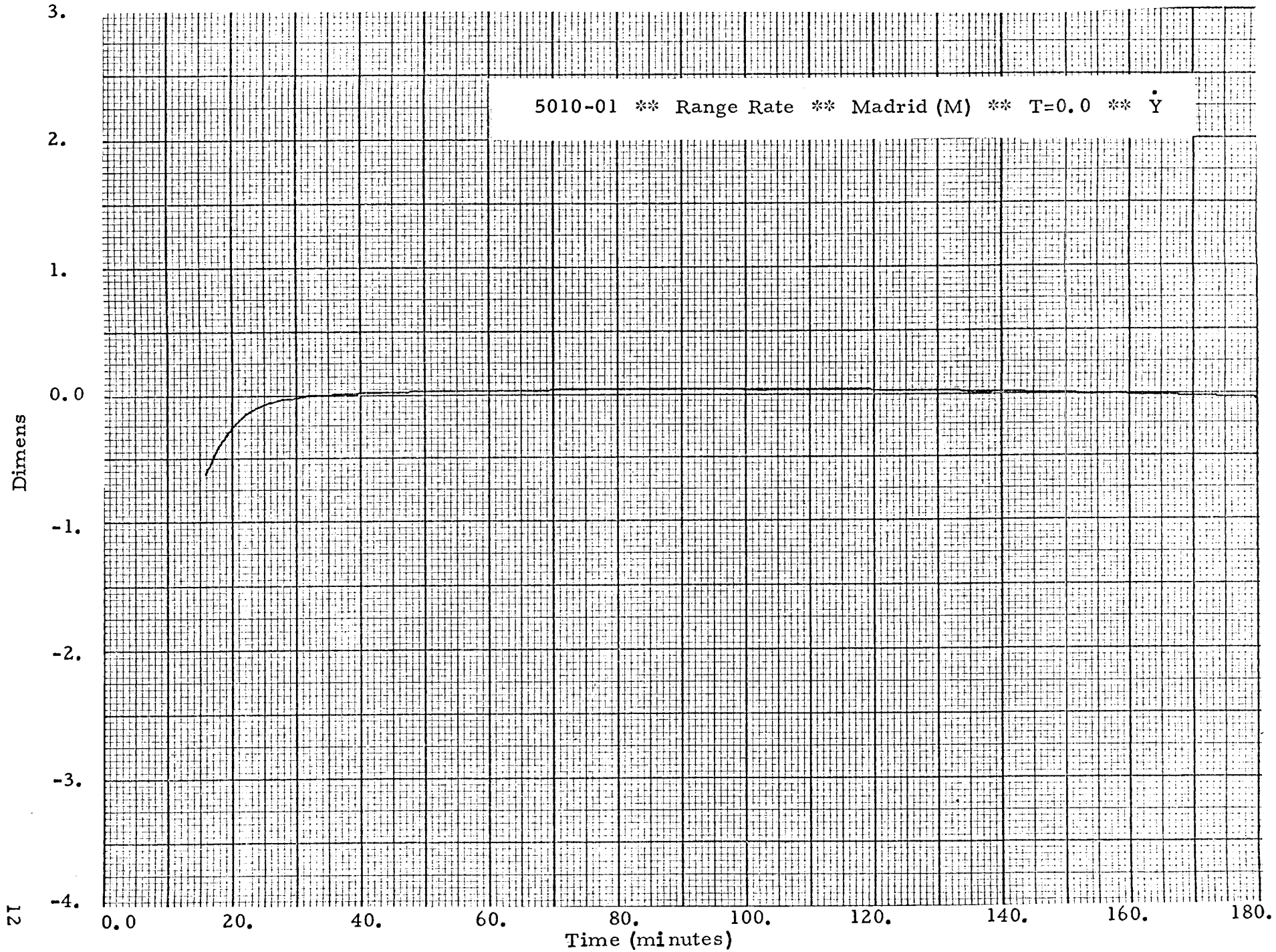
5010-01 ** Range Rate ** Madrid (M) ** T=0.0 ** Ẏ
3.
2.
1.
0.0
-1.
-2.
-3.
-4.
Dimens
0.0
20.
40.
60.
80.
100.
120.
140.
160.
180.
Time (minutes)

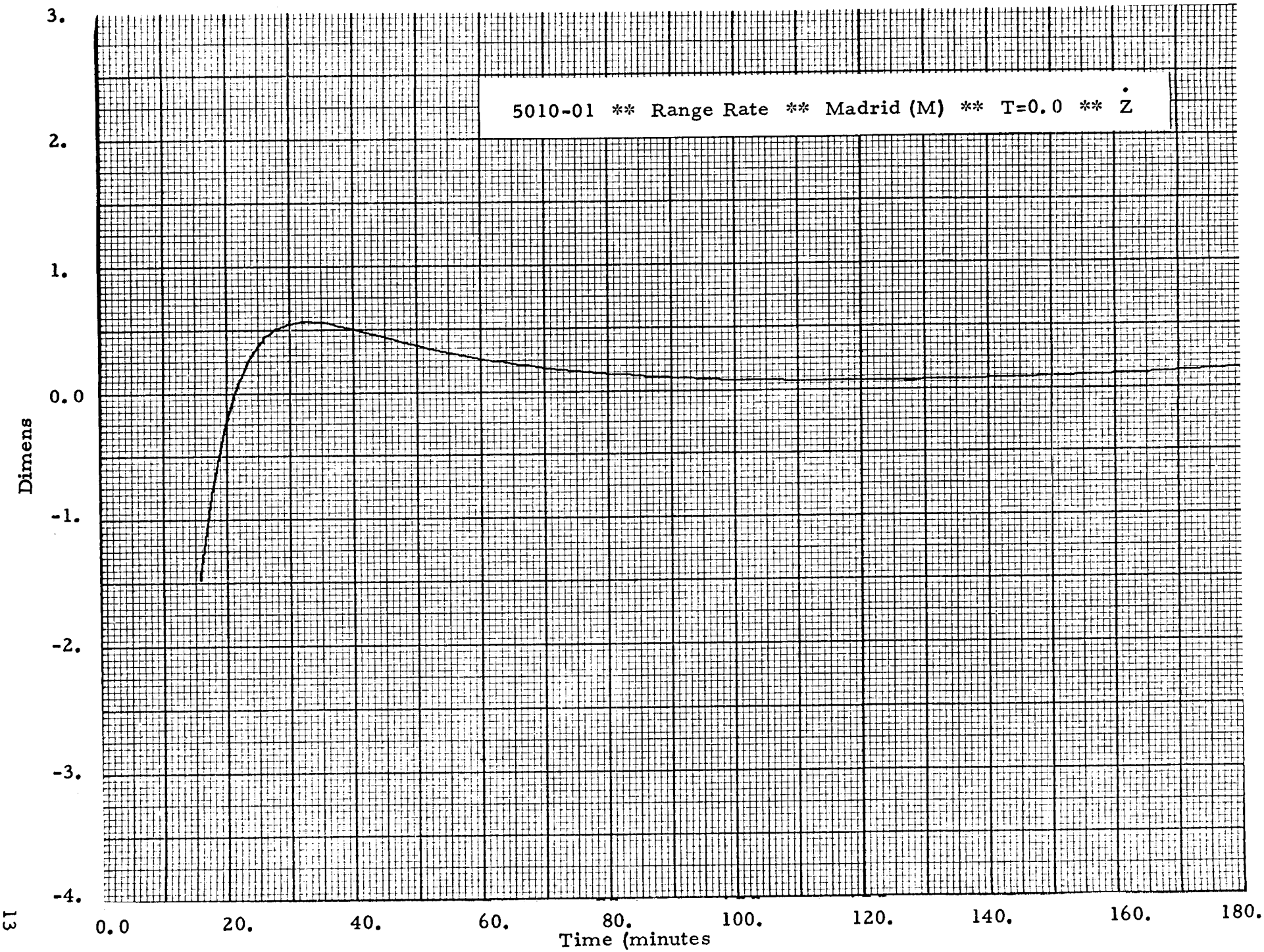
5010-01 ** Range Rate ** Madrid (M) ** T=0.0 ** Ż
3.
2.
1.
0.0
-1.
-2.
-3.
-4.
Dimens
0.0
20.
40.
60.
80.
100.
120.
140.
160.
180.
Time (minutes

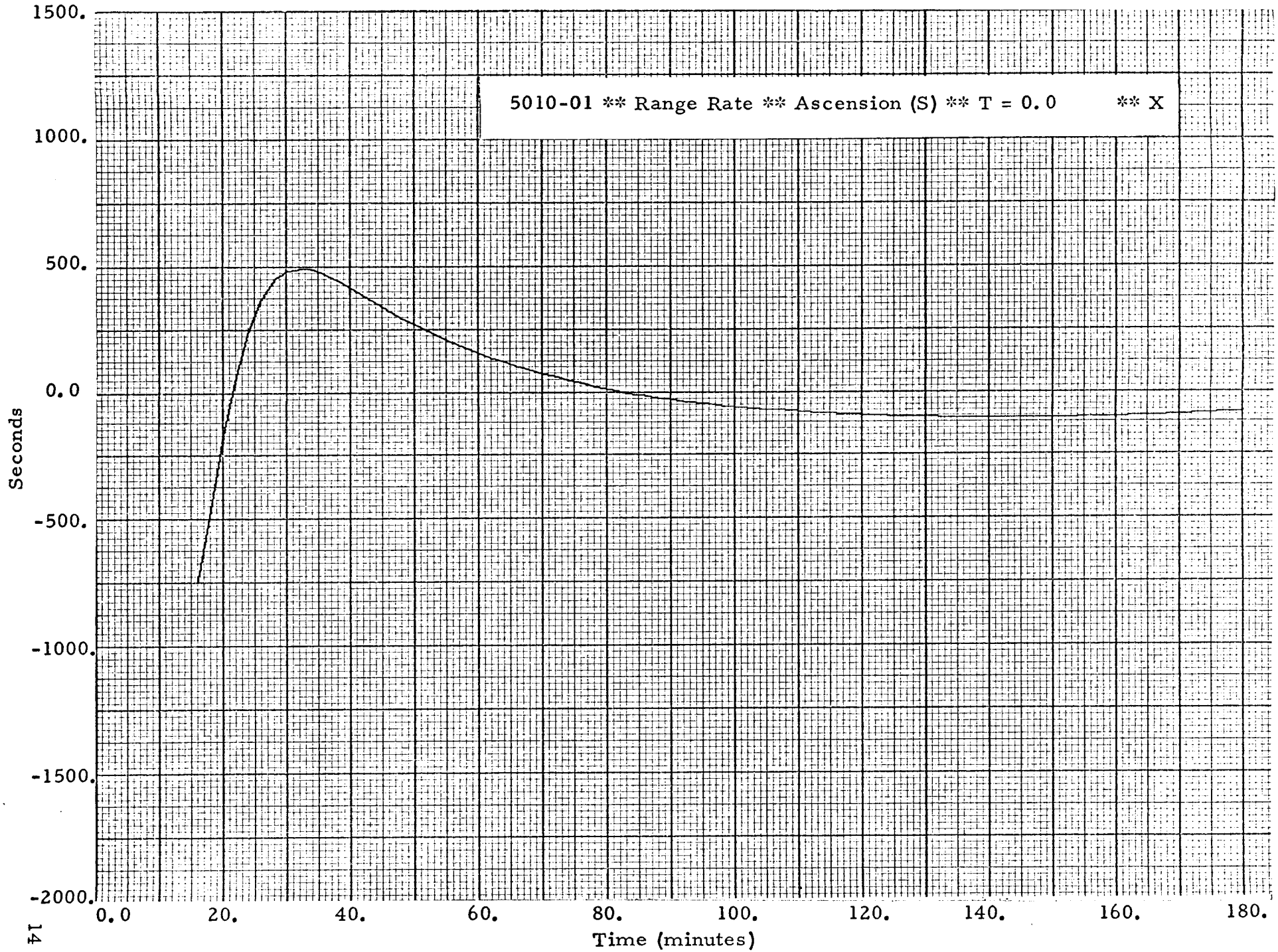
5010-01 ** Range Rate ** Ascension (S) ** T = 0.0 ** X
1500.
1000.
500.
0.0
-500.
-1000.
-1500.
-2000.
Seconds
0.0
20.
40.
60.
80.
100.
120.
140.
160.
180.
Time (minutes)

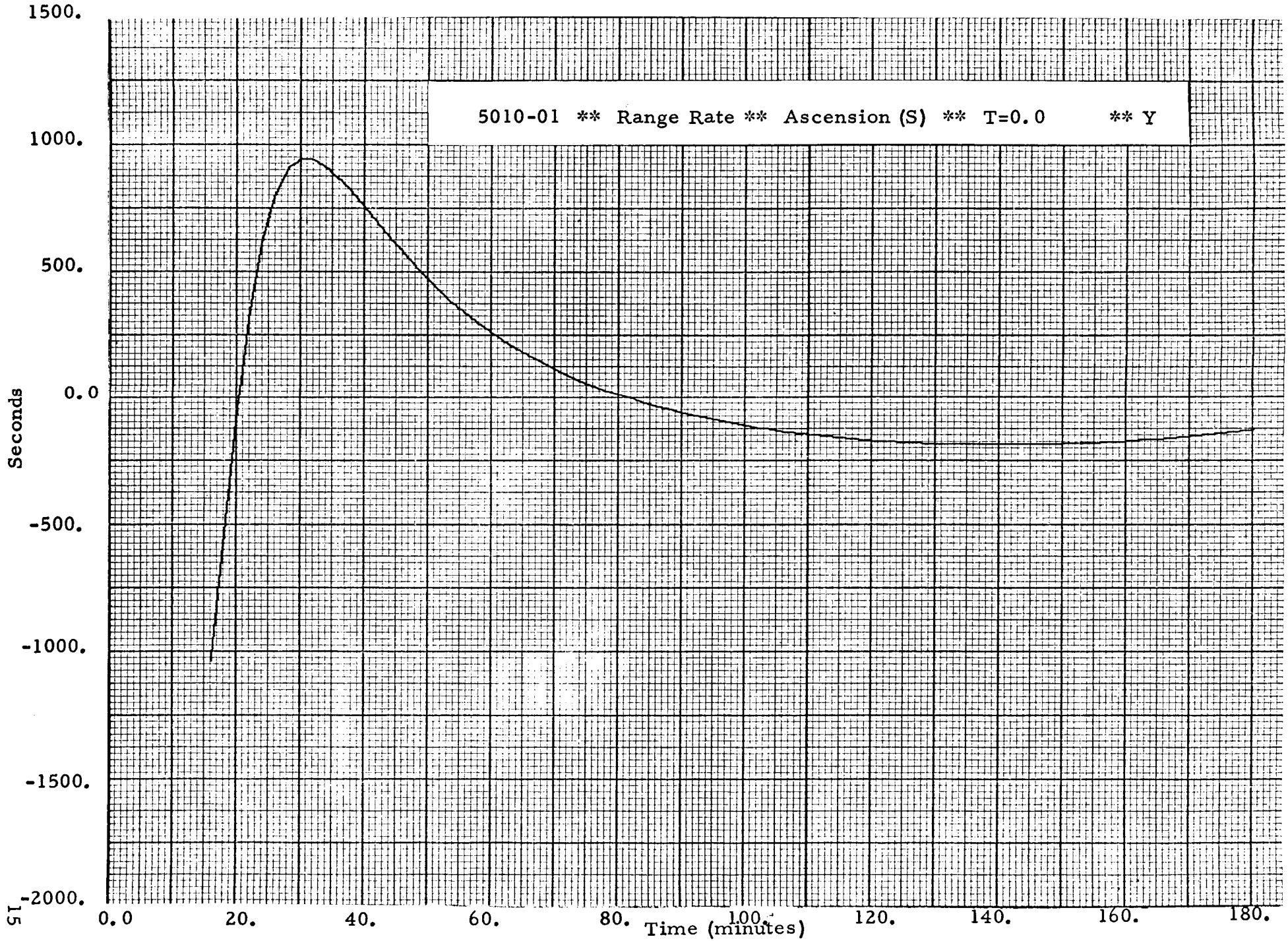
5010-01 ** Range Rate ** Ascension (S) ** T=0.0 ** Y
1500.
1000.
500.
0.0
-500.
-1000.
-1500.
-2000.
Seconds
0.0
20.
40.
60.
80.
100.
120.
140.
160.
180.
Time (minutes)

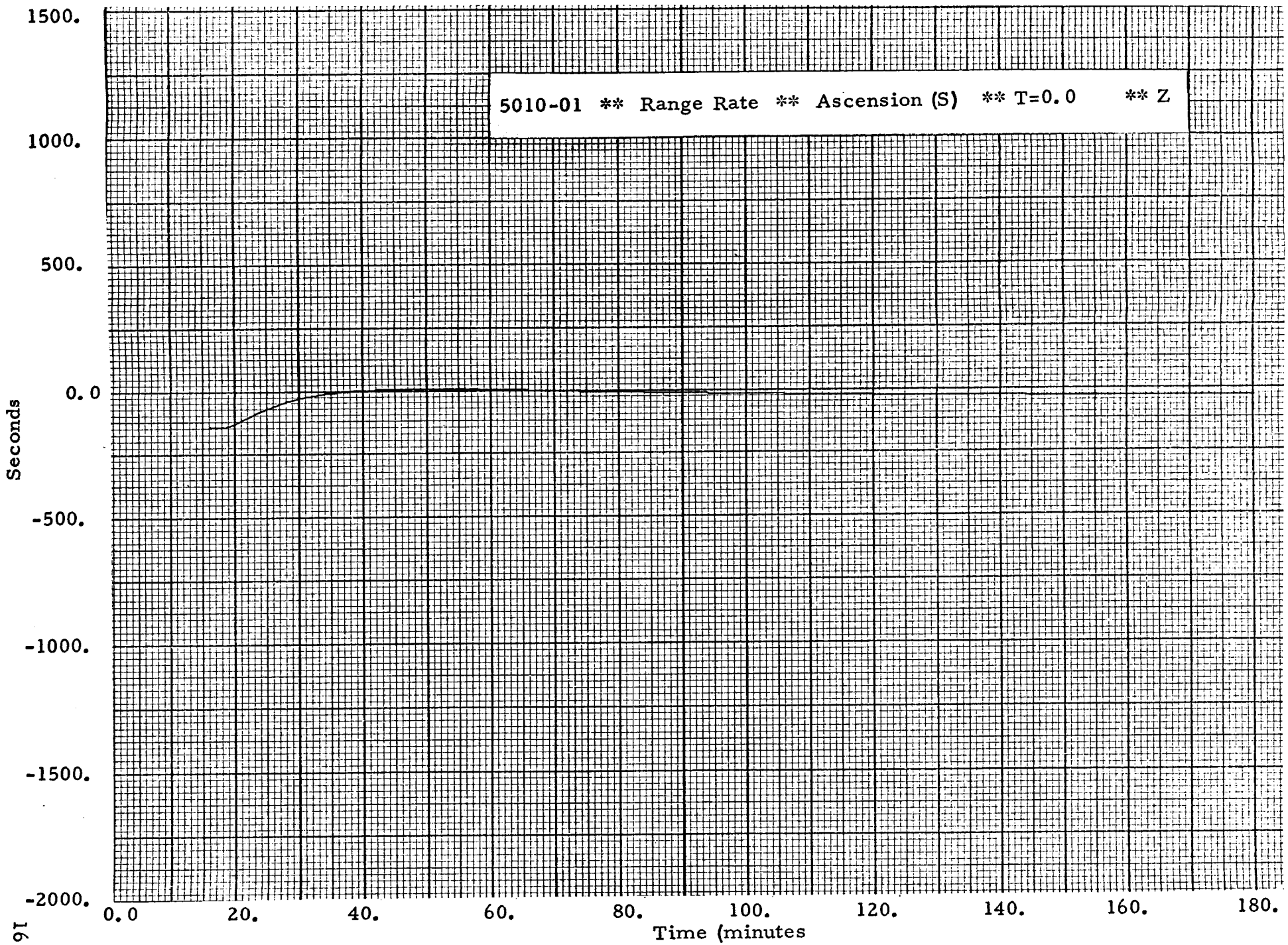
5010-01 ** Range Rate ** Ascension (S) ** T=0.0 ** Z
1500.
1000.
500.
0.0
-500.
-1000.
-1500.
-2000.
Seconds
0.0
20.
40.
60.
80.
100.
120.
140.
160.
180.
Time (minutes

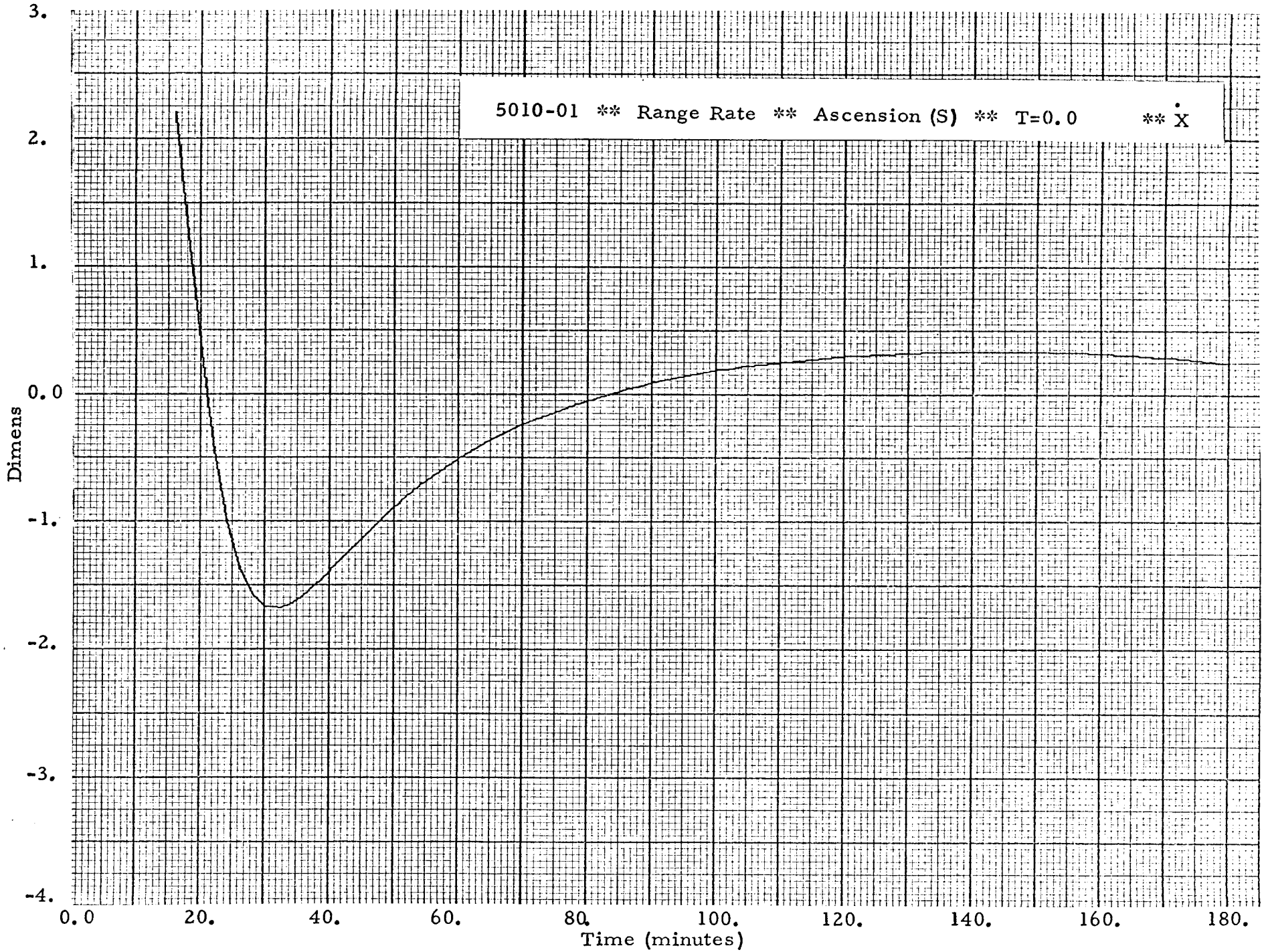
5010-01 ** Range Rate ** Ascension (S) ** T=0.0 ** $\dot{X}$
3.
2.
1.
0.0
-1.
-2.
-3.
-4.
Dimens
0.0
20.
40.
60.
80.
100.
120.
140.
160.
180.
Time (minutes)

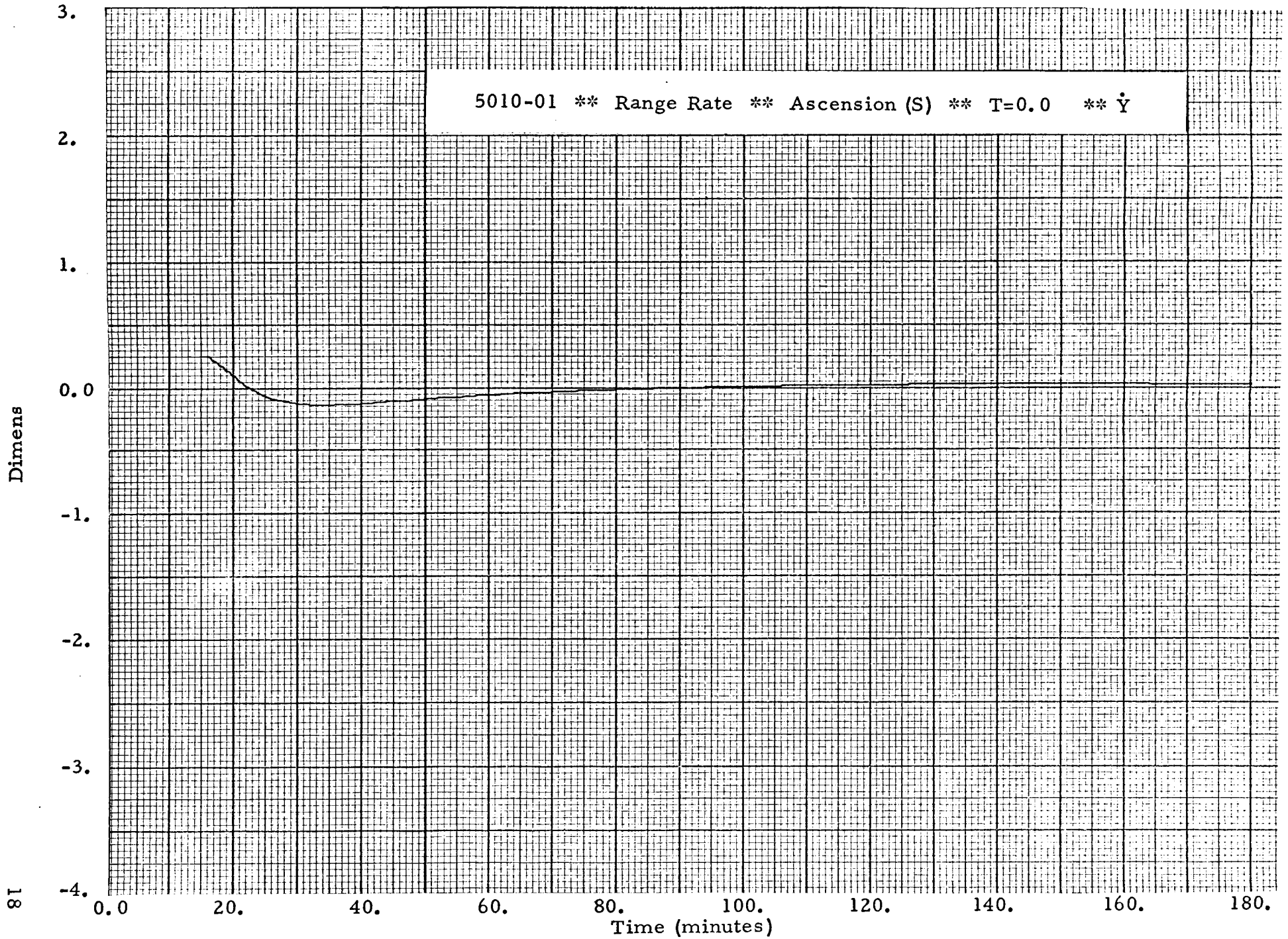
5010-01 ** Range Rate ** Ascension (S) ** T=0.0 ** Ẏ
3.
2.
1.
0.0
-1.
-2.
-3.
-4.
Dimens
0.0
20.
40.
60.
80.
100.
120.
140.
160.
180.
Time (minutes)

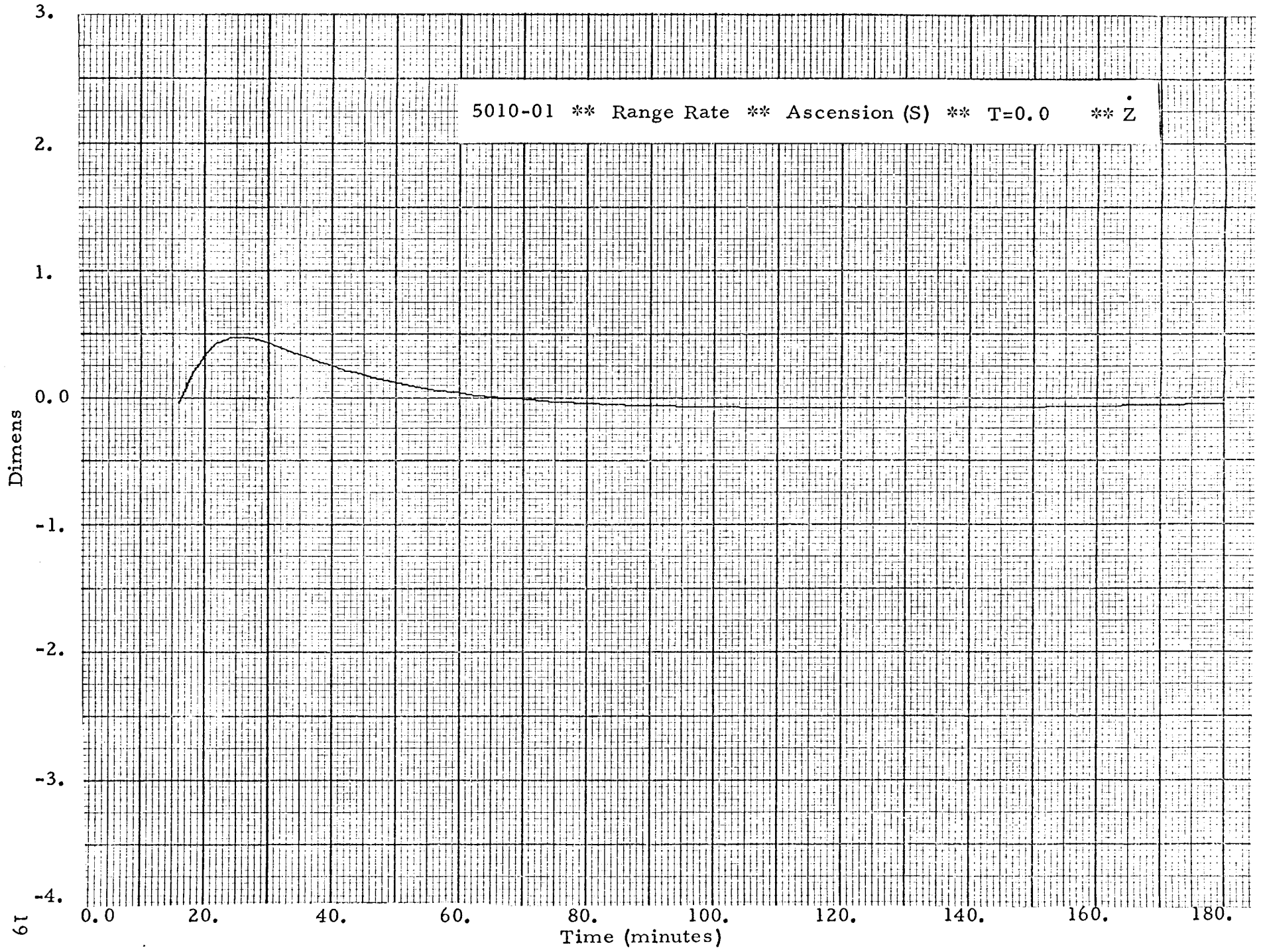
5010-01 ** Range Rate ** Ascension (S) ** T=0.0 ** $\dot{Z}$
3.
2.
1.
0.0
-1.
-2.
-3.
-4.
Dimens
0.0
20.
40.
60.
80.
100.
120.
140.
160.
180.
Time (minutes)

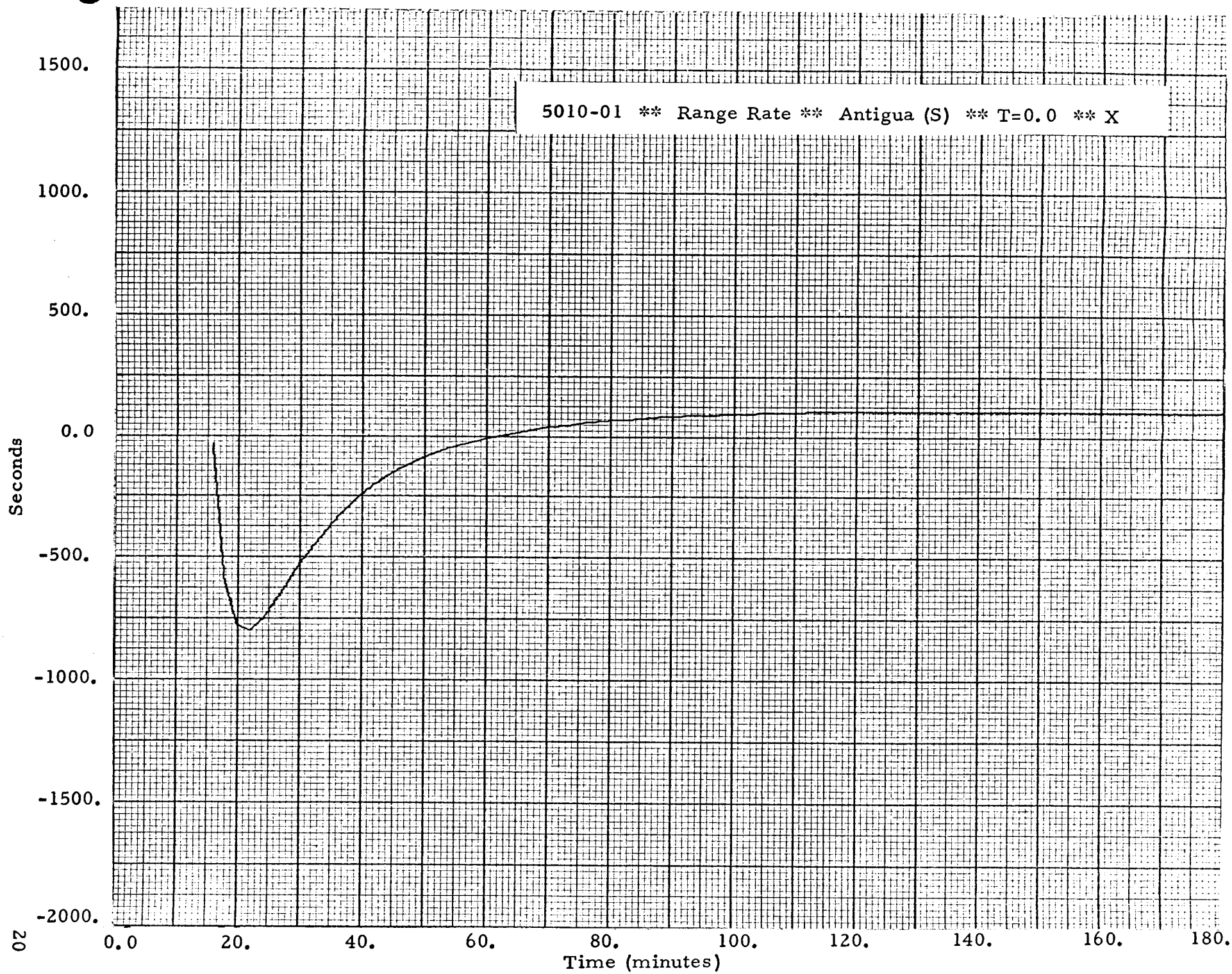
5010-01 ** Range Rate ** Antigua (S) ** T=0.0 ** X
1500.
1000.
500.
0.0
-500.
-1000.
-1500.
-2000.
Seconds
0.0
20.
40.
60.
80.
100.
120.
140.
160.
180.
Time (minutes)

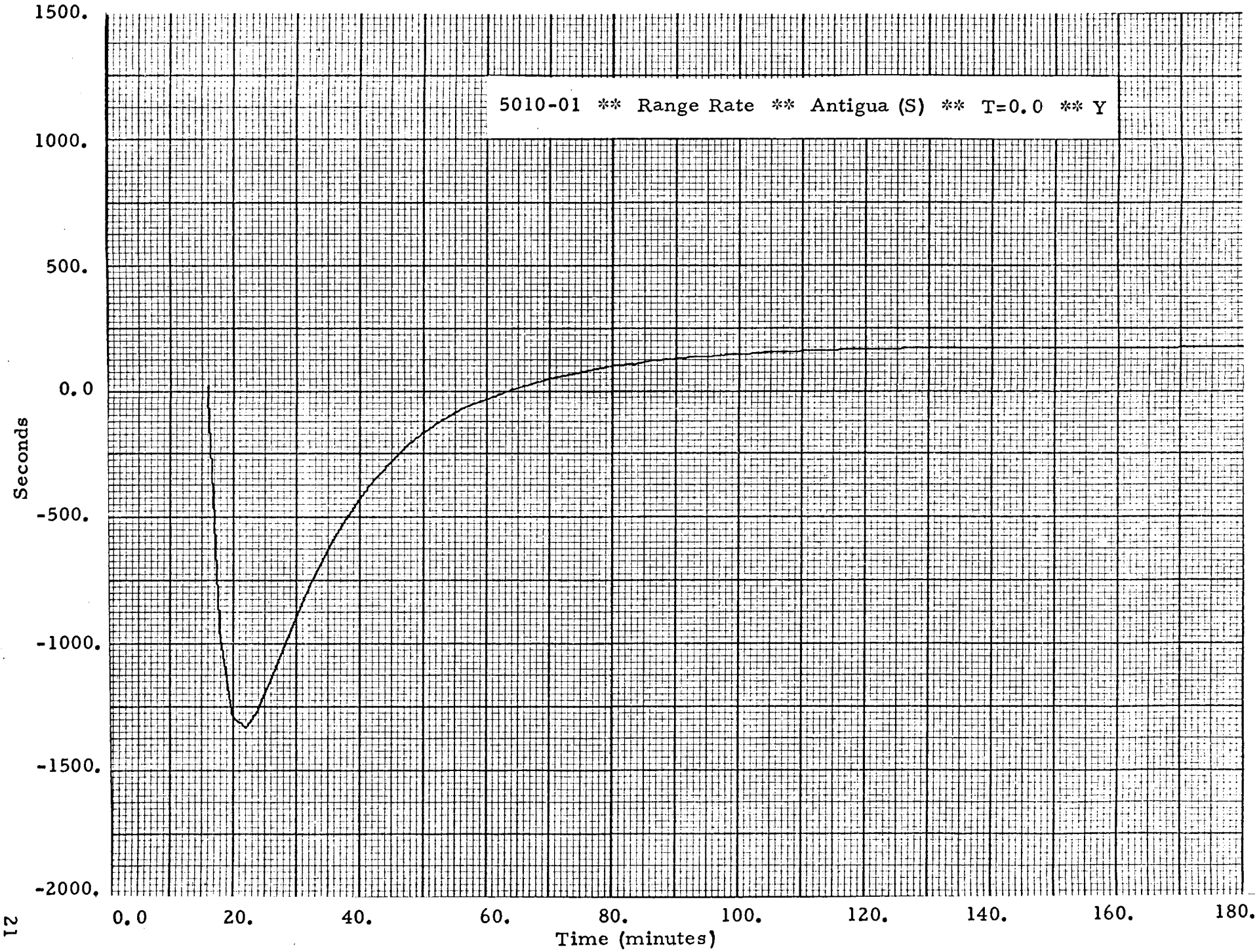
5010-01 ** Range Rate ** Antigua (S) ** T=0.0 ** Y
1500.
1000.
500.
0.0
-500.
-1000.
-1500.
-2000.
Seconds
0.0
20.
40.
60.
80.
100.
120.
140.
160.
180.
Time (minutes)

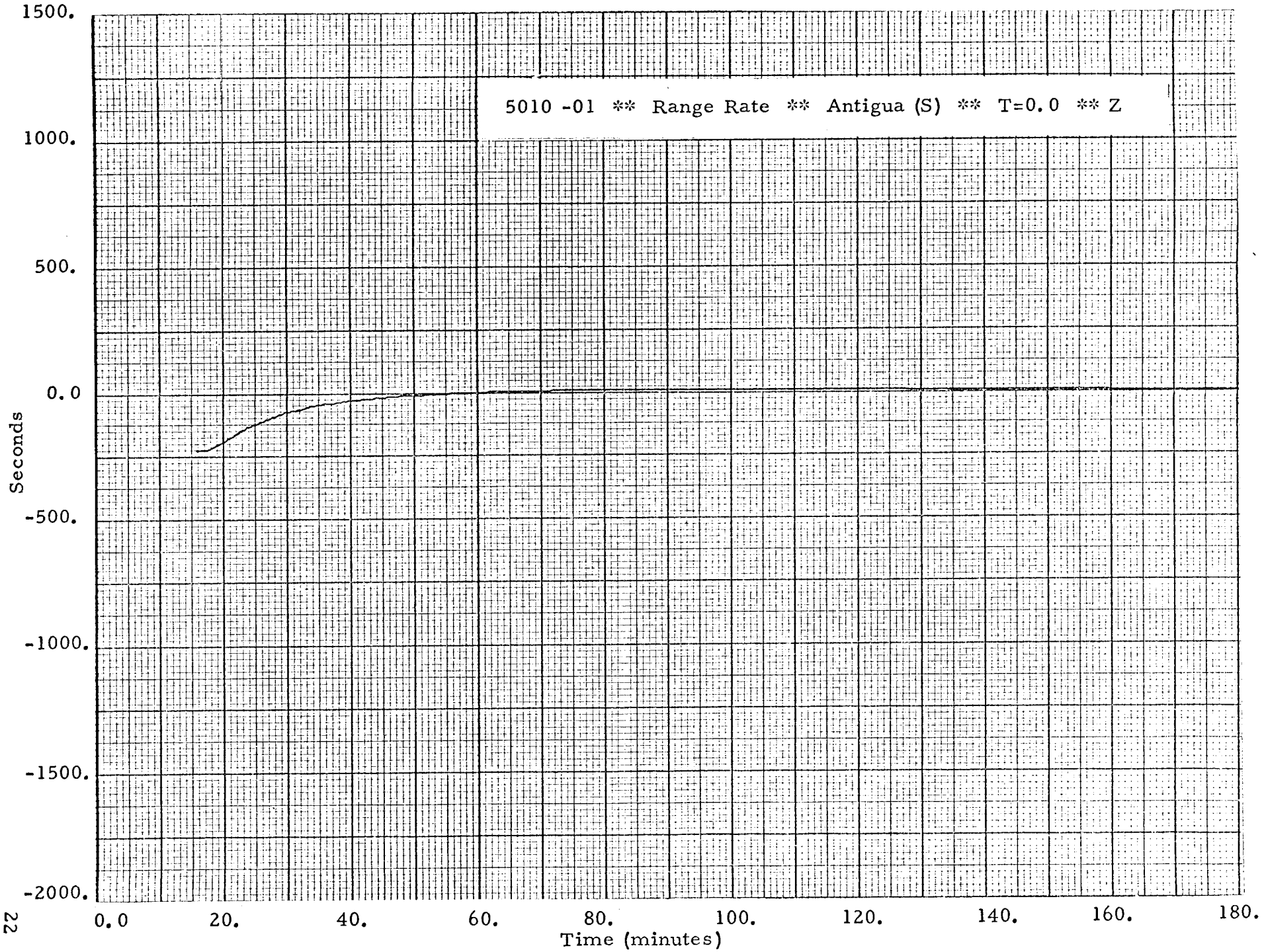
5010 -01 ** Range Rate ** Antigua (S) ** T=0.0 ** Z
1500.
1000.
500.
0.0
-500.
-1000.
-1500.
-2000.
Seconds
0.0
20.
40.
60.
80.
100.
120.
140.
160.
180.
Time (minutes)

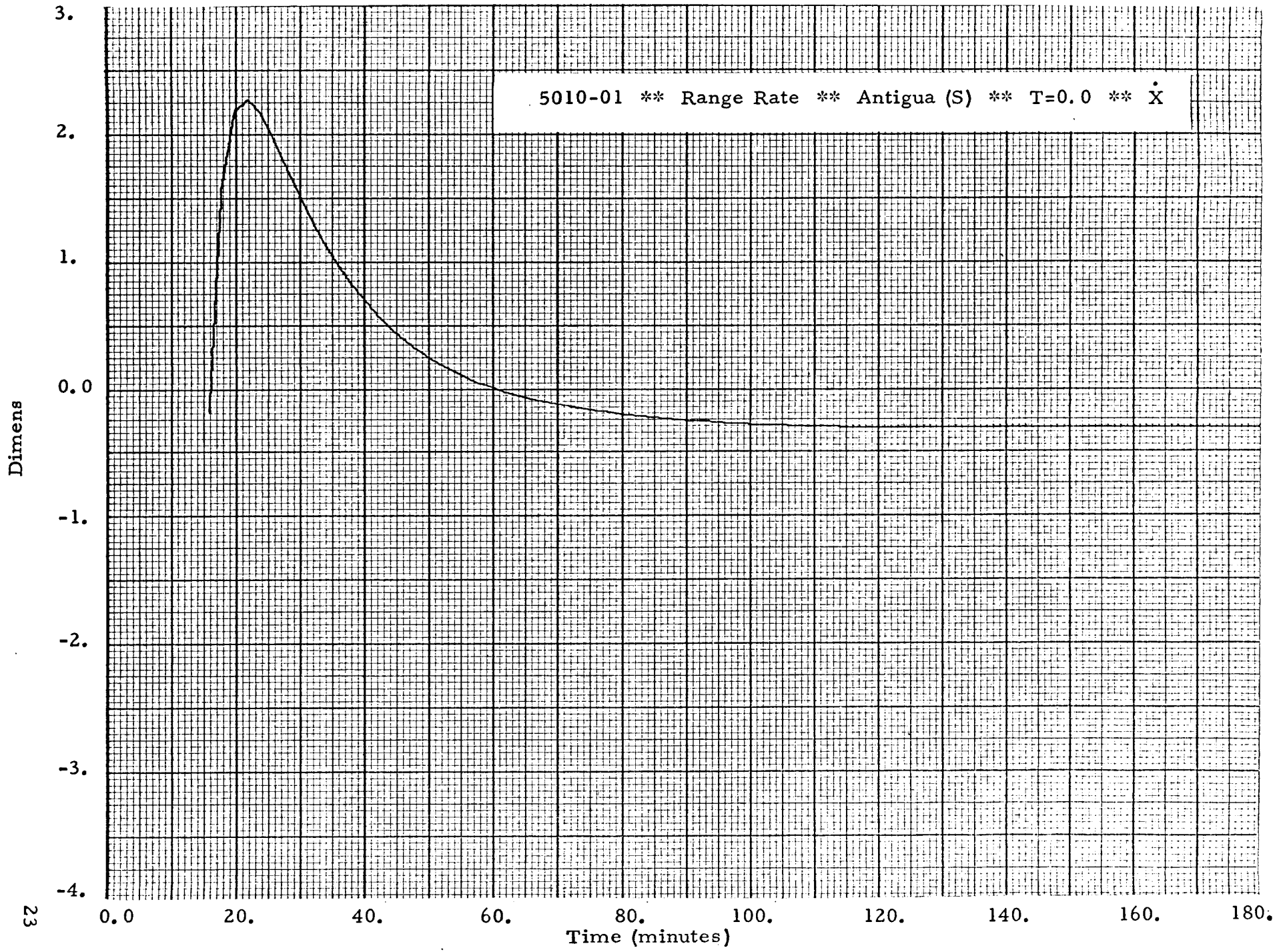
5010-01 ** Range Rate ** Antigua (S) ** T=0.0 ** $\dot{X}$
3.
2.
1.
0.0
-1.
-2.
-3.
-4.
Dimens
0.0
20.
40.
60.
80.
100.
120.
140.
160.
180.
Time (minutes)

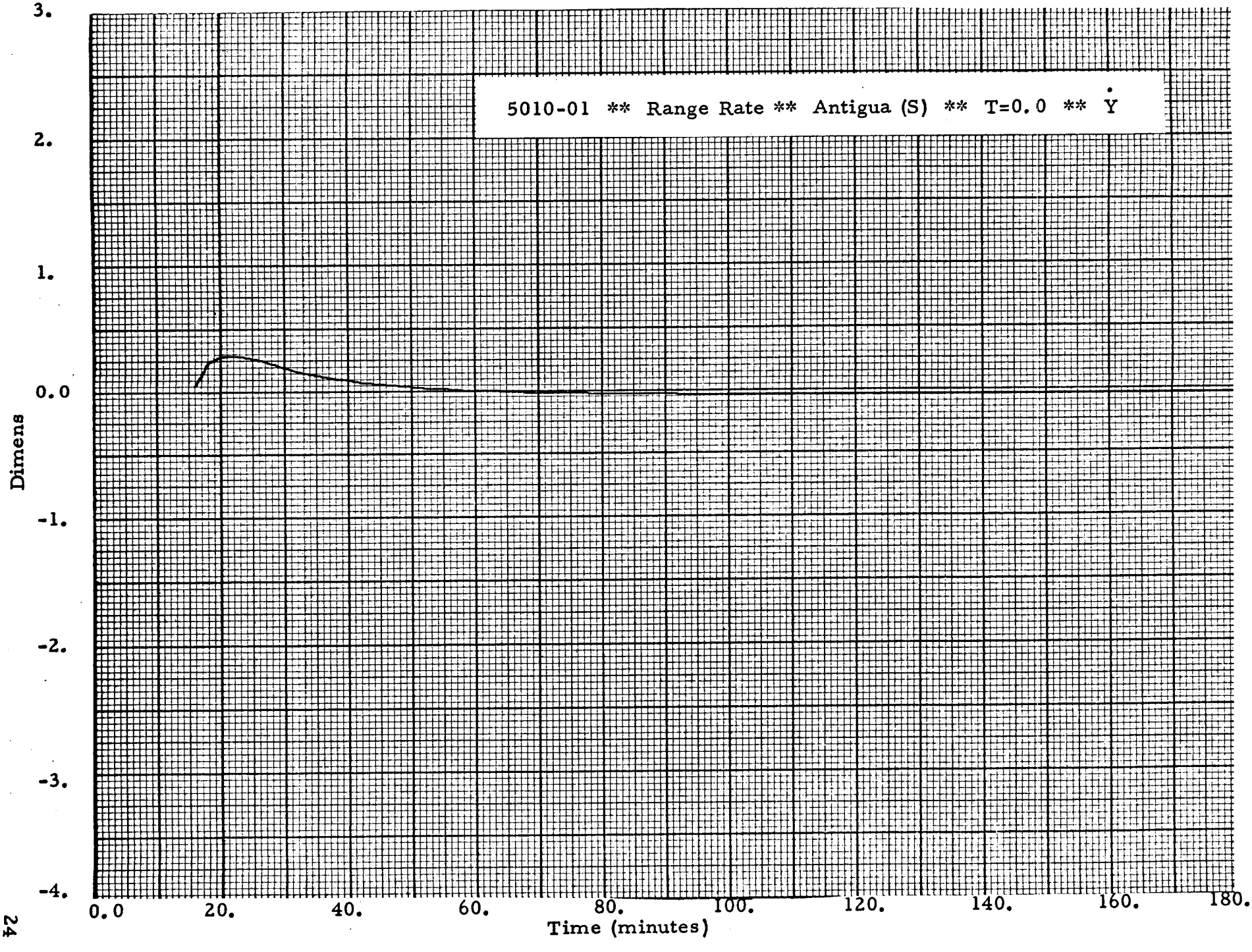
5010-01 ** Range Rate ** Antigua (S) ** T=0.0 ** $\dot{Y}$
3.
2.
1.
0.0
-1.
-2.
-3.
-4.
Dimens
0.0
20.
40.
60.
80.
100.
120.
140.
160.
180.
Time (minutes)

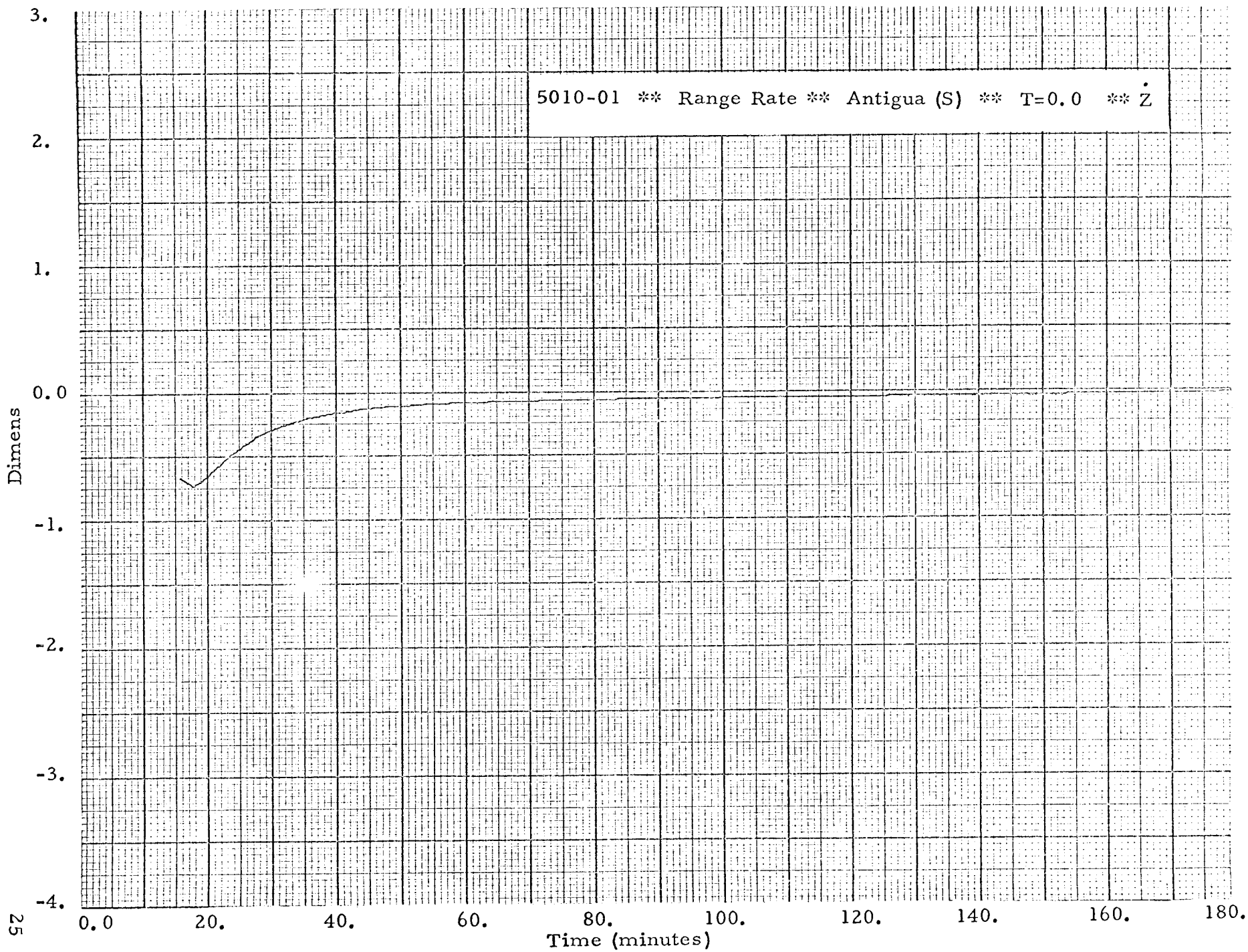
5010-01 ** Range Rate ** Antigua (S) ** T=0.0 ** Ż
3.
2.
1.
0.0
-1.
-2.
-3.
-4.
Dimens
0.0
20.
40.
60.
80.
100.
120.
140.
160.
180.
Time (minutes)

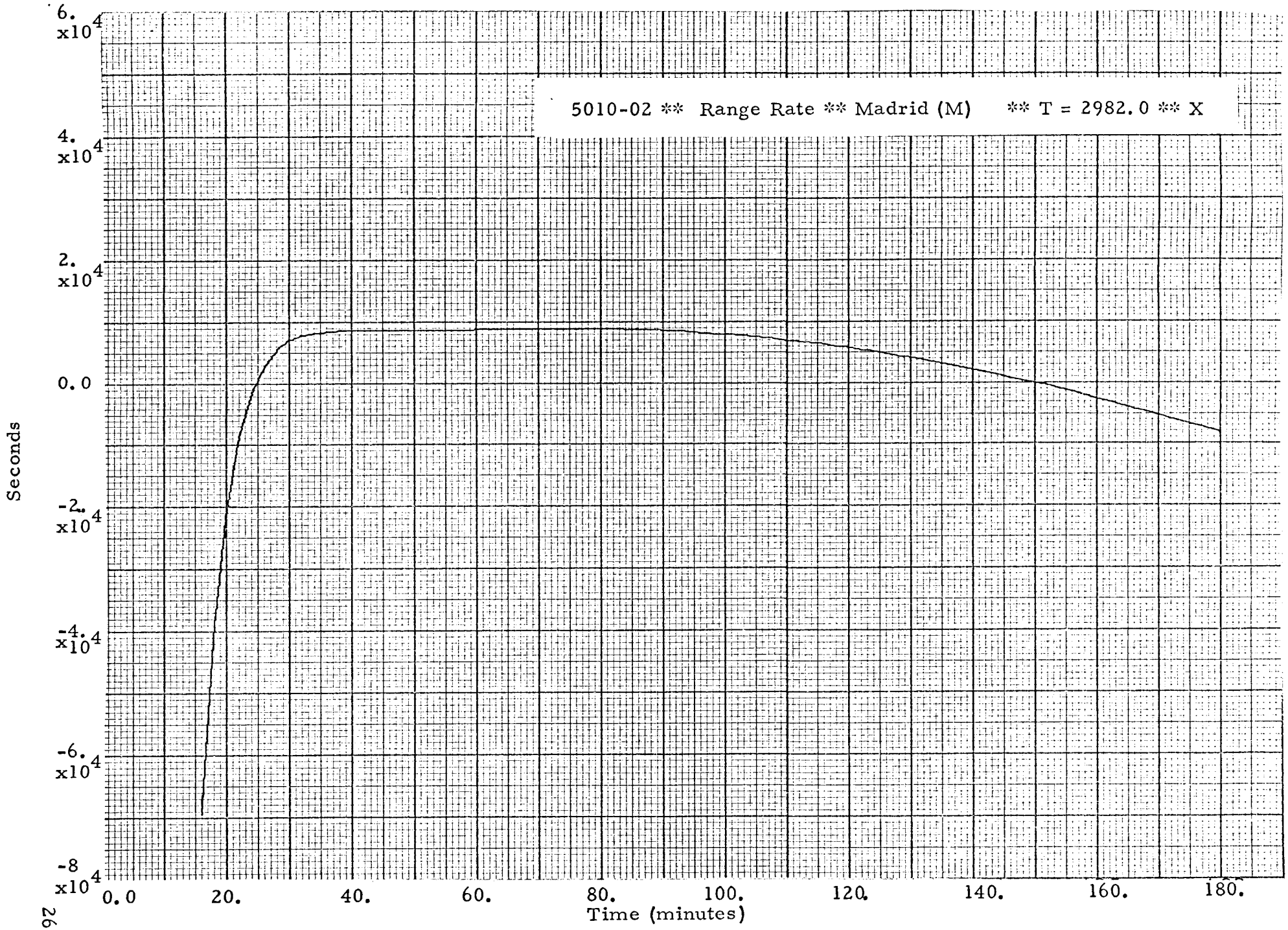
5010-02 ** Range Rate ** Madrid (M) ** T = 2982.0 ** X
6. x10^4
4. x10^4
2. x10^4
0.0
-2. x10^4
-4. x10^4
-6. x10^4
-8 x10^4
Seconds
0.0
20.
40.
60.
80.
100.
120.
140.
160.
180.
Time (minutes)

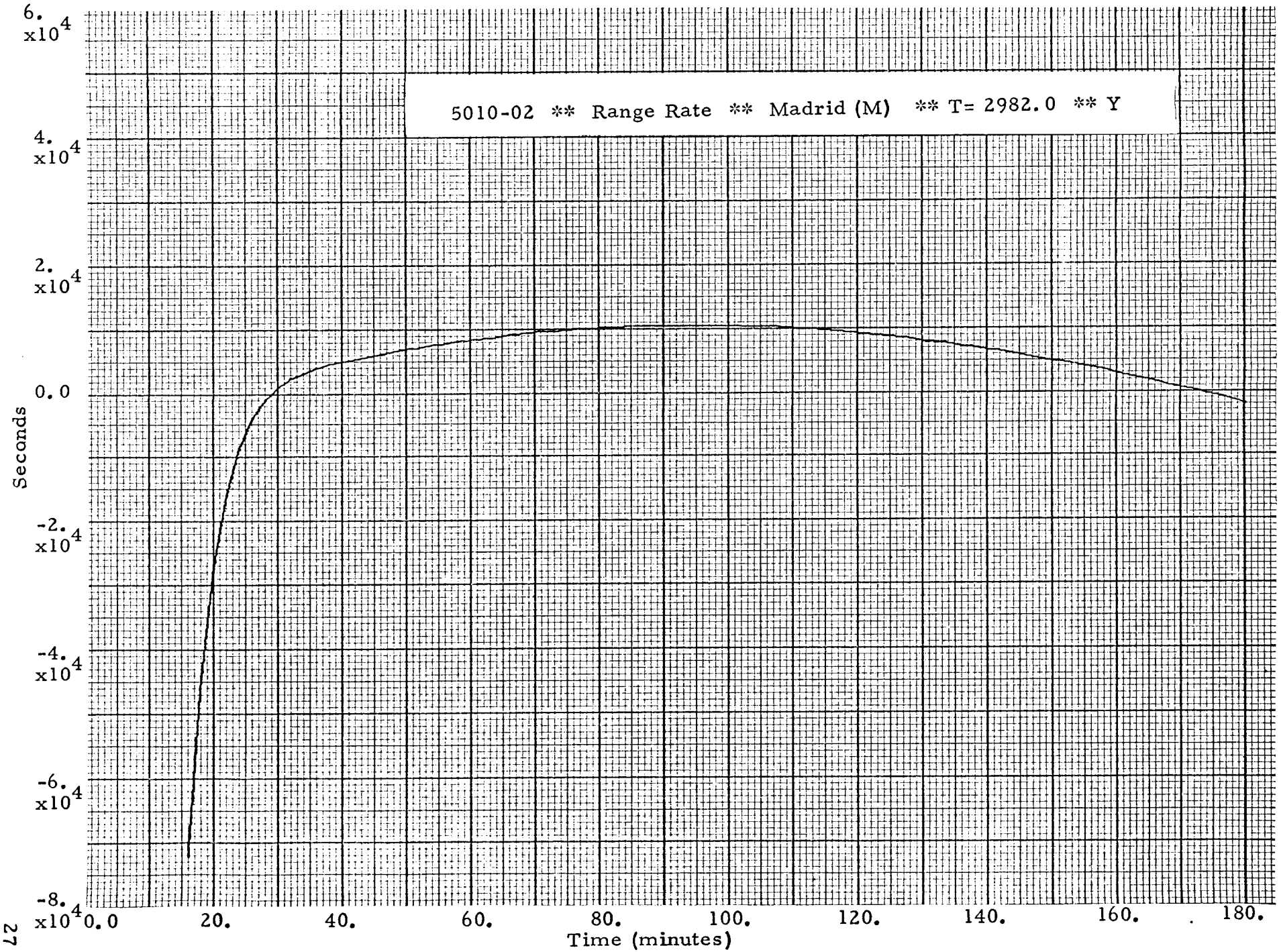
5010-02 ** Range Rate ** Madrid (M) ** T= 2982.0 ** Y
6. x10^4
4. x10^4
2. x10^4
0.0
-2. x10^4
-4. x10^4
-6. x10^4
-8. x10^4
Seconds
0.0
20.
40.
60.
80.
100.
120.
140.
160.
180.
Time (minutes)

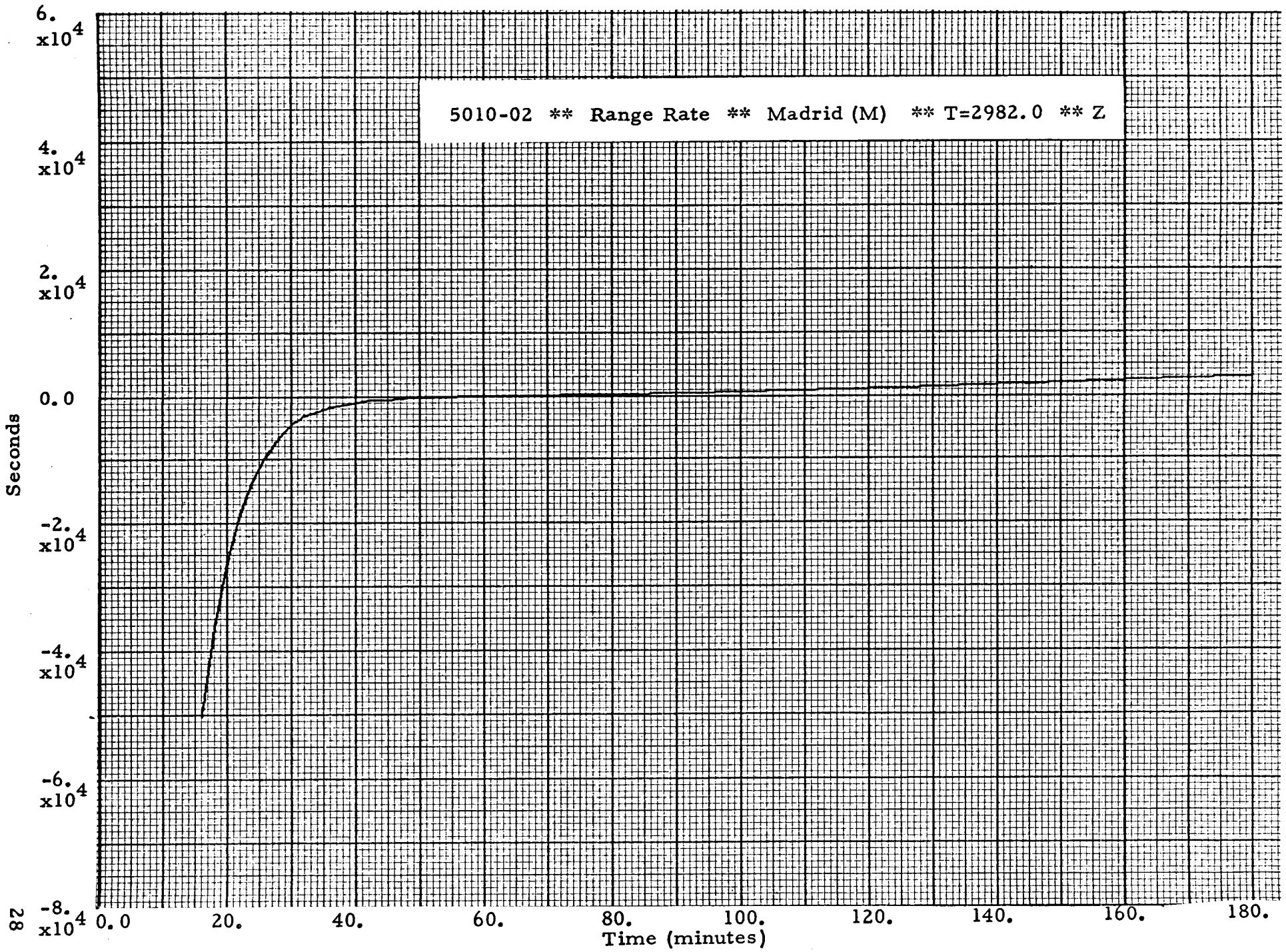
5010-02 ** Range Rate ** Madrid (M) ** T=2982.0 ** Z
6. x10^4
4. x10^4
2. x10^4
0.0
-2. x10^4
-4. x10^4
-6. x10^4
-8. x10^4
Seconds
0.0
20.
40.
60.
80.
100.
120.
140.
160.
180.
Time (minutes)

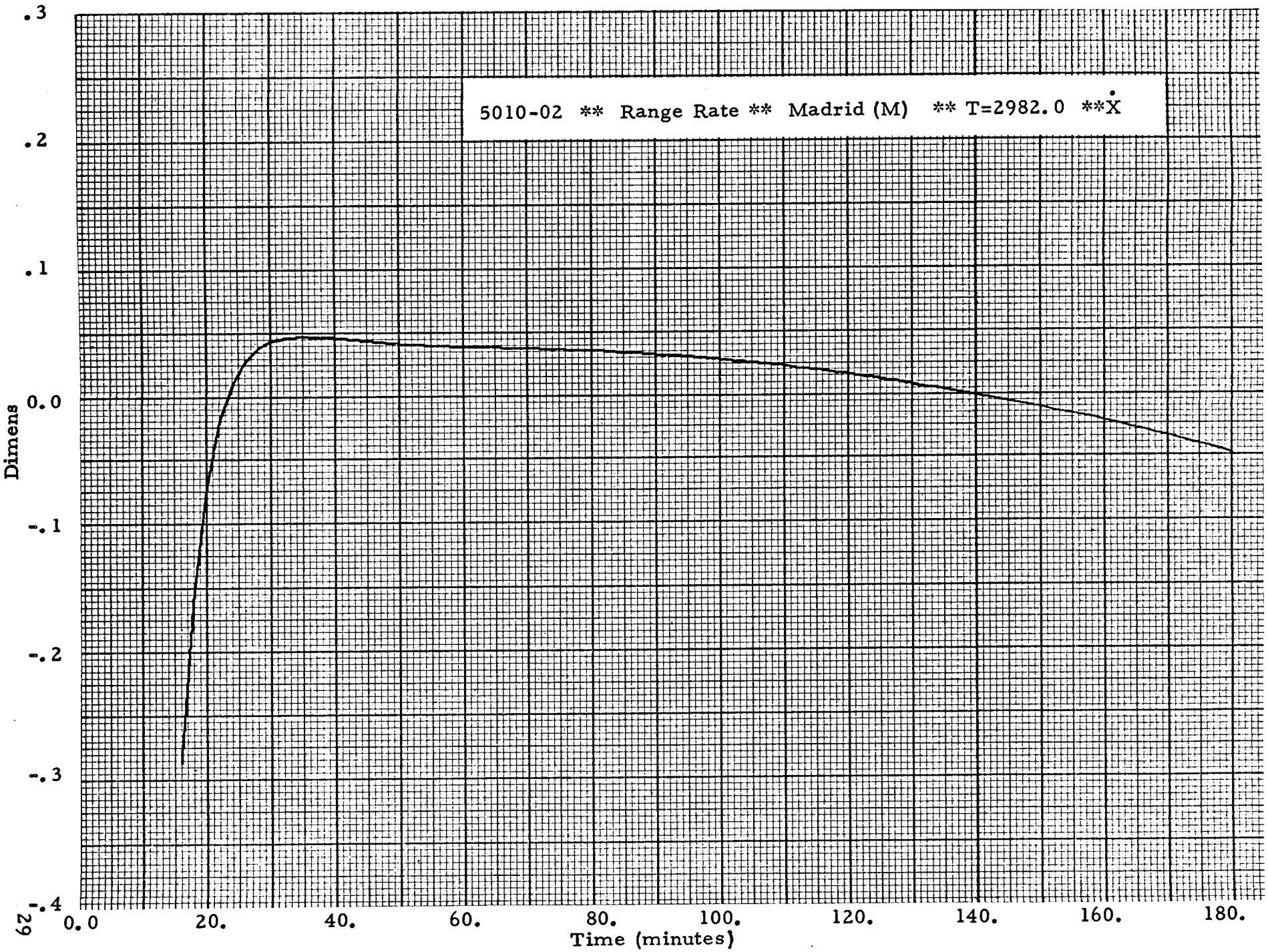
5010-02 ** Range Rate ** Madrid (M) ** T=2982.0 **Ẋ
Dimens
.3
.2
.1
0.0
-.1
-.2
-.3
-.4
0.0
20.
40.
60.
80.
100.
120.
140.
160.
180.
Time (minutes)

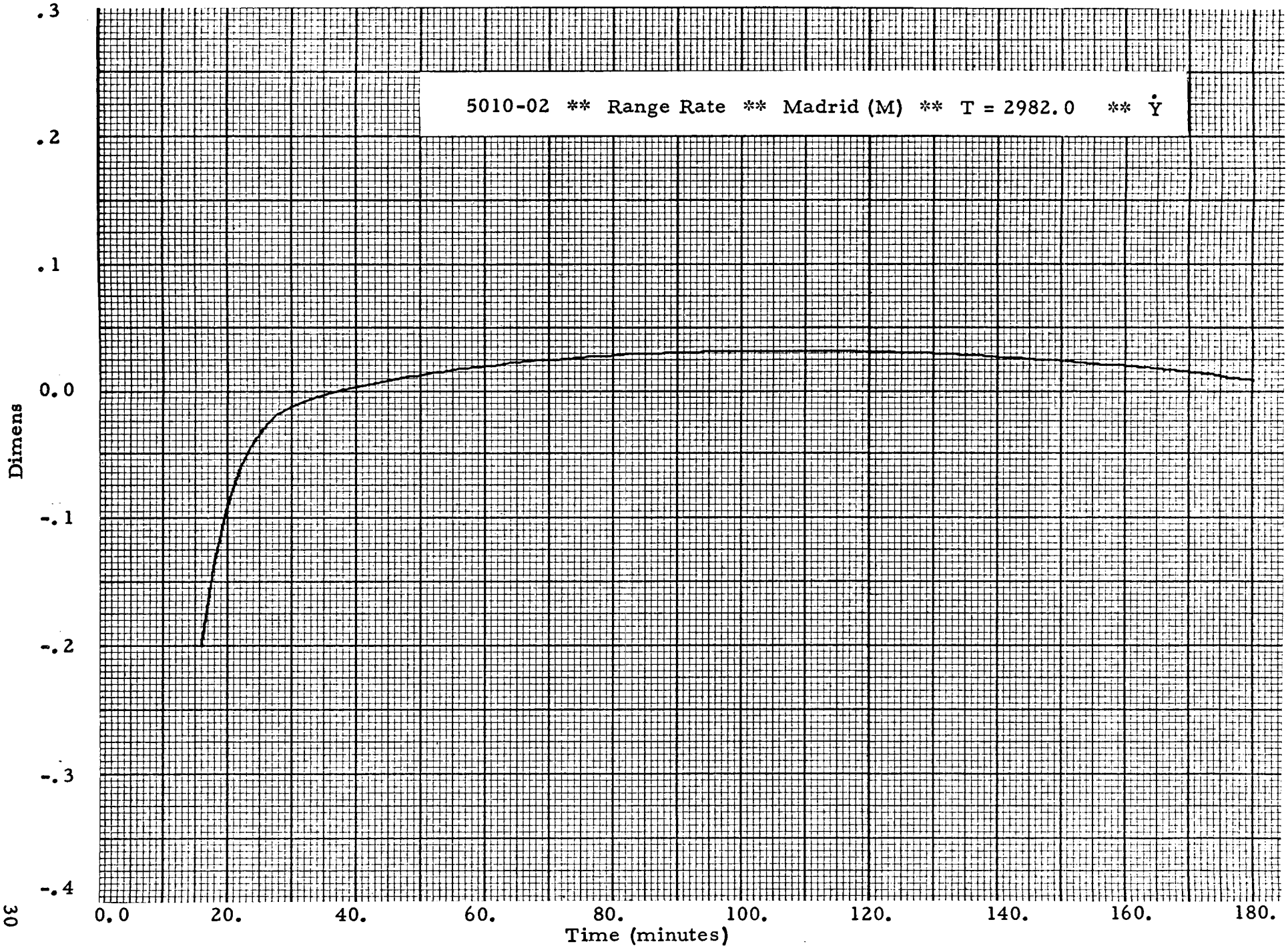
5010-02 ** Range Rate ** Madrid (M) ** T = 2982.0 ** Ẏ
.3
.2
.1
0.0
-.1
-.2
-.3
-.4
Dimens
0.0
20.
40.
60.
80.
100.
120.
140.
160.
180.
Time (minutes)

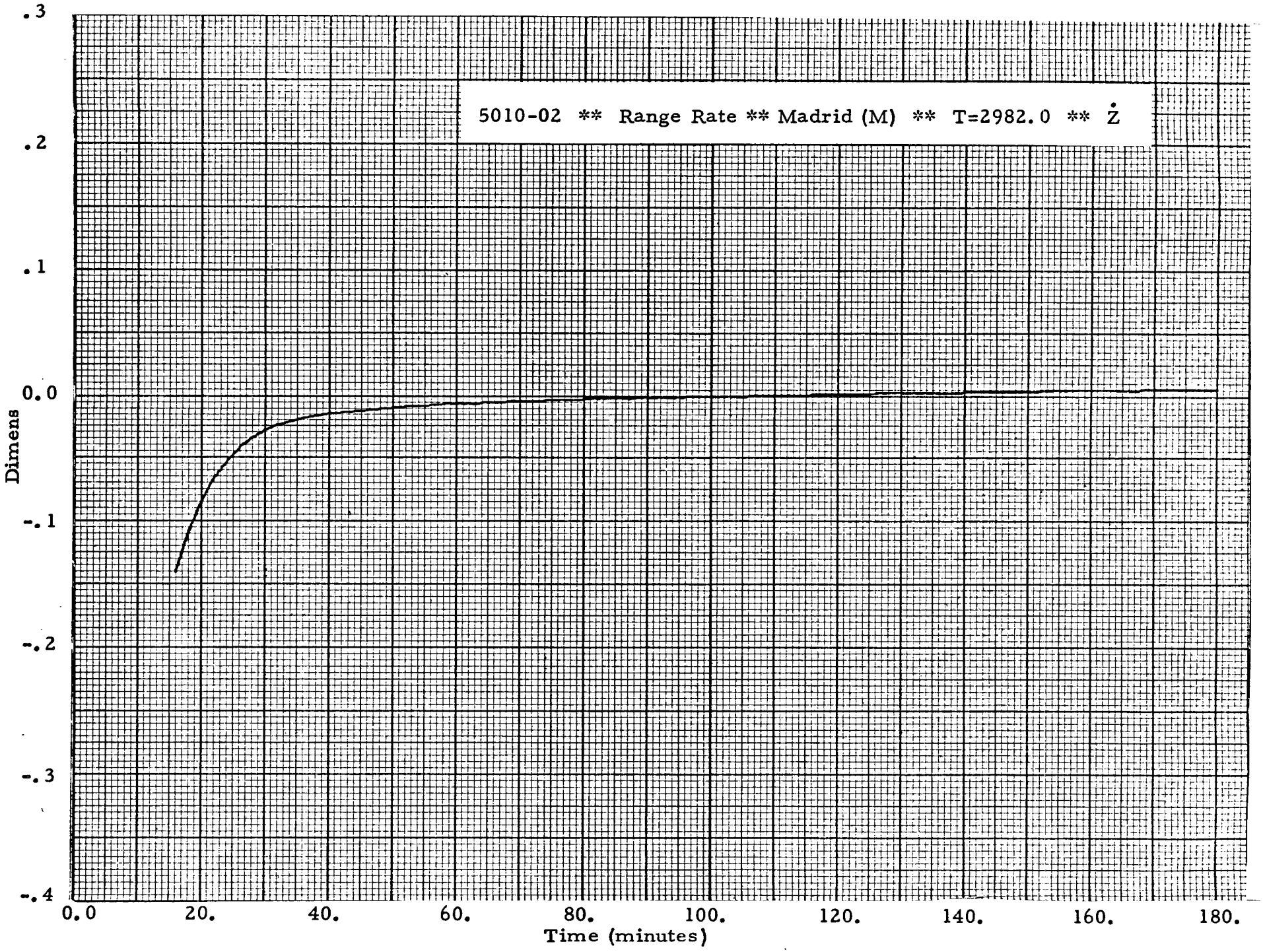
5010-02 ** Range Rate ** Madrid (M) ** T=2982.0 ** Ż
.3
.2
.1
0.0
-.1
-.2
-.3
-.4
Dimens
0.0
20.
40.
60.
80.
100.
120.
140.
160.
180.
Time (minutes)

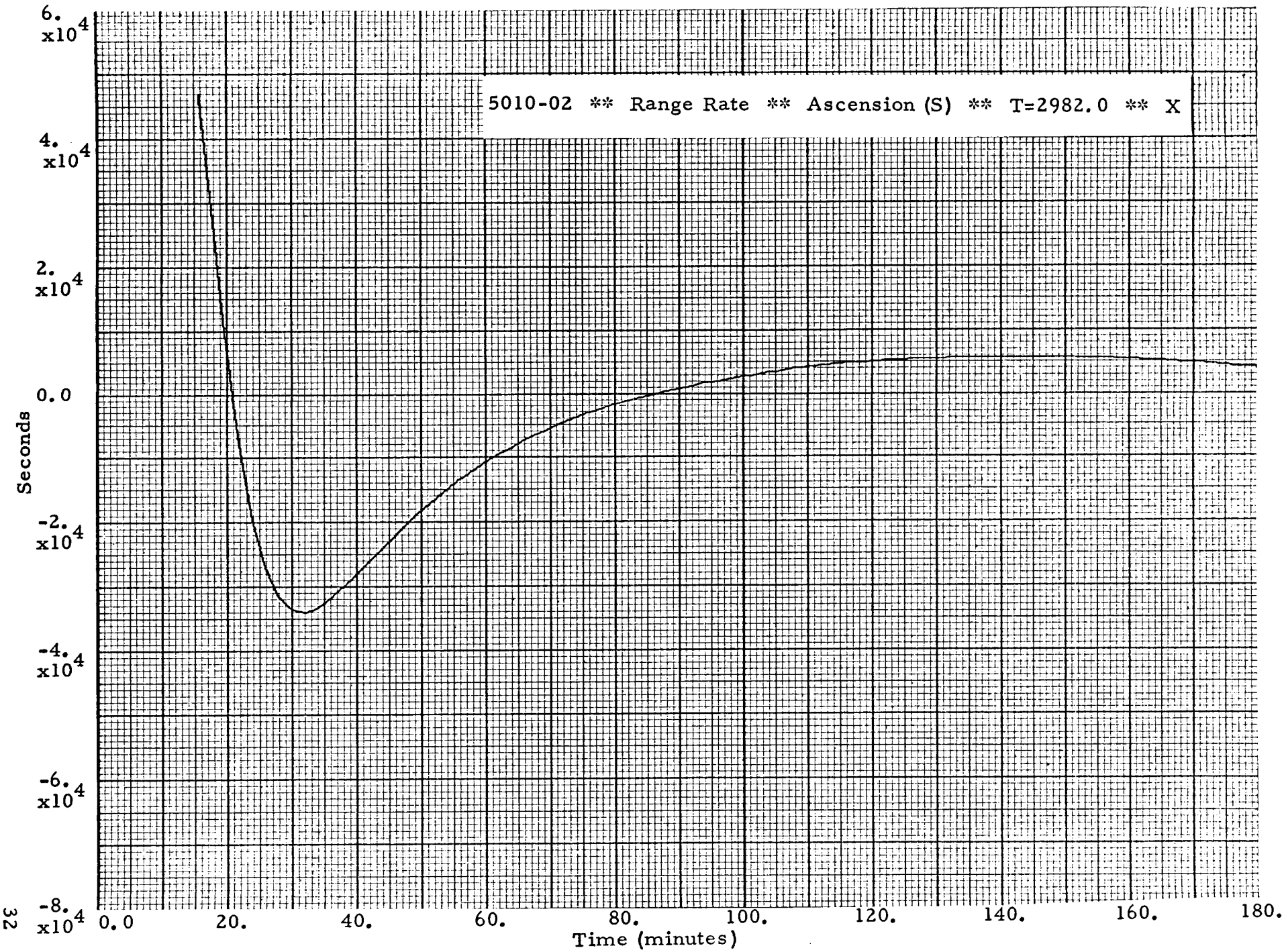
5010-02 ** Range Rate ** Ascension (S) ** T=2982.0 ** X
6. x10^4
4. x10^4
2. x10^4
0.0
-2. x10^4
-4. x10^4
-6. x10^4
-8. x10^4
Seconds
0.0
20.
40.
60.
80.
100.
120.
140.
160.
180.
Time (minutes)

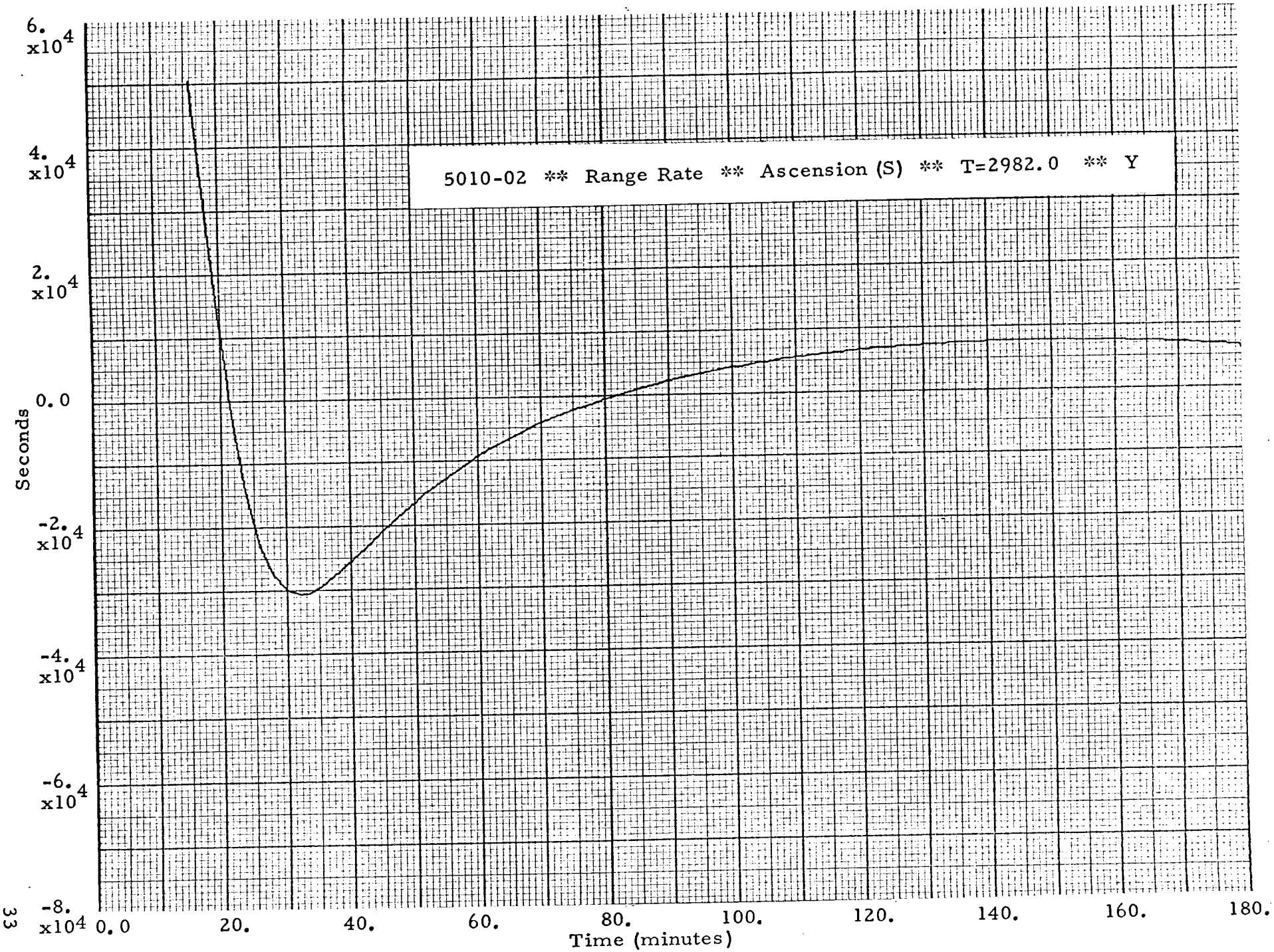
5010-02 ** Range Rate ** Ascension (S) ** T=2982.0 ** Y
6. x10^4
4. x10^4
2. x10^4
0.0
-2. x10^4
-4. x10^4
-6. x10^4
-8. x10^4
Seconds
0.0
20.
40.
60.
80.
100.
120.
140.
160.
180.
Time (minutes)

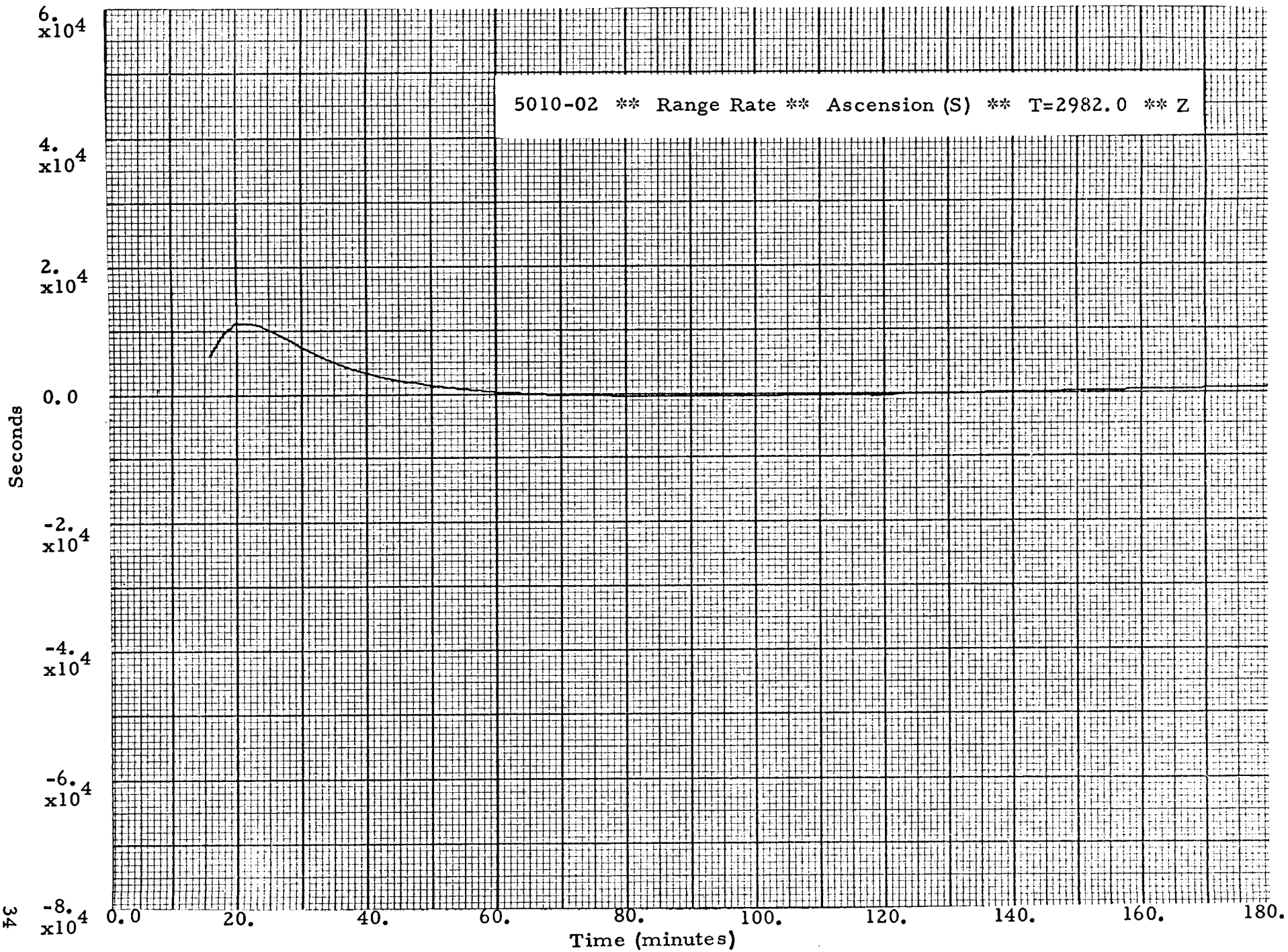
5010-02 ** Range Rate ** Ascension (S) ** T=2982.0 ** Z
6. x10^4
4. x10^4
2. x10^4
0.0
-2. x10^4
-4. x10^4
-6. x10^4
-8. x10^4
Seconds
0.0
20.
40.
60.
80.
100.
120.
140.
160.
180.
Time (minutes)

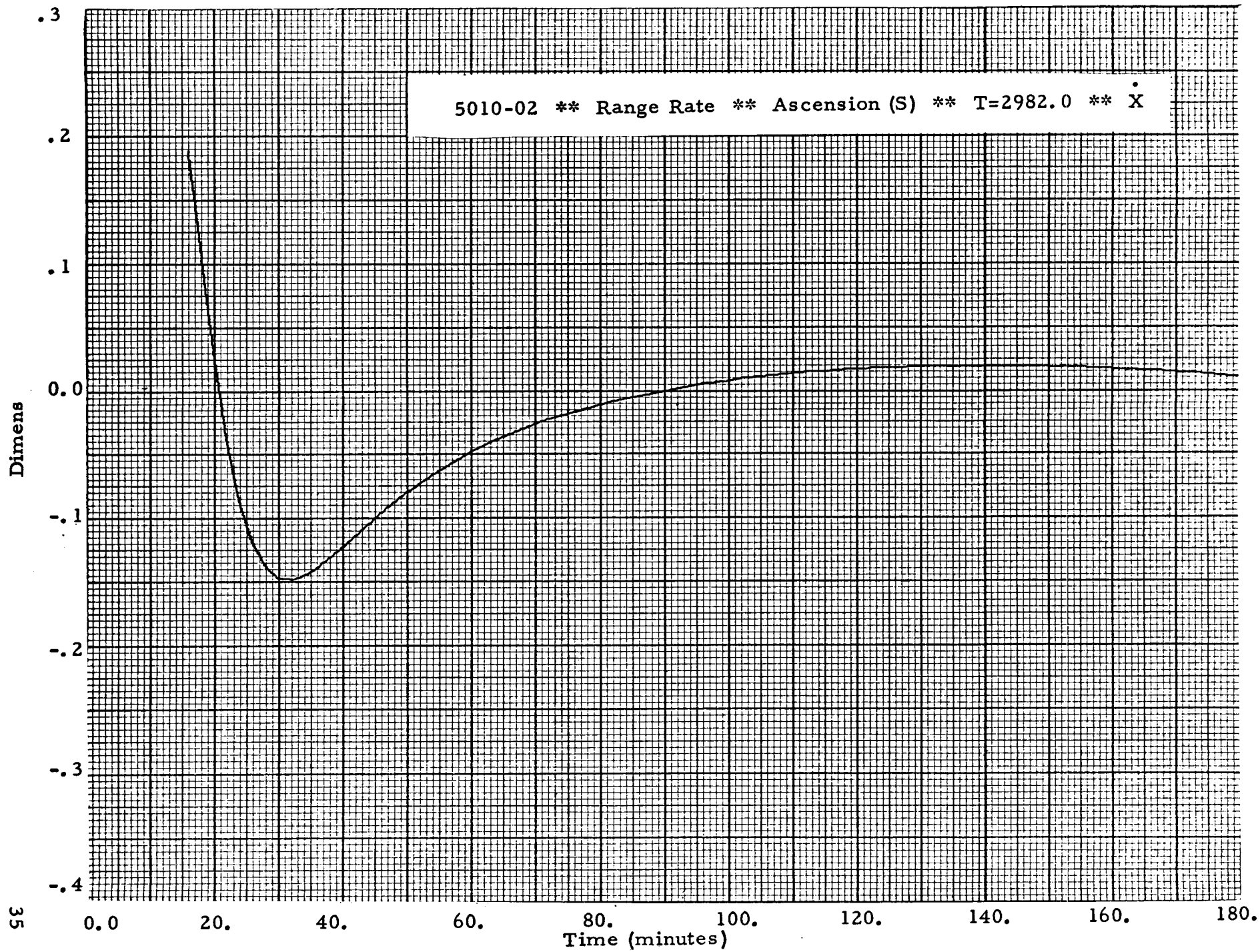
5010-02 ** Range Rate ** Ascension (S) ** T=2982.0 ** $\dot{X}$
Dimens
.3
.2
.1
0.0
-.1
-.2
-.3
-.4
0.0
20.
40.
60.
80.
100.
120.
140.
160.
180.
Time (minutes)

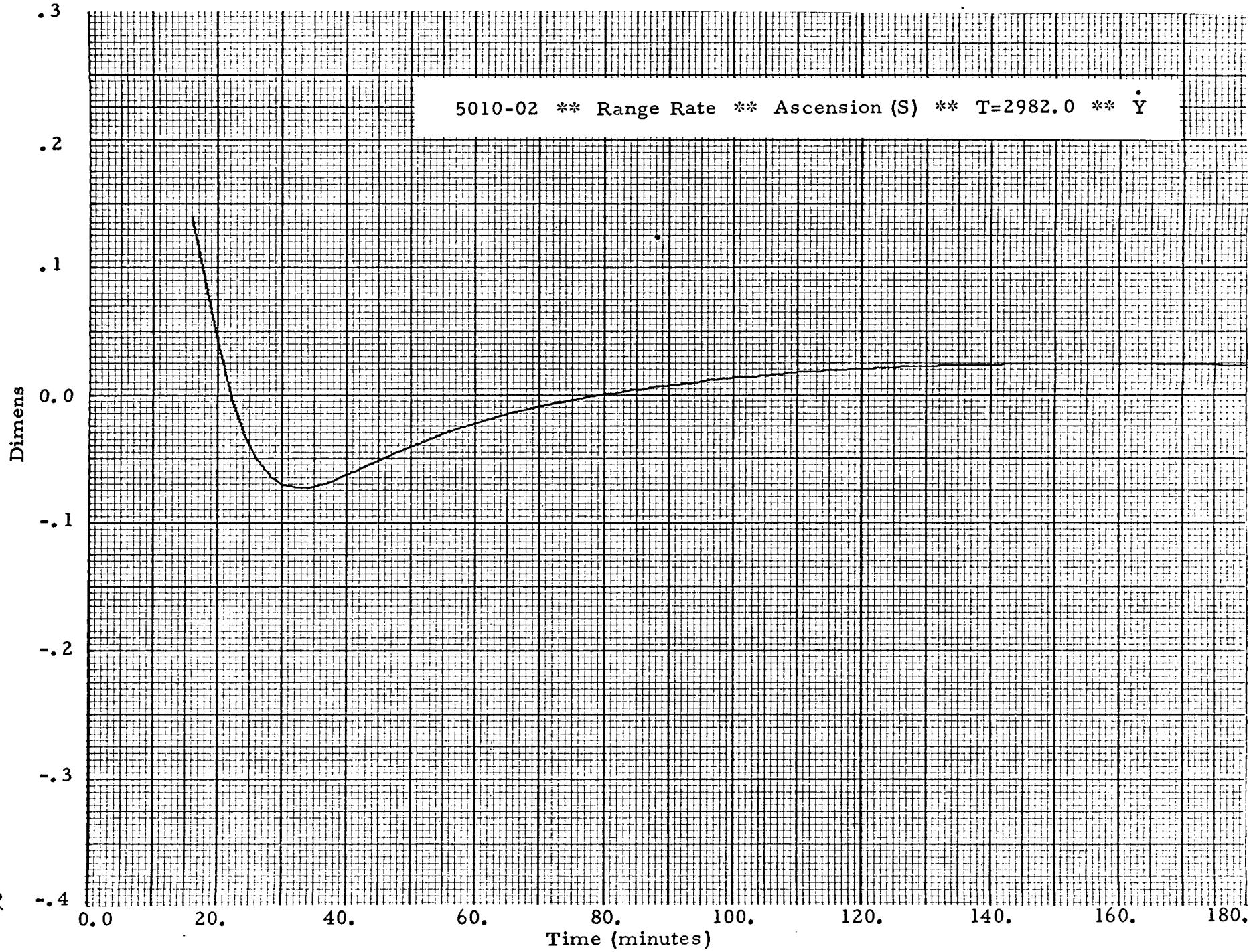
5010-02 ** Range Rate ** Ascension (S) ** T=2982.0 ** $\dot{Y}$
Dimens
.3
.2
.1
0.0
-.1
-.2
-.3
-.4
0.0
20.
40.
60.
80.
100.
120.
140.
160.
180.
Time (minutes)

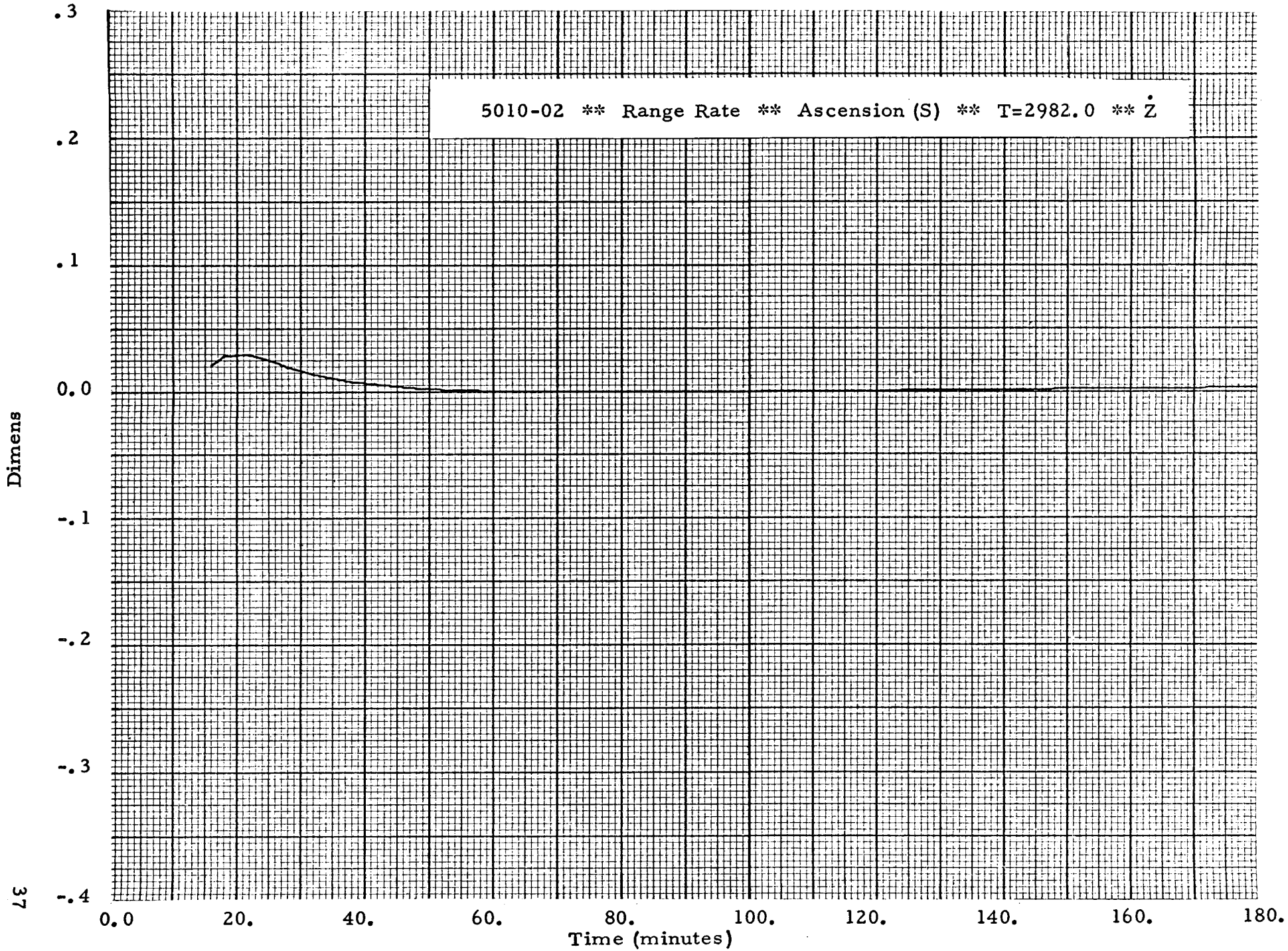
5010-02 ** Range Rate ** Ascension (S) ** T=2982.0 ** Ż
.3
.2
.1
0.0
-.1
-.2
-.3
-.4
Dimens
0.0
20.
40.
60.
80.
100.
120.
140.
160.
180.
Time (minutes)

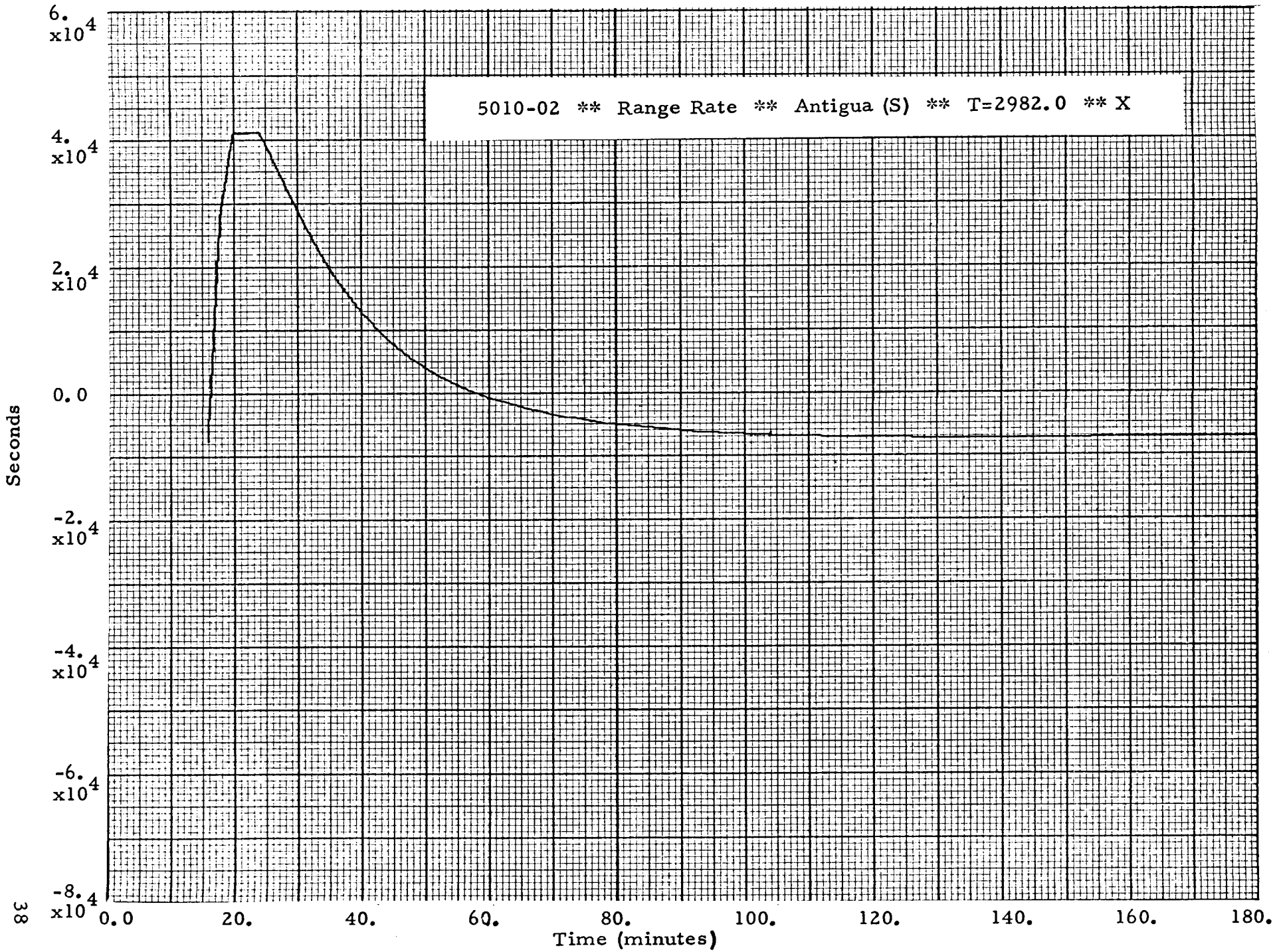
5010-02 ** Range Rate ** Antigua (S) ** T=2982.0 ** X
6. x10^4
4. x10^4
2. x10^4
0.0
-2. x10^4
-4. x10^4
-6. x10^4
-8. x10^4
Seconds
0.0
20.
40.
60.
80.
100.
120.
140.
160.
180.
Time (minutes)

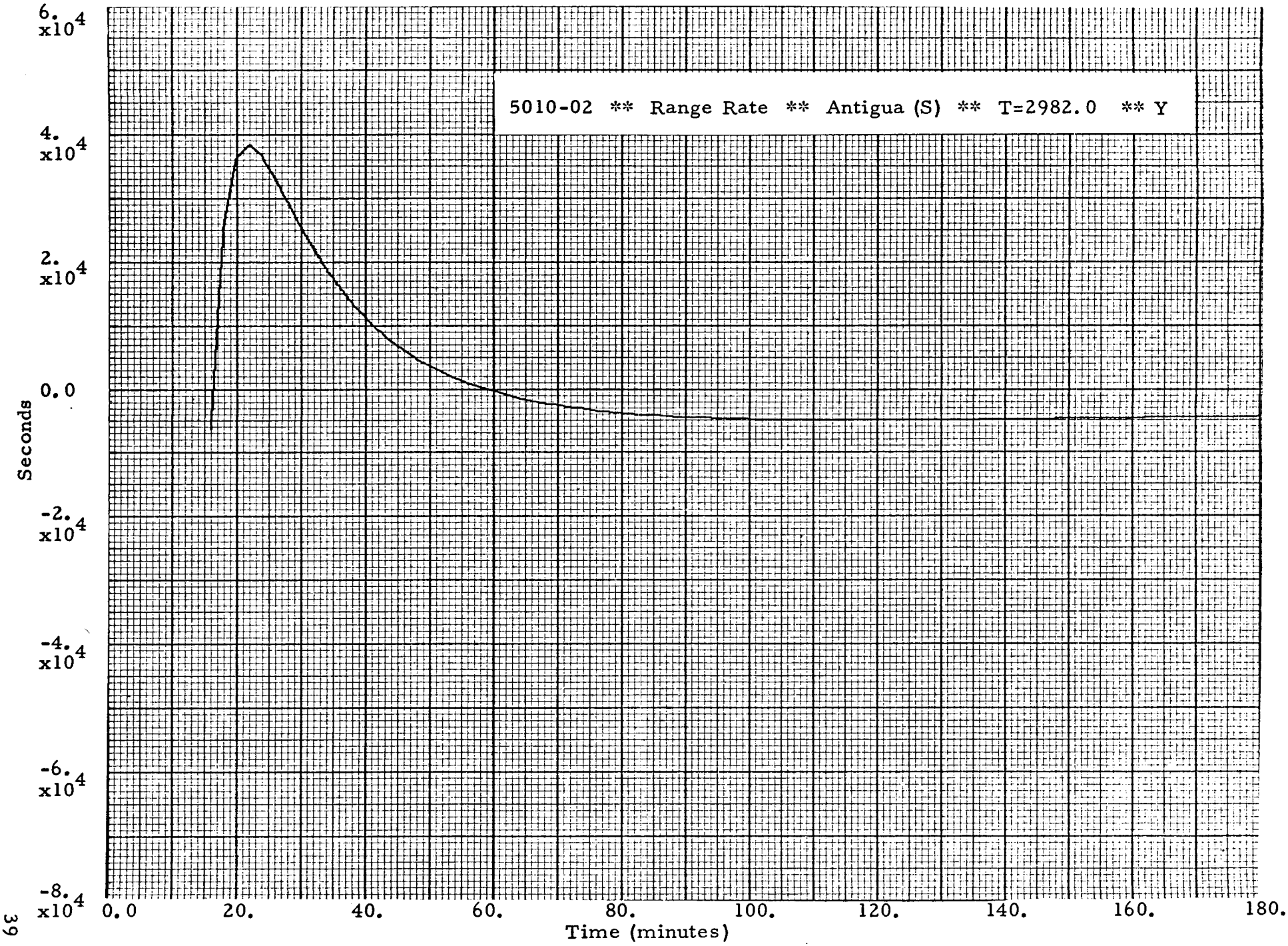
5010-02 ** Range Rate ** Antigua (S) ** T=2982.0 ** Y
6. x10^4
4. x10^4
2. x10^4
0.0
-2. x10^4
-4. x10^4
-6. x10^4
-8. x10^4
Seconds
0.0
20.
40.
60.
80.
100.
120.
140.
160.
180.
Time (minutes)

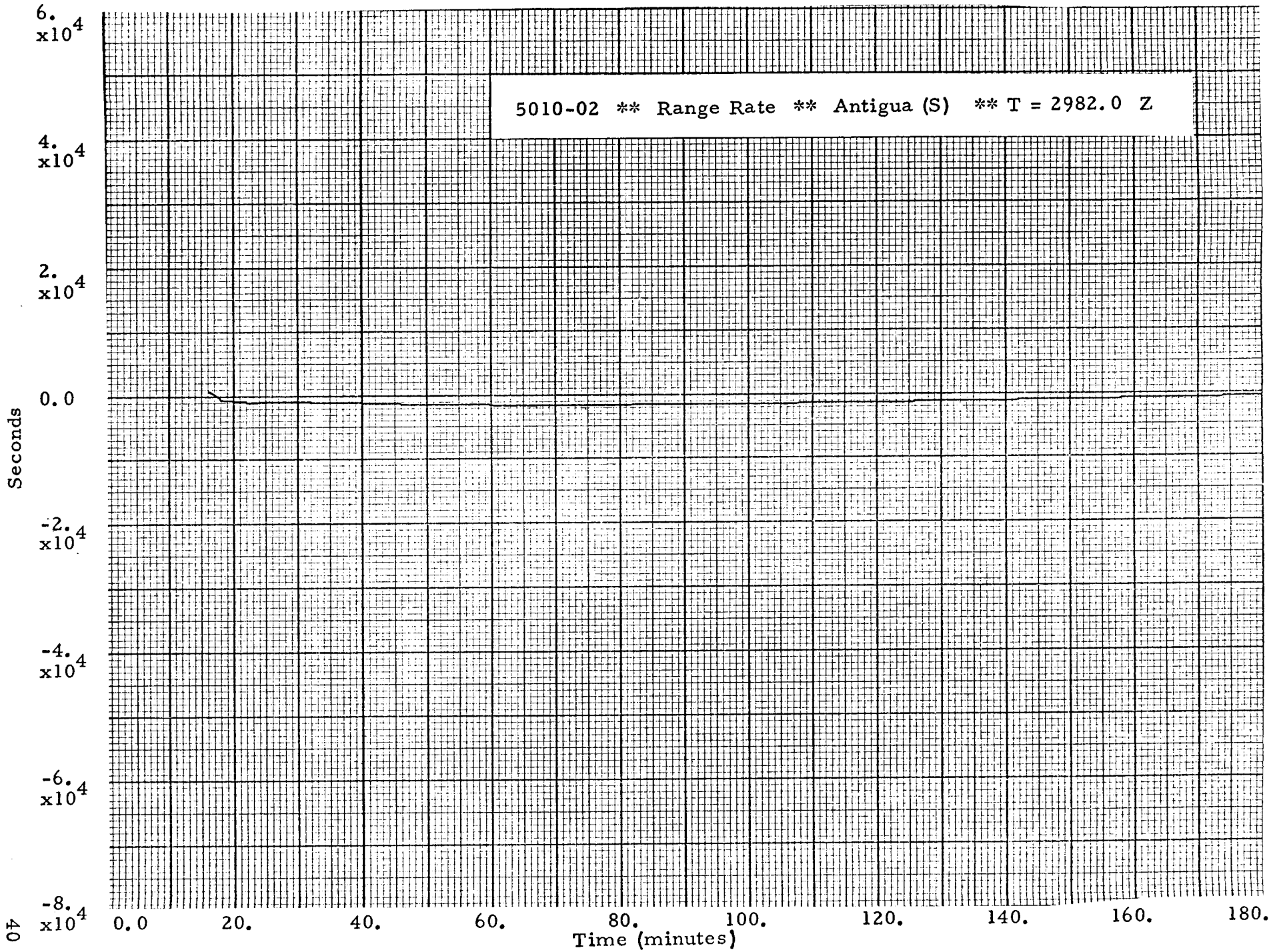
5010-02 ** Range Rate ** Antigua (S) ** T = 2982.0 Z
6. x10^4
4. x10^4
2. x10^4
0.0
-2. x10^4
-4. x10^4
-6. x10^4
-8. x10^4
Seconds
0.0
20.
40.
60.
80.
100.
120.
140.
160.
180.
Time (minutes)

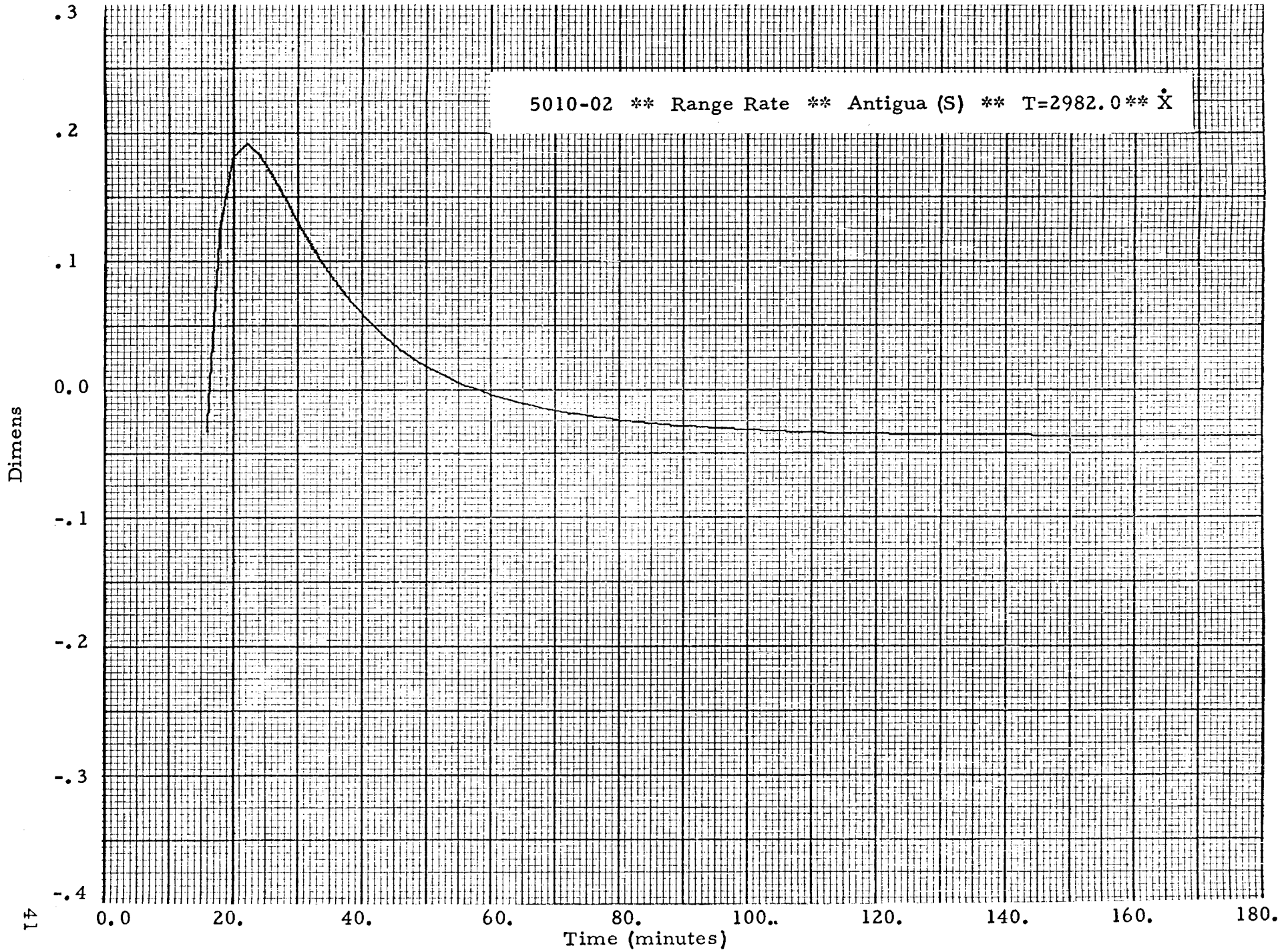
5010-02 ** Range Rate ** Antigua (S) ** T=2982.0** $\dot{X}$
.3
.2
.1
0.0
-.1
-.2
-.3
-.4
Dimens
0.0
20.
40.
60.
80.
100.
120.
140.
160.
180.
Time (minutes)

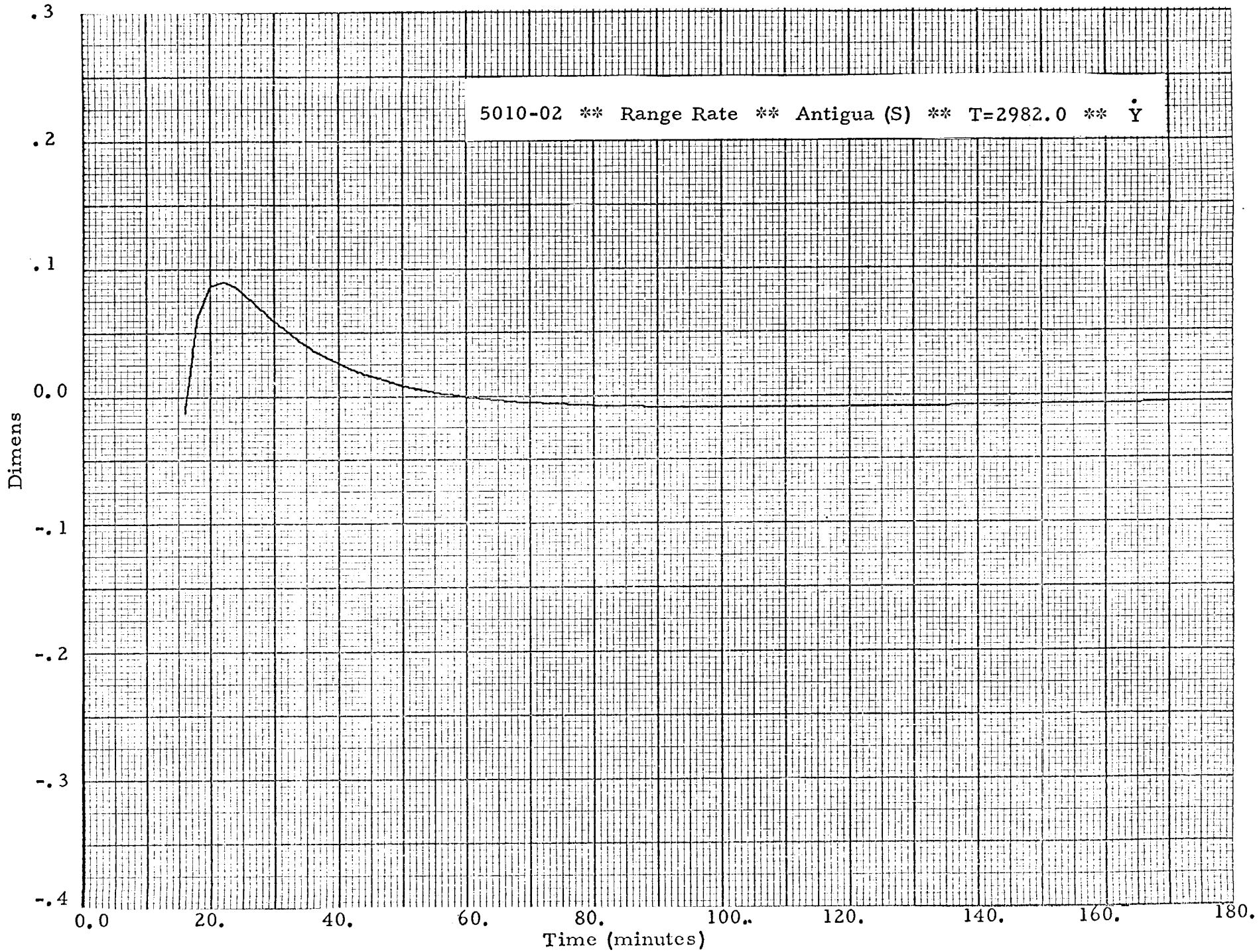
5010-02 ** Range Rate ** Antigua (S) ** T=2982.0 ** $\dot{Y}$
.3
.2
.1
0.0
-.1
-.2
-.3
-.4
Dimens
0.0
20.
40.
60.
80.
100.
120.
140.
160.
180.
Time (minutes)

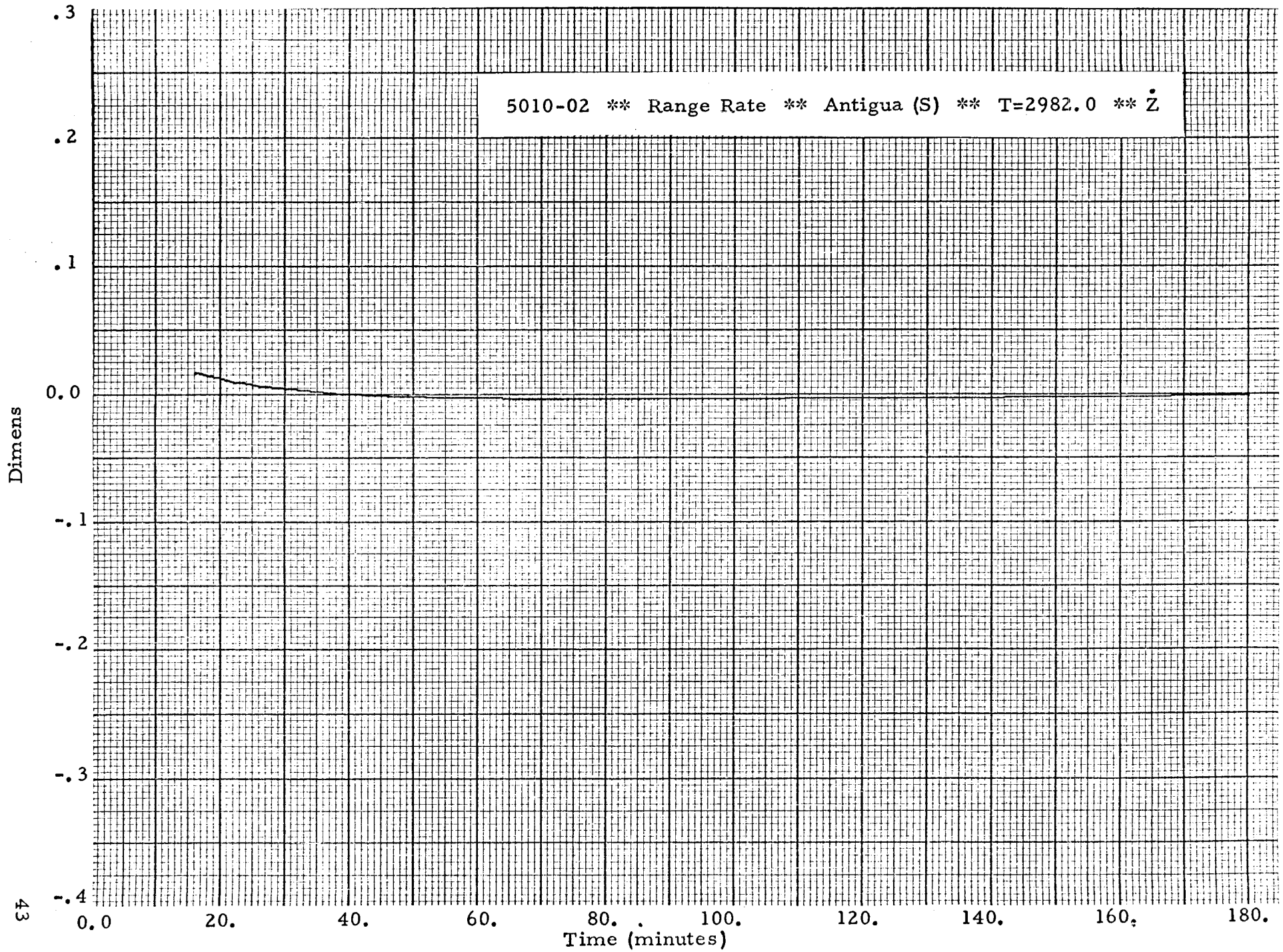
5010-02 ** Range Rate ** Antigua (S) ** T=2982.0 ** Ż
.3
.2
.1
0.0
-.1
-.2
-.3
-.4
Dimens
0.0
20.
40.
60.
80.
100.
120.
140.
160.
180.
Time (minutes)

APOLLO NOTE NO. 354
(Task I - Item I(B))

B. Murphy
6 July 1965

COMPARISON OF ONE-DIMENSION AND THREE-DIMENSION TROPOSPHERE MODELS

In an effort to obtain a more accurate representation of the troposphere (or ionosphere) to arrive at more meaningful radar range and angle errors, the program described in Apollo Note No. 293, Appendix B and C was written. The first model used (for the refractivity) is:

$$N(h, \gamma, \Omega) = \begin{cases} N_o \, \delta \, e^{-\frac{\delta h}{H}} & 0 \leq h \leq H_2 \\ 0 & h > H_2 \end{cases}$$

where:

$$\delta = \left[1 - \alpha' (\gamma - \gamma_o) - \beta' (\Omega - \Omega_o) \right]$$

γ_o = station longitude

Ω_o = station co-latitude

$$\alpha' = - \frac{1}{N_o} \frac{\partial N}{\partial \gamma} \bigg|_{h=0}$$

$$\beta' = - \frac{1}{N_o} \frac{\partial N}{\partial \Omega} \bigg|_{h=0}$$

h = height above surface of Earth

H = scale height

To a large extent, two parameters characterize the exponential troposphere model, the surface refractivity (N_o) and the zenith range error (N_oH). Note that for this troposphere model, N_oH is independent of co-latitude (Ω) or longitude (γ) while N_o [N (h=0)] is a linear function of these angles.

These parameters were chosen to give a best fit to the 1959 ARDC troposphere model. Neglecting water vapor, the surface refractivity is proportional to surface temperature, thus α' and β' are chosen to give extremes in surface temperature variation [a 10°F variation in temperature in 10° of latitude (or longitude) is effected by β' (or α') = .11].

A one-dimensional standard for comparison is obtained from the program described in Apollo Note No. 308 (combined troposphere-ionosphere) using only the troposphere portion of this program. The model used for this program is

$$N(h) = \begin{cases} N_o e^{-\frac{h}{H}} & 0 \leq h \leq H_2 \\ 0 & h > H_2 \end{cases}$$

where N_o and H are again chosen to give a good fit to the 1959 ARDC model, which are

$$N_o = .27286296 \cdot 10^{-3}$$

$$H = .84672269 \cdot 10^{4} \text{ meters}$$

The results of this one-dimensional program in addition to the various combinations of α', β', and θ (azimuth) for the three-dimensional program (including the case $\alpha' = \beta' = 0$, yielding a one-dimension representation) are compiled in Table 1 for two values of H_f, 127 km and the limiting case as H_f goes to infinity. From this table, it is seen that even for the extremes in surface temperature variation,

100°F in 10° of longitude ($\alpha' = 1.1$) and 40°F in 10° of latitude ($B' = .44$) along with an initial azimuth of 90°, for the worst case ($\phi_o = 5^{\circ}$) there is no more than 27 cm difference between this run and the one-dimensional situation. At $\phi_o = 30^{\circ}$, this difference is reduced to 1.2 cm. Note also that this difference is roughly proportional to this longitude coefficient α'(for $\theta_o = 90^{\circ}$) so that for $\phi_o = 5^{\circ}$, $\alpha' = .55$, and $\beta' = .22$, the difference is about 13 cm. The $\Delta\phi$ difference corresponding to the first case is 14 microradians. These differences, for Apollo purposes, are negligible.

Having shown that the three-dimensional effects in the N_o parameters are insignificant, the 3-D effects of the zenith range error (N_oH) are next investigated. The model used for this situation is

$$N(h, \gamma, \Omega) = \begin{cases} N_o e^{-\frac{\delta h}{H}} & 0 \leq h \leq H_2 \\ 0 & h > H_2 \end{cases}$$

where the variables employed are the same as the first model with the exception that

$$\alpha' = \left(\frac{1}{N_oH}\right) \frac{\partial\left(\int_0^{H_2} N\, dh\right)}{\partial\gamma} \Bigg|_{\substack{\Omega = \Omega_o \\ \gamma = \gamma_o}}$$

$$\beta' = \left(\frac{1}{N_oH}\right) \frac{\partial\left(\int_0^{H_2} N\, dh\right)}{\partial\Omega} \Bigg|_{\substack{\Omega = \Omega_o \\ \gamma = \gamma_o}}$$

That is, α' and β' are the percent rate of change zenith range error as a function of longitude and co-latitude, respectively. Since the zenith range error is highly correlated with surface barometric pressure, a choice of $\alpha' = .003$, $\beta' = .003$, (corresponding to a 3% change in barometric pressure in 10° of latitude or longitude) can be considered an extreme case. The results of this run are compiled in Table 2.

From this table, it is seen that the maximum difference from the one-dimension case is about .2 cm (at $\alpha' = .003$, $\beta' = .006$, $\phi_o = 5^{\circ}$, $\theta = 0^{\circ}$). This difference is quite obviously insignificant and can be entirely neglected. The $\Delta\phi$ difference, while not tabulated, is under no conditions more than a few tenths of a microradian, again insignificant.

It is possible to conclude, based on these data, that three-dimensional effects of the troposphere are negligible, and that the one-dimensional model is entirely satisfactory for Apollo purposes. The largest difference is that due to the three dimensional effects of surface refractivity (1/4 meter in ΔR for an extremal case). These results are important in that

1. A simpler and quicker program can be used to compute ΔR and $\Delta\phi$.
2. Fewer number of parameters are needed to characterize the troposphere (two instead of 4), meaning only two additional nuisance parameters for the Error Analysis Program.
3. The requirement of finding a good three-dimensional troposphere model is eliminated.

While these conclusions are based on troposphere investigations, the same conclusions in all probability apply to the ionosphere as the ionosphere accounts for only one-sixth of the total ΔR error at the low elevation angles where the three-dimensional effects are the largest and effective angle of incidence to the ionosphere is always higher because of its height.

Table 1a

ΔR (H_f = 127 km) - Meters

1-D vs. 3-D Model #1 Troposphere Error Models

$N_o = .27286296 \cdot 10^{-3}$ $H = .8467269 \cdot 10^4$ m. θ = Azimuth

ϕ_o	1-D	3-D Co-Lat = 70°; Long. = 0°				
		$\alpha' = 0$, $\beta' = 0$, $\theta = 0$	$\alpha' = 1.1$, $\beta' = .44$, $\theta = 90°$	$\alpha' = .55$, $\beta' = .22$, $\theta = 90°$	$\alpha' = 1.1$, $\beta' = .44$, $\theta = 0°$	$\alpha' = .55$, $\beta' = .22$, $\theta = 0°$
5°	23.70963	23.71090	23.9752	23.8383	23.6200	23.6649
10°	12.87027	12.87070	12.9698	12.9191	12.8355	12.8529
30°	4.605184	4.605387	4.61768	4.61148	4.60080	4.60305
60°	2.666791	2.666813	2.66920	2.66800	2.66591	2.66636
90°	2.310391	2.310391	2.31039	2.31039	2.31039	2.31039
		ΔR ($H_f = \infty$) - Meters				
5°	23.73846	23.73884	24.0040	23.8667	23.6477	23.6927
10°	12.87446	12.87463	12.9738	12.9231	12.8394	12.8567
30°	4.605449	4.605513	4.61781	4.61161	4.60093	4.60318
60°	2.666818	2.666822	2.66920	2.66801	2.66593	2.66637
90°	2.310392	2.310392	2.31039	2.31039	2.31039	2.31039

Table 1b

$\Delta\phi$ (H_f = 127 km) Milliradians

ϕ	1-D	3-D				
		$\alpha' = 0$, $\beta' = 0$, $\theta = 0$	$\alpha' = 1.1$, $\beta' = .44$, $\theta = 90^\circ$	$\alpha' = .55$, $\beta' = .22$, $\theta = 90^\circ$	$\alpha' = 1.1$, $\beta' = .44$, $\theta = 0^\circ$	$\alpha' = .55$, $\beta' = .22$, $\theta = 0^\circ$
5°	2.5144	2.5144	2.5001	2.5073	2.5198	2.5171
10°	1.3769	1.3769	1.3742	1.3755	1.3779	1.3774
30°	.4384	.4384	.4382	.4383	.4384	.4384
60°	.1468	.1468	.1467	.1467	.1468	.1468
90°	0	10^{-3}	10^{-3}	10^{-3}	10^{-3}	10^{-3}
		$\Delta\phi$ ($H_f = \infty$) - Milliradians				
5°	2.7708	2.7710	2.7607	2.7658	2.7751	2.7731
10°	1.4924	1.4924	1.4914	1.4918	1.4920	1.4927
30°	.4703	.4703	.4703	.4703	.4703	.4703
60°	.1573	.1573	.1573	.1573	.1573	.1573
90°	0	10^{-4}	10^{-4}	10^{-4}	10^{-4}	10^{-4}

Table 2

1-D vs. 3-D (Model #2) Troposphere Error Models

ΔR - (H_f = 127 km) Meters

ϕ_o	1-D	$\alpha' = .003$ $\beta' = .003$ $\theta = 90^o$	$\alpha' = .003$ $\beta' = .003$ $\theta = 0^o$	$\alpha' = .003$ $\beta' = .006$ $\theta = 90^o$	$\alpha' = .003$ $\beta' = .006$ $\theta = 0^o$
5°	23.70963	23.71251	23.7093	23.7125	23.7077
10°	12.87027	12.87125	12.8700	12.8713	12.8696
30°	4.605184	4.60545	4.60526	4.60545	4.60520
60°	2.666791	2.66683	2.66679	2.66682	2.66678
90°	2.310391	2.31039	2.31039	2.31039	2.31039
	ΔR - ($H_f = \infty$)				
5°	23.73846	23.74046	23.7372	23.7405	23.7357
10°	12.87446	12.875175	12.8740	12.8752	12.8734
30°	4.605449	4.60558	4.60539	4.60558	4.60532
60°	2.666818	2.66683	2.66680	2.66683	2.66679
90°	2.310392	2.31039	2.31039	2.31039	2.31039

The Bissett-Berman Corporation 2941 Nebraska Avenue, Santa Monica, California EXbrook 4-3270

APOLLO NOTE NO. 355
(Task II - Item II)

H. Engel
9 July 1965

ARBITRARY WEIGHTING OF DATA

For various reasons, a technique of data processing other than that of finding the maximum likelihood estimate of parameters may be employed. The purpose of this note is to show how the covariance matrices of the errors in the estimates of the parameters may be computed for arbitrary weighting of the data.

We start by reviewing the derivation of the covariance matrix for a maximum likelihood estimate, using a single measurable y with standard deviation σ. We have

$$S = \sum_i \frac{(y_{mi} - y_{ci})^2}{\sigma^2}$$

In order to find the maximum likelihood estimate we set the first partial derivatives of S with respect to each of the parameters to zero.

$$\frac{1}{2}\frac{\partial S}{\partial a_j} = 0 = \sum_i \frac{1}{\sigma^2}\left(y_{mi} - y_{ci} - \sum_k \frac{\partial y_{ci}}{\partial a_k}\Delta a_k\right)\frac{\partial y_{ci}}{\partial a_j}$$

Now, defining C and e as matrices

$$C_{jk} = \sum_i \frac{1}{\sigma^2}\frac{\partial y_{ci}}{\partial a_j}\frac{\partial y_{ci}}{\partial a_k}$$

$$e_j = \sum_i \frac{1}{\sigma^2}\frac{\partial y_{ci}}{\partial a_j}(y_{mi} - y_{ci})$$

$$= \sum_i \frac{1}{\sigma^2}\frac{\partial y_{ci}}{\partial a_j} n_i$$

in which n_i is the noise on the ith measurement, we have

$$C \, \Delta a = e$$

$$\Delta a = C^{-1} e$$

and, since Δa is an unbiased estimator the covariance of the error in the estimates of the parameters is $\overline{\Delta a \, \Delta a^T}$.

$$\overline{\Delta a \, \Delta a^T} = C^{-1} \, \overline{e \, e^T} \, C^{-1}$$

Now,

$$\overline{e_j \, e_k} = \overline{\left(\sum_i \frac{1}{\sigma^2} \frac{\partial y_{ci}}{\partial a_j} n_i \right) \left(\sum_\ell \frac{1}{\sigma^2} \frac{\partial y_{c\ell}}{\partial a_k} n_\ell \right)}$$

$$= \sum_{i,\ell} \frac{1}{\sigma^4} \frac{\partial y_{ci}}{\partial a_j} \frac{\partial y_{c\ell}}{\partial a_k} \overline{n_i \, n_\ell} \, \delta_{i\ell}$$

$$= \sum_i \frac{1}{\sigma^2} C_{jk} \, \sigma^2$$

$$= C_{jk}$$

so

$$\overline{e \, e^T} = C$$

and

$$\overline{\Delta a \, \Delta a^T} = C^{-1} \, C \, C^{-1} = C.$$

Next, let us examine the effect of using an incorrect value σ_e for the standard deviation of the errors in the measurable. We will let $\mathbb{C}$ and $\mathbb{e}$ be the values computed using σ_e instead of σ. The apparent covariance of the estimators is $\overline{(\Delta a\, \Delta a^T)}_e$

$$\overline{(\Delta a\, \Delta a^T)}_e = \mathbb{C}^{-1}\, \mathbb{C}\, \mathbb{C}^{-1} = \mathbb{C}^{-1}$$

The actual covariance is different because the correct value of $\overline{ee^T}$ in this case is <u>not</u> $\mathbb{C}$. Instead, it is C, so

$$\overline{\Delta a\, \Delta a^T} = \mathbb{C}^{-1}\, C\, \mathbb{C}^{-1}$$

In this particular example,

$$C = \frac{\sigma_e^2}{\sigma^2}\, \mathbb{C}$$

so in this example

$$\overline{\Delta a\, \Delta a^T} = \mathbb{C}^{-1}\, \frac{\sigma_e^2}{\sigma^2}\, \mathbb{C}\, \mathbb{C}^{-1}$$

$$= \frac{\sigma_e^2}{\sigma^2}\, \mathbb{C}^{-1} = C$$

That is, in this case the <u>actual</u> covariance matrix of the estimators is the maximum likelihood processing value.

As our next example we consider the case in which there are two measurables, called y and z. We have

$$S = \sum_i \frac{y_{mi} - y_{ci}}{\sigma_{ye}^2} + \sum_\ell \frac{z_{m\ell} - z_{c\ell}}{\sigma_{ze}^2}$$

$$\frac{1}{2}\frac{\partial S}{\partial a_j} = 0 = \frac{1}{\sigma_{ye}^2}\sum_i \left(n_{yi} - \sum_k \frac{\partial y_{ci}}{\partial a_k}\Delta a_k \right)\frac{\partial y_{ci}}{\partial a_j}$$

$$+ \frac{1}{\sigma_{ze}^2}\sum_\ell \left(n_{z\ell} - \sum_k \frac{\partial z_{c\ell}}{\partial a_k}\Delta a_k \right)\frac{\partial z_{c\ell}}{\partial a_j}$$

and letting

$$\mathbb{C} = \frac{1}{\sigma_{ye}^2}\sum_i \frac{\partial y_{ci}}{\partial a}\frac{\partial y_{ci}}{\partial a} + \frac{1}{\sigma_{ze}^2}\sum_\ell \frac{\partial z_{c\ell}}{\partial a}\frac{\partial z_{c\ell}}{\partial a}$$

$$= \mathbb{C}_y + \mathbb{C}_z$$

$$e = \frac{1}{\sigma_y^2}\sum_i n_{yi}\frac{\partial y_{ic}}{\partial a} + \frac{1}{\sigma_z^2}\sum_\ell n_{z\ell}\frac{\partial z_{\ell c}}{\partial a}$$

we find

$$\mathbb{C}\,\Delta a = e$$

$$\Delta a = \mathbb{C}^{-1} e$$

$$\overline{\Delta a\,\Delta a^T} = \mathbb{C}^{-1}\,\overline{ee^T}\,\mathbb{C}^{-1}$$

$$= \mathbb{C}^{-1}\,C\,\mathbb{C}^{-1}$$

$$= \left[\mathbb{C}_y + \mathbb{C}_z\right]^{-1}\left[\frac{\sigma_y^2}{\sigma_{ye}^2}\mathbb{C}_y + \frac{\sigma_z^2}{\sigma_{ze}^2}\mathbb{C}_z\right]\left[\mathbb{C}_y + \mathbb{C}_z\right]^{-1}$$

As another example, let us consider the case in which the measurables are range, azimuth and elevation (R, A, E), that the measurables are resolved into a fixed x, y, z coordinate system and that these resolved quantities are assigned equal variances σ_e^2. Then we have,

$$S = \frac{1}{\sigma_e^2} \left[\sum_i (R_{mi} \sin E_{mi} - z_{ci})^2 + \sum_i (R_{mi} \cos E_{mi} \cos A_{mi} - x_{ci})^2 \right.$$

$$\left. + \sum_i (R_{mi} \cos E_{mi} \sin A_{mi} - y_{ci})^2 \right]$$

$$\frac{1}{2} \frac{\partial S}{\partial a_j} = 0 = \frac{1}{\sigma_e^2} \left[\sum_i \left(R_{mi} \sin E_{mi} - z_{ci} - \sum_k \frac{\partial z_{ci}}{\partial a_k} \Delta a_k \right) \frac{\partial z_{ci}}{\partial a_j} \right.$$

$$+ \sum_i \left(R_{mi} \cos E_{mi} \cos A_{mi} - x_{ci} - \sum_k \frac{\partial x_{ci}}{\partial a_k} \Delta a_k \right) \frac{\partial x_{ci}}{\partial a_k}$$

$$\left. + \sum_i \left(R_{mi} \cos E_{mi} \sin A_{mi} - y_{ci} - \sum_k \frac{\partial y_{ci}}{\partial a_k} \Delta a_k \right) \frac{\partial y_{ci}}{\partial a_k} \right]$$

Now, apply the assumption of linearity,

$$R_{mi} \sin E_{mi} - z_{ci} = n_{ri} \sin E_i + n_{Ei} R_i \cos E_i$$

$$R_{mi} \cos E_{mi} \cos A_{mi} - x_{ci} = n_{ri} \cos E_i \cos A_i - n_{Ei} R_i \sin E_i \cos A_i$$

$$- n_{Ai} R_i \cos E_i \sin A_i$$

$$R_{mi} \cos E_{mi} \sin A_{mi} - y_{ci} = n_{ri} \cos E_i \sin A_i - n_{Ei} R_i \sin E_i \sin A_i$$

$$+ n_{Ai} R_i \cos E_i \cos A_i$$

We let

$$\mathbb{C} = \frac{1}{\sigma_e^2} \sum_i \left[\frac{\partial x}{\partial a} \frac{\partial x}{\partial a} + \frac{\partial y}{\partial a} \frac{\partial y}{\partial a} + \frac{\partial z}{\partial a} \frac{\partial z}{\partial a} \right]$$

$$\mathbb{e} = \frac{1}{\sigma_e^2} \sum_i \Big[(n_{ri} \sin E_i + n_{Ei} R_i \cos E_i) \frac{\partial z}{\partial a} + (n_{Ri} \cos E_i \cos A_i$$

$$- N_{Ei} R_i \sin E_i \cos A_i - n_{Ai} R_i \cos E_i \sin A_i) \frac{\partial x}{\partial a}$$

$$+ (n_{ri} \cos E_i \sin A_i - n_{Ei} R_i \sin E_i \sin A_i$$

$$+ n_{Ai} R_i \cos E_i \cos A_i) \frac{\partial y}{\partial a} \Big]$$

Then,

$$\overline{\mathcal{E}\mathcal{E}^T} = \frac{1}{\sigma_e^4} \sum_i \Bigg[\sigma_r^2 \Bigg\{ \sin^2 E_i \frac{\partial z}{\partial a} \frac{\partial z}{\partial a} + \cos^2 E_i \cos^2 A_i \frac{\partial x}{\partial a} \frac{\partial x}{\partial a}$$

$$+ \cos^2 E_i \sin^2 A_i \frac{\partial y}{\partial a} \frac{\partial y}{\partial a} + 2 \sin E_i \cos E_i \cos A_i \frac{\partial z}{\partial a} \frac{\partial x}{\partial a}$$

$$+ 2 \sin E_i \cos E_i \sin A_i \frac{\partial z}{\partial a} \frac{\partial y}{\partial a}$$

$$+ 2 \cos^2 E_i \sin A_i \cos A_i \frac{\partial x}{\partial a} \frac{\partial y}{\partial a} \Bigg\}$$

$$+ \text{ equally complicated expressions in } \sigma_E^2 \text{ and } \sigma_A^2 \Bigg]$$

and

$$\overline{\Delta a \, \Delta a^T} = \mathbb{C}^{-1} \, \overline{\mathcal{E}\mathcal{E}^T} \, \mathbb{C}^{-1}.$$

As a final example we consider a case of arbitrary weighting with some parameters (b) not updated. As it is the most complicated we continue with the immediately preceding case. We have,

$$\frac{1}{2} \frac{\partial S}{\partial a_j} = 0 = \frac{1}{\sigma^2} \Bigg[\sum_i \Bigg(R_{mi} \sin E_{mi} - z_{ci} - \sum_k \frac{\partial z_{ci}}{\partial a_k} \Delta a_k - \sum_u \frac{\partial z_{ci}}{\partial b_u} \Delta b_u \Bigg) \frac{\partial z_{ci}}{\partial a_j}$$

$$+ \text{ similar expressions in x and y.} \Bigg]$$

We let

$$\mathbb{C}_{11} = \frac{1}{\sigma_e^2} \sum_i \left(\frac{\partial x}{\partial a} \frac{\partial x}{\partial a} + \frac{\partial y}{\partial a} \frac{\partial y}{\partial a} + \frac{\partial z}{\partial a} \frac{\partial z}{\partial a} \right)$$

$$\mathbb{C}_{12} = \frac{1}{\sigma_e^2} \sum_i \left(\frac{\partial x}{\partial a} \frac{\partial x}{\partial b} + \frac{\partial y}{\partial a} \frac{\partial y}{\partial b} + \frac{\partial z}{\partial a} \frac{\partial z}{\partial b} \right)$$

$\mathbb{e}_1$ = the value of $\mathbb{e}$ defined above, for the updated paramters a.

Then we have,

$$\mathbb{C}_{11} \Delta a = \mathbb{e}_1 - \mathbb{C}_{12} \Delta b$$

$$\Delta a = \mathbb{C}_{11}^{-1} \left[\mathbb{e}_1 - \mathbb{C}_{12} \Delta b \right]$$

$$\overline{\Delta a \, \Delta a^T} = \mathbb{C}_{11}^{-1} \left[\overline{\mathbb{e}_1 \mathbb{e}_1^T} + \mathbb{C}_{12} \, \overline{\Delta b \, \Delta b^T} \, \mathbb{C}_{12}^T \right] \mathbb{C}_{11}^{-1}$$

In summary we may say that:

1. If only the incorrect values for the variances of the measurements are used, it is a simple matter to compute the covariance of the estimator errors,

2. If the actual data processing differs in some other way from the maximum likelihood processing, the program changes required to compute the covariance of the estimator errors are extensive and must be done individually for each different kind of data processing to be investigated.

The reader is also referred to Apollo Note No. 269.

The Bissett-Berman Corporation 2941 Nebraska Avenue, Santa Monica, California EXbrook 4-3270

APOLLO NOTE NO. 356
(Task II - Item II)

H. Engel
9 July 1965

ESTIMATION OF LEM/CSM RELATIVE POSITION

We have been informed by MSC that if only the six orbit parameters are updated, then the LEM position uncertainty at rendezvous is too large. One way of avoiding this difficulty, of course, is to update some of the nuisance parameters. For various reasons this solution is not at present acceptable.

Another alternative that should be investigated is that of determining the position of the LEM relative to the CSM when the positions of both are obtained updating only the six orbit parameters of each. If the CSM and LEM are observed by the same radars, then since their trajectories are very nearly alike, it is hoped that the effects of errors in the nuisance parameters will tend to cancel out when the relative position is computed.

Following notation of previous Apollo notes, and using the subscripts C and L to denote CSM and LEM, we have

$$C_{L,11}\,\Delta a_L = e_L - C_{L,12}\,\Delta b$$

$$\Delta a_L = C_{L,11}^{-1}\left[e_L - C_{L,12}\,\Delta b\right]$$

$$C_{C,11}\,\Delta a_C = e_C - C_{C,12}\,\Delta b$$

$$\Delta a_C = C_{C,11}^{-1}\left[e_C - C_{C,12}\,\Delta b\right]$$

The error in the estimate of the state vector of the LEM with respect to that of the CSM at a later time is ΔX

$$\Delta X = Q_L\,\Delta a_L - Q_C\,\Delta a_C$$

and its covariance is

$$\overline{\Delta X \, \Delta X^T} = \overline{(Q_L \, \Delta a_L - Q_C \, \Delta a_C)(Q_L \, \Delta a_L - Q_C \, \Delta a_C)^T}$$

$$= Q_L \, \overline{\Delta a_L \, \Delta a_L^T} \, Q_L^T + Q_C \, \overline{\Delta a_C \, \Delta a_C^T} \, Q_C^T$$

$$- Q_L \, \overline{\Delta a_L \, \Delta a_C^T} \, Q_C^T - Q_C \, \overline{\Delta a_C \, \Delta a_L^T} \, Q_L^T$$

$$= Q_L \left[C_{L,11}^{-1} + (C_{L,11}^{-1} C_{L,12}) \, \overline{\Delta b \, \Delta b^T} \, (C_{L,11}^{-1} \, C_{L,12})^T \right] Q_L^T$$

$$+ Q_C \left[C_{C,11}^{-1} + (C_{C,11}^{-1} \, C_{C,12}) \, \overline{\Delta b \, \Delta b^T} \, (C_C^{-1} \, C_{C,12})^T \right] Q_C^T$$

$$- Q_L \, (C_{L,11}^{-1} \, C_{L,12}) \, \overline{\Delta b \, \Delta b^T} \, (C_{C,11}^{-1} C_{C,12})^T \, Q_C^T$$

$$- Q_C \, (C_{C,11}^{-1} \, C_{C,12}) \, \overline{\Delta b \, \Delta b^T} \, (C_{L,11}^{-1} C_{L,12})^T \, Q_L^T$$

$$= Q_L \, C_{L,11}^{-1} \, Q_L^T + Q_C \, C_{C,11}^{-1} \, Q_C^T$$

$$+ (Q_L C_{L,11}^{-1} \, C_{L,12} - Q_C \, C_{C,11}^{-1} \, C_{C,12})$$

$$\overline{\Delta b \, \Delta b^T} \, (Q_L \, C_{L,11}^{-1} \, C_{L,12} - Q_C \, C_{C,11}^{-1} C_{C,12})^T$$

Hopefully, the third term, above will be small.

APOLLO NOTE NO. 357
(Task II - Item II)

J. R. Holdsworth
13 July 1965

RELATIVE EFFICIENCY OF UNWEIGHTED LEAST SQUARES ORBIT PARAMETER ESTIMATORS WHERE THE NOISE SAMPLES ARE EXPONENTIALLY AUTO-CORRELATED

The purpose of this note is to report upon further numerical results relating to the loss in estimator efficiency incurred by using unweighted least squares estimates for the orbit parameters when, in fact, the noise samples are auto-correlated in time. Apollo Notes No. 291 and 298 gave numerical comparisons of the optimal and least squares r.m.s. initial position and velocity errors for a particular noise correlation model where successive noise samples were correlated only with their neighbors occurring at adjacent sampling times. This was referred to as the one lag correlation model and Notes 291 and 298 gave numerical results for a 100 mile Earth parking orbit where range data with an error of $\sigma_R = 15$ meters was obtained by the tracking stations. Note 291 assumed that only one station was tracking the vehicle while Note 298 assumed that three tracking stations were involved.

It may be recalled that in these notes it turned out that over a large range of the one lag correlation parameter the unweighted least squares estimates yielded position and velocity error variances which were quite close to those achieved by the optimal filter.

The purpose of this note is to report the same calculations as in Note 298, i.e., the three station case, under the assumption that the noise samples are obtained from a stationary stochastic process with a normalized exponential or exponential cosine correlation function. That is, if observations from each station are taken at

equal increments of time then the normalized correlation between a noise sample at time t_i and one at t_j is given by:

$$C(t_i, t_j) = \rho^{|i-j|} \tag{1}$$

where:

$$-1 \leq \rho \leq +1 \tag{2}$$

The expressions for the error matrices of the orbit parameters for the least squares and optimal filter are directly obtainable from formulae developed in earlier Apollo notes, e.g., Apollo Notes 273 and 115. As the inversion of the correlation matrices of the noise samples given by (1) is quite straightforward, we'll just write down the equations for the estimator error matrices for the least squares and optimal filters. Before doing so we note that the only correlation assumed is between noise samples obtained at the same station -- i.e., there is no cross-correlation between noise samples obtained from different stations.

If the parameters to be estimated are $\theta_1, \ldots \theta_6$, say and if the range measurement error is σ_R from each station and if N_a, N_b, N_c are the numbers of observations made from each station then for the least squares filter the covariance matrix of the estimator errors may be shown to be:

$$\text{cov}\, \Delta\overline{\theta} = \sigma_R^2 (\quad)^{-1} \left[\quad \right] (\quad)^{-1} \tag{3}$$

where the i, j th elements of the matrices ( ) and $\left[\quad \right]$ are given by:

$$
(\quad)_{i,j} = \sum_{k=1}^{N_a} \frac{\partial R_a(k)}{\partial \theta_i} \frac{\partial R_a(k)}{\partial \theta_j} + \sum_{\ell=1}^{N_b} \frac{\partial R_b(\ell)}{\partial \theta_i} \frac{\partial R_b(\ell)}{\partial \theta_j} + \sum_{m=1}^{N_c} \frac{\partial R_c(m)}{\partial \theta_i} \frac{\partial R_c(m)}{\partial \theta_j} \tag{4}
$$

for $1 \leq i, j \leq 6$

and,

$$
\begin{aligned}
[\quad]_{i,j} = & \sum_{k=1}^{N_a} \sum_{\ell=1}^{N_a} \rho^{|k-\ell|} \frac{\partial R_a(k)}{\partial \theta_i} \frac{\partial R_a(\ell)}{\partial \theta_j} \\
& + \sum_{m=1}^{N_b} \sum_{n=1}^{N_b} \rho^{|m-n|} \frac{\partial R_b(m)}{\partial \theta_i} \frac{\partial R_b(n)}{\partial \theta_j} \\
& + \sum_{p=1}^{N_c} \sum_{q=1}^{N_c} \rho^{|p-q|} \frac{\partial R_c(p)}{\partial \theta_i} \frac{\partial R_c(q)}{\partial \theta_j}
\end{aligned} \tag{5}
$$

for

$1 \leq i, j \leq 6,$ respectively.

Similarly, if $\Delta\hat{\theta}$ denotes the estimator error vector obtained by using the optimal filter, we have the following expression for the error matrix.

$$\operatorname{cov} \Delta\hat{\theta} = \sigma_R^2 \, (M_a + M_b + M_c)^{-1} \tag{6}$$

where the i, jth element of M_a is given explicitly by:

$$\left.\begin{aligned}
(M_a)_{i,j} = \frac{1}{1-\rho^2} \Bigg\{ & \frac{\partial R_a(1)}{\partial \theta_i} \left(\frac{\partial R_a(1)}{\partial \theta_j} - \rho \, \frac{\partial R_a(2)}{\partial \theta_j} \right) \\
& + (1+\rho^2) \sum_{k=2}^{N_a-1} \frac{\partial R_a(k)}{\partial \theta_i} \, \frac{\partial R_a(k)}{\partial \theta_j} \\
& - \rho \sum_{k=2}^{N_a-1} \frac{\partial R_a(k)}{\partial \theta_i} \left(\frac{\partial R_a(k-1)}{\partial \theta_j} + \frac{\partial R_a(k+1)}{\partial \theta_j} \right) \\
& + \frac{\partial R_a(N_a)}{\partial \theta_i} \left(\frac{\partial R_a(N_a)}{\partial \theta_j} - \rho \, \frac{\partial R_a(N_a-1)}{\partial \theta_j} \right) \Bigg\}
\end{aligned}\right\} \tag{7}$$

where:

$1 \leq i, j \leq 6$

The explicit expressions for typical elements of the matrices M_b and/or M_c are immediately obtained by merely replacing the subscript a in Equation (7), by either b or c.

The numerical results were obtained under assumptions identical to those in Note 298 except of course for the exponential noise correlation model with which we currently replace the one lag correlation model of Note 298. That is, the vehicle is assumed to be in a 100 nautical mile Earth parking orbit with its orbital plane inclined at an angle of 28.5° to the Earth's equator. At time zero the vehicle is at 27° North

latitude and 60.5° West longitude, and is tracked from the Bermuda, Carnarvon and Guaymas stations exactly as described in the earlier note, so that each station makes about 100 range observations with a range measurement error of 15 meters. Furthermore, as in that note, it is assumed that the one lag auto-correlation of the noise samples are equal for each of the three stations even though the time increment between successive samples varies from station to station due to different visibility times.

In statistical estimation the relative efficiency of two estimates of the same parameter is defined to be the reciprocal of the ratio of their mean square errors, or variances if they are unbiased. The parameters to be estimated are the 6 components of the position and velocity vectors at time zero, hence for a particular value of ρ, the relative efficiency of the least squares estimate of θ_i would be:

$$\frac{\mathrm{Var}\ \hat{\theta}_i}{\mathrm{Var}\ \bar{\theta}_i} \tag{8}$$

where $\hat{\theta}_i$ and $\bar{\theta}_i$ are the optimal and unweighted least squares estimates of the parameter θ_i respectively. That is, we would have 6 different expressions as in (8) which we could plot as a function of the quantity ρ for $-1 \leq \rho \leq +1$. These numbers will all be less than or equal to one and in a sense measure the cost in estimate efficiency which one incurs by using the least squares in lieu of the optimal filter, component by component.

To reduce the amount of tabulation we shall use the term estimator efficiency in a somewhat different sense. For a particular value of ρ, we shall define the relative position efficiency of the least squares estimate to be:

$$P_{eff} = \frac{\sigma^2_{\hat{\theta}_1} + \sigma^2_{\hat{\theta}_2} + \sigma^2_{\hat{\theta}_3}}{\sigma^2_{\bar{\theta}_1} + \sigma^2_{\bar{\theta}_2} + \sigma^2_{\bar{\theta}_3}} \tag{9}$$

and the relative velocity efficiency of the least squares estimator to be:

$$N_{eff} = \frac{\sigma_{\hat{\theta}_4}^2 + \sigma_{\hat{\theta}_5}^2 + \sigma_{\hat{\theta}_6}^2}{\sigma_{\bar{\theta}_4}^2 + \sigma_{\bar{\theta}_5}^2 + \sigma_{\bar{\theta}_6}^2} \tag{10}$$

These quantities are just the ratios of the traces of the partitioned submatrices of the optimal and least squares covariance matrices.

Thus to conclude, a computer program was written to evaluate the matrices cov $\Delta\bar{\theta}$ and cov $\Delta\hat{\theta}$ for values of ρ between $\pm .9$.

Figure 1 shows the initial root-mean-square position error together with the relative position efficiency of the least squares filter as a function of ρ.

Figure 2 shows comparable results for the initial r.m.s. velocity errors. Examination of both of these tables reveals the comforting fact that over a very wide range of values of ρ there is very little increase in error variance due to using the unweighted least squares instead of the optimal estimates.

Thus, for exponentially correlated noise, as well as the one lag model, the least square estimate appears to render good service.

Relative Efficiency	L.S. $\sqrt{(\sigma_{x_o}^2 + \sigma_{y_o}^2 + \sigma_{z_o}^2)}$ in meters	Opt. $\sqrt{\sigma_{x_o}^2 + \sigma_{y_o}^2 + \sigma_{z_o}^2}$ in meters	ρ
.8735	2.33	2.18	-0.9
.9422	3.25	3.15	-0.8
.9721	4.03	3.97	-0.7
.9810	4.77	4.72	-0.6
.9902	5.48	5.45	-0.5
.9920	6.21	6.20	-0.4
.9973	6.93	6.93	-0.3
.9990	7.70	7.70	-0.2
1.000	8.51	8.51	-0.1
1.000	9.39	9.39	0.0
0.999	10.37	10.37	0.1
0.998	11.46	11.46	0.2
0.996	12.73	12.70	0.3
0.994	14.22	14.18	0.4
0.991	16.06	15.98	0.5
0.982	18.45	18.29	0.6
0.973	21.73	21.44	0.7
0.950	26.87	26.19	0.8
0.891	36.50	35.18	0.9

Figure 1.

Optimal and Least Square R.M.S. Initial Position Errors

In Meters and Relative Efficiency

Relative Efficiency	L.S. $\sqrt{(\sigma_{\dot{x}_o}^2 + \sigma_{\dot{y}_o}^2 + \sigma_{\dot{z}_o}^2)}$ in cm/sec	Opt. $\sqrt{\sigma_{\dot{x}_o}^2 + \sigma_{\dot{y}_o}^2 + \sigma_{\dot{z}_o}^2}$ in cm/sec	ρ
0.803	3.38	3.04	-0.9
0.906	4.61	4.40	-0.8
0.954	5.65	5.54	-0.7
0.968	6.67	6.59	-0.6
0.984	7.63	7.58	-0.5
0.986	8.63	8.58	-0.4
0.996	9.61	9.60	-0.3
0.998	10.66	10.65	-0.2
1.000	11.77	11.76	-0.1
1.000	12.98	12.98	0.0
0.999	14.31	14.30	0.1
0.998	15.80	15.79	0.2
0.994	17.52	17.51	0.3
0.990	19.54	19.53	0.4
0.985	22.00	21.90	0.5
0.970	25.23	24.90	0.6
0.955	29.56	28.90	0.7
0.918	36.32	34.9	0.8
0.848	48.44	44.6	0.9

Figure 2.

Optimal and Least Squares R.M.S. Initial Velocity Errors In Centimeters Per Second and Relative Efficiency

APOLLO NOTE NO. 358
(Task II - Item II)

H. Engel
20 July 1965

OPTIMUM SAMPLING INTERVAL

The measured change in range from t_i to t_{i+1} is ΔR_i,

$$\Delta R_i = R_{i+1} - R_i + \int_i^{i+1} \mathcal{E}(t)\, dt + n_{i+1} - n_i$$

in which

$\int_i^{i+1} \mathcal{E}(t)\, dt$ is the clock drift in the interval

n_i is a bounded range noise on the measurement,

and $t_{i+1} - t_i$ is large enough (1 second or more) that the clock noise is uncorrelated from sample to sample and that n_{i+1} is uncorrelated with n_i. This noise model is consistent with Ranger data (see Apollo Notes, Vol. IX). We let

$$N_i = \int_i^{i+1} \mathcal{E}(t)\, dt + n_{i+1} - n_i$$

Then we have

$$C \Delta a = e = \frac{1}{\sigma^2} \sum_i \frac{\partial \Delta R_i}{\partial a} N_i$$

and

$$E(\Delta a\, \Delta a^T) = C^{-1} E(ee^T) C^{-1}$$

Now

$$C = \frac{1}{\sigma^2} \sum_i \frac{\partial \Delta R_i}{\partial a} \frac{\partial \Delta R_i}{\partial a}$$

in which

$$\sigma^2 = E \left(\int_i^{i+1} \mathcal{E}(t)\, dt \right)^2 + E\, (n_{i+1} - n_i)^2$$

$$= \sigma_c^2 + 2\, \sigma_n^2$$

The correlation coefficient of the noise is

$$\rho = \frac{E\,(N_i\, N_{i+j})}{E\,(N_i)^2}$$

$$= \begin{cases} 1 & \text{for} \quad j = 0 \\ -\dfrac{\sigma_n^2}{\sigma^2} & j = \pm 1 \\ 0 & \text{all other } j \end{cases}$$

From this we find

$$\sigma_n^2 = -\rho\, \sigma^2$$

and

$$\sigma_c^2 = \sigma^2 - 2\, \sigma_n^2 = \sigma^2\, (1 + 2\rho)$$

Then,

$$E(ee^T) = \frac{1}{\sigma^4} \sum_i \frac{\partial \Delta R_i}{\partial a} N_i \sum_j \frac{\partial \Delta R_j}{\partial a} N_j$$

$$= \frac{1}{\sigma^4} \sum_i \left[-\sigma_n^2 \frac{\partial \Delta R_{i+1}}{\partial a} \frac{\partial \Delta R_i}{\partial a} + \sigma^2 \frac{\partial \Delta R_i}{\partial a} \frac{\partial \Delta R_i}{\partial a} - \sigma_n^2 \frac{\partial \Delta R_{i-1}}{\partial a} \frac{\partial \Delta R_i}{\partial a} \right]$$

Now, the one approximation we make is to replace $\sum (\partial \Delta R_{i+1}/\partial a)(\partial \Delta R_i/\partial a)$ by $\sum (\partial \Delta R_i/\partial a)^2$.

Then,

$$E(ee^T) = \frac{1}{\sigma^4} (1 + 2\rho) \sigma^2 \sum_i \frac{\partial \Delta R_i}{\partial a} \frac{\partial \Delta R_i}{\partial a}$$

$$= (1 + 2\rho) C$$

It follows that

$$E(\Delta a \Delta a^T) = C^{-1} \left[(1 + 2\rho) C \right] C^{-1}$$

$$= (1 + 2\rho) C^{-1}$$

and this equation is important because it tells us how the true covariance of Δa is related to C^{-1} when the data is treated as uncorrelated in the data processing. A separate Apollo Note, Number 291, compares the quantity $(1 + 2\rho) C^{-1}$ with the covariance obtained if the data is properly treated as correlated, and finds that except for ρ very

nearly equal to -0.5 the covariances least square estimates and optimal estimates are very nearly equal. Thus in our error analyses we can estimate the true covariance matrix by using $(1 + 2\rho)\, C^{-1}$.

Now, continuing with our particular example, we write

$$E\,(\Delta a\ \Delta a^T) = (1 + 2\rho_T) \left[\frac{1}{\sigma_T^2} \sum_i \left(\frac{\partial \Delta R_i}{\partial a}\right)_T \left(\frac{\partial \Delta R_i}{\partial a}\right)_T \right]^{-1}$$

in which the subscripts T refer to samples taken at intervals of T seconds. Now

$$\left(\frac{\partial \Delta R_i}{\partial a}\right)_T = T \left(\frac{\partial \Delta R_i}{\partial a}\right)_1$$

and over the total sampling time there may be only 1/T as many samples at intervals of T seconds as at intervals of one second, so

$$E\,(\Delta a\ \Delta a^T) = \frac{(1 + 2\rho_T)\,\sigma_T^2}{\sigma_T^2} \left[\frac{\sigma_1^2}{\sigma_T^2}\ \frac{1}{T}\ \frac{1}{\sigma_1^2} \sum T^2 \left(\frac{\partial \Delta R}{\partial a}\right)_1 \left(\frac{\partial \Delta R}{\partial a}\right)_1 \right]^{-1}$$

$$= \frac{\sigma_{cT}^2}{\sigma_T^2}\ \frac{\sigma_T^2}{\sigma_1^2}\ \frac{1}{T}\ C_1^{-1}$$

Now, the clock noise is a random walk and has the property that

$$\sigma_{cT}^2 = T\ \sigma_{c1}^2$$

so that by substitution we find

$$E\,(\Delta a\ \Delta a^T) = \frac{\sigma_{c1}^2}{\sigma_1^2}\ C_1^{-1}$$

$$= (1 + 2\rho_1)\, C_1^{-1}$$

That is, no matter what the sampling interval (so long as the number of samples is large) the covariance of Δa independent of the sampling interval.

Other samples in which taking the smallest possible sampling interval is not the optimum thing to do are given in a letter to the Editor "On the Estimation of the Mean of a Random Process," T. Fine and N. Johnson, Proceedings of the IEEE, February 1965, (pp187, 188).

APOLLO NOTE NO. 359

C. H. Dale
21 April 1965

CALCULATION OF INFORMATION MATRICES BASED UPON SEXTANT DATA TAKEN BETWEEN STARS AND EARTH OR MOON DISKS

(Task II - Item II)

The assumption is that an Apollo astronaut may take sextant measurements, measuring the angle between a star and either the Earth or Moon. The present "Program A" cannot easily handle such information. This note suggests a modified form of the computer program to be used only when vehicle-based sextant measurements are taken between stars and the Earth or Moon disks.

The data input sheet should look like (see Apollo Note 297):

(1)	A1	(16)	LIST OF TJ (s)
(2)	A4	(17)	Not used
(3)	A5	(18)	BIG L
(4)	GAM ID	(19)	SMA L
(5)	BETA	(20)	Not used
(6)	XI	(21)	Not used
(7)	ETA	(22)	Q IND
(8)	ZETA	(23)	Q F
(9)	Not used	(24)	Not used
(10)	Not used	(25)	Not used
(11)	OMEGA E	(26)	Not used
(12)	OMEGA M	(27)	TI (init)
(13)	RHO E = O	(28)	TI (inter)
(14)	RHO M	(29)	DIMENS
(15)	MU	(30)	Not used

(31) Not used

(32) Not used

(33) EARTH/MOON ORBIT IND (1 if Earth)

(34) LAT STR (in degrees)

(35) LON STR (in degrees)

(36) E D IND (1 if EARTH ANGLE)

(37) M D IND (1 if MOON ANGLE)

The new inputs, (33) through (37) are defined as follows: (33) tells the program whether the vehicle is in the Earth's or Moon's sphere of influence; (34) and (35) give the latitude and longitude of the Earth substellar point of the star to be tracked, at T = 0. (36) and (37) are indicators which denote which angles, i. e., Earth-to-Star and Moon-to-Star, are to be used in forming information matrices.

First, let us assume that input (33) is zero, indicating that the vehicle is in the lunar sphere of influence.

The direction of the star with respect to the Earth at T = 0 allows direction cosings of the unit vector pointing at the star to be computed in the x, y, z system:

$$\cos \alpha_s \equiv \cos (\text{LAT STR}) \cos (\text{LON STR}) \tag{1}$$

$$\cos \beta_s \equiv \cos (\text{LAT STR}) \sin (\text{LON STR}) \tag{2}$$

$$\cos \gamma_s \equiv \sin (\text{LAT STR}) \tag{3}$$

Now, we may define the unit vector in the x, y, z system which points to the star

$$u_s = \begin{bmatrix} \cos \alpha_s \\ \cos \beta_s \\ \cos \gamma_s \end{bmatrix} \tag{4}$$

Define:

$\theta E, E \equiv$ Earth Orbit, Angle between star and Earth

$\theta E, M \equiv$ " " , Angle between star and Moon

$\theta M, E \equiv$ Moon Orbit, Angle between star and Earth

$\theta M, M \equiv$ " " , Angle between star and Moon

Now we wish to calculate the partials of the above angles with respect to the parameters, a_j.

<u>First Case:</u> Lunar orbit, Angle from star to Earth, $\theta M, E$

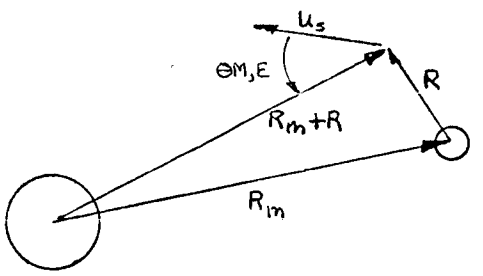

$\theta M, E$ is less than π

$$\cos \theta M, E = -u_s \cdot (R_m + R) \tag{5}$$

This last equation, written in terms of Apollo Note 82, is:

$$\cos (\theta M, E) = \frac{-u_s \cdot (K^T \tilde{X}_m + K^T L^T X')}{|\tilde{X}_m + L^T X'|} \tag{6}$$

Now the following relation

$$\frac{\partial \cos \theta}{\partial a_j} = -\sin \theta \frac{\partial \theta}{\partial a_j}$$

may be used to give,

$$\frac{\partial (\theta M, E)}{\partial a_j} = \frac{1}{\sin (\theta M, E)} \frac{\partial \left[\frac{u_s \cdot (K^T \tilde{X}_m + K^T L^T X')}{|\tilde{X}_m + L^T X'|} \right]}{\partial a_j}$$

Now since $\theta M, E$ is always positive and since u_s, K, and L are not a function of a_j, then

$$\frac{\partial\,(\theta M, E)}{\partial\, a_j} = \frac{}{\sqrt{1 - \cos^2(\theta M, E)}} \left[\frac{u_s \cdot (K^T \frac{\partial \widetilde{X}_m}{\partial\, a_j} + K^T L^T \frac{\partial\, X'}{\partial\, a_j})}{|\widetilde{X}_m + L^T X'|} - \left(\frac{u_s \cdot (K^T \widetilde{X}_m + K^T L^T X')}{|\widetilde{X}_m + L^T X'|^2} \right) \left(\frac{(K^T \widetilde{X}_m + K^T L^T X') \cdot (K^T \frac{\partial\, \widetilde{X}_m}{\partial\, a_j} + K^T L^T \frac{\partial\, X'}{\partial\, a_j})}{|\widetilde{X}_m + L^T X'|} \right) \right]$$

Now in the notation of the program, $\frac{\partial\, X_m}{\partial\, a_j}$ is defined as R_j' for J = 25 through 30 and is given in the primed coordinate system, while $\frac{\partial\, X'}{\partial\, a_j}$ is defined as R'_j for j = 1 through 24. This conveniently allows us to write,

$$\frac{\partial\,(\theta M, E)}{\partial\, a_j} = \frac{1}{\sqrt{1 - \cos^2(\theta M, E)}} \left[\frac{LK\, u_x \cdot R'_j}{|L\widetilde{X}_m + X'|} - \frac{LK\, u_s \cdot (L\widetilde{X}_m + X')}{|L\widetilde{X}_m + X'|^3} \left\{ L\widetilde{X}_m + X') \cdot R'_j \right\} \right] \tag{7}$$

where R'_j means $\frac{\partial\, X'}{\partial\, a_j}$ for j = 1 through 24, and L $\frac{\partial\, X_m}{\partial\, a_j}$ for j = 25 through 30.

Second Case: Lunar Orbit, Angle from Star-to-Moon, $\theta M, M$

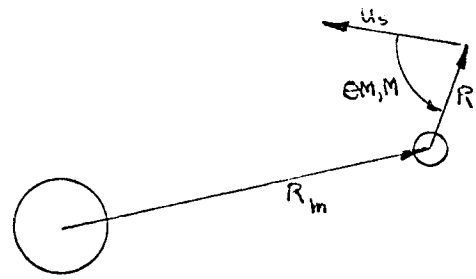

$\theta M, M$ is less than π (8)

$$\cos(\theta M, M) = \frac{-u_s \cdot (K^T L^T X')}{|X'|} \tag{9}$$

$$\frac{\partial(\theta M, M)}{\partial a_j} = \frac{1}{\sqrt{1-\cos^2(\theta M, M)}}\left[\frac{KL\, u_s \cdot R_j'}{|X'|} - \frac{KL\, u_s \cdot X'}{|X'|^3}(X' \cdot R_j')\right] \tag{10}$$

Third Case: Earth Orbit, Angle from Star-to-Earth, $\theta E, E$

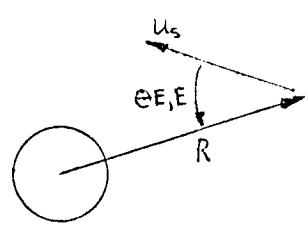

In the Earth orbit cases XI, ETA, and ZETA are used to produce an L matrix which rotates the x, y, z coordinates into x', y', z' coordinates. Here the x' axis is directed along $\overline{R}_o$ (from the center of the Earth to the vehicle). y' is directed horizontally in the planes of $\overline{R}_o$ and $\dot{\overline{R}}_o$ such that $\dot{y}_o'$ is positive, and z' follows a right-hand rule. This re-definition of L

frees the Moon and allows the Moon to be placed for disk sittings.

$$\theta E, E \text{ is less than } \pi \tag{11}$$

$$\cos(\theta E, E) = \frac{-u_s \cdot (L^T X')}{|X'|} \tag{12}$$

$$\frac{\partial(\theta E, E)}{\partial a_j} = \frac{1}{\sqrt{1 - \cos^2(\theta E, E)}} \left[\frac{u_s \cdot (L^T R_j')}{|X'|} - \frac{u_s \cdot (L^T X')}{|X'|^3} (X' \cdot R_j') \right] \tag{13}$$

Note here that no terms should exist for j = 25 through 30.

<u>Fourth Case:</u> Earth Orbits, Angle from Star-to-Moon, $\theta E, M$

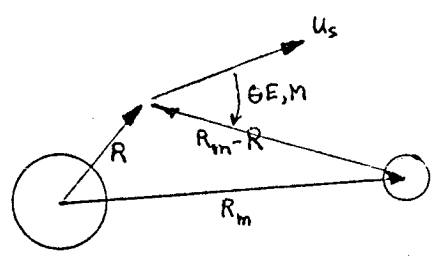

$$\theta E, M \text{ is less than } \pi \tag{14}$$

$$\cos(\theta E, M) = \frac{-u_s \cdot (K^T \tilde{X}_m - L^T X')}{|K^T X_m - L^T X'|} \tag{15}$$

Note whereas the absolute value of $R_m + R$ may be expressed in the tilda system in equation (6), the more complicated notation is required in

equation (15) since the L matrix has been redefined.

$$\frac{\partial(\theta E, M)}{\partial a_j} = \frac{1}{\sqrt{1 - \cos^2(\theta E, M)}} \left[\frac{u_s \cdot (K^T R'_{j2} - L^T R'_{j1})}{|K^T \tilde{X}_m - L^T X'|} \right.$$

$$\left. - \frac{u_s \cdot (K^T \tilde{X}_m - L^T X')}{|K^T \tilde{X}_m - L^T X'|} (K^T \tilde{X}_m - L^T X') \cdot (K^T R'_{j2} - L^T R'_{j1}) \right]$$

where:

for j = 1 through 24, $R'_{j1} = R'_j$ and $R'_{j2} = 0$

and,

for j = 25 through 30, $R'_{j2} = R'_j$ and $R'_{j1} = 0$

APOLLO NOTE NO. 360
(Task II - Item II)

C. Siska/
M. Blasgen
9 August 1965

THE INTEGRATED TRAJECTORY ERROR ANALYSIS PROGRAM

1. Introduction

At the present time, a computer program exists at Bissett-Berman Corporation which develops information matrices involving parameters of a non-central force field. These parameters include a selected list of sectorial and tesseral harmonic coefficients of the pertinent central body, and the principal gravitational constant and semi-major axis of a perturbing body.

Vehicle trajectories are obtained by means of an Encke integration of the dynamical equations for the following situations: 1) the Earth as the central body with the Moon in circular orbit about it and the Sun also in a relative circular motion about the Earth; and (2) the Moon as a central body and the Earth and Sun in relative circular motion about the Moon. The above simplifications involving circular motion are considered satisfactory for use in an error analysis program.

A description of the elements of the program and its use follows.

2. Trajectory Perturbations

The differential equations of motion, which are integrated using the Runge-Kutta method, are outlined in Apollo Note No. 319. For convenience, the governing potential equation is written here as

$$U = \frac{\mu}{r} + \frac{\mu}{a} \sum_{n=2}^{5} J_n \left(\frac{a}{r}\right)^{n+1} P_n (\sin\phi)$$

$$+ \frac{\mu}{a} \sum_{n=2}^{5} \left(\frac{a}{r}\right)^{n+1} \sum_{m=1}^{5} (C_{nm} \cos m\lambda + S_{nm} \sin m\lambda) P_{nm} (\sin\phi)$$

$$- \frac{\mu_2}{r_2} \sum_{n=2}^{4} \left(\frac{r}{r_2}\right)^{n} P_n (\cos S_2) - \frac{\mu_s}{r_s} \sum_{n=2}^{3} \left(\frac{r}{r_s}\right)^{n} P_n (\cos S_s)$$

where the last two terms represent approximations for the potential contributions of body 2 (normally the Moon) and the Sun.

In addition to the reference trajectory (1), the program integrates 19 perturbed trajectories (in parallel) for the following parameter values,

2. $\Delta x_o = 200$ m
3. $\Delta y_o = 400$ m
4. $\Delta z_o = 400$ m
5. $\Delta \dot{x}_o = 3$ m/s
6. $\Delta \dot{y}_o = 3$ m/s
7. $\Delta \dot{z}_o = 3$ m/s
8. $\Delta\mu = .0003\ \mu\ m^3/s^2$
9. $\Delta J_2 = 0.1\ J_2$
10. $\Delta J_3 = J_3$
11. $\Delta J_4 = J_4$
12. $\Delta J_5 = J_5$
13. $\Delta C_{22} = C_{22}$
14. $\Delta C_{31} = C_{31}$
15. $\Delta C_{32} = C_{32}$
16. $\Delta S_{22} = S_{22}$
17. $\Delta S_{31} = S_{31}$
18. $\Delta S_{32} = S_{32}$
19. $\Delta\mu_2 = 0.2\ \mu_2\ m^3/s^2$
20. $\Delta r_2 = 0.2\ r_2$ m

The basic trajectory outputs, for all 20 trajectories, are $\Delta x(t)$, $\Delta y(t)$, $\Delta z(t)$, $\Delta \dot{x}(t)$, $\Delta \dot{y}(t)$, $\Delta \dot{z}(t)$, which represent position and velocity changes from the $t = 0$ osculating Kepler orbit.

These outputs are later used in the error analysis section to form finite difference partials, such as,

$$\frac{\partial x}{\partial x_o}(t) = \frac{\Delta x\,(x_o + \Delta x_o, t) - \Delta x_{ref}(x_o, t)}{\Delta x_o}$$

The remaining tesseral harmonic coefficients appearing in the potential equation, are not perturbed in the manner indicated. If one wishes to obtain perturbed trajectories involving C_{33}, C_{41}, etc., one must compute two different reference trajectories using two different values, say for example, C_{33}.

During the integration, the initial integration step size can be changed to one other value, the time for switching to the next step size as well as the two step sizes being input parameters. Similarly, there are two print intervals, the first interval switching at the same time as the initial integration step size. This enables one to control the amount of trajectory printout.

It is noted in passing, that the present program does not have the capability of rectifying the initial Kepler orbit. Further, if any J, C, or S value is input as zero (nominal value) the program bypasses the calculation of the associated perturbation acceleration.

There is a choice of two different sets of initial condition inputs, which are described subsequently.

Integration ceases at the input value of T MAX.

3. Selection of Central Body

An input indicator (EAIND) determines whether or not body 2 (normally the Moon) is the central body for the trajectory integration.

If EAIND = 1.0, then the central body (primary body parameters) is the Earth and body 2 (Moon) is a perturbing body. In this system, the inertial coordinates x, y, lie in the Earth's equatorial plane with z as the Earth spin axis.

If EAIND = 0, then the central body (primary body parameters) is the Moon and body 2 is the Earth. In this case, the inertial coordinates x, y lie in the Earth-Moon plane with the x axis pointing toward the Earth and collinear with the Earth-Moon line at t = 0. The z axis is the Moon's spin axis. Additional inputs (transformation parameters) are now needed in order to transform these inertial coordinates in the error analysis section to the Earth's equatorial system. Also required is the position of Greenwich prime meridian at t = 0, so that station coordinates are properly computed for the error analysis. Trajectory outputs are given in the Earth-Moon plane coordinate system and for purposes of computing gravitational potential effects, this plane is also considered the Moon's equatorial plane.

4. Error Analysis Section

Up to 20 stations can be processed with a single run of the program; however, only up to 3 stations can be processed simultaneously.

Each station will have an initial (TI) and a final (TF) time of observation and all stations will have the same sampling interval $\Delta\tau$. In this program, the first sample is obtained at TI + $\Delta\tau$. The values $\Delta\tau$, TI, and TF must be a multiple of the integration step sizes.

The stations must be indexed according to increasing values of TI, the first three then being the first subset to be processed. Processing is done for each station in the subset only if the time during the trajectory integration coincides with a sample time. If a sample time is indicated, then the contribution to the information matrix for each desired measurable is computed. The partials are computed via the chain rule using the finite difference partials of Section 2.

Measurables to be computed for each station are defined by input indicators and can be any combination of the following three categories,

1. Slant Range Data
2. Angle Data (either AZ - EL or X - Y mount)
3. Slant Range Rate Data (either Master or Slave station)

When the integration time becomes equal to a station's TF time in the subset of three stations, the pertinent information matrices are recorded on an output tape and then the station is replaced by the next one in sequence. It is noted here, that at any given time, there can be no duplication of TF's and only one master station.

Information matrices can also be recorded at sample times during an observation period. Ten values of time (TRP) are available for this purpose.

State transition matrices, labelled U MATRIX, (instead of the former Q matrix), can be obtained at five different times (TU), which need not be a multiple of the integration step sizes. However, an input indicator (Q IND) is available, which will permit a U MATRIX to be recorded at every TF time and TRP time. Note that if one inputs a J, C, or S value of zero, the corresponding row of values will be identically zero in the matrix.

The column headings on the information matrix printout are, for the most part, self-explanatory. Those which require some elucidation follow.

(US, VS, WS) - these pertain to errors in the location of the designated station (whether master or slave) in directions Eastward, Northward, and toward Zenith.

(UM, VM, WM)- similar to above except they pertain to the master station location, if the designated station is a slave in the 3-way Doppler mode (the only case in which the columns are non-zero).

The following columns pertain primarily to clock parameters, but these have more than one interpretation because of an imposed upper limit of 30 columns required for Program B (the matrix inversion program). Equations involving the parameters RM, AM, BS, RS, AS appear in Apollo Note No. 320, and pertain to the relations for estimated time at the master and slave stations, $\hat{t}_M = t_M + (BM) + (RM)\, t_M + \frac{1}{2}$ $(AM)\, t_M^2$, $\hat{t}_S = t_S + (BS) + (RS)\, t_S + \frac{1}{2}\, (AS)\, t_S^2$.

(RM, AM, BS, RS, AS) - these require the following interpretation:

1. <u>Range Rate Data (3-way Doppler Mode)</u>

   (RM, AM) refer to master station clock but the RM column will be zero.

   (BS, RS, AS) refer to slave station clock.

2. <u>Range Rate Data (Master Station Operating Singly)</u>

   (RM, AM) - refer to station clock parameters RM, AM.
   (BS) - refers to station clock parameter BM.
   (RS, AS) - are not applicable, but are printed with value zero.

3. Range Data (any station operating as transmitter and receiver)

(RM, AM) refer to the designated station's clock.

(BS) is a bias in the range measurable.

(RS, AS) are not applicable and are not included in the printout.

4. Angle Data

(RM, AM) are not applicable but are printed with value zero.

(BS) is a bias in the angle measurable.

(RS, AS) are not applicable and are not included in the printout for angle data.

5. List of Inputs

Inputs are categorized by printed headings. The group of input cards following each heading can be read into the program in any order except for the first input indicated, which must be the first input in the group. Whenever nominal values appear, no input card is required unless one wishes to change the value via an input card.

Card No.	Symbol/Units	Definition	Index No.	Nominal Value
PRIMARY BODY PARAMETERS (Central Body)				
14	MU (m^3/s^2)	gravitational constant		
23	J_2	zonal harmonics	02	0
	J_3		03	0
	J_4		04	0
	J_5		05	0
24	C_{22}	tesseral harmonics which can appear in information matrix	22	0
	C_{31}		13	0
	C_{32}		23	0

Card No.	Symbol/Units	Definition	Index No.	Nominal Value
24	C_{33}	tesseral harmonics which do not appear in information matrix, but which can be included in the trajectory determination	33	0
	C_{41}		14	0
	C_{42}		24	0
	C_{43}		34	0
	C_{44}		44	0
	C_{51}		15	0
	C_{52}		25	0
	C_{53}		35	0
	C_{54}		45	0
	C_{55}		55	0
25	S_{22}	tesseral harmonics which can appear in information matrix	22	0
	S_{31}		13	0
	S_{32}		23	0
	S_{33}	tesseral harmonics which do not appear in information matrix, but which can be included in the trajectory determination	33	0
	S_{41}		14	0
	S_{42}		24	0
	S_{43}		34	0
	S_{44}		44	0
	S_{51}		15	0
	S_{52}		25	0
	S_{53}		35	0
	S_{54}		45	0
	S_{55}		55	0

Card No.	Symbol/Units	Definition	Index No.	Nominal Value
29	R (m)	equatorial radius		
26	ω (rad/sec)	spin rate of primary body		
37	APM (deg.)	right ascension of prime meridian		
44	EAIND	primary body indicator (1.0 is for Earth; 0 is for Moon)		
BODY TWO PARAMETERS				
19	MU_2 (m^3/s^2)	gravitational constant		
20	R_2 (m.)	circular orbit radius from primary body		
21	PHI 2 (deg.)	declination in central body coordinates		
22	V2 (deg.)	right ascension in central body coordinates		
33	GAMID2	$\pm$ 1.0 - the sign is chosen as minus the sign of $\dot{z}_0$ of body two		
34	I_2 (deg.)	orbit plane inclination angle		
60	ω_2 (rad/sec)	circular orbit angular velocity about the Earth		
BODY THREE PARAMETERS				
15	MUS (m^3/s^2)	gravitational constant		
16	RSUN (m)	circular orbit radius from primary body		
17	PHISUN (deg.)	declination in central body coordinates		
18	VSUN (deg.)	right ascension in central body coordinates		
31	GAMIDS	$\pm$ 1.0 - the sign is chosen as minus the sign of $\dot{z}_0$ of body three		
32	ISUN (deg.)	orbit plane inclination angle		

Card No.	Symbol/Units	Definition	Index No.	Nominal Value
TRANSFORMATION PARAMETERS (only if EAIND = 0)				
46	PHITO (deg.)	declination of Moon at t = 0		
47	VTO (deg.)	right ascension of Moon at t = 0		
45	IT (deg.)	Moon orbit plane inclination		
48	APMT (deg.)	right ascension of Earth's prime meridian		
59	GAMIDT	$\pm$ 1.0 - the sign is chosen as minus the sign of $\dot{z}_o$ of Moon at t = 0		
ERROR ANALYSIS PARAMETERS				
27	DELT 1 (min)	integration step size $0 = \leq t \leq$ TSWITCH		
35	DELT 2 (min)	integration step size TSWITCH $< t \leq$ TMAX		
39	PRINT 1 (min)	trajectory print interval, $0 \leq t \leq$ TSWITCH		
40	PRINT 2 (min)	trajectory print interval, TSWITCH $\leq t \leq$ TMAX		
36	TSWITCH (min)	time for switching DELT 1 to DELT 2 and PRINT 1 to PRINT 2		1.0 +08
30	TMAX (min)	maximum time of integration		
38	KEPLER ITER (sec)	bound on time solution of Kepler equation		
49	DEL TAU (min)	time interval between observation samples		

Card No.	Symbol/Units	Definition	Index No.	Nominal Value
41	TU MATRIX (min)	time for printout of U matrix	01	1.0 + 08
			02	1.0 + 08
			.	.
			.	.
			.	.
			.	.
			5	1.0 + 08
42	TRP (min)	time for printout of information matrix other than time TF	01	1.0 + 08
			02	1.0 + 08
			03	1.0 + 08
			.	.
			.	.
			.	.
			.	.
			.	.
			.	.
			10	1.0 + 08
43	QIND	+1.0 - will print U matrix at times TRP and times TF 0 - will not print U matrix		
13	INPUT IND	0 - will input initial conditions on cards 1 through 6 1.0 - will input initial conditions on cards 7 through 12		
57	STATION (NAME) DATA SET (3 digits)		01 to 20	
50	LONGITUDE (deg.)		01 to 20	0
51	LATITUDE (deg.)		01 to 20	0

Card No.	Symbol/Units	Definition	Index No.	Nominal Value
52	ANG ID	-1.0 - AZ-EL data 0 - no data +1.0 - x-y mount data	01 to 20	
53	RIND	+1.0 - range data 0 - no data	01 to 20	
54	RDIND	-1.0 - master/slave data (3-way Doppler) 0 - no data +1.0 - master range rate data	01 to 20	
58	MSIND	+1.0 - station is a master 0 - station is a slave NOTE: Needed only if RDIND = -1.0	01 to 20	
55	TI (min)	time for start of observation interval	01 to 20	1.0 + 08
56	TF (min)	time for stop of observation interval	01 to 20	

ORBIT INITIAL CONDITIONS

1	Ω (deg.)	right ascension of ascending node
2	I (deg.)	orbit plane inclination
3	U (deg.)	argument of perifocus plus true anomaly
4	r (m)	radius
5	VR (m/s)	radial velocity (inertial)
6	VT (m/s)	tangential velocity (inertial)

Card No.	Symbol/Units	Definition	Index No.	Nominal Value
7	x_o	inertial system coordinates for initial condition		
8	y_o			
9	z_o			
10	$\dot{x}_o$			
11	$\dot{y}_o$			
12	$\dot{z}_o$			

NOTE: If input cards 7 through 12 are used, the program will also compute and print out the variables appearing on cards 1 through 6 and in addition will print the argument of perifocus, OMEGA (SM), and eccentricity, ECC. If input cards 1 through 6 are used, the variables appearing on cards 7 through 12 will appear heading the t = 0 trajectory printout.

6. Restrictions to Input Values

1. The values of TI, TF, TSWITCH, TRP, DEL TAU, must be multiples of the integration step sizes.
2. Each station must have a different TF.
3. Only one master station must exist at any given time, i.e., the observation periods of master stations must not overlap.
4. Stations must be indexed according to increasing values of TI.
5. Only three stations can be processed simultaneously, i.e., observation periods of all stations cannot overlap more than three at a time.

6. J, C, and S harmonic coefficients cannot be input as zero in order to get U MATRIX and information matrix elements for these coefficients.

7. I2, ISUN, R2, RSUN, should all be non-zero.

8. To avoid exceeding the number of iteration cycles for the time solution of Kepler's equation, use the following inequality in determining the value of KEPLER ITER,

$$\text{KEPLER ITER} > \text{TMAX (sec.)} \times 10^{-7}$$

7. Input Card Format

Program A Cards (information matrix program)

1. Program A Card

   Cols. 1 - 7; PROGRAM

   Col. 9 ; A

   Col. 11-12; xx if this is the first item on a new tape, blank otherwise

2. Program A apriori card

   Cols. 1-7, PROGRAM

   Col. 9 , A

   Cols. 11-12, xx if this is the first item on a new tape, blank otherwise

   Col. 15 , A

   Cols. 31-33, data set number (greater than data set numbers appearing on cards 57 if cards 57 precede this card in deck and vice versa).

3. Cards for apriori covariance matrix

   Cols. 1-2, row number of element

   Cols. 4-5, column number of element

   Cols. 7-20, value of element, $\pm$ x.xxxxxxx E $\pm$ xx

4. Numbered input cards (appearing in text)

   Col. 1-2, card number

   Col. 4-5, Index number when applicable, blank otherwise.

   Col. 7-20, parameter value, $\pm$ x. xxxxxxx E $\pm$ xx

   Col. 25-37, parameter name (eg. MU OF SUN)

   NOTE: on card 57, cols. 7-20 give data set number for each station in floating point.

5. A blank card must end each Program A deck.

Program B Cards (matrix inversion program)

The format for Program B cards is shown in Figure 1.

8. Assembly of Input Card Deck

The manner in which each set of cards comprising the input deck is sequenced is described in the following sample arrangement. If there is an acceptable nominal value for some specific card it need not be included.

Sequence Number	Card No. or Description	Comments
1.	Program A card	
2.	14	
3.	23, 24, 25, 26, 29, 37, 44	arbitrary order
4.	19	
5.	20, 21, 22, 33, 34, 60	arbitrary order
6.	15	
7.	16, 17, 18, 31, 32	arbitrary order
8.	46	
9.	45, 47, 48, 59	arbitrary order
10.	27	

Sequence Number	Card No. or Description	Comments
11.	13, 30, 35, 36, 38, 39, 40, 41, 42, 43, 49	arbitrary order
12.	7, 8, 9, 10, 11, 12 or 1, 2, 3, 4, 5, 6	the set of initial conditions used depends on card 13
13. (a)	57	this block is repeated for each station with stations arranged according to increasing values of TI
13. (b)	50, 51, 52, 53, 54, 58, 55, 56	
14	Blank Card	
15. (a)	Program A apriori card	this block is repeated for each apriori matrix included
15. (b)	apriori covariance matrix cards (card for each element)	
15. (c)	Blank Card	
16. (a)	Program B card	this block is repeated for each case where a co-variance matrix is desired
16. (b)	cards for each data set to be included in the matrix for inversion	
16. (c)	Blank Card	

NOTES:

1. In above sample, if new tape is used, columns 11 and 12 on Program A card and Program A apriori card will respectively have xx and blank registered. Furthermore, data set numbers on Program A apriori cards will be greater in value than those on cards 57.

2. It is permissible to have block 15 cards above precede blocks 1 through 14; but then columns 11 and 12 will be xx on the first Program A apriori card only and blank on the remaining cards, including the Program A card. Furthermore, data set numbers on the Program A apriori cards must be lower than those on cards 57.

PROGRAM B

DATA INPUT SHEET

Keypunch: Punch a card for each row checked (✓)

✓ 1 PROGRAM B 9

Data Case Set No.

31 33 35 36

Matrix Rotation Angles (± xxx. xxx in degrees)

45 52 55 62 65 72

Data Set 1 3 | Case No. 4 5 | Measurable 6 7 | Time (TJ) ± x. x x x x x E x x x 8 19 | σ ± x. x x x x x E ± x x 20 31 | 6 x 6 32 | 33

Indicators for control of Matrix Format

07	08	09	10	11	12	13	14	15	16	17	18	19	20	21
MU	J2	J3	J4	J5	C1	C2	C3	S1	S2	S3	M2	R2	US	VS

Indicators continued

22	23	24	25	26	27	28	29	30
WS	UM	VM	WM	RM	AM	BS	RS	AS

80

FIGURE 1.

APOLLO NOTE NO. 361
(Task II - Item II)

E. Cortina
10 August 1965

RE-ENTRY – EQUATIONS OF MOTION

INTRODUCTION

Presented in this note are the equations of motion of the Apollo Command Module during re-entry. This is preliminary to the writing of a computer program for computing re-entry trajectories with the ultimate objective of developing error covariance matrices for predicting landing point dispersion and for evaluating the MSFN's ability to contribute to the guidance of the re-entry vehicle.

The nominal trajectory and Apollo Command Module characteristics used were taken from the NASA document titled, "Preliminary Apollo Reference Trajectory", dated February 1964. The exception to this data source is the guidance rules for controlling the orientation of the vehicle lift force. It is understood that the rules described therein are being modified, and are therefore not used in this note. Instead, the lift force was arbitrarily resolved into components in and normal to the plane of motion relative to the Earth, with the control variable, the resolving angle, left in general form.

The assumptions made in developing the equations of motion are:

1. A spherical rotating Earth.

2. The Apollo Command Module is a lifting body with constant lift-to-drag ratio.

3. The spacecraft rolls about the relative wind vector such that the vertical and lateral lift components are controlled simultaneously.

4. The ARDC, 1962 model of the atmosphere was used.

DEFINITION OF COORDINATE SYSTEMS

The coordinate systems which are useful in developing the equations of motion are defined as follows:

$\hat{x}, \hat{y}, \hat{z}$ Inertial coordinate system, Earth centered with the z-axis along the Earth's angular velocity vector and the x-axis in the plane of the prime meridian at time equal zero.

x, y, z Earth centered coordinate system rotating with the Earth. The z-axis is along the Earth's angular velocity vector, the x-axis is initially aligned with the $\hat{x}$-axis.

$\hat{x}, \hat{y}, \hat{z}$ Earth stabilized coordinate system rotating with the Earth. The $\hat{y}$-axis is along the vehicle velocity vector (relative to the Earth) and the $\hat{z}$-axis is normal to the plane defined by the vehicle velocity and radius vectors.

The relative orientation of these frames of reference can be expressed in terms of three Euler angles where:

E_1 rotation about z-axis

E_2 rotation about new x-axis (line of nodes)

E_3 rotation about final z-axis

Hence,

$$\begin{bmatrix} x' \\ y' \\ z' \end{bmatrix} = \begin{bmatrix} \ell_{11} & \ell_{12} & \ell_{13} \\ \ell_{21} & \ell_{22} & \ell_{23} \\ \ell_{31} & \ell_{32} & \ell_{33} \end{bmatrix} \begin{bmatrix} x \\ y \\ z \end{bmatrix} \tag{1}$$

where

$$\begin{aligned}
\ell_{11} &= \text{Cos } E_3 \text{ Cos } E_1 - \text{Cos } E_2 \text{ Sin } E_1 \text{ Sin } E_3 \\
\ell_{12} &= \text{Cos } E_3 \text{ Sin } E_1 + \text{Cos } E_2 \text{ Cos } E_1 \text{ Sin } E_3 \\
\ell_{13} &= \text{Sin } E_3 \text{ Sin } E_2 \\
\ell_{21} &= -\text{Sin } E_3 \text{ Cos } E_1 - \text{Cos } E_2 \text{ Sin } E_1 \text{ Cos } E_3 \\
\ell_{22} &= -\text{Sin } E_3 \text{ Sin } E_1 + \text{Cos } E_2 \text{ Cos } E_1 \text{ Cos } E_3 \\
\ell_{23} &= -\text{Cos } E_3 \text{ Sin } E_2 \\
\ell_{31} &= \text{Sin } E_2 \text{ Sin } E_1 \\
\ell_{32} &= \text{Sin } E_2 \text{ Cos } E_1 \\
\ell_{33} &= \text{Cos } E_2
\end{aligned} \tag{2}$$

The Euler angles used to describe the transformations are shown in Figures 1a and 1b. The following notation will be used in referencing them.

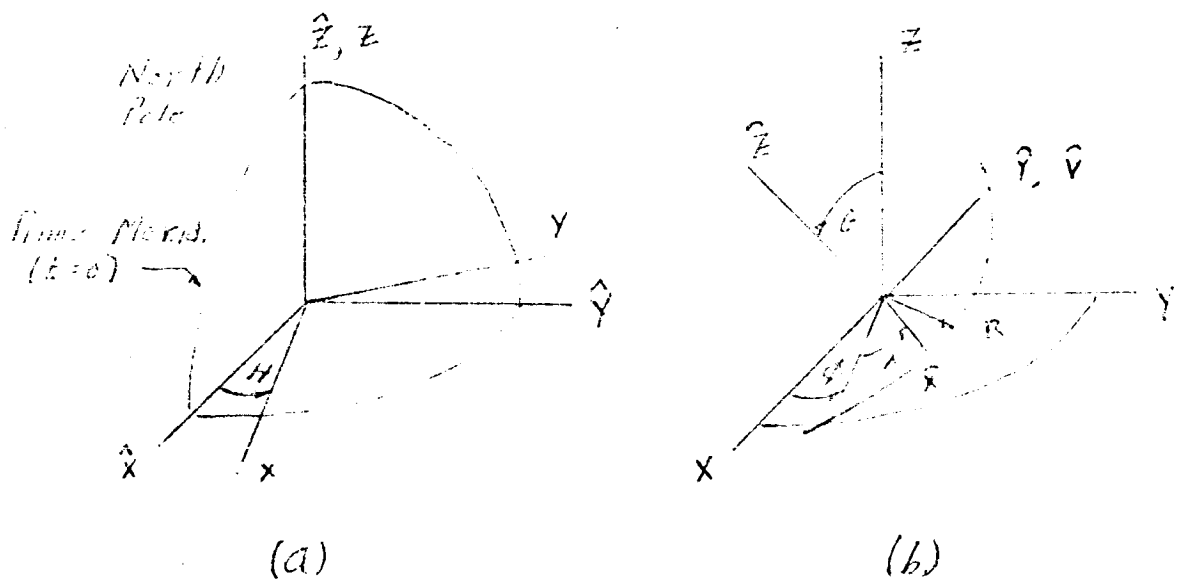

COORDINATE SYSTEMS

Figure 1

$$\begin{bmatrix} x' \\ y' \\ z' \end{bmatrix} = \begin{bmatrix} E_1 \\ E_2 \\ E_3 \end{bmatrix} \begin{bmatrix} x \\ y \\ z \end{bmatrix}$$

$$\begin{bmatrix} x \\ y \\ z \end{bmatrix} = \begin{bmatrix} H \\ 0 \\ 0 \end{bmatrix} \begin{bmatrix} x \\ y \\ z \end{bmatrix} \tag{3}$$

$$\begin{bmatrix} \hat{x} \\ \hat{y} \\ \hat{z} \end{bmatrix} = \begin{bmatrix} \phi \\ \theta \\ \lambda \end{bmatrix} \begin{bmatrix} x \\ y \\ z \end{bmatrix} \tag{4}$$

In addition, the Euler angles can be defined in terms of the vehicle coordinates and the known angular rate of the Earth.

The angle, H, which describes the relative orientation of the inertial ($\hat{x}$, $\hat{y}$, $\hat{z}$) to the Earth fixed (x, y, z) polar systems is given by,

$$H = \Omega t + H_0$$

$\Omega =$ Earth's angular rate.

By definition the two systems are aligned 0 + time equal zero, thus

$$H_0 = 0$$

and

$$H = \Omega t \tag{5}$$

From the general transformation matrix (3),

$$\begin{bmatrix} x \\ y \\ z \end{bmatrix} = \begin{bmatrix} \text{Cos Ht} & \text{Sin Ht} & 0 \\ \text{-Sin Ht} & \text{Cos Ht} & 0 \\ 0 & 0 & 1 \end{bmatrix} \begin{bmatrix} \hat{x} \\ \hat{y} \\ \hat{z} \end{bmatrix} \tag{6}$$

The spacecraft radius and relative velocity vectors in the Earth fixed coordinate system (x, y, z) are defined as follows:

$$\overline{R} = \begin{bmatrix} x \\ y \\ z \end{bmatrix}$$

$$\overline{V} = \begin{bmatrix} \dot{x} \\ \dot{y} \\ \dot{z} \end{bmatrix} = \begin{bmatrix} V_x \\ V_y \\ V_z \end{bmatrix}$$

From the definition of the $\hat{x}$, $\hat{y}$, $\hat{z}$ system,

$$\overline{\hat{y}} = \frac{\overline{V}}{V} \quad ; \overline{\hat{y}} \text{ unit vector in } \hat{y} \text{ direction}$$

$$\overline{\hat{z}} = \frac{\overline{R} \times \overline{V}}{RV \text{ Sin } \alpha} \quad ; \overline{\hat{z}} \text{ unit vector in } \hat{z} \text{ direction}$$

$$\text{Cos } \alpha = \frac{\dot{R}}{V}$$

$$\text{Sin } \alpha = +\sqrt{1 - \text{Cos}^2 \alpha}$$

$$\bar{\hat{x}} = \bar{\hat{y}} \times \bar{\hat{z}} \; ; \text{ unit vector in } \hat{x} \text{ direction}$$

$$= \frac{\bar{V} \times (\bar{R} \times \bar{V})}{RV^2 \operatorname{Sin} \alpha}$$

$$= \frac{(\bar{V} \cdot \bar{V})\, \bar{R} - (V \cdot \bar{R})\, \bar{V}}{RV^2 \operatorname{Sin} \alpha}$$

$$\bar{V} \cdot \bar{V} = V^2$$

$$\bar{V} \cdot \bar{R} = VR \operatorname{Cos} \alpha$$

$$\bar{\hat{x}} = \frac{\bar{R}}{R} \frac{1}{\operatorname{Sin} \alpha} - \frac{\bar{V}}{V} \cot \alpha$$

It may be noted that for $\alpha = 0, \pi$, these unit vectors are undefined. However, this occurs only at the terminal portion of the trajectory where the vehicle is descending vertically down. By this time, all essential features of the trajectory are determined and the trajectory computations can be stopped.

The transformation matrix can be expressed by,

$$\begin{bmatrix} \hat{x} \\ \hat{y} \\ \hat{z} \end{bmatrix} = \begin{bmatrix} \hat{\ell}_{11} & \hat{\ell}_{12} & \hat{\ell}_{13} \\ \hat{\ell}_{21} & \hat{\ell}_{22} & \hat{\ell}_{23} \\ \hat{\ell}_{31} & \hat{\ell}_{32} & \hat{\ell}_{33} \end{bmatrix} \begin{bmatrix} x \\ y \\ z \end{bmatrix} \tag{7}$$

where

$$\ell_{11} = \bar{\hat{x}} \cdot \bar{x} = \frac{1}{\operatorname{Sin}\alpha} \frac{X}{R} - \frac{V_x}{V} \cot \alpha$$

$$\ell_{12} = \bar{\hat{x}} \cdot \bar{y} = \frac{1}{\operatorname{Sin}\alpha} \frac{Y}{R} - \frac{V_y}{V} \cot \alpha$$

$$\ell_{13} = \bar{\hat{x}} \cdot \bar{z} = \frac{1}{\operatorname{Sin}\alpha} \frac{Z}{R} - \frac{V_z}{V} \cot \alpha$$

$$\ell_{21} = \bar{\hat{y}} \cdot \bar{x} = \frac{V_x}{V}$$

$$\ell_{22} = \bar{\hat{y}} \cdot \bar{y} = \frac{V_y}{V}$$

$$\ell_{23} = \bar{\hat{y}} \cdot \bar{z} = \frac{V_z}{V}$$

$$\ell_{31} = \bar{\hat{z}} \cdot \bar{x} = \frac{Y\,V_z - Z\,V_y}{RV\,\mathrm{Sin}\,\alpha}$$

$$\ell_{32} = \bar{\hat{z}} \cdot \bar{y} = \frac{Z\,V_x - X\,V_z}{RV\,\mathrm{Sin}\,\alpha}$$

$$\ell_{33} = \bar{\hat{z}} \cdot \bar{z} = \frac{X\,V_y - Y\,V_x}{RV\,\mathrm{Sin}\,\alpha}$$

KINEMATICS

The significant forces affecting the spacecraft motion during re-entry are aerodynamic and gravitational. Equation (8) is the general expression relating these forces to the vehicle acceleration.

$$\bar{D} + \bar{L} + \bar{G} = \bar{a}_I \tag{8}$$

$\bar{D}$ and $\bar{L}$ are the components of the aerodynamic force resolved parallel and normal to the relative wind velocity. Neglecting wind motion relative to the Earth, the relative wind velocity is simply the vehicle velocity with respect to the Earth.

The drag force, $\bar{D}$, is defined to be in the negative direction of the relative velocity. Thus,

$$\bar{D} = -D\,\frac{\bar{V}}{V}$$

$$= \frac{-D}{V}\left[V_x i + V_y j + V_z k\right] \tag{9}$$

The only constraint on the direction of the lift force is that it be normal to the relative velocity vector. Thus, the orientation of the plane defined by $\bar{L} X \bar{V}$ can be arbitrarily specified. Control of this degree of freedom is in fact the proposed method of maneuvering the re-entry vehicle to the desired landing area. For convenience, the lift vector will be resolved into components normal and parallel to the plane of motion. That is, the components of lift are along the $\hat{X}$ and $\hat{Z}$ axis.

Let

$$\hat{\bar{L}} = L (\text{Cos}\, \beta\, \hat{i} + \text{Sin}\, \beta\, \hat{k})$$

where,

L is the lift force magnitude per unit mass

and

β, the resolving angle, is the control variable.

Using the transformation matrix (7),

$$\bar{L} = L_x i + L_y j + L_z k \tag{10}$$

where,

$$L_x = L (\ell_1 \text{Cos}\, \beta + n_1 \text{Sin}\, \beta)$$

$$L_y = L (\ell_2 \text{Cos}\, \beta + n_2 \text{Sin}\, \beta)$$

$$L_z = L (\ell_3 \text{Cos}\, \beta + n_3 \text{Sin}\, \beta)$$

It may be noted from the definition of the control variable that for $0 \leq \beta \leq \pi/2$, the lift is oriented away from the center of the Earth ("up lift") and tending to increase the inclination of the plane of motion, i.e., $L \text{Sin}\, \beta \Rightarrow + V \dot{\theta}$.

The vector $\bar{G}$ represents the acceleration due to the Earth's gravitational force.

$$\bar{G} = \frac{-\mu}{R^3} \bar{R} \tag{11}$$

The inertial acceleration expressed in a rotating coordinate system can be obtained as follows:

$$\bar{V}_I = \dot{\bar{R}} + \bar{\Omega} X \bar{R}$$

$\bar{V}_I$ = inertial velocity

$\dot{\bar{R}} \triangleq \bar{V}$ = velocity w.r.t. Earth fixed system

$\bar{\Omega}$ = angular velocity of the Earth

$$\bar{a}_I = \frac{d\bar{V}_I}{dt} + \bar{\Omega} X (\bar{V}_I)$$

$$\bar{a}_I = \dot{\bar{V}} + \dot{\bar{\Omega}} X \bar{R} + 2 \bar{\Omega} X \dot{\bar{R}} + \bar{\Omega} X (\bar{\Omega} X \bar{R})$$

since,

$$\dot{\bar{\Omega}} = 0$$

$$\dot{\bar{R}} = \bar{V}$$

and,

$$A X (B X C) = (\bar{A} \cdot \bar{C}) \bar{B} - (\bar{A} \cdot \bar{B}) \bar{C}$$

$$a_I = \dot{\bar{V}} + 2 \bar{\Omega} X \bar{V} + (\bar{\Omega} \cdot \bar{R}) \bar{\Omega} - \Omega_e^2 \bar{R} \tag{12}$$

$$\bar{R} = X i + Y j + Z k$$

$$\bar{V} = V_x i + V_y j + V_z k$$

$$\dot{\bar{V}} = V_x i + V_y j + V_z k$$

$$\bar{\Omega} = \Omega_e k$$

Expanding (12)

$$\left.\begin{aligned} \mathcal{a}_{xI} &= \dot{V}_x - 2 V_y \Omega e - X\Omega_e^2 \\ \mathcal{a}_{yI} &= \dot{V}_y + 2 V_x \Omega_e - Y\Omega_e^2 \\ \mathcal{a}_{zI} &= \dot{V}_z \end{aligned}\right\} \qquad (13)$$

Combining equations (8), (9), (10), (11), and (12)

$$\left.\begin{aligned} \dot{V}_x &= 2 V_y \Omega_e + X\Omega_e^2 - \frac{\mu X}{R^3} - \frac{D V_x}{V} + L_x \\ \dot{V}_y &= -2 V_x \Omega_e + Y\Omega_e^2 - \frac{\mu Y}{R^3} - \frac{D V_y}{V} + L_y \\ \dot{V}_z &= \frac{\mu Z}{R^3} - \frac{D V_z}{V} + L_z \end{aligned}\right\} \qquad (14)$$

Ancillary Equations

$$D = \frac{1}{2} \rho (h) \frac{C_D A}{M} V^2$$

$$L = \frac{1}{2} \rho (h) \frac{C_L A}{M} V^2$$

ρ (h) is determined from the ARDC Air Density Tables, 1962.

The altitude "h" is defined by

$$h = R - R_e$$

R_e = Earth's radius

$\frac{C_D A}{M}$ and $\frac{C_L A}{M}$ for the Apollo Command Module are defined by,

$$C_L/C_D = 1/2$$

$$\frac{C_D A}{M} = 0.43 \text{ ft}^3/\text{lb-sec}^2$$

In addition to the basic variables involved in equations of motion, other flight parameters are of interest. Among these are:

A. The instantaneous distance to the nominal landing point. This distance will be expressed in terms of altitude above the Earth and the central angles to the nominal landing point in and normal to the plane of motion.

B. The instantaneous value of the local flight path angle.

Let $\overline{R}_T$ and $\widehat{R}$ be the radius vectors to the nominal landing point and vehicle, respectively.

$$\overline{R}_T = X_T i + Y_T j + Z_T k$$

$$\widehat{R} = Xi + Yj + Zk$$

Expressing both vectors in the $\hat{X}$, $\hat{Y}$, $\hat{Z}$ coordinate system by transformation matrix (7)

$$\hat{\bar{R}}_T = \hat{X}_T \hat{i} + \hat{Y}_T \hat{j} + \hat{Z}_T \hat{k}$$

$$\hat{\bar{R}} = \hat{X}\hat{i} + \hat{Y}\hat{j} + \hat{Z}\hat{k}$$

where

$$\hat{X}_T = \ell_1 X_T + \ell_2 Y_T + \ell_3 Z_T$$

$$\hat{Y}_T = m_1 X_T + m_2 Y_T + m_3 Z_T$$

$$\hat{Z}_T = n_1 X_T + n_2 Y_T + n_3 Z_T$$

$$\hat{X} = \ell_1 X + \ell_2 Y + \ell_3 Z$$

$$\hat{Y} = m_1 X + m_2 Y + m_3 Z$$

$$\hat{Z} = n_1 X + n_2 Y + n_3 Z$$

let,

Δ_1 be the angle between the vehicle radius vector and the $\hat{X}$ axis and Δ_2 the angle between the projection of $\hat{R}_T$ on the $\hat{X}$, $\hat{Y}$ plane such that,

$$\text{Sin}\, \Delta_1 = \frac{\hat{Y}}{R}$$

$$\text{Sin}\, \Delta_1 = \frac{\hat{Y}_T}{R_T}$$

Then, the in plane range is given by,

$$\Delta = \Delta_2 - \Delta_1$$

$$= \text{Sin}^{-1} \frac{\hat{Y}_T}{R_T} - \text{Sin}^{-1} \frac{\hat{Y}}{R} \qquad (15)$$

The out-of-plane range, e, is simply,

$$e = \sin^{-1} \frac{\hat{Z}_T}{R_T} \tag{16}$$

Local Flight Path Angle γ.

$$\sin\gamma = \frac{\hat{Y}}{R} \tag{17}$$

PROGRAM FORMAT

Inputs

Earth's Rotation Rate, Ω_e	OMEGAE = 0.7292116×10^{-4} $\frac{rad}{sec}$
Equatorial Radius, R_e,	RADE = 0.2092574×10^{8} ft
Gravitational Parameter, μ	FMU = 0.1407528×10^{17} ft^3/sec^2
Lift-to-Drag Ratio, (L/D)	LOVERD = 0.5
Ballistic Coefficient, $(W/C_D A)$	WOVCDA = 0.748×10^{2} $16/ft^2$
Processing Increments, ΔT	DELTA T =

Initial Vehicle Coordinates
Inertial

$\hat{X}_0, \hat{Y}_0, \hat{Z}_0$ — XZEROI, YZEROI, ZZEROI

Initial Vehicle Velocity
Inertial

$\hat{V}_{x0}, \hat{V}_{y0}, \hat{V}_{z0}$ — XDOTOI, YDOTOI, ZDOTOI

Landing Point Coordinates

X_T, Y_T, Z_T — XTARG, YTARG, ZTARG

Equations

$$X_0 = \hat{X}_0$$

$$Y_0 = \hat{Y}_0$$

$$Z_0 = \hat{Z}_0$$

$$V_{X0} = \hat{V}_{X0} + \Omega_e Y_0$$

$$V_{Y0} = \hat{V}_{Y0} - \Omega_e X_0$$

$$V_{Z0} = \hat{V}_{Z0}$$

$$R = \pm\sqrt{X^2 + Y^2 + Z^2}$$

$$V = \pm\sqrt{V_X^2 + V_Y^2 + V_Z^2}$$

$$\dot{R} = \frac{X V_X + Y V_Y + Z V_Z}{R}$$

$$\cos\alpha = \frac{\dot{R}}{V}$$

$$\sin\alpha = \pm\sqrt{1 - \cos^2\alpha}$$

$$\cot\alpha = \frac{\cos\alpha}{\sin\alpha}$$

$$L = \begin{bmatrix} \ell_{11} & \ell_{12} & \ell_{13} \\ \ell_{21} & \ell_{22} & \ell_{23} \\ \ell_{31} & \ell_{32} & \ell_{33} \end{bmatrix}$$

$$\ell_{11} = \frac{X/R}{\sin\alpha} - \frac{V_X}{V}\cot\alpha$$

$$\ell_{12} = \frac{Y/R}{\sin\alpha} - \frac{V_Y}{V}\cot\alpha$$

$$\ell_{13} = \frac{Z/R}{\sin\alpha} - \frac{V_Z}{V}\cot\alpha$$

$$\ell_{21} = V_X/V$$

$$\ell_{22} = V_Y/V$$

$$\ell_{23} = V_Z/V$$

$$\ell_{31} = \frac{Y\,V_Z - Z\,V_Y}{RV\sin\alpha}$$

$$\ell_{32} = \frac{Z\,V_X - X\,V_Z}{RV\sin\alpha}$$

$$\ell_{33} = \frac{X\,V_Y - Y\,V_X}{RV\sin\alpha}$$

$$h = R - R_e$$

$\rho(h)$ computed from 1962 ARDC atmosphere model.

$$g = \frac{\mu}{R_e^2}$$

$$\begin{bmatrix} L_X/D \\ L_Y/D \\ L_Z/D \end{bmatrix} = L^T \begin{bmatrix} \hat{L}_X/D \\ \hat{L}_Y/D \\ \hat{L}_Z/D \end{bmatrix}$$

$$\begin{bmatrix} \hat{L}_X/D \\ \hat{L}_Y/D \\ \hat{L}_Z/D \end{bmatrix} = \begin{bmatrix} (L/D) \cos\beta \\ 0 \\ (L/D) \sin\beta \end{bmatrix}$$

$$\left.\begin{matrix} \cos\beta \\ \sin\beta \end{matrix}\right\} \quad \text{To be specified in subsequent notes.}$$

<u>Differential Equations</u>

$$\dot{V}_X = 2 V_Y \Omega_e + X\Omega_e^2 - \frac{\mu X}{R^3} + \frac{1}{2}\rho(h) V^2 + \frac{C_D A}{W} g \left[- \frac{V_X}{V} + \frac{L_X}{D} \right]$$

$$\dot{V}_Y = -2V_X\Omega_e + Y\Omega_e^2 - \frac{\mu Y}{R^3} + \frac{1}{2}\rho(h)\frac{C_D A}{W} g \left[-\frac{V_Y}{V} + \frac{L_Y}{D} \right]$$

$$\dot{V}_Z = -\frac{\mu Z}{R^3} - \frac{1}{2}\rho(h)\frac{C_D A}{W} g \left[-\frac{V_Z}{V} + \frac{L_Z}{D} \right]$$

$$X = X + V_X \Delta T + \frac{1}{2}\dot{V}_X (\Delta T)^2$$

$$V_X = \dot{V}_X \Delta T$$

$$Y = Y + V_y \Delta T + \frac{1}{2}\dot{V}_Y (\Delta T)^2$$

$$V_Y = \dot{V}_Y \Delta T$$

$$Z = Z + V_Z \Delta T + \frac{1}{2}\dot{V}_Z (\Delta T)^2$$

$$V_Z = \dot{V}_Z \Delta T$$

<u>Auxiliary Calculations</u>

$$\begin{bmatrix} \hat{X}_T \\ \hat{Y}_T \\ \hat{Z}_T \end{bmatrix} = L \begin{bmatrix} X_T \\ Y_T \\ Z_T \end{bmatrix}$$

$$\begin{bmatrix} \hat{X} \\ \hat{Y} \\ \hat{Z} \end{bmatrix} = L \begin{bmatrix} X \\ Y \\ Z \end{bmatrix}$$

$$\sin \Delta_1 = \frac{\hat{Y}}{R}$$

$$\cos \Delta_1 = \frac{\hat{X}}{R}$$

$$R_T = +\sqrt{X_T^2 + Y_T^2 + Z_T^2}$$

$$\sin \Delta_2 = \frac{\hat{Y}_T}{R_T}$$

$$\cos \Delta_2 = \frac{\hat{X}_T}{R_T}$$

$$\Delta = \Delta_2 - \Delta_1$$

$$e = \sin^{-1} \frac{\hat{X}_T}{R_T} \quad -\pi/2 \leq e \leq \pi/2$$

$$\gamma = \frac{\hat{Y}}{R} \quad -\pi/2 \leq \gamma \leq \pi/2$$

APOLLO NOTE NO. 362
(Task 2, Item II)

J. W. Childress, III,
L. Lustick
11 August 1965

CHECKOUT OF THE LATITUDE, LONGITUDE, ORBITAL INCLINATION, FLIGHT PATH ANGLE AND INERTIAL HEADING ROUTINES OF THE ERROR ANALYSIS PROGRAM

INTRODUCTION

This note is the first of a series of notes which will describe the checkout procedures used to verify the accuracy of various special routines which have been added to the Error Analysis Program (EAP). These special routines are used to determine features such as latitude, longitude, the flight path angle, etc. of an orbiting vehicle. This memo discusses the checkout of the routines used to compute the latitude, longitude, orbital inclination, flight path angle and inertial heading.

COMPUTATIONAL PROCEDURE

The method used to determine the latitude, longitude, orbital inclination, flight path angle and inertial heading is described in Apollo Note No. 352.

CHECKOUT PROCEDURE

Earth Orbit

Figure 1 shows the input data used in the first checkout case. Figure 2 shows the Q and QE matrices at the time T = 0. Following the printing of the Q matrix is shown Sin $(\theta-\theta_o)$, Cos $(\theta-\theta_o)$, R, X', Y', $\dot{X}'$, $\dot{Y}'$, L (latitude, ℓ longitude), i (orbital inclination), γ (flight path angle), and Az (inertial heading).

Since θ and θ_o are equal at $T = 0$, the sine of $(\theta-\theta_o)$ should be identically zero. The non-zero value represents the roundoff error in the computational procedure used to compute Sin $(\theta-\theta_o)$. Sin $(\theta-\theta_o)$ is computed from Sin θ Cos θ_o-Cos θ Sin θ_o. The θ_o computations are handled fairly accurately and consistently, but the θ computations are inherently less accurate and less consistent. (The computations are considered consistent if both the sine and the cosine are computed from the same argument. This problem is currently being studied.)

The R and X' values are correct to the number of digits (7) shown but the Y' value reflects the error in the computation of the sine. It should be zero. This is not significant, however, since this is less than one millimeter if the input data was errorless. The $\dot{X}'$ and $\dot{Y}'$ calculations agree exactly with the input data. This does not indicate that the calculations which were used to determine X' and Y' are more accurate than those used to determine Y'; merely that absolute error is considerably smaller than the printed values. Likewise the latitude, longitude and the orbital inclination agree exactly with the input values. The flight path angle appears to be correct at least two fire digits. The inertial heading is exactly correct. The errors in the QE matrix will be discussed in detail in another paper. It is interesting to note that the 1-4, 2-2, 2-4, and 2-5 elements should be identically zero. Thus the non-zero values represent the roundoff (truncation) error in the determinations of $\frac{\partial H}{\partial a_4}$, $\frac{\partial r}{\partial a_2}$, $\frac{\partial r}{\partial a_4}$, and $\frac{\partial r}{\partial a_5}$. (Similar comments could be made reagarding the certain partials of velocity, V, and flight path angle with respect to the a_j's.)

It should also be noticed that this example indicates the magnitude of some of the roundoff errors in Q since the off-diagonal elements should be zero. The error in the 1-2 term is due primarily to the error in the determination of $\frac{\partial r}{\partial a_2}$. (The error due to Y' is $-.5227874.\ 10^{-11}$.) Likewise, Sin $(\theta-\theta_o)$ is primarily responsible for the error in $\frac{\partial r}{\partial a_4}$.

The error in the 2-1 term is due to both Sin $(\theta-\theta_o)$ and $\frac{\partial r}{\partial a_1}$ errors. The error in the 2-4 term is due to the Sin $(\theta-\theta_o)$ error. In a like manner all of the error sources for each of the terms is easily found. These will be treated in detail in a later note.

Lunar Orbit

Figure 2 shows the input data used in the second test case. In this case a lunar rather than an earth orbit was selected. Notice that parameters 05, 06, 08, 14 and 15 are changed.

The error sources in the Q matrix are unchanged.

The error in the computation of Sin $(\theta-\theta_o)$ has increased significantly. Its cause is unchanged from the previous example. This increased error in the determination of Sin $(\theta-\theta_o)$ produces a proportionately larger error in the determination of Y'. In addition, the error in R and X' becomes apparent in the seventh significant digit due to the error in Sin $(\theta-\theta_o)$.

While the latitude determination did not reveal any error, the longitude determination contains an error in the sixth significant digit. This error is due to the errors in Y and X, as well as the matrix rotation process. The inclination error is due to the same sources which produced the longitude errors. The error is smaller however. The flight path error has increased and becomes apparent in the fifth significant digit. (Ideally it would not differ from the value computed in the first example earth orbit due to the values selected.)

Since Z' and Z are zero, the angle of inclination is independent of coordinate rotation when 7 is zero. Likewise, the flight path angle is unchanged when a coordinate rotation is made with n equal to zero.

The determination of the inertial heading was exactly correct. Thus, the latitude, longitude, orbital incoination, flight path angle and inertial heading routines have been successfully checked out numerically as well as theoretically.

INPUT DATA

01	0.6635332E 07	A1
02	0.9832780E 03	A4
03	0.6874121E 04	A5
04	0.1000000E 01	GAM ID
05	0.2356725E 02	BETA
06	-0.	XI
07	-0.	ETA
08	-0.	ZETA
09	0.3217408E 02	LAMBDA
10	-0.6465364E 02	ALPHA
11	-0.	OMEGAE
12	-0.	OMEGAM
13	0.6378165E 07	RHOE
14	-0.	RHOM
15	0.3986032E 15	MU
16	-0.	D TIME
17	0.6645332E 07	REENTRY RAD
18	0.2356725E 02	BIG L
19	-0.6570400E 02	SMA L
20	-0.	RRATE IND
21	0.1000000E 01	RANGE IND
22	0.1000000E 01	Q IND
23	-0.	QF IND
24	0.1000000E 01	ANG 1 IND
25	0.1000000E 01	ANG 2 IND
26	0.1000000E 01	PVW IND
27	-0.	T INIT
28	0.1666660E-01	T INCR
29	0.7000000E 01	DIMENS
30	-0.	LAMBDA2
31	-0.	ALPHA2
32	-0.1000000E 01	M-S IND

Figure 1

```
                                   Q MATRIX        6     Q        T =   -0,

 0,100000E 01  0,902889E-12  0,            0,613127E-08  0,149419E-08  0,
 0,131223E-10  0,100000E 01 -0,            0,326314E-08  0,147725E-07 -0,
 0,            0,            0,100000E 01  0,            0,            0,504627E-08
-0,370256E-14 -0,186385E-14  0,            1,000000E 00 -0,157721E-10  0,
-0,102119E-15 -0,101854E-13 -0,           -0,640490E-12  1,000000E 00 -0,
 0,            0,           -0,953742E-14  0,            0,            1,000000E 00

                         SIN(TH-THO) =  0,5227874E-11      COS(TH-THO) =  1,0000000E 00

  R =  0,6635332E 07   XP =  0,6635332E 07   YP =  0,3468868E-04   XDP =  0,9832780E 03   YDP =  0,6874121E 04

                           LATITUDE =  0,2356725E 02        LONGITUDE = -0,6570400E 02

ORB INCL =  0,2356725E 02              FL PATH ANGLE =  0,8140400E 01                    INERT HEAD =  0,9000000E 02


                                  QE MATRIX        6     QE       T =   -0,

 0,687412E 04 -0,983278E 03  0,            0,254110E-20  0,663533E 07  0,            0,
 0,100000E 01  0,613076E-11  0,            0,613127E-08  0,149419E-08  0,            0,
-0,625370E-15 -0,103467E-13  0,            0,141599E-00  0,989924E 00  0,            0,
-0,135901E-19 -0,308358E-08 -0,           -0,291679E-05  0,417219E-06 -0,           -0,
```

Figure 2

INPUT DATA

01	0.6635332E 07	A1
02	0.9832780E 03	A4
03	0.6874121E 04	A5
04	0.1000000E 01	GAM ID
05	0.3178484E 02	BETA
06	0.1800000E 03	XI
07	-0.	ETA
08	0.1000000E 02	ZETA
09	0.3217408E 02	LAMBDA
10	-0.6465364E 02	ALPHA
11	-0.	OMEGAE
12	-0.	OMEGAM
13	0.6378165E 07	RHOE
14	0.3850000E 06	RHOM
15	0.4896000E 13	MU
16	-0.	D TIME
17	0.6645332E 07	REENTRY RAD
18	0.2356725E 02	BIG L
19	-0.6570400E 02	SMA L
20	-0.	RRATE IND
21	0.1000000E 01	RANGE IND
22	0.1000000E 01	Q IND
23	-0.	QF IND
24	0.1000000E 01	ANG 1 IND
25	0.1000000E 01	ANG 2 IND
26	0.1000000E 01	PVW IND
27	-0.	T INIT
28	0.1666660E-01	T INCR
29	0.7000000E 01	DIMENS
30	-0.	LAMBDA2
31	-0.	ALPHA2
32	-0.1000000E 01	M-S IND

Figure 3

Q MATRIX T Q T = -0.

0.100000E 01	-0.277491E-15	0.	0.194024E-02	0.150592E-11	0.
-0.379979E-16	1.000000E 00	-0.	-0.522373E-12	0.194024E-02	-0.
0.	0.	1.000000E 00	0.	0.	0.194024E-02
0.650337E-10	0.962772E-16	0.	0.100000E 01	0.603342E-17	0.
0.973899E-16	-0.325168E-10	-0.	0.156053E-15	1.000000E 00	-0.
0.	0.	-0.325168E-10	0.	0.	1.000000E 00

SIN(TH-THO) = 0.2010062E-05 COS(TH-THO) = 1.0000000E 00

R = 0.6635334E 07 XP = 0.6635334E 07 YP = 0.1333743E 02 XDP = 0.9832778E 03 YDP = 0.6874121E 04

LATITUDE = -0. LONGITUDE = 0.1000011E 02

ORB INCL = 0.5729578E-08 FL PATH ANGLE = 0.8140513E 01 INERT HEAD = 0.9000000E 02

QE MATRIX T QE T = -0.

0.687412E 04	-0.983278E 03	0.	-0.244341E-14	0.663533E 07	0.	0.
1.000000E 00	0.201006E-05	0.	0.194024E-02	0.390150E-08	0.	0.
0.920882E-11	-0.321892E-10	0.	0.141599E-00	0.989924E 00	0.	0.
0.600867E-14	-0.308367E-08	-0.	-0.291687E-05	0.417225E-06	-0.	-0.

Figure 4

The Bissett-Berman Corporation 2941 Nebraska Avenue, Santa Monica, California EXbrook 4-3270

APOLLO NOTE NO. 363
(Task 88, Item I(2))

J. B. Murphy
11 August 1965

ONE-DIMENSIONAL COMBINED TROPOSPHERE-IONOSPHERE MODELS AND ASSOCIATED TRACKING ERRORS

In the past, studies of the effect of the troposphere and ionosphere on radar have been made independently under the assumption that the perturbations were small. It was assumed that a good approximation to the actual situation was simply the respective algebraic sum of the range and angle errors introduced by the individual programs.

However, it is more desirable and more accurate to treat the troposphere and the ionosphere together in a single program. For this reason, a program implementing the equations of Apollo Note No. 308 has been written in which the troposphere and ionosphere are treated as a continuum.

For standard model of the troposphere, an exponential refractivity model with a scale height (H) and ground level refractivity (N_o) of:

$$H = .84672268 \cdot 10^4 m$$
$$N_o = .27286296 \cdot 10^{-3}$$

has been chosen so as to give a best fit to the 1959 ARDC troposphere model. The standard ionosphere model used is a parabolic one with a scale height (H_i), maximum height of ionization (H_{max}), and M_{max} of:

$$H_i = 6 \cdot 10^4 m$$
$$H_{max} = 3 \cdot 10^5 m$$
$$H_{max} = .25 \cdot 10^{-4}$$

so as to effect a 1 meter zenith range error. A parabolic model is a good approximation of the ionosphere near the maximum ionization level and has been shown to differ little from a more complex model with the same zenith range error (see Apollo Note No. 315)

The combined program, in addition to separate troposphere and ionosphere programs, was run utilizing these models. The combined program range and angle differences are compiled in Table I and Table II respectively, using the parameters indicated in these tables for various initial elevation angles (ϕ_o) and find altitudes (H_f). In addition, the quantities δR and $\delta\phi$ where:

$$\delta R = \Delta R \text{ (combined program)} - \Delta R \text{ (separate troposphere)} - \Delta R \text{ (separate ionosphere)}$$

$$\delta\phi = \Delta\phi \text{ (combined)} - \Delta\phi \text{ (troposphere)} - \Delta\phi \text{ (ionosphere)}$$

are tabulated.

As can be seen from Table I and II, the differences between the combined and the summed separate runs for this typical case are, in general, very small. At the worst, the range difference is about 1 cm. ($\phi_o = 5^o, H_f \geq H_2$) and the angle difference is .5 microradian ($\phi_o = 5^o$, $H_f \leq H_2$). Both of these errors, especially the angles are negligible.

In addition, the effects of varying the ionosphere parameters on the combined run are of some interest. Tables III, IV, and V give range error for the combined program, where the parameters are the same except as noted. Table III is the result of doubling the density of the ionosphere, Table IV is the result of making the ionosphere thinner by halving the scale height (H_i) and doubling the density, and Table V shows the effect of increasing the height of maximum ionization by 100 km. to 400 km. It is seen that the δR error is, to a large extent, proportional to density, independent of thickness, and inversly proportional to the height of the ionosphere. Nevertheless, the differences in range and angle errors between the combined program and the sum of separate programs is insignificant for most conceivable troposphere and ionosphere models.

COMBINED TROPOSPHERE
AND IONOSPHERE

$H_t = .84672268 \cdot 10^4 m$ $\quad$ $H_i = .60 \cdot 10^4 m$

$N_o = .27286296 \cdot 10^3$ $\quad$ $M_{max} = .25 \cdot 10^{-4}$

$R_o = .63781 \cdot 10^7 m$ $\quad$ $H_{max} = .3 \cdot 10^6 m$

TABLE I (RANGE)

	$H_f = 300$ km		$H_f = 360$ km		$H_f \rightarrow \infty$	
ϕ_o	ΔR-m	δR-Cm	ΔR	δR-Cm	ΔR	δR
5°	25.4095	+. 58	26.9915	+1.03	27.0055	+1.00
10°	14.3892	. 37	15.8292	.69	15.8308	.66
30°	5.50228	.057	6.38617	.11	6.38620	.11
60°	3.23652	.013	3.80510	.027	3.80510	.026
90°	2.81040	10^{-4}	3.31040	10^{-4}	3.31040	10^{-4}

TABLE II (ANGLE)

	$H_f = 300$ km		$H_f = 360$ km		$H_f \rightarrow \infty$	
ϕ_o	$\Delta\phi$-MRAD	$\delta\phi$-μRAD	$\Delta\phi$	$\delta\phi$	$\Delta\phi$	$\delta\phi$
5°	2.63123	+.44	2.64997	+.44	2.77575	+.14
10°	1.43827	.22	1.44854	.22	1.49604	.008
30°	.45879	.07	.46264	.06	.47101	-.008
60°	.15373	.02	.15508	.02	.15712	-.025
90°	0	0	0	0	0	0

TABLE III ($M_{max} = .5 \cdot 10^{-4}$)

	$H_f = 300$ km		$H_f = 360$ km		$H_f \rightarrow \infty$	
ϕ_o	ΔR-m	δR-Cm	ΔR	δR	ΔR	δR
5°	27.0969	+1.15	30.2599	+2.06	50.2735	+1.99
10°	15.9064	.74	18.7865	1.37	18.7879	1.33
30°	6.3993	.11	8.1671	.22	8.1671	.22
60°	3.8063	.027	4.9434	.053	4.9434	.052
90°	3.31042	10^{-4}	4.31045	10^{-4}	4.31045	10^{-4}

TABLE IV ($H_i = .3 \cdot 10^6$, $M_{max} = .5 \cdot 10^{-4}$)

	$H_f = 300$ km		$H_f = 360$ km		$H_f \rightarrow \infty$	
ϕ_o	ΔR-m	δR-m	ΔR	δR	ΔR	δR
5°	25.3798	+.53	26.9858	+1.01	26.9999	+.99
10°	14.3683	.36	15.8259	.68	15.8276	.65
30°	5.4980	.056	6.3860	.11	6.3860	.11
60°	3.2362	.039	3.8051	.078	3.8051	.078
90°	2.81041	10^{-4}	3.31042	10^{-4}	3.31042	10^{-4}

TABLE V ($H_{max} = .4 \cdot 10^6$)

	$H_f = 400$ km	$H_f = 460$ km	$H_f = \infty$	
ϕ_o	ΔR	ΔR	ΔR	δR
5°	25.2014	26.6093	26.6211	+.68
10°	14.2342	15.5416	15.5430	.47
30°	5.4744	6.3321	6.3321	.10
60°	3.2340	3.8002	3.8002	.018
90°	2.81040	3.31041	3.31041	10^{-4}

The Bissett-Berman Corporation 2941 Nebraska Avenue, Santa Monica, California EXbrook 4-3270

APOLLO NOTE NO. 364
(Task 2, Item II)

B. Buffington
C. Siska
12 August 1965

MODIFICATIONS TO THE STATION VISIBILITY PROGRAM

INTRODUCTION

Two modifications have been added to the Station Visibility Program described in Apollo Note No. 310. These modifications permit one (via an input indicator) to obtain for a given orbit, either the rise/set times for up to 20 stations, or the ground track.

RISE/SET TIMES

If Column 9 of the PROGRAM card has the value zero, then rise/set times are recorded. Up to 20 station cards are permitted with the first card of the sequence containing the number (NRSTAT) of the stations comprising the set. The values of LAMBDA and ALPHA (Cards 9 and 10) for the set of stations must be arranged in the same order as the station cards (in order to pertain to the proper station.) Remaining inputs are executed as in the past. The changes required are incorporated on the input sheet shown in Figure 1.

With this modification, the computer, at any given time interval, searches the input set of stations for any rise or set times and records those that occur. A considerable reduction in running time is obtained over that required in the past. An example printout is shown in Figure 2.

GROUND TRACK

If Column 9 of the PROGRAM card has the value 1.0, the program will compute the longitude and latitude of the sub-vehicle position at each time interval. An example printout is shown in Figure 3.

STATION VISIBILITY PROGRAM

DATA INPUT SHEET

Keypunch:
Punch a card
for each row
checked ( )

***

✓	1 – 9	21 – 34 TI(Initial)	41 – 54 TI(Interval)
✓	PROGRAM	± . E ±	± . E ±

✓	1 – 8 Station	9 – 12 (NRSTAT) **
✓		

✓	1 2	7 – 20			
	01	. E	A1	m	Initial Orbit radius
	02	. E	A4	m/sec	Initial Orbit radial velocity
	03	. E	A5	m/sec	Initial Orbit tangent velocity
	04	. E	GAM ID		+1 if $\lvert\gamma\rvert \leq \pi/2$, -1 otherwise
	05	. E	BETA	deg	Inclin. of E-M orbit to Eq.
	06	. E	XI	deg	Euler angles relating
	07	. E	ETA	deg	x'y'z' coordinates to
	08	. E	ZETA	deg	$\tilde{x}\tilde{y}\tilde{z}$ coordinates
	09	. E	LAMBDA **	deg	Station latitude
	10	. E	ALPHA **	deg	Station longitude
	11	. E	OMEGA E	rad/sec	Earth angular rate
	12	. E	OMEGA M	rad/sec	Earth-Moon angular rate
	13	. E	RHO E	m	Radius of Earth
	14	. E	RHO M	m	Earth-Moon distance
	15	. E	MU	m^3/sec^2	Gravitational constant
	16	. E	D-Time	min	Maximum time of observation
	18	. E	BIG L	deg	Lat. sublunar pt at T = 0
	19	. E	SMA L	deg	Long. sublunar pt at T = 0
✓	20	+0.00000000E+00	RR IND*		1: calc. R; otherwise 0
✓	21	+0.00000000E+00	R IND*		1: calc. R; otherwise 0
✓	22	+0.00000000E+00	Q IND*		1: calc. Q; otherwise 0
✓	23	+0.00000000E+00	QF*	min	Time for additional Q
✓	24	+0.00000000E+00	PS1 IND*		1: calc. Ang 1; otherwise 0
✓	25	+0.00000000E+00	PS2 IND*		1: calc. Ang 2; otherwise 0
✓	26	+0.00000000E+00	PVW IND*		1: x-y mount; otherwise 0
	27	. E	$\mathcal{E}$		Limiting Elevation Angle
		±x.xxxxxxxxE±xx			

* Does not need to be repeated after the first set.
Every set of Data must be followed by a blank card.
Only parameters that change need to be inserted in each new set.

** Listing up to 20 stations with first station card containing NRSTAT.
Lambda and Alpha arranged in same sequence as stations.

*** On PROGRAM card in Column 9, insert 1 for ground track output, or 0 for Station Visibility rise/set times.

REMARKS:

Figure 1.

STATION VISIBILITY

INPUT DATA

01	0.6563420E 07	A1
02	0.	A4
03	0.7797638E 04	A5
04	0.1000000E 01	GAM ID
05	0.8900000E 02	BETA
06	0.	XI
07	0.	ETA
08	0.	ZETA
09	0.2661600E 02	LAMBDA
10	-0.7834800E 02	ALPHA
11	0.7291160E-04	OMEGAE
12	0.	OMEGAM
13	0.6378100E 07	RHOE
14	0.	RHOM
15	0.3990762E 15	MU
	0.	T INITIAL
	0.1000000E 01	T INTERVAL
16	0.2700000E 03	D TIME
18	0.3300000E 02	BIG L
19	-0.1200000E 03	SMA L
20	0.	SD IND
21	0.	S IND
22	0.	PS1IND
23	0.	Q IND
24	0.	QF IND
25	0.	PS2IND
26	0.	PVWIND
27	0.5000000E 01	E

Figure 2.

STATION	LATITUDE(DEGREES)	LONGITUDE(DEGREES)
G TURK I	21.4340	-71.1450
ANTIGUA	17.1430	-61.7930
ASCENS	-7.9520	-14.4130
BERMUDA	32.3480	-64.6540
GR CAN	27.7360	-15.6000
CARNARV	-24.8670	113.6330
HAWAII	22.1250	-159.6710
GUAYMAS	27.9580	-110.7210
EGLIN	30.4220	-86.7980
GUAM	13.5830	144.9250
CORP CHR	27.6550	-97.3800
PT ARGU	34.5830	-120.5610
WH SANDS	32.3580	-106.3700
CANBERRA	-35.3120	149.1360
MADRID	40.4170	-3.6670
GOLDSTON	35.3900	-116.8490
CAPE K	28.4820	-80.5770
GBI	26.6160	-78.3480

PT ARGU SET	T(Y)=	1.96
GOLDSTONSET	T(Y)=	1.69
GUAYMAS SET	T(Y)=	2.18
HAWAII RISE	T(Y)=	176.83
HAWAII SET	T(Y)=	180.94
MADRID RISE	T(Y)=	236.26
MADRID SET	T(Y)=	240.54

Figure 2. (cont.)

GROUND TRACK

INPUT DATA

01	0.6563420E 07	A1
02	0.	A4
03	0.7797638E 04	A5
04	0.1000000E 01	GAM ID
05	0.8900000E 02	BETA
06	0.	XI
07	0.	ETA
08	0.	ZETA
09	0.2143400E 02	LAMBDA
10	-0.7114500E 02	ALPHA
11	0.7291160E-04	OMEGAE
12	0.	OMEGAM
13	0.6378100E 07	RHOE
14	0.	RHOM
15	0.3990762E 15	MU
	0.	T INITIAL
	0.2000000E 01	T INTERVAL
16	0.9000000E 02	D TIME
18	0.3300000E 02	BIG L
19	-0.1200000E 03	SMA L
20	0.	SD IND
21	0.	S IND
22	0.	PS1IND
23	0.	Q IND
24	0.	QF IND
25	0.	PS2IND
26	0.	PVWIND
27	0.5000000E 01	E

Figure 3.

TIME	LATITUDE	LONGITUDE
0.	33.00	-120.00
2.00	24.83	-120.31
4.00	16.67	-120.65
6.00	8.50	-121.00
8.00	0.33	-121.36
10.00	-7.84	-121.72
12.00	-16.00	-122.07
14.00	-24.17	-122.41
16.00	-32.34	-122.73
18.00	-40.50	-123.01
20.00	-48.67	-123.23
22.00	-56.83	-123.33
24.00	-65.00	-123.22
26.00	-73.15	-122.56
28.00	-81.29	-119.82
30.00	-88.89	-62.51
32.00	-82.25	45.26
34.00	-74.11	48.61
36.00	-65.96	49.38
38.00	-57.79	49.54
40.00	-49.63	49.45
42.00	-41.46	49.24
44.00	-33.30	48.96
46.00	-25.13	48.65
48.00	-16.96	48.31
50.00	-8.79	47.96
52.00	-0.63	47.60
54.00	7.54	47.25
56.00	15.71	46.89
58.00	23.87	46.55
60.00	32.04	46.24
62.00	40.21	45.95
64.00	48.37	45.73
66.00	56.54	45.62
68.00	64.70	45.72
70.00	72.86	46.35
72.00	81.00	48.93
74.00	88.73	94.29
76.00	82.54	-146.06
78.00	74.41	-142.49
80.00	66.25	-141.68
82.00	58.09	-141.51
84.00	49.92	-141.59
86.00	41.76	-141.80
88.00	33.59	-142.07
90.00	25.42	-142.38

Figure 3. (cont.)

The Bissett-Berman Corporation 2941 Nebraska Avenue, Santa Monica, California EXbrook 4-3270

APOLLO NOTE NO. 365
(Task 2, Item II)

M. Blasgen
16 August 1965

TIME-SIGMA SCALING IN THE BISSETT-BERMAN ERROR ANALYSIS PROGRAM

INTRODUCTION

This note documents a short experiment to show that the Bissett-Berman Error Analysis Program will, as stated in Apollo Note No. 186, accept $\sigma - t_{incr}$ scaling. We have long maintained that for convenience in computing, a much longer sampling interval can be used in Program A as long as the standard deviation used in Program B is scaled appropriately. The equation to be used is:

$$\sigma_{\text{Program B}} = \sqrt{\frac{\text{No. of sample pts. in Prog. A}}{\text{Actual No. of sample pts.}}} \quad \sigma_{\text{actual}} \tag{1}$$

This is not an exact expression, but as will be shown in a following paragraph, it is quite satisfactory for a fairly large number of samples.

ANALYSIS

Each total information matrix element is formed from a sum of values f, where:

$$f(t) = \frac{\partial M(t)}{\partial a_i} \frac{\partial M(t)}{\partial a_j}$$

The entry in the matrix is then:

$$I_1 = \underbrace{f(o) + f(1) + \ldots f(n)}_{n+1 \text{ terms}} \tag{2}$$

where sampling takes place every 1 time unit. If we scale time, this same term will be:

$$I_2 = \frac{f(o) + f(r) + f(2r) + \ldots . f(n)}{n/r + 1 \text{ terms}} \tag{3}$$

Using a linear approximation in Equation (2) that:

$$f(1) + f(2) + \ldots f(r-1) = \frac{r-1}{2} (f(o) + f(r))$$

etc., one obtains the result that:

$$I_1 = f(o) + \frac{r-1}{2} (f(o) + f(r)) + f(r) + \frac{r-1}{2} (f(r) + f(2n)) + \ldots f(n)$$

$$= rI_2 - \frac{r-1}{2} (f_o + f_n) \tag{4}$$

rearranging:

$$I_2 = \frac{I_2}{r} + \frac{r-1}{2r} (f_o + f_n) \tag{5}$$

If in Program B we use I_1 with a sigma of 1, then Equation (1) says to use I_2 with a sigma of :

$$\sqrt{\frac{n/r + 1}{n + 1}}$$

in order for it to be the same as I_1:

$$I_1^B = \frac{n + 1}{n/r + 1} \; I_2 \stackrel{?}{=} I_1$$

and using Equation (5) we have:

$$I_1^B = \frac{n+1}{n/r+1} \left[\frac{I_1}{r} + \frac{r-1}{2r} (f_o + f_n) \right]$$

$$= \frac{n+1}{n+r} \left[I_1 + \frac{r-1}{2} (f_o + f_n) \right] \tag{6}$$

$$\Delta I = I_1^B - I_1 = \frac{n+1}{n+r} I_1 - I_1 + \frac{n+1}{n+r} \frac{r-1}{2} (f_o + f_n)$$

$$= \frac{1-r}{n+r} \left[I_1 - \frac{n+1}{2} (f_o + f_n) \right] \tag{7}$$

If you let $I_1 = (n+1)\bar{f}$ where $\bar{f}$ is an average value of f over the n+1 data points, then:

$$\Delta I = \frac{1-r}{n+r} \left[(n+1)\bar{f} - \frac{n+1}{2} (f_o + f_n) \right] \tag{8}$$

or:

$$\frac{\Delta I}{I} = \frac{r-1}{n+r} \left[\frac{f_o + f_n}{2\bar{f}} - 1 \right] \tag{9}$$

where n+1 is the original number of sample points, and r is the ratio of the two sampling intervals. Note that if the average of the first and last sampling points is equal to the average value, then the error is zero. Also, note the more important result that the error decreases with larger and larger n.

RESULTS

Test cases were set up using three stations, (Madrid, Antigua, and Ascension) tracking in range rate, with a translunar trajectory. Tracking began at 16 minutes and ended at 180 minutes. Three different sampling intervals were used, 1/2, 1, and 2 minutes.

The covariance matrices which resulted from this study are presented in Figures 1, 2, and 3; along with the sigmas used in Program B.

DISCUSSION

The results for the three cases agree to within a few percent, which is consistent with the analysis presented in this report.

Translunar Trajectory

3 Stations Tracking in Range Rate for 164 minutes

Covariance Matrix

0.289406E 03	0.474371E 03	0.470743E 02	-0.855734E 00	-0.100838E-00	0.979679E-01
0.474371E 03	0.793965E 03	0.662478E 02	-0.142095E 01	-0.162181E-00	0.195125E-00
0.470743E 02	0.662478E 02	0.257425E 02	-0.120124E-00	-0.197831E-01	0.172451E-01
-0.855734E 00	-0.142095E 01	-0.120124E-00	0.256234E-02	0.292780E-03	-0.313401E-03
-0.100838E-00	-0.162181E-00	-0.197831E-01	0.292780E-03	0.360516E-04	-0.303374E-04
0.979679E-01	0.195125E-00	0.172451E-01	-0.313401E-03	-0.303374E-04	0.211420E-03

MISS TIME = 0.9487336E 00

MINIMUM MISS = 0.1775242E 02

REND MISS = 0.3330335E 02

SQRT((2,2)+(3,3)) = 0.2863054E 02

SQRT((4,4)+(5,5)+(6,6)) = 0.5300768E-01

SQRT(1, 1) = 0.1701193E 02

SQRT(2, 2) = 0.2817739E 02

SQRT(3, 3) = 0.5073709E 01

SQRT(4, 4) = 0.5061959E-01

SQRT(5, 5) = 0.6004296E-02

SQRT(6, 6) = 0.1454027E-01

Sampling Interval = 1/2 Minutes

Sigma = 0. 5375547 - 02 m/sec.

Figure 1.

Translunar Trajectory

3 Stations Tracking in Range Rate for 164 minutes

Covariance Matrix

0.284556E 03	0.467882E 03	0.456582E 02	-0.842408E 00	-0.989697E-01	0.101538E-00
0.467882E 03	0.785350E 03	0.644189E 02	-0.140304E 01	-0.159694E-00	0.200371E-00
0.456582E 02	0.644189E 02	0.250697E 02	-0.116615E-00	-0.191733E-01	0.179078E-01
-0.842408E 00	-0.140304E 01	-0.116615E-00	0.252514E-02	0.287746E-03	-0.323380E-03
-0.989697E-01	-0.159694E-00	-0.191733E-01	0.287746E-03	0.353155E-04	-0.316778E-04
0.101538E-00	0.200371E-00	0.179078E-01	-0.323380E-03	-0.316778E-04	0.206487E-03

MISS TIME = 0.9435725E 00 MINIMUM MISS = 0.1759617E 02 REND MISS = 0.3309042E 02

SQRT((2,2)+(3,3)) = 0.2846788E 02

SQRT((4,4)+(5,5)+(6,6)) = 0.5260171E-01

SQRT(1, 1) = 0.1686878E 02

SQRT(2, 2) = 0.2802410E 02

SQRT(3, 3) = 0.5006965E 01

SQRT(4, 4) = 0.5025075E-01

SQRT(5, 5) = 0.5942684E-02

SQRT(6, 6) = 0.1436965E-01

Sampling Interval = 1 Minute

Sigma = 0. 3806858 - 02 m/sec.

Figure 2.

Translunar Trajectory

3 Stations Tracking in Range Rate for 164 minutes

Covariance Matrix

0.275871E 03	0.456260E 03	0.432728E 02	-0.818349E 00	-0.956584E-01	0.108309E-00
0.456260E 03	0.769921E 03	0.614131E 02	-0.137063E 01	-0.155301E-00	0.210516E-00
0.432728E 02	0.614131E 02	0.238622E 02	-0.110812E-00	-0.181273E-01	0.190639E-01
-0.818349E 00	-0.137063E 01	-0.110812E-00	0.245726E-02	0.278780E-03	-0.342492E-03
-0.956584E-01	-0.155301E-00	-0.181273E-01	0.278780E-03	0.340181E-04	-0.341873E-04
0.108309E-00	0.210516E-00	0.190639E-01	-0.342492E-03	-0.341873E-04	0.198522E-03

MISS TIME = 0.9342576E 00 MINIMUM MISS = 0.1731281E 02 REND MISS = 0.3270557E 02

SQRT((2,2)+(3,3)) = 0.2817416E 02

SQRT((4,4)+(5,5)+(6,6)) = 0.5186325E-01

SQRT(1, 1) = 0.1660937E 02

SQRT(2, 2) = 0.2774745E 02

SQRT(3, 3) = 0.4884893E 01

SQRT(4, 4) = 0.4957072E-01

SQRT(5, 5) = 0.5832503E-02

SQRT(6, 6) = 0.1408980E-01

Sampling Interval = 2 minutes

Sigma = 0.2700000 - 02 m/sec.

Figure 3.

The Bissett-Berman Corporation 2941 Nebraska Avenue, Santa Monica, California EXbrook 4-3270

APOLLO NOTE NO. 366
(Task III, Item b)

G. F. Floyd
2 September 1965

OPTIMUM POWERED FLIGHT TRACKING AND MONITORING

AVAILABLE DATA

During powered flight, the information available to the ground consists of a sequence of telemetered inertial measurements, (I_n), and a sequence of ground based measurements, (M_n).

The (I_n) will be components along some preselected inertial axes of the inertial estimates of vector position $\overline{R}_I(t_n)$, velocity $\overline{V}_I(t_n)$, and possibly acceleration $\overline{A}_I(t_n)$. The ground-based measurements (M_n) will be some set of range rate, (more precisely range change in a time to interval), range, or angle from particular Earth-based stations. Thus the complete data set (D) with which we have to work may be written symbolically as:

$$D = I_1, M_1, \ldots . I_n, M_n$$

$$= (\overline{R}_I(t_n), \overline{V}_I(t_n), M_n), \quad n = 1 \ldots N \tag{1}$$

and we wish to process this general message optimally to get the best estimate of the present position $\overline{R}(t)$, and velocity $\overline{V}(t)$ of the spacecraft.

NATURE OF THE DATA

Let $\overline{R}_I(t)$ and $V_I(t)$ be the inertial system estimates of the present spacecraft position $\overline{R}(t)$ and velocity $\overline{V}(t)$.

Then we can always write:

$$\overline{R}_I(t) = \overline{R}(t) + \overline{e}_{\overline{r}}(t)$$
$$\overline{V}_I(t) = \overline{V}(t) + \overline{e}_{\overline{v}}(t) \tag{2}$$

where $\overline{e}_{\overline{r}}(t)$ and $\overline{e}_{\overline{v}}(t)$ are the errors in the inertial system estimates. Similarly, for a particular ground-based measurement (M_n) we have:

$$M_n = C_n + e_n \tag{3}$$

where (C_n) is defined as the correct value of the measurable and (e_n) is the error in (M_n).

Next we have that:

$$C_n = T\left[\overline{R}(t_n),\ \overline{V}(t_n)\right] \tag{4}$$

where the operation (T) means that (T) is the coordinate transformation which maps the true position or velocity of the spacecraft into the coordinate systems of the measuring station, and so includes station location and the coordinate system used for the measurable, (doppler from the master or slave, scalar range at the station or angular data).

NATURE OF THE ERRORS

The errors (e_n) in the ground-based measurables are fundamentally random quantities with perhaps biases, thus they are <u>noise-like.</u> On the other hand, the errors $\overline{e}_r(t)$ and $\overline{e}_v(t)$ in the inertial data have negligible noise-like components but are fundamentally <u>multiple time integrations</u> of unknown constants (a_i) which define gyro drift rates, accelerometer biases, initial platform misalignments,

integration scale factors, etc. Thus we may write:

$$\bar{e}_{\bar{r}}(t) = \bar{f}(a_i, t)$$
$$\bar{e}_{\bar{v}}(t) = \bar{g}(a_i, t) \tag{5}$$

where $\bar{f}$ and $\bar{g}$ are <u>known</u> vector functions of a finite set of <u>parameter</u> values (a_i) which define the errors in the inertial system. Thus combining (5) and (2) we can solve for the true $\bar{R}(t)$ and $\bar{V}(t)$ as:

$$\bar{R}(t) = \bar{R}_I(t) - \bar{f}(a_i, t)$$
$$\bar{V}(t) = \bar{V}_I(t) - \bar{g}(a_i, t) \tag{6}$$

and using (6) in (4), the result in (3) and solving for e_n we get:

$$\boxed{e_n = M_n - T\left[\bar{R}_I(t_n) - \bar{f}(a_i, t_n); \bar{V}_I(t_n) - \bar{g}(a_i, t_n)\right]} \tag{7}$$

which expresses the noise-like variable (e_n) in terms of the complete data set (D) as given by (1), and the finite set of unknown parameters (a_i).

From this point on the analysis of the optimization is <u>exactly</u> the same as in Apollo Note No. 347 if we simply identify the inertial system error parameters (a_i) used here with the orbit parameters, (also denoted by (a)), of Apollo Note No. 347.

Then since we have reduced the powered flight tracking problem to the identical mathematical problem of Note 347 we know that the solution will be the same so there is no point in wasting time re-deriving the same answers as obtained there. In particular, we can immediately draw the computational block diagram for the optimum powered flight tracking program by simply referencing Figure 2. of Note No. 347 and using the definitions of terms used in this note.

The result is then shown in Figure 1. of this note.

In particular, rules for the use of a priori estimates of the inertial error parameters are then exactly the same as before and the precise definitions of the optimum filters are also as before, namely the partial derivative of the predict with respect to the parameter.

We can use a little insight into the nature of the optimum filters as follows. The form of $\bar{e}_{\bar{n}}(t)$ and $\bar{e}_{\bar{v}}(t)$ due to say a vector acceleration bias $(\bar{a})$ will be simply:

$$\bar{e}_{\bar{v}}(t) = \bar{a}\, t$$
$$\bar{e}_{\bar{v}}(t) = \frac{1}{2}\, \bar{a}\, t^2 \tag{8}$$

Therefore, when the spacecraft is very far away, so the observing station is effectively at the center of the Earth, we have for an $(\dot{r})$ type of measurable:

$$m(t) = \bar{e}_{\bar{v}}(t) \cdot \bar{1}_{\ell os}$$
$$= k\, a\, t \tag{9}$$

where k is a known direction cosine. Thus, in this case (M_n) would be of the form:

$$M_n = k\, a\, n \tag{10}$$

and so:

$$\frac{\partial M_n}{\partial a} = k\, n \tag{11}$$

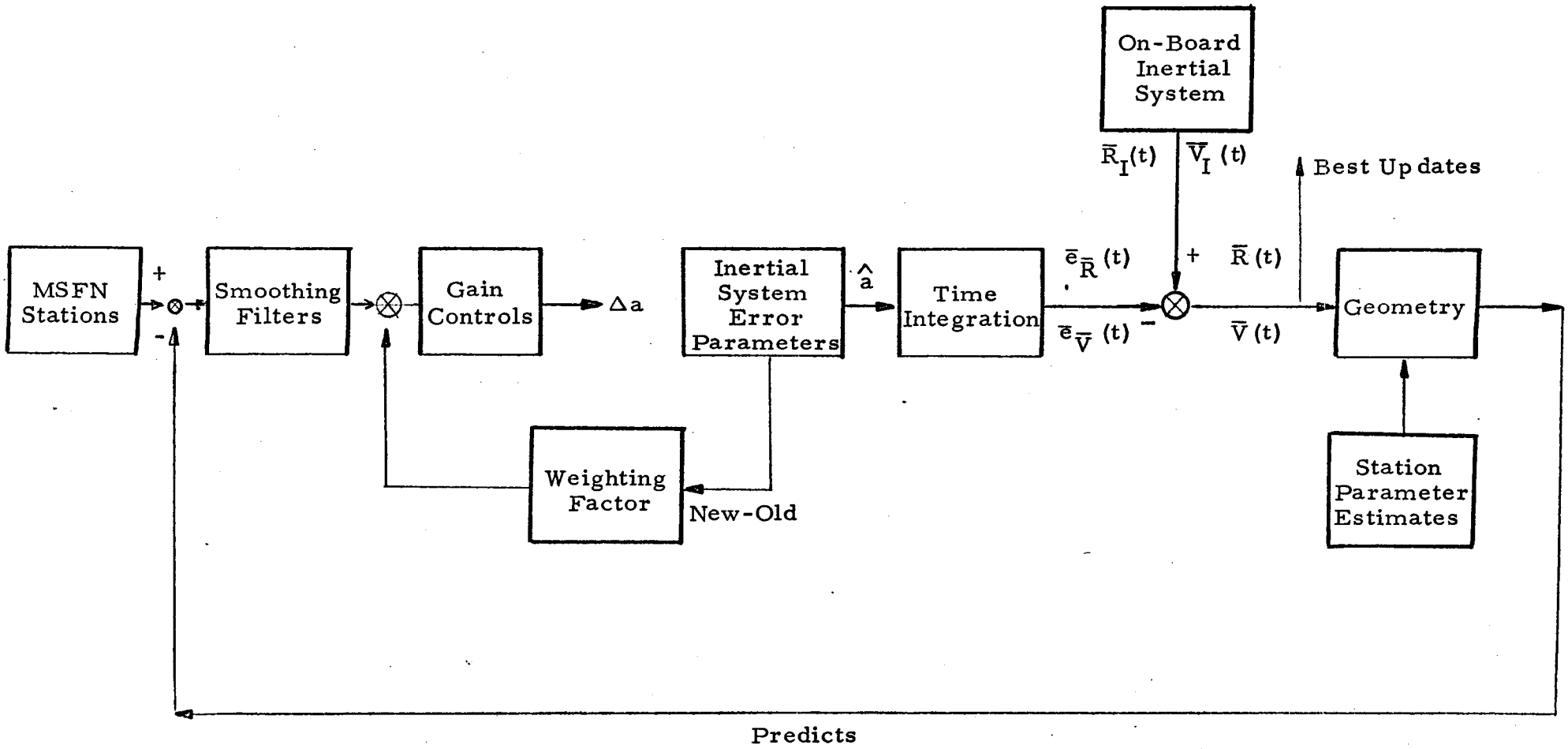

OPTIMUM POWERED FLIGHT TRACKING PROGRAM

Figure 1.

hence the optimum filter would be a simple ramp function. Now since powered phases last a short time, the transformation (T) may not have time to charge much when the spacecraft is not in Earth orbit. Hence, it may be essentially constant over the observation time. When this is true, the above then shows that the optimum filter will simply be the well-known class of optimum filter designed to get polynomial coefficients out of noise.

MONITORING

The processing needed here is simply a special case of Figure 2. where we don't update the initial error parameter estimates, (we might set all the error parameter to zero), and simply calculate the indicated changes (Δa). Then if any of these are too large we say the inertial system is "out of bounds" and could shift to a back-up However, since the system automatically computes the needed corrections to the inertial estimates, we could in fact, continue to operate with a high-drift gyro and use the calculated corrections, since we would get these for free from a system like Figure 2.

STUDY PROGRAM

There are many possibilities here and a careful study of both the <u>detection</u> and <u>correction</u> capabilities of the optimum processing system shown in Figure 2. is now needed. This will involve a considerable amount of analysis, programming and many computer runs to cover the many cases of operational interest.

START ON ERROR ANALYSIS

To start on the error analysis we let (r_n) be the differenoe between the measurable (M_n) and the predicts (P_n) of Figure 1. Thus:

$$r_n = M_n - P_n \tag{12}$$

with:

$$M_n = T\left[\overline{R}(t_n),\ \overline{V}(t_n)\right] + e_n \tag{13}$$

where $\overline{R}(t)$ and $\overline{V}(t)$ are the true values and e_n is the error on the measurable. Now from Figure 1.

$$P_n = T\left[\overline{R}_I(t) - \overline{f}(\tilde{a}_i,\ t_n),\ \overline{V}_I(t) - \overline{g}(\tilde{a}_i\ t_n)\right] \tag{14}$$

where $\overline{R}_I(t)$, $\overline{V}_I(t)$ are the inertial estimates and $\tilde{a}_i$ are our estimates of the error parameters. However, from (6):

$$\begin{aligned} \overline{R}_I(t) &= \overline{R}(t) + \overline{f}(a_i,\ t) \\ \overline{V}_I(t) &= \overline{V}(t) + \overline{g}(a_i,\ t) \end{aligned} \tag{15}$$

Where (a_i) are the true values of the parameters. Then using (15) in (14) and using the fact that the given coordinate transformation will be linear, (if the errors don't change the transformation), we have:

$$\begin{aligned} P_n &= T\left[\overline{R}(t_n) + \overline{f}(\tilde{a},\ t_n) - \overline{f}(a,\ t_n);\ \overline{V}(t) + \overline{g}(a,\ t_n) - g(\tilde{a},\ \tilde{t}_n)\right] \\ &= T\left[\overline{R}(t_n),\ \overline{V}(t_n)\right] + T\left[\overline{f}(a,\ t_n) - \overline{f}(\tilde{a},\ t_n),\ \overline{g}(a,\ t_n) - \overline{g}(\tilde{a},\ t_n)\right] \end{aligned} \tag{17}$$

Thus on substitution of (13) and (17) in (12), the main terms cancel and we have:

$$r_n = e_n + T\left[\overline{f}(a,\ t_n) - f(\tilde{a},\ t_n),\ \overline{g}(a,\ t_n) - \overline{g}(\tilde{a},\ t_n)\right] \tag{18}$$

Now if we assume the error n in our estimates of the parameters are small, we may write:

$$\bar{f}(a, t_n) \approx \bar{f}(\tilde{a}, t_n) + \frac{\partial \bar{f}}{\partial a} \Delta a$$

$$\bar{g}(a, t_n) \approx \bar{g}(\tilde{a}, t_n) + \frac{\partial \bar{g}}{\partial a} \Delta a. \tag{19}$$

Where

$$\Delta a = a - \tilde{a} \tag{20}$$

and so is our error in the estimate of (a)

Thus on use of (19) in (18), we get:

$$\boxed{r_n = e_n + T \left[\frac{\partial \bar{f}}{\partial a} \Delta a, \ \frac{\partial \bar{g}}{\partial a} \Delta a \right]} \tag{21}$$

Now a coordinate transformation takes the input and multiplies it by trignometric fuction, therefore, we can factor the (Δa) terms out in (21) getting:

$$\boxed{r_n = e_n + \Delta a \ T \left[\frac{\partial \bar{f}}{\partial a}, \ \frac{\partial \bar{g}}{\partial a} \right]} \tag{22}$$

The form of the matrices involved will be exactly the same as before as may be seen as follows. When the MSFN noise is Gaussian the maximum likelihood become minimum variance as well and minimizes the mean square value of the computed residual. Hence we will change our estimates of (a) until:

$$0 = \frac{\partial}{\partial \hat{a}} \left(\sum_1^n r_n^2 \right) = 2 \sum_1^n r_n \frac{\partial r_n}{\partial a} \tag{23}$$

and from (21):

$$\frac{\partial r_n}{\partial a} = \frac{\partial r_n}{\partial \Delta a} = T \left[\frac{\partial \bar{f}}{\partial \bar{a}} , \frac{\partial \bar{g}}{\partial a} \right] \tag{24}$$

Thus, substituting (22) and (24) into (23) and solving for Δa, we will have:

$$\Delta a \sum_{1}^{n} T \left[\frac{\partial \bar{f}}{\partial a} , \frac{\partial \bar{g}}{\partial a} \right] \left\{ T \left[\frac{\partial \bar{f}}{\partial a} , \frac{\partial \bar{g}}{\partial a} \right] \right\}^{\text{transpose}} = \sum_{1}^{n} e_n T \left[\frac{\partial \bar{f}}{\partial a} , \frac{\partial \bar{g}}{\partial a} \right] \tag{25}$$

which is exactly the same form as we have in the orbit case. Thus, for the Gaussian noise case we will get:

$$\boxed{\text{Cov}\ (\Delta a) = \sigma^2 C^{-1}} \tag{26}$$

$$\boxed{C \triangleq \sum_{1}^{n} T \left[\frac{\partial \bar{f}}{\partial a} , \frac{\partial \bar{g}}{\partial a} \right] \left\{ T \left[\frac{\partial \bar{f}}{\partial a} , \frac{\partial \bar{g}}{\partial a} \right] \right\}^{\text{transpose}}} \tag{27}$$

Since the transformation (T) depends on the true trajectory, in the analysis we will let it be the nominal trajectory for error study purposes. Thus, the error studies will consist in calculating covariance matrices for the (Δa) as a function of observation time in much the same way we have done for orbit analysis.

APOLLO NOTE NO. 367

(Task II - Item II)

H. Dale
H. Engel
L. Lustick
30 August 1965

CHANGES AND CORRECTIONS TO APOLLO NOTES NOS. 329, 328, 320 and 295

Note No. 329

In the Orbit Error Analysis Program (OEA Program), we used to have σ_r^2, σ_v^2, σ_γ^2 at fixed time t as the 1, 1 2, 2 and 3, 3 elements of the matrix product

$$QE(t) \ \ cov_o \ \ QE(t)^T$$

in which

$$QE(t) = \begin{bmatrix} \partial U/\partial X \\ \partial \gamma/\partial X \end{bmatrix} Q(t)$$

in which $\partial U/\partial X$ and $\partial \gamma/\partial X$ were obtained as outlined in Apollo Note No. 239, and Q(t) is the Q matrix used in obtaining cov_t from cov_o. This formulation could become indeterminate if the radial velocity were zero. Furthermore, this formulation did not take into account venting uncertainty. The new expression for QE(t) is

$$QE(t) = \begin{bmatrix} \partial r(t)/\partial a_j \\ \partial v(t)/\partial a_j \\ \partial \gamma(t)/\partial a_j \end{bmatrix} \quad , \ j = 1, \ldots, 6, \mu, a_v$$

in which QE(t) is a 3 x 8 matrix, $\partial r(t)/\partial a_j$ is obtained from Part A of the OEA Program,

$$\frac{\partial r(t)}{\partial a_j} = \left[\cos(\theta - \theta_o),\ \sin(\theta - \theta_o),\ 0, 0, 0, 0, 0, 0\right] \quad Q(t)$$

$$\frac{\partial v(t)}{\partial a_j} = \left[0, 0, 0,\ \frac{x'}{v},\ \frac{y'}{v},\ 0, 0, 0\right] \quad Q(t)$$

and

$$\frac{\partial \gamma(t)}{\partial a_j} = \left[\frac{y'}{r^2},\ \frac{-x'}{r^2},\ 0,\ \frac{-y'}{v^2},\ \frac{x'}{v^2},\ 0, 0, 0\right] \quad Q(t)\ .$$

Note No. 328

Apollo Note No. 328 contains several difficult to locate errors that have been found, and the solution for the Euler angles has been reformulated. The eigenvalues and p_{11}, p_{21}, p_{31}, p_{12}, p_{22}, and p_{32} are found as in Note No. 328. The direction cosines for λ_1 and λ_2 are also found as in that note. Letting ν be the rotation matrix from the prime coordinate system to the principal axis system we have

$$\nu = \begin{bmatrix} \frac{1}{p_{11}} & \frac{p_{21}}{p_{11}} & \frac{p_{31}}{p_{11}} \\ \frac{1}{p_{12}} & \frac{p_{22}}{p_{12}} & \frac{p_{32}}{p_{12}} \\ \nu_{31} & \nu_{32} & \nu_{33} \end{bmatrix}$$

in which we now obtain the direction cosines of λ_3 as the cross product of the unit vectors in the directions of λ_1 and λ_2. We have

$$\nu_{31} = \nu_{12}\ \nu_{23} - \nu_{13}\ \nu_{22}$$

$$\nu_{32} = \nu_{13}\ \nu_{21} - \nu_{11}\ \nu_{23}$$

$$\nu_{33} = \nu_{11}\ \nu_{22} - \nu_{12}\ \nu_{21}$$

Next we assume the line of nodes has direction cosines in the ratio of ν_{32}, $-\nu_{31}$ and 0, so

$$\cos\phi = \frac{\nu_{32}}{(\nu_{31}^2 + \nu_{32}^2)^{1/2}}$$

$$\sin\phi = \frac{-\nu_{31}}{(\nu_{31}^2 + \nu_{32}^2)^{1/2}}$$

Letting λ_i denote the eigenvector, and LON the line of nodes unit vector, we have

$$\cos\psi = \frac{\lambda_1}{|\lambda_1|} \cdot \text{LON} = \nu_{11}\cos\phi + \nu_{12}\sin\phi$$

$$\sin\psi = \frac{\lambda_2}{|\lambda_2|} \cdot \text{LON} = -\nu_{21}\cos\phi - \nu_{22}\sin\phi$$

$$\cos X = \nu_{33}$$

and

$$\sin X = \nu_{13} / \sin\psi.$$

Note No. 320

There is a sign error in Apollo Note No. 320. The correct expression for $e_{\dot{M}}$ for three-way Doppler is

$$e_{\dot{M}} = c\left(\beta_s + \alpha_s \hat{t}_s - \beta_m - \alpha_m \hat{t}_s + \alpha_m \frac{\left|\bar{R}_s(\hat{t}_s) - \bar{R}_v(\hat{t}_s)\right| + \left|\bar{R}_v(\hat{t}_s) - \bar{R}_m(\hat{t}_s)\right|}{c}\right)$$

$$- \left(b_s + \beta_s \hat{t}_s + \frac{\alpha_s}{2}\hat{t}_s^{\,2}\right)\left\{\frac{\left[\bar{R}_s(\hat{t}_s) - \bar{R}_v(\hat{t}_s)\right] \cdot \left[\frac{d^2\bar{R}_s(\hat{t}_s)}{dt_s^{\,2}} - \frac{d^2\bar{R}_v(\hat{t}_s)}{dt_s^{\,2}}\right]}{\left|\bar{R}_s(\hat{t}_s) - \bar{R}_v(\hat{t}_s)\right|}\right.$$

$$\left. + \frac{\left[\bar{R}_v(\hat{t}_s) - \bar{R}_m(\hat{t}_s)\right] \cdot \left[\frac{d^2\bar{R}_v(\hat{t}_s)}{dt^2} - \frac{d^2\bar{R}_m(\hat{t}_s)}{dt^2}\right]}{\left|\bar{R}_v(\hat{t}_s) - \bar{R}_m(\hat{t}_s)\right|}\right\}$$

and for the two-way Doppler this reduces to

$$e_{\dot{M}} = 2\alpha_m\left|\bar{R}_v(t_m) - \bar{R}_m(t_m)\right| - 2\left(b_m + \beta_m t_m + \frac{\alpha_m}{2} t_m^{\,2}\right) \cdot$$

$$\left\{\frac{\left[\bar{R}_v(t_m) - \bar{R}_m(t_m)\right] \cdot \left[\frac{d^2\bar{R}_v(t_m)}{dt_m^{\,2}} - \frac{d^2\bar{R}_m(t_m)}{dt_m^{\,2}}\right]}{\left|\bar{R}_v(t_m) - \bar{R}_m(t_m)\right|}\right\}$$

This last quantity to be divided by 2 for use in the OEA Program.

Note No. 295

The lunar ephemeris calculations outlined in Apollo Note No. 295 are unnecessarily complicated since much of the computation can be done using the existing Part A of the OEA Program. The trick is to consider the Moon as a vehicle in orbit about the Earth with a tracking station located at the center of the Earth.

The lunar ephemeris is important only in the lunar sphere of influence, at which time only range and range rate measurements are used.

For the lunar ephemeris calculations, which assume a circular lunar orbit, the inputs used for other parts of Part A of the OEA Program are used in a different fashion. The inputs used in the portion of the program are as follows. They do not require additional inputs on the program input sheet.

A1 = RHOM (= Earth-Moon distance)*

A4 = 0

A5 = OMEGAM x RHOM*

GAMID =
BETA = } Same as on program input sheet

XI = ETA = ZETA = LAMBDA = ALPHA = 0

OMEGAE = OMEGAM** = RHO = RHOM** = 0

MU = $.399689 \times 10^{15}\ m^3\ sec^2$

TJ(i) =
BIG L =
SMA L = } Same as on program input sheet
RRIND =
RIND =

QIND = QF = PSIND = PSZIND = PVW IND = 0

$$\left.\begin{array}{l}\text{TI(init)} \quad = \\ \text{TI(interval)} \quad =\end{array}\right\} \text{Same as on program input sheet}$$

DIMENSION = 6

LAMBDA 2 = ALPHA2 = M − SIND = 0

*If A1 or A5 are 0 or not specified on program input sheet, use $A1 = .385 \times 10^9$ m or $A5 = .10256 \times 10^4$ m/sec.

**These values are the ones to be used in this subroutine as inputs and are not the values used to compute A1 and A5.

Using this subroutine, we compute R_j' and $\dot{R}_j'$ for the 6 values of j corresponding to the lunar orbit parameters. Since XI, ETA and ZETA are zero, the prime coordinates used in this subroutine are the same as the tilda coordinates used in this subroutine, and these in turn are the same as the tilda coordinates used in the main portion of Part A. To find the prime components in the prime system of the <u>vehicle</u> orbit, we use $\mathbb{L}$ matrix from the main portion of the program, and calculate

$$R_i' = \mathbb{L}\, R_j'$$

$$\dot{R}_j' = \mathbb{L}\, \dot{R}_j'$$

in which R_i' and $\dot{R}_i'$ are in vehicle prime coordinates, R_j' and $\dot{R}_j'$ and in lunar (subroutine) prime coordinates. Next calculate

$$\frac{\partial s}{\partial a_j} = \frac{1}{s} \left(X_s'\right)^T \left(R_i'\right)$$

$$\frac{\partial \dot{s}}{\partial a_j} = \frac{1}{s} \left\{ X_s'^{\,T} \dot{R}_i' + \left[X_s' - \frac{\dot{s}}{s} X_s' \right] R_i' \right\}$$

for the six values of j corresponding to lunar orbit parameters.

Treat the Master-Slave problem in the ordinary way, with

$$\frac{\partial \dot{s}}{\partial a_j} = \frac{\partial \dot{s}_{master}}{\partial a_j} + \frac{\partial \dot{s}_{slave}}{\partial a_j}$$

as before.

The Bissett-Berman Corporation 2941 Nebraska Avenue, Santa Monica, California EXbrook 4-3270

APOLLO NOTE NO. 368
(Item 2, Task II)

C. H. Dale
25 August 1965

A MODIFICATION OF THE ERROR ANALYSIS PROGRAM TO PERMIT ANGLE MEASURABLES FROM ONE VEHICLE TO ANOTHER, BOTH IN ELLIPTIC ORBITS

(Apollo Note No. 337, continued)

In the above referenced Apollo Note, range and range rate measurables were considered. Angle measurements, described in this note, depend upon the equipment used. Although I don't know exactly how vehicle-to-vehicle measurements would be taken I will assume that any pair of somewhat orthogonal measurements referenced to the navigational base will yield nearly equivalent results. The notation in Apollo Note No. 337 is difficult; we are about to achieve the impossible.

Define (as in Apollo Note No. 337):

$\overline{R}_1 \equiv$ vector from Moon center to Vehicle$_1$, the vehicle which is doing the tracking.

$\overline{R}_2 \equiv$ vector from Moon center to Vehicle$_2$, the target.

$\overline{r} \equiv$ vector from Vehicle$_1$ to Vehicle$_2$.

$r \equiv$ magnitude of $\overline{r}$ where $\overline{r} = \overline{R}_2 - \overline{R}_1$.

a_j's defined in Apollo Note No. 337 for $j = 1$ through 14.

Now if the platform of the tracker were perfectly aligned, its axes would coincide with the x', y', z' axes which define the first vehicle's position at time zero. Actually we will assume that the vehicle's axes are in unknown error by θ_1, θ_2, and θ_3 (in that order.)

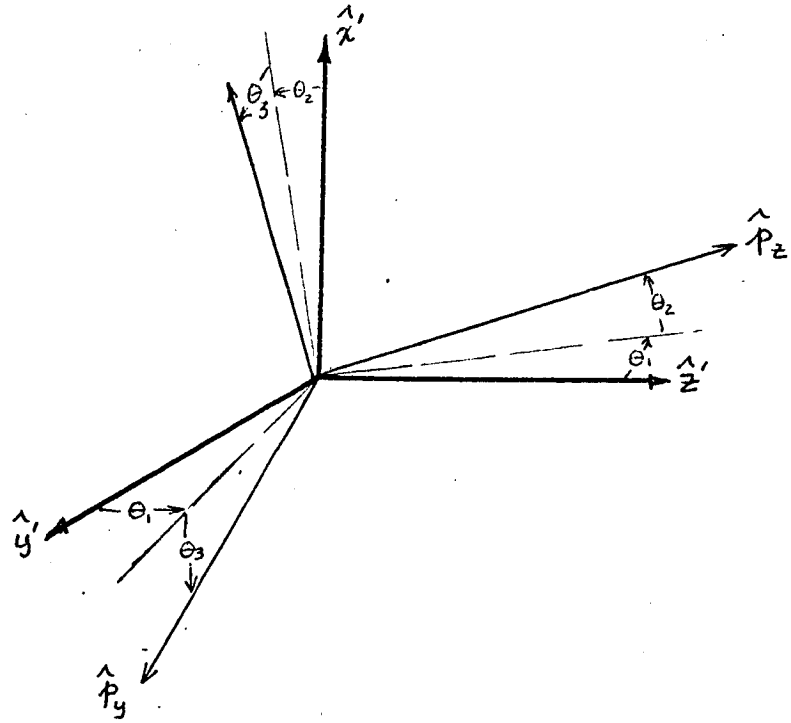

Any vector with components x', y', z' may thus be expressed in the platform coordinate x_p, y_p, z_p by the following:

$$\begin{bmatrix} x_p \\ y_p \\ z_p \end{bmatrix} = \begin{bmatrix} (\cos\theta_3\cos\theta_2) & (+\cos\theta_3\sin\theta_2\sin\theta_1+\sin\theta_3\cos\theta_1) & (-\cos\theta_3\sin\theta_2\cos\theta_1+\sin\theta_3\sin\theta_1) \\ (-\sin\theta_3\cos\theta_2) & (-\sin\theta_3\sin\theta_2\sin\theta_1+\cos\theta_3\cos\theta_1) & (+\sin\theta_3\sin\theta_2\cos\theta_1+\cos\theta_3\sin\theta_1) \\ (+\sin\theta_2) & (-\cos\theta_2\sin\theta_1) & (\cos\theta_2\cos\theta_1) \end{bmatrix} \begin{bmatrix} x' \\ y' \\ z' \end{bmatrix}$$

This transformation matrix may be approximated to first order for small angles as:

$$\begin{bmatrix} (1) & (\theta_3) & (-\theta_2) \\ (-\theta_3) & (1) & (\theta_1) \\ (+\theta_2) & (-\theta_1) & (1) \end{bmatrix}$$

Now the vector position of tracked vehicle with respect to the tracking vehicle is $\bar{r}$ whose components in the x'y'z' are described by the vector $r' = \mathbb{L}\,\mathbb{L}_2^T\,(R_2)'_2 - R'_1$ as discussed in Apollo Note No. 337. In the platform system we will define the relative range vector as r_p where:

relative range in platform coordinates

$$r_p = \begin{bmatrix} r_p(x) \\ r_p(y) \\ r_p(z) \end{bmatrix} = \begin{bmatrix} (1) & (\theta_3) & (-\theta_2) \\ (-\theta_3) & (1) & (\theta_1) \\ (\theta_2) & (-\theta_1) & (1) \end{bmatrix} r'$$

relative range in x'y'z' coordinates

we may now define further nuisance parameters:

$$a_{15} = \theta_1$$

$$a_{16} = \theta_2$$

$$a_{17} = \theta_3$$

for this special problem. These parameters are nominally all zero and the above matrix is nominally a unity matrix.

Now the measurables, Az and El may be described in the platform system from which they are actually measured. r is the magnitude of r' or r_p.

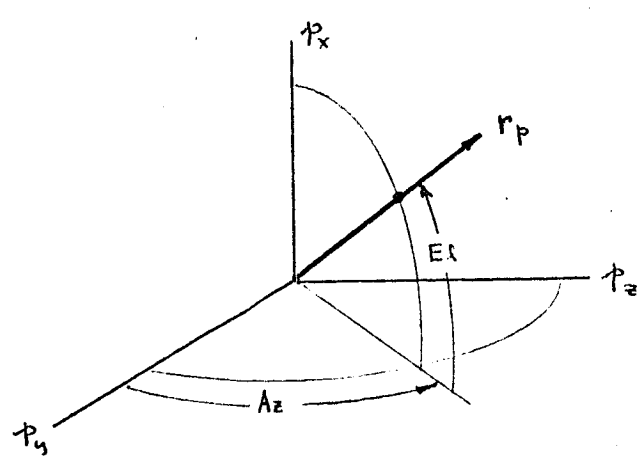

Now if:

$$\mathbb{P}_x = [(1)\ (\theta_3)\ (-\theta_2)]$$

$$\mathbb{P}_y = [(-\theta_3)\ (1)\ (\theta_1)]$$

$$\mathbb{P}_z = [(\theta_2)\ (-\theta_1)\ (1)]$$

$$\mathbb{P} = \begin{bmatrix} \mathbb{P}_1 \\ \mathbb{P}_2 \\ \mathbb{P}_3 \end{bmatrix}$$

Then:

$$\frac{\partial r_p(x)}{\partial a_j} = \frac{\partial \mathbb{P}_x}{\partial a_j} r' + \mathbb{P}_x \frac{\partial r'}{\partial a_j}$$

$$\frac{\partial r_p(y)}{\partial a_j} = \frac{\partial \mathbb{P}_y}{\partial a_j} r' + \mathbb{P}_y \frac{\partial r'}{\partial a_j}$$

$$\frac{\partial r_p(z)}{\partial a_j} = \frac{\partial \mathbb{P}_z}{\partial a_j} r' + \mathbb{P}_y \frac{\partial r'}{\partial a_j}$$

Now from the previous figure:

$$\sin(E\ell) = \frac{r_p(x)}{r}$$

where:

$$r = |r'| = +\sqrt{(r')^T r'}$$

as described in Apollo Note No. 337.

And:

$$\cos(E\ell) = +\sqrt{1-\sin^2(E\ell)} = +\sqrt{1-\left(\frac{r_p(x)}{r}\right)^2}$$

Then the partials of the first measurable are:

$$\frac{\partial(E\ell)}{\partial a_j} = \frac{1}{\cos(E\ell)}\,\frac{d\sin(E\ell)}{\partial a_j} = \frac{1}{\sqrt{1-\left(\frac{r_p(x)}{r}\right)^2}}\,\frac{d\left(\frac{r_p(x)}{r}\right)}{\partial a_j}$$

$$= \frac{1}{\sqrt{1-\left(\frac{r_p(x)}{r}\right)^2}}\left\{\frac{1}{r}\,\frac{\partial r_p(x)}{\partial a_j} - \frac{r_p(x)}{r^2}\,\frac{\partial r}{\partial a_j}\right\}$$

where $\frac{\partial r}{\partial a_j}$ is given in Apollo Note No. 337, and is not to be confused with $\frac{\partial r'}{\partial a_j}$ where:

$$\frac{\partial r'}{\partial a_j} = \mathbb{L}\,\mathbb{L}_2^T\,\frac{\partial R'_2}{\partial a_j} - \frac{\partial R'_1}{\partial a_j}$$

The second angle is given by:

$$\sin(A_z) = \frac{r_p(z)}{\left(r_p^2(z) + r_p^2(y)\right)^{1/2}}$$

$$\cos(A_z) = \frac{r_p(y)}{\left(r_p^2(z) + r_p^2(y)\right)^{1/2}}$$

Then the partials of the second measurable are:

$$\frac{\partial(A_z)}{\partial a_j} = \frac{1}{\cos(A_z)} \frac{\partial \sin(A_z)}{\partial a_j} = \frac{(r_p^2(z) + r_p^2(y))^{1/2}}{r_p(y)} \frac{\partial\left\{\dfrac{r_p(z)}{(r_p^2(z)+r_p^2(y))^{1/2}}\right\}}{\partial a_j}$$

or:

$$\frac{\partial(A_z)}{\partial a_j} = \frac{[r_p^2(z)+r_p^2(y)]^{1/2}}{r_p(y)} \left\{ \frac{\dfrac{\partial r_p(z)}{\partial a_j}}{[r_p^2(z)+r_p^2(y)]^{1/2}} - \frac{r_p(z)\left[r_p(z)\dfrac{\partial r_p(z)}{\partial a_j} + r_p(y)\dfrac{\partial r_p(y)}{\partial a_j}\right]}{[r_p^2(z)+r_p^2(y)]^{3/2}} \right\}$$

Now nominally the relative-range vector is identical in the platform coordinate system and in the x'y'z' coordinate system. Thus, the equations to be programmed are: (following Apollo Note No. 337)

$$\begin{bmatrix} r'(x) \\ r'(y) \\ r'(z) \end{bmatrix} \equiv r' \tag{1}$$

$$\left.\begin{aligned}
\frac{\partial r_p(x)}{\partial a_j} &= [(1)\ (0)\ (0)]\ \frac{\partial r'}{\partial a_j} && \text{for } j = 1 \text{ through } 14 \\
&= 0 && \text{for } j = 15 \\
&= [(0)\ (0)\ (-1)]\ r' && \text{for } j = 16 \\
&= [(0)\ (1)\ (0)]\ r' && \text{for } j = 17
\end{aligned}\right\} \tag{2}$$

$$\left.\begin{aligned}
\frac{\partial r_p(y)}{\partial a_j} &= [(0)\ (1)\ (0)]\ \frac{\partial r'}{\partial a_j} && \text{for } j = 1 \text{ through } 14 \\
&= [(0)\ (0)\ (1)]\ r' && \text{for } j = 15 \\
&= \quad 0 && \text{for } j = 16 \\
&= [(-1)\ (0)\ (0)]\ r' && \text{for } j = 17
\end{aligned}\right\} \tag{3}$$

$$\left.\begin{aligned}
\frac{\partial r_p(z)}{\partial a_j} &= [(0)\ (0)\ (1)]\ \frac{\partial r'}{\partial a_j} && \text{for } j = 1 \text{ through } 14 \\
&= [(0)\ (-1)\ (0)]\ r' && \text{for } j = 15 \\
&= [(1)\ (0)\ (0)]\ r' && \text{for } j = 16 \\
&= \quad 0 && \text{for } j = 17
\end{aligned}\right\} \tag{4}$$

$$\sin(E\ell) = \frac{r'(x)}{r} \tag{5}$$

$$\cos(E\ell) = +\left(1 - \sin^2(E\ell)\right)^{1/2} \tag{6}$$

$$\frac{\partial(E\ell)}{\partial a_j} = \frac{1}{\cos(E\ell)} \left\{\frac{1}{r}\ \frac{\partial r_p(x)}{\partial a_j} - \frac{r'(x)}{r^2}\ \frac{\partial r}{\partial a_j}\right\} \tag{7}$$

where $\frac{\partial r}{\partial a_j}$ is defined in Apollo Note No. 337:

$$\cos(A_z) = \frac{r'(y)}{\left(r'(y)^2 + r'(z)^2\right)^{1/2}} \tag{8}$$

$$\frac{\partial(A_z)}{\partial a_j} = \frac{1}{\cos(A_z)} \left\{ \frac{r'(y)^2 \frac{\partial r_p(z)}{\partial a_j} - r'(z)\, r'(y) \frac{\partial r_p(y)}{\partial a_j}}{\left[r'(z)^2 + r'(y)^2\right]^{3/2}} \right\} \tag{9}$$

It should be remembered that:

$$\left.\begin{aligned} a_{15} &\equiv \theta_1 \\ a_{16} &\equiv \theta_2 \\ a_{17} &\equiv \theta_3 \end{aligned}\right\} \quad \text{which are all nominally zero.}$$

The Bissett-Berman Corporation 2941 Nebraska Avenue, Santa Monica, California EXbrook 4-3270

APOLLO NOTE NO. 369
(Task III, Item b)

C. H. Dale
8 September 1965

SOME THOUGHTS ON "POWERED FLIGHT ECT." FROM A WORK LOAD POINT OF VIEW

We wish to build an "Error Analysis Program" which will show how well the MSFN can evaluate the IMU-AGC performance during powered flight. This note is intended to show what must be done to accomplish the task of writing the program. It is felt that time spent in preliminary blocking out of the problem may save future pitfalls.

From Apollo Note No. 366 it is seen that the first desired output of the above program is a covariance matrix. The terms in this covariance matrix refer to uncertainties in all relevant MSFN biases and IMU and AGC biases. From this covariance matrix it is assumed that statements regarding detection and false alarm probabilities, (gyros, accelerometers, initial condition constants, etc.) may be generated.

The above mentioned covariance matrix will be the inverse of an information matrix, the terms of which will be sums of partials of the MSFN measurable with respect to parameters of interest. This is all old hat:

$$\text{Information matrix term, } C_{ij} = \frac{1}{\sigma^2} \sum_{t_k}^{K} \frac{\partial m(t_k)}{\partial a_i} \frac{\partial m(t_k)}{\partial a_j}$$

where σ is the known mean noise on the radar for a sampling interval, $t_{k+1} - t_k$; $m(t_k)$ is the measurable (say range, angle, or range-rate) at a time, t_k; and a_i and a_j are a couple of the many uncertain parameters which might affect the measurable.

Now the next relevant question should be, "How do we get $\frac{\partial m(t_k)}{\partial a_j}$?"

We plagerize the Final Report on Contract NASw-688, "Capabilities of MSFN for Apollo Guidance and Navigation", dated 2 March 1964, Page 3-51 and environs:

A partial of a measurable, say range (s), with respect to a parameter a_j may be expressed:

$$\frac{\partial s}{\partial a_j} = \frac{1}{s} (R'_s)^T \left(\frac{\partial R'_s}{\partial a_j}\right)$$

where R'_s is the vector range for a nominal trajectory, s is its magnitude and $\frac{\partial R'_s}{\partial a_j}$ is the 1 x 3 vector expressing the partial of R'_s with respect to the particular parameter of interest, a_j. The above equation is a dot product; it is evaluated along the nominal trajectory; and the prime denotes a particular coordinate system within which the dot product is taken (any will do). It is important to realize that equations similar to the above exist for any MSFN measurable, and that they involve only the <u>nominal</u> vector range (R'_s) and vector velocity ($\dot{R}'_s$), their absolute magnitudes (s and $\dot{s}$), and such quantities as:

$$\frac{\partial R'_s}{\partial a_j} \text{ and } \frac{\partial \dot{R}'_s}{\partial a_j}$$

expressed in a working coordinate system.

All the above is pure plagerism. The next question is, "How do we get the four quantities":

$$R'_s, \dot{R}'_s, \frac{\partial R'_s}{\partial a_j} \text{ and } \frac{\partial \dot{R}'_s}{\partial a_j} \text{ ?}$$

Let us look at the geometry involved:

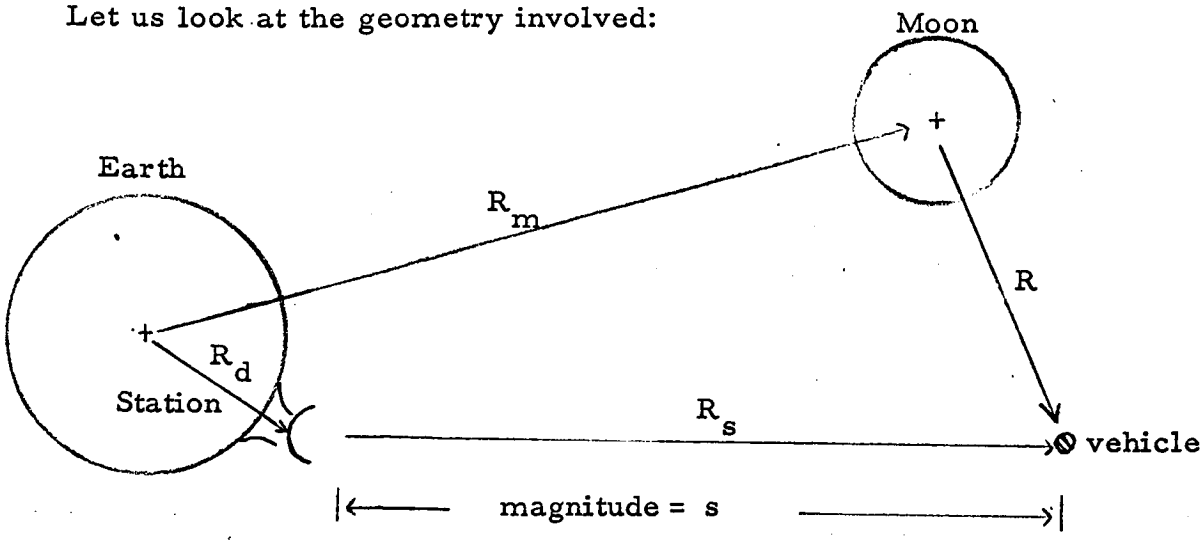

$R_s = R_m + R - R_d$ for any coordinate system.

$R'_s = R'_m + R' - R'_d$ for a particular inertial system defined at t = o with a center at the point of qravitational attraction, $\hat{x}'$ pointed at the vehicle and $\hat{y}'$ in the plane of motion with $\dot{y}'$ (t= o) positive.

$$s = \left[(R'_s)^T R'_s \right]^{1/2}$$

$$\dot{R}'_s = \dot{R}'_m + \dot{R}' - \dot{R}'_d$$

$$\dot{s} = \frac{1}{s} (R'_s)^T \dot{R}'_s$$

Now from the above it is seen that for R'_s and $\dot{R}'_s$ we need R_m and R_d as before but we also need R and $\dot{R}$ which are no longer described by Keplerian orbits. What we may do is define some inertial coordinate system such as the primed one. Then R and $\dot{R}$ may be generated as six polynomials from existing thrusting trajectory data in an appropriate inertial frame. Say:

$$R'(t) = \begin{bmatrix} p_x(t) \\ p_y(t) \\ p_z(t) \end{bmatrix} ; \qquad \dot{R}'(t) = \begin{bmatrix} p_{\dot{x}}(t) \\ p_{\dot{y}}(t) \\ p_{\dot{z}}(t) \end{bmatrix}$$

where the p's are polynomial data fits. If the data is not in the (') system a simple transformation will take care of that.

Now we are left with generating $\frac{\partial R'_s}{\partial a_j}$ and $\frac{\partial \dot{R}'_s}{\partial a_j}$. We have:

$$\frac{\partial R'_s}{\partial a_j} = \left(\frac{\partial R_m}{\partial a_j}\right)' + \frac{\partial R'}{\partial a_j} - \left(\frac{\partial R_d}{\partial a_j}\right)'$$

$$\frac{\partial \dot{R}'_s}{\partial a_j} = \left(\frac{\partial \dot{R}_m}{\partial a_j}\right)' + \frac{\partial \dot{R}'}{\partial a_j} - \left(\frac{\partial R_d}{\partial a_j}\right)'$$

where for the a_j's which involve the IMU and AGC only for the $\frac{\partial R'}{\partial a_j}$ and $\frac{\partial \dot{R}'}{\partial a_j}$ terms exist. For the MSFN a_j's some of the other terms exist. For instance station location uncertainties are tied up in $\frac{\partial R'_d}{\partial a_j}$. The MSFN type parameters have been discussed at length before, thus the remainder of this note involves:

Getting $\frac{\partial R'}{\partial a_j}$ and $\frac{\partial \dot{R}'}{\partial a_j}$ for IMU and AGC Parameters:

Define:

a_1 through a_k as MSFN Parameters (biases).

The platform defined to be aligned with x' y' z'.

a_{k+1} = positive x' acceleration error, i. e. the platform reads the actual $\ddot{x}'$ + $\overrightarrow{grav.}$ (in x') - a_{k+1}

a_{k+2}, a_{k+3} = the above for y' and z'

a_{k+4} = positive platform initial rotational misalignment about x'

.
.
.

etc. to include accelerometer and gyro offsets, non or orthogonalities, scale factor errors, etc.

Now for the first case of x' accelerometer additive error, we assume that the nominal trajectory is R' and $\dot{R}'$ while the actual trajectory is:

$$\dot{R}'_{actual}(t) = \dot{R}'(t) + \begin{bmatrix} (a_{k+1})t \\ 0 \\ 0 \end{bmatrix}$$

$$R'_{actual}(t) = R'(t) + \begin{bmatrix} (a_{k+1})t^2/2 \\ 0 \\ 0 \end{bmatrix}$$

and $\frac{\partial \dot{R}'}{\partial a_{k+1}}$ would just equal $\begin{bmatrix} t \\ 0 \\ 0 \end{bmatrix}$

while $\frac{\partial R'}{\partial a_{k+1}}$ would equal $\begin{bmatrix} t^2/2 \\ 0 \\ 0 \end{bmatrix}$

If the a_{k+4} term involves a positive rotation about the x' axis (alignment error) then the actual $\dot{R}'$ and R' would be:

$$\dot{R}'_{actual} = \begin{bmatrix} 1 & 0 & 0 \\ 0 & \cos a_j & \sin a_j \\ 0 & -\sin a_j & \cos a_j \end{bmatrix} \dot{R}'$$

and:

$$\frac{\partial \dot{R}'}{\partial a_{k+4}} \text{ would equal } \begin{bmatrix} 0 & 0 & 0 \\ 0 & -\sin a_j & \cos a_j \\ 0 & -\cos a_j & -\sin a_j \end{bmatrix} \dot{R}'; \text{ etc.}$$

Hopefully all of the IMU and AGC bias parameters, i. e. all of the $a_{k+4} \cdots a_n$, may be handled in so simple a manner. The old parameters regarding the MSFN uncertainties, $a_1, \ldots\ldots a_k$ must be re-looked at in light of the new definition of $R'(t)$ and $\dot{R}'(t)$, that is thrusting trajectories rather than Keplerian orbits; however, no problems are foreseen.

APOLLO NOTE NO. 370
(Task I, Item IB)

H. R. Wright
20 September 1965

A PEAK ELECTRON DENSITY MODEL FOR REFRACTIVE INDEX PREDICTIONS IN THE ANOMALOUS QUIET IONOSPHERE

1. INTRODUCTION

Irrespective of the refractive index profile finally adopted, the F-2 peak electron density must be specified for any prediction model based on current understanding of the anomalous ionosphere. At least one density-height distribution, that proposed by Seddon[1], also requires a knowledge of the corresponding density in the daytime E region. On the other hand, neither the F-1 nor the F-1-1/2 layers are accounted for by any models set forth to date. The latter ionospheric features, when they can be detected, appear only during daylight and at altitudes well below the peak--say the 140 to 200 km levels. Although distinct echoes are observed frequently enough to interest communications, these layers blend smoothly into the F region contour when the data are reduced to electron density-height profiles and appear as insignificant distortions. They will be ignored in this discussion.

Details in the D region also will be ignored. That this is reasonable follows, first of all, from the low ionization levels which even during the day are some two orders of magnitude below those prevailing in the F2 region. Even fairly large D region profile distortions have little influence on propagation predictions through the ionosphere at S band frequencies. At night, conditions are even more favorable because at these low altitudes, about 50 to 90 km, collision frequencies are high and the layer essentially disappears by recombination shortly after ionization production ceases at sunset.

Conditions in the E-layer will be discussed but mainly because they assume importance in Seddon's widely cited mid-latitude electron

density profile. As a matter of practice the F region dominates the refractive index profile at S band frequencies. In this connection, it is an unfortunate fact that although fairly simple laws governing the E-layer have been discovered, the real F region is extremely anomalous. Further, like the F-1 and F-1-1/2 regions but excluding F-2, rather than maximum density regions, all "layers" are now known to be inflection points on an otherwise smooth density-height curve.

A prediction model for the anomalous ionosphere will be described in a later note with the actual profile being accounted for rather closely. For this, the discussion to be given here regarding N_m predictions will be useful. More immediately, it also will be useful as a first step in accounting for the anomalies by exploiting the fact that a fairly realistic estimate of refraction effects through the ionosphere may be made if the peak electron density is known near the region penetrated by the ray. In order to do this, a greatly simplified model is adopted in which profile details are ignored. Then, as a first approximation, the ionosphere may be considered a uniform slab with a total electron content that is proportional to the peak electron density. It is customary to write this relation in the form

$$n_t = yN_m \tag{1.1}$$

where n_t is the total electron content, y is the equivalent slab thickness and N_m is the F-2 peak electron density. It will be recalled that at S band this relation may be used to obtain an excellent estimate for ionospheric path length changes $\Delta\ell$ through the simple relation[2]

$$\begin{aligned} \Delta\ell &= 1,600\ n_t/\omega^2 \\ &= 1,600\ yN_m/\omega^2 \end{aligned} \tag{1.2}$$

where ω is the transmitted angular frequency and rmks units are used unless otherwise noted. This is equivalent to a slab with a uniform index of refraction given by

$$\mu = [1 - 80.6\, N_m/f^2]^{1/2}$$
$$\cong 1 - 40.3\, N_m/f^2 \qquad (1.3)$$

where μ is the refractive index and f is the transmitted frequency.

Now if it may be assumed that although N_m is anomalous on a global scale, the density height profile itself is not seriously distorted, then it is well known that

$$n_t \cong 4.133\, N_m H$$
$$\text{or} \qquad (1.4)$$
$$y \cong 4.133\, H$$

where H is the scale height and equality obtains in the last two relations if the profile is rigorously described by an alpha-Chapman distribution. Here H refers to the ionizable constituent and has the value

$$H = kT/Mg \qquad (1.5)$$

in which M, the mean molecular weight, may be taken to be that for atomic oxygen, T is the temperature of the essentially isothermal ionosphere, g is the acceleration of gravity near the F-2 peak and k is Boltzmann's constant. While it is known that both M and T vary with time, there is little reason to anticipate large sudden changes in either quantity or their ratio. Support for this has been offered by Ross[3] who found the summer daytime slab thickness remained quite constant even when N_m varied widely. In the equatorial ionosphere, Blumle[4] found that y varied in phase with T except for about a four hour period centered at sunrise. More recently, Bhonsle, et al,[5] described the mean diurnal variation of the mid-latitude y as having a maximum near dawn with somewhat irregular variations through the day. On the other hand when the latter workers calculated y based on individual observations, they found a rather smooth and gradual decrease from the immediate post dawn period, through the day and into the evening.

It must be recognized that the scale height is a much more complicated parameter than this discussion has indicated and it will be the subject of a later note. Nonetheless a constant scale height for periods measured in hours is not a completely unrealistic assumption for the slab approximation. If desired, H variations from the post dawn period until approximately midnight may be estimated more closely by calculating T as described in Apollo 317[6] and taking M as 16 atomic mass units in equation 1.6. After midnight, and especially in the dawn period, this approach breaks down but since n_t is reduced by about a factor of five or six from its midday value during this time (see Apollo 281, Figure 7)[7] the error in ignoring the sunrise "runaway temperature" in the F-2 layer is not serious at this level of approximation. Arbitrarily, the base of the slab may be taken to be at an altitude of about 250 km at night and about 150 km during the day (see Apollo 303, figure 4).[2] Its thickness and refractive index are given by equations 1.5 and 1.3, respectively.

The global F-2 critical frequency model put forward by Bazzard and Minnis[8] is suggested as a basis for predicting N_m. Variations are accounted for both through the seasons and the solar activity cycle. A description of this model is given in Section 8, but there is an important gap in that the diurnal variations must be extrapolated from noon conditions. This will be filled shortly in another note giving a detailed description of the geomagnetic anomaly which exerts an important influence over much of the earth and must be considered when treating diurnal variations on a global scale.

2. PEAK ELECTRON DENSITY VARIATIONS WITH SOLAR ACTIVITY

Ionospheric observatories normally report F-2 critical frequencies rather than N_m. For reference, it will be noted here that at the peak ionization level the ordinary ray critical reflection frequency f_m (commonly written f_o F2) is related to the maximum ionization density N_m, through the well known relation

$$N_m = 4\pi^2 e_o \; m f_m^{\;2}/e^2 \tag{2.1}$$

in which e_o is the free space permitivity, m the electron mass and e the electron charge. Numerically, in rmks units

$$f_m = 9.0 \sqrt{N_m} \tag{2.2}$$

(or $N = 12,400 \; f^2_m$ for N in electrons/cu. cm. and f_m in mc)

Vast f_m data taken over many years exists from which a strong correspondence with solar activity has been established. Figure 2.1 given by Wright[9] illustrates this through the equivalent N_m variations that are superposed on seasonal changes. Here "Sunspot number" is the "Wolf number" R for which data are available over more than a 200 year period and which remains the most widely used solar activity index. It is weighted more heavily by the number of spot groups than by the actual number of spots[10] being defined as proportional to the number of individual sunspots plus ten times the number of sunspot groups. The proportionality constant is not very precisely defined and depends on the observatory itself as well as the observation technique. Data are provided as averages on a daily, monthly and annual basis and as the "Zurich relative sunspot number". The latter is a running average over the preceding and following six month periods.

Sunspot periodicity, which plays such an important role in ionospheric physics, is illustrated for the latest solar cycle in Figure 2.2 and over a long time period in Figure 2.3. While average periods are

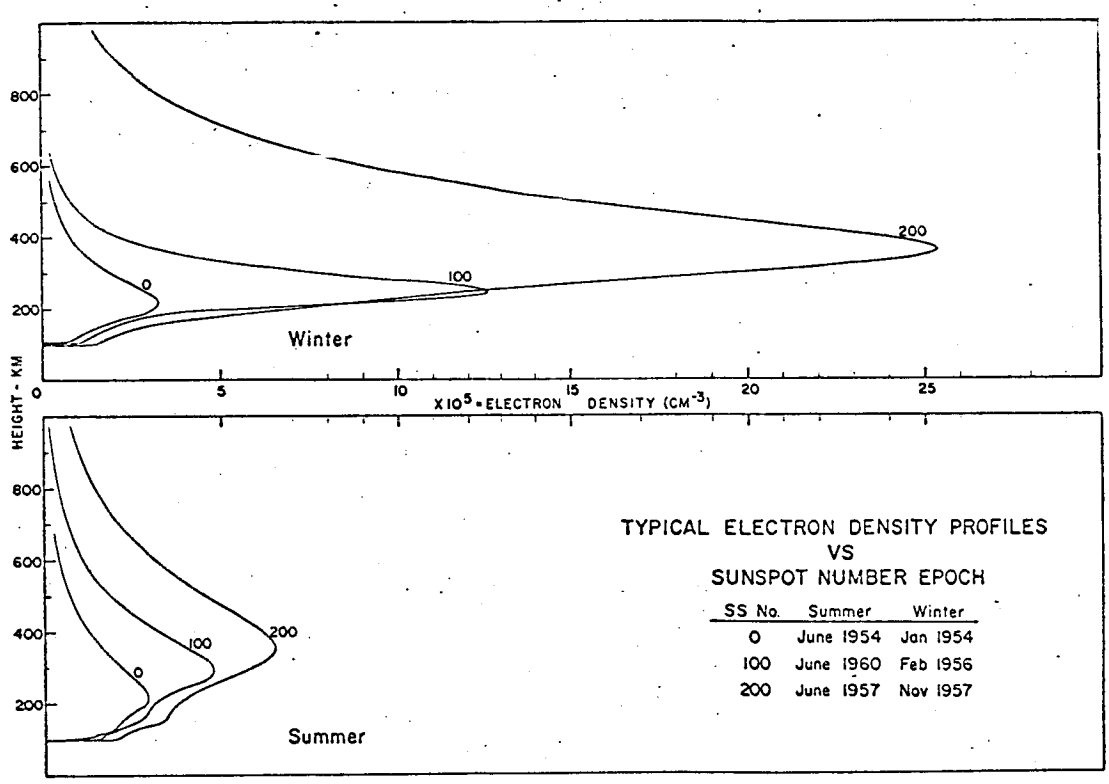

Figure 2.1. Dependence of the Noon Electron Density-Height Profiles on the Solar Cycle, After Wright (Ref 23)

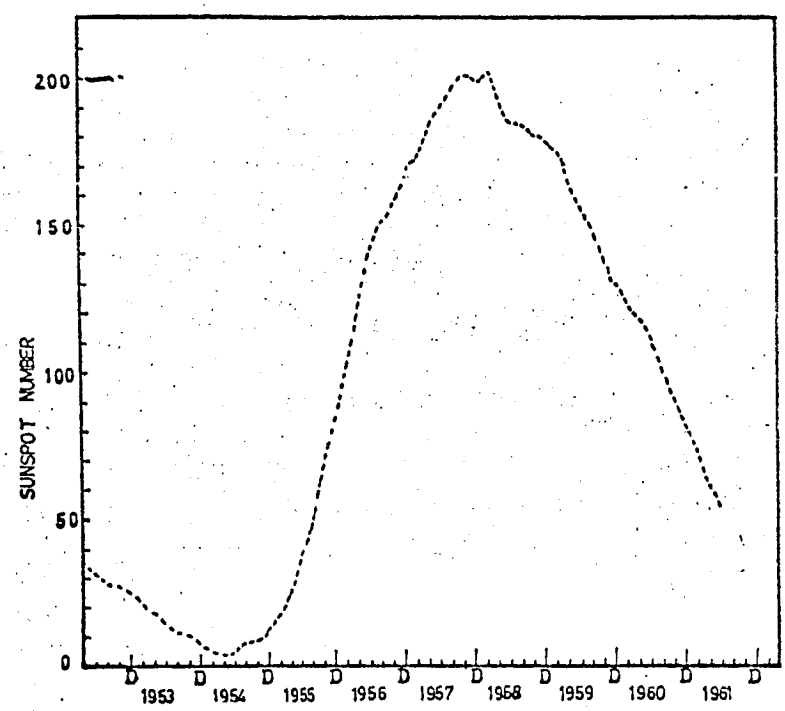

Figure 2.2. Sunspot Activity During the Period 1953-1961 After Singleton (Ref 11)

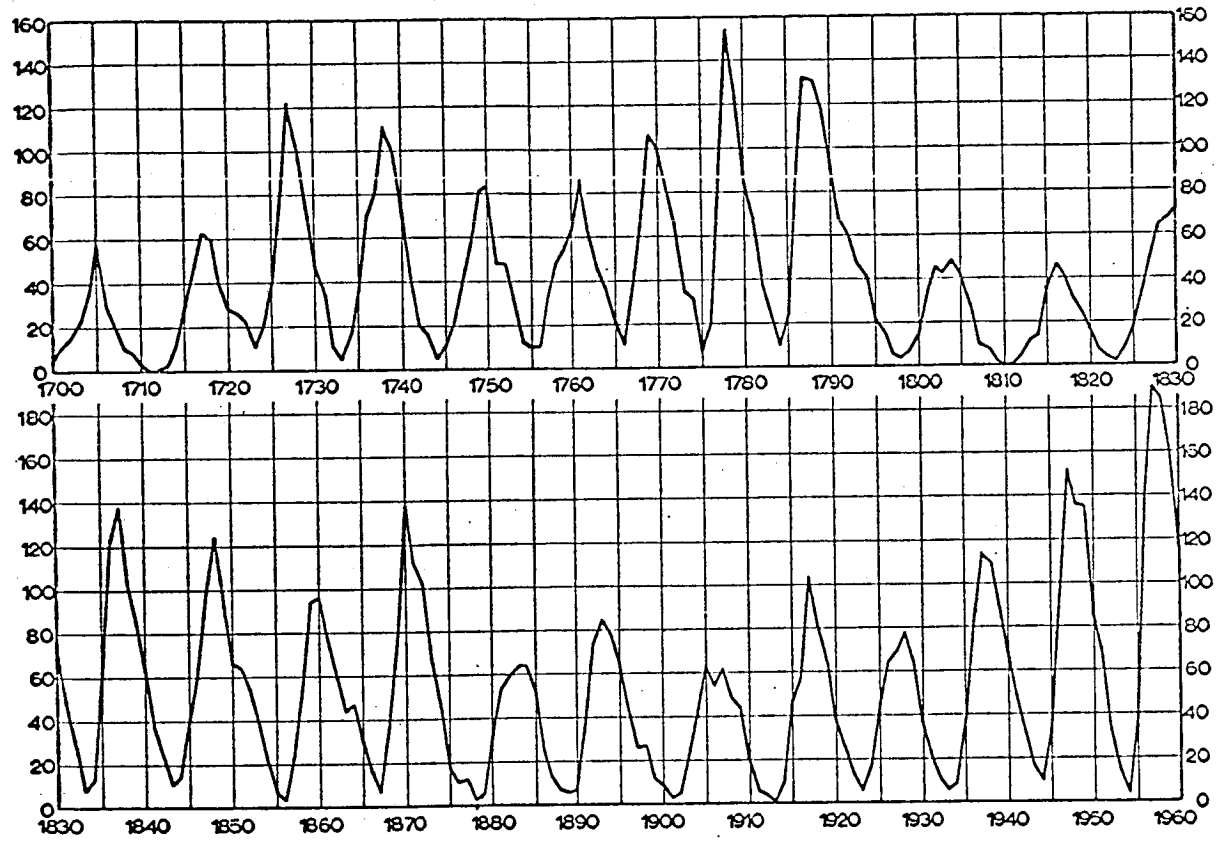

Figure 2.3. Sunspot Activity Over the Years 1700 to 1960
After Davies (Ref. 12)

about 11 years, it is to be noted there is great variation and that the intervals between minima may lie anywhere between about 8.5 and 14 years while those for the maxima are between 7.3 and 17 years[12]. The annual minimum R values fall between 0 and 10 while the maxima are between 50 and 190. In contrast to this rather limited range of annual averages, daily R values may exceed 355. Care must be taken when assigning model R values because authors are not always careful to state which average they are discussing.

Russian workers recognize three classes of f_m dependence on R[13]. The first, representing the monthly median, is linear until R approaches 200; the second is linear for moderate R values, say less than 100 to 140, but is flat for higher values in a condition known as "saturation"; and the third exhibits two linear regions beginning with a small positive slope for low R values, say less than 80, and terminating with a distinctly steeper positive slope. Vasil'yeva [14] has given coefficients for the linear relation holding when $0 < R < 100$ from which monthly median f_oF2 geographical variations may be calculated showing the diurnal and seasonal changes by the hour.

A relation that is also valid at higher R values but which gives less detail, has been suggested by Lal[15] who noted the data are all fairly well represented by

$$\sum \overline{f}_m = \sqrt{R + 100\, C_i} \qquad (2.3)$$

where $\sum \overline{f}_m$ is the monthly mean diurnal f_m average, R is the monthly relative sunspot number and C_i is the international geomagnetic character figure which is a rather crude solar activity measure being defined in terms of magnetic conditions by

C_i = 0 for quiet days

C_i = 1 for moderately disturbed days, and

C_i = 2 for disturbed magnetic days

Data fits exhibited by Lal to support his suggestion are shown as Figure 2.4.

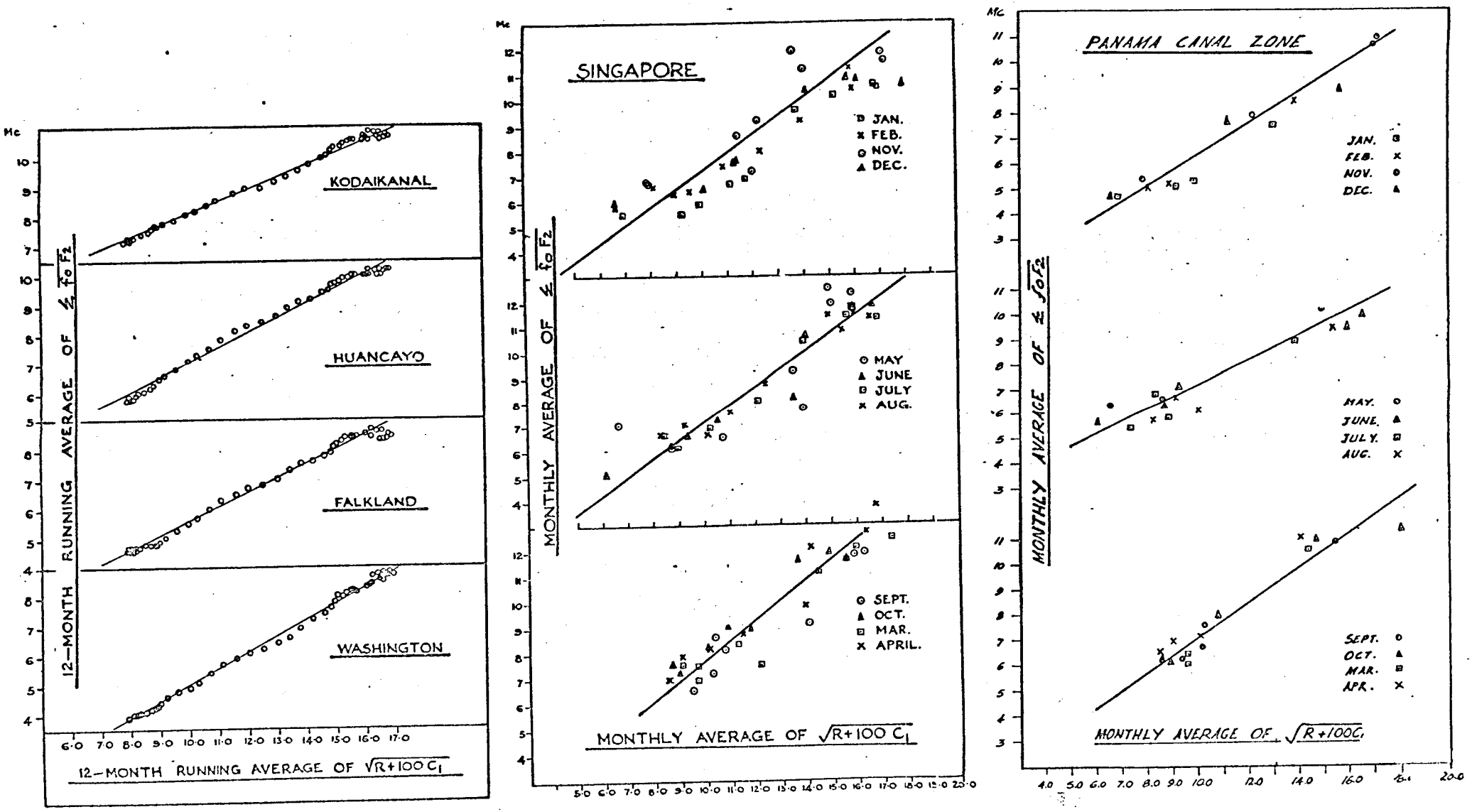

Figure 2.4 . Dependance of the Diurnal Average Monthly Mean F2 Critical Frequency on the Relative Sunspot Member and Geomagnetic Activity as Exhibited by Lal. (Ref. 15)

3. PEAK ELECTRON DENSITY SEASONAL ANOMALIES

Extrapolation of electron density profiles above the F-2 peak based on bottomside observations led Wright[9] to conclude that in reality the "seasonal anomaly" is a summer anomaly in the sense that the winter height profiles N(h) follow a Chapman law over a wide latitude range but that the daytime summer total electron content n_t is anomalously low. The amplitude of this N_m difference between winter noon and summer noon increases with solar activity and may be greater for other hours since the winter maximum is often observed in the evening hours rather than at noon[16]. However, at night, both N_m and n_t are in general greater in summer than in winter.

In winter the moderate latitude F-layer ionization decays much more slowly before sunrise than after sunset. A generally accepted explanation for this behavior has yet to be offered. In fact, not even the general principles governing maintenance of the night time ionosphere are agreed upon by all authors. One suggestion is that at night the ions diffuse upward to regions where recombination is low[17]. Another proposal appeals to a mechanism in which electrons with greater than thermal energy are the source of ionization production[18], while a recent and widely accepted atmospheric model invokes an unspecified "second source" of energy[19] with a maximum at 9 or 10 LT.

4. PEAK ELECTRON DENSITY MAXIMUM GEOGRAPHICAL ANOMALIES

Both intuition and simple theory suggest that maximum ionization production should occur in regions where the sun is directly overhead. A simple and well known analysis, which will not be reproduced here, shows that if losses are proportional to N^2, as in a recombination process, then N_m should vary as $\sqrt{\cos \chi}$ where χ is the solar zenith angle and the region is known as "alpha-Chapman". When losses are proportional to N, as is the case in an attachment process, N_m should vary as $\cos \chi$ and the region is called "beta-Chapman." These laws are so seriously violated in the F-region that the geographical N_m dependence is highly anomalous.

Magnetic dip, rather than solar zenith angle, geographic or geomagnetic latitude, is the most convenient coordinate for a general discussion of how the peak ionization density varies with position. Ship based ionograph critical frequency measurements reported by Yamada and Ogata[20] show f_m peaked at about 30° dip angle North and South at all seasons of 1962 but that the ionospheric equator minimum was at $0\text{-}5^\circ$ dip angle south. These results are in general agreement with those published earlier by Eyfrig[21] who found, as shown in Figure 4.1 that in 1953 the dip and ionospheric equators did not match exactly in the Western hemisphere. In the Eastern hemisphere the ionospheric equator was very near the dip equator at that time with ionization peaking symmetrically as a function of the dip angle North and South.

Recent Alouette topside sounder data[22] for 1962 shows the ionospheric and dip equators then matched quite well and that the equatorial geomagnetic anomaly, taking the form of N maxima both sides of the magnetic equator and separated by a trough, was most pronounced near the 20° dip angle. The latter anomaly, which will be discussed further in another note, reaches a maximum near 1500 LST and essentially disappears between 2000 and 2200 LST during years of the relatively quiet sun. At the peak of the solar cycle, the anomaly may persist through the night until about 0300 LST.

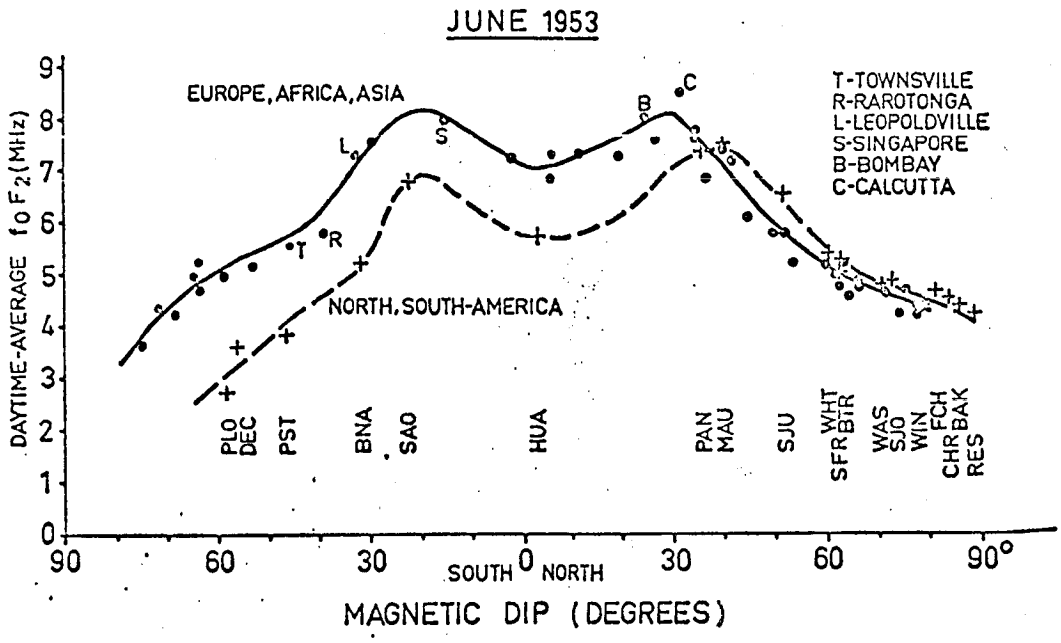

Figure 4.1. Daytime Average (06 Hours, 18 Hours, Mean) F2 Critical Frequency Latitudinal Variation During the Northern Solstice of a Low-Sunspot Year, 1953. (Ref. 21)

Wright[23] found the diurnal maximum N_m was reached as late as 1800 LT at high latitudes in summer but that a more representative time was 1300 LT, or later, as shown in the contours of Figure 4.2. Since the center of the atmospheric bulge produced by diurnal heating lags about two hours behind the sun[24], a reasonable assumption is that N_m attains its daily maximum at about 1400 LT except at high latitudes. Purely for convenience, it may be assumed that the post sunrise climb of N_m starts at ground level sunrise although it is recognized that N_m actually bottoms out as early as 0400. This is not unreasonable, because if the layer is at high altitude, especially in summer, sunrise and the onset of ionization production occur at an early hour but with a time lag before solar energy absorption becomes important. In this connection it is important to note that although the morning N_m increase is spectacular once it starts, it is preceded by an hour or two period during which conditions are almost static as illustrated in Figure 4.3.

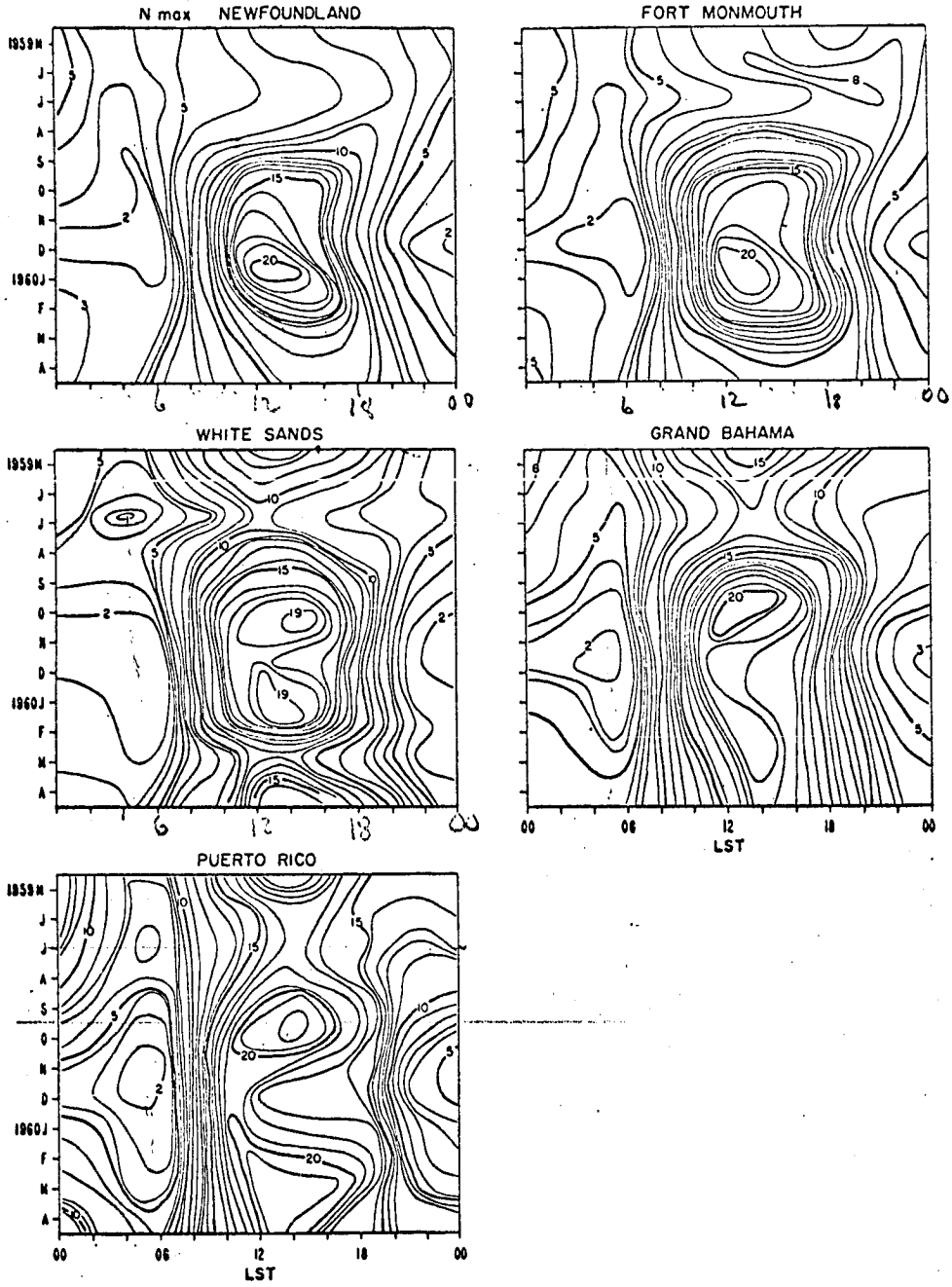

Figure 4.2. Dirunal and Seasonal N_m Variations at Mid Latitude Stations With Contours Given in(Electrons/cm^3) X 10^{-5} (Ref. 23)

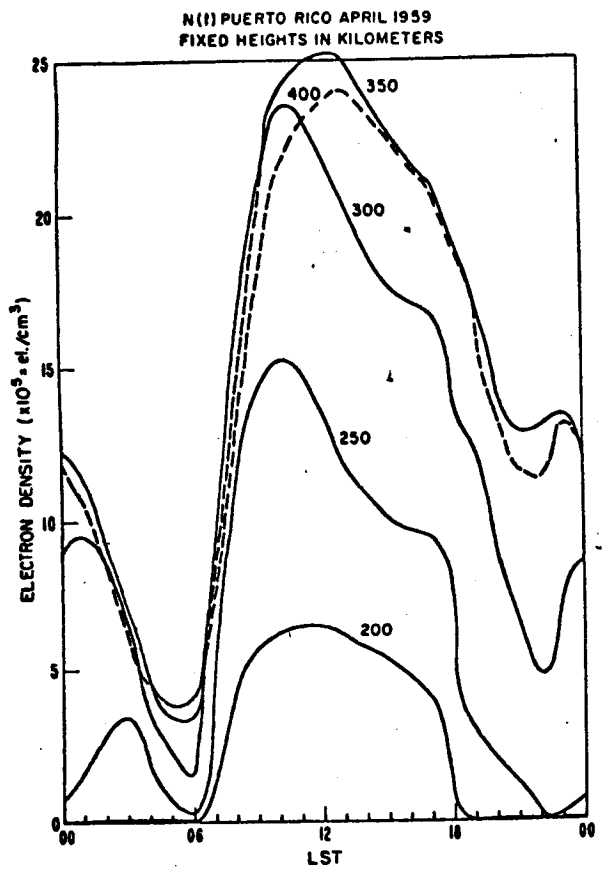

Figure 4.3. Diurnal Variation of Electron Density at Fixed Heights With Contours Given in Kilometers. (Ref. 23)

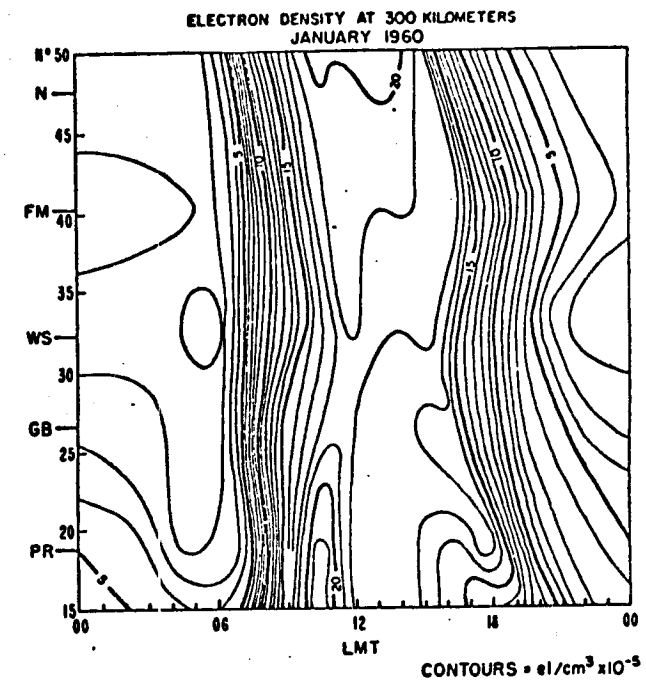

Figure 4.4. Latitude Versus Local-Time Isoionic Map at 300 km With Contours Given in Electrons Per $cm^3 \times 10^{-5}$ (Ref. 23)

5. HIGH LATITUDE ANOMALIES

Marked diurnal electron density variations are not observed when the sun remains above the horizon all day[25]. On the other hand, when the sun remains below the horizon there are pronounced diurnal variations. At such times the N_m maximum lags about 2-3 hours behind local noon. When the f_oF2 isolines corresponding to these electron density variations are plotted geographically, the most complicated patterns occur during the equinoxes and the simplest, essentially concentric ellipses, occur in summer[26].

An asymmetry exists between the two hemispheres in that peak electron densities observed during the IGY were higher over the northern than the southern polar cap for all seasons. Thus, the estimate of conditions in the high latitude southern hemisphere, where there are few observatories, based on behavior of the arctic ionosphere, must be accepted with caution.

An important high latitude anomaly is the appearance of high electron densities in the darkened hemisphere. In auroral regions the maximum of the anomalous N_m occurs during the early morning hours and, according to Yudovich[27], moves back through midnight to early evening hours with increasing geomagnetic latitude. Greatest intensity of the anomaly occurs at geomagnetic latitudes 82° - 87° [28]. Table 5.1 gives the frequency at which the anomalous f_oF2 exceeds 5 Mc/s (3.1×10^{11} el/cu. m) and 7 Mc/s (6.1×10^{11} el/cu. m). In the auroral zone electron densities exceeding 6×10^{11} el/cu. m are observed in the winter early morning hours 20% of the time and for 60% of the time these intense ionozation levels appear in the polar regions during the afternoon and evening hours. The isolines giving frequency of appearance of this anomalous ionization take the form of concentric ovals centered on the pole of the eccentric dipole. Considering the great day to day ionospheric variability, this indicates an anomalously high N_m is the best assumption for use in a refractive index model.

Table 5.1. Frequency of Appearance of Anomalous f_oF2 in the Winter High Latitudes, After Yudovich (English Ed. 1965)

Station	Geomagnetic Coordinates		Total No. of Values	Mean for Winter, %		Average Winter Monthly Mean, %		
	Latitude	Longitude		> 5 Mc	> 7 Mc	> 5 Mc	> 7 Mc	
Thule	88.1 N	1.1	186	91	63	92	63	November 1957 - February 1958
Eureka	86.5	236.9	318	92	66	92	66	
Alert	85.9	165.7	294	92	65	92	65	
Fletcher	82.5	231	279	80	56	82	58	
Tikhaya Bak	71.5	155.5	203	85	40	84	39	
Narsarssuaq	71.2	37.6	168	81	22	79	20	
Reykjavik	70.1	70.2	54	66	18	63	17	
Tromso	67.2	117.3	167	78	24	81	27	
Kiruna	65.3	115.5	356	85	33	85	35	
Murmansk	64.1	126.5	84	83	34	85	36	
Dixon	63.0	161.5	139	82	24	84	26	
Lulea	63.0	114.7	235	75	23	77	21	
Luxele	62.7	110.8	315	77	22	78	23	
Vostok	89.1 S	71.9	168	73	44	80	49	August 1958
Scott	79.0	294.4	291	94	73	94	72	
South Pole	78.5	0	247	78	28	78	29	
Little America	74.0	312.0	189	86	49	88	53	
Byrd	70.6	336.0	319	80	31	80	31	
Ellsworth	66.9	14.2	239	38	3	38	3	
Halley Bay	65.8	24.3	273	28	2	24	1	

Another striking high latitude anomaly is that although the diurnal N_m may be said to lag 2-3 hours behind the sun, the ionosphere is actually under universal, rather than local time control near the magnetic poles. Ionization maxima occur above all stations there at about 0600 UT in the antarctic and at about 1800 UT in the arctic.[29]. The times of these maxima correspond to local noon at the geomagnetic poles and are most pronounced in the antarctic. This anomaly is stronger in winter than in summer.

One of the most familiar high latitude anomalies is the fact the electron densities do not decrease with latitude nearly as rapidly during the day as simple theory indicates. At night N_m actually increases with latitudes above 60° geographic. A number of theories have been advanced to account for these phenomena. One of the most recent, due to Gintzburg[18] ascribes this excess ionization to the effects of dumping "soft" electrons with energies of about 1 kev which move along magnetic field lines with velocities high enough to penetrate approximately the 120 km level.

6. ELECTRON DENSITY: LUNAR TIDAL EFFECTS

Evidence of lunar ionospheric tidal phenomena was first given by Martyn in 1947. Rastogi[30] later studied F2 critical frequency variations for 18 stations located over a geographical range $\pm 40^{\circ}$ latitude and found lunar variation depends on geomagnetic latitude. Relatively strong F2 lunar tides have been detected by Rastogi and Alurkar[31] over Ahmedabad during the day with a critical frequency amplitude as great as 0.34 mc/s corresponding to about 10^8 electrons per cu. meter but with a 24 hour average of only 0.08 mc/s or less than 10^7 electrons per cu. meter. Equatorial type variation is greatest at about 04 lunar hours while the maximum does not occur until about 10 lunar hours at higher magnetic latitudes with a phase reversal taking place at about $\pm 11^{\circ}$ magnetic latitude. There may be a shift as much as 150° in the semi-diurnal variation between the winter and summer solstices according to Rangaswamy[32] who suggests these seasonal changes may be under the influence of solar activity. Latitude dependence is also evident from sharp maxima at the magnetic equator and $\pm 20^{\circ}$ magnetic.

Table 1, which was given by Kotadia[33], illustrates the amplitude and phase of the semi-diurnal midday f_oF2 mean. Relative changes from 3 day mean critical frequencies amount to at most about $\pm 4\%$. Pre-sunrise maxima of 9.7% during equinoxes; 7.7% during the summer and 6.9% during the winter at the tropical station Nhatrang have been reported by Rastogi[34] but it should be remembered that these changes refer to times when f_oF2 is at its diurnal minimum. For comparison at the mid latitude station Lindau, the pre-sunrise maxima were 2.8% in winter and 1.2% at the equinoxes.

According to Thomas,[35] semi-diurnal tides are significant where the dip angle is less than 20° and then only between 1900 and 2300 LST. Rastogi[34] estimated the lunar tide maximum to occur slightly before noon at equatorial stations and at 1400-1500 LT at higher latitude tropical stations.

The significance of the word "maximum" here may be inferred from the fact that a virtual height tidal drop of 20 km is considered a large effect. More typical are the virtual F2 height variations due to lunar tidal effects investigated by Zagulyayeva[36] who found 2 km to be approximately the maximum amplitude.

Further evidence for the weakness of lunar tidal effects has been offered by Burkhard[37] who deduced that the M2 lunar tide is significant only in winter months over Puerto Rico at which time the electron density follows

$$N(h) = N_o(h) + N_1(h) \sin(\omega t + \alpha) \qquad (6.1)$$

where the height dependence is strong for the phase but weak for N_o/N_1 and where $0.02 < N_1/N_o < 0.06$. These results are more or less in agreement with theoretical conclusions reached by Gliddon and Kendall[38] to the effect that F2 tidal electrodynamic drift is about 0.5 mc/sec and causes a f_oF2 variation of about 3%.

From this discussion, it appears it would not be an insuperable task to incorporated model parameters accounting for lunar tidal variations, but the phenomena will be ignored since the effects will probably be obscured by other uncertainties.

Table 6-1

Amplitude Δf and Phase t_2 of Lunar Variation in f_oF2 Mean from 1000-1400 Hours for 1954

(Min. Solar Activity)

	Magnetic dip N	Δf (mc)	t_2 (lunar hours) (first max)
Delhi	42.4	0.9	9.7
Ahmedabad	34.0	0.35	10.2
Bombay	24.8	0.24	10.0
Madras	10.5	0.14	3.8
Tiruchy	4.8	0.13	2.8
Kodaikanal	3.5	0.21	3.9

7. DAY-TO-DAY VARIABILITY

Peak electron density exhibits considerable day-to-day variability even during periods when the geomagnetic field is undisturbed. In general, the relative variability is greater by night than by day, as would be expected, since a small absolute change becomes relatively important during the night when densities are low. There is also a tendency for an increase with latitude. The latter effect is just what would be anticipated from the effects of irregular ionization increases ascribed to the increased importance of charged particle dumping as the auroral zone is approached. Diurnal and latitudinal dependence of the relative variability, expressed as the ratio of the N_m standard deviation to N_m in %, has been given by Wright[23] and reproduced here as Figure 7.1. Any possible seasonal effects have been wiped out there by taking averages over the period May 1959 - April 1960. Note that at high dip angles, say St. Johns at 72°N dip as an example, even the daytime N variability becomes serious.

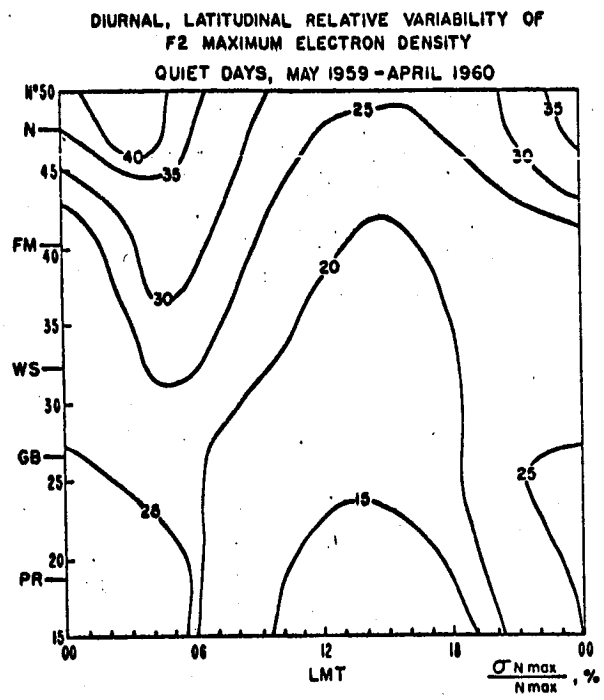

Figure 7.1. Relative Diurnal N_m Percentage Variability Contours as a Function of Latitude for Quiet Mean Values Averaged Over the Period May 1959-April 1960. (Ref. 23)

8. GEOGRAPHICAL REPRESENTATION OF THE PEAK ELECTRON DENSITY SHOWING DEPENDENCE ON SOLAR ACTIVITY AND SEASONS

A somewhat more complicated but at the same time more useful N_m relation for the present purposes than those discussed in Section 2 has been given by Bazzard and Minnis[39]. With it they are able to describe the seasonal variations on a global scale with account being taken of the changes due to the solar cycle. While these investigators did not include the diurnal components, there was less data smoothing than is typical in simplified models. They considered the average noon critical frequency, f_{om}, rather than monthly average critical frequency. The resulting representation exploits the well known facts that at all stations f_{om} exhibits variations containing a cyclic component with a one year period and that this component varies both with geographical location and solar activity. At many stations a strong second harmonic is also present. Taken together these variations are often referred to as seasonal components, but here are treated separately as the annual and semi-annual components. A new solar activity indix I_{F2}[8] was invented by the authors to account for the noon f_{om} geographical distribution in statistical relations taking the form

$$f_{om} = p(\theta) + q(\theta) I_{F2} \tag{8.1}$$

in which $p(\theta)$ and $q(\theta)$ are oscillating functions with a one year period. As an indication of magnitudes, the index I_{F2} varies from zero at solar activity minimum to about 150 at solar activity maximum. When θ is taken to be zero in mid-January these functions may be represented by

$$p(\theta) = \alpha_1 \cos\theta + \beta_1 \cos 2\theta + \gamma_1 \tag{8.2}$$

$$f(\theta) = \alpha_2 \cos\theta + \beta_2 \cos 2\theta + \gamma_2 \tag{8.3}$$

in which the α, β, γ are constants for a given location. First and second harmonic coefficients were calculated for 61 stations and

Table 8.1 shows the results for eleven representative stations. World-wide contour maps of the α, β, γ coefficients of Equations 8.2 and 8.3 are shown in Figure 8.1.

Figure 8.2 illustrates the annual and semi-annual noon f_{om} variations at three representative stations for the solar cycle minimum and maximum. The seasonal variations are shown in Figure 8.3 with greater detail for one of those stations, Panama (dip $\cong$ 39.2°N), during the IGY (high activity). These diurnal patterns depict ionospheric characteristics in the transition region near the 40° dip angle which roughly separates the geomagnetic anomaly from the mid latitudes.

Table 8.1 Representative Annual f_{om} Variation Coefficients (Bazzard and Minnis 1961)

	α_1	β_1	γ_1	α_2x100	β_2x100	γ_2x100	Dip Angle
Baguio	0.40	-0.85	8.65	0.8	0.4	3.2	19.5°N
Brisbane	0.75	-0.40	6.35	-0.1	-0.4	3.7	57.5°S
Capetown	0.75	-1.00	6.50	-0.3	-0.2	3.7	64°S
Huancayo	0.55	-0.65	7.00	0.9	0.2	3.5	0.5°N
Johannesburg	0.80	-0.70	6.75	-0.1	-0.2	3.6	62.5°S
Puerto Rico	0.05	-0.85	7.25	0.1	-0.1	3.7	51.5°N
San Francisco	0.70	0.05	5.90	1.3	-0.7	3.8	62°N
Slough	0.45	0	5.00	1.3	-0.4	3.8	68°N
Washington	0.70	-0.15	5.55	1.8	-0.4	3.5	72°N
Watheroo	0.45	-0.95	5.95	-0.4	-0.5	3.7	64°S
White Sands	1.15	-0.23	6.15	0.4	-0.3	3.8	60°N
Winnipeg	0.55	0.18	4.90	1.7	-0.3	3.2	78°N

Except for a narrow high northern latitude range the second harmonic phase is the same all over the earth.

Naismith and Smith[40] plotted I_{F2} against sunspot numbers R from data taken over the past 20 years and found a linear relation between R and I_{F2} which at times reached equality, as in 1947. Later Barclay[41] analyzed the data for more than two solar cycles and found a non linear

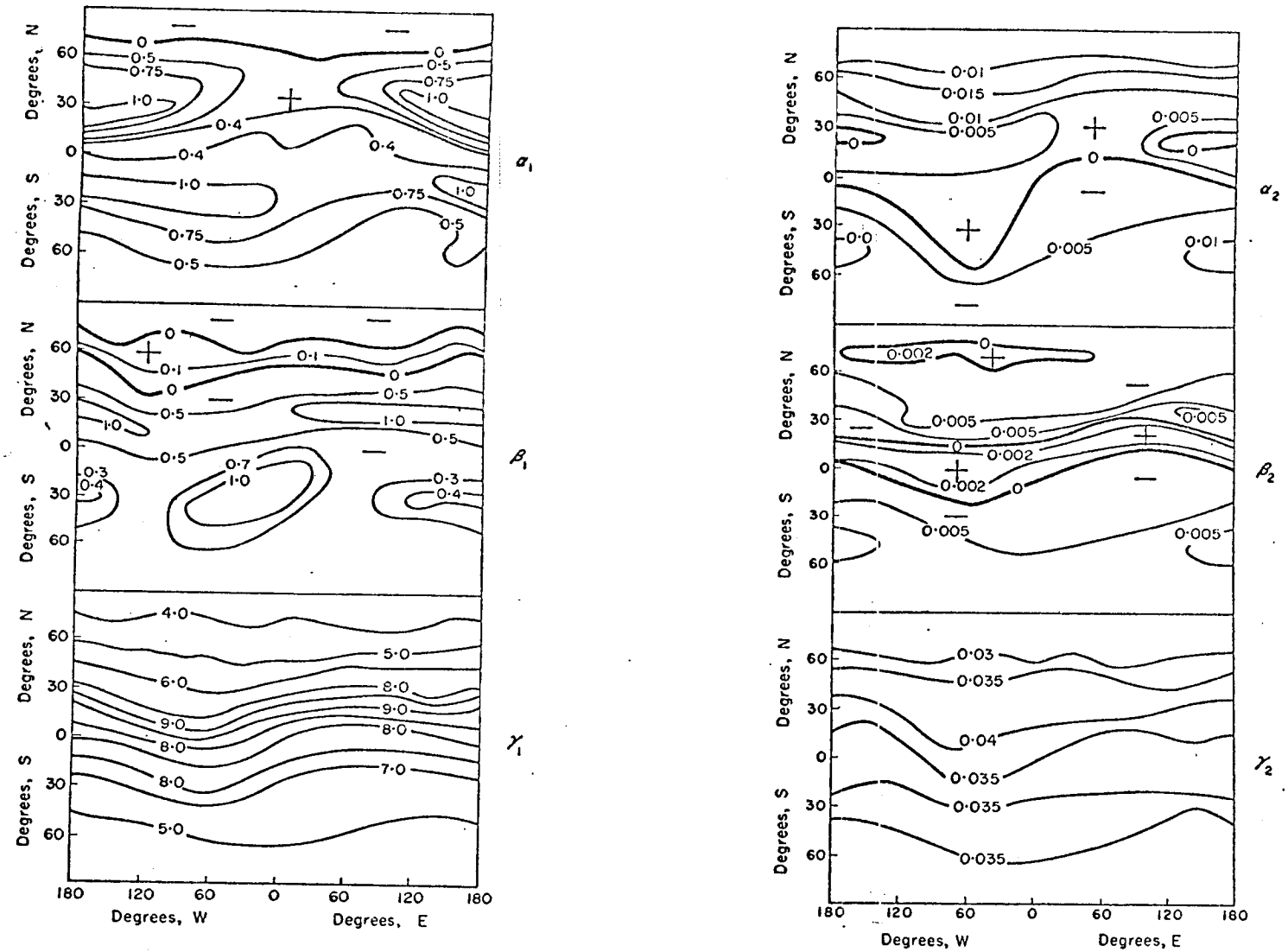

Figure 8.1. Contour Maps of the Coefficients Appearing in Equations 8.2 and 8.3

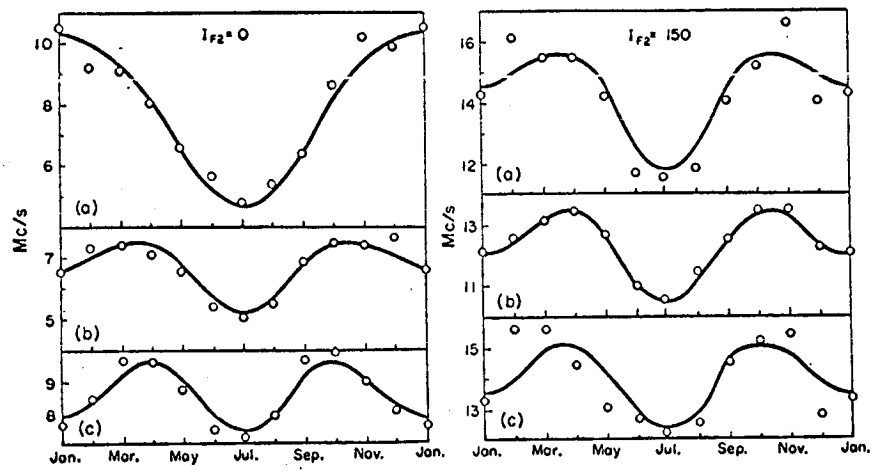

Figure 8.2. The Annual f_m Noon Variation at (a) Rarotonga (b) Johannesburg and (c) Panama C. Z. (o) Experimental Values; (____) Fitted Curves. (Ref. 39)

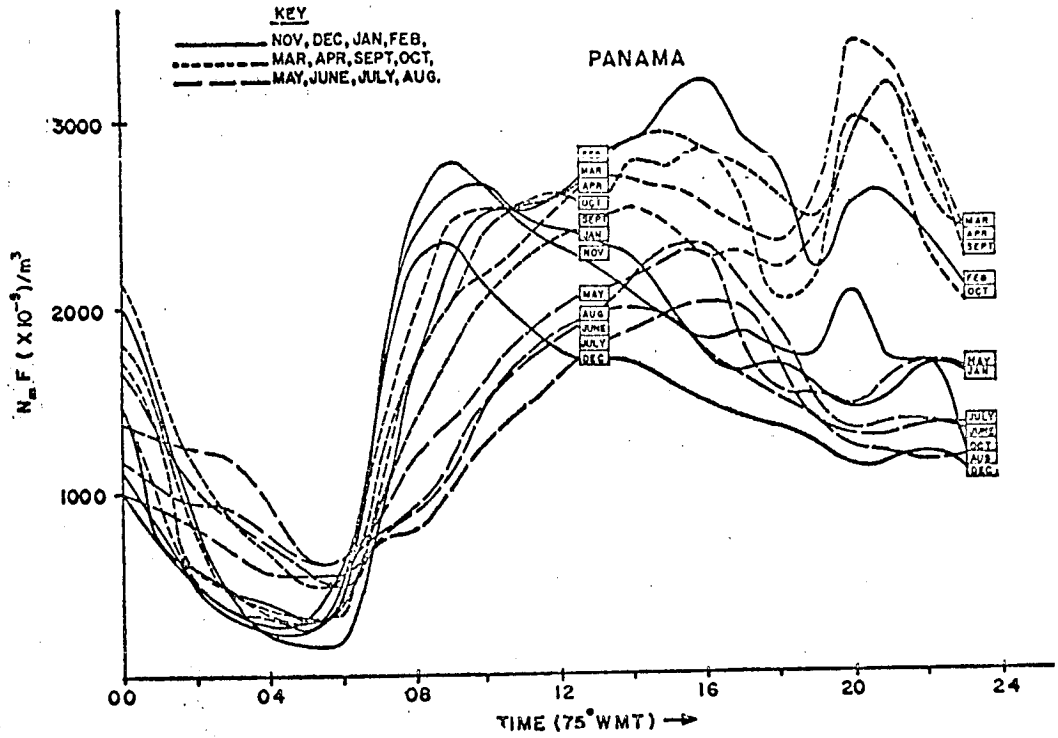

Figure 8.3. Average N_m Diurnal Variation at Panama for the IGY Months September 1957 through August 1958 After Somayajulu.

relation between the R and I_{F2} indices which he wrote

$$R = 11.44 + 0.478\, I_{F2} + 0.00278\, (I_{F2})^2 \qquad (8.4)$$

Minnis is quoted by Barclay to have found that if $I_{F2} \leq 120$, then a valid relation is

$$R = 5 + 0.88\, I_{F2} \qquad (8.5)$$

Thus, the ionospheric index may be obtained quite simply from published sunspot numbers. The noon f_{om} for a specified station then may be calculated from the Table of f_{om} variation coefficients.

Regardless of the model profile finally chosen, it is suggested that N_m predictions be made by first calculating the noon peak electron density N_{om}, based on the noon f_{om} predicted by Bazzard and Minnis. In spite of the fact that their technique appears more complex than that proposed by others, by Lal for example, it has the advantage that the needed coefficients over wide geographical areas are available. There are, of course, the further advantages of a more detailed representation and one which is obtained with an index that is free of seasonal effects.

Considering the great ionospheric variability, briefly discussed in Section 7, it might be argued that this detail is not warranted. Nonetheless, since trends are described at a time near the diurnal maximum, the model is of greater value than those proposed by others in which the daily maximum N_m estimates may be distorted by weighting given to N_m values at other times of day.

9. MIDDAY E-LAYER VARIATIONS

Although it appears the existance of an E-layer as a distinct entity maybe ignored in this application, Seddon's model [1] involves a daytime parameter $N_m(E)$, the E-layer electron density maximum, which was assumed to be located at the 100 km level. In effect he too ignores the E-layer because his model profile joins $N_m(E)$ smoothly and neglects electron densities at lower levels. No studies seem to have been reported correlating the geographical dependence of this parameter, or its equivalent f_E, the E-layer critical penetration frequency. A possible reason for this is that f_E is not precisely defined because E region virtual height curves produced by sounders typically show several breaks, one of which is arbitrarily selected and associated with f_E. Further, it is now known that the profile in this region is continuous when the data are reduced to N(h) curves.

For many years it has been accepted that f_E depends both on the sunspot number and solar zenith angle. A quantitative statement of this dependence at midday in southeast England has recently been established by Appleton[42] in the form

$$f_{En}^{\ 2} = 10.2\ (1 + 0.0039R)\ \sqrt{\cos\ \chi_n} \qquad (9.1)$$

where f_{En} is the critical E-layer penetration frequency at noon in mc/s, R is the Zurich sunspot number and χ_n is the noon solar zenith angle.

A similar relation, but one that is independent of the solar angle was shown by Noonkester[43] to hold at Washington, D. C. It takes the form

$$f_E = 3.12 + 0.0051R \qquad (9.2)$$

for f_{En} in mc/s. Noonkester found that for R values between the maximum and minimum there was a strong 27 day periodicity which became quite weak when R was either a maximum or a minimum. No periodicities were found in the E-layer virtual height h_E' but in contrast to Appleton's work it was found that the solar zenith angle dependence appeared in the latter parameter through the following relation

$$h_E' = 101 + 11.5 \ln \sec \overline{\chi}_n \qquad (9.3)$$

for h_E' in kilometers and where χ_n is the monthly average noon solar zenith angle. Since the electron content below E is relatively small, even at midday, real and virtual heights should not differ greatly so it is interesting that this relation has the same form as the real layer height predicted by Chapman theory. While this in no way proves the real height equation is valid, when taken with Appleton's findings that the E layer electron density follows the $\sqrt{\cos \chi}$ law, it does suggest the layer is Chapman-like, at least for our purposes. Thus, in spite of the serious violation of the isothermal assumption in the E layer, Chapman theory is a reasonable basis for making estimates even though it is not rigorously applicable.

Then for S band refractive index models it is not unreasonable to assume the E layer is without anomalies during the day (at night it may be ignored) and write

$$N_{mE} = 1.25 \times 10^5 (1 + 0.004R) \sqrt{\cos \chi} \qquad (9.4)$$

where now χ is taken to be the existing solar zenith angle rather than its noon value or its monthly noon average. The height at which E_m is located will be approximated as

$$h_{mE} = h_o + H \ln \sec \chi \qquad (9.5)$$

in which H is the E layer scale height. Scale heights will be discussed in a later note but for the present purposes H may be taken to be that corresponding to conditions in the E-layer. For example, at 100 km $T = 212^o$, $g = 950$ cm/sec^2 [44] and assuming as usually done, that the ionizable constituent is atomic oxygen, then H is 11.6 km which when combined with equation 6.3, gives added confidence that the layer may be treated with Chapman theory. Considering this agreement, $h_o = 100$ km seems to be a realistic, if arbitrary choice.

LIST OF REFERENCES

1. J. C. Seddon, "A Model of the Quiet Ionosphere", NASA TN D-1670, February 1963

2. H. R. Wright, "The Quiet Ionosphere as It Relates to Precision Tracking at S Band", Apollo Note 303, January 25, 1965

3. W. J. Ross, "The Determination of Ionospheric Electron Content from Satellite Doppler Measurements: 1. Method of Analysis, 2. Experimental Results", Journal of Geophysical Research, 65, No. 9, September 1960, p. 2601

4. L. J. Blumle, "Satellite Observations of the Equatorial Ionosphere", Journal of Geophysical Research, 67, 1962, pp. 4601-05 (1962), "Satellite Observation of the Equatorial Ionosphere", NASA Tech. Note D-1756, June 1963

5. R. V. Bhonsle, Aldo V. Da Rosa and O. K. Garriott, "Measurements of the Total Electron Content and the Equivalent Slab Thickness of the Mid-latitude Ionosphere", Journal of Research, National Bureau of Standards, 69D, No. 7, July 1965, pp. 929-937

6. H. R. Wright, "A Simple Time Dependent World-Wide Ionospheric Refractive Index Model", Apollo 317, April 6, 1965

7. H. R. Wright, "Correction of Range Errors Induced by Ionospheric Disturbances", Apollo 281, November 10, 1964

8. C. M. Minnis and G. H. Bazzard, Journal of Atmospheric and Terrestrial Physics, 18, 1960, p. 181

9. J. W. Wright, "Dependence of the Ionospheric F Region on the Solar Cycle", Nature 194, May 5, 1962, p. 461

10. G. Godoli and C. W. Allen, "The Indices of Solar Activity", Planetary and Space Science, 12, No. 5, pp. 349-354

11. D. G. Singleton, "The Spread F Equator", Journal of Atmospheric and Terrestrial Physics, Volume 25, No. 3, March 1963, pp. 121-149

12. K. Davies, " Ionospheric Radio Propagation", National Bureau of Standards 80, April 1, 1965

13. T. N. Vasil'yeva and T. S. Kerblay, "Various Types of Dependencies of f_oF2 Solar Activity", Geomagnetism and Aeronomy, Volume IV, No. 5, 1964, English Edition, April 1965, pp. 669-671

14. T. N. Vasil'yeva, "Parameters of the Linear Dependence of f_oF2 and M3000 F2 on Solar Activity", Geomagnetism and Aeronomy IV, No. 4, 1964, English Edition, February 1965

15. Chaman Lal, "Solar Corpuscular Activity and Ionization Density in the F-2 Layer of the Ionosphere", Proceedings of the IEEE, Vol. 51, No. 11, November 1963, P. 1471

16. G. S. Ivanov-Kholodny, "On the Interpretation of the Seasonal Variations of Electron Density in the F2 Region of the Ionosphere", Space Research IV, 1963 Warsaw Proceedings, John Wiley and Sons, Inc., 1964, pp 525-533

17. W. B. Hanson and T. N. L. Patterson, "The Maintenance of the Night-Time F-Layer", Planetary Space Science, Volume 12, No. 10, October 1964, pp 979-997

18. M. A. Gintzburg, "Interpretation of Pioneer I Magnetic Field Measurements", Phys. Rev. Letters 14, No. 16, April 19, 1965, pp 625-626

19. I. Harris and W. Priester, "Of the Diurnal Variation of the Upper Atmosphere", Journal of Atmospheric Science, American Meteorological Society, Volume 22, No. 1, January 1965, pp 3-10

20. K. Yamada and T. Ogata, "Geomagnetic Dependence of the F2 Layer by Observations on Board Ship", J. Radio Res. Lab., Japan, Volume 11, No. 55, May 1964, pp 137-146

21. R. Eyfrig, "The Geographical Distribution of Ionization at the Equator in the F2 Layer", Journal of Geophysical Research, Volume 67, 1962, pp 1679-1682

22. J. W. King, P. A. Smith, D. Eccles, G. F. Fooks and H. Helm, "Preliminary Investigation of the Structure of the Upper Ionosphere as Observed by the Topside Sounder Satellite, Alouette", Journal of Geophysical Research, Volume 68, 1963, pp 464-487

23. J. W. Wright, "Diurnal and Seasonal Changes in Structure of the Mid-Latitude Quiet Ionosphere", National Bureau of Standards, Journal of Research, Volume 66D, May-June 1962, pp 297-312

24. L. G. Jacchia, "Variations in the Earth's Upper Atmosphere as Revealed by Satellite Drag", Rev. Mod. Physics, Volume 35, No. 1, October 1964, p 973

25. J. A. Ratcliffe, "Advances in Ionospheric Physics 1960-1963", Progress in Radio Science 1960-1963, Volume III, Elsevier Publication Company, New York, 1965, p 1013

26. N. V. Mednikova, "The Main Results in the IGY Program of Ionospheric Vertical Soundings in the USSR", JATP 27, No. 1, January 1965, pp 31-45

27. L. A. Yudovich, "Temporal Patterns in the Occurence of Anomalous Ionization in the F-2 Layer at High Latitudes", Geomagnetism and Aeronomy, Volume 3, No. 6, 1963, (English Translation August 1964) pp 843-845

28. L. A. Yudovich, "Spatial Distribution of Anomalous Ionization in the F2 Layer at High Latitudes", Geomagnetism and Aeronomy, IV, No. 3, English Edition, January 1965, pp 411-415

29. R. A. Duncan and W. Priester, Journal of Atmospheric Science, Vol. 19, 1962, p 286

30. R. G. Rastogi, "The Morphology of Lunar Semi-Diurnal Variation in f_oF2 Near Solar Noon", Journal of Atmospheric and Terrestrial Physics, Volume 22, No. 4, December 1961, pp 290-297

31. R. G. Rastogi and S. K. Alurkar, "Lunar Tides in the F-2-Layer of the Ionosphere Over Ahmedabad", Journal of Atmospheric and Terrestrial Physics, Volume 26, No. 5, June 1964, pp 641-658

32. S. Rangaswamy, "Lunar Control of Noon Critical Frequencies of the F-2 Region", Journal of Atmospheric and Terrestrial Physics, 25, No. 9, September 1963, pp 545-549

33. K. M. Kotadia, "Lunar Tidal Variation of Mid-day Critical Frequencies of the F-2 Layer of the Ionosphere in Low Latitudes", Journal of Atmospheric and Terrestrial Physics, Volume 24, July 1962, pp 659-661

34. R. G. Rastogi, "Large Lunar Tidal Effects in f_oF2 in Pre-sunrise Hours," Journal of Atmospheric and Terrestrial Physics 25, No. 9, September 1963, pp 515-518

35. J. A. Thomas, "Lunar Semi-Diurnal Tides in h'F and Their Influence on Transequatorial Radio Propagation", National Bureau of Standards, Journal of Research, Volume 68D, No. 4, April 1964, pp 419-427

36. V. A. Zagulyayeva, "Lunar Tidal Variations of the Minimum Virtual Heights of the F-2 Layer", Geomagnetism and Aeronomy, Volume 3, No. 6 (1963), (English Edition, August 1964), pp 911-913

37. O. M. Burkhard, "Height-Variability of Lunar Tides in the Ionospheric F-Region", Journal of Atmospheric and Terrestrial Physics, 27, January 1965, pp 113-114

38. J. E. C. Gliddon and P. C. Kendall, "Perturbation of a Model F2-Region by a Small Arbitrary Time Dependent Electrodynamic Drift", Journal of Atmospheric and Terrestrial Physics, 26, No. 7, July 1964, pp 721-728

39. G. H. Bazzard and C. M. Minnis, "The Geographical Distribution of the Harmonics of the Annual Variation in the Critical Frequency of the F2-Layers at Noon", Journal of Atmospheric and Terrestrial Physics, 1961, November, Volume 22, Pergamon Press Ltd., Printed in Northern Ireland, pp 192-199

40. R. Naismith and P. A. Smith, "Further Evidence of Long Term Variation in the Relationship of Solar Activity to the Ionosphere", Journal of Atmospheric and Terrestrial Physics, Volume 22, No. 4, December 1961, pp 270-274

41. L. W. Barclay, "Variations in the Relation Between Sunspot Number and I_{F2}", Journal of Atmospheric and Terrestrial Physics, Volume 24, June 1962, pp 547-549

42. E. Appleton, "Sunspot Control of Ionospheric and Geomagnetic Variations", Journal of Atmospheric and Terrestrial Physics, 26, No. 6, June 1964, pp 633-640

43. V. R. Noonkester, "Non-diurnal E-layer Variations at Washington, D.C.", Journal of Atmospheric and Terrestrial Physics, 26, No. 10, October 1964, pp 964-977

44. H. Kallman-Bijl, R.L.F. Boyd, H. Lagow, S.M. Poloskov and W. Priester, Compilers, "Cospar International Reference Atmosphere, 1961", North Holland Publishing Company, Amsterdam 1961

APOLLO NOTE NO. 371
(Task II, Item II)

L. Bonin
21 October 1965

EFFECT OF LUNAR EPHEMERIS ERRORS ON THE EXPECTED ORBIT OF A SATELLITE OF THE MOON

The degree of accuracy achieved when predicting the orbit of a lunar satellite depends to some extent on the errors associated with the lunar ephemeris. A cursory analysis was conducted to determine the variation of satellite ephemeris errors due to errors in the lunar ephemeris. This analysis showed that the expected lunar ephemeris errors produce neglectable short term effects on the satellite's dispersion. The error model used in this analysis is discussed below.

The satellite is assumed to be in a circular parking orbit, 80 n.mi. above the lunar surface. The orbit is inclined 180 degrees t_o the lunar equator with the satellite located 90 degrees relative to the Earth-Moon line at time zero. The Moon, at time zero, is located at a latitude of 4 degrees and a longitude of 60 degrees from the prime meridian. The inclination of the lunar orbit is 18.308 degrees relative to the Earth's equator.

Range-rate tracking data is obtained from three stations operating in the Doppler mode. The tracking station at Madrid, Spain is considered the master, with the stations at Ascension and Carnarvon considered slaves. The geographic location of these stations are:

Station	Latitude	Longitude
Madrid (Master)	40.4	-3.7
Ascension (Slave)	-7.9	14.3
Carnarvon (Slave)	-24.87	113.7

The relative geometry between the radar sites and the lunar satellite allows at least 30 minutes of continual tracking. A standard deviation of 0.003 m/sec is used for one minute observations. The a priori standard deviation in station location for three tracking sites are

$$\sigma_x^2 = 4.4 \times 10^3 m^2$$

$$\sigma_y^2 = 3.8 \times 10^3 m^2$$

$$\sigma_z^2 = 3.5 \times 10^3 m^2.$$

The bias in the measurable is $4.6 \times 10^{-4} m^2/sec^2$ for the master and $1.8 \times 10^{-3} m^2/sec^2$ for the slaves.

At time zero, the satellite's position is assumed to be known within a standard deviation of 1 km in the x', y', and z' directions. Its velocity is known within 3 m/sec along each axis of the same coordinate system. The uncertainty in the gravitational potential of the Moon is assumed to be $5.7 \times 10^8 m^3/sec^2$.

These errors provide a nominal case for solution in the Bissett-Berman OEA Program. The satellite ephemeris errors resulting from this case are compared with a second case that includes the expected errors in the lunar ephemeris. The expected 1 - sigma deviations in the lunar ephemeris are

$$\sigma_{\tilde{x}} = 1 \times 10^3 m \qquad \sigma_{\dot{\tilde{x}}} = 1 \times 10^{-3} m/sec$$

$$\sigma_{\tilde{y}} = 2 \times 10^3 m \qquad \sigma_{\dot{\tilde{y}}} = 1 \times 10^{-3} m/sec$$

$$\sigma_{\tilde{z}} = 1 \times 10^3 m \qquad \sigma_{\dot{\tilde{z}}} = 1 \times 10^{-3} m/sec$$

The attached table shows the agreement achieved between the two cases in the rendezvous miss distance ($\sqrt{P_{11} + P_{22} + P_{33}}$) and the magnitude of the total velocity error ($\sqrt{P_{44} + P_{55} + P_{66}}$). The data are presented for tracking times of 5 and 30 minutes. The effect of updating all nuisance parameters is also shown. Errors in the lunar ephemeris increase the satellite's position error by at most 1 part in 10,000 and its velocity error at most 3 parts in 10,000. Because variations of this order of magnitude are inconsequential from an error analysis point of view, lunar ephemeris errors of the magnitude studied here may be neglected in the future.

EFFECT OF LUNAR EPHEMERIS ERRORS

ON A SATELLITE IN A LUNAR PARKING ORBIT

	Tracking Time (Minutes)			
	5		30	
	Without Lunar Errors	With Lunar Errors	Without Lunar Errors	With Lunar Errors
Rendezvous Miss, (m) $\sqrt{P_{11} + P_{22} + P_{33}}$				
No nuisance parameters updated	1257	1257	3870	3870
All nuisance parameters updated	1107	1107	805.5	805.5
Velocity Errors, (m/sec) $\sqrt{P_{44} + P_{55} + P_{66}}$				
No nuisance parameters updated	5.39	5.39	3.65	3.65
All nuisance parameters updated	2.90	2.90	0.755	0.755

APOLLO NOTE NO. 372
(Task 2, Item II)

ADDITION OF REFRACTION PARAMETERS TO ORBIT ERROR ANALYSIS PROGRAM

L. Lustick
4 October 1965

PURPOSE

The purpose of this note is to describe the parameters required to represent the effect of the static troposphere on the MSFN measurables and to indicate the functional equations required to include them in the Orbit Error Analysis Program.

INTRODUCTION

Previous studies have indicated that the results for three dimensional refractivity profiles differ negligibly from studies with one dimensional profiles (see Apollo Note 354). There does not appear to be any significant azimuth angle error. The effect of wet and dry standard atmosphere refractivity profiles can be represented almost exactly by an exponential refractivity profile with the same zenith range error (N_oH) and the same index of refraction at the station (see Apollo Notes 293 and 311).

In summary, there are two parameters which define the troposphere effects on the MSFN measurables: (1) the zenith range error (N_oH) and, (2) the surface refractivity (N_o).

ASSUMPTIONS

1. The effects of the troposphere on the measurables are independent of altitude for altitudes in excess of 200 kilometers (see Apollo Note 293).
2. For elevation angles in excess of 5 degrees the range error and elevation angle error

have the following approximate forms:

$$\Delta R = \frac{N_o H}{\sin E\ell_a} \qquad (1)$$

$$\Delta \phi = N_o \operatorname{ctn} E\ell_a \qquad (2)$$

} See Apollo Note 293 Appendix D

In order to see the nature of this approximation let us compare

$$\frac{\partial(\Delta R)}{\partial(N_o H)}, \quad \frac{\partial(\Delta R)}{\partial N_o}, \quad \frac{\partial(\Delta\phi)}{\partial(N_o H)}, \quad \frac{\partial\Delta\phi}{\partial N_o}$$

with those obtained from the exact perturbation analysis (see Apollo Note 293, Appendix E).

$E\ell_a$	$\left[\frac{\partial(\Delta R)}{\partial(N_o H)}\right]_{N_o}$		$\left[\frac{\partial(\Delta R)}{\partial N_o}\right]_{N_o H}$ meters		$\left[\frac{\partial(\Delta\phi)}{\partial(N_o H)}\right]_{N_o}$ rad/meter		$\left[\frac{\partial(\Delta\phi)}{\partial N_o}\right]_{N_o H}$ rad	
	exact	eq. (1)	exact	eq. (1)	exact	eq. (2)	exact	eq. (2)
5°	9.21	11.5	8.45×10^3	0	-1.24×10^{-4}	0	11.1	11.5
10°	5.37	5.75	1.59×10^3	0	-2.38×10^{-5}	0	5.65	5.7
30°	1.99	2.00	62.2	0	-1.06×10^{-6}	0	1.73	1.73
60°	1.15	1.15	4.10	0	-1.2×10^{-7}	0	.577	.577
90°	1.0	1.00	0	0	0	0	0	0

It can be seen from this table that the agreement between equation 1 and 2 and the exact perturbation analysis is excellent down to 5° with the exception of the

$$\left[\frac{\partial(\Delta R)}{\partial N_o}\right]_{N_o H} \quad \text{and} \quad \left[\frac{\partial(\Delta\phi)}{\partial(N_o H)}\right]_{N_o}.$$

However, if we look at the magnitude of N_o (3×10^{-4}) a 1% error in N_o results in a ΔR of about 2.4 centimeters at $E\ell_a = 5^o$, whereas a 1% error in N_oH (.024 meters) results in an error in ΔR of about 24 centimeters, about 10 times as much. Hence, the leading parameter in the range equation is N_oH the zenith range error. On the other hand, if we compare the error in elevation angle, $\Delta\phi$, at 5° due to a 1% error in N_o, we obtain an error of about (.03 milliradians) whereas a 1% error in (N_oH) results in an angle error of only (.003 milliradians). Hence, the leading term for angle errors is the surface refractivity, N_o.

In summary, we will adopt equations (1) and (2) for our initial refractive model which implies that the range error is only dependent on N_oH and the angle error is only dependent on the parameter, N_o.

DEVELOPMENT OF EQUATIONS FOR MSFN MEASURABLES

Range Measurable

$$R_c = R(a_i) + \frac{N_oH}{\sin E\ell_a}$$

$$\frac{\partial R_c}{\partial (N_oH)} = \frac{1}{\sin E\ell_a} \cong \frac{1}{\sin E\ell_{ref}}$$

Even at 5° elevation, where the angle errors will be a maximum, the elevation angle error is 2.6 milliradians where 5° corresponds to approximately 90 milliradians

$$\frac{\partial R_c}{\partial N_o} = 0$$

Angle Measurables

$$E\ell_a = E\ell(a_i) + N_o \operatorname{ctn} E\ell_a$$

$$\frac{\partial E\ell}{\partial N_o} = \operatorname{ctn} E\ell_{ref} \qquad \frac{\partial A_z}{\partial N_o} = 0$$

$$\frac{\partial E\ell}{\partial N_o H} = 0 \qquad \frac{\partial A_z}{\partial N_o H} = 0$$

Range Rate Measurable (Two-Way Mode)

$$\dot{R}_c = \dot{s}(a_i) + \frac{d}{dt}\left(\frac{N_o H}{\sin E\ell_a}\right)$$

$$\dot{R}_c = \dot{s}(a_i) - (N_o H)\frac{\operatorname{ctn} E\ell_a}{\sin E\ell_a}\frac{d\,E\ell_a}{dt}$$

$$\frac{\partial \dot{R}_c}{\partial (N_o H)} \cong \frac{-\operatorname{ctn} E\ell_{ref}}{\sin E\ell_{ref}}\frac{d\,E\ell_{ref}}{dt}$$

$$\frac{\partial \dot{R}_c}{\partial N_o} = 0$$

Range Rate Measurable (Three-Way Mode)

$$\frac{\partial \dot{R}_{slave}}{\partial (N_o H)_{master}} = \left[\frac{-\operatorname{ctn} E\ell_{ref}}{\sin E\ell_{ref}}\frac{d\,E\ell_{ref}}{dt}\right]_{master}$$

$$\frac{\partial \dot{R}_{slave}}{\partial (N_o H)_{slave}} = \left[\frac{-\operatorname{ctn} E\ell_{ref}}{\sin E\ell_{ref}}\frac{d\,E\ell_{ref}}{dt}\right]_{slave}$$

Notice that there are two different columns required for master N_oH and slave N_oH. We also need an expression for

$$\frac{d\, E\ell_{ref}}{dt}$$

and trigonometric functions of the elevation angle

$$\begin{pmatrix} \hat{x} \\ \hat{y} \\ \hat{z} \end{pmatrix} = BA\, K^T L^T X'_s$$

$$\begin{pmatrix} \dot{\hat{x}} \\ \dot{\hat{y}} \\ \dot{\hat{z}} \end{pmatrix} = BA\, K^T L^T \dot{X}'_s + B\mathring{A} K^T L^T X'_s$$

where

$$\dot{A} = \omega_E \begin{bmatrix} -\sin\left(\omega_E T + \alpha\right) & \cos\left(\omega_E T + \alpha\right) & 0 \\ -\cos\left(\omega_E T + \alpha\right) & -\sin\left(\omega_E T + \alpha\right) & 0 \\ 0 & 0 & 1 \end{bmatrix}$$

All the above quantities, with the exception of $\mathring{A}$, already exist in the program. However, the required terms of $\dot{A}$ do exist in A, but must be multiplied by ω_E

$$\tan E\ell_{ref} = \frac{\hat{x}}{+\sqrt{\hat{y}^2 + \hat{z}^2}}$$

if $\hat{y}^2 + \hat{z}^2 = 0$

set $\operatorname{ctn} E\ell = 0$

$\sin E\ell = 1.0$

$\cos E\ell = 0$

the sin $E\ell$ and cos $E\ell$ can be defined from the above equations, both are taken as positive.

$$\frac{\text{ctn } E\ell}{\sin E\ell} \quad \frac{d\,E\ell}{dt} = \frac{1}{\hat{x}^2 \sin E\ell} \left\{ \hat{x}\,\dot{\hat{x}} \cos^2 E\ell - \sin^2 E\ell \left[\hat{y}\,\dot{\hat{y}} + \hat{z}\,\dot{\hat{z}} \right] \right\}$$

If $\tan E\ell_{ref} < \tan 5^{\circ}$, then do not include point in any information matrix.

SUMMARY

There are two new parameters to be added to Part A of the Orbit Error Analysis Program (N_oH and N_o). The Elevation angle information matrix will have one additional column, N_o. The Range information matrix will have one additional column (N_oH). The two-way mode doppler information matrix will have one additional column, N_oH. The three-way mode doppler measurable will have two additional columns $(N_oH)_{master}$ and $(N_oH)_{slave}$.

APOLLO NOTE NO. 373
(Task 2, Item II)

J. C. Childress, III,
L. Lustick
October 10, 1965

CHECKOUT OF THE SHIP VELOCITY PROGRAM

INTRODUCTION

This memo describes the checkout of the ship velocity routine addition to the Error Analysis Program (EAP). The ship velocity routine considers the use of a moving ship as a master station during the running of the EAP. It is assumed that the ship's position is specified by nuisance parameters a_8, a_9, a_{10}, while its velocity is specified by nuisance parameters a_{18}, and a_{19}. These parameters are topocentric coordinates, $\hat{x}$, $\hat{y}$, and $\hat{z}$: up, east and north for position and $\dot{\hat{y}}$ and $\dot{\hat{z}}$ for velocity. If a slave station is present, then its position is specified by nuisance parameters a_{15}, a_{16}, and a_{17}.

In order to operate the EAP with a velocity uncertainty, a -1 must be set into the Master-Slave Indicator - input parameter 32 of Program A. The velocity uncertainties may be in either range, range rate, or angle (remember that the input parameters 24 and 25 of Program A are set to +1 or -1 depending on whether an x-y or AZ-Eℓ mount is used - see Apollo Note 327).

CHECKOUT PROCEDURE

The equations described in Apollo Note 301 were programmed. These equations, as well as the theory which led to these equations, were checked and found to be valid. The parameters designations in the Note are no longer correct, however. A_{12} is μ, a_{13} is obsolete,

a_{18} and a_{19} rather than a_{25} and a_{26} are the master station velocities, a_{20} to a_{24} are the clock errors (range and range rate) which will be described in a subsequent Note, while a_{25} to a_{30} contain the lunar ephemeris data also described in a subsequent Note.

In order to check the accuracy of the routine in the EAP, the variables listed in Apollo Note 301, such as $\partial\overline{R}_s/\partial a_j$, $\partial\dot{\overline{R}}_s/\partial a_j$, $\overline{R}$ $\dot{\overline{R}}d$, 1B, A, $\partial R'_s/\partial a_j$, and $\partial\dot{R}'_s/\partial a_j$, were computed by hand and compared with the machine (7094) computed values. Since some of the quantities are not normally printed during the running of the EAP, a core dump was used to obtain the machine computed values.

Fig. 1 shows the actual Program A input data. Figs. 2 and 3 show the Q and QE matrices, while Figs. 4 and 5 show the range rate and range information matrices for the test station (moving ship) (these are 24 x 24 since the lunar ephemeris was not computed, i. e., Program A input parameter number 29 was less than 25). Fig. 6 is a printout of the matrix QP. Chart I shows the machine and hand-computed values of the parameters compared. There is obviously good agreement between the two values given. The growth of the error is easily traced in these computations since the primary errors are known. The sine and cosine routines are accurate to the eighth significant digit - see B_{j3}. The errors in $\partial R'_s/\partial a_9$, for example, are due to the errors in the computation of $\mathrm{Sin}(\omega_E T + \alpha)$ and $\mathrm{Cos}(\omega_e T + \alpha)$. Although the errors in partials of R'_s and $\dot{R}'_s$ would have been slightly larger if it had not been assumed that the LK matrix was an identity matrix, this does not affect the validity of the programming of the ship's velocity (moving master) routine of the EAP.

Due to the smallness of the errors in the calculations of the partials, it is apparent that the ship's velocity (moving master) routine of the EAP is functionally correct and programmed in a manner which should keep round-off and/or truncation errors small.

CHART I

Usual Name	Fortran Name	EAP Value	Calculator Value
$\partial R'_s/\partial a_8$*	RP1I(8)	-.74034985 -.44931292 -.5000000	-.74034986 -0.44931290 -.500000
$\partial R'_s/\partial a_9$*	RP1I(9)	.51882186 -.85488237 0.0	.51882183 -.85488238 0.0
$\partial R'_s/\partial a_{10}$*	RP1I(10)	.42744118 .25941093 -.86602541	.42744119 .25941092 -.866025404
$\partial R'_s/\partial a_{18}$*	RP1I(18)	155.64656 -256.46471 0.0	155.646558 -256.464714 0.0
$\partial R'_s/\partial a_{19}$*	RP1I(19)	128.23235 77.823280 -259.80762	128.232324 77.823279 -259.80762
$\partial \dot{R}'_s/\partial a_8$*	RDP1I(8) $\cdot 10^{+4}$	.32760123 -.53980092 0.0	.327601232 -.539800927 0.0
$\partial \dot{R}'_s/\partial a_9$*	RDP1I(9) $\cdot 10^{+4}$	.62330841 .37828132 0.0	.623308421 .378281319 0.0
$\partial \dot{R}_s/\partial a_{10}$*	RDP1I(10) $\cdot 10^{+4}$	-.18914066 .3116542 0.0	-.1891406596 .311654211 0.0
$\partial \dot{R}_s/\partial a_{18}$*	RDP1I(18)	.53752112 -.84353393 0.0	.5375211126 -.84353394 0.0
$\partial \dot{R}_s/\partial a_{19}$*	RDP1I(19)	-.42176696 .26870056 -.86602541	-.42176697 .268760556 -.866025404

*LK = I and $\partial R''_d/\partial a_j$ of A. N. 301 (p. 5) is actually $\partial R_d/\partial a_j$, i. e. $-\partial R'_s/\partial a_j$.

CHART I (Cont'd.)

Usual Name	Fortran Name	EAP Value	Calculator Value
B_{i1}	B_{I1}	.86602541 0.0 -.500000	.866025404 0.0 -.50000
B_{i2}	B_{I2}	0.0 1.0 0.0	0.0 1.0 0.0
B_{i3}	B_{I3}	.5000000 0.0 .86602541	.5000000 0.0 .866025404
A_{i1}	A_{I1}	.85488237 -.51882186 0.0	.85483238 -.51882185 0.0
A_{i2}	A_{I2}	.51882186 .85488237 0.0	.51882185 -.85488238 0.0
A_{i3}	A_{I3}	0.0 0.0 1.00000	0.0 0.0 1.0000000
BA_{i1}	BA_{I1}	.74034985 -.86602541 -.42744118	.740349859 -.866025404 -.42744119
BA_{i2}	BA_{Ia}	.44931292 .51882186 -.25941093	.44931290 .51882183 -.25941092
BA_{i3}	BA_{I3}	.50000000 0.00 .86602541	.5000000 0.00 .866025404
Rd	X_{SuBD} $\cdot 10^{-7}$	.47220255 .28657627 .31890499	.47220254 .286576268 .318905
$\dot{R}_d$	D_{XP11} $\cdot 10^{-3}$	-.20894734 .34429042 0.0	-.208947342 .344290429 0.0

01	0.3850000F 09	A1
02	-0.	A4
03	0.1025563E 04	A5
04	0.1000000F 01	GAM IN
05	-0.	BETA
06	-0.	XI
07	-0.	ETA
08	-0.	ZETA
09	0.3000000F 02	LAMBDA
10	0.3000000F 02	ALPHA
11	0.7291160F-04	OMEGAE
12	-0.	OMEGAM
13	0.6378100F 07	RHOE
14	-0.	RHOM
15	0.3996890E 15	MU
16	0.5000000F 01	D TIME
17	-0.	REENTRY RAD
18	-0.	BIG L
19	-0.	SMA L
20	0.1000000F 01	RRATE IND
21	0.1000000F 01	RANGE IND
22	0.1000000F 01	Q IND
23	-0.	QF IND
24	-0.	ANG 1 IND
25	-0.	ANG 2 IND
26	-0.	PVW IND
27	-0.	T INIT
28	0.5000000F 01	T INCR
29	0.2400000F 02	DIMENS
30	-0.	LAMBDA2
31	-0.	ALPHA2
32	-0.1000000F 01	M-S IND

FIGURE 1.

INPUT DATA

0.100000E 01	0.251869F-09	-0.	0.300000F 03	0.381032E-07	-0.	0.	0.
0.251869E-09	1.000000E 00	0.	0.379084E-07	0.300000E 03	0.	0.	0.
0.	0.	1.000000F 00	0.	0.	0.300000F 03	0.	0.
0.420234E-08	0.251869F-11	0.	0.100000E 01	0.503739E-09	0.	0.	0.
0.251869E-11	-0.210117E-08	-0.	0.503739E-09	1.000000E 00	-0.	0.	0.
0.	0.	-0.210117F-08	0.	0.	1.000000F 00	0.	0.
0.	0.	0.	0.	0.	0.	0.100000F 01	0.
0.	0.	0.	0.	0.	0.	0.	0.100000E 0
0.	0.	0.	0.	0.	0.	0.	0.
0.	0.	0.	0.	0.	0.	0.	0.
0.	0.	0.	0.	0.	0.	0.	0.
0.	0.	0.	0.	0.	0.	0.	0.
0.	0.	0.	0.	0.	0.	0.	0.
0.	0.	0.	0.	0.	0.	0.	0.

0.	0.	0.	-0.303593E-12	0.	-0.119871F 02
0.	0.	0.	-0.808710E-16	0.	0.450000F 05
0.	0.	0.	0.	0.	0.
0.	0.	0.	-0.202395E-14	0.	-0.119871E-00
0.	0.	0.	-0.808710E-18	0.	0.300000F 03
0.	0.	0.	0.	0.	0.
0.	0.	0.	0.	0.	0.
0.	0.	0.	0.	0.	0.
0.100000E 01	0.	0.	0.	0.	0.
0.	0.100000F 01	0.	0.	0.	0.
0.	0.	0.100000F 01	0.	0.	0.
0.	0.	0.	0.100000F 01	0.	0.
0.	0.	0.	0.	0.100000F 01	0.
0.	0.	0.	0.	0.	0.100000F 01

STN(TH-THO) = 0.7991399E-03 COS(TH-THO) = 0.9999997E 00

R = 0.3850000E 09 XP = 0.3849999F 09 YP = 0.3076689E 06 XDP = -0.8089505E 00 YDP = 0.1025563E 04

LATITUDE = -0. LONGITUDE = -0.1207471F 01

ORB INCL = 0.5729578E-08 FL PATH ANGLE = 0.5931924F-03 INERT HEAD = 0.9000000E 0:

FIGURE 2.

Q MATRIX

0.	0.	0.	0.	0.	0.	0.	0.
0.100000E 01	0.799140F-03	0.	0.300000E 03	0.239742E-00	0.	-0.303592E-12	0.239742E 02
-0.796057E-12	-0.210117E-08	0.	-0.788787E-03	0.999999E 00	0.	0.787755E-18	0.300000E 03
-0.202191E-11	-0.259740F-08	0.	-0.975074E-03	-0.154835E-05	0.	0.197350E-17	-0.230738E-03

FIGURE 3.

QE MATRIX

0.434965E-15	0.524586E-13	0.129803E-15	0.293052E-07	-0.195322E-09	-0.245751E-09	0.293069E-07	0.932153E-12
0.524586E-13	0.640349E-11	0.158162E-13	0.357846E-05	-0.240628E-07	-0.300093E-07	0.357867E-05	0.113604E-09
0.129803E-15	0.158162E-13	0.390755E-16	0.883811E-08	-0.593526E-10	-0.741169E-10	0.883862E-08	0.280662E-12
0.293052E-07	0.357846E-05	0.883811E-08	0.199977E 01	-0.134505E-01	-0.167702E-01	0.199988E 01	0.634826E-04
-0.195322E-09	-0.240628E-07	-0.593526E-10	-0.134505E-01	0.910471E-04	0.112799E-03	-0.134513E-01	-0.426384E-06
-0.245751E-09	-0.300093E-07	-0.741169E-10	-0.167702E-01	0.112799E-03	0.140637E-03	-0.167712E-01	-0.532369E-06
0.293069E-07	0.357867E-05	0.883862E-08	0.199988E 01	-0.134513E-01	-0.167712E-01	0.200000E 01	0.634862E-04
0.932153E-12	0.113604E-09	0.280662E-12	0.634826E-04	-0.426384E-06	-0.532369E-06	0.634862E-04	0.201588E-08
0.178466E-11	0.218081E-09	0.538561E-12	0.121874E-03	-0.820156E-06	-0.102205E-05	0.121881E-03	0.386844E-08
-0.538328E-12	-0.656078E-10	-0.162085E-12	-0.366619E-04	0.246241E-06	0.307449E-06	-0.366640E-04	-0.116419E-08
0.587292E-05	0.715743E-03	0.176826E-05	0.399960E 03	-0.268633E 01	-0.335409E 01	0.399983E 03	0.127007E-01
-0.330180E-22	-0.363283E-20	-0.911891E-23	-0.202372E-14	0.125235E-16	0.169684E-16	-0.202383E-14	-0.653770E-19
0.	0.	0.	0.	-0.	-0.	0.	0.
-0.335598E-07	-0.369244E-05	-0.926855E-08	-0.205693E 01	0.127290E-01	0.172468E-01	-0.205704E 01	-0.664499E-04
0.	0.	0.	0.	-0.	-0.	0.	0.
0.	0.	0.	0.	-0.	-0.	0.	0.
0.	0.	0.	0.	-0.	-0.	0.	0.
0.154315E-07	0.187716E-05	0.463885E-08	0.104890E 01	-0.703539E-02	-0.879616E-02	0.104897E 01	0.333178E-04
0.126681E-07	0.154909E-05	0.382515E-08	0.865721E 00	-0.582884E-02	-0.726003E-02	0.865771E 00	0.274760E-04
-0.109157E-06	-0.120101E-04	-0.301469E-07	-0.669039E 01	0.414025E-01	0.560971E-01	-0.669075E 01	-0.216135E-03
0.111446E 02	0.136086E 04	0.336106E 01	0.760495E 09	-0.511509E 07	-0.637758E 07	0.760539E 09	0.241419E 05
-0.657812E-09	-0.803892E-07	-0.198522E-09	-0.449253E-01	0.302344E-03	0.376748E-03	-0.449279E-01	-0.142597E-05
0.	0.	0.	0.	-0.	-0.	0.	0.
0.	0.	0.	0.	-0.	-0.	0.	0.

0.178466E-11	-0.538328E-12	0.587292E-05	-0.330180E-22	0.	-0.335598E-07	0.	0.
0.218081E-09	-0.656078E-10	0.715743E-03	-0.363283E-20	0.	-0.369244E-05	0.	0.
0.538561E-12	-0.162085E-12	0.176826E-05	-0.911891E-23	0.	-0.926855E-08	0.	0.
0.121874E-03	-0.366619E-04	0.399960E 03	-0.202372E-14	0.	-0.205693E 01	0.	0.
-0.820156E-06	0.246241E-06	-0.268633E 01	0.125235E-16	-0.	0.127290E-01	-0.	-0.
-0.102205E-05	0.307449E-06	-0.335409E 01	0.169684E-16	-0.	0.172468E-01	-0.	-0.
0.121881E-03	-0.366640E-04	0.399983E 03	-0.202383E-14	0.	-0.205704E 01	0.	0.
0.386844E-08	-0.116419E-08	0.127007E-01	-0.653770E-19	0.	-0.664499E-04	0.	0.
0.742780E-08	-0.223406E-08	0.243723E-01	-0.122532E-18	0.	-0.124543E-03	0.	0.
-0.223406E-08	0.672333E-09	-0.733478E-02	0.377559E-19	-0.	0.383755E-04	-0.	-0.
0.243723E-01	-0.733478E-02	0.800184E 05	-0.411938E-12	0.	-0.418698E 03	0.	0.
-0.122532E-18	0.377559E-19	-0.411938E-12	0.409589E-29	-0.	0.416311E-14	-0.	-0.
0.	-0.	0.	-0.	0.	-0.	0.	0.
-0.124543E-03	0.383755E-04	-0.418698E 03	0.416311E-14	-0.	0.423143E 01	-0.	-0.
0.	-0.	0.	-0.	0.	-0.	0.	0.
0.	-0.	0.	-0.	0.	-0.	0.	0.
0.	-0.	0.	-0.	0.	-0.	0.	0.
0.639100E-04	-0.192414E-04	0.209913E 03	-0.109834E-14	0.	-0.111637E 01	0.	0.
0.527649E-04	-0.158677E-04	0.173107E 03	-0.864858E-15	0.	-0.879051E 00	0.	0.
-0.405089E-03	0.124820E-03	-0.136186E 04	0.135410E-13	-0.	0.137632E 02	-0.	-0.

0.463476E 05	-0.139422E 05	0.152101E 12	-0.769661E-06	0.	-0.782291E 09	0.	0.
-0.273806E-05	0.823514E-06	-0.898405E 01	0.451365E-16	-0.	0.458772E-01	-0.	-0.
0.	-0.	0.	-0.	0.	-0.	0.	0.
0.	-0.	0.	-0.	0.	-0.	0.	0.

0.	0.154315E-07	0.126681E-07	-0.109157E-06	0.111446E 02	-0.657812E-09	0.	0.
0.	0.187716E-05	0.154909E-05	-0.120101E-04	0.136086E 04	-0.803892E-07	0.	0.
0.	0.463885E-08	0.382515E-08	-0.301469E-07	0.336106E 01	-0.198522E-09	0.	0.
0.	0.104890E 01	0.865721E 00	-0.669039E 01	0.760495E 09	-0.449253E-01	0.	0.
-0.	-0.703539E-02	-0.582884E-02	0.414025E-01	-0.511509E 07	0.302344E-03	-0.	-0.
-0.	-0.879616E-02	-0.726003E-02	0.560971E-01	-0.637758E 07	0.376748E-03	-0.	-0.
0.	0.104897E 01	0.865771E 00	-0.669075E 01	0.760539E 09	-0.449279E-01	0.	0.
0.	0.333178E-04	0.274760E-04	-0.216135E-03	0.241419E 05	-0.142597E-05	0.	0.
0.	0.639100E-04	0.527649E-04	-0.405089E-03	0.463476E 05	-0.273806E-05	0.	0.
-0.	-0.192414E-04	-0.158677E-04	0.124820E-03	-0.139422E 05	0.823514E-06	-0.	-0.
0.	0.209913E 03	0.173107E 03	-0.136186E 04	0.152101E 12	-0.898405E 01	0.	0.
-0.	-0.109834E-14	-0.864858E-15	0.135410E-13	-0.769661E-06	0.451365E-16	-0.	-0.
0.	0.	0.	-0.	0.	-0.	0.	0.
-0.	-0.111637E 01	-0.879051E 00	0.137632E 02	-0.782291E 09	0.458772E-01	-0.	-0.
0.	0.	0.	-0.	0.	-0.	0.	0.
0.	0.	0.	-0.	0.	-0.	0.	0.
0.	0.	0.	-0.	0.	-0.	0.	0.
0.	0.550828E 00	0.453879E-00	-0.363111E 01	0.398890E 09	-0.235580E-01	0.	0.
0.	0.453879E-00	0.374841E-00	-0.285921E 01	0.329226E 09	-0.194504E-01	0.	0.
-0.	-0.363111E 01	-0.285921E 01	0.447662E 02	-0.254449E 10	0.149221E-00	-0.	-0.
0.	0.398890E 09	0.329226E 09	-0.254449E 10	0.289210E 18	-0.170847E 08	0.	0.
-0.	-0.235580E-01	-0.194504E-01	0.149221E-00	-0.170847E 08	0.100931E-02	-0.	-0.
0.	0.	0.	-0.	0.	-0.	0.	0.
0.	0.	0.	-0.	0.	-0.	0.	0.

FIGURE 4.

TEST STATION VELOCITY

0.199976E 01	-0.139890F-01	-0.167716F-01	0.299966E 03	-0.201784E 01	-0.251554F 01	0.199988F 01	-0.147562E 01
-0.139890E-01	0.980016E-04	0.117323E-03	-0.201784E 01	0.135738E-01	0.169218E-01	-0.139898E-01	0.103250E-01
-0.167716E-01	0.117323E-03	0.140659E-03	-0.251554E 01	0.169218E-01	0.210956E-01	-0.167726E-01	0.123757E-01
0.299966E 03	-0.201784F 01	-0.251554E 01	0.899896E 05	-0.605352E 03	-0.754662E 03	0.299983E 03	-0.219915E 03
-0.201784E 01	0.135738E-01	0.169218E-01	-0.605352E 03	0.407214E 01	0.507654E 01	-0.201796E 01	0.147935E 01
-0.251554E 01	0.169218E-01	0.210956E-01	-0.754662E 03	0.507654E 01	0.632868F 01	-0.251569E 01	0.184423E 01
0.199988E 01	-0.139898F-01	-0.167726E-01	0.299983E 03	-0.201796E 01	-0.251569E 01	0.200000E 01	-0.147571E 01
-0.147562E 01	0.103250E-01	0.123757E-01	-0.219915E 03	0.147935E 01	0.184423E 01	-0.147571E 01	0.108890E 01
0.103074E 01	-0.720546E-02	-0.864458E-02	0.157354E 03	-0.105850E 01	-0.131958E 01	0.103080E 01	-0.760494E 00
0.871316E 00	-0.609661F-02	-0.730753E-02	0.129873E 03	-0.873641E 00	-0.108913E 01	0.871367E 00	-0.642968E 00
0.760495E 09	-0.531989F 07	-0.637810E 07	0.114083E 12	-0.767428E 09	-0.956715E 09	0.760540E 09	-0.561167E 09
-0.303557E-12	0.204200E-14	0.254566E-14	-0.910671E-10	0.612600E-12	0.763698E-12	-0.303574E-12	0.222548E-12
0.299983E 03	-0.201795F 01	-0.251569E 01	0.899948E 05	-0.605387E 03	-0.754706E 03	0.300000E 03	-0.219928E 03
-0.314662E 03	0.211670E 01	0.263878E 01	-0.943985E 05	0.635010E 03	0.791635E 03	-0.314680E 03	0.230689E 03
-0.	0.	0.	-0.	0.	0.	-0.	0.
-0.	0.	0.	-0.	0.	0.	-0.	0.
-0.	0.	0.	-0.	0.	0.	-0.	0.
0.157354E 03	-0.105850F 01	-0.131958E 01	0.472061E 05	-0.317551E 03	-0.395875F 03	0.157363E 03	-0.115361E 03
0.129873E 03	-0.873641E 00	-0.108912E 01	0.389618E 05	-0.262092E 03	-0.326738E 03	0.129880E 03	-0.952141E 02
0.760495E 09	-0.531989F 07	-0.637810E 07	0.114083E 12	-0.767428E 09	-0.956715E 09	0.760540E 09	-0.561167E 09
0.114083E 12	-0.767428E 09	-0.956715E 09	0.342250E 14	-0.230228E 12	-0.287014F 12	0.114090E 12	-0.836384E 11

0.	-0.	-0.	0.	-0.	-0.	0.	-0.
0.	-0.	-0.	0.	-0.	-0.	0.	-0.
0.	-0.	-0.	0.	-0.	-0.	0.	-0.

0.103074E 01	0.871316F 00	0.760495E 09	-0.303557E-12	0.299983E 03	-0.314662E 03	-0.	-0.
-0.720546E-02	-0.609661F-02	-0.531989E 07	0.204200E-14	-0.201795E 01	0.211670E 01	0.	0.
-0.864458E-02	-0.730753E-02	-0.637810E 07	0.254566E-14	-0.251569E 01	0.263878E 01	0.	0.
0.157354E 03	0.129873E 03	0.114083E 12	-0.910671E-10	0.899948E 05	-0.943985E 05	-0.	-0.
-0.105850E 01	-0.873641E 00	-0.767428E 09	0.612600E-12	-0.605387E 03	0.635010E 03	0.	0.
-0.131958E 01	-0.108913F 01	-0.956715E 09	0.763698E-12	-0.754706E 03	0.791635E 03	0.	0.
0.103080E 01	0.871367F 00	0.760540E 09	-0.303574E-12	0.300000E 03	-0.314680E 03	-0.	-0.
-0.760494E 00	-0.642968F 00	-0.561167E 09	0.222548E-12	-0.219928E 03	0.230689E 03	0.	0.
0.531443E 00	0.449053F-00	0.391983E 09	-0.159238E-12	0.157363E 03	-0.165063E 03	-0.	-0.
0.449053E-00	0.379656E-00	0.331354E 09	-0.131428E-12	0.129880E 03	-0.136235E 03	-0.	-0.
0.391983E 09	0.331354F 09	0.289210E 18	-0.115449E-03	0.114090E 12	-0.119673E 12	-0.	-0.
-0.159238E-12	-0.131428E-12	-0.115449E-03	0.921574E-25	-0.910723E-10	0.955287E-10	0.	0.
0.157363E 03	0.129880F 03	0.114090E 12	-0.910723E-10	0.900000E 05	-0.944039E 05	-0.	-0.
-0.165063E 03	-0.136235E 03	-0.119673E 12	0.955287E-10	-0.944039E 05	0.990233E 05	0.	0.
-0.	-0.	-0.	0.	-0.	0.	0.	0.
-0.	-0.	-0.	0.	-0.	0.	0.	0.
-0.	-0.	-0.	0.	-0.	0.	0.	0.
0.825434E 02	0.681276F 02	0.598450F 11	-0.477713E-10	0.472088E 05	-0.495188F 05	-0.	-0.
0.681276E 02	0.562295E 02	0.493934E 11	-0.394283E-10	0.389640E 05	-0.408706F 05	-0.	-0.
0.391983E 09	0.331354E 09	0.289210E 18	-0.115449E-03	0.114090E 12	-0.119673E 12	-0.	-0.
0.598450E 11	0.493934F 11	0.433884E 20	-0.346348E-01	0.342270E 14	-0.359018E 14	-0.	-0.
0.	0.	0.	-0.	0.	-0.	-0.	-0.
0.	0.	0.	-0.	0.	-0.	-0.	-0.
0.	0.	0.	-0.	0.	-0.	-0.	-0.

-0.	0.157354E 03	0.129873F 03	0.760495E 09	0.114083E 12	0.	0.	0.
0.	-0.105850F 01	-0.873641E 00	-0.531989E 07	-0.767428E 09	-0.	-0.	-0.
0.	-0.131958E 01	-0.108912F 01	-0.637810E 07	-0.956715E 09	-0.	-0.	-0.
-0.	0.472061E 05	0.389618E 05	0.114083E 12	0.342250E 14	0.	0.	0.
0.	-0.317551E 03	-0.262092E 03	-0.767428E 09	-0.230228E 12	-0.	-0.	-0.
0.	-0.395875E 03	-0.326738F 03	-0.956715E 09	-0.287014E 12	-0.	-0.	-0.
-0.	0.157363E 03	0.129880F 03	0.760540E 09	0.114090E 12	0.	0.	0.
0.	-0.115361E 03	-0.952141E 02	-0.561167E 09	-0.836384E 11	-0.	-0.	-0.
-0.	0.825434F 02	0.681276E 02	0.391983E 09	0.598450E 11	0.	0.	0.
-0.	0.681276E 02	0.562295E 02	0.331354E 09	0.493934E 11	0.	0.	0.
-0.	0.598450E 11	0.493934E 11	0.289210E 18	0.433884E 20	0.	0.	0.
0.	-0.477713E-10	-0.394283E-10	-0.115449E-03	-0.346348E-01	-0.	-0.	-0.
-0.	0.472088E 05	0.389640E 05	0.114090E 12	0.342270E 14	0.	0.	0.
0.	-0.495188F 05	-0.408706E 05	-0.119673E 12	-0.359018E 14	-0.	-0.	-0.
0.	-0.	-0.	-0.	-0.	-0.	-0.	-0.
0.	-0.	-0.	-0.	-0.	-0.	-0.	-0.
0.	-0.	-0.	-0.	-0.	-0.	-0.	-0.
-0.	0.247630F 05	0.204383E 05	0.598450E 11	0.179535E 14	0.	0.	0.
-0.	0.204383F 05	0.168688E 05	0.493934E 11	0.148180E 14	0.	0.	0.
-0.	0.598450F 11	0.493934E 11	0.289210E 18	0.433884E 20	0.	0.	0.
-0.	0.179535E 14	0.148180E 14	0.433884E 20	0.130165E 23	0.	0.	0.
-0.	0.	0.	0.	0.	0.	0.	0.
-0.	0.	0.	0.	0.	0.	0.	0.
-0.	0.	0.	0.	0.	0.	0.	0.

FIGURE 5.

TEST STATION VELOCITY

1.000000E 00	-0.	-0.	-0.	-0.186265E-07	-0.	-0.

FIGURE 6.

QP MATRIX

APOLLO NOTE NO. 374
(Task 2, Item II)

J. C. Childress, III
21 October 1965

CHECKOUT OF THE $QE(Cov_0)QE^T$ ROUTINE OF THE ORBIT ERROR ANALYSIS PROGRAM

INTRODUCTION

The $QE\ (Cov_0)\ QE^T$ routine of the Orbit Error Analysis (OEA) Program computes the standard deviation in the radius vector, $\overline{r}$ velocity vector, $\overline{v}$, and flight path angle, γ, at a fixed time. This routine is analytically described in Apollo Note 367. There is a minor change, however: the first row of the matrix $\partial U/\partial X$ (see Apollo Note 329) no longer contains the partials of H with respect to the state vector (this row now contains all zeros). Thus, the expression for QE given in Apollo Note 367 is not quite correct since QE is a 4 x 8 with the first row identically zero. Likewise, the 2:2, 3:3, and 4:4 rather than the 1:1, 2:2, and 3:3 elements of $QE(t)\ (Cov_0)\ QE(t)^T$ produce the standard deviations in r, v, and γ.

COMPUTATIONAL PROCEDURE

Since the fundamental underlying assumption, which has been shown to be valid, in the OEA Program is that the error in any quantity which is a function of the nuisance parameters and the time, e.g., $\psi(a_i, t)$, can be estimated from

$$\left[\frac{\partial \psi}{\partial a_j}\right] \left[Cov_0\right] \left[\frac{\partial \psi}{\partial a_j}\right]^T \tag{1}$$

it is sufficient to show that the $\partial\psi/\partial a_j$'s, the partials of r, v, and γ with respect to the a_j's, in this case, are being correctly computed

in this routine. Prior analysis has shown that the matrices (Cov_0) and Q(t) are being correctly computed in the OEA Program.

CHECKOUT PROCEDURE

After writing QE(t) as

$$QE(t) = \begin{bmatrix} \partial U/\partial X \\ \partial \gamma/\partial X \end{bmatrix} Q(t) \qquad (2)$$

$$= \begin{bmatrix} QEH \end{bmatrix} Q(t)$$

the elements of the QEH matrix, i.e.,

$$QEH = \begin{bmatrix} 0 & 0 & 0 & 0 & 0 & 0 & 0 & 0 \\ \text{Cos } x & \text{Sin } x & 0 & 0 & 0 & 0 & 0 & 0 \\ 0 & 0 & 0 & \frac{\dot{x}'}{v} & \frac{\dot{y}'}{v} & 0 & 0 & 0 \\ \frac{y'}{r^2} & \frac{-x'}{r^2} & 0 & \frac{-\dot{y}'}{v^2} & \frac{\dot{x}'}{v^2} & 0 & 0 & 0 \end{bmatrix} \qquad (3)$$

where

$$\begin{aligned} &a \quad \text{Cos } x = \text{Cos } (\theta - \theta_0), \\ &b \quad \text{Sin } x = \text{Sin } (\theta - \theta_0) \end{aligned} \qquad (4)$$

were checked. Figure 1 shows the input data; while Figure 2 shows the Q matrix, Sin x, Cos x, R, x', y', $\dot{x}'$, $\dot{y}'$, latitude, longitude, orbital inclination (ι), flight path angle (γ), inertial heading (β), and the QE matrix computed.

The errors in the computation of the above quantities have already been discussed in Apollo Note 362 and will not be discussed here. It was found in that Note that the method of computing these quantities is correct. It was determined that the proper quantities were being inserted in the matrix QEH by means of a core dump containing the matrix QEH - a 4 x 8.

Next, the elements of QEH were multiplied by the elements of Q(t) to determine the elements of QE, i.e.,

$$QE_{ij} = \sum_{k=1}^{8} QEH_{ik} \cdot Q_{kj}. \tag{5}$$

Obviously, the first row of the QE matrix is identically zero and is not printed (see Figure 2), likewise, the third and sixth columns (see Apollo Note 362).

With the exception of the eighth element, all elements of the second row of QE computed agreed to the last digit given in the printout of QE. For the eighth element, the last digit differed by one unit, i.e., 5 instead of 6. The elements of the second and third rows are slightly more inaccurate dut to more complex computational process. There is little, if anything, which can be done to reduce roundoff and/or truncation error in the computation of the third row. The fourth row (of QE) calculations could be improved slightly by computing (Sin x)/r and (Cos x)/r rather than y'/r^2 and x'/r^2, but these changes would not change the accuracies by more than one significant digit, generally (also the use of $(2\mu/r + |E|)$, i.e., v^2, in place of v . v should be more accurate since v was originally found by taking the square root of v^2). The uncertainty (error) in the third row of QE appears in the seventh (not shown) significant digit assuming that the

program inputs are errorless. The uncertainty in the fourth row is of the same order of magnitude as that of the third row although the computations are slightly more complex.

Thus, the $QE(Cos_0)QE^T$ routine of the OEA Program appears to be very accurate.

01	0.6635332E 07	A1
02	0.9832780E 03	A4
03	0.6874121E 04	A5
04	0.1000000E 01	GAM ID
05	0.3178484E 02	BETA
06	-0.	XI
07	-0.	ETA
08	-0.	ZETA
09	0.3217408E 02	LAMBDA
10	-0.6465364E 02	ALPHA
11	0.7292115E-04	OMEGAE
12	-0.	OMEGAM
13	0.6378165E 07	RHOE
14	-0.	RHOM
15	0.3986032E 15	MU
16	0.4999980E-00	D TIME
16	0.3183321E 01	D TIME
17	0.	REENTRY RAD
18	0.2356725E 02	BIG L
19	-0.6570400E 02	SMA L
20	0.1000000E 01	RRATE IND
21	0.1000000E 01	RANGE IND
22	0.1000000E 01	Q IND
23	-0.	QF IND
24	0.1000000E 01	ANG 1 IND
25	0.1000000E 01	ANG 2 IND
26	0.1000000E 01	PVW IND
27	-0.	T INIT
28	0.1666660E-01	T INCR
29	0.3000000E 02	DIMENS
30	-0.	LAMBDA2
31	-0.	ALPHA2
32	-0.1000000E 01	M-S IND

FIGURE 1.

INPUT DATA

0.100122E 01	0.189119E-04	-0.	0.300121E 02	0.283188E-03	-0.	0.	0.
0.189189E-04	0.999389E 00	0.	0.283225E-03	0.299938E 02	0.	0.	0.
0.	0.	0.999389E 00	0.	0.	0.299938E 02	0.	0.
0.813278E-04	0.188548E-05	0.	0.100122E 01	0.376569E-04	0.	0.	0.
0.188663E-05	-0.406197E-04	-0.	0.376638E-04	0.999392E 00	-0.	0.	0.
0.	0.	-0.406586E-04	0.	0.	0.999391E 00	0.	0.
0.	0.	0.	0.	0.	0.	0.100000E 01	0.
0.	0.	0.	0.	0.	0.	0.	0.100000E 01
0.	0.	0.	0.	0.	0.	0.	0.
0.	0.	0.	0.	0.	0.	0.	0.
0.	0.	0.	0.	0.	0.	0.	0.
0.	0.	0.	0.	0.	0.	0.	0.
0.	0.	0.	0.	0.	0.	0.	0.
0.	0.	0.	0.	0.	0.	0.	0.

0.	0.	0.	-0.101923E-10	0.	-0.466009E 01
0.	0.	0.	-0.105241E-12	0.	0.449924E 03
0.	0.	0.	0.	0.	0.
0.	0.	0.	-0.678598E-12	0.	-0.465891E-00
0.	0.	0.	-0.105046E-13	0.	0.299902E 02
0.	0.	0.	0.	0.	0.
0.	0.	0.	0.	0.	0.
0.	0.	0.	0.	0.	0.
0.100000E 01	0.	0.	0.	0.	0.
0.	0.100000E 01	0.	0.	0.	0.
0.	0.	0.100000E 01	0.	0.	0.
0.	0.	0.	0.100000E 01	0.	0.
0.	0.	0.	0.	0.100000E 01	0.
0.	0.	0.	0.	0.	0.100000E 01

SIN(TH-TH0) = 0.3093970E-01 COS(TH-TH0) = 0.9995212E 00

R = 0.6663959E 07 XP = 0.6660768E 07 YP = 0.2061809E 06 XDP = 0.7128965E 03 YDP = 0.6869937E 04

LATITUDE = 0.2289380E 02 LONGITUDE = -0.6404449E 02

ORB INCL = 0.3178484E 02 FL PATH ANGLE = 0.7697401E 01 INERT HEAD = 0.6732655E 02

QE MATRIX 1 QE T = 0.50

0.100074E 01	0.309397E-01	0.	0.299977E 02	0.928282E 00	0.	-0.101907E-10	0.926266E 01
0.102709E-04	-0.402081E-04	0.	0.103379E-00	0.994058E 00	0.	-0.804908E-13	0.297820E 02
-0.703823E-08	-0.150776E-06	0.	-0.144046E-03	0.104308E-04	0.	0.975370E-16	0.447764E-03

FIGURE 2.

QE AND Q MATRIX

APOLLO NOTE NO. 375
(Task 2, Item II)

J. C. Childress, III
22 October 1965

CHECKOUT OF THE LUNAR EPHEMERIS ROUTINE OF THE ERROR ANALYSIS PROGRAM

INTRODUCTION

The lunar ephemeris routine of the Error Analysis Program (EAP) computes an ephemeris for the Moon. If a matrix larger than 24 x 24 is requested during the running of Program A, i. e., the 29th input parameter is greater than 24 then a lunar ephemeris is computed. The six parameters used to comprise this ephemeris are called nuisance parameters 25 to 30. Only range and range rate data is acceptable for the measurables, i. e., angle data is not acceptable.

COMPUTATIONAL PROCEDURE

Since it can be assumed that the EAP is computing trajectories correctly, it was only necessary to compute the trajectory of the moon, assumed to be a point mass about the Earth, when a 7 x 7 matrix is requested, and compare it with the trajectory which the lunar ephemeris routine computed. Apollo Notes 295 and 367 describe the use of the lunar ephemeris parameters in the EAP as nuisance parameters. (The parameters are now numbered 25 to 30.) Thus the elements of a 6 x 6 ϕ matrix which corresponds to the trajectory of the Moon relative to the center of the Earth were compared with the 25-30 elements of the partials of the position and velocity vectors before they were transferred to the lunar reference via the L matrix.

CHECKOUT PROCEDURE

Fig. 1 shows the input data used to compute the epheremis for the Moon relative to a station located at the center of the Earth. Fig. 2 shows the Q and QE matrices which result. Fig 3 shows the information matrices which were found for the test case. The input data for the computations using the lunar ephemeris routine is shown in Fig. 4. The partials of the radius and velocity vectors with respect to the 25 to 30 nuisance parameters at times T = 1, . . . ,5 are given in Fig. 6. Notice that the last printout is the transpose of the first Q matrix. The error in the 29-1 element is due to the computational procedure and although the error is relatively large, it is unimportant because of its absolute magnitude. The Q and QE matrices are shown in Fig. 6.

Since the philosophy inherent in the design of the test case is shown and the results consistant with those respected, it is concluded that the lunar ephemeris routine is correctly programmed.

01	0.3850000E 09	A1
02	-0.	A4
03	0.1025563E 04	A5
04	0.1000000E 01	GAM ID
05	0.1830800E 02	BETA
06	-0.	XI
07	-0.	ETA
08	-0.	ZETA
09	-0.	LAMBDA
10	-0.	ALPHA
11	-0.	OMEGAE
12	-0.	OMEGAM
13	-0.	RHOE
14	-0.	RHOM
15	0.3996890E 15	MU
16	0.5000000E 01	D TIME
16	0.5805000E 02	D TIME
17	-0.	REENTRY RAD
18	0.4000000E 01	BIG L
19	0.6000000E 02	SMA L
20	0.1000000E 01	RRATE IND
21	0.1000000E 01	RANGE IND
22	0.1000000E 01	Q IND
23	0.5805000E 02	QF IND
24	0.1000000E 01	ANG 1 IND
25	0.1000000E 01	ANG 2 IND
26	-0.	PVW IND
27	0.1000000E 01	T INIT
28	0.1000000E 01	T INCR
29	0.7000000E 01	DIMENS
30	-0.	LAMBDA2
31	-0.	ALPHA2
32	0.1000000E 01	M-S IND

FIGURE 1.

INPUT DATA

Q MATRIX 12 Q T = 5.00

0.100000E 01	0.251869E-09	-0.	0.300000E 03	0.381032E-07	-0.
0.251869E-09	1.000000E 00	0.	0.379084E-07	0.300000E 03	0.
0.	0.	1.000000E 00	0.	0.	0.300000E 03
0.420234E-09	0.251869E-11	0.	0.100000E 01	0.503739E-09	0.
0.251869E-11	-0.210117E-08	-0.	0.503739E-09	1.000000E 00	-0.
0.	0.	-0.210117E-08	0.	0.	1.000000E 00

SIN(TH-THO) = 0.7991399E-03 COS(TH-THO) = 0.9999997E 00

R = 0.3850000E 09 XP = 0.3849999E 09 YP = 0.3076689E 06 XDP = -0.8089505E 00 YDP = 0.1025563E 04

LATITUDE = 0.3985941E 01 LONGITUDE = 0.6004368E 02

ORB INCL = 0.1830800E 02 FL PATH ANGLE = 0.5931924E-03 INERT HEAD = 0.7211664E 02

QE MATRIX 12 QE T = 5.00

0.102556E 04	0.	0.	0.	0.385000E 09	0.	0.
0.100000E 01	0.799140E-03	0.	0.300000E 03	0.239742E-00	0.	0.
-0.796057E-10	-0.210117E-08	0.	-0.788787E-03	0.999999E 00	0.	0.
-0.202191E-11	-0.259740E-08	0.	-0.975074E-03	-0.154835E-05	0.	0.

FIGURE 2.

QE AND Q MATRIX

0.945952E-17	0.165709E-13	-0.	0.622077E-08	0.729119E-11	-0.	0.622077E-08
0.165709E-13	0.354791E-10	-0.	0.133190E-04	0.127725E-07	-0.	0.133190E-04
-0.	-0.	0.	-0.	-0.	0.	-0.
0.622077E-08	0.133190E-04	-0.	0.500000E 01	0.479484E-02	-0.	0.500000E 01
0.729119E-11	0.127725E-07	-0.	0.479484E-02	0.561990E-05	-0.	0.479484E-02
-0.	-0.	0.	-0.	-0.	0.	-0.
0.622077E-08	0.133190E-04	-0.	0.500000E 01	0.479484E-02	-0.	0.500000E 01

LUN EPH TEST 12 R T = 5.00

0.500000E 01	0.239742E-02	0.	0.900000E 03	0.527432E 00	0	0.500000E 01
0.239742E-02	0.140497E-05	0.	0.527432E 00	0.344857E-03	0.	0.239742E-02
0.	0.	0.	0.	0.	0.	0.
0.900000E 03	0.527432E 00	0.	0.198000E 06	0.129461E 03	0.	0.900000E 03
0.527432E 00	0.344857E-03	0.	0.129461E 03	0.900308E-01	0.	0.527432E 00
0.	0.	0.	0.	0.	0.	0.
0.500000E 01	0.239742E-02	0.	0.900000E 03	0.527432E 00	0.	0.500000E 01

LUN EPH TEST 12 A1 T = 5.00

0.136437E-23	-0.232708E-20	0.119694E-19	0.334986E-21	-0.512191E-18	0.263416E-17	-0.236199E-11
-0.232708E-20	0.484981E-17	-0.249498E-16	-0.512191E-18	0.873592E-15	-0.449335E-14	0.492433E-08
0.119694E-19	-0.249498E-16	0.128354E-15	0.263416E-17	-0.449335E-14	0.231117E-13	-0.253332E-07
0.334986E-21	-0.512191E-18	0.263416E-17	0.874695E-19	-0.125755E-15	0.646700E-15	-0.519756E-09
-0.512191E-18	0.873592E-15	-0.449335E-14	-0.125755E-15	0.192278E-12	-0.988872E-12	0.886698E-06
0.263416E-17	-0.449335E-14	0.231117E-13	0.646700E-15	-0.988872E-12	0.508569E-11	-0.456076E-05
-0.236199E-11	0.492433E-08	-0.253332E-07	-0.519756E-09	0.886698E-06	-0.456076E-05	0.500000E 01

LUN EPH TEST 12 A2 T = 5.00

0.913335E-23	-0.155851E-19	0.303004E-20	0.224181E-20	-0.342869E-17	-0.666682E-18	-0.611261E-11
-0.155851E-19	0.325043E-16	0.631828E-17	-0.342869E-17	0.585070E-14	0.113749E-14	0.127484E-07
-0.303004E-20	0.631828E-17	0.122816E-17	-0.666681E-18	0.113749E-14	0.221149E-15	0.247807E-08
0.224181E-20	-0.342869E-17	-0.666681E-18	0.585260E-18	-0.841583E-15	-0.163651E-15	-0.134477E-08
-0.342869E-17	0.585070E-14	0.113749E-14	-0.841583E-15	0.128714E-11	0.250275E-12	0.229470E-05
-0.666682E-18	0.113749E-14	0.221149E-15	-0.163651E-15	0.250275E-12	0.486639E-13	0.446132E-06
-0.611261E-11	0.127484E-07	0.247807E-08	-0.134477E-08	0.229470E-05	0.446132E-06	0.500000E 01

COS(EL) = 0.867101E 00

CP MATRIX 12 QP

1.000000E 00	-0.	-0.	-0.	-0.186265E-07	-0.	-0.

FIGURE 3.

LUNAR EPHEMERIS TEST

```
0.100008E 01  0.394151E-06 -0.            0.348310E 04  0.686413E-03 -0.
0.394161E-06  0.999958E 00  0.            0.686418E-03  0.348295E 04  0.
0.            0.            0.999958E 00  0.            0.            0.348295E 04
0.487884E-07  0.339488E-09  0.            0.100008E 01  0.788291E-06  0.
0.339502E-09 -0.243921E-07 -0.            0.788301E-06  0.999958E 00 -0.
0.            0.           -0.243942E-07  0.            0.            0.999958E 00
```

```
                    SIN(TH-THO) =  0.9277879E-02     COS(TH-THO) =  0.9999570E 00

R =  0.3850002E 09   XP =  0.3849836E 09   YP =  0.3571985E 07   XDP = -0.9391778E 01   YDP =  0.1025519E 04

                    LATITUDE =  0.3836632E 01       LONGITUDE =  0.6050705E 02

ORB INCL =  0.1830800E 02            FL PATH ANGLE =  0.6886867E-02                INERT HEAD =  0.7208503E 02
```

```
                    QE MATRIX      12     QE      T =    58.05

0.102556E 04  0.            0.            0.            0.385000E 09  0.            0.
0.100004E 01  0.927788E-02  0.            0.348295E 04  0.323151E 02  0.            0.
-0.107301E-09 -0.243942E-07 0.           -0.915767E-02  0.999916E 00  0.            0.
-0.234740E-10 -0.259729E-08 0.           -0.975033E-03 -0.179760E-04  0.            0.
```

INPUT DATA

```
01    0.1752500E 07    A1
02   -0.               A4
03    0.1701720E 04    A5
04    0.1000000E 01    GAM ID
05    0.1830800E 02    BETA
06   -0.               XI
07    0.1800000E 03    ETA
08    0.1800000E 03    ZETA
09    0.4040000E 02    LAMBDA
10   -0.3700000E 01    ALPHA
11    0.7291160E-04    OMEGAE
12    0.2663800E-05    OMEGAM
13    0.6378100E 07    RHOE
14    0.3850000E 09    RHOM
15    0.4896000E 13    MU
16    0.5000000E 01    D TIME
16    0.5805000E 02    D TIME
17   -0.               REENTRY RAD
18    0.4000000E 01    BIG L
19    0.6000000E 02    SMA L
20    0.1000000E 01    RRATE IND
21    0.1000000E 01    RANGE IND
22    0.1000000E 01    Q IND
23    0.5805000E 02    QF IND
24    0.1000000E 01    ANG 1 IND
25    0.1000000E 01    ANG 2 IND
26   -0.               PVW IND
27    0.1000000E 01    T INIT
28    0.1000000E 01    T INCR
29    0.3000000E 02    DIMENS
30   -0.               LAMBDA2
31   -0.               ALPHA2
32    0.1000000E 01    M-S IND
```

FIGURE 4.

INPUT DATA

25	0.1000000E 01	0.2014955E-11	0.	0.8404681E-09	0.1007477E-12	0.
26	0.2014955E-11	1.0000000E 00	0.	0.1007477E-12	-0.4202340E-09	0.
27	-0.	0.	1.0000000E 00	0.	-0.	-0.4202341E-09
28	0.6000000E 02	0.1851184E-09	0.	0.1000000E 01	0.4029910E-11	0.
29	0.4557228E-09	0.6000000E 02	0.	0.4029910E-11	1.0000000E 00	0.
30	-0.	0.	0.6000000E 02	0.	-0.	1.0000000E 00
25	0.1000000E 01	0.1611964E-10	0.	0.1680936E-08	0.4029910E-12	0.
26	0.1611964E-10	0.9999999E 00	0.	0.4029910E-12	-0.8404680E-09	0.
27	-0.	0.	0.9999999E 00	0.	-0.	-0.8404681E-09
28	0.1200000E 03	0.1086182E-08	0.	0.1000000E 01	0.3223928E-10	0.
29	0.1528543E-08	0.1200000E 03	0.	0.3223928E-10	0.9999999E 00	0.
30	-0.	0.	0.1200000E 03	0.	-0.	0.9999999E 00
25	0.1000000E 01	0.5440379E-10	0.	0.2521404E-08	0.9067298E-12	0.
26	0.5440378E-10	0.9999999E 00	0.	0.9067297E-12	-0.1260702E-08	0.
27	-0.	0.	0.9999999E 00	0.	-0.	-0.1260702E-08
28	0.1800000E 03	0.5023917E-08	0.	0.1000000E 01	0.1088076E-09	0.
29	0.5478629E-08	0.1800000E 03	0.	0.1088076E-09	0.9999999E 00	0.
30	-0.	0.	0.1800000E 03	0.	-0.	0.9999999E 00
25	0.1000000E 01	0.1289571E-09	0.	0.3361872E-08	0.1611964E-11	0.
26	0.1289571E-09	0.9999998E 00	0.	0.1611964E-11	-0.1680935E-08	0.
27	-0.	0.	0.9999998E 00	0.	-0.	-0.1680936E-08
28	0.2400000E 03	0.1556670E-07	0.	0.1000000E 01	0.2579142E-09	0.
29	0.1578189E-07	0.2400000E 03	0.	0.2579142E-09	0.9999998E 00	0.
30	-0.	0.	0.2400000E 03	0.	-0.	0.9999998E 00
25	0.1000001E 01	0.2518694E-09	0.	0.4202340E-08	0.2518694E-11	0.
26	0.2518693E-09	0.9999997E 00	0.	0.2518693E-11	-0.2101169E-08	0.
27	-0.	0.	0.9999997E 00	0.	-0.	-0.2101170E-08
28	0.3000001E 03	0.3791561E-07	0.	0.1000001E 01	0.5037387E-09	0.
29	0.3811951E-07	0.3000000E 03	0.	0.5037386E-09	0.9999997E 00	0.
30	-0.	0.	0.3000000E 03	0.	-0.	0.9999997E 00

FIGURE 5.

EPHEMERIS DATA

0.108118E 01	0.116565E-01	-0.	0.307933E 03	0.174472E 01	-0.	0.	0.
0.119449E-01	0.961083E 00	0.	0.175917E 01	0.296237E 03	0.	0.	0.
0.	0.	0.959375E 00	0.	0.	0.295929E 03	0.	0.
0.536510E-03	0.114800E-03	0.	0.107766E 01	0.229733E-01	0.	0.	0.
0.119578E-03	-0.246201E-03	-0.	0.232612E-01	0.964536E 00	-0.	0.	0.
0.	0.	-0.268788E-03	0.	0.	0.959435E 00	0.	0.
0.	0.	0.	0.	0.	0.	0.100000E 01	0.
0.	0.	0.	0.	0.	0.	0.	0.100000E 01
0.	0.	0.	0.	0.	0.	0.	0.
0.	0.	0.	0.	0.	0.	0.	0.
0.	0.	0.	0.	0.	0.	0.	0.
0.	0.	0.	0.	0.	0.	0.	0.
0.	0.	0.	0.	0.	0.	0.	0.
0.	0.	0.	0.	0.	0.	0.	0.

0.	0.	0.	-0.147349E-07	0.	-0.422408E 04
0.	0.	0.	-0.146088E-08	0.	0.443876E 05
0.	0.	0.	0.	0.	0.
0.	0.	0.	-0.987459E-10	0.	-0.412891E 02
0.	0.	0.	-0.148584E-10	0.	0.291993E 03
0.	0.	0.	0.	0.	0.
0.	0.	0.	0.	0.	0.
0.	0.	0.	0.	0.	0.
0.100000E 01	0.	0.	0.	0.	0.
0.	0.100000E 01	0.	0.	0.	0.
0.	0.	0.100000E 01	0.	0.	0.
0.	0.	0.	0.100000E 01	0.	0.
0.	0.	0.	0.	0.100000E 01	0.
0.	0.	0.	0.	0.	0.100000E 01

SIN(TH-THO) = 0.2869279E-00 COS(TH-THO) = 0.9579522E 00

R = 0.1755103E 07 XP = 0.1681304E 07 YP = 0.5035880E 06 XDP = -0.4710512E 03 YDP = 0.1632690E 04

LATITUDE = -0.1593382E-10 LONGITUDE = -0.1671991E 02

ORB INCL = 0.1800000E 03 FL PATH ANGLE = 0.5806204E 00 INERT HEAD = 0.2700000E 03

QE MATRIX 13 QE T = 5.00

0.170172E 04	0.	0.	0.	0.175250E 07	0.	0.
0.103918E 01	0.286928E-00	0.	0.295490E 03	0.866699E 02	0.	-0.145345E-07
-0.338317E-04	-0.268376E-03	0.	-0.276384E-00	0.920368E 00	0.	0.130968E-10
-0.152627E-06	-0.547410E-06	0.	-0.563745E-03	-0.331739E-03	0.	0.566653E-13

FIGURE 6.

QE AND Q MATRIX

APOLLO NOTE NO. 376
(Task I, Item IB)

H. R. Wright
25 October 1965

SOME COMMENTS CONCERNING EQUIVALENT SLAB THICKNESS AND SCALE HEIGHT INTERPRETATIONS IN RELATION TO THE QUESTION OF THERMAL EQUILIBRIUM

INTRODUCTION

Physically, the scale height H and the equivalent slab thickness y, are about as simple to interpret as the layer height, h_m. Briefly stated, y or the more commonly used H, are measures of total ionization along the ray provided the vehicle being tracked is not actually in the ionosphere. Both are more critical parameters than h_m. Quantitatively, H appears as the quarter layer thickness in the parabolic approximation obtained by expanding the Chapman function for an overhead sun near the F-2 peak ionization level. It varies directly with the temperature, T, and inversely with the molecular mass, M, through

$$H = kT/Mg \tag{1}$$

where k is Boltzmann's constant and g, the acceleration of gravity, may be treated as a constant through the ionosphere only for rough approximations.

SOME PRACTICAL CONSIDERATIONS CONCERNING THE MEANING OF THE TERM "SCALE HEIGHT"

For the single component Chapman layer M is most frequently taken to be that for atomic oxygen in spite of the fact that only at levels well above h_m and below 900 km or so is this even approximately true. From this simplified point of view, "scale height" is a direct measure of the temperature as well as the thickness of the ionosphere.

Such an approximation is very useful for making rough refractive index estimates, but its limitations should be recognized. To begin with, the real atmosphere near h_m is a varying multicomponent gas. If this variation is allowed for and M is taken to be the mean molecular mass near h_m, then the definition (1) is identical with the scale height for that region as defined by the familiar barometric equation for a neutral perfect gas atmosphere, but now the temperature is not determined by a measurement of H alone.

Despite this implied definition, the term "scale height" has come to be somewhat ambiguous. In Chapman theory, it is the quantity kT/Mg with reference to the ionizable particles near h_m, but to avoid confusion and, unless otherwise noted, this convention will be followed here and the notation H_m will be used. At the same time, some workers, King et. al.[19] for example, use "scale height" as the quantity H which fits electron density data to an exp-h/H curve where here h is the height above some reference level. They find the equilibrium electron density distribution is determined through

$$-1/H = d/d\zeta \ (\log N) = -M_i g/k(T_i+T_e) - 1/(T_i+T_e) \cdot d/d\zeta \ (T_i+T_e) \qquad (2)$$

where N is the electron density and ζ, the "geopotential altitude", is defined by

$$\zeta = hR/(R + h) \qquad (3)$$

with R being the Earth radius, h the altitude and the subscripts e and i refer to electrons and ions, respectively. Others, Baxter and Kendall[2] for instance, refer to "scale height" as $kT/M_i g$ for ions, a quantity that is sometimes referred to as the "electron scale height". Keep in mind that the latter usage implies thermal equilibrium exists in a strict sense because then the neutrals, electrons and ions must be at the same temperature. When the last two definitions

are used, the data often are fitted to an exp-(h/2H) curve in contrast to the convention followed by King, et al.[19].

Under conditions where it may not be assumed that electron and ion temperatures are necessarily equal, but where each species has attained an equilibrium distribution, "electron scale height" for the ion-electron gas in a one component ionosphere has been taken to be

$$H_e = k(T_e+T_i)/(M_i+M_e) \simeq k(T_e+T_i)/M_i g \tag{4}$$

as was done by Nelms[21]. Effectively, a factor of two or more is thus introduced. Its use is justified by the fact that well above h_m diffusive processes dominate gravitational forces with ionization and recombination being negligible. If losses may be ignored under these conditions, Bourdeau[4] has taken the corresponding electron distribution law to be that of a hydrostatic process with the right term of equation (2) omitted. The ionization then follows a distribution as though it is at a temperature T_e+T_i. Thus, even at equilibrium, the electron scale height is twice that of the neutrals as was realized earlier by Johnson[18].

Usually, it is only the electrons that are assumed to be hotter than the neutrals, but Hines[17] has emphasized that if diffusive equilibrium exists and the distribution is controlled by hydrostatic as well as ballistic processes, as it is in the exosphere, then even the ions have a greater scale height than the neutrals. In this case, the definition is $H_i = -N_i dh/dN_i$. When defined in this manner, he attributes the greater "ion scale height" to differential diffusion of electrons and ions, a process in which the ions, although much more massive than the electrons, are also heated in response to the resultant electric field. Despite the complexity of this situation, the classical temperatures corresponding to T, T_e and T_i are defined for the neutral, electron and ion populations provided only that each obeys a Maxwellian velocity distribution. In what follows the ionospheric plasma then will be considered to be at equilibrium even though $T < T_i < T_e$.

When departures from equilibrium exist, the situation is more complicated than just indicated. Such a situation exists, for example, while electrons or protons are being reduced to thermal energies after injection into the ionosphere by energetic photo processes or from the solar flux. Particle acceleration, especially electrons, in ionospheric electric fields also add non-thermalized charge populations at higher altitudes where the collision frequency is low. Current theory is not well developed concerning non-equilibrium distributions, however, and it will not be pursued further. This lack of theoretical guidance, notwithstanding, the scale height or the related "equivalent slab thickness", whether deduced from an equilibrated distribution or not, is such an important model parameter that a separate and more detailed discussion of the experimental evidence will be given in a later note.

THE EQUILIBRIUM QUESTION AS IT RELATES TO THE SCALE HEIGHT OR EQUIVALENT SLAB THICKNESS

Serious departures from thermal equilibrium in the ionosphere are now recognized by most investigators. This complicates the interpretation of both y and H_m as well as the related parameter Y_m (the "parabolic layer half thickness"), and the NBS parameter "Scat" = $Y_m/2$ ("Scale height at the F2 peak"). In simplified theory, any one of these parameters, together with N_m, the F2 peak electron density, is proportional to n_t, the ionospheric electron content. Since the latter is proportional to the S-band phase path decrease produced by the ionosphere, it is clear that any deviation from equilibrium has a direct bearing on refractive index calculations.

Non-equilibrium data applications related to any of the parameters y, Y_m, H or Scat in refractive index calculations become involved, first of all, by the fact that when the electron temperature T_e and ion temperature T_i differ, the relation between Scat, for example, and the ionizable neutral scale height must be written [26]

$$H = 2\,\mathrm{Scat}/(1 + T_e/T_i) \tag{5}$$

Secondly, not only must T_e/T_i be established before definite scale height interpretations are possible, but a knowledge of M_i is required also as has been stressed by Nelms[21].

Striking effects are implied by equation (5). Dalgarno and McElroy[8] found in fact that rough theory indicates T_e should "run away" for a short period at dawn. Since there is no reason to expect a similar response from either the massive ions or neutrals, then H would also "run away". While this point is still in question, accumulating experimental evidence [10] supports an earlier theoretical conclusion by Dalgarno, et. al. [9] that even when the sunrise period is excluded T_e may be expected to exceed T_i by as much as 1500°K at altitudes between 120 km and 400 km in an undisturbed ionosphere. This would decrease H to 0.67 Scat for typical conditions.

Evans and Lowenthal[15] find that as observed from the Millstone Observatory T_e/T_i is close to unity only after sunset when backscatter experiments indicate a sharp drop in T_e[11]. This more or less confirms earlier experiments of an entirely different nature conducted by Nagey et. al. [20] in which electrostatic probes were ejected over Eglin Air Force Base near midday August 3, 1963 and midnight October 26, 1962. Conditions near the F2 peak were found to be far from thermal equilibrium on the midday flight with T_e/T estimated as 2750°K/1650°K. At midnight, however, it appeared that T_e/T_i was unity. Rocket and satellite experiments conducted from Kuhlungsborn in East Germany also indicate the daytime T_e greatly exceeds T,[23] especially in summer. Further support for these findings are the daytime departures from equilibrium that have been inferred from topside sounder ionograms by Bauer and Blumle[1].

Based on rocket flown electrostatic probe data, Spencer et. al. [24] concluded that not even ions and neutrals equilibrated

below 420 km either over Fort Churchill or Wallops Island. In this connection, however, Bourdeau[4] has noted that equilibrium appears to be established above 450 km except for a brief period at dawn. Evans[12] has noted the doubtful validity of assuming $T_e = T_i = T$, but argues that even if the assumption $T_e/T_i = 1$ is invalid, it is still reasonable to take $T_i = T$ because of the essential mass equality of the ions and neutrals. More recently the latter author [13] observed, however, that vertical radar backscatter experiments at Millstone Hill show that T_i may exceed T in the upper F region.

Based on Ariel I satellite probe measurements between 400 and 1200 km, Bowen, et. al., [5] concluded that T_e is closely linked with the Earth's magnetic field, being almost symmetrical and increasing with latitude. The latter investigators found no evidence for a dawn T_e "run away", however. Finally, Explorer 17 electrostatic probe measurements [7] also indicated departures from equilibrium having marked increases with latitude during the day.

At variance with the departure from equilibrium observed in temperate latitudes, Bowles, et. al.[6] report that except at daybreak, electrons and ions in the equatorial ionosphere are in equilibrium near the maximum ionization levels as determined by incoherent scatter echoes.

Despite the active investigations now in progress for the purpose of clarifying the equilibrium question, available data are inadequate as a basis on which to make definite statements regarding either Scat or H. Harris and Priester[16], for example, very recently advised caution even regarding the assumption that temperature and density are in phase. Stein and Walker[25] find, in fact, that densities may be made to agree with drag data over a wide range of boundary conditions and this, of course, places previously accepted temperatures in question. They point out that drag inferred temperatures may be in error by as much as 25%, primarily due to uncertainty

regarding the atomic oxygen population.

Further reasons for caution in statements regarding either temperatures or any of the thickness parameters arise from the fact that the three principal measurement techniques; rocket, satellite and radar backscatter experiments; yield results that are difficult to reconcile. Evans[14] has compared T_e determinations by these methods and emphasizes that daytime temperate latitude results obtained by Ariel I and Explorer 17 satellites are in marked disagreement. Both Explorer 17 data and the Millstone radar indicate a diurnal pattern for the spring of 1963 in the F regions with T_e rising from about 1000° - 1200°K before ionospheric dawn to about 2300-3000°K at about 06-08h EST. Ariel results, on the other hand, indicate that T_e peaks at less than 1750°K shortly after 08h EST.

Another matter about which there is conflicting evidence is the T_e height gradient. Rocket experiments made during the day indicate T_e is probably isothermal but both satellite and radar results show a small height gradient having the order of 1°K/km. At night all techniques indicate T_e increases monotonically with height but the radar measurements consistently show higher nocturnal T_e values than the satellites.

All things considered, it must be assumed that outside equatorial regions, T_e/T_i reaches values at least as high as 2.2 and probably 2.5. The diurnal pattern is not well established, but it appears that the Explorer results[7] do not exclude a shape following the slab model proposed in Apollo Note 317, with Figure 5 of that report scaled up by an appropriate factor.

LIST OF REFERENCES

1. Bauer, S. J. and L. J. Blumle, "Mean Diurnal Variation of the Topside Ionosphere at Mid-Latitudes", J. Geophsy. Res., No. 17, pp 3613-3618, Sept. 1, 1964.

2. Baxter, R. G. and P. C. Kendall, "Diffusive Equilibrium of the Topside Electron Density in the F2 Region", JATP 27, No. 2, February 1965, pp. 129-132.

3. Bourdeau, R. E., "Rocket and Satellite Investigations of the Ionosphere", American Geophysical Union, Vol. 44, p. 443-446, 1963.

4. Bourdeau, R. E., "Space Flight Studies of the Ionosphere", Geophysics and Astronomy in Space Exploration, NASA SP-13, p. 7, December 1962.

5. Bowen, P. J., R. L. F. Boyd, C. L. Henderson, W. J. Raitt, and A. P. Willmore, "Ionospheric Results Using Langmuir Probes in the ' Ariel I' Satellite", Space Research IV, 1963 Warsaw Proceedings, John Wiley and Sons, Inc., (1964) pp 471-472.

6. Bowles, K. L., G. R. Ocho, and J. L. Gron, "On The Absolute Intensity of Incoherent Scatter Echoes From the Ionosphere", NBS J. Res. Vol. 66D, No. 4, July-August 1962, pp. 395-407.

7. Brace, L. H. and N. W. Spencer, "First Electrostatic Probe Results from Explorer 17", J. Geophys. Res., 69, No. 21, Nov. 1, 1964, pp 4686-4689.

8. Dalgarno, A. and M. B. McElroy, "Ionospheric Electron Temperatures Near Dawn", Planet Space Sciences, Vol. 13, No. 2, pp 143-145, February 1965.

9. Dalgarno, A., M. B. McElroy and R. J. Moffett, "Planetary Aeronomy VI: Electron Temperatures in the Ionosphere", NASA CR-12, September 1963

10. Evans, J. V., "Midlatitude Ionospheric Temperatures on Magnetically Quiet and Disturbed Days", Journal of Geophysical Research, Vol. 70, No. 11, pp 2726-2732, June 1, 1965.

11. Evans, J. V., "Cause of the Mid-Latitude Evening Increase in f_oF2", Journal of Geophysical Research 70, No. 5, March 1965, pp 1175-1185.

LIST OF REFERENCES (continued)

12. Evans, J. V., "Electron to Ion Temperature Ratios", Electron Density Distribution in Ionosphere and Exosphere, E. Thrane, Ed., pp 387-392, North Holland Publishing Co., 1964.

13. Evans, J. V., "Mid-Latitude Ionospheric Temperatures on Magnetically Quiet and Disturbed Days", Journal of Geophysical Research, 70, No. 11, pp 2726-2732, June 1, 1965.

14. Evans, J. V., "A Comparison of Rocket, Satellite, and Radar Determination of Electron Temperature at Mid-Latitude", Journal of Geophysical Research, 70, No. 17, pp 4365-4374, September 1, 1965.

15. Evans, J. V. and M. Loewenthal, "Ionospheric Backscatter Observations", Planetary and Space Science, Vol. 12, No. .10, October 1964, pp 915-944.

16. Harris, I. and W. Priester, "Of the Diurnal Variation of the Upper Atmosphere", Journal of Atmospheric Science, American Meteorological Society, Vol. 22, No. 1, January 1965, pp 3-10.

17. Hines, C. O., "Symposium on the Exosphere and Upper F Region, Summary of the Proceedings", Journal of Geophysical Research, Vol. 65, No. 9, September 1960, pp 2563-2569.

18. Johnson, F. S., "The Exosphere and Upper F Region", Journal of Geophysical Research, Vol. 65, No. 9, September 1960, pp 2571- 2575.

19. King, J. W., P. A. Smith, D. Eccles, G. F. Fooks and H. Helm, "Preliminary Investigation of the Structure of the Upper Ionosphere as Observed by the Topside Sounder Satellite, Alouette", Journal of Geophysical Research, Vol. 68, pp 464-487, 1963.

20. Nagy, A. F., L. H. Brace, G. R. Carignan and M. Kanal, "Direct Measurements Bearing on the Extent of Thermal Non-Equilibrium in the Ionosphere", Journal of Geophysical Research 68, No. 24, Dec. 15, 1963, pp 6401-6412.

21. Nelms, G. L., "Scale Heights of the Upper Atmosphere From Topside Soundings", Canadian Journal of Physics, 41, pp 202-206, 1963.

22. Nelms, G. L., "Ionospheric Results from the Topside Sounder Alouette", Space Research IV, 1963 Warsaw Proceedings, John Wiley and Sons Inc., pp 437-448, 1964.

LIST OF REFERENCES (Continued)

23. Schmelovsky, K. H., "Plasma Temperatures and Recombination Parameters in the Outer Ionosphere", Space Research IV, 1963 Warsaw Proceedings, John Wiley and Sons, Inc., pp 508-515, 1964.

24. Spencer, N. W., L. H. Brace and G. R. Carignan, "Electron Temperature Evidence for Nonthermal Equilibrium in the Ionosphere", Journal of Geophysical Research Vol. 67, No. 1, pp 157-175, January 1962.

25. Stein, J. A. and J. C. G. Walker, "Models of the Upper Atmosphere for a wide Range of Boundary Conditions", Journal of Atmospheric Science, American Meteorological Society, Vol. 22, No. 1, pp 11-17, January 1965.

26. Wright, J. W., "On the Implication of Diurnal, Seasonal and Geographical Variations in Composition of the High Atmosphere, From F-Region Measurements", Electron Density Distribution in Ionosphere and Exosphere, Edited by E. Thrane, pp 186-198, North-Holland Publishing Co., 1964.

APOLLO NOTE NO. 377
(Task I, Item IB)

H. R. Wright
25 October 1965

COMPUTATIONAL PROCEDURE FOR REFRACTIVE INDEX ESTIMATES BASED ON A GLOBAL TIME DEPENDENT SLAB MODEL IONOSPHERE

INTRODUCTION

Justification of the principles on which the model presented here is based was offered in Section 3, Apollo Note 317 and will not be repeated. Steps suggested for making an application are set down without comment and where they are not substantitated in Apollo Note 317 or discussed in Apollo Note 303 and Apollo Note 370, the details will be described in later notes. This particularly applies to analytical forms which are substituted for ionospheric station data.

Although an attempt was made to keep notation close to accepted practices in ionospheric literature, this was not always convenient. Consequently, an appendix has been added summarizing the conventions used. Also listed there are definitions for a number of symbols which in the interest of brevity do not appear in the text.

Computational methods for median conditions are given in the next section where it is assumed the vertical electron density profile over any given location is alpha-Chapman. Ionospheric anomalies are not treated specifically, but a procedure for estimating the variations obscured by their neglect is given beginning on Page 11. It is important to keep in mind that this model ignores the fact that the earth magnetic and rotation axes do not coincide. For that reason, longitudinal anisotropies do not appear nor are allowances made for variations in the times of the diurnal maximum and minimum which here were chosen to occur at 20 h and 14 h solar time, respectively.

Nonetheless, in the absence of solar storms or other disturbances, estimates of phase path length rate of change limits will be realistic because it is only at high magnetic latitudes that the diurnal phase shifts to universal time from solar time.

THE MEDIAN CONDITION MODEL

Equation (3.5) of Apollo Note 317 describes the total electron content variation in a vertical column through the locally uniform ionospheric model slab. For a given place on earth and any season, time of day or period in the solar cycle, the equation is

$$n_t = n_\pi \left[1 + \sqrt{(T - T_\pi)/T_1}\right] . \tag{1}$$

The parameter T_1 is not very sensitive and was taken to be 10°K in Apollo Note 317, but a better fit to the data exhibited there and to more recently reported observations is $T_1 = 1.6^\circ$K.

Numerically, equation (1) may be written

$$n_t = n_\pi \left[1 + 0.79\sqrt{T - T_\pi}\right]. \tag{1a}$$

When the inequality of the neutral gas, ion and electron temperatures is ignored, as it is when discussing a non-anomalous ionosphere, equation (1a) may be greatly simplified and written

$$n_t = n_\pi \left[1 + 0.5 \cos^2 (\psi/2)\sqrt{T_N}\right]. \tag{1b}$$

However, since estimates are desired of the effects of neglected anomalies, the application will be described as though the dependence on T is not simply removed by equation (1b). The first step when using either equation (1a) or (1b) is to establish the slab geometry,

illustrated in Figure 1, by finding the base height h_b at which the ray enters, the height h_c at which it leaves and the slab thickness at these two points. Begin by calculating the altitude h_m near the point where a rough estimate indicates the ray penetrates the F2 peak ionization level. It is suggested that this be done through

$$h_m = (1500/MUF) - 200 \quad (km) \tag{2}$$

If M(3000)F2 factors are not available for the time and location of interest, an alternate estimate may be made with

$$\begin{aligned} h_m = {} & 270\,(1+0.22\,\psi_o \sin\theta_3)\,(1+\cos^2\theta_5 \cos^6 1.5\,\psi_o)\,(1+0.001R) \\ & + 10 \sin^6 (\psi/2)\,(9+\psi_o \sin\theta_3)\,(1+0.0026R)\,(T/T_\pi) \end{aligned} \tag{3}$$

The daily sunspot numbers, R, are published in the "Quarterly Bulletin on Solar Activity", by the International Astronomical Union, M. Waldmeier, editor, Eidgen, Sternwarte, Zürich. Illustrative calculations may be made using the R value and $\bar{R}$, its monthly mean as given in Table 1. While these values are representative, it should be kept in mind that R may at times reach 350. When R is not known, take $R = 1.75\,\bar{R}$ (see Figure 2) and as a first approximation assume

$$T/T_\pi = 1 + 0.4 \cos^4 (\psi/2) \tag{4}$$

with ψ_{om} and ψ_m corresponding to the point where the ray reaches, say, the 300 km level by day and 400 km by night in the northern hemisphere and 200 km, day or night, in the southern hemisphere.

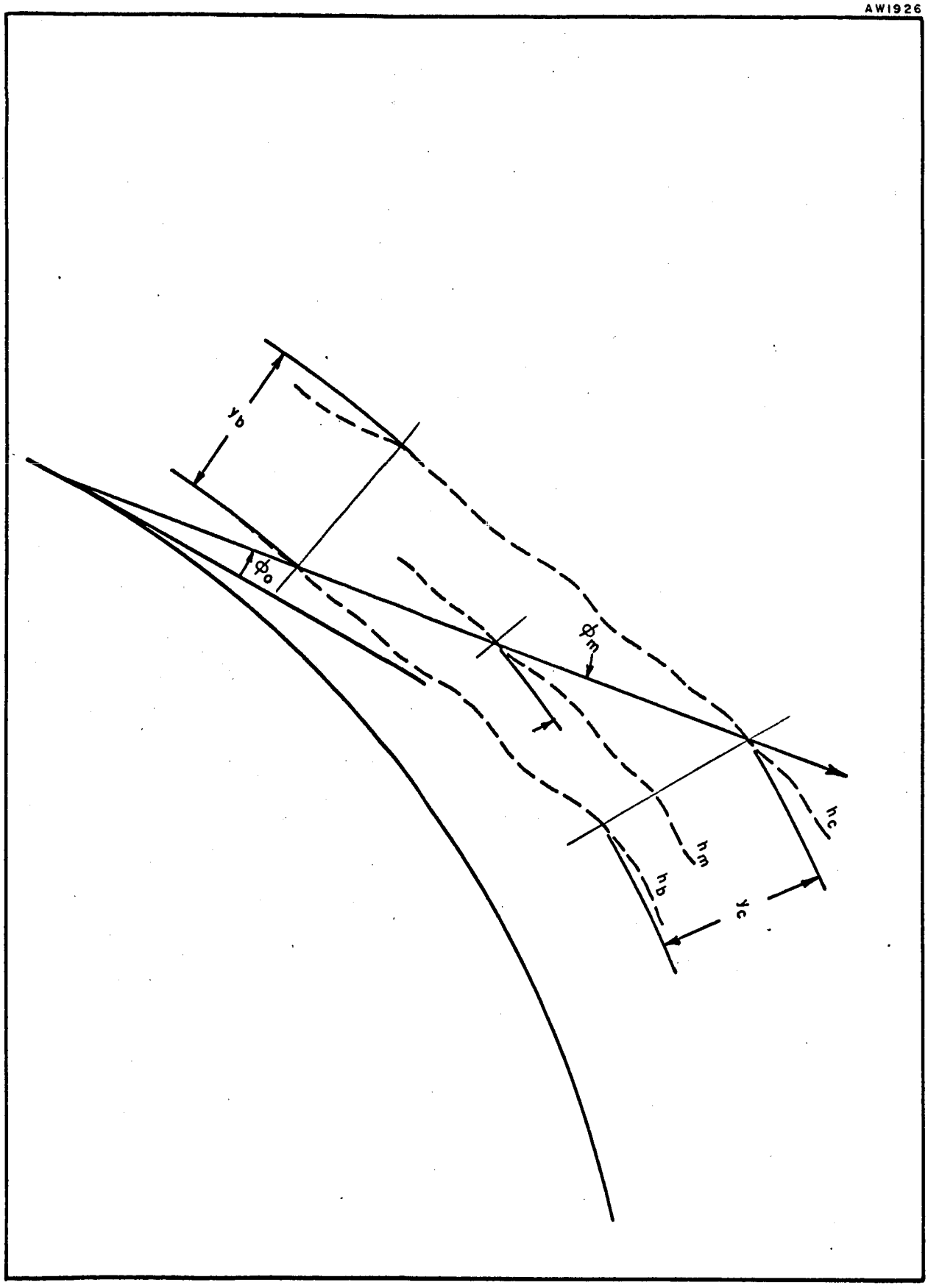

Figure 1. Geometry for the Uniform Slab model Ionosphere

TABLE 1.

Zurich Sunspot Numbers
For July through September, 1959
According to Waldmeier
(Intl. Astro. Union; Qtrly Bulletin on Solar Activity, No. 127, Feb. 1960)

1959	July	August	September
	R	R	R
1	147	194	290
2	118	210	256
3	138	213	202
4	158	225	161
5	136	212	148
6	127	207	152
7	120	179	135
8	131	175	136
9	129	170	157
10	127	155	141
11	133	180	155
12	135	160	170
13	160	125	148
14	180	139	151
15	176	144	161
16	190	157	130
17	193	166	87
18	195	174	100
19	184	182	120
20	160	180	149
21	132	200	143
22	94	204	157
23	113	205	143
24	108	217	155
25	118	212	132
26	134	220	110
27	156	231	102
28	181	274	91
29	182	301	87
30	193	292	86
31	190	284	
Mean = $\bar{R}$	149.6	199.6	145.2

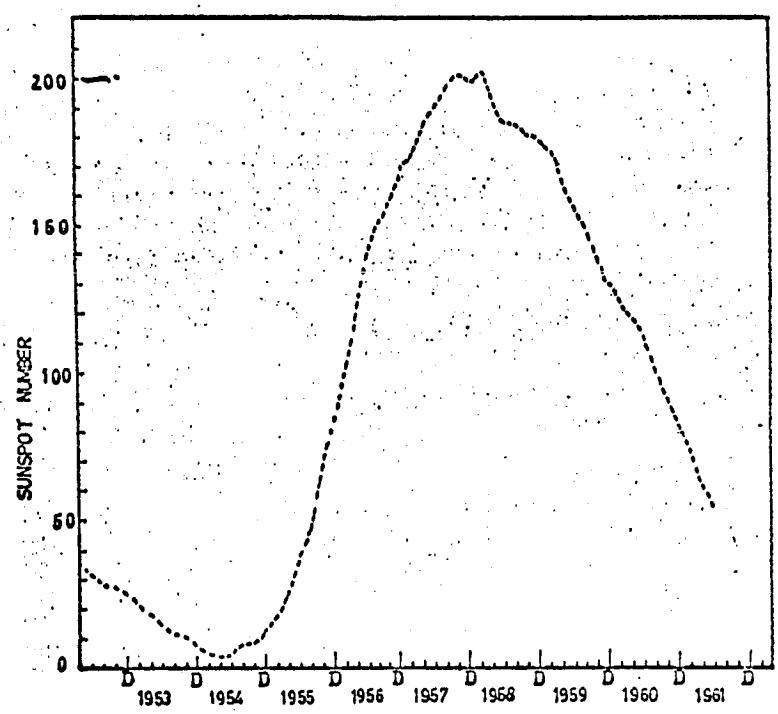

Figure 2. Sunspot activity as indicated by the parameter $\bar{R}$ during the period 1953-1961 after Singleton (JATP, 25, pp 121-149, 1963). More intensive data are given by M. Waldmeier, (editor) Quarterly Bulletin on Solar Activity, International Astronomical Union, Schulthess and Co., Zürich.

These angles may be calculated from

$$\cos \psi = \sin \lambda \sin\delta + \cos \lambda \cos\delta \cos \theta_4 \tag{5}$$

and the angle ψ_o is simply

$$\psi_o = \lambda - \delta \tag{6}$$

Note, however, that ψ_o may vary along an oblique ray with a north-south component.

Estimates are required for the ionospheric temperatures where the ray penetrates and leaves the slab. To obtain these, first estimate T_m by using the approximate ψ_m just computed for ψ in the relation

$$\begin{aligned} T = {} & (635^\circ + 0.3^\circ \bar{F} + 0.012^\circ \bar{F}^2) \left[1 + 0.4 \cos^4 (\psi/2)\right] \\ & + 2.5^\circ (F - \bar{F}) + 0.5^\circ \bar{F} \cos \theta_1 \\ & + 1.0^\circ a_p + 125^\circ \left[1 - \exp - (0.08\, a_p)\right] \end{aligned} \tag{7}$$

At any time either F or a_p are unknown, take $F = \bar{F}$ (see Figure 3), and $a_p = 0$ for quiet solar conditions. Evaluate T_π by setting $\psi = \pi$ in equation (7). Next, using the values estimated above, calculate the slab thickness where the ray penetrates the F2 peak from the equation

$$y = 0.2191\,(1 + 0.003R) \left\{ 180\, \psi_o \sin \theta_3 + T \left(\frac{6378 + h_m}{6378} \right)^2 . \right\} \tag{8}$$

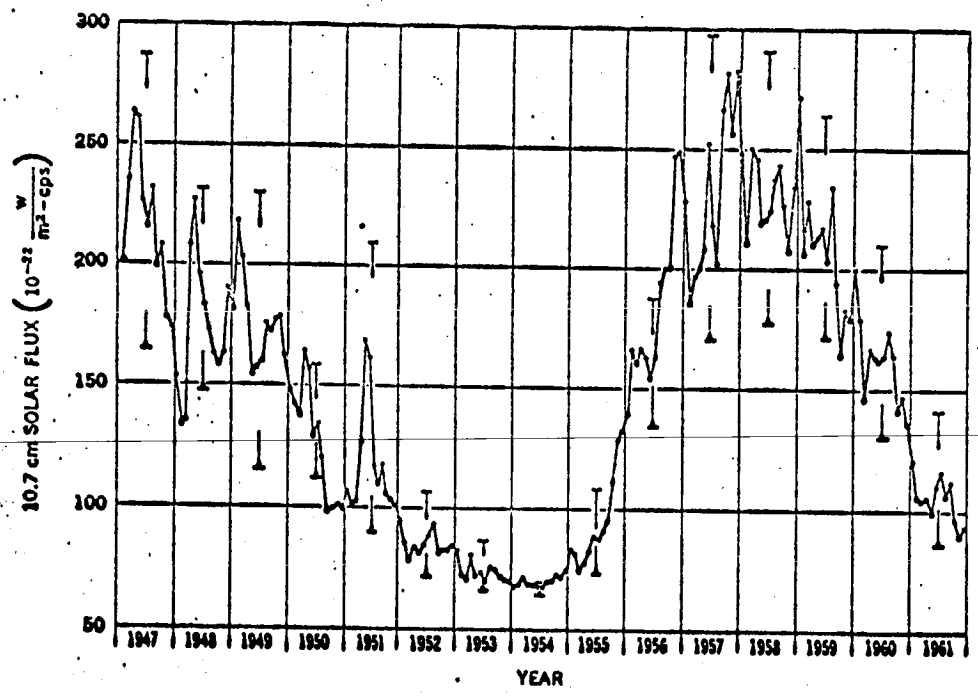

Figure 3. Variation of the Monthly Averages of the 10.7 cm Solar Flux According to Measurements by the National Research Council of Canada. Bars indicate the Maximum and Minimum of the Fluctuations in June and July of each year. Harris and Priester, NASA TND-1444, August 1962.

Its base is assumed to be located at the level

$$h_b = h_{mb} - 0.31\, y_b \tag{9}$$

and its top at the level

$$h_c = h_{mc} + 0.69\, y_c \tag{10}$$

Ignore the h_m and y variations along the ray to obtain first estimates for T_b and T_c from equation (7). This implies using the ψ_b value at a distance $0.31\, y_m \cot \phi_m$ along the slab base in the plane of the ray toward the ground station; and for ψ_c, the evaluation is made a corresponding distance $0.69\, y_m \cot \phi$ away from the ground station.

Under normal median conditions T variations along the ray are not so serious that further iteration would be profitable. On the other hand, when allowance is made for non-equilibrium conditions along a ray close to the normal of the dawn meridian, calculations for T_b and T_c may not converge rapidly. At such times, a single mean value of conditions at the slab entrance and exit points may not be realistic and it may prove necessary to determine the temperature at a number of points along the ray.

After the slab geometry and temperatures are established, the electron content calculation is simple. First extrapolate n_π to its value at the universal time of the observation using equation (3.3) in Apollo Note 317. The suggested numerical form is

$$n_\pi = 2 \times 10^{10}\, (1 + 0.02\, R) \sqrt{T_\pi} \tag{11}$$

Using equation (1), the electron content now may be calculated for points along the ray and the corresponding slab electron density variation found through

$$N_m = 10^{-5} n_t/y . \tag{12}$$

One procedure for calculating the electron content along the ray is to take an average determined from a number of points and write

$$n_S = \bar{N}_m S \times 10^5 . \tag{13}$$

An alternate method is to consider only mean N_m variations along the ray and estimate the content from

$$n_S = n_c S(1 + \sqrt{T_b/T_c})/(2y_c). \tag{14}$$

For most purposes, equation (14) is adequate and considerably simpler than equation (13). Using equation (14) the phase path length change introduced by the ionosphere is

$$\Delta \ell = -2.013 \times 10^7 n_c S (1 + \sqrt{T_b/T_c}) / (y_c f^2) \text{ (cm)}. \tag{15}$$

When using equation (13) the corresponding estimate for the change is

$$\Delta \ell = -4.026 \times 10^{12} \bar{N}_m S/f^2 \text{ (cm)} \tag{16}$$

where $\bar{N}_m$ is in electrons/cc and S is in km.

DIURNAL VARIATION RATE NEAR THE VERTICAL THROUGH A MEDIAN CONDITION SLAB WHEN THE QUIET SUN IS AT STEADY STATE

For an illustration, the diurnal phase path rate of change has been calculated for conditions so static that a_p, F and $\overline{F}$ may be considered constant but without otherwise restricting the time in the solar cycle. The one way result for near normal slab incidence is

$$\frac{\partial(\Delta\ell)}{\partial t} = 10^{17}\sqrt{T_\pi}\,(1+0.02R)\left\{0.5\sqrt{T_N}\cos\lambda\cos\delta\sin\theta_4 + 8\cot\phi\left[1+0.5\sqrt{T_N}\cos^2(\psi/2)\right]\frac{\partial\phi}{\partial t}\right\}/(f^2\sin\phi)\ \left(\frac{\text{cm}}{\text{hour}}\right) \tag{17}$$

Near the peak of the solar cycle R may reach 350, at which times T_N may be 2000°K so that for a 1 kmc signal in equatorial regions this would indicate a rate of about 0.22 cm/sec in the vertical at 08h and 20h. As another example, when the rate is calculated for the conditions of Figure 1, Apollo Note 281, which is for the 1960 summer solstice with an average λ for the subionospheric point $\overline{\lambda} \cong 48°$N, $R \cong 200$ and $T_N \cong 1100°$K, the corresponding rate is about 0.04 cm/sec while the published data indicate a higher diurnal rate of about 0.12 cm/sec. This is what would be expected, however, when allowance is made for the fact that the electron temperature considerably exceeds that of the ions during the dawn period at ionospheric levels. It should be noted however that the summer afternoons appear to be anomalous as is evident from the post 14h rise in n_t shown in that figure. For median conditions and low to moderate geomagnetic latitudes, see Figure 24, Apollo Note 303, as a more representative picture of the diurnal and seasonal variations. A good example of the diurnal variations at low latitude is Figure 4, Apollo Note 317.

It is important that this example not be considered as a demonstration of the most extreme $\Delta\ell$ variation rate possible. A vehicle parked in an orbit which passes through the F2 peak in the sunlit southern hemisphere, but where the F2 layer is at great heights in

other parts of the orbit, is one possible example where a higher $\Delta \ell$ rate may be anticipated.

DEVIATIONS FROM THE MEDIAN

A. Departures from Equilibrium Across the Dawn Meridian

Even in quiet conditions the temperature along a ray from the dark hemisphere across the dawn meridian may increase by a factor of between 1.5 and 2 in a distance corresponding to less than an hour time difference. The ratio T_c/T_b also changes by this factor since one factor refers to darkness and the other to light. This phenomenon is still under study but the basic mechanism seems to be understood. The cause of this situation is that electrons, three or four orders of magnitude less massive than the ions or neutrals, respond to solar heating very rapidly. Subsequently, they approach equilibrium by coulomb encounters with oxygen ions. An acceptable model for this process as it relates to refractive index calculations could undoubtedly be constructed, but in order to bracket the magnitude of the effect, consider the effective temperature changes linearly by a factor of two from T_b to T_c, increasing in the direction of dawn.

B. Changes in the 3-Hour Geomagnetic Index

At the peak of the strongest solar storms a_p may rise from about 0 to its defined upper limit of 400 (when $K_p = 9$) in a period of about 20 hours as during the strongest storm of the last cycle which occurred 13 November 1960 with conditions returning to normal in slightly less than two days. During a moderate solar event a_p may be taken to rise and fall at a rate of say, 4/hour, with 10/hour a possibility. Far more important than this in its direct relation to T is the fact that the electrons heat quickly as a_p rises with the net result that the effective T could rise above normal by a factor of say 50% in an hour or less after the onset of a moderate disturbance. For estimating limits on phase path length rates, assume this change is linear in time. In auroral zones this heating rate increases by a factor of four or five.

A model accounting for heating following a_p variations has not been derived but it should be remembered that since solar disturbances conform to relatively definite patterns, it may well prove feasible to predict refractive index changes, which may be expected to lag a_p by about five hours, based on monitored values of one of the solar activity indices.

C. Decimetric Solar Flux Variations

In general, the monthly average flux $\overline{F}$ does not change rapidly; further, the term $2^{\circ}.5\ (F - \overline{F})$ appearing in equation (7) often changes smoothly with a 27 day average period. Nonetheless, the daily F may show sudden and erratic changes even for relatively quiet solar conditions. Deviations of F from $\overline{F}$ at a rate in excess of 1.0 decimetric flux unit/hour should not be considered a "disturbed" condition.

D. Change in the Top-to-Bottom Electron Content Ratio

It has been observed for some years that the ratio of the electron content above and below the F2 peak can vary widely from the alpha-Chapman value of 2.15. However, since the F2 peak is quite broad, h_m may move quite appreciably without serious effect on either the total electron content or the top-to-bottom ratio. It is believed this effect may be ignored when calculating rates of change.

APPENDIX

List of Abbreviations used in Text

a_p = Three hour geomagnetic index.

d = Number of the day of the year.

$\bar{F}$ = Monthly average of the 10.7 cm solar flux in units of 10^{-22} watts/sq. meter-cps (see Figure 3).

F = Daily value of the 10.7 cm solar flux.

f = Transmitted Frequency (cps).

h_b = Slab height where the ray enters (km).

h_c = Slab height where ray leaves (km).

h_m = Altitude at which the peak F-2 ionization level is located (km).

h_{mb} = Value of h_m above point where ray enters slab (km).

h_{mc} = Value of h_m below point where ray leaves slab (km).

(MUF) = Maximum usable frequency for a 3000 km range - see hourly median (M3000) F-2 factors (mc) in "Annals of the IGY", Vols. XIII, XIV, and XV.

N = Electron density (electrons/cu cm).

N_m = Electron density at the level h_m.

n_b = Electron content along the vertical above point where ray penetrates slab base (electrons/cc).

n_c = Electron content along the vertical above point where ray penetrates top of slab (electrons/cc).

n_S = Electron content along the ray (electrons/cc).

n_t = Electron content in a vertical column above the sub-ionospheric point at the angle ψ (electrons/sq. cm).

R = Daily sunspot number.

$\bar{R}$ = Mean sunspot number (see Figure 3).

S = Path length through the slab for an undeviated ray (km)

T = Isothermal ionospheric temperature at the angle ψ (^{o}K).

T_b = Value of T at a point where ray penetrates slab base (^{o}K).

T_c = Value of T where ray penetrates top of slab (^{o}K).

T_m = Temperature at point where ray reaches the F2 peak ionization level (^{o}K).

T_N = $635^{o} + 0^{o}.3\ \bar{F} + 0^{o}.012\ \bar{F}^2$ (^{o}K).

T_π = Value of T when $\psi = \pi$.

t = Local solar time (hours) with noon at 12h and 26h = 02h.

y = Equivalent thickness of an ionosphere with uniform density equal to N_m (km).

y_b = Value of y where ray penetrates base of the slab (km).

y_c = Value of y where ray penetrates top of the slab (km).

δ = Solar declination-positive to the North

$\Delta\ell$ = Phase path length change (cm).

θ_1 = $4\pi/365\ \left[d - 97\right]$

θ_2 = $4\pi/365\ \left[d - 173\right]$

θ_3 = $2\pi/365\ \left[d - 80\right]$

θ_4 = $\pi/12\ (t - 14)$; $02 \leq t \leq 26$

θ_5 = $\pi/12\ (t - 20)$; $08 \leq t \leq 32$

λ = Geographic latitude - positive to the North.

ϕ_m = Ray elevation angle where it penetrates the F2 peak, plus the geocentric angular distance from the ground based station.

ψ = Geocentric angular distance to an ionospheric point measured from 14 hours local solar time along the solar track.

ψ_b = Value of ψ where ray enters slab.

ψ_c = Value of ψ where ray leaves slab.

ψ_m = Value of ψ where the ray penetrates the F2 peak ionization level.

ψ_o = Diurnal minimum of ψ; positive to North of solar track $= (\lambda - \delta)$.

ψ_{om} = Diurnal minimum of ψ at point where ray reaches F2 peak.

The Bissett-Berman Corporation 2941 Nebraska Avenue, Santa Monica, California EXbrook 4-3270

APOLLO NOTE NO. 378
(Task I, Item IB)

H. R. Wright
27 October 1965

PEAK IONIZATION LEVEL HEIGHT ANOMALIES

INTRODUCTION

According to simple Chapman layer formation theory, the maximum ionization production above a flat earth for a given solar zenith angle χ should occur at a height given by[19]

$$h_m = h_o + H_m \log_e \sec \chi \qquad (1)$$

where the base height, h_o, is determined when $\chi = 0$, that is, the peak ionization level at the subsolar point and H_m is the Chapman scale height. Although $\sec \chi$ in equation (1) should be replaced with a complicated function allowing for the additional atmosphere in the path of a solar ray to a spherical earth, the errors are not significant for χ less than about 60-75°. Maxima in both the ion production rate and the ion density are assumed to be at the same level, but this simplification is not at all suitable for latitude extrapolation and h_m is said to be anomalous. More detailed theory has been offered. One example is that of the "Bradbury Layer" where N_m, the peak electron density, is at an altitude considerably higher than that where ion production is a maximum. Unfortunately, even these more elaborate treatments are of limited value here. To illustrate, Shapiro[20] has analyzed routine station data from wide areas of Asia as a function of solar activity and finds that h_m often decreases toward the poles in conflict with simple theory. A similar afternoon trend appears over North America in NBS true height analyses[26].

GENERAL CONSIDERATIONS CONCERNING VERTICAL MOVEMENT OF THE F-2 LAYER

Maintenance of nighttime ionization is yet to be explained without qualification. One simple suggestion that at least accounts for

trends in F layer movements at night has been made by Hanson and Patterson[6]. They note a possibility exists that the F layer is maintained at night by an upward drift to regions where collisions are infrequent and, hence, where recombination is not a dominant process. On this basis, the F layer nocturnal midlatitude height variations, at least during the early evening, are not grossly anomalous since h_m is greater by night than by day. On the other hand, these variations are not really well described by theory even for relatively small solar angles. A difficulty pointed out by Becker[5] in commenting on a paper by Haubert and Laloe[7], is that universal time appears to correlate better with height changes than does local time in disagreement with Equation (1). Further, a striking feature of the diurnal h_m pattern is its rapid rise beginning about 0800 LT in a narrow belt centered on the magnetic equator. This "fountain effect" in the vertical ionization drift does not find an explanation in terms of any elementary theory.

Some workers have found that with all its limitations, the theoretical Chapman layer height for a spherical earth is a useful concept at sunrise near the magnetic equator[12]. It is not, however, realistic at moderate-to-high latitudes. This is illustrated in Figure 1, which was plotted based on the results of calculations reported by Shapiro[20] for two values of the mean sunspot number, $\overline{R}$. Consider the April diurnal pattern near 06h and 18h LT when $\chi \cong 90^\circ$ at Sverdlovsk. While there is a sharp drop at about 06h LT, as expected from equation (1), there is no corresponding rise at 06h LT. Further evidence for the extremely anomalous h_m variations is shown in Figures 2, 3, and 4 which were drawn by replotting data for a quiet ionosphere reported by Wright[26].

Another important height anomaly is observed at the peak of the sunspot cycle. Then h_m data show a marked asymmetry about the magnetic equator during the evening enhancement of the geomagnetic anomaly[13, 17] which is observed to occur first on the side nearest

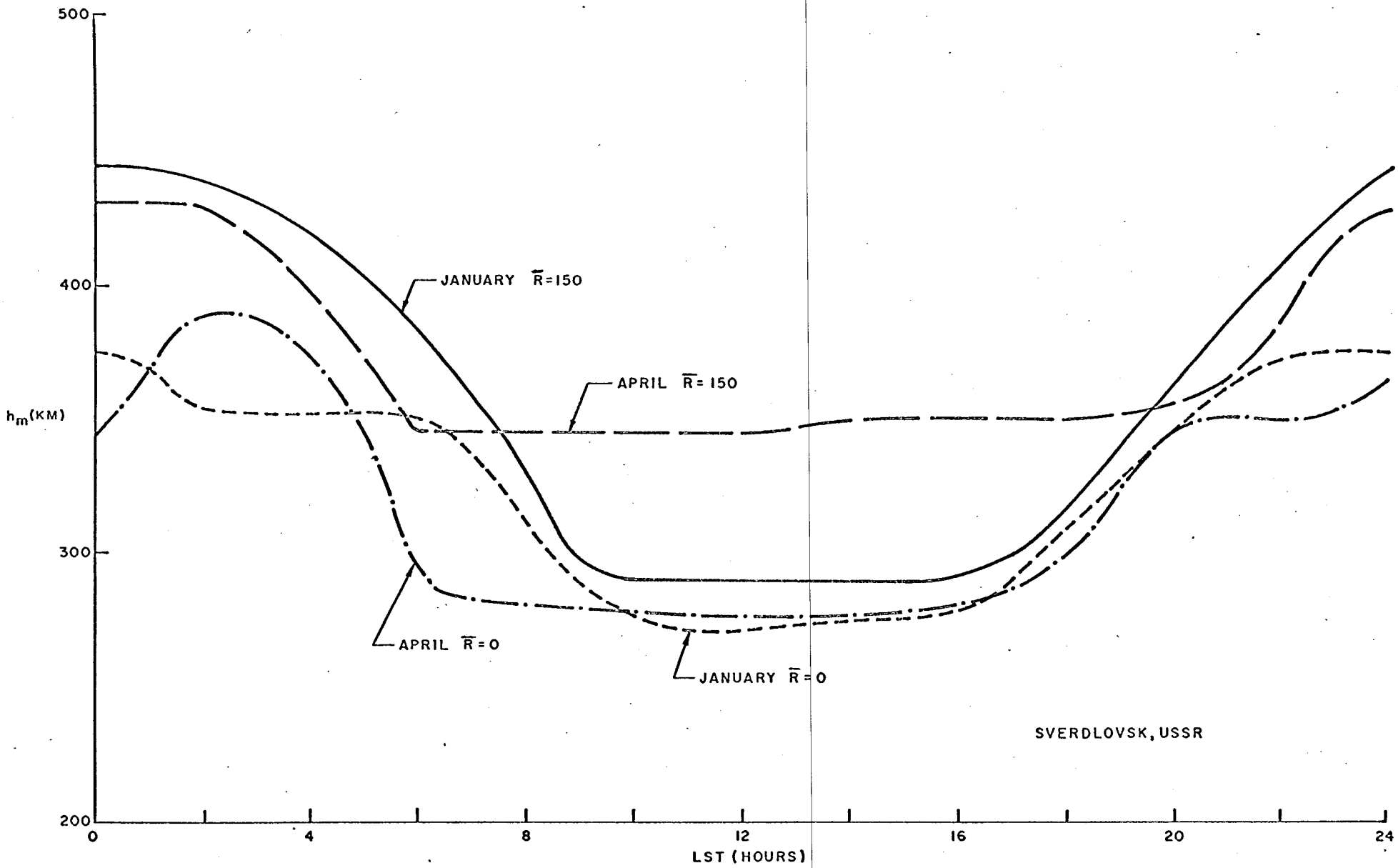

Figure 1 . Peak Ionization Level Diurnal Variation at Sverdlovsk (Magnetic Dip ≅ 72°N) Based on Computations Reported By Shapiro. (Ref. 20)

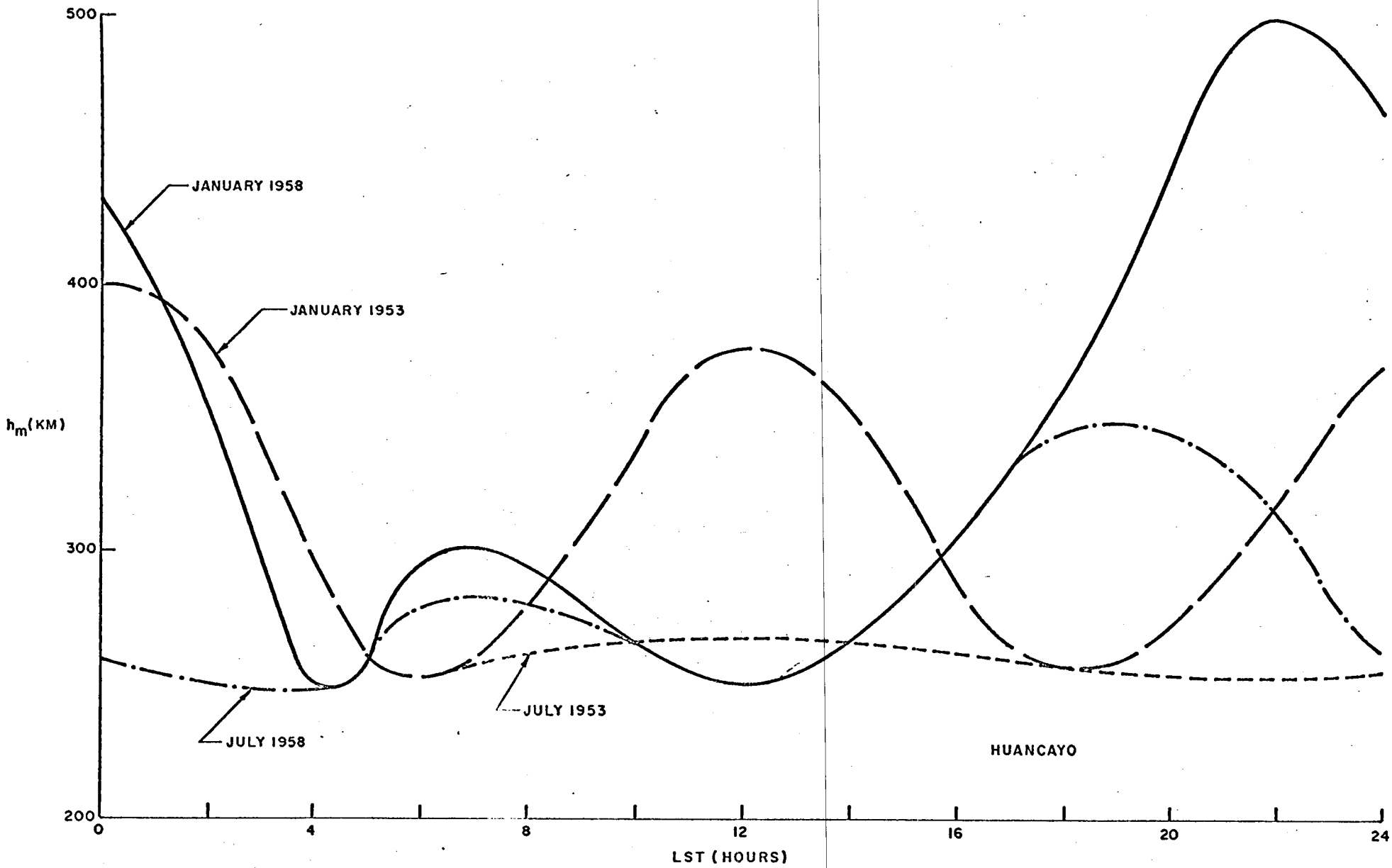

Figure 2 . Peak Ionization Level Diurnal Variation at Huancayo Replotted From Contour Maps Published by Wright. (Ref. 26)

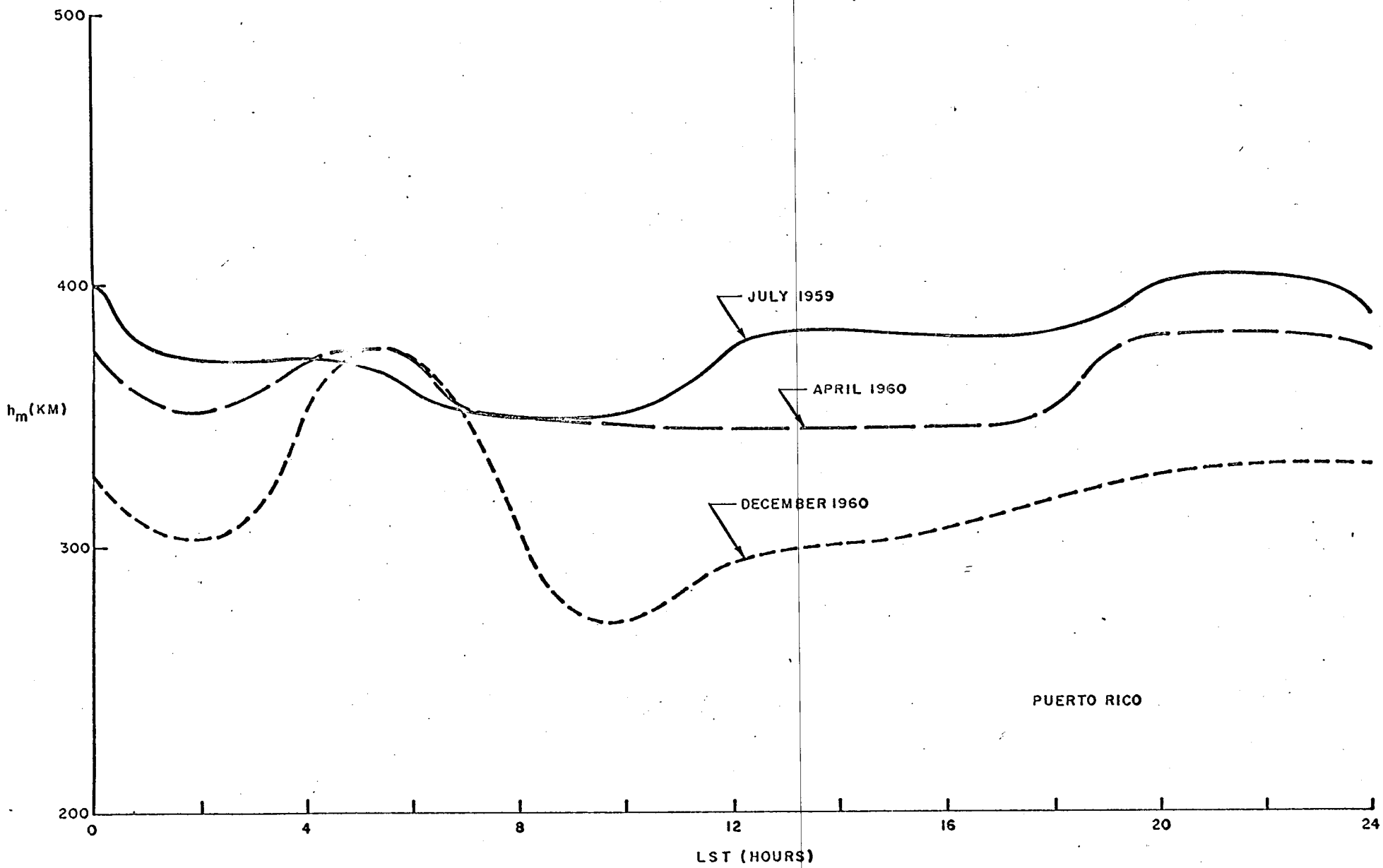

Figure 3 . Peak Ionization Level at Puerto Rico Replotted From Contour Maps Published by Wright. (Ref. 26)

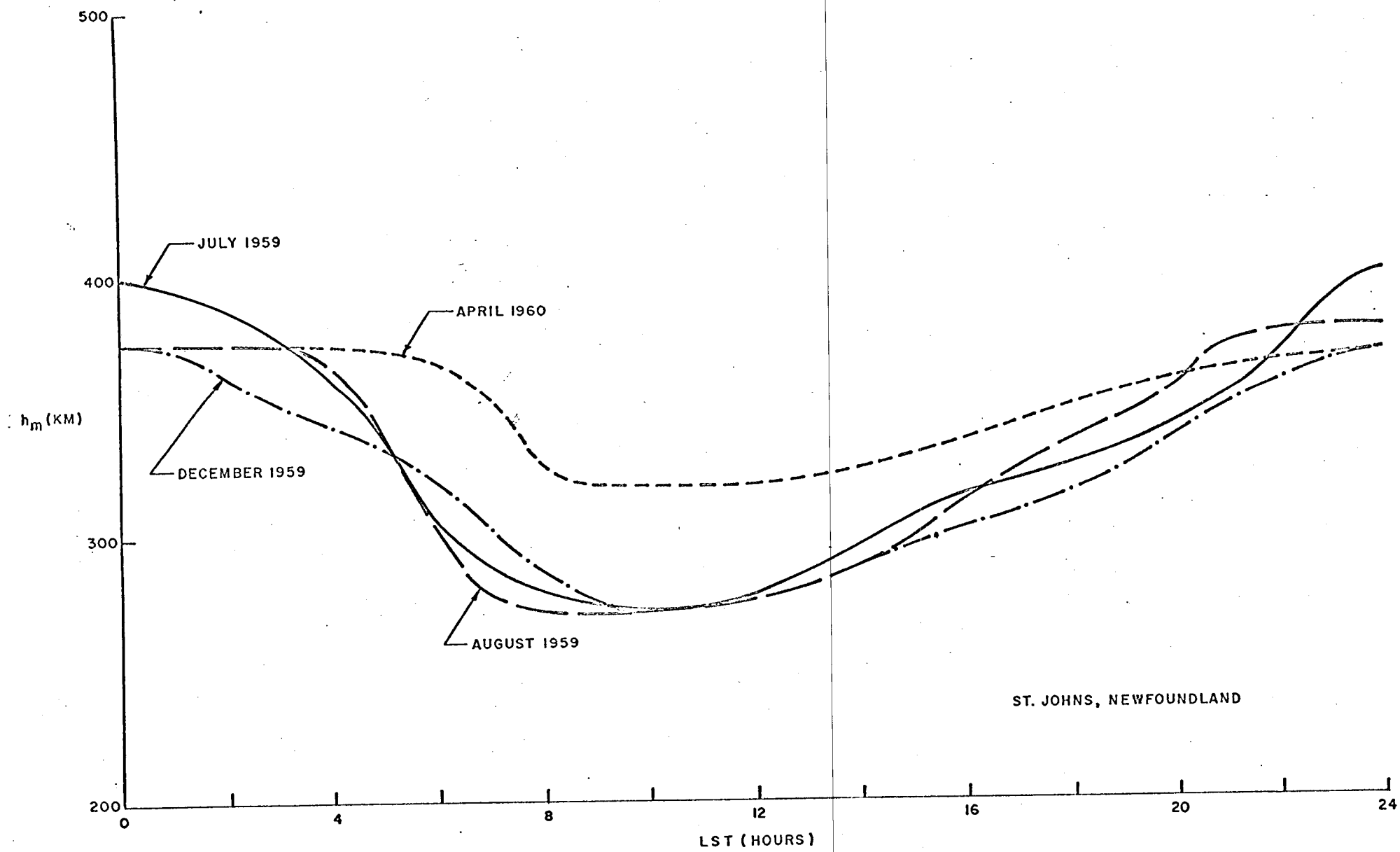

Figure 4 . Peak Ionization Level Diurnal Variation at Newfoundland Replotted From Contour Maps Published by Wright. (Ref. 26)

the geographic equator. Greater h_m values are reached in Northern latitudes of the American sector while in the African and West Asian sectors the southern heights are greatest. In the belts 10-20° magnetic, north and south, this difference may be the order of 100 km. An asymmetry also is observed during solstitial periods with h_m being lower in the winter hemisphere than in the summer hemisphere.

MODERATE AND HIGH LATITUDE F LAYER HEIGHT VARIATIONS

Even at midlatitudes where extensive observations have been made, there are difficulties in assigning h_m values. In the first place, although electron densities, N, as independently determined by the NASA Argo D4 check flight are in excellent agreement with Alouette soundings, there is usually considerable uncertainty in individual h_m values deduced from routine soundings. As an example, N accuracy on the carefully instrumented Argo D4 flight was as high as 2% below the 600 km level, 5% below 700 km and 15% below 860 km[3], but h_m, the most inaccurately measured ionospheric parameter, does not approach this precision. Furthermore, data variability is very serious. Indeed, Becker[4] reports that on comparable magnetically quiet nights at Lindau, West Germany, the layer height differences are as great as 100 km. Even on a given night, layer height changes were as great as 60 km and lasted about 2 hours. No seasonal effects appeared to be involved in the rise and fall of the F2 layer but such effects could be obscured by the data. Indicative of the h_m data reliability is the fact that Nisbet[14, 15] reports that nocturnal true heights at and above h_m as determined from ionograms appeared to be 20-40 km lower than those measured by rocket flights even though daytime results were in satisfactory agreement.

Wright[26] has examined the question of h_m variability and how it relates to Scat (NBS "scale height at F2 maximum") variability. He finds, as illustrated by Figure 5, that for quiet conditions in 1959-1960, h_m was about twice as variable at night as in the day

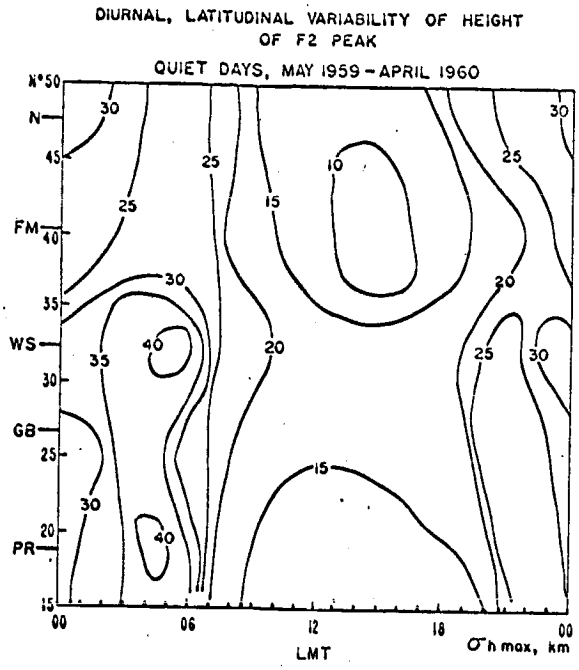

Figure 5 Diurnal h_m Variability Dependence on Latitude Expressed As the Average Standard Deviation in Kilometers for the Period May 1959 Through April 1960; Abbreviations: N, Newfoundland; FM, Fort Monmouth; WS, White Sands; GB, Grand Bahama; PR, Puerto Rico. (Ref. 26)

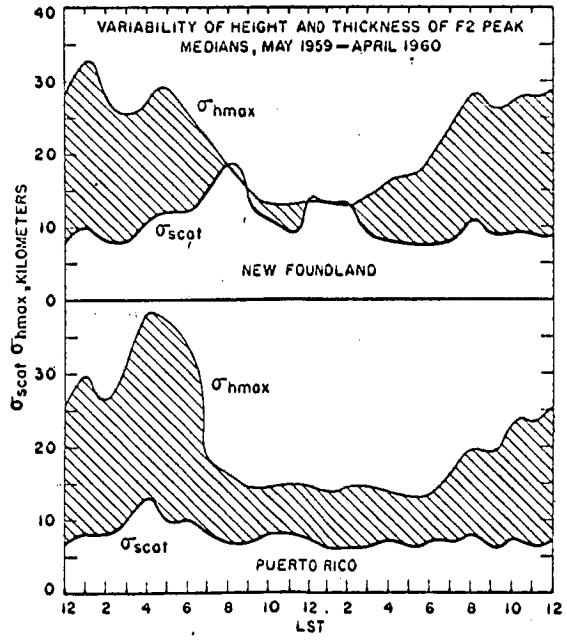

Figure 6 Comparative Diurnal Scat and h_m Variability, in Terms of Average Standard Deviation, at Two Stations for the Period May 1959 Through April 1960. (Ref. 26)

with post midnight, especially at lower latitudes, being the most variable period. Scat variability, on the other hand, is greatest at high latitudes in the early morning or sunrise intervals. The question arises as to whether or not the h_m variability may actually be due to layer thickness variability, as would be the case if the layer remained fixed in position and merely varied in thickness. Wright concludes that this is not the case. Although there is some correlation between the parameters, Scat and h_m, indications are that except at high latitudes at night, the layer may be at greatly different altitudes with little change in thickness. Thus, the large neutral scale height variability, which will be described in a later note, is exceeded by that of h_m in most applications. At high latitudes, however, they are about equal. The shaded area of Figure 6 illustrates the part of the variability that cannot be accounted for by the variability of one of the parameters. There σ is the standard deviation and h_{max} is the height of the F2 peak.

In spite of data variability, King and Scott[9] nonetheless attribute the day-to-day changes in the F2 layer height to the daily sunspot number. For the present purposes, however, a more directly applicable result is obtained when the day-to-day variations are smoothed out by taking the monthly noon median. Then a dependence on solar activity becomes quite evident. This is illustrated for Christchurch, New Zealand, in Table 1. An interesting observation in passing is that layer heights were much lower over the southern hemisphere station than those above comparable northern regions. To illustrate, Christchurch's northern counterpart would have a dip angle about midway between those at White Sands and Ft. Monmouth where, for example, on a summer noon in 1959, a year of high solar activity, a representative layer height was about 325 km. Another comparison region for which data exist is that near Hannover where the dip angle ($\cong 67^{\circ}$N) is also about the same as at Christchurch. There, during a high solar activity year such as 1958, the December

TABLE 1.

Solar Cycle Variations of December Noon Median Ionospheric Parameters at Christchurch (43°S, 172.5E, 48°S Geomag) After King and Lawden[8]

H_O = Oxygen Scale Height

Year	10.7 cm Solar Flux (watts/sq. m-cps)	Mean Sunspot No. $\bar{R}$	$N_m \times 10^{-5}$/cc	H_O (km)	h_m (km)
1949	160		3.84	41.1	189
1950	125		2.66	38.9	169
1951	100	40	2.75	38.0	165
1952	75	30	2.30	32.0	153
1953	50	25	2.21	27.0	167
1954	50	5	2.20	33.7	160
1955	125	10	3.18	39.0	185
1956	175	80	4.18	52.0	185
1957	225	160	4.44	58.2	181
1958	275	200	4.84	68.2	191
1959	175	130	3.15	45.8	171

noon layer height was about 340 km as opposed to 191 km at Christchurch. Corresponding northern and southern heights for the low activity year, 1954, were about 200 km and 160 km respectively. Note that the last example does not allow for the seasonal difference between the hemispheres. If this were done, the comparison would be even more striking because, counter to theory, generally h_m is higher at noon in summer than in winter[26].

Stubbe[23] describes the magnetically quiet noon mean December F layer height dependence on the Zürich daily sunspot number R at Lindau, West Germany, through

$$h_m = 196.5 + 0.79\,R - 1.10 \times 10^{-3}\,R^2 \text{ (kilometers)} \qquad (2)$$

and the corresponding midnight (2330-0200 LT) height by

$$h_m = 298.7 + 0.60\,R \text{ (kilometers)} \qquad (3)$$

Figures 7 and 8 illustrate these relations and the data from which they were deduced. The extreme variability for a given time of day and sunspot number particularly should be noted. Even the average diurnal changes exhibit extreme variability as indicated by Figure 9.

EQUATORIAL F LAYER HEIGHT

At the dip equator the F layer maximum ionization level, unlike that in any other part of the world, rises from a diurnal morning low to great heights in the late afternoon. Experimental work related to this matter has been severely hampered because bottomside data are nonexistent over most of the equatorial regions. True height determinations at the few stations reporting indicate, however, that typically in September the altitude range of h_m extends from 325 km at 0700 LT to 500 km by 1200 LT[16]. Recent topside Alouette

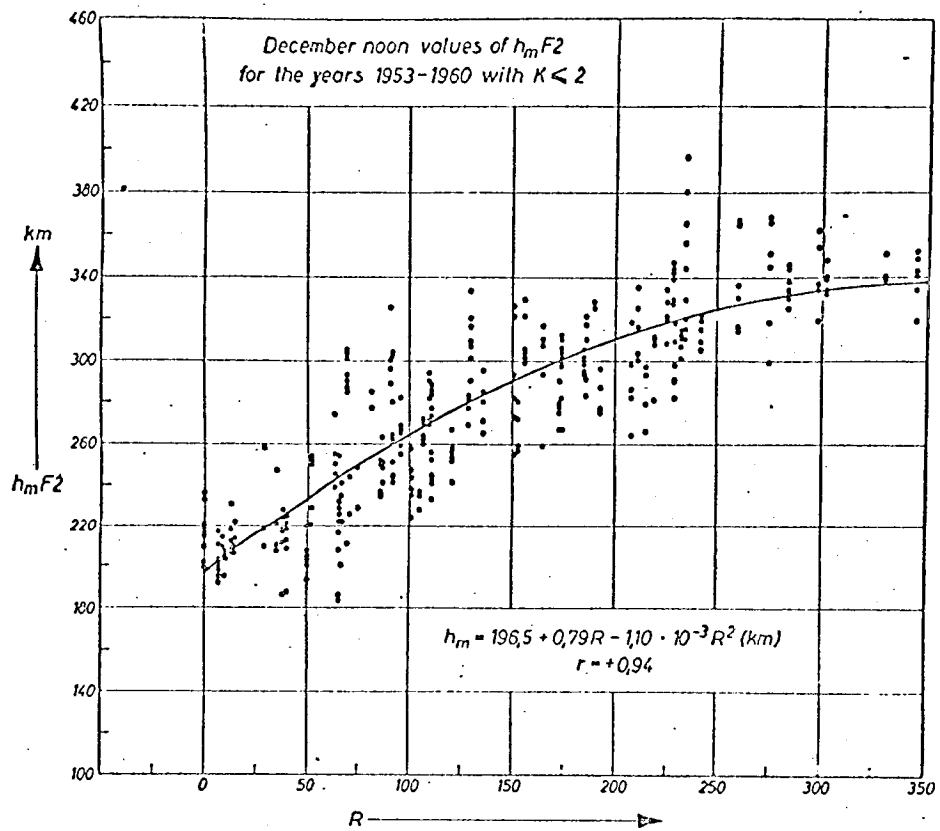

Figure 7 Noon Mean h_m Values Plotted Against Daily Zurich Sunspot Number R for Magnetically Quiet December Days from 1953 to 1960 as Deduced by Stubbe from Ionograms Taken at Lindau/Harz. (Ref. 23)

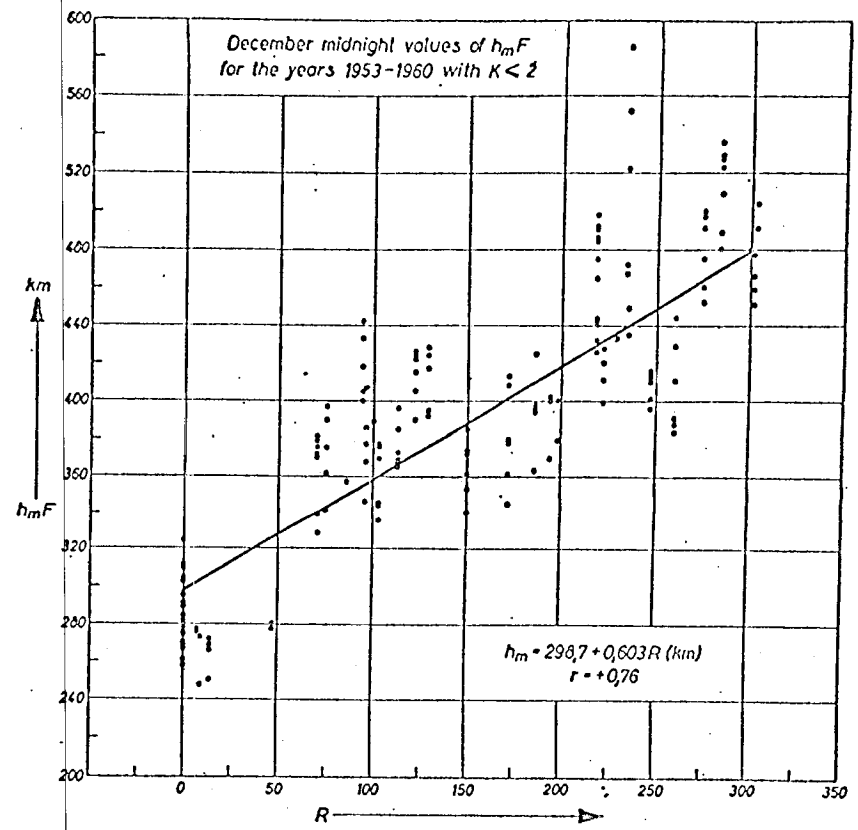

Figure 8 Midnight Mean h_m Values Plotted Against Daily Zurich Sunspot Number R for Magnetically Quiet December Nights from 1953 to 1960 as Deduced by Stubbe from Ionograms Taken at Lindau/Harz. (Ref. 23)

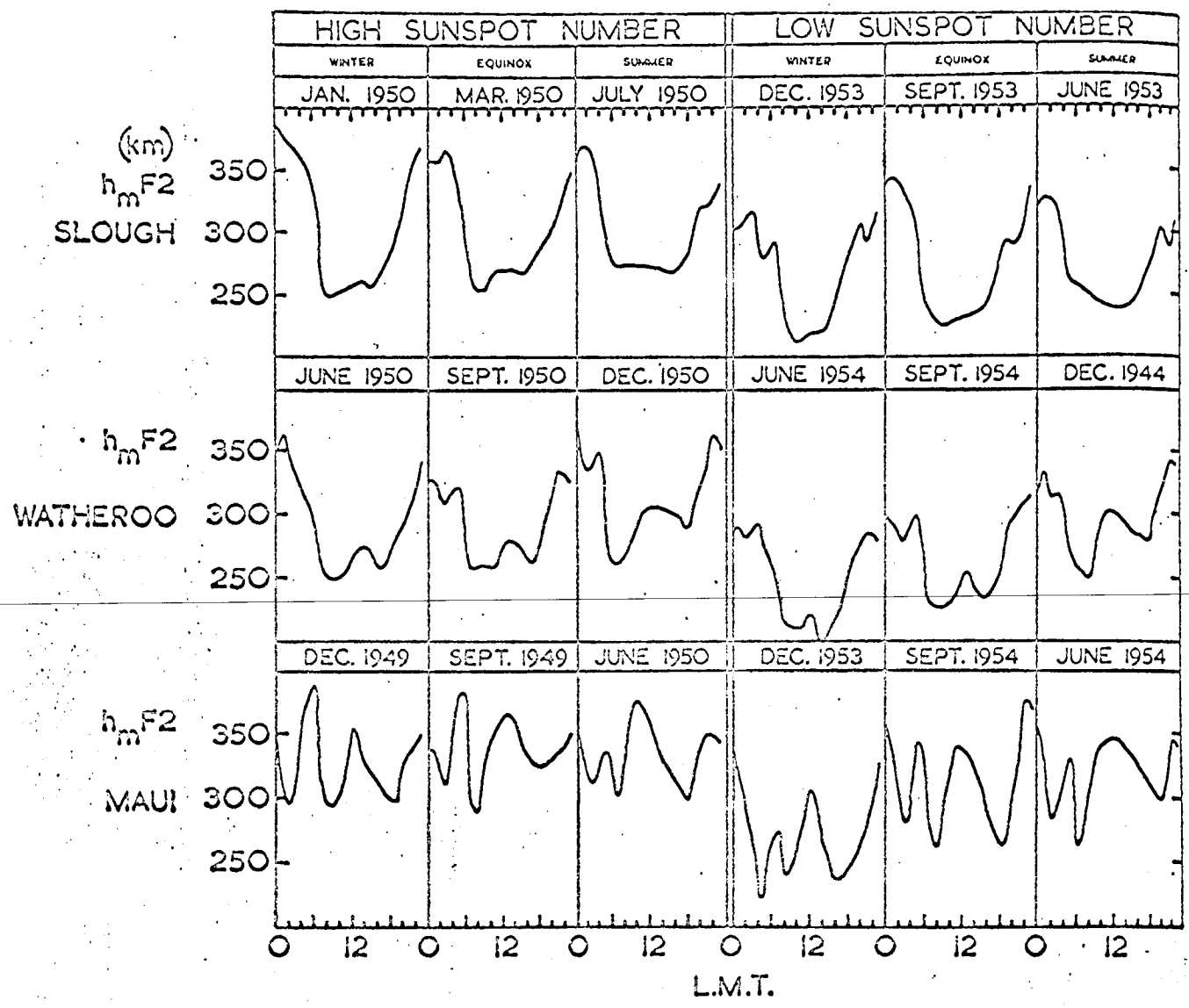

Figure 9 The Average Variation of hmF2 for Ten International Quiet Days in Each Month for Three Seasons in Years of High and Low Sunspot Number at Slough (51°30'N, 00° 36'W), Watheroo (30°19'S, 115°53'E), and Maui (20°48'N, 156°30'W). (Ref. 24)

sounder ionograms have given new insight with respect to this phenomenon by providing height profiles at increments of not more than one degree of latitude in contrast to the data previously available from the isolated and fixed ionospheric sounding stations. Figures 10 and 11, which were given by Lockwood and Nelms[10], show clearly the smooth h_m latitude variation. Unfortunately, interpretation of this data is not always as simple as it might at first appear. Since Alouette must orbit for more than a month to obtain about half the diurnal cycle, the interpretation problem actually is quite difficult because seasonal effects are superimposed. For the present, it is probably better to accept bottomside station-to-station variability when attempting to estimate diurnal trends.

Figures 12 and 13 were given by Somayajulu[21] as examples of the seasonal and diurnal variations at two such stations during the peak of the solar cycle. A plot showing the seasonal variations in the post sunset F layer height at those stations is drawn in Figure 14. Somayajulu finds that seasonal post sunset h_m variations are correlated with $\cos \chi_n$ where χ_n is the noon zenith angle. This is illustrated in Figure 15.

The evening equatorial F2 layer rise indicated in Figures 11, 12 and 13, occurs only during years of peak solar activity[1]. There is also an evening N_m increase in the transition zone between the geomagnetic anomaly and the midlatitudes. A seasonal correlation between the two phenomena has been demonstrated by Somayajulu[22] and illustrated in Figure 16 where N_m is for Panama at 39.2°N dip, considered to be a transition zone station, and h_m is for Talara, an equatorial station at 13°N dip. This is taken as strong evidence that the equatorial and transition regions are connected by diffusion along magnetic field lines.

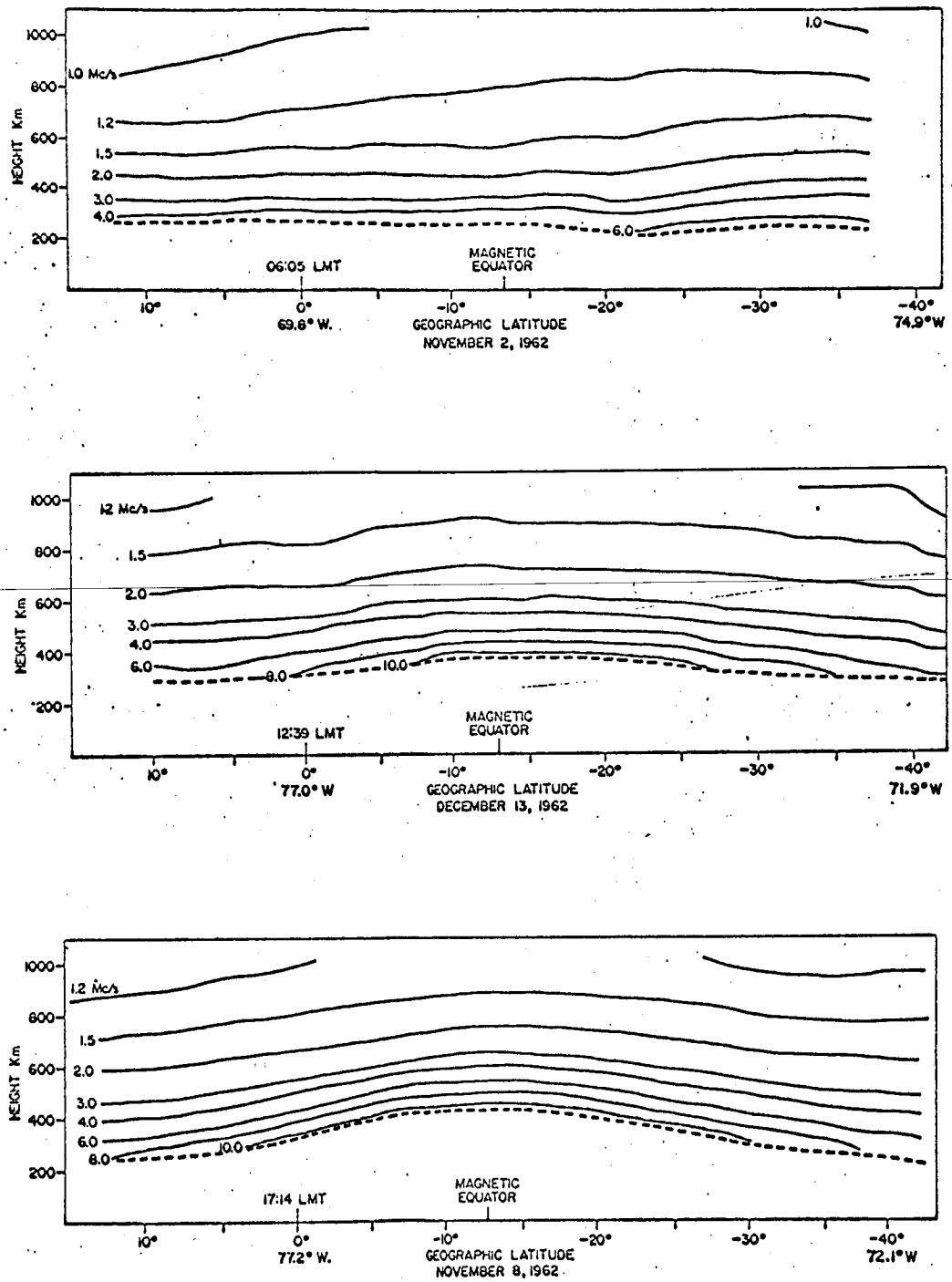

Figure 10 Constant Electron Density Contours at 0605, 1239 and 1714 Local Time. The Dashed Line is an Estimation of the Height of the Peak of the F-Layer. (Ref. 10)

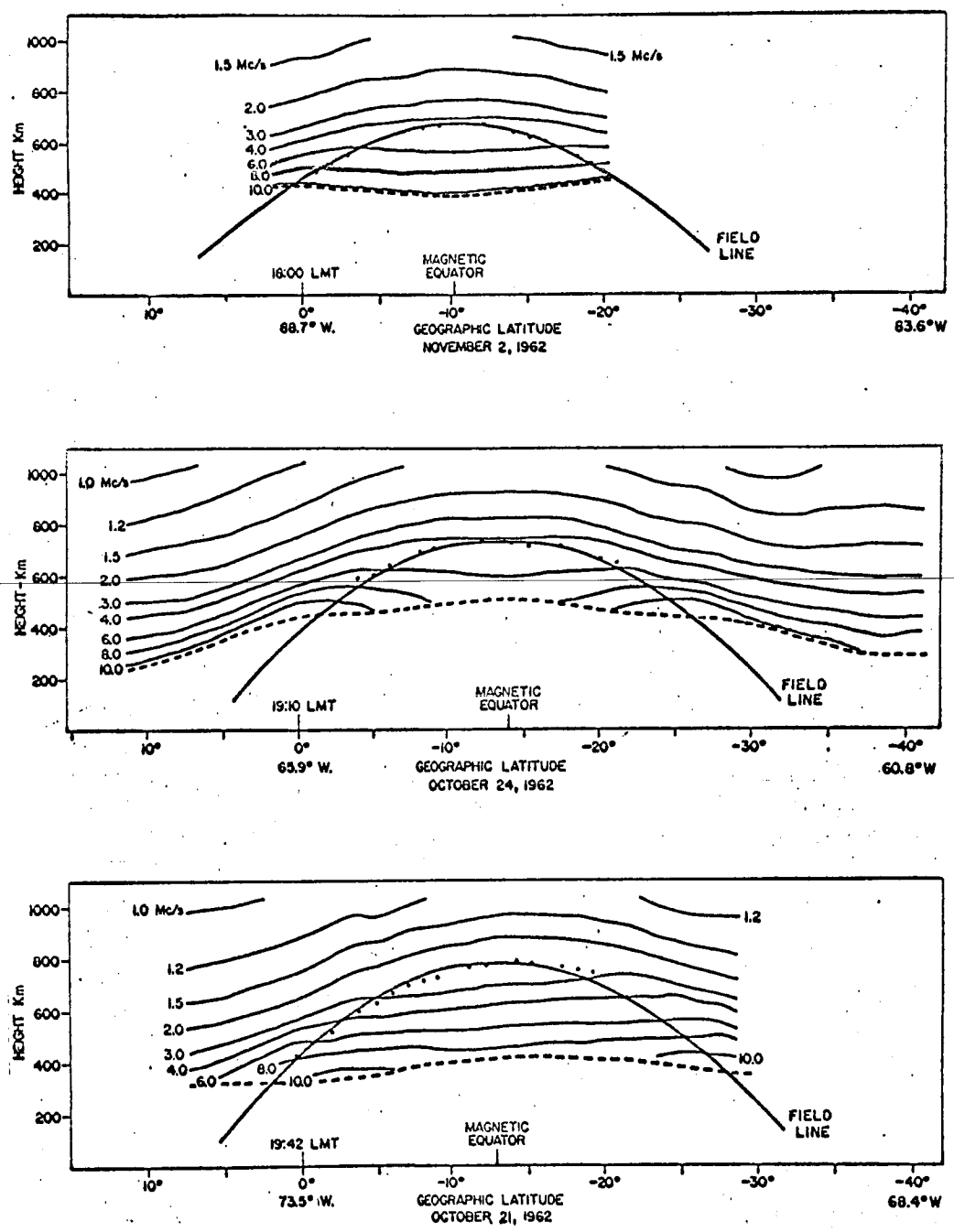

Figure 11 Constant Electron Density Contours at 1800, 1910 and 1942 Local Time. The Dashed Line is an Estimation of the Height of the Peak of the F-Layer. (Ref. 10)

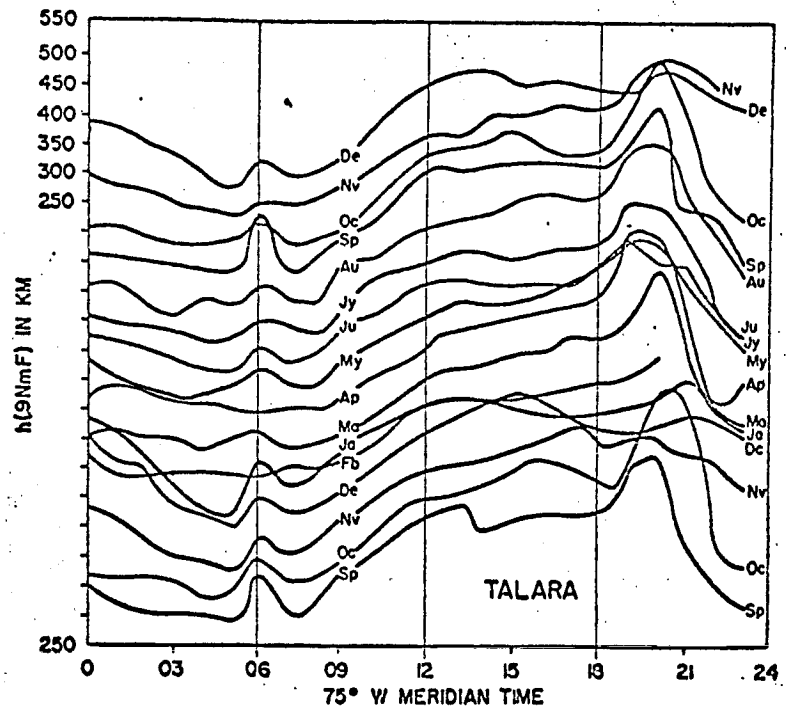

Figure 12 Mean Quiet Day Variations in $h(.9N_mF)$ at Talara for IGY Months. (Ref. 21)

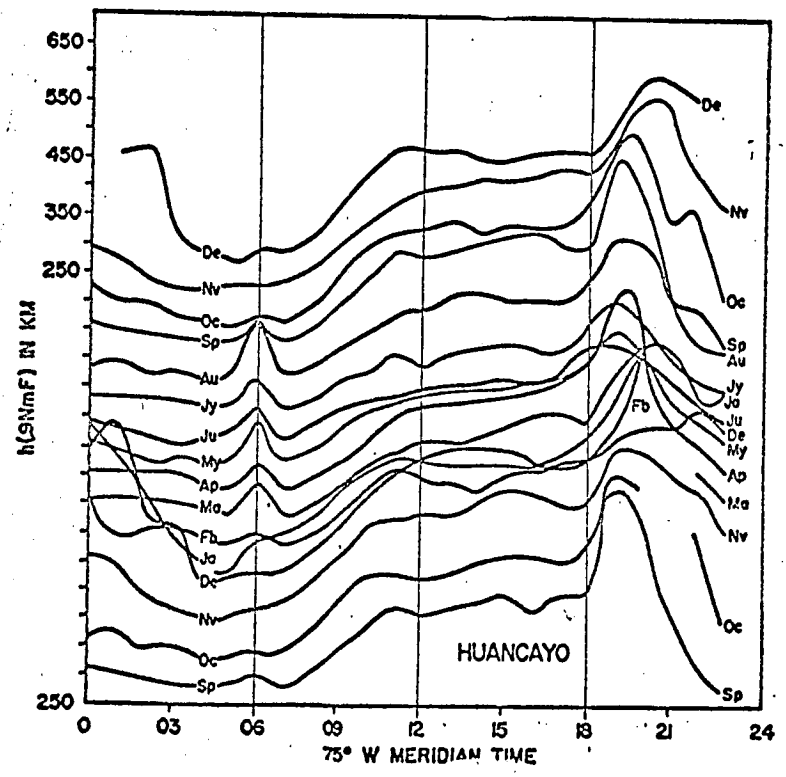

Figure 13 Mean Quiet Day Variations in $h(.9N_mF)$ at Huancayo for IGY Months. (Ref. 21)

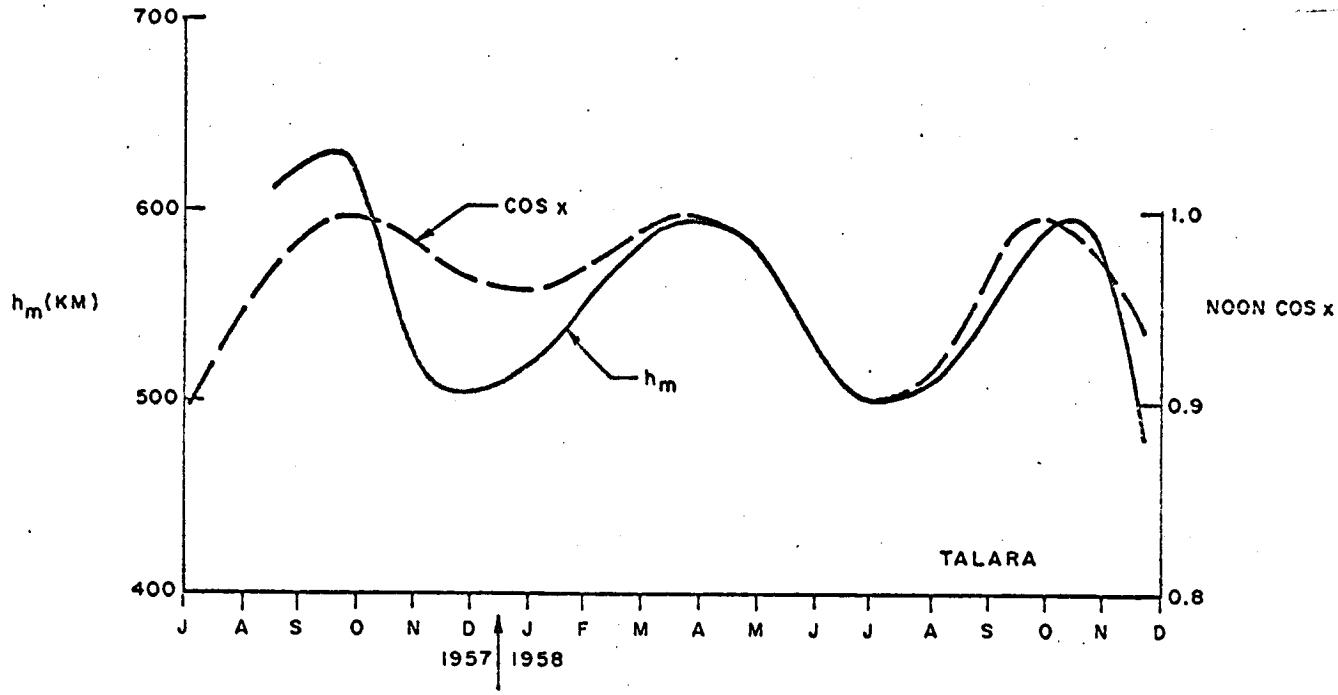

Figure 14 Post Sunset F2 Layer Diurnal Maximum Height During a Magnetically Quiet Period of High Solar Activity Based on $h(.9N_m)$ Data Given by Somayajulu, April 1964 (Ref. 21)

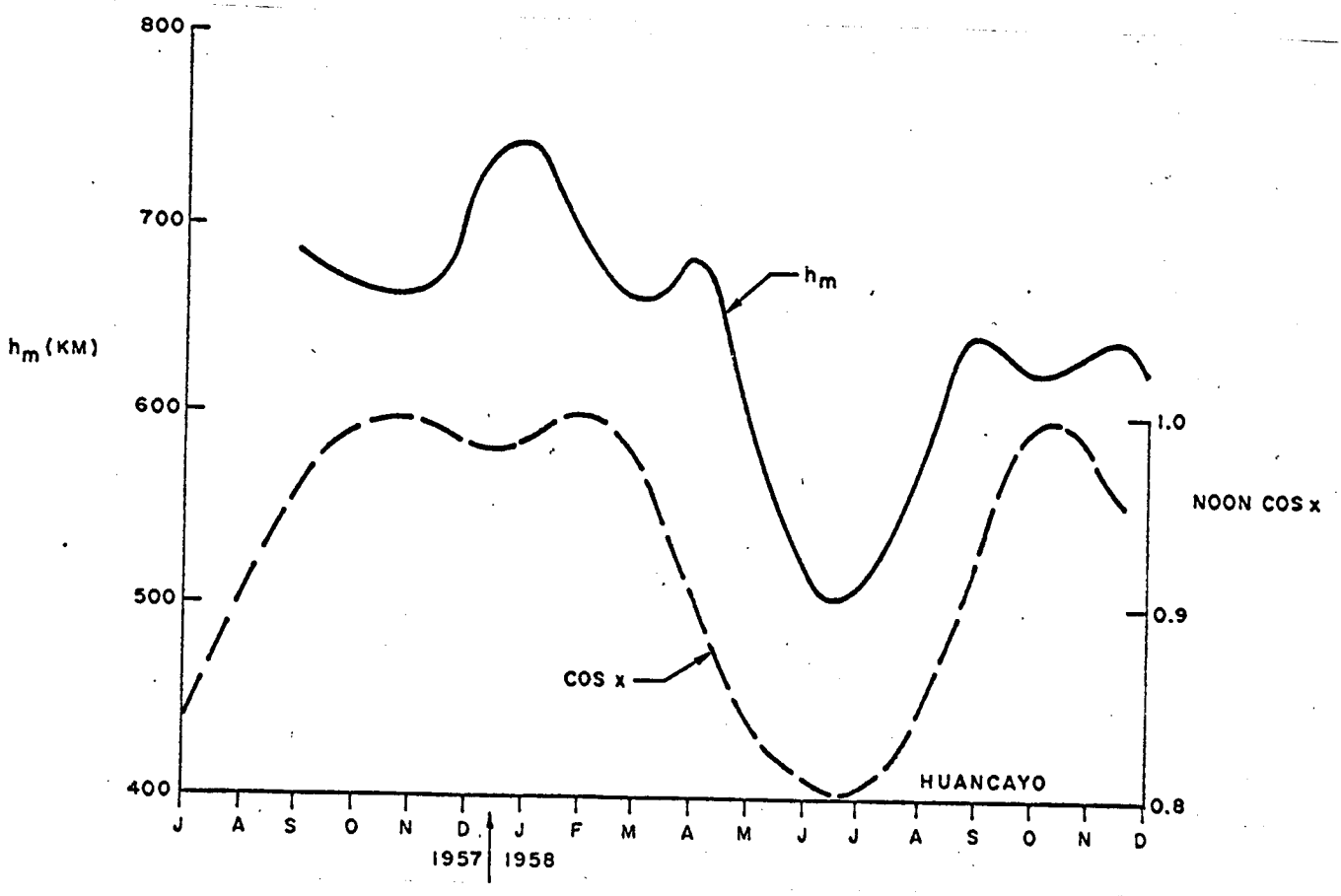

Figure 15 Correlation of the Noon Solar Zenith Angle and h_m as Exhibited by Somayajulu (Ref. 21).

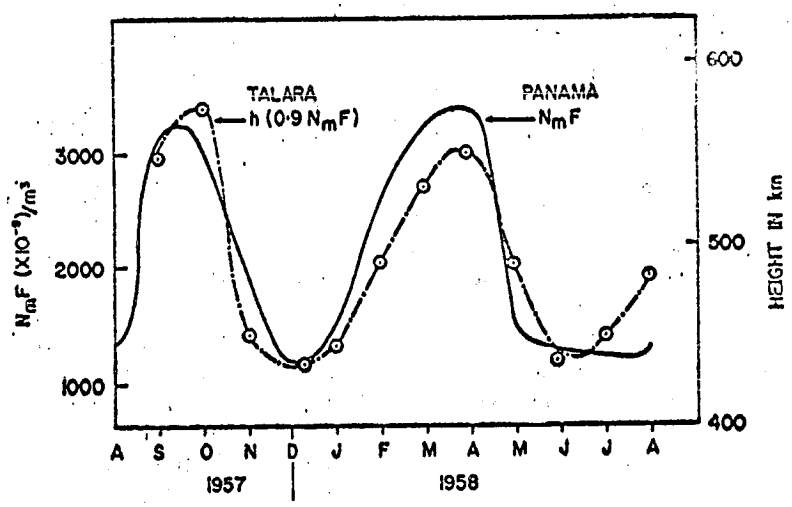

Figure 16 Seasonal Correlation Between the Respective Evening Rises in N_m at Panama and h_m at Talara. (Ref. 22)

ESTIMATE OF THE PEAK IONIZATION LEVEL BASED ON MAXIMUM USABLE FREQUENCY DATA

Although ionospheric observatories report the virtual heights of the levels represented by the parameters h'F2, h'F, h'E, and $h'E_s$, only infrequently are the extensive computations carried out that are necessary to make the conversion to true heights. On the other hand, many stations for each hour report the monthly median maximum usable frequency for a 3000 km range by reflection from the F2 layer. This parameter, designated M(3000)F2 varies as the reflection layer moves up or down. A thin layer approximation relating true reflection height h for a range D and a maximum usable frequency M is given by the classical Appleton-Beynon equation

$$h = -(D^2/r) + (D/2M)\,(1 - 1/M^2)^{-1/2} \tag{4}$$

in which r is the earth radius. In spite of the approximations involved, this is a surprisingly accurate relation. Lyon[11] reports that over the altitude range 250-700 km the simplification

$$h_m = -a + b/M \tag{5}$$

is good to within $\pm 2\%$ near the magnetic equator with a = 280 km, b = 1908 km/sec, and M = M(3000)F2. Optimum a and b values depend only slightly on season and latitude, but may show variations between day and night. The approximation taking the form of equation (5) is frequently referred to as Shimazaki's formula for the true height of a parabolic layer h_p. Lyon and Thomas[13] used it in the form

$$h_p = 1658/M - 225 \text{ (km)} \tag{6}$$

to estimate h_m variations in an equatorial region where true height determinations are too sparse for meaningful interpretations. Also

using Shimizaki's formula to represent equatorial F2 layer heights, Rastogi and Sanatani[18] wrote

$$h_p = 1490/M - 176 \text{ (km)} \tag{7}$$

to represent layer height variations for the latter half of 1958 with the results shown in Figure 17. Argence, et. al.[2], studying total electron content, n_t, also cite equation (7) but without specifying the additive constant, 176 km. An example of the winter midday M3000F2 contours was given by Argence, et. al., and reproduced as Figure 18.

Shimazaki's formula, when used in the present application, is subject to a valid criticism in that it does not represent F2 layer height over the station of interest. When the extreme variability and low accuracy of h_m data is considered, however, the more or less mean F2 layer height at a distance of 1500 km from the station is quite an acceptable compromise for h_m. Then too, the wide availability of M(3000)F2 data in contrast to the relatively sparse h_m data make h_p a very practical substitute. In this connection, considerable geographical extrapolation of even h_p data is required because supposing M(3000)F2 data were available from all sounding stations; the average separation then would exceed 2000 km and in many important parts of the world, the separation would be much larger.

Extrapolation is simple, nonetheless, if the findings of Yamada and Ogata[27] are accepted. Ship based soundings made during a 1962 voyage provided data from which it was deduced that the dependence of h_p on the dip angle was nearly linear. In December h_p appeared to increase monotonically from 200 km at 60°N dip to about 500 km at 40°S dip. It does not seem advisable to attempt extrapolation over such a great distance as this but certainly data variability make acceptable a linear extrapolation from zone-to-zone of the model. For example, considering the diurnal changes the extrapolation to a dip

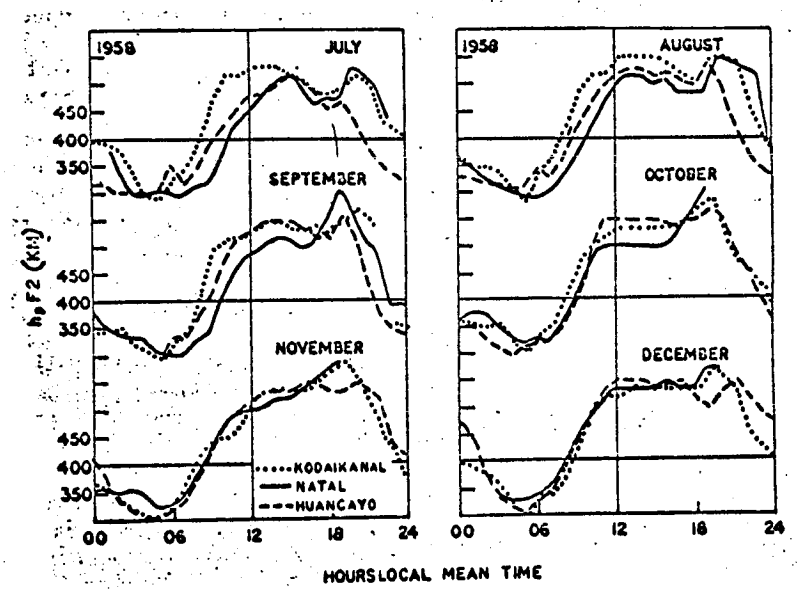

Figure 17 Diurnal h_m Variations at Three Low Latitude Stations for Six Months of 1958 Based On Equation 7. (Ref. 18)

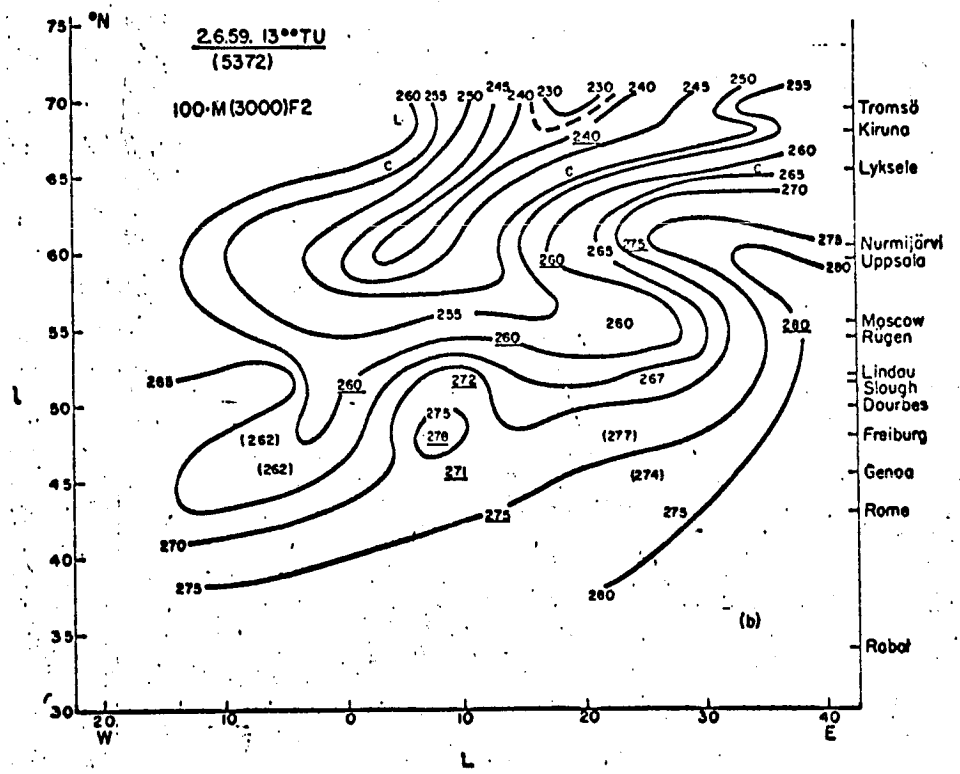

Figure 18 An Example of a Map of M(3000)F2 at Mid-day After E. Argence, et. al. (Ref. 1)

angle I could be written at time t in the form

$$h_p (I, t) = h_{p1} + (I - I_1) (h_{p2} - h_{p1}) / (I_2 - I_1) \tag{8}$$

where $h_{p1} = h_p(I_1, t)$ and $h_{p2} = h(I_2, t)$ are the layer heights calculated from M(3000)F2 data taken at the dip angles I_1 and I_2.

As an illustration, two suitable stations for extrapolation in the equatorial trough at about 75°W longitude are Huancayo at 75.3°W, 2°N dip; Bogota 74°15'W, 33°N dip; and Panama at 79.9°W, 39.2°N dip. In the midlatitudes the extrapolation could be made from Panama to Grand Bahama, 78.2°W, 60°N dip and then to Fort Monmouth at 74°.0W, 71.5°N dip. There are no auroral stations near 75°W and Winnepeg, 97°24'W, ≅ 77.5°N dip is probably the best compromise. Thule 68°50'W, 86.2°N dip is an excellent choice for a polar station.

The form of Shimazaki's formula suggested for trial is

$$h_p = 1500/M - 200 \text{ (km)} \tag{9}$$

where M is in mc. This is known to give a good daytime representation in equatorial regions and for the present purposes also should prove adequate at other latitudes for any time of day. Table 2 shows the M factors at Fort Monmouth, an example of a moderately high latitude station (dip ≅ 71.5°N) and the scale heights calculated using the last equation for both night and day. True height data were not available but the range of heights Δh_p is consistent with Wright's observation that the range is usually about 100 km. Certainly these results are within the limits of the day-to-day variability.

Although it is suggested that M(3000)F2 values be taken from past observations for times that approximate anticipated conditions, it may prove feasible to extrapolate observations to some extent.

TABLE 2.

Monthly Mean M(3000)F2 Factors for 1958
at Fort Monmouth and Calculated Layer Heights

	M(Max) (mc)	M(Min) (mc)	h_p(Min)	h_p(Max)	Δh_p
January	3.1026	2.7022	285 km	360 km	75 km
February	3.2026	2.6820	270	360	90
March	3.0025	2.5013	300	400	100
April	2.8023	2.3521	340	440	100
May	2.7526	2.4025	350	430	80
June	2.8024	2.4025	340	430	90
July	2.8228	2.4024	330	430	100
August	2.9530	2.5031	310	400	90
September	3.0027	2.5025	300	400	100
October	3.0525	2.5526	245	390	95
November	3.1528	2.7228	280	350	70
December	3.1530	2.7028	280	360	80

Vasil'Yeva[25], for example, finds M(3000)F2 is linear in R for $R \leq 120$, and writes

$$M(3000)F2 = c - dR .$$

He presents values for the constants c and d in graphical form showing the diurnal variations in equatorial regions.

BIBLIOGRAPHY

1. Appleton, E. V., "Some Ionospheric Results Obtained During the IGY", Elsevier Publishing Company, Amsterdam, 1960.

2. Argence, E., Eyfrig, R., Hess, H. A., Paul, A., and Rawer, K., "Equivalent Thickness of the Outer Ionosphere by Evaluation of Faraday Records", Planet Space Science, Volume 11, pp 1431-1457 (1963).

3. Bauer, S. J., Blumle, L. J., Donley, J. L., Fitzenreiter, R. J., and Jackson, J. E., "Simultaneous Rocket and Satellite Measurements of the Topside Ionosphere", Journal of Geophysical Research, Vol. 69, No. 1, January 1, 1964, pp 186-189.

4. Becker, W., "The Varying Electron Density Profile of the F Region During Magnetically Quiet Nights", J. A. T. P., Vol. 22, No. 4, December 1961, pp 275-289.

5. Becker, W., "Discussion on the Diurnal Variation of Electron Density in the F-Region", Electron Density Distribution in the Ionosphere and Exosphere, E. Thrane, Ed., John Wiley and Sons pp 243 (1964).

6. Hanson, W. B., and Patterson, T. N. L., "The Maintenance of the Nighttime F-Layer", Planetary Space Science, Vol. 12, No. 10, pp 979-997, October 1964.

7. Haubert, A., and Laloe, F., "L' Ionisation de la Region F all Lever du Soleil", Electron Density Distribution in the Ionosphere and Exosphere, E. Thrane, Ed., John Wiley and Sons, pp 222-225, (1964).

8. King, G. A. M., and Lawden, M. D., "Variations of Some Ionospheric Parameters Over a Solar Cycle", J. A. T. P., Vol. 24, July 1962, pp 565-568.

9. King, J. W., and Scott, J. L., "Variations of the Peak of the Ionospheric F2 Layer", J. A. T. P., Vol. 24, July 1962, pp 569-572.

10. Lockwood, G. E. K, and Nelms, G. L., "Topside Sounder Observations of the Equatorial Anomaly in the 75°W Longitude Zone", J. A. T. P., Vol. 26, No. 5, pp 569-580, May 1964.

11. Lyon, A. J., "The Geomagnetic Anomaly", Proc. Int. Conf. on the Ionosphere, London, 1962, pp 88-93, Inst. of Phys. and the Phys. Soc., Chapman and Hall, (1963).

Bibliography (continued)

12. Lyon, A.J., and Awojobi, O.A., "The F-Layer at Sunrise Near the Magnetic Equator", J.A.T.P., Vol. 27, No. 1, pp 53-56, January, 1965.

13. Lyon, A.J., and Thomas, L., "The F2 Region Equatorial Anomaly in the African, American and East Asian Sectors During Sunspot Maximum", J.A.T.P., Vol. 25, No. 7, July 1963, pp 373-386.

14. Nisbet, J.S., "Electron-Density Distribution in the Upper Ionosphere from Rocket Measurements", J. Geophys. Res. 65, No. 9, September 1960, pp 2597-2599.

15. Nisbet, J.S., "Factors Controlling the Shape of the Upper F Region Under Daytime Equilibrium Conditions", J. Geophys. Res., Vol. 68, No. 22, Nov. 15, 1963, pp 6099-6112.

16. Norton, R.B., and Van Zandt, T.E., "The Daytime Equatorial F Layer", J.A.T.P., Vo. 26, No. 11, 1964, pp 1047-1054.

17. Rao, C.S.R., and Malthotra, P.L., "A Study of Geomagnetic Anomaly During IGY", J.A.T.P., Vo. 26, No. 11, November 1964, pp 1075-1085.

18. Rastogi, R.G. and Sanatani, S., "Longitudinal Effect in the Equatorial F2 Region of the Ionosphere", J.A.T.P, Vol. 25, (1963), pp 739-742.

19. Ratcliffe, J.A., and Weekes, K., "The Ionosphere", Physics of the Upper Atmosphere, pp 378-470, J.A. Ratcliffe, editor Academic Press, (1960).

20. Shapiro, B.S., "Compilation of Predictions of the Geometric Parameters and the h'f Frequency-Height Curves of the Ionosphere", Akad. Nauk. SSSR, Trudy Zem. Mag., Ion. Rasp. Rad., No. 17 (27) pp 216-239 (1960, ASTIA translation 298207

21. Somayajulu, Y.V., "Some Features of the F Region Electron Density and Height Variations in the Equatorial Regions", J. Geophys. Res. Vol. 69, No. 7, April 1, 1964, pp 1329-1339.

22. Somayajulu, Y.V., "Evidence on the Horizontal Diffusion of F Region Ionization Along the Magnetic Lines of Force in Equatorial Latitudes", J. Geophys. Res., Vol. 69, No. 3, pp 561-563, February 1, 1964.

23. Stubbe, P., "Temperature Variation at the F Layer Maximum During a Sunspot Cycle", J.A.T.P., Vol. 26, No. 11, Nov. 1964, pp 1055-1068.

Bibliography (continued)

24. Thomas, J. O., "The Distribution of Electrons in the Ionosphere," Proc. IRE, 47, No. 1, p. 162, January 1959.

25. Vasil-Yeva, T. N., "Parameters of the Linear Dependence of f_o F2 and M(300) F2 on Solar Activity", Geomag. and Aeronomy IV, No. 4 (1964) English Edition Feb. 1965.

26. Wright, J. W., "Diurnal and Seasonal Changes in Structure of the Mid-latitude Quiet Ionosphere," NBS J. Res., 66D, 3, pp 297-310, (May-June 1962).

27. Yamada, K., and Ogata, T., "Geomagnetic Dependence of the F2 Layer by Observations on Board Ship," J. Radio Res. Lab. (Japan) 11, No. 55, pp 137-146, May 1964.

APOLLO NOTE NO. 379
(Task I, Item IB)

H. R. Wright
28 October 1965

IONOSPHERIC PHASE PATH SENSITIVITY TO CHAPMAN PARAMETER VARIATIONS

INTRODUCTION

A good approximation for the S-band phase path length decrease through the ionosphere below that for free space in rmks units is (see Apollo Note No. 303, Section 2)

$$\Delta \ell = (1,600/\omega^2) \int_0^{\ell_v} N \, d\ell \tag{1}$$

where N is the electron density at the height h, ω is the wave angular frequency, ℓ is distance along the ray and the subscript v refers to the vehicle. The simplest ionospheric model commonly cited in the literature is the "alpha Chapman" electron density distribution, and somewhat surprisingly it comes fairly close to satisfying our requirements. Flat layers in a single component gas at quasi-equilibrium are assumed with an electron production rate proportional to the square of the electron density. Monochromatic ionizing solar radiation is incident on an isothermal atmosphere. With these assumptions, well-known and simple analysis then leads to the Chapman electron density height profile

$$N = N_m (\cos \chi)^{1/2} \, Ch(\chi, z) \tag{2}$$

where χ is the solar zenith angle and Ch (χ, z), the Chapman alpha function for a flat earth, is defined by

$$Ch\,(\chi, z) = \exp\left[(1 - z - \sec\chi \exp - z)/2\right] \tag{3}$$

in which z, the reduced height, vanishes at the peak ionization level, h_m, in accordance with a height dependence given by

$$z = (h-h_m)/H_m \tag{4}$$

where H_m is the Chapman "scale height" which it will be remembered is defined by

$$H_m = kT/Mg \tag{5}$$

where k is Boltzmann's constant, T is the ionospheric temperature, M the mass of the ionizable constituent (which is usually taken to be atomic oxygen), g is the acceleration of gravity and the parameter is evaluated near the altitude, h_m.

Before discussing the $\Delta\ell$ variations implied by equation (1) in any detail, it is informative to consider the special case when the vehicle is above the ionosphere with the sun overhead. The $\Delta\ell$ dependence on the Chapman parameters then is very simple because after substituting equation (2) in (1) and performing the integration it is found that for a one way vertical transmission that

$$\Delta\ell = 167.5\, N_m H_m/f^2 \qquad \text{(meters)} \tag{6}$$

in which f is the transmitted frequency (cps) with N_m and H_m in mks units as before. Conditions vary widely but as an illustration take

$N_m = 5 \times 10^{11}$ eℓ/cubic meter, $H_m = 5 \times 10^4$ meter and $f = 3 \times 10^9$ cps. Then a 10% variation in either N_m or H_m varies $\Delta\ell$ by about 0.05 meter.

Choice of this example for illustration was dictated by the ease of analysis and since propagation through the entire ionosphere was postulated it is not surprising that equation (6) shows the h_m independence characterizing a situation in which the actual location of the ionosphere is immaterial. This is only approximately true, as will become evident later. Nonetheless an upper $\Delta\ell$ limit for one way vertical transmission is thus established. Keep in mind, however, that equations (1) - (5) of themselves do not make it immediately evident that when the vehicle is in the ionosphere a guarantee may be offered that parametric variations, say even $\partial\Delta\ell / \partial h_m$, will be negligible.

THE EFFECT OF N_m VARIATIONS WHEN THE VEHICLE IS WITHIN AN EQUILIBRIUM IONOSPHERE

For a given integration of equation (1), the ray passes through a definite h_m where H_m may be assigned a fixed value. Then from equation (4),

$$d\ell = H_m \, dz / \sin \phi \tag{7}$$

where ϕ is the elevation angle which to avoid earth curvature complications will be restricted to values greater than 15°-30°. Using equations (2), (4), and (7) in (1) and converting to frequency f (cps) from angular frequency results in

$$\Delta\ell = \left[40.53\ H_m N_m\ (\cos\chi)^{1/2}\ /\ (f^2 \sin\phi)\right] \int_{-z_o}^{z_v} Ch(\chi, z)\ dz \tag{8}$$

where

$$z_o = h_m / H_m \tag{9}$$

$$z_v = (h_v / H_m) - z_o. \tag{10}$$

Before attempting to differentiate equation (8), a reasonable assumption employed by workers at Stanford University and NBS, Boulder will be invoked. This is the fact that at equilibrium, the electron density should be proportional to $1/\sqrt{T}$ at a constant pressure level. Further, h_m should occur at the same pressure level independent of the temperature. On this basis, the Chapman parameters are not independent. The relation becomes simple if it is also assumed that h_m varies directly with T (see Apollo Note 317, Section 4), and while the latter may not hold rigorously, certainly $dz_o/dN_m \cong 0$. On the other hand, it follows that

$$dz_v/dN_m = 2\ h_v/(H_m N_m) \tag{11}$$

and that

$$\frac{d}{dN_m}(N_m H_m) = -\ H_m. \tag{12}$$

The negative sign in equation (12) may seem surprising until it is noted that while a temperature drop increases N_m, there is a decrease in

the overall electron content which, according to Chapman theory is proportional to $N_m H_m$.

Based on these results, the total derivative of equation (8) is

$$d\Delta\ell/dN_m = \left[40.53\ (\cos\chi)^{1/2}/(f^2 \sin\phi)\right] X$$

$$\left[2\ h_v\ Ch\ (\chi, z_v) - H_m \int_{-z_o}^{z_v} Ch(\chi, z)\ dz\right] \tag{13}$$

Again take the example of an overhead sun and vertical incidence at $f = 3 \times 10^9$ cps. Now consider a vehicle parked at $z_v = 0$. Corresponding local noon values for h_m and H_m at the peak of the solar cycle in the southern hemisphere are typically 180 km and 60 km, respectively. The integral in equation (13) has a value of about 2.15 so that for this example

$$\frac{d\Delta\ell}{dN_m} = \frac{40.53}{9 \times 10^{18}} \left[2 \times 1.8 \times 10^5 - 6 \times 10^4 \times 2.15\right]$$

$$= 1.03 \times 10^{-12} \text{ meters/(electron/cu meter)}.$$

A 10% variation in N_m would be the order of 10^{11} electrons/cu meter corresponding to a $\Delta\ell$ variation of about 0.1 meters which is greater than the variation when the entire ionosphere is included. To verify this, note from equation (3) that when z_v is large, $2h_v\ Ch\ (\chi, z_v)$ appearing in equation (13) is very small compared to the term with

the integral which then has the value 4.133 H_m. Including the entire ionosphere in this example thus results in

$$\frac{d\Delta\ell}{dN_m} = -167.5\ H_m/f^2 = -167.5 \times 6 \times 10^4/9 \times 10^{18}$$
$$= -1.1 \times 10^{-12} \text{meters/(electron/cu meter)} \tag{14}$$

It is rather interesting that under an overhead sun the phase path derivatives for vertical penetration of the ionosphere are related through

$$\frac{d\Delta\ell}{dN_m} = -\frac{\partial\Delta\ell}{\partial N_m} \tag{15}$$

which is an expression of the fact that when N_m increases without compensating changes in the other parameters, the entire N(h) profile is scaled upward through equations (2) and (3). On the other hand when the other parameters are allowed to change, the temperature drop accompanying an N_m increase causes $N_m H_m$ and hence the total ionization, to decrease, as pointed out above.

THE EFFECTS OF H_m VARIATIONS

The total derivative will be calculated using

$$\frac{d\Delta\ell}{dH_m} = \frac{d\Delta\ell}{dN_m}\ \frac{dN_m}{dH_m} \tag{16}$$

where, on the basis of the preceding discussion,

$$\frac{dN_m}{dH_m} = - \frac{N_m}{2H_m} \tag{17}$$

These two equations together with (13) result in

$$\frac{d\Delta\ell}{dH_m} = -\left[40.53 \, (\cos \chi)^{1/2} / \, (f^2 \sin \phi) \right] x \left[(h_v N_m / H_m) \, Ch \, (\chi, z_v) - (N_m/2) \int_{-z_o}^{z_v} Ch(\chi, z) dz \right] \tag{18}$$

Again consider the vehicle parked at $z_v = 0$ with $h_m = 180$ km; $H_m = 60$ km, $z_o = 3$, $N_m = 10^{12}$ electrons/cu meter. In this case,

$$\frac{d\Delta\ell}{dH_m} = -8.9 \times 10^{-6} \quad \frac{\text{meter}}{\text{meter}}$$

and a 10% change in H_m would amount to about 0.07 meters.

When H_m is allowed to change but the other parameters are fixed, equation (8) shows that

$$\frac{\partial \Delta\ell}{\partial H_m} = 40.53 \, N_m \, (\cos \chi)^{1/2} / \, (f^2 \sin \phi) \; x \left[\int_{-z_o}^{z_v} Ch(\chi, z) \, dz - z_v \, Ch \, (\chi, z_v) - z_o \, Ch(\chi, -z_o) \right] \tag{19}$$

Using the parameter values for the preceding example results in

$$\frac{\partial \Delta \ell}{\partial H_m} = 0.52 \times 10^{-5} \text{ meters/meter}$$

in which case a 10% H_m change varies $\Delta \ell$ about 0.03 meters.

THE INFLUENCE OF h_m CHANGES

Differentiating N_m with respect to h_m based on the assumptions made above results in

$$\frac{dN_m}{dh_m} = -\frac{N_m}{2h_m} \tag{20}$$

which asserts that as the temperature drops, N_m increases but h_m moves to lower levels. When the result is applied in equation (8) it follows that

$$\frac{d\Delta \ell}{dh_m} = \left[40.53\, N_m (\cos \chi)^{1/2} / (h_m f^2 \sin \phi) \right] \times \left[(H_m/2) \int_{-z_o}^{z_v} Ch(\chi, z)\, dz - h_v\, Ch(\chi, z_v) \right] \tag{21}$$

For the example of the parking orbit at 180 km through the F2 peak in the southern hemisphere,

$$\frac{d\Delta \ell}{dh_m} \cong -5 \times 10^{-6} \frac{\text{meters}}{\text{meter}}$$

so a 10% rise in h_m reduces $\Delta \ell$ by about 0.1 meters.

When only h_m varies the result is

$$\frac{\partial \Delta \ell}{\partial h_m} = - \left[40.53 \, N_m \, (\cos \chi)^{1/2} / (f^2 \sin \phi \right] \times$$

$$\left[Ch(\chi, z_v) - Ch(\chi, -z_o) \right] \tag{22}$$

and substituting values for the example of the vehicle near the F2 peak yields

$$\frac{\partial \Delta \ell}{\partial h_m} \cong - 2.3 \times 10^{-6} \text{ meter/meter}$$

here a 10% rise in h_m reduces the phase path retardation by about 0.08 meters.

Note that since $Ch(0, -3) = 3 \times 10^{-4}$ is a typical value for $Ch(0, -z_o)$ and that above the ionoshpere $Ch(0, z_v) = 0$, then for one way vertical transmission through the ionosphere

$$\frac{\partial \Delta \ell}{\partial h_m} \cong 0.012 \, N_m / f^2 \tag{23}$$

which for the present example is only the order of 10^{-9} meters/meter and may be ignored, but note that now the sign corresponds to an increase in the phase path retardation. From equation (21) the corresponding total derivative is

$$\frac{d\Delta \ell}{dh_m} = 84.0 \, N_m H_m / (h_m f^2) \tag{24}$$

or 3.1×10^{-6} meters/meter in this example with $\Delta \ell$ increasing about 0.02 meters for a 10% increase in h_m.

The Bissett-Berman Corporation 2941 Nebraska Avenue, Santa Monica, California EXbrook 4-3270

APOLLO NOTE NO. 380
(Task 2, Item II)

L. Bonin
15 November 1965

EFFECT OF CLOCK ERRORS ON THE EPHEMERIS OF A LUNAR SATELLITE

An analysis was conducted to determine the effect of tracking clock errors on the expected position and velocity of a satellite in a lunar parking orbit. The clocks at the master and slave stations are assumed to possess an initial offset error (b), to run at the wrong rate (β) and to have rates linearly varying with time (α). In Apollo Note No. 320, the time ($\hat{t}$) indicated by the station clocks is assumed to vary with the real time (t) according to the relation:

$$\hat{t} = b + (1 + \beta)\, t + \frac{\alpha}{2}\, t^2 .$$

The Bissett-Berman OEA Program is used to study the effect of small values of b, β, and α on the satellite's ephemeris. As a result of this analysis, the a priori clock errors are found to contribute significantly to ephemeris errors, however, updating these nuisance parameters is not warranted from the standpoint of improved accuracy. A discussion of this analysis is presented in this note.

Before discussing the analysis, a brief explanation of the significance of updating the nuisance parameters is justified. In the basic orbit determination problem, radar tracking data is used to improve an a priori estimate of a satellite's orbit. This a priori estimate is a function of some assumed initial position and velocity components plus a model of the gravitational force field acting on the satellite. Because the gravitational force field is not exactly known, the initial estimate of the satellite's orbit is influenced by this uncertainty in addition to the uncertainties in initial position and velocity. For this reason, the gravitational force field is considered a nuisance parameter because it affects the accuracy of the satellite's orbit even though we are not primarily

interested in determining its actual value.

When radar data are used to improve the orbit estimate, the number of nuisance parameters is increased, e. g., station location errors, bias in the measurables, etc. In essence, updating these nuisance parameters is equivalent to considering them as additional orbit parameters and utilizing the tracking data to improve their estimates. In practice, any or all of the nuisance parameters may be updated, however as more parameters are updated the complexity of the orbit determination problem is increased. Even though the best accuracy is obtained by updating all nuisance parameters, updating a particular parameter does not always improve the orbit accuracy. This fact is illustrated in the present investigation.

The importance of tracking site clock errors is determined by comparing a nominal error case that neglects clock errors with perturbed cases that include clock errors. The tracking stations and errors used in this nominal case are identical to those assumed for the nominal case discussed in Apollo Note No. 371. The geometric conditions between the satellite and the Moon, and the Moon and the Earth, at time zero, are also the same. A restatement of these nominal conditions is not required in this note.

For the perturbed case, the assumed 1 - sigma deviations of the tracking station clocks are:

σ_b (clock offset) = 1 millisecond

σ_β (clock rate) = 1×10^{-10} seconds per second

σ_α (clock drift rate) = 10^{-10} parts/part/hour = 2.8×10^{-14} seconds/second^2.

These errors are assumed for both the master and the slaves. The dispersion due to these errors is determined by comparing the perturbed error case with the nominal case after 30 minutes of range-rate tracking.

The increased dispersion caused by each of the assumed clock errors is shown in Table 1. The clock offset is shown to produce a negligible effect on both the rendezvous uncertainty and the velocity error. The clock rate, however, increases the dispersion in rendezvous uncertainty distance by almost 1 kilometer and the velocity error by about 1 meter per second. Adding the drift rate error further increases the rendezvous uncertainty only about 250 meters with negligible effect on the velocity error. Based on these results some consideration must be given to updating the clock rate error.

Before investigating the effect of updating particular nuisance parameters, the effect of updating all nuisance parameters is considered. This type of filtering system provides the most accurate estimate possible with a given amount of tracking information. Table 2 shows the accumulative effect of clock errors when all parameters are updated. In this case, both the clock offset and rate errors produce negligible effects, but the drift rate error is significant. A detailed analysis of the drift rate error showed that it is updated at a very slow rate. Most of this error is contributed by the a priori deviations assumed for the slave tracking stations. As a consequence, attempting to update this parameter with only 30 minutes of tracking information is unwarranted.

The last part of the analysis is devoted to determining the effect of updating particular nuisance parameters. The main parameter selected is the bias in the range-rate measurable. The main contributors to this source of error are frequency dispersions caused by ionization effects in the ionosphere, spacecraft wobble, and clock rate and other

TABLE 1.

EFFECT OF INDIVIDUAL CLOCK ERRORS*
(No Nuisance Parameters Updated)

	Rendezvous Uncertainty, (m) $\sqrt{P_{11} + P_{22} + P_{33}}$	Velocity Error, (m/sec) $\sqrt{P_{44} + P_{55} + P_{66}}$
Nominal Case (no clock errors)	3870	3.66
Clock Offset	3883	3.66
Clock Offset and Rate	4736	4.46
Clock Offset Rate and Drift Rate	4989	4.49

* Three stations, Doppler tracking for 30 minutes.

TABLE 2.

EFFECT OF UPDATING ALL NUISANCE PARAMETERS

	Rendezvous Uncertainty	Velocity Error
Nominal Case (no clock errors)	805	0.755
Clock Offset	814	0.771
Clock Offset and Rate	817	0.776
Clock Offset, Rate and Drift Rate	868	1.206

*Three Stations, Doppler tracking for 30 minutes.

TABLE 3.

EFFECT OF UPDATED SELECTED NUISANCE PARAMETERS*

	Rendezvous Uncertainty	Velocity Error
Nominal Case (bias in the measurable updated)	855	0.81
Clock Offset (bias in the measurable updated)	864	0.83
Clock Offset and Rate (bias in the measurable and clock rate updated)	879	0.84
Clock Offset, Rate and Drift Rate (bias in the measurable and clock rate updated)	961	1.39
Clock Offset, Rate and Drift Rate (bias in the measurable updated)	950	1.38

*Three Stations, Doppler tracking for 30 minutes.

instrumentation errors of a bias nature. In the present analysis, clock rate errors are investigated as a separate nuisance parameter. The a priori estimate of the range rate bias used in this study is the value currently in use at MSC. Table 3 shows the effect of clock errors when the bias in the measurable is always updated. In the nominal case, all clock errors are ignored. Comparing this case with the nominal case shown in Table 1 shows that updating the measurable bias reduces the rendezvous uncertainty about 3 kilometers and the velocity error about 3 meters per second. Taking into account the clock offset error produces a negligible increase in both distance and velocity.

In the third and fourth cases, both the clock rate and the bias in the measurable is updated. The main increase in satellite position and velocity error is caused by the clock drift rate error. Updating this parameter, however, is not considered for the reason discussed previously.

A particularly interesting case is obtained when all clock errors are included but only the bias in the measurable is updated. In this case, which is the last case shown in Table 3, the position and velocity errors are less than that obtained when both the measurable bias and the clock rate error are updated. This means that updating the clock rate error actually increases the satellite's expected dispersion. The effect is caused by a cross-correlation between the clock rate error and the non-updated nuisance parameters. A cursory check of the cross-correlation functions associated with the clock rate error suggest that the major contribution to this result is caused by not updating the gravitational potential of the Moon. Since the effect of the clock rate error, like the other clock errors, is small in the first place, updating the clock nuisance parameters is considered unnecessary.

The Bissett-Berman Corporation 2941 Nebraska Avenue, Santa Monica, California EXbrook 4-3270

APOLLO NOTE NO. 381
(Task 2, Item II)

J. R. Holdsworth
11 October 1965

OPTIMAL WEIGHTING FUNCTIONS II

The purpose of this note is to continue the discussion of certain topics initiated in Apollo Note No. 205. In particular, we shall extend our considerations to the joint estimation of two parameters and will consider a different error correlation model than that which postulated for Apollo Note No. 205. This will permit a closer examination of the relative effects of using the non-optimal unweighted least squares estimates for the parameters involved. We shall also give an example of how prediction errors behave as a function of time by the use of what have been called Q matrices in earlier notes.

We shall assume that we are interested in predicting the constant velocity one-dimensional motion of a particle at some prediction time t_p. That is, we assume that the actual position of the particle at any arbitrary time t may be written as:

$$X(t_p) = X(\bar{t}) + \dot{X}(t_p - \bar{t}) \tag{1}$$

where $\dot{X}$ and $X(t_p)$ are constant but unknown quantities to be estimated. The estimators $\hat{X}(t_p)$, $\hat{\dot{X}}$ must be functions of observations $y(t_1), \ldots . y(t_N)$ which have been corrupted by additive noise.

That is, we assume that the kth observation $y(t_k)$ may be written as:

$$y(t_k) = X(t_k) + e_k . \tag{2}$$

or:

$$y(t_k) = X(\bar{t}) + \dot{X}(t_k - \bar{t}) + e_k \tag{3}$$

where the e_k's are equi-spaced samples from a Gaussian, zero mean stationary, exponentially auto-correlated random process, with a known correlation function so that:

$$E\, e_k \equiv 0 \tag{4}$$

and:

$$E\left[e_k\, e_{k+\ell}\right] = \sigma_e^2\ \rho^{|\ell|} \tag{5}$$

with:

$$|\rho| \leq 1 \tag{6}$$

To compute the estimates $\hat{X}(t_p)$ and $\hat{\dot{X}}$, it is convenient to first assume that the prediction time t_p is given by:

$$t_p = \bar{t} = \frac{1}{N} \sum_{i=1}^{N} t_i \tag{7}$$

Then aside from in-essential constants, the logarithm of the joint likelihood function of the N observations $y_1, \ldots y_N$ is given by:

$$\begin{aligned} \log L = {} & (y_1 - X(\bar{t}) - \dot{X}(t_1 - \bar{t}))^2 + (y_N - X(\bar{t}) - \dot{X}(t_N - \bar{t}))^2 \\ & + (1+\rho^2) \sum_{k=2}^{N-1} (y_k - X(\bar{t}) - \dot{X}(t_k - \bar{t}))^2 \\ & - 2\rho \sum_{k=1}^{N-1} (y_k - X(\bar{t}) - \dot{X}(t_k - \bar{t}))(y_{k+1} - X(\bar{t}) - \dot{X}(t_{k+1} - \bar{t})) \end{aligned} \tag{8}$$

The maximum likelihood estimators $X(\bar{t})$, $\dot{X}$ are obtained by computing:

$$\frac{\partial \log L}{\partial X(\bar{t})} = 0$$

$$\frac{\partial \log L}{\partial \dot{X}} = 0 \tag{9}$$

which yields:

$$\hat{X}(\bar{t}) = \frac{y_1 + (1-\rho) \sum_{k=2}^{N-1} y_k + y_N}{2 + (N-2)(1-\rho)} \tag{10}$$

and:

$$\hat{\dot{X}} = \frac{\left[(t_1-\bar{t}) - \rho(t_2-\bar{t})\right] y_1 + (1-\rho)^2 \sum_{k=2}^{N-1} (t_k-\bar{t}) y_k + \left[(t_N-\bar{t}) - \rho(t_{N-1}-\bar{t})\right] y_N}{(t_1-\bar{t})^2 + (1+\rho^2) \sum_{k=2}^{N-1} (t_k-\bar{t})^2 - 2\rho \sum_{k=1}^{N-1} (t_k-\bar{t})(t_{k+1}-\bar{t}) + (t_N-\bar{t})^2} \tag{11}$$

It is not hard to show from Equations (10) and (11), and (3) through (5) that:

$$E\,\hat{X}(\bar{t}) = X(\bar{t}) \tag{12}$$

$$E\,\hat{\dot{X}} = \dot{X} \tag{13}$$

$$\mathrm{Var}\,\hat{X}(\bar{t}) = \frac{(1+\rho)\,\sigma_e^2}{N(1-\rho) + 2\rho} \tag{14}$$

$$\mathrm{Var}\,\hat{\dot{X}} = \frac{(1-\rho^2)\,\sigma_e^2}{\sum_{k=1}^{N}(t_k-\bar{t})^2 - 2\rho\sum_{k=1}^{N-1}(t_{k+1}-\bar{t})(t_k-\bar{t}) + \rho^2\sum_{k=2}^{N-1}(t_k-\bar{t})^2} \tag{15}$$

Assuming that N is reasonably large and letting $T = t_N - t_1$ it may be shown that Equation (15) may be written:

$$\mathrm{Var}\,\hat{\dot{X}} \approx \frac{\frac{12}{NT^2}(1-\rho^2)\,\sigma_e^2}{(1-\rho)^2 + \frac{6}{N}\rho(1-\rho) + \frac{6}{N^2}\rho(1+\rho)} \tag{15a}$$

In addition we have:

$$E\left[(\hat{X}(\bar{t}) - X(\bar{t})(\hat{\dot{X}} - \dot{X})\right] = 0 \tag{16}$$

so that the covariance matrix of the estimators $\hat{X}(\bar{t})$, $\hat{\dot{X}}$ is:

$$\mathrm{Cov}\,(\hat{X}(\bar{t}),\ \hat{\dot{X}}) = \begin{pmatrix} \mathrm{Var}\,\hat{X}(\bar{t}) & 0 \\ 0 & \mathrm{Var}\,\hat{\dot{X}} \end{pmatrix} \tag{17}$$

We mention here that these formulas are valid only for the special case where the prediction time t_p is chosen to be equal to the average of the observation times $\bar{t}$, which for equally spaced observations is the mid-point of the tracking interval. Furthermore we note that since $X(t_p)$ will vary as t_p is varied that we should expect that its estimator $\hat{X}(t_p)$ would also vary as t_p. On the other hand, since $\dot{X}(t_p) = \dot{X}$ is constant for all t_p by assumption, we anticipate that its estimator $\hat{\dot{X}}(t_p) = \hat{\dot{X}}$ together with its variance will not depend upon the prediction time t_p. However, the independence of $\hat{X}(\bar{t})$ and $\hat{\dot{X}}$ does depend upon t_p equaling $\bar{t}$.

To investigate the situation for values of t_p not equal to $\bar{t}$ it is convenient to consider the two-dimensional state vector, the first component of which is $X(t)$, the second $\dot{X}$. From Equation (1) we may clearly write:

$$\begin{pmatrix} X(t_p) \\ \dot{X} \end{pmatrix} = \begin{pmatrix} X(\bar{t}) + \dot{X}(t_p - \bar{t}) \\ \dot{X} \end{pmatrix} \tag{18}$$

or:

$$\begin{pmatrix} X(t_p) \\ \dot{X} \end{pmatrix} = \begin{pmatrix} 1 & t_p - \bar{t} \\ 0 & 1 \end{pmatrix} \begin{pmatrix} X(\bar{t}) \\ \dot{X} \end{pmatrix} \tag{19}$$

so that if we define:

$$Q(t_p, \bar{t}) = \begin{pmatrix} 1 & t_p - \bar{t} \\ 0 & 1 \end{pmatrix} \tag{20}$$

then the state vector at an arbitrary prediction time t_p may be calculated from the state vector at time $\bar{t}$ by operating upon it with the matrix $Q(t_p, \bar{t})$.

Now for a fixed set of equally spaced observations $y_1, \ldots y_N$, it may be shown that the best estimate of the state vector at an arbitrary prediction time t_p, is obtained by:

$$\begin{pmatrix} \hat{X}(t_p) \\ \hat{\dot{X}} \end{pmatrix} = Q(t_p, \bar{t}) \begin{pmatrix} \hat{X}(\bar{t}) \\ \hat{\dot{X}} \end{pmatrix} \tag{21}$$

where the components of the estimated vector at $\bar{t}$ are given by Equations (10) and (11).

Since by definition:

$$\mathrm{Cov}\,(\hat{X}(t_p), \hat{\dot{X}}) = E\left[\begin{pmatrix} \hat{X}(t_p) - X(t_p) \\ \hat{\dot{X}} - \dot{X} \end{pmatrix} \begin{pmatrix} \hat{X}(t_p - X(t_p) \\ \hat{\dot{X}} - \dot{X} \end{pmatrix}^T\right] \tag{22}$$

we obtain:

$$\mathrm{Cov}\,(\hat{X}(t_p), \hat{\dot{X}}) = Q(t_p, \bar{t})\ \mathrm{Cov}\,(\hat{X}(\bar{t}), \hat{\dot{X}})\ Q^T(t_p, \bar{t}) \tag{23}$$

which from (17) may be expressed solely as functions of Var $\hat{X}(\bar{t})$, Var $\hat{\dot{X}}$, and $t_p - \bar{t}$ as:

$$\mathrm{Cov}\,(\hat{X}(t_p), \hat{\dot{X}}) = \begin{pmatrix} 1 & t_p - \bar{t} \\ 0 & 1 \end{pmatrix} \begin{pmatrix} \mathrm{Var}\,\hat{X}(\bar{t}) & 0 \\ 0 & \mathrm{Var}\,\hat{\dot{X}} \end{pmatrix} \begin{pmatrix} 1 & 0 \\ t_p - t & 1 \end{pmatrix} \tag{24}$$

or:

$$\mathrm{Cov}\,(\hat{X}(t_p), \hat{\dot{X}}) = \begin{pmatrix} \mathrm{Var}\,\hat{X}(\bar{t}) + (t_p - \bar{t})^2\,\mathrm{Var}\,\hat{\dot{X}} & (t_p - \bar{t})\,\mathrm{Var}\,\hat{\dot{X}} \\ (t_p - \bar{t})\,\mathrm{Var}\,\hat{\dot{X}} & \mathrm{Var}\,\hat{\dot{X}} \end{pmatrix} \tag{25}$$

Equation (25) concisely displays several interesting results. First, we note that unless t_p equals $\bar{t}$, the off diagonal terms do not vanish, hence, the midpoint of the observation interval is the only value of t_p such that the estimates of $X(t_p)$ and X are uncorrelated. Second, inspection of the first term of the matrix shows that the variance in predicted position is minimized when the position to be predicted is that at the midpoint at the observation interval. Third, we note that since Var $\hat{\dot{X}}$ does not depend upon t_p that the variance of both predicted position and velocity are minimized at $t_p = \bar{t}$.

The coefficient of correlation between $\hat{X}(t_p)$, $\hat{\dot{X}}$ is obtained from (25) by dividing the off diagonal term by the square root of the product of the diagonal terms and may be written:

$$\rho\,[\,\hat{X}(t_p), \hat{\dot{X}}\,] = \frac{t_p - \bar{t}}{\sqrt{(t_p - \bar{t})^2 + \dfrac{\mathrm{Var}\,\hat{X}(\bar{t})}{\mathrm{Var}\,\hat{\dot{X}}}}} \tag{26}$$

so that as the magnitude of the difference between the prediction time and the midpoint of the smoothing interval becomes very large, the

estimator errors become perfectly correlated either positively or negatively, depending upon whether the prediction time follows or precedes the middle of the smoothing interval. That is, from (26) we see that:

$$\lim_{|t_p - \bar{t}| \to \infty} \rho \left[\hat{X}(t_p), \hat{\dot{X}} \right] = \pm 1 \tag{27}$$

which, of course, implies the singularity in the limit of the matrix $\mathrm{Cov}\left[\hat{X}(t_p), \hat{\dot{X}}\right]$.

This could pose numerical problems in the actual orbit determination problem for the following reasons. Suppose that initially data were obtained at times $t_{11}, \ldots . t_{1N_1}$, to yield the estimates $\hat{X}(\bar{t}_1)$, $\hat{\dot{X}}_1$. Now suppose that $\hat{X}(\bar{t}_1)$, $\hat{\dot{X}}_1$ are to be combined in some fashion with N_2 measurements made at a different set of times $t_{21}, t_{22}, \ldots . t_{2N_2}$, in order to predict the value of the state vector at some time t_p quite distant from $\bar{t}_1$. Then the determination of the proper weighting to assign to $\hat{X}(\bar{t}_1)$, $\hat{\dot{X}}_1$, in combination with the second set of measurements, requires the inversion of the matrix $\mathrm{Cov}\left[\hat{X}_1(t_p), \hat{\dot{X}}_1\right]$. But if $|t_p - \bar{t}_1|$ is large, then this matrix will be nearly singular and very likely ill conditioned which will make its numerically accurate inversion extremely difficult.

We now consider the unweighted least squares estimates of $X(t_p)$ and $\dot{X}$, which we shall denote by $\bar{X}(t_p)$ and $\bar{\dot{X}}$ respectively in order to compare their prediction variances with those of the optimal estimators which we have just discussed.

The unweighted least squares estimates $\bar{X}(t_p)$, $\bar{\dot{X}}$ are those functions of the data which minimize the observed sum of squared differences shown on the following page.

$$D = \sum_{k=1}^{N} \left[y_k - X(t_p) - \dot{X}(t_k - t_p) \right]^2 \tag{28}$$

and are obtained by solving the equations:

$$\frac{\partial D}{\partial X(t_p)} = 0 \tag{29}$$

$$\frac{\partial D}{\partial \dot{X}} = 0$$

for $\overline{X}(t_p)$, $\overline{\dot{X}}$ as functions of the measurements $y_1, \ldots y_N$

Again by first assuming that $t_p = \overline{t}$ the solutions of (27) are easily shown to be:

$$\overline{X}(\overline{t}) = \frac{1}{N} \sum_{i=1}^{N} y_i \tag{30}$$

and:

$$\overline{\dot{X}} = \frac{\sum_{i=1}^{N} (t_i - \overline{t})\, y_i}{\sum_{i=1}^{N} (t_i - \overline{t})^2} \tag{31}$$

As in the former case the least squares estimates for an arbitrary prediction time t_p are obtained by operating on the state vector estimator at $t_p = \overline{t}$ by the Q matrix so that:

$$\begin{pmatrix} \overline{X}(t_p) \\ \overline{\dot{X}} \end{pmatrix} = Q(t_p, \overline{t}) \begin{pmatrix} \overline{X}(\overline{t}) \\ \overline{\dot{X}} \end{pmatrix} \tag{32}$$

To compare the prediction variance of $\overline{X}(t_p)$ with that of $\hat{X}(t_p)$ it is first necessary to calculate the covariance matrix $\mathrm{Cov}(\overline{X}(\overline{t}), \overline{X})$ of the estimator errors at $t_p = \overline{t}$. Having this, the error matrix for these estimators at an arbitrary t_p are obtained by:

$$\mathrm{Cov}\left[\overline{X}(t_p), \overline{\dot{X}}\right] = Q(t_p, \overline{t})\ \mathrm{Cov}\left[\overline{X}(\overline{t}), \overline{\dot{X}}\right] Q^T(t_p, \overline{t}) \tag{33}$$

From Equation (30), we have:

$$E\,\overline{X}(\overline{t}) = \frac{1}{N}\sum_{i=1}^{N} E\,y_i = X(\overline{t}) \tag{34}$$

hence:

$$E\left[(\overline{X}(\overline{t}) - X(\overline{t}))^2\right] = \mathrm{Var}\,\overline{X}(\overline{t})$$

$$= \frac{1}{N^2}\sum_{i=1}^{N}\sum_{j=1}^{N} E(e_i\,e_j)$$

$$= \frac{1}{N^2}\sum_{i=1}^{N}\sum_{j=1}^{N} \sigma_e^2\,\rho^{|i-j|}$$

or:

$$\mathrm{Var}\,\overline{X}(\overline{t}) = \frac{\sigma_e^2}{N}\left[1 + 2\rho\left\{\frac{N(1-\rho) - (1-\rho^N)}{N(1-\rho)^2}\right\}\right] \tag{35}$$

The calculation of the mean square error of the least squares estimate of the velocity seems to be a bit more complicated. From Equation (3) and (31) it follows that the estimator error is:

$$\Delta\overline{\dot{X}} = \overline{\dot{X}} - \dot{X} \tag{36}$$

or:

$$\Delta\overline{X} = \frac{\sum_{i=1}^{N} (t_i - \overline{t})\ e_{(i)}}{\sum_{i=1}^{N} (t_i - \overline{t})^2} \tag{37}$$

Equation (37) shows that the estimate $\overline{\dot{X}}$ is unbiased so that the mean square error and variance of $\overline{\dot{X}}$ are the same which permits us to write:

$$\mathrm{Var}\ \overline{\dot{X}} = E\left[(\Delta\overline{\dot{X}})^2\right] \tag{38}$$

$$= \frac{\sum_{i=1}^{N} \sum_{j=1}^{N} (t_i - \overline{t})(t_j - \overline{t})\ E\left[e_{(i)}\ e_{(j)}\right]}{\left[\sum_{i=1}^{N} (t_i - \overline{t})^2\right]^2}$$

or:

$$\mathrm{Var}\ \overline{\dot{X}} = \frac{\sigma_e^2 \sum_{i=1}^{N} \sum_{j=1}^{N} (t_i - \overline{t})(t_j - \overline{t})\ \rho^{|i-j|}}{\left[\sum_{i=1}^{N} (t_i - \overline{t})^2\right]^2} \tag{39}$$

Recalling that:

$$t_i - \bar{t} = \left(\frac{i-1}{N-1} - \frac{1}{2}\right) T \tag{40}$$

and that for large N:

$$\sum_{i=1}^{N} \left(\frac{i-1}{N-1} - \frac{1}{2}\right)^2 \approx \frac{N}{12} \tag{41}$$

equation (37) reduces to:

$$\mathrm{Var}\,\bar{\dot{X}} \approx \frac{12\sigma_e^2}{NT^2} + \frac{288\sigma_e^2}{N^2T^2} \sum_{i=1}^{N-1} \sum_{j=i+1}^{N} \left(\frac{i-1}{N-1} - \frac{1}{2}\right)\left(\frac{j-1}{N-1} - \frac{1}{2}\right)\rho^{j-1} \tag{42}$$

where the first term in (42) is the variance of the least squares estimate of $\dot{X}$ when the noise samples are uncorrelated.

The double summation appearing in the last term of Equation (42) may be explicitly evaluated although the calculation is a bit tedious. For completeness, however, we state that it may be shown that:

$$\sum_{i=1}^{N-1} \sum_{j=i+1}^{N} \left(\frac{i-1}{N-1} - \frac{1}{2}\right) \left(\frac{j-1}{N-1} - \frac{1}{2}\right) \rho^{j-i} \tag{43}$$

$$= \frac{1}{(N-1)^2} S_1 - \frac{1}{2(N-1)} S_2 - \frac{1}{2(N-1)} S_3 + \frac{1}{4} S_4$$

where:

$$S_1 = \frac{N(N-1)\rho^2}{2(1-\rho)^2} - \frac{\rho^2}{(1-\rho)^4}\left[N(1-\rho) - (1-\rho^N)\right]\left[1 + N(1-\rho)\right] + \frac{N(N-1)(N+1)\rho}{3(1-\rho)} \tag{44}$$

$$S_2 = \frac{(N-1)(N+2)\rho}{2(1-\rho)} + \frac{\rho^2}{(1-\rho)^3}\left[(1-\rho^{N-1})(2-\rho) - (N-\rho^{N-1})(1-\rho)\right] \tag{45}$$

$$S_3 = \frac{(N-1)\rho(2\rho-1)}{(1-\rho)^2} + \frac{(N-1)(N+2)\rho}{2(1-\rho)} - \frac{\rho^2(1-\rho^{N-1})}{(1-\rho)^3}\left[\rho + N(1-\rho)\right] \tag{46}$$

$$S_4 = \frac{(N-1)\rho}{1-\rho} - \frac{\rho^2(1-\rho^{N-1})}{(1-\rho)^2} \tag{47}$$

Lack of tenacity coupled with a suspicion that any further simplification of the last term in (42) would not be justified by the probable labor required, discouraged further efforts to obtain a tidier expression for Var $\dot{\bar{X}}$.

Equations (14) and (15a) and (35) and (42), which give the error variances for the optimal and unweighted least squares estimates respectively, of $X(\bar{t})$ and $\dot{X}$ permit some interesting comparisons. First consider the expressions given by Equations (14) and (15a) which are the error variances Var $\hat{X}(\bar{t})$ and Var $\hat{\dot{X}}$ of the optimal estimates of $X(\bar{t})$ and $\dot{X}$. From (14) we see that in one

cent noise samples are perfectly positively correlated, we see that $\mathrm{Var}\ \hat{X}(\bar{t}) = \sigma_e^2$ so that we effectively get information from only one observation, $y(\bar{t})$, in our entire data record.

From (15a), on the other hand, we see that for both $\rho = -1$ and $\rho = +1$ that $\mathrm{Var}\ \hat{\dot{X}} = 0$. In other words, perfect error correlation of adjacent noise samples either positive or negative, permits the exact error free determination of the velocity $\dot{X}$. This is rather interesting since it is in contrast with the case of the optimal estimate of center position $\hat{X}(\bar{t})$ whose error variance decreases as ρ becomes negative, but increases as it grows in a positive direction.

These results for the behavior of the optimal estimator variances as a function of the one lag noise correlation may be conveniently summarized by the following equations:

$$\lim_{\rho \to -1} \mathrm{Var}\ \hat{X}(\bar{t}) = 0 \tag{48}$$

$$\lim_{\rho \to 0} \mathrm{Var}\ \hat{X}(\bar{t}) = \frac{\sigma_e^2}{N} \tag{49}$$

$$\lim_{\rho \to +1} \mathrm{Var}\ \hat{X}(\bar{t}) = \sigma_e^2 \tag{50}$$

and:

$$\lim_{\rho \to -1} \mathrm{Var}\ \hat{\dot{X}} = 0 \tag{51}$$

$$\lim_{\rho \to 0} \quad \mathrm{Var}\ \hat{\dot{X}} = \frac{12\sigma_e^2}{NT^2} \tag{52}$$

$$\lim_{\rho \to +1} \quad \mathrm{Var}\ \hat{\dot{X}} = 0 \tag{53}$$

When we investigate the corresponding behavior of the least squares error variances Var $\overline{X}(\overline{t})$ and Var $\overline{\dot{X}}$ for these limiting values of the one lag noise auto-correlation ρ, we find some interesting differences. For example, if in the expression for Var $\overline{X}(\overline{t})$ as given by (35) we let $\rho \longrightarrow -1$ we see that two distinct contingencies arise, depending upon whether the number of observations is an even or an odd integer. In the first case,a little reflection show that when $\rho = -1$, Var $\overline{X}(\overline{t}) = 0$. On the other hand if N is an odd integer then from (35) we see that $\rho = -1$ implies that Var $\overline{X}(\overline{t}) = \sigma_e^2/N^2$. That is, when N is moderate in size, in the limiting case where $\rho = -1$ there is a considerable change in Var $\overline{X}(\overline{t})$ caused by the fortuitous parity of the number of data points.

At the other end of the spectrum, we see from Equation (35) that if we allow ρ to approach + 1, that the expression for Var $\overline{X}(\overline{t})$ becomes a 0/0 indeterminate form. A precise limit does exist however, and may be obtained by applying L'Hospital's rule to Equation (35) as $\rho \longrightarrow +1$. The result is that for $\rho = +1$, Var $\overline{X}(\overline{t}) = \sigma_e^2$ which was the same result obtained at this limit for the optimal estimator.

The error variance, Var $\overline{\dot{X}}$, of the least squares estimate $\overline{\dot{X}}$ of the velocity does not exhibit such whimsical behavior in any of its limiting cases. If one ponders upon Equations (39) and (42) it becomes clear that Var $\overline{\dot{X}} = 0$ whenever $\rho = \pm 1$, which was what we found for optimal velocity estimate $\hat{\dot{X}}$.

These results for the unweighted least squares error variances are summarized by the following equations:

$$\lim_{\rho \to -1} \quad \mathrm{Var}\ \overline{X}(\overline{t}) = 0 \quad \text{if N is an even integer} \tag{54}$$

$$\lim_{\rho \to -1} \quad \mathrm{Var}\ \overline{X}(\overline{t}) = \frac{\sigma_e^2}{N^2} \quad \text{if N is an odd integer} \tag{55}$$

$$\lim_{\rho \to 0} \quad \mathrm{Var}\ \overline{X}(\overline{t}) = \frac{\sigma_e^2}{N} \tag{56}$$

$$\lim_{\rho \to +1} \quad \mathrm{Var}\ \overline{X}(\overline{t}) = \sigma_e^2 \tag{57}$$

$$\lim_{\rho \to -1} \quad \mathrm{Var}\ \overline{\dot{X}} = 0 \tag{58}$$

$$\lim_{\rho \to 0} \quad \mathrm{Var}\ \overline{\dot{X}} = \frac{12\,\sigma_e^2}{NT^2} \tag{59}$$

$$\lim_{\rho \to +1} \quad \mathrm{Var}\ \overline{\dot{X}} = 0 \tag{60}$$

In the last two sets of equations we have included the $\rho = 0$ case merely to re-emphasize the fact that the optimal and unweighted least squares estimates are identical when adjacent noise samples are uncorrelated.

Having computed the estimator error variances $\mathrm{Var}\,\hat{X}(\bar{t})$, $\mathrm{Var}\,\hat{\dot{X}}$, $\mathrm{Var}\,\bar{X}(\bar{t})$, $\mathrm{Var}\,\bar{\dot{X}}$, we are now able to write the equations for both the optimal and unweighted least square, mean square prediction errors for any arbitrary prediction time t_p. These prediction error variances for an arbitrary prediction time t_p are easily shown to be given by:

$$\mathrm{Var}\,\hat{X}(t_p) = \mathrm{Var}\,\hat{X}(\bar{t}) + (t_p - \bar{t})^2\,\mathrm{Var}\,\hat{\dot{X}} \tag{61}$$

and:

$$\mathrm{Var}\,\bar{X}(t_p) = \mathrm{Var}\,\bar{X}(\bar{t}) + (t_p - \bar{t})^2\,\mathrm{Var}\,\bar{\dot{X}} \tag{62}$$

where in (61) the quantities $\mathrm{Var}\,\hat{X}(\bar{t})$ and $\mathrm{Var}\,\hat{\dot{X}}$ are given by Equations (14) and (15a) respectively, while the quantities $\mathrm{Var}\,\bar{X}(\bar{t})$ and $\mathrm{Var}\,\bar{\dot{X}}$ in (62) are those given by Equation (35) and (42).

We have purposely written the optimal and least squares prediction variances at the arbitrary prediction time t_p in terms of their position and velocity error variances at the midpoint of the tracking interval. The reason for doing this was to avail ourselves of the extra convenience afforded by the fact that the estimator errors of position and velocity are uncorrelated when the reference position is that at the center of the smoothing interval. This is true for both the optimal and unweighted least squares estimates in spite of the fact that the noise samples are auto correlated.

Thus with Equations (61) and (62) we may undertake a large number of numerical comparisons of the relative performance of the optimal and unweighted least squares predictors form as functions of the one lag correlation parameters, ρ, the prediction time distance $t_p - \bar{t}$, length of smoothing time T, etc.

We shall close this note with a brief discussion of the asymptotic limiting forms which our results assume when we obtain the tracking data continuously instead of discretely, over the interval:

$$0 \leq t \leq T \tag{63}$$

We now assume that at a particular instant of time t, in the interval that we observe:

$$y(t) = X(T/2) + \dot{X}(t - T/2) + e(t) \tag{64}$$

where:

$$E\left[e(t) \right] \equiv 0 \tag{65}$$

and where it is now more convenient to write the auto covariance function of the additive noise as:

$$E\left[e(t)\, e(t+\tau) \right] = \sigma_e^2\, e^{-\frac{\tau}{\theta}} \tag{66}$$

If one should wish to, the correlation time θ in (66) may be related to the one lag auto correlation parameter ρ and the time between successive samples Δt as follows:

$$\theta = \frac{\Delta t}{\log 1/\rho} \tag{67}$$

or:

$$\theta = \frac{t_N - t_1}{N \log 1/\rho} \tag{68}$$

To make a long story short, by an extension of Weiner's prediction method, e.g., Ref. 1, it is possible to show that in the continuous tracking case, the optimal estimates of $X(T/2)$ and $\dot{X}$ are given by:

$$\hat{X}(T/2) = \frac{\theta\,(y(o) + y(T)) + \int_o^T y(t)\,dt}{T + 2\theta} \tag{69}$$

and:

$$\hat{\dot{X}} = \frac{\frac{T\theta}{2}\,(y(T) - y(o)) + \int_o^T (t - T/2)\,y(t)\,dt}{\frac{T^2}{12}\,(6\,\theta + T)} \tag{70}$$

In these latter equations, $T/2$, being the midpoint of the smoothing interval plays the part of $\bar{t}$ in the discrete case.

Substituting (64) into (69) and (70) shows that the optimal estimator errors in the continuous case are:

$$\Delta\hat{X}(T/2) = \hat{X}(T/2) - X(T/2) \tag{71}$$

or:

$$\Delta\hat{X}(T/2) = \frac{\theta\,(e(o) + e(T)) + \int_o^T e(t)\,dt}{T + 2\theta} \tag{72}$$

$$\Delta\hat{\dot{X}} = \hat{\dot{X}} - \dot{X} \tag{73}$$

or:

$$\Delta\hat{\dot{X}} = \frac{\frac{T\theta}{2}\,(e(T) - e(o)) + \int_o^T (t - T/2)\,e(t)\,dt}{\frac{T^2}{12}\,(6\theta + T)} \tag{74}$$

Among other things, these expressions show that in the continuous case, the optimal estimates are unbiased also; hence, their mean square errors are their variances.

The variance of $\hat{X}(T/2)$ is obtained in a straightforward manner by squaring both sides of (72) and taking the expected value. Recalling that the expected value operator may be taken inside the integration with respect to time, the resulting integrals may be easily evaluated to yield:

$$\mathrm{Var}\,\hat{X}(T/2) = \frac{2\sigma_e^2\,\theta}{T + 2\theta} \tag{75}$$

The variance of $\hat{\dot{X}}$ is calculated by squaring both sides of (74) and proceeding in a similar manner. The algebra is a little messier but a moderate amount of perserverance yields the following equation.

$$\mathrm{Var}\,\hat{\dot{X}} = \frac{24\sigma_e^2\,\theta}{T(T+6\theta)^2} + \frac{72\,\sigma_e^2\,\theta^2}{T^2(T+6\theta)^2}\left(1 - e^{-T/\theta}\right)$$

$$+ \frac{288\,\sigma_e^2\,\theta^4}{T^4(T+6\theta)^2}\left(1 - \frac{T}{2\theta}\right)\left[\left(1 - \frac{T}{2\theta}\right) - e^{-T/\theta}\left(1 + \frac{T}{2\theta}\right)\right] \tag{76}$$

As in the discrete sampling case, the estimator errors $\Delta\hat{X}(T/2)$ and $\Delta\hat{\dot{X}}$ are uncorrelated so that just as before, we may write the following equation for the prediction error variance for an arbitrary prediction time t_p.

$$\mathrm{Var}\,\hat{X}(t_p) = \mathrm{Var}\,\hat{X}(T/2) + (t_p - T/2)^2\,\mathrm{Var}\,\hat{\dot{X}} \tag{77}$$

where the terms $\mathrm{Var}\,\hat{X}(T/2)$ and $\mathrm{Var}\,\hat{\dot{X}}$ in (77) are those given by Equation (75) and (76) which we have just discussed for the continuous case.

It is a little tricky to rigorously prove directly, that in the continuous limit, the estimators $\hat{X}(\bar{t})$, $\hat{\dot{X}}$ given by Equations (10) and (11) assume the forms shown in (69) and (70). As suggested earlier, the best way perhaps is not to attempt to work with the discrete equations and pass to the limit, but to approach the problem on its own merits as an extended Weiner filtering or prediction problem. The details together with the necessary descriptive preliminaries required to obtain Equations (69) and (70) are too long to reproduce here. To the interested reader who would like to go through the mathematical development, we repeat our recommendation that he consult the paper by Zadeh and Ragazzini in Reference (1). With this background, a reasonably simple alteration of one of the examples they discuss, will yield Equations (69) and (70) as we have written them. Another very interesting paper which treats an overlapping class of problems is that by R. E. Vowels in Reference (2).

The continuous limit of the unweighted least squares estimates is much easier to obtain. By direct analogy with the discrete tracking case, the continuous unweighted least squares estimates of $X(T/2)$ and $\dot{X}$, are those functionals of the observed data function $y(t)$ which minimize the following error integral.

$$Q = \int_0^T \left[y(t) - X(T/2) - (t - T/2)\,\dot{X} \right]^2 dt \tag{78}$$

Just as before, the unweighted least squares estimates $\bar{X}(T/2)$ and $\bar{\dot{X}}$ are those functionals of the observed data $y(t)$ obtained by the simultaneous solution of:

$$\frac{\partial Q}{\partial X(T/2)} = 0 \tag{79}$$

$$\frac{\partial Q}{\partial \dot{X}} = 0 \tag{80}$$

These calculations are easily made, and the equations are readily solved to yield the following expressions for the unweighted least squares estimates when the data are taken continuously.

$$\bar{X}\ (T/2) = \frac{1}{T} \int_o^T y\ (t)\ dt \tag{81}$$

$$\bar{\dot{X}} = \frac{12}{T^3} \int_o^T (t - T/2)\ y\ (t)\ dt \tag{82}$$

The estimators $\bar{X}\ (T/2)$ and $\bar{\dot{X}}$ just given are unbiased and may also be shown to be uncorrelated. The resulting estimator errors $\Delta\bar{X}\ (T/2)$ and $\Delta\bar{\dot{X}}$ are thus given by:

$$\Delta\bar{X}\ (T/2) = \frac{1}{T} \int_o^T e\ (t)\ dt \tag{83}$$

$$\Delta\bar{\dot{X}} = \frac{12}{T^3} \int_o^T (t - T/2)\ e\ (t)\ dt \tag{84}$$

The variances of those unweighted least squares estimates are obtained by squaring (83) and (84) and taking the expected values. That is:

$$\mathrm{Var}\ \bar{X}\ (T/2) = E\left[\ \Delta\bar{X}^2\ (T/2)\ \right] \tag{85}$$

$$= \frac{1}{T^2} \int_o^T \int_o^T E\left[\ e\ (u)\ e\ (v)\right] du\ dv \tag{86}$$

$$= \frac{\sigma_e^2}{T^2} \int_o^T \int_o^T e^{-\frac{|u-v|}{\theta}}\ du\ dv \tag{87}$$

or:

$$\mathrm{Var}\ \bar{X}\ (T/2) = \frac{2\ \sigma_e^2}{T} - \frac{2\ \sigma_e^2\ \theta^2}{T}\ (1 - e^{-T/\theta}) \tag{88}$$

Likewise, from (84) we get:

$$\mathrm{Var}\,\overline{\dot{X}} = E\left[(\Delta\overline{\dot{X}})^2\right] \tag{89}$$

$$= \left(\frac{12}{T^3}\right)^2 \int_o^T \int_o^T (u - T/2)(v - T/2)\, E\left[e(u)\, e(v)\right] du\, dv$$

$$= \sigma_e^2 \left(\frac{12}{T^3}\right)^2 \int_o^T \int_o^T (u - T/2)(v - T/2)\, e^{-\frac{|u-v|}{\theta}}\, du\, dv \tag{90}$$

or:

$$\mathrm{Var}\,\overline{\dot{X}} = \frac{24\,\sigma_e^2\,\theta}{T^3} - \frac{72\,\sigma_e^2\,\theta^2}{T^4}\left(1 + \frac{2\theta}{T}\right)\left[e^{-\frac{T}{\theta}} + \left(1 - \frac{2\theta}{T}\right)\right] \tag{91}$$

This wraps everything up and should permit almost any sort of numerical comparison one wishes for the continuous case.

References

1. Zadeh and Ragazzini, An Extension of Wiener's Theory of Prediction, Journal of Applied Physics, 21, pp 645-655 July, 1950.

2. Vowels, R. E., The Application of Statistical Methods to Servo Mechanisms, Australian Journal of Applied Sciences, Vol. 4, pp 469-488, 1953.

APOLLO NOTE NO. 382
(Task 2, Item II)

J. W. Childress, III
11 November 1965

CONSTANT, LINEAR ECCENTRICITY

INTRODUCTION

This note describes a rendezvous technique which includes the use of coaxial ellipses in the procedure. This technique was proposed by NASA-Houston. The study determines the boost requirements in magnitude and direction for general rendezvous as well as the orbits needed. Thus, four distinct orbits are used. The burnout conditions (or state) define the initial orbit. It is assumed that the nominal position and velocity vectors will be the same after each launch. The launch time will also be a constant (this does not limit the analysis since the time from launch to rendezvous is the critical parameter. For this reason the launch time, t_L, could be identically zero or any other constant.) The assumption that the burnout conditions are constant does not restrict the rendezvous altitude to altitudes higher than the burnout altitude. (Obviously, it would be necessary to reverse the directions of the "orbit-changing" boosts but the magnitudes are unchanged.) The first "orbit-changing" boost, which comes when the true anomaly is 90° greater than the true anomaly at burnout is the only "free" boost. It is called "free" because it is not constrained by primary mission objectives. While it is obvious that one of the primary objectives is rendezvous, another primary objective is to achieve the transfer to the orbit preceding the rendezvous orbit via a particular coaxial orbit transfer; i. e., constant linear eccentricity. Minimization of the specific fuel requirements, i. e. fuel per unit mass, is a secondary objective.

The second "orbit-changing" boost is constrained by the coaxial orbit transfer condition, while the third "orbit-changing" boost is constrained by the rendezvous requirements. Figure 1 shows the proposed trajectory. Table I is a list of symbols used in the analysis.

AW1947

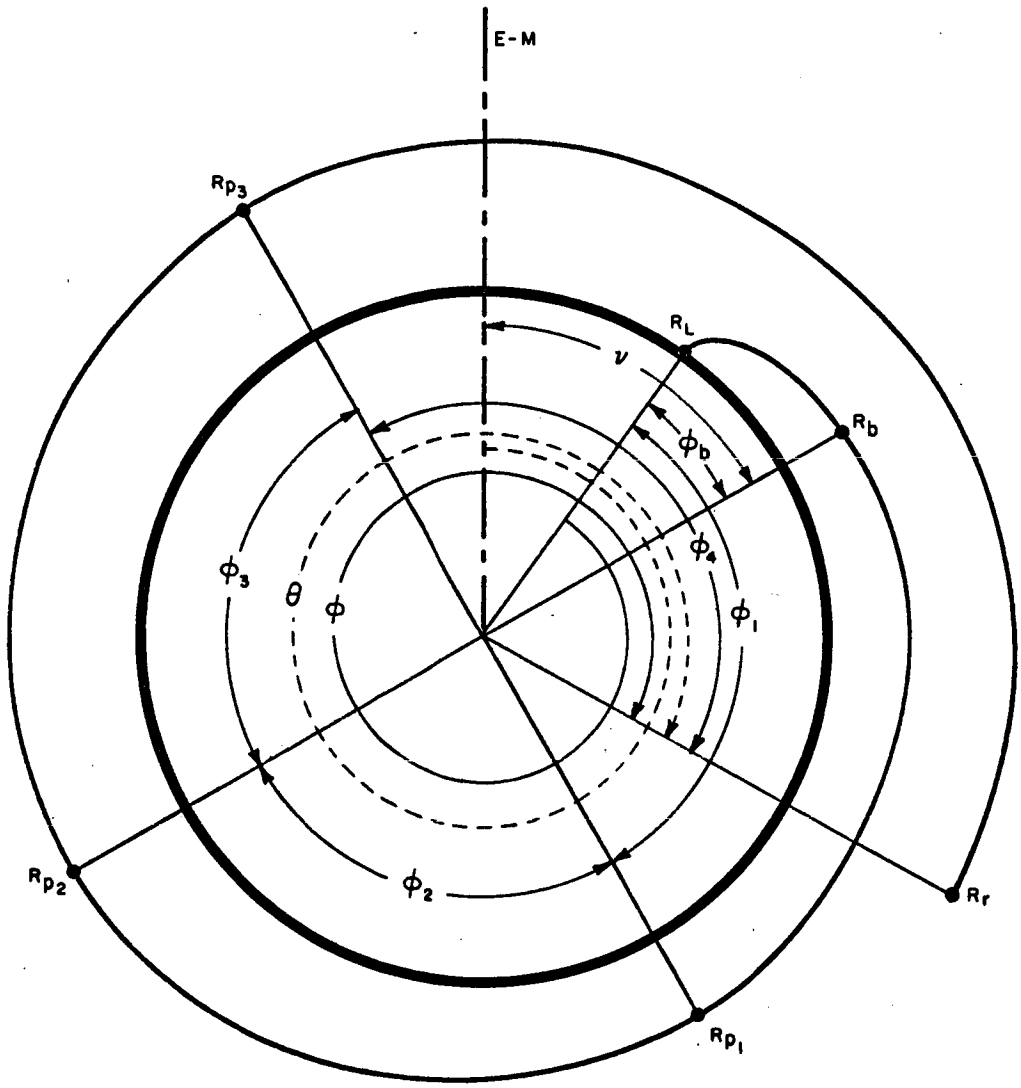

Figure 1

TABLE OF SYMBOLS

$\overline{X}_i$	the ith state vector $(\overline{R}_i, \overline{V}_i)^T$
$\overline{R}_i$	the ith position vector
r_i	the ith scalar range
$\overline{V}_i$	the angle between velocity nodes
E - M	the Earth-Moon line
Az	the flight path azimuth, i.e., the angle between the orbit plane and the meridian containing the rocket at burnout
u	the angle between the line of nodes and $\overline{R}_L$
v	the true anomaly
ϕ_b	the angle between $\overline{R}_L$ and $\overline{R}_b$
θ	the angle between E - M and $\overline{R}_r (2\pi \leq \theta \leq 3\pi)$
ϕ	the angle between $\overline{R}_L$ and $\overline{R}_r (2\pi \leq \theta \leq 3\pi)$
ϕ_1	the angle between $\overline{R}_L$ and $\overline{R}_{p1}$
ϕ_2	the angle between $\overline{R}_{p1}$ and $\overline{R}_{p2}$
ϕ_3	the angle between $\overline{R}_{p2}$ and $\overline{R}_{p3}$
ϕ_4	the angle between $\overline{R}_{p3}$ and $\overline{R}_r$

Table of Symbols (continued)

e_i	the eccentricity after the ith boost
a_i	the major axis after the ith boost
b_i	the minor axis after the ith boost
c_i	the linear eccentricity after the ith boost
α_b	the right ascension after burnout
α_L	the right ascension at launch
δ_b	the declination after burnout
δ_L	the declination at launch
θ_b	the longitude at burnout
θ_L	the longitude at launch
β	the flight path angle; i. e., the angle between $\overline{R}_i$ and $\overline{V}_i$
$\overline{i}, \overline{j}, \overline{k}$	the unity vectors in the x, y, z (or x', y', z' system if the mean is the reference body) - normally $\overline{i}$ points to the vernal equinox
t_i	the transit time between R_{pi} and R_{pi-1} (t_4 is the transit time between R_r and R_{p3}
h_i	the angular momentum after the ith boost
ι	the inclination of the orbit plane

Table of Symbols (continued)

Ω	the longitude of the ascending node
$\Delta\lambda$	the right ascension
ω	the requirement of the pericenter
$\dot{V}_i$	the rate at which the time anomaly changes after the ith boost
b(subscript)	refers to burnout
L "	refers to launch
PI "	refers to i^{th} impulsive boost
r "	refers to rendezvous position
p_i or p "	refers to perigee
a_i or a "	refers to apogee
'(superscript)	refers to state before boost while the absence of the prime denotes the state after boost

ANALYSIS

In order to simplify the analysis orbital plane transfers were not permitted. In addition, two-dimensional analysis was used for further simplification. Either or both of these assumptions could be eliminated without seriously affecting the analysis. The out-of-plane transfers are tricky because the out-of-plane velocity boost must be taken out when the out-of-plane transfer is completed. The equations needed for 3-D analysis are included below:

$$\cos \iota = \sin Az \cos \phi_b, \tag{1}$$

$$\tan \Delta\lambda = \tan Az \sin \phi_b, \text{ and} \tag{2}$$

$$\cos u = \cos Az \cos \phi_b, \tag{3}$$

where ι is the inclination of the orbit plane, $\Delta\lambda$ is the right ascension, ϕ_b is the angle between $\overline{R}_L$ and $\overline{R}_b$, u is the angle between the line of nodes and $\overline{R}_L$, and Az is the flight path azimuth.

The state vector at rendezvous $\overline{X}_r = (\overline{R}_r, \overline{V}_r, t_r)^T$ defines one point on the final orbit. If a minimum energy expenditure constraint, between two fixed end points in a conservative field, is applied, then one additional constraint will define the rendezvous orbit and the preceding orbits. Ideally the rendezvous time, t_r could be adjusted by adjusting the launch time or burnout time, t_b. Since:

$$t_r = t_b + t_1 + t_2 + t_3 + t_4, \tag{4}$$

where the t_i (i = 1, 2, 3) are the R_{Pi} to R_{Pi-1} and t_4 is the transit time between R_{P3} and R_r, there is an opportunity to adjust t_r; i. e., during t_2. Since it is assumed that the burnout conditions are fixed, the eccentricity for the first orbital segment is given by:

$$e_1 = -1 + \frac{V_b^2 r_b}{\mu} \tag{5}$$

where V_b is the burnout velocity, r_b is the magnitude of the burnout radius, and μ is the gravitational constant when burnout occurs at pericenter. When burnout does not occur at the pericenter, the analysis becomes far more complex and the trajectory becomes less efficient from a fuel economy point of view.

The other parameters are given by:

$$a_1 = \left[\frac{2}{r_b} - \frac{V_b^2}{\mu}\right]^{-1}, \tag{6}$$

$$V_{pb} = V_b, \tag{7}$$

$$r_{pb} = r_b, \tag{8}$$

$$V_{ab} = \frac{\mu}{a_1 V_b}, \tag{9}$$

$$r_{ab} = a_1(1 + e_1), \text{ and} \tag{10}$$

$$b_1 = \left[a_1(1 + e_1)\, r_b\right]^{1/2}, \tag{11}$$

where r is the magnitude of the radius vector, V is the velocity vector magnitude, a is the semi-major axis, b is the semi-minor axis, and the subscripts p, a, b and 1 refer to the periapsis (pericenter), apoapsis (apocenter), b burnout and first orbit, respectively.

The final orbit parameters are:

$$e_4 = e_r = 1 - \frac{V_r^2 r_r}{\mu}, \tag{12}$$

$$a_4 = a_r = \left[\frac{2}{r_p} - \frac{V_p^2}{\mu}\right]^{-1}, \tag{13}$$

$$V_{ar} = V_r , \tag{14}$$

$$r_{ar} = r_r , \tag{15}$$

$$V_{pr} = \frac{\mu}{a_4 V_r} , \tag{16}$$

$$r_{pr} = a_4(1 - e_4), \text{ and} \tag{17}$$

$$b_4 = \left[a_4(1 + e_4)\, r_p\right]^{1/2} \tag{18}$$

where the subscripts 4 and r indicate the 4th or rendezvous orbits, when it is assumed that rendezvous occurs at apocenter. If rendezvous does not occur at apocenter, but the last impulsive boost is given at pericenter, then Equations (12) through (18) become:

$$e_4 = 1 - \frac{V_{P3}\, r_{P3}}{\mu} , \tag{19}$$

$$a_4 = a_r = \left[\frac{2}{r_{P3}} - \frac{V_{P3}^2}{\mu}\right]^{-1} , \tag{20}$$

$$V_{pr} = V_{P3} , \tag{21}$$

$$r_{pr} = r_{P3} , \tag{22}$$

$$V_{ar} = \frac{\mu}{a_4 V_{P3}} , \tag{23}$$

$$r_{ar} = a_4(1 + e_4), \text{ and} \tag{24}$$

$$b_4 = \left[a_4(1 + e_1)\, r_{P3}\right]^{1/2} , \tag{25}$$

where the subscripts P_i refer to the state vector $\overline{X}$ at the point R_{Pi}.

Regardless of which set of equations are used; i.e., 12-19 or 19-25, the following relationships must exist between orbits 3 and 4:

$$C_3 = a_3 e_3 = a_4 e_4 = C_4 \tag{26}$$

(the linear eccentricity condition which was imposed by NASA).

When rendezvous occurs at the apocenter, the state vector after the final "orbit-changing" boost at R_{p3} is found from:

$$r_{P3} = \frac{P_4}{1 + e_4 \cos(-\theta + \frac{\pi}{2} + 2)}, \text{ where} \tag{27}$$

$$P_4 = \frac{(V_{ar} V_{ar})^2}{\mu}, \text{ and} \tag{28}$$

$$V_{P3} = \left[\mu \frac{2}{r_{P3}} - \frac{1}{a_4}\right]^{1/2}, \tag{29}$$

when P is the orbit parameter, θ is the angle between the Earth-Moon line and the rendezvous position. Since $\left[\overline{X}_{P3}\right]$ is not, in general, one of the apses, it is necessary to compute the flight path angle at $\overline{R}_{p3}$ in order to determine the boost requirements at that point. The flight path angle can be determined from:

$$(r_r V_r / V_{P3} r_{P3}) = \sin \beta_3 . \tag{30}$$

When $\left[\overline{X}_{P3}\right]$ is at the pericenter, the $\left[\overline{X}_r\right]$ is found from:

$$r_r = \frac{P_4}{1 + e_4 \cos(\theta - 3\frac{\pi}{2} - v)}, \text{ where} \tag{31}$$

$$P_4 = r_{P3}(1 + e_4), \tag{32}$$

and v is the true anomaly.

In this case, the flight path angle is zero at $\left[\overline{X}_{P3}\right]$.

Notice that knowledge of $\left[\overline{X}_r\right]$ and e is required in order to solve the problem so all of Equations (12) to (32), except (26), are completely determined by the assumption that rendezvous occurs at the apocenter or that the last impulsive "orbit-changing" boost occurs at the pericenter. Both assumptions are considered because of minimum energy considerations, as well as for simplifications. If the final orbit is to be circular, then:

$$r_{P3} = r_r = a_4 = b_4 = p_4 , \tag{33}$$

$$V_{P3} = V_r , \text{ and} \tag{34}$$

$$\beta_4 = 0 = e_4 . \tag{35}$$

Unless the $\left[\overline{X}_{Pi}\right]$ are π rather than $\pi/2$ degrees apart, the rendezvous cannot be conducted on a minimum energy basis. This is apparent since each of the boosts cannot occur at an apsis. An attempt will be made to minimize the energy requirement subject to the $\pi/2$ boost constraints and the constraint imposed by Equation (26).

In order to minimize the fuel consumption, as well as to simplify the analysis, it will be assumed that either $\left[\overline{X}_{P3}\right]$ or $\left[\overline{X}_{P2}\right]$ defines an apsis. If $\left[\overline{X}_{P3}\right]$ is an apsis, for the 3rd orbit:

$$C_3 = a_3 - r_{P3} = \frac{1}{2}\left[a_3(1 + e_3) - r_{P3}\right] \tag{36}$$

when the apsis is a pericenter, or:

$$C_3 = -a_3 + r_{P3} = \frac{1}{2}\left[r_{P3} - a_3(1 - e_3)\right] \tag{37}$$

when the apsis is apocenter. In any case:

$$r_{P2} = p_3 . \tag{38}$$

If the $\left[\overline{X}_{P3}\right]$ is a pericenter after the final transfer and an apocenter before, then the required boost is given by:

$$\Delta V_3 = V_{P3} - V_{a3} \tag{39}$$

Since C_3, C_4 and $\overline{X}_{P3}$ are known, a_3 can be computed from Equation (37). Subsequently, e_3 is found from:

$$e_3 = \frac{r_{P3}}{a_3} - 1 \tag{40}$$

Now:

$$\begin{aligned} V_{a3} &= \left[\frac{\mu}{r_{P3}} (1 - e_3)\right]^{1/2} \\ &= \left[\frac{\mu}{r_{P3}} \left(2 - \frac{r_{P3}}{a_3}\right)\right]^{1/2} = \left[\frac{2\mu}{r_{P3}} - \frac{\mu}{a_3}\right]^{1/2} \\ &= \mu^{1/2} \left[\frac{2}{r_{P3}} - \frac{1}{(r_{P3} - C_4)}\right] \quad \text{and} \end{aligned} \tag{41}$$

$$V_{P3} = \left[V_r^2 + 2\mu \left(\frac{1}{r_{P3}} - \frac{1}{r_r}\right)\right]^{1/2} \tag{42}$$

in terms of the rendezvous coordinates and Equations (31) and (32) give r_{P3} in terms of r_r. Equation (13) gives a_4 in terms of r_r and V_r so e_4, i.e.:

$$e_4 = \left[1 - \frac{V_r^2 r_r}{\mu} \left(2 - \frac{V_r^2 r_r}{\mu}\right) \sin \beta_r\right]^{1/2}, \text{ and} \tag{43}$$

$$p_4 = \frac{V_r^2 r_r^2 \sin^2 \beta_r}{\mu} = r_{P3}(1 + e_4) \tag{44}$$

are sufficient to define the final orbit. Alternatively, Equation (42) may be written:

$$V_{P3} = \left(\frac{\mu}{p_4}\right)^{1/2} (1 + e_4) = \left[\frac{\mu}{p_4(1+e_4)}\left(2 - \frac{(1+e_4)}{a_4}\right)\right]^{1/2} \tag{45}$$

$$= \left[\frac{\mu}{r_{P3}} (1 + e_4)\right]^{1/2}$$

If $\left[\overline{X}_{P3}\right]$ is an apocenter after the final transfer and a pericenter before, then the required boost is given by:

$$\Delta V_3 = V_{P3} - V_{P3} \tag{46}$$

(< 0, i.e. opposite direction from Equation 39). Equations (13), (43), and (44) define the final orbit so:

$$r_{P3} = p_4/(1 - e_4) = r_{a4} \tag{47}$$

defines the apocenter and:

$$V_{P3} = V_{ar} = \left[\frac{\mu}{r_{P3}} (1 - e_4)\right]^{1/2} = \left[\left(\frac{\mu}{r_{P3}}\right)\left(2 - \frac{r_{P3}}{a_4}\right)\right]^{1/2} \tag{48}$$

defines the velocity at the apocenter. Now V_{P3} is found by noting that Equations (26), (36) and (47) yield a_3 which leads to:

$$V_{P3} = \left[\frac{\mu}{r_{P3}} \left(2 - \frac{r_{P3}}{a_3}\right)\right]^{1/2} \tag{49}$$

Thus, the state vector and the orbit before the final corrective boost have been determined as well as the final "orbit-changing" boost.

The perigee-perigee and apogee-apogee cases are described by combinations of equations already found.

If the rendezvous occurs at a pericenter, then the state vector is found from the following equations:

$$r_{P3} = \frac{p_4}{1 + e_4 \cos\left(\theta - \frac{3\pi}{2} - v\right)} , \tag{50}$$

$$p_4 = (r_r V_r)^2/\mu = r_r(1 + e_4) , \tag{51}$$

$$V_{P3} = \left[V_r^2 + 2\mu\left(\frac{1}{r_{P3}} - \frac{1}{r_r}\right)\right]^{1/2} , \tag{52}$$

$$e_4 = \frac{V_r^2 r_r}{\mu} , \text{ and} \tag{53}$$

$$\sin \beta_3 = \frac{r_r V_r}{V_{P3} V_{P3}} . \tag{54}$$

At this point, the state vectors at $\overline{X}_{P3}$ and $\overline{X}_r$ have been defined as well as the required velocity increments; i.e., the "orbit-changing" boosts. In addition, the state vector at burnout $\overline{X}_b$ has been determined, hence the state vectors at R_{p1} and R_{p2} are partially determined.

Now:

$$r_{P2} = p_3 \tag{55}$$

if R_{p3} is an apsis.

In order to determine the state vectors when rendezvous occurs at an apsis, it is necessary to make some assumption regarding the orbit before the second corrective boost. The simplest assumption is(1) the flight path angle is unchanged during the second "orbit-changing" boost, or (2) the second boost occurred at an apsis. Before selecting either of these assumptions, it is worthwhile to evaluate the effects of the initial orbit on the final since the second orbit "patches" orbits 1 and 3 together. The first and third orbits

are somewhat arbitrary with the second orbit obviously determined by the first and third. If it is decided that either rendezvous or the last boost occurs at an apsis, then this assumption, along with Equation (26) determines r_{P2}. Since the endpoint of the trajectory is always specified, it is possible to drop the apsis assumption and replace it with some other constraint, but this will not be done at this time.

Assuming that the burnout conditions define the pericenter, R_{P1} is given by:

$$R_{P1} = r_b(1 + e_1). \tag{56}$$

The velocity before the first "orbit-changing" boost is given by:

$$V'_{P1} = \left[V_b^2 + 2\mu \left(\frac{1}{R_{P1}} - \frac{1}{r_b}\right)\right]^{1/2} ; \tag{57}$$

while the flight path angle is given by:

$$\sin \beta_1 = \frac{V_b \, r_b}{V_{P1} \, r_{P1}} \tag{58}$$

Since R_{P1} and R_{P2} are fixed by the initial conditions and Equation (26), there is only one "free" variable associated with this rendezvous technique. Thus, one additional assumption will completely specify the complete trajectory. If it is assumed that the point R_{P1} serves as a pericenter for the second orbit, then the second orbit is determined. This is shown by noting that R_{P2} is determined by the rendezvous conditions while R_{P1} is determined by the launch conditions. Thus:

$$r = \frac{p_2}{1 + e_2 \cos v} \tag{59}$$

describes the second orbit. The parameters p_2 and e_2 are found noting that:

$$r_{P1} = \frac{p_2}{1 + e_2} \tag{60}$$

and that:

$$r_{P2} = p_2 \tag{61}$$

If it is assumed that the point R_{P1} is an apocenter, then Equation (59) has solutions:

$$r_{P1} = \frac{p_2}{1 - e_2} \quad \text{and} \tag{62}$$

$$r_{P2} = p_2. \tag{63}$$

If the point R_{P2} is a pericenter, then Equation (59) has solutions:

$$r_{P2} = \frac{p_2}{1 + e_2} \quad \text{and} \tag{64}$$

$$r_{P1} = p_2. \tag{65}$$

On the other hand, if R_{P2} is an apocenter, then:

$$r_{P2} = \frac{p_2}{1 - e_2} \tag{66}$$

and

$$r_{P1} = p_2. \tag{67}$$

In each of these cases, the velocity at the point which is not an apsis is given by:

$$V = \left[V_a^2 + 2\mu \left(\frac{1}{r} - \frac{1}{r_a}\right)\right]^{1/2} \tag{68a}$$

$$V = \left[V_p^2 + 2\mu \left(\frac{1}{r} - \frac{1}{r_p}\right)\right]^{1/2}, \tag{68b}$$

where 68a is used if the apsis is an apocenter while 68b is used if the apsis is a pericenter.

Since a_2 is found from:

$$a_2 = \frac{r_{P1}}{1 - e_2}, \tag{69a}$$

$$= \frac{r_{P2}}{1 + e_2}, \tag{69b}$$

$$= \frac{r_{P2}}{1 - e_2}, \quad \text{or} \tag{69c}$$

$$= \frac{r_{P2}}{1 + e_2}; \tag{69d}$$

when r_{P1} is a pericenter or apocenter, or if r_{P2} is a pericenter or an apocenter, respectively; and:

$$V_{P1} = \left[\left(\frac{\mu}{R_{P1}}\right) \left(2 - \frac{R_{P1}}{a_2}\right)\right]^{1/2} \tag{70}$$

when R_{P1} is an apsis, or:

$$V'_{P2} = \left[\left(\frac{\mu}{R_{P2}}\right) \left(2 - \frac{R_{P2}}{a_2}\right)\right]^{1/2} \tag{71}$$

when R_{P2} is an apsis.

Since the velocity at R_{P2} after the second orbit-changing boost is given by:

$$V_{P2} = \left[V'_{P3} + 2\mu \left(\frac{1}{r_{P2}} - \frac{1}{r_{P3}}\right)\right]^{1/2} \tag{72}$$

the minimum boost required is:

$$\Delta V_2 = V_{P2} - V'_{P2} \tag{73}$$

This boost is the minimum required to achieve the magnitude of V_{P2} desired since it assumes that no boost is required to change the flight path angle which is $\pi/2$. If the flight path angle is to be changed, then:

$$\Delta V_2 = \frac{V'_{P3}\, r_{P3}}{r_{P2}} \frac{\sin \beta'_3}{\sin \beta_2} - \frac{V'_{P1}\, r_{P1}}{r_{P2}} \frac{\sin \beta_1}{\sin \beta'_2} \tag{74}$$

or:

$$\Delta V_2 = \left[V^2_{P2} + V^{2'}_{P2} - 2V_{P2}\, V'_{P2} \cos (\beta_2 - \beta'_2)\right]^{1/2} \tag{75}$$

when the flight path angle is changed from β'_2 to β_2. Obviously, Equation (74) is simplified if β_1 and β'_3 are $\pi/2\ (2n + 1)(n = 0, 1, \ldots)$. A practical choice seems to be $\pi/2$ which could correspond to apses at r_{P1} and r_{P3}. Equation (74) may be more useful than Equation (75) since knowledge of V_{P2} and V'_{P2} is not required and β_2 and β'_2 are known if the state vectors at R_{P1} and R_{P3} are known. Since:

$$\Delta V_1 = V_{P1} - V'_{P1}, \tag{76}$$

where V_{P1} is given by either Equation (68) or (70), and V'_{P1} is given by Equation (57); all of the required boosts have been determined.

From Equation (75), it is noted that a change in the flight path angle requires additional boost $\Delta V_{\Delta\beta}$. This additional boost may be determined by subtracting $(V_{P2} - V'_{P2})$ from Equation (75); i. e.,

$$\Delta V_{\Delta\beta} = \Delta V_2 - V_{P2} + V'_{P2}$$

$$= \left[V_{P2}^2 + (V'_{P2})^2 - 2V_{P2}V'_{P2}\cos(\beta_2 - \beta'_2)\right]^{1/2} - V_{P2} + V'_{P2} \quad (77)$$

If the vehicle must be rotated in order to thrust in the proper direction, then additional energy will be required to start and stop the rotation needed. While more thrust is required to change the flight path angle, this is not necessarily derogatory. If the flight path angle increases toward $\pi/2$, while the magnitude of the velocity is increasing, then the angular momentum is increased.

EVALUATION OF OPTIONS

In order to select the most promising options, some of the least promising must be eliminated. Although it was not given much consideration during the analysis, it is obviously possible to inject into a circular orbit following the last boost. This is not feasible in this case since Equation (26) must be satisfied. If the fourth orbit is circular; i. e., $e = 0$, then the third orbit must be circular and thus the final boost is not required. This somewhat degenerate case will not be considered further. Another plausible assumption might be in the case of an initial circular orbit. This does not appear to be desirable when the rendezvous altitude is greater than the burnout altitude since the circular velocity requirements increase with lower altitudes, the thrust control requirements are more severe, and possible drag losses greater. From these considerations, it seems practical to consider circularization of the second orbit only. This possibility will be discussed in greater detail later. Since Hohmann transfers have been shown to be most efficient for coplanar

orbits, it seems desirable to maximize the number used or to maximize the velocity increments given during a Hohmann transfer relative to the velocity increments given during a non-Hohmann transfer.

Since there are only four boost or burnout points on the trajectory, and none of these are 180° apart, it seems impossible to include more than two Hohmann transfers (H. T.) in the maneuver. With the first three injection points being only 90° apart, only two H. T.'s seem feasible and these cannot be consecutive. On closer inspection, it is seen that two H. T.'s are possible, if R_{P1} and R_{P3} are the transfer points; i. e., apsides, while the burnout point could be an apsis it would not be an H. T. point and the next apsis should occur at R_{P2}. Although this would utilize only one H. T., this is not altogether undesirable since rendezvous could be made to occur near an apsis with relatively little trouble; i. e., the flight path angle would require little change at R_{P3}. From an implementation point-of-view, it might be simpler to achieve an apsis at burnout rather than at R_{P1} since the latter state would require a flight path angle other than $(2n + 1)\,\pi/2$ (which is easy to determine).

If:

$$R_r > R_b \tag{78}$$

then it does not seem desirable to utilize R_{P1} as a pericenter for orbit. In order to do so, it is necessary that:

$$R_b > R_{P1}\,. \tag{79}$$

But this is undesirable since energy is wasted going from a higher to a lower to a higher altitude. Thus, R_{P1} should be used as an apocenter when Equation (78) holds and it is desirable to use R_{P1} as an apsis. Likewise, R_b should not be used as an apocenter

when Equation (78) holds. If the equality sign in Equation (78) is reversed, then the words apocenter and pericenter should be interchanged in the foregoing discussion.

When:

$$R_p > R_{P1} \tag{80}$$

and Equation (78) holds, then R_{P1} after the first orbit-changing boost should be a pericenter. In the absence of the boost at R_{P2}, R_{P3} becomes an apocenter. The boosts at R_{P2} and R_{P3} should allow rendezvous to be achieved and Equation (26) to be satisfied.

When R_b is a pericenter, then R_{P2} should be an apocenter in the absence of a boost at R_{P1}; and in the absence of a boost of R_{P3}, rendezvous should be near an apsis. In general, it is desirable to achieve rendezvous near an apocenter when Equation (78) holds. It is difficult and probably undesirable to achieve rendezvous exactly at an apocenter since the rendezvous point will not be an integral multiple of $\pi/2$ degrees from any of the boost points—hence, an additional flight path correction would be required. As before, if Equation (78) does not hold, then apocenter and pericenter points should be interchanged. In order to limit the performance requirements of the primary booster system, it is probably desirable to fix the furnout conditions independently of the rendezvous conditions. The mass to be accelerated or rotated is smaller during the later stages of the flight, and hence more easily controlled. This restriction would not require that burnout occur at an apsis; only that burnout be independent of θ (or ϕ). Thus, there appears to be two most favorable options. These are (1) burnout 90° before an apocenter, H. T. to a pericenter at R_{P1}, flight path change at R_{P2}, H. T. from an apocenter to a pericenter at R_{P3}; or (2) burnout at a pericenter, flight path change at R_{P1}, an H. T. from an apocenter to a pericenter at R_{P2}, and a flight path change at R_{P3}. Since the first option uses two H. T.'s, it is in general preferable.

Option I

The first orbit is defined by Equation (6) and:

$$r_{P1} = \frac{p_1}{1 - e_1} \tag{81}$$

$$p_1 = r_b \tag{82}$$

$$e_1 = \left[1 - \frac{V_b^2 r_b}{\mu}\left(2 - \frac{V_b^2 r_b}{\mu}\right) \sin \beta_b\right]^{1/2} \tag{83}$$

and

$$V'_{P1} = \left[\left(\frac{\mu}{r_{P1}}\right)\left(2 - \frac{r_{P1}}{a_1}\right)\right]^{1/2} \tag{84}$$

The second orbit is partially determined since Equations (60) and (61) hold. The eccentricity and semi-major axes are not specified, however.

The fourth orbit is defined by Equations (13, (43) through (45), while the third orbit is partially determined by Equation (32). Assuming that r_{P3} is an apocenter prior to the last boost, p_3 can be determined in terms of e_3; i.e., using:

$$p_3 = r_{P3}(1 - e_3) \tag{85}$$

Now Equations (26) and (37) yield a_3 and subsequently e_3. These equations complete the determination of the third orbit; hence, V'_{P3} and V_{P2} can be found using Equations (49) (priming the left side), and (72), respectively. Now, Equations (60) and (61) yield:

$$r_{P2} = p_2 = r_{P1}(1 + e_2). \tag{86}$$

Let:

$$r_{P2} = p_3 \tag{87}$$

so:

$$e_2 = \frac{p_3}{r_{P1}} - 1 \tag{88}$$

Now that the perigee and eccentricity of the second orbit are known, the velocity at perigee:

$$V_{P1} = \left[\left(\frac{\mu}{r_{P1}}\right)(1 + e_2)\right]^{1/2} \tag{89}$$

and the velocity at R_{P2}, i. e.

$$V'_{P2} = \left[V_{P1}^2 + 2\mu\left(\frac{1}{r_{P2}} - \frac{1}{r_{P1}}\right)\right]^{1/2} \quad \text{(Eq. 68)}, \tag{90}$$

are determined. While the boost requirements are given by:

$$\Delta V_i = V_{Pi} - V'_{Pi} \; (i = 1, 2, 3) \; , \tag{91}$$

when i = 2, the flight path angle is changed and the orientation of the velocity must be considered carefully (see Section II and Equations (76) and (77)). Since the flight path angle before the second boost is given by:

$$\sin \beta'_2 = \frac{V_{P1}\, r_{P1}}{V'_{P2}\, r_{P2}} \tag{92}$$

while the flight path angle, β, after boost is:

$$\sin \beta_2 = \frac{V'_{P3}\, r_{P3}}{V_{P2}\, r_{P2}} \tag{93}$$

the change in β required is easily ascertained, as well as the desired boost direction. Obviously, the required velocity increment could have been determined from:

$$\Delta V_2^2 = V_{P2}^2 + (V'_{P2})^2 - 2V_{P2}\, V'_{P2} \cos (V'_{P2}, V_{P2}) \qquad (94)$$

$$= V_{P2}^2 + (V'_{P2})^2 - 2V_{P2}\, V'_{P2} \cos (\beta_2 - \beta'_2)$$

$$= V_{P2}^2 + (V'_{P2})^2 - 2V_{P2}V'_{P2}\left\{\left[(1-\sin^2 \beta_2)(1-\sin^2 \beta'_2)\right] + \sin \beta'_2 \sin \beta_2\right\}$$

Once ΔV_2 is determined, the thrust angle ϕ_T, i. e. the angle between thrust vector and the velocity vector, can be found from:

$$\phi_T = \cos^{-1}\left[\frac{-(V_{P2})^2 + (V_{P2})^2 + (\Delta V_2)^2}{(2V_{P2}\, \Delta V_2)}\right] \qquad (95)$$

Option II

The first orbit is defined by Equation (5) through (11). So R_{P1} V_{P1} and β_1 are given by Equations (56), (57), and (58). The fourth orbit is defined by Equations (13), (14) and:

$$e_4 = \left[1 - \frac{V_r^2\, r'_r}{\mu}\left(2 - \frac{V_r^2\, r_r}{\mu}\right) \sin^2 \beta_r\right] \qquad (96)$$

Since neither R_r nor R_{P3} is an apsis, the true anomaly must be found from:

$$v^* = \tan^{-1}\left[\frac{p_4 \cot \beta_r}{p_4 - r_r}\right]$$

$$= \cos^{-1}\left[\frac{p_4 - r_r}{e_4\, r_r}\right]$$

$$= \sin^{-1}\left[\frac{p_4}{e_4\, r_r}\right] \cot \beta_r \tag{97}$$

Now the true anomaly at R_{P3} is:

$$v^*_{P3} = v^* - \phi_4 \tag{98}$$

so:

$$r_{P3} = \frac{p_4}{1 + e_4 \cos (v^* - \phi_4)}$$

$$= \frac{p_4}{1 + e_4 \left[\cos v^* \operatorname{cov} \phi_4 + \sin v^* \sin \phi_4\right]} \tag{99}$$

Equation (43) may be used to find the velocity at R_{P3} and now Equation (26) does not completely determine the third orbit since neither R_r nor R_{P3} is an apsis. In a later analysis it will be assumed that the last thrust is toward the CSM which will serve as an additional constraint.

In order to save the energy spent rotating the thrust axis of the vehicle, it will be assumed that the impulses given at R_{P3} and R_{P1} will be in the direction of the velocity vector and that the flight path angles will be unchanged.

Noting that the flight path angle at R_{P3} after boost is:

$$\sin \beta_3 = \frac{V_r\, r_r \sin \beta_r}{V_{P3}\, r_{P3}} \tag{100}$$

and before boost:

$$\sin \beta_3' = \frac{V_{P2}\, r_{P2}}{V'_{P3}\, r_{P3}} \tag{101}$$

the assumption:

$$\beta_3 = \beta_3' \tag{102}$$

yields V_{P3}' in terms of r_{P2} and V_{P2}. Likewise, the assumption:

$$\beta_1 = \beta_1' \tag{103}$$

yields V_{P2}' in terms of r_{P2} and V_{P1} since:

$$\sin \beta_1' = \frac{V_b \, r_p \sin \beta_b}{V_{P1}' \, r_{P1}} \tag{104}$$

and:

$$\sin \beta_1 = \frac{V_{P2} \, r_{P2}}{V_{P1} \, r_{P1}} \tag{105}$$

The requirement that R_{P2} be a pericenter after boost determines r_{P2} and V_{P2} since Equations (26) and (100 through 102) can be solved simultaneously (use the fact that:

$$C_4 = C_3 = a_3 - r_{P2} \tag{106}$$

with:

$$a_3 = \left[\frac{2}{r_{P2}} - \frac{V_{P2}^2}{\mu}\right]). \tag{107}$$

Finally, the second orbital parameters are found through the elimination of r_{P2} in Equations (103 through 105), so that V_{P2}' can be found solely in terms V_{P1} (see Equation (70)). In addition:

$$r_{P2} = \frac{p_2}{(1 - e_2)} \tag{108}$$

and:

$$r_{P1} = p_2 \tag{109}$$

so that e_2 is specified. With e_1 known, V_{P2} is given by:

$$V'_{P2} = \left[\left(\frac{\mu}{r_{P2}}\right)(1 - e_2)\right]^{1/2} \text{ (See Equation 84).} \tag{110}$$

Thus:

$$V_{P1} = \left[(V'_{P2})^2 + 2\mu\left(\frac{1}{r_{P1}} - \frac{1}{r_{P2}}\right)\right]^{1/2} \text{ (See Equation 69)} \tag{111}$$

Equation (91) can now be used to determine the required boosts. Since none of the flight path angles were changed during boost, it is obvious that Equation (91) can be used to determine all three of the orbit-changing boosts without modification. In a later analysis this option will be compared with one in which the last thrust is in the direction of the CSM.

TIMING

Now that various trajectories have been given for accomplishing the desired rendezvous, it is necessary to determine launch and boost times. Equation (4) gives the rendezvous time from launch. The burn time, t_b, is considered known and fixed. The time, measured from periapsis passage, is given by:

$$\begin{aligned} t &= \frac{(p/\mu)}{(1-e)^2}\left\{p(1-e^2)^{-1/2}\left[\sin^{-1}\left(\frac{+\cos v}{1+e\cos v}\right) - \frac{\pi}{2}\right] - \frac{e_p \sin v}{1+e\cos v}\right\} \\ &= \frac{(p/\mu)^{1/2}}{(1-e^2)}\left\{p(1-e^2)^{1/2}\left[\sin^{-1}\left(\frac{a-r}{c}\right) - \frac{\pi}{2}\right] - \left[2pr - r^2(1-e^2) - p^2\right]^{1/2}\right\} \end{aligned} \tag{112}$$

If:

$$v = 2 \tan^{-1} \left[\left(\frac{1 + e}{1 - e} \right)^{1/2} \tan \frac{E}{2} \right] \tag{113}$$

is used to convert from E to v or vice versa, then other forms of Equation (112) may be used. Throughout this analysis, however, an attempt will be made to avoid the use of the eccentric, E, or mean, M, anomalies.

Option 1 - Timing

For Option 1:

$$t_1 = \frac{(p_1/\mu)^{1/2}}{(1-e_1^2)} \left\{ p_1 (1-e_1^2)^{-1/2} \left(\sin^{-1} e_1 - \frac{\pi}{2} \right) e_1 p_1 \right\}, \tag{114}$$

$$t_2 = \frac{(p_2/\mu)^{1/2}}{(1-e_2^2)} \left\{ p_2 (1-e_2^2)^{1/2} \left(\sin^{-1} e_2 - \frac{\pi}{2} \right) - e_2 p_2 \right\}, \tag{115}$$

$$t_3 = \frac{(p_3/\mu)^{1/2}}{(1-e_3^2)} \left\{ p_3 (1-e_3^2)^{-1/2} \left(\sin^{-1} e_3 - \frac{\pi}{2} \right) - e_3 p_3 \right\}, \text{ and:} \tag{116}$$

$$t_4 = \frac{(p_4/\mu)^{1/2}}{(1-e_4^2)} \left\{ p_4 (1-e_4^2)^{-1/2} \left(\sin^{-1} e_4 - \frac{\pi}{2} \right) - e_4 p_4 \right\}.$$

While p can be fairly easily determined from t and e, it is obviously far more difficult to find e in terms of t and p. This is an important consideration whenever it is desirable to use t as a constraint on an orbit. During an actual mission one of the t's might be shorter or longer than planned, requiring a slow-down or speed-up of the orbit velocity. In this case, β, or ΔV_i could be changed to correct for the timing error.

Option II - Timing

For Option II, Equations (114 through 116) hold; while t_4 is found by means of Equation (112) and:

$$v = v_4 = \cos^{-1}\left[\frac{1}{e_4}\ \frac{(r_r V_r^2 \sin^2\beta_1)}{\mu} - 1\right] \tag{118}$$

where:

$$-\pi \leq v \leq 0 \tag{119}$$

is implied from:

$$\beta = \frac{\pi}{2} \tag{120}$$

and:

$$0 < v < \pi \tag{121}$$

is implied from:

$$\beta > \frac{\pi}{2} \tag{122}$$

Since most of the periods involve angles of $\pm\frac{\pi}{2}$, it may be useful to use the eccentric anomaly for timing, i. e.,

$$E = \sin^{-1}\left[\frac{r}{b}\ \sin v\right]$$

$$= 2\sin^{-1}\left\{\left[\frac{r}{a(1-e)}\right]^{1/2} \sin v/2\right\}, \text{ or} \tag{123}$$

$$= \cos^{-1}\left[\frac{r\cos v + ae}{a}\right];$$

and:

$$t = \left(\frac{a^3}{\mu}\right)^{1/2} (E - e \sin E)$$

$$= \frac{\tau}{2\pi} (E - e \sin E) \tag{124}$$

Thus:

$$E_1' = \sin^{-1}\left(\frac{r_{P1}}{b_1}\right) = 2 \sin^{-1}\left[\left(\frac{r_{P1}}{a_1(1-e_1)}\right)^{1/2} \frac{\phi_2}{2}\right] = \cos^{-1} (e_1) \tag{125}$$

implies:

$$t_1 = \left(\frac{a_1^3}{\mu}\right)^{1/2} \left[(\cos^{1} e_1 - e_1 (1-e_1^2)^{1/2}\right]$$

$$= \frac{T_1}{2\pi} \left[\cos^{-1} e_1 - e_1 (1 - e_1^2)^{1/2}\right] \tag{126}$$

Similar expressions are found for Equations (115 and 116) Since a is proportional to the pericenter and for a given periapsis increases with e, the period increases with e for a given periapsis. Thus, reductions in the eccentricity cause reductions in the orbital periods and vice versa.

ENERGY REQUIREMENTS

The absolute energy requirements cannot be easily determined unless relative masses are known. For example, it is usually assumed that maximum orbital payload is achieved if burnout occurs at periapsis. Thus, burnout to rendezvous fuel requirements might be greater for Option II than for Option I yet smaller for the overall mission, i. e.,

energy/unit mass of payload, are more easily determined.

The relative energy is given by:

$$
\begin{aligned}
W &= -\frac{\mu}{2a}, \\
&= \frac{V^2}{2} - \frac{\mu}{r}, \\
&= -\frac{\mu}{2r_a}(1+e), \text{ or} \\
&= -\frac{\mu}{2r_p}(1+e)
\end{aligned}
\tag{127}
$$

From this equation it is seen that if r_b is the same in both options, then the energy requirement of Option II is greatest at burnout, i. e.

$$W_{II} < W_I \tag{128}$$

or:

$$|W_{II}| > |W_I| \tag{129}$$

From a lift-off to rendezvous point-of-view the two methods should require identical amount of energy per unit mass since when it is assumed that the vehicle moves in a conservative system with fixed end points. However, energy is expended changing the flight path angle or rotating the thrust axis hence Option II should be more expensive if two flight path angle changes are made. In the actual evaluation of the velocity requirements for Option II, it was not assumed that the flight path angle changed, hence, Option II was computed more efficiently than Option I where a flight path angle change was included. In a subesequent analysis Option II will include at least one flight path angle change in order to

thrust in the direction of the CSM. In general, options can be compared through comparisons of the sum of the ΔV_i's (i = 1, 2, 3) for each option. In particular, the cost of the linear eccentricity requirement can be determined from Equations (26) and (127); i. e.,

$$e_4 W_3 = e_3 W_4 \tag{130}$$

Thus, the ratio between the eccentricities before and after the final boost will determine the ratio of the specific (relative) energies before and after boost. Since W is negative in this analysis, the smaller magnitude represents the higher magnitude; hence, decreases in e correspond to increases in W. Since e_4 and W_4 are determined by the rendezvous conditions and e_3 found through Equation (26), W_3 can be determined exactly. In general,

$$e_4 < e_3 \tag{131}$$

does not necessarily imply inefficiency since energy is needed to assume the higher orbit. On the other hand,

$$e_4 > e_3 \tag{132}$$

would imply inefficiency since the energy was reduced by an amount ΔW_3, where

$$\begin{aligned} \Delta W_3 &= W_4 - W_3 \\ &= \left(\frac{e_4}{e_3} - 1\right) W_3 \text{, or} \\ &= \left(1 - \frac{e_3}{e_4}\right) W_4 . \end{aligned} \tag{133}$$

If it is assumed that at least ΔW_3 was spent in achieving the higher energy state (orbit), then $2\Delta W_3$ must be a lower bound on the energy wasted when Equation (132) is valid. Since the end points of the trajectory are assumed known; i.e., the burnout and rendezvous points, the minimum specific energy change required is given by:

$$\Delta W^* = W_r - W_b = W_r(1 - \frac{a_4}{a_1}) = W_4 - W_1 . \tag{134}$$

The actual requirement is:

$$\Delta W = \sum_{i=1}^{3} (\Delta W_i + \Delta W_{ri}) , \tag{135}$$

where ΔW_{ri} is used to denote energy dissipated changing flight path angles or thrust vectors, and

$$\Delta W_i = W_{i+1} - W_i . \tag{136}$$

Due to the constant linearity condition, ΔW^* does not equal ΔW, in general, even if the ΔW_{ri}'s are zero. The ΔW^* and ΔW are equal, when the ΔW_{ri}'s are zero, if:

$$a_1 < a_2 < a_3 < a_4 \tag{137a}$$

or

$$a_1 > a_2 > a_3 > a_4 \tag{137b}$$

Although estimates of ΔW_{ri} can be made using Equation (94), for example, ΔW_{ri} includes the torquing energy required to change the thrust axis and to hold it in the new position during the thrusting as well as the energy realign the thrust axis and the velocity vector.

Finally, Equation (136), which can be written:

$$\Delta W_i = W_{i+1} \left(1 - \frac{a_{i+1}}{a_i}\right) \tag{138}$$

shows that Equation (133) gives a minimum energy expenditure when Equation (131) holds, while Equation (137b) as well as (137a) give a minimum energy condition. There is an inherent waste in a procedure which uses (137b) since a_1 greater than a_4 implies a waste. Obviously Equation (134) is not equivalent to:

$$\Delta V^* = V_r - V_b \tag{139}$$

since r_r and r_b fixed (actually Equation (134) equals:

$$\Delta W^* = \frac{(V_r^2 - V_b^2)}{\mu} - 2\left(\frac{1}{r_r} - \frac{1}{r_b}\right) \Big), \tag{140}$$

where ΔV^* is the idealized velocity (boost) requirement. Ideally, ΔV^* should be given by:

$$\Delta V^* = V_r - V_b^2 + 2\left(\frac{1}{r_r} - \frac{1}{r_b}\right)^{1/2}, \tag{141}$$

actually it is given by:

$$\Delta V = \sum_{i=1}^{3} \Delta V_i \tag{142}$$

The required velocity increment, ΔV, is greater than the theoretical requirement ΔV^*, because of the flight path angle changes as well as the moments required.

APOLLO NOTE NO. 383 H. Engel

(Task II - Item II) 23 November 1965

EFFECT OF CHANGING UPDATED PARAMETERS

In the actual mission data processing only a few nuisance parameters will be updated. In fact, the selection of parameters that are updated will change from time-to-time throughout the mission as different ground stations are employed. It is the purpose of this note to show that the orbit parameter estimates (not the nuisance parameter estimates) obtained with this kind of data processing are the same as would be obtained if all of the nuisance parameters, that are estimated at one time or another, were estimated at all times.

We show this, not because this fact is important relative to mission data processing, but because it is important relative to our guidance and navigation evaluation programs. It is convenient in our G and N Evaluation Program not to change from time-to-time the selection of nuisance parameters to be updated. Avoiding changing saves a very large amount of bookkeeping. We shall first present an argument and then a proof.

We let a denote the column vector of parameters that are always updated; ordinarily, these will be only the six orbit parameters. We let b be the column vector of nuisance parameters that are updated using the first batch of data, c the nuisance parameters that are updated using the second batch of data, and d the nuisance parameters that are not updated.

In the actual data processing $\begin{bmatrix} \Delta\hat{a}_1 \\ \Delta\hat{b}_1 \end{bmatrix}$ is evaluated using the first batch of data, $\begin{bmatrix} \Delta\hat{a}_2 \\ \Delta\hat{c}_2 \end{bmatrix}$ is evaluated using the second batch of data, and $\begin{bmatrix} \Delta\hat{a} \\ \Delta\hat{c} \end{bmatrix}$ is determined as a weighted average of Δa_1 and $\begin{bmatrix} \Delta\hat{a}_2 \\ \Delta\hat{c}_2 \end{bmatrix}$. In our

argument, we shall restrict ourselves to the case in which errors in c do not affect the measurements in the first batch of data and errors in b do not affect the measurements in the second batch of data. This is a reasonable restriction since c is likely to correspond to biases or station location errors associated with the measurables in the second set of data, while b is likely to correspond to biases or station location errors associated with measurables in the first set of data. Initially, we shall also assume that there are no non-updated nuisance parameters; this assumption will be abandoned later. In this case, we can represent $\begin{bmatrix} \Delta\hat{a}_1 \\ \Delta\hat{b}_1 \end{bmatrix}$ as the output of filter 1, and $\begin{bmatrix} \Delta\hat{a}_2 \\ \Delta\hat{b}_2 \end{bmatrix}$ as the output of filter 2. We can also regard $\Delta\hat{c}_1$ as an output of filter 1, and $\Delta\hat{b}_2$ as an output of filter 2, both with infinite variance since they do not affect the measurables. The outputs of these two filters are then combined in filter 3 to obtain best estimates $\begin{bmatrix} \Delta\hat{a}^* \\ \Delta\hat{b}^* \\ \Delta\hat{c}^* \end{bmatrix}$ as in Figure 1a. We use the asterisks to distinguish these estimates from estimates that will be obtained later.

Now, what is filter 1? It obtains a best estimate of Δa and Δb based on data set 1. Viewed in another way, it is a filter that obtains a best estimate of Δa independent of the value of Δb. In like fashion, filter 2 obtains a best estimate of Δa independent of the value of Δc. Filter 3 then combines these two estimates of Δa to obtain a best estimate $\Delta\hat{a}^*$ of Δa independent of the values of Δb and Δc. On the other hand, what the optimum filter that uses both data sets does is obtain the best estimate $\Delta\hat{a}$ of Δa independent of the values of Δb and Δc. That is, $\Delta\hat{a}^*$ and $\Delta\hat{a}$ are both best estimates of Δa independent of

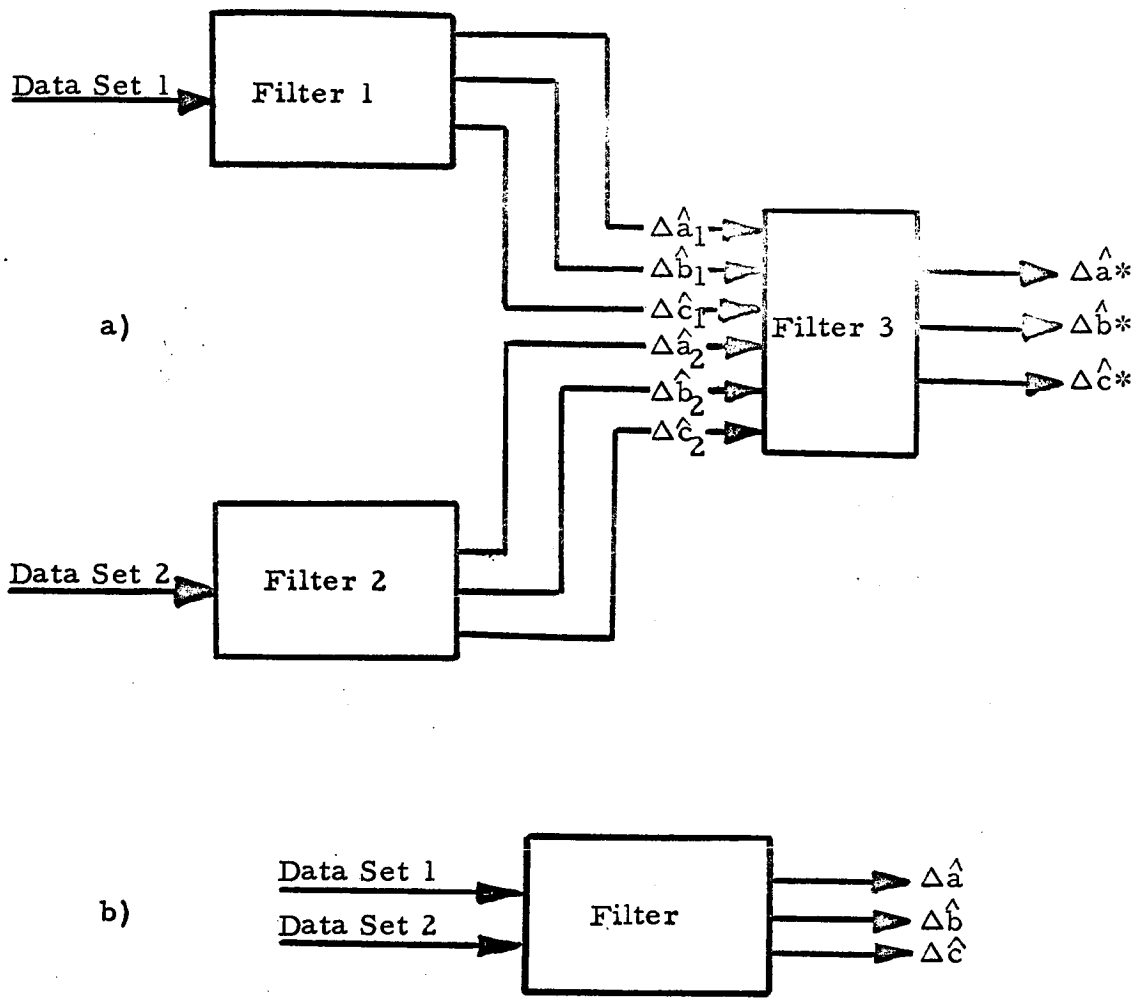

Figure 1.

the values of Δb and Δc, and hence, they are the same, and apply the same weights to the input data to obtain $\Delta\hat{a}*$ and $\Delta\hat{a}$.

Now, let us drop the assumption that there are no non-updated nuisance parameters. Since the two kinds of data processing apply the same weights to the input data, the effect of having non-updated parameters will be the same on the estimates of Δa obtained in both data processing techniques. Hence, they are equivalent.

Next, we shall demonstrate mathematically that the two data processing schemes give the same estimates of Δa, still with the

restriction that errors in Δc do not affect the measurements in the first set of data and errors in Δb do not affect the measurements in the second set of data.

We have,

$$\begin{bmatrix} A_{11} & A_{12} \\ A_{21} & A_{22} \end{bmatrix} \begin{bmatrix} \Delta\hat{a}_1 \\ \Delta\hat{b}_1 \end{bmatrix} = \begin{bmatrix} e_{1a} \\ e_{1b} \end{bmatrix} - \begin{bmatrix} A_{13} \\ A_{23} \end{bmatrix} \Delta\hat{d}$$

and

$$\begin{bmatrix} B_{11} & B_{12} \\ B_{21} & B_{22} \end{bmatrix} \begin{bmatrix} \Delta\hat{a}_2 \\ \Delta\hat{c}_2 \end{bmatrix} = \begin{bmatrix} e_{2a} \\ e_{2c} \end{bmatrix} - \begin{bmatrix} B_{13} \\ B_{23} \end{bmatrix} \Delta\hat{d}$$

which are the usual linear matrix equations for the estimates of the difference of the parameters from their actual values.

We find it convenient to introduce α and β

$$\alpha = \begin{bmatrix} \alpha_{11} & \alpha_{12} \\ \alpha_{21} & \alpha_{22} \end{bmatrix} = \begin{bmatrix} A_{11} & A_{12} \\ A_{21} & A_{22} \end{bmatrix}^{-1} = A^{-1}$$

$$\beta = \begin{bmatrix} \beta_{11} & \beta_{12} \\ \beta_{21} & \beta_{22} \end{bmatrix} = \begin{bmatrix} B_{11} & B_{12} \\ B_{21} & B_{22} \end{bmatrix}^{-1} = B^{-1}$$

Then,

$$\begin{bmatrix} \Delta\hat{a}_1 \\ \Delta\hat{b}_1 \end{bmatrix} = \alpha \begin{bmatrix} e_{1a} \\ e_{1b} \end{bmatrix} - \alpha \begin{bmatrix} A_{13} \\ A_{23} \end{bmatrix} \Delta\hat{d}$$

$$\begin{bmatrix} \Delta\hat{a}_2 \\ \Delta\hat{c}_2 \end{bmatrix} = \beta \begin{bmatrix} e_{2a} \\ e_{2c} \end{bmatrix} - \beta \begin{bmatrix} B_{13} \\ B_{23} \end{bmatrix} \Delta\hat{d}$$

$$E\left\{ \begin{bmatrix} \Delta\hat{a}_1 \\ \Delta\hat{b}_1 \end{bmatrix} \begin{bmatrix} \Delta\hat{a}_1^T & \Delta\hat{b}_1^T \end{bmatrix} \right\} = \alpha + \alpha \begin{bmatrix} A_{13} \\ A_{23} \end{bmatrix} \operatorname{cov} \Delta\hat{d} \begin{bmatrix} A_{13}^T & A_{23}^T \end{bmatrix} \alpha$$

$$E\left\{ \begin{bmatrix} \Delta\hat{a}_2 \\ \Delta\hat{c}_2 \end{bmatrix} \begin{bmatrix} \Delta\hat{a}_2^T & \Delta\hat{c}_2^T \end{bmatrix} \right\} = \beta + \beta \begin{bmatrix} B_{13} \\ B_{23} \end{bmatrix} \operatorname{cov} \Delta\hat{d} \begin{bmatrix} B_{13}^T & B_{23}^T \end{bmatrix} \beta$$

and it follows that

$$E\left[\Delta\hat{a}_1 \Delta\hat{a}_1^T\right] = \alpha_{11} + \left[\alpha_{11} A_{13} + \alpha_{12} A_{23}\right] \operatorname{cov} \Delta\hat{d} \left[\alpha_{11} A_{13} + \alpha_{12} A_{23}\right]^T$$

$$E\left[\Delta\hat{a}_1 \Delta\hat{a}_2^T\right] = \left[\alpha_{11} A_{13} + \alpha_{12} A_{23}\right] \operatorname{cov} \Delta\hat{d} \left[\beta_{11} B_{13} + \beta_{12} B_{23}\right]^T$$

In determining $\begin{bmatrix} \Delta\hat{a} \\ \Delta\hat{c} \end{bmatrix}$ we should properly weight $\Delta\hat{a}_1$, the only part of $\begin{bmatrix} \Delta\hat{a}_1 \\ \Delta\hat{b}_1 \end{bmatrix}$ retained, according to α_{11}^{-1}.

Then,

$$\begin{bmatrix} \Delta\hat{a} \\ \Delta\hat{c} \end{bmatrix} = \left\{ \begin{bmatrix} \alpha_{11}^{-1} & 0 \\ 0 & 0 \end{bmatrix} + \begin{bmatrix} B_{11} & B_{12} \\ B_{21} & B_{22} \end{bmatrix} \right\}^{-1} \left\{ \begin{bmatrix} \alpha_{11} & 0 \\ 0 & 0 \end{bmatrix} \begin{bmatrix} \Delta\hat{a}_1 \\ 0 \end{bmatrix} + \begin{bmatrix} B_{11} & B_{12} \\ B_{21} & B_{22} \end{bmatrix} \begin{bmatrix} \Delta\hat{a}_2 \\ \Delta\hat{c}_2 \end{bmatrix} \right\}$$

Letting

$$\begin{bmatrix} \quad \end{bmatrix}_1 \text{ denote } \begin{bmatrix} \alpha_{11}^{-1} + B_{11} & B_{12} \\ B_{21} & B_{22} \end{bmatrix}$$

we have

$$\begin{bmatrix} \quad \end{bmatrix}_1^{-1} = \begin{bmatrix} \phi_{11} & \phi_{12} \\ \phi_{21} & \phi_{22} \end{bmatrix}$$

and

$$\Delta\hat{a} = \begin{bmatrix} \phi_{11} & \phi_{12} \end{bmatrix} \left\{ \begin{bmatrix} \alpha_{11}^{-1} & \Delta\hat{a}_1 \\ & 0 \end{bmatrix} + \begin{bmatrix} B_{11}\Delta\hat{a}_2 + B_{12}\Delta\hat{c}_2 \\ B_{21}\Delta\hat{a}_2 + B_{22}\Delta\hat{c}_2 \end{bmatrix} \right\}$$

$$= \phi_{11}\alpha_{11}^{-1}\Delta\hat{a}_1 + \phi_{11}B_{11}\Delta\hat{a}_2 + \phi_{11}B_{12}\Delta\hat{c}_2 + \phi_{12}B_{21}\Delta\hat{a}_2 + \phi_{12}B_{22}\Delta\hat{c}_2$$

$$= \phi_{11}\alpha_{11}^{-1}\Delta\hat{a}_1 + \left[\phi_{11}B_{11} + \phi_{12}B_{21}\right]\Delta\hat{a}_2 + \left[\phi_{11}B_{12} + \phi_{12}B_{22}\right]\Delta\hat{c}_2$$

$$= \phi_{11}\alpha_{11}^{-1}\left[\alpha_{11}e_{1a} + \alpha_{12}e_{1b} - (\alpha_{11}A_{13} + \alpha_{12}A_{23})\Delta\hat{d}\right]$$

$$+ \left[\phi_{11}B_{11} + \phi_{12}B_{21}\right]\left[\beta_{11}e_{2a} + \beta_{12}e_{2c} - (\beta_{11}B_{13} + \beta_{12}B_{23})\Delta\hat{d}\right]$$

$$+ \left[\phi_{11}B_{12} + \phi_{12}B_{22}\right]\left[\beta_{21}e_{2a} + \beta_{22}e_{2c} - (\beta_{21}B_{13} + \beta_{22}B_{23})\Delta\hat{d}\right]$$

$$= \phi_{11} e_{1a} + \phi_{11} \alpha_{11}^{-1} \alpha_{12} e_{1b} + \left\{ \left[\phi_{11} B_{11} + \phi_{12} B_{21} \right] \beta_{11} + \left[\phi_{11} B_{12} + \phi_{12} B_{22} \right] \beta_{21} \right\} e_{2a}$$

$$+ \left\{ \left[\phi_{11} B_{11} + \phi_{12} B_{21} \right] \beta_{12} + \left[\phi_{11} B_{12} + \phi_{12} B_{22} \right] \beta_{22} \right\} e_{2c}$$

$$- \left\{ \left[\phi_{11} B_{11} + \phi_{12} B_{21} \right] \left[\beta_{11} B_{13} + \beta_{12} B_{23} \right] + \left[\phi_{11} B_{12} + \phi_{12} B_{22} \right] \left[\beta_{21} B_{13} + \beta_{22} B_{23} \right] \right.$$

$$\left. + \left[\phi_{11} A_{13} + \phi_{11} \alpha_{11}^{-1} \alpha_{12} A_{23} \right] \right\} \Delta \hat{d}$$

Next, we are going to simplify this expression for $\Delta \hat{a}$, taking term by term, and using the formulas for matrix inversion by partition. Using those formulas, we have

$$\beta_{11} = (B_{11} - B_{12} B_{22}^{-1} B_{21})^{-1}$$

$$\beta_{22} = (B_{22} - B_{21} B_{11}^{-1} B_{12})^{-1}$$

$$\beta_{12} = - B_{11}^{-1} B_{21} \beta_{22} = - \beta_{11} B_{12} B_{22}^{-1}$$

$$\beta_{21} = \beta_{12}^{T}$$

and

$$\alpha_{11} = (A_{11} - A_{12} A_{22}^{-1} A_{21})^{-1}$$

$$\alpha_{22} = (A_{22} - A_{21} A_{11}^{-1} A_{12})^{-1}$$

$$\alpha_{12} = A_{11}^{-1} A_{21} \alpha_{22} = - \alpha_{11} A_{12} A_{22}^{-1}$$

$$\alpha_{21} = \alpha_{12}^{T}$$

and

$$\phi_{11} = (\alpha_{11}^{-1} + B_{11} - B_{12} B_{22}^{-1} B_{21})^{-1} = (A_{11} + B_{11} - A_{12} A_{22}^{-1} - A_{21} - B_{12} B_{22}^{-1} B_{21})^{-1}$$

$$\phi_{22} = \left(B_{22} - B_{21} (\alpha_{11}^{-1} + B_{11})^{-1} B_{12}\right)^{-1}$$

$$\phi_{12} = (\alpha_{11}^{-1} + B_{11}) B_{21} \phi_{22} = - \phi_{11} B_{12} B_{22}^{-1}$$

$$\phi_{21} = \phi_{12}^{T}$$

$$\left[\phi_{11} B_{11} + \phi_{12} B_{21}\right] \beta_{11} + \left[\phi_{11} B_{12} + \phi_{12} B_{22}\right] \beta_{21}$$

$$= \phi_{11} \left[(B_{11} + \phi_{11}^{-1} \phi_{12} B_{21}) \beta_{11} + (B_{12} + \phi_{11}^{-1} \phi_{12} B_{22}) \beta_{21}\right]$$

$$= \phi_{11} \left[(B_{11} - B_{12} B_{22}^{-1} B_{21}) (B_{11} - B_{12} B_{22}^{-1} B_{21})^{-1} + (B_{12} - B_{12} B_{22}^{-1} B_{22}) \beta_{21}\right]$$

$$= \phi_{11} \left[I - 0 \beta_{21}\right]$$

$$= \phi_{11}$$

and

$$\left[\phi_{11} B_{11} + \phi_{12} B_{21}\right] \beta_{12} + \left[\phi_{11} B_{12} + \phi_{12} B_{22}\right] \beta_{22}$$

$$= \phi_{11} \left[(B_{11} + \phi_{11}^{-1} \phi_{12} B_{21}) \beta_{12} + (B_{12} + \phi_{11}^{-1} \phi_{12} B_{22}(\beta_{22}\right]$$

$$= \phi_{11} \left[(B_{11} - B_{12} B_{22}^{-1} B_{21}) (- \beta_{11} B_{12} B_{22}^{-1}) + (B_{12} - B_{12} B_{22}^{-1} B_{22}) \beta_{22}\right]$$

$$= - \phi_{11} B_{12} B_{22}^{-1}$$

$$= \phi_{12}$$

and

$$\left[\phi_{11} B_{11} + \phi_{12} B_{21}\right] \left[\beta_{11} B_{13} + \beta_{12} B_{23}\right] + \left[\phi_{11} B_{12} + \phi_{12} B_{22}\right] \left[B_{21} B_{13} + \beta_{22} B_{23}\right]$$

$$= \phi_{11} B_{13} + \phi_{12} B_{23}$$

so

$$\Delta\hat{a} = \phi_{11} e_{1a} + \phi_{11} \alpha_{11}^{-1} \alpha_{12} e_{1b} + \phi_{11} e_{12} e_{2c}$$

$$- (\phi_{11} B_{13} + \phi_{12} B_{23} + \phi_{11} A_{13} - \phi_{11} A_{12} A_{22}^{-1} A_{23}) \hat{d}$$

$$= \phi_{11} (e_{1a} + e_{2a}) - \phi_{11} A_{12} A_{22}^{-1} e_{1b} - \phi_{12} e_{2c}$$

$$- (\phi_{11} B_{13} + \phi_{12} B_{23} + \phi_{11} A_{13} - \phi_{11} A_{12} A_{22}^{-1} A_{23}) \hat{d}$$

$$= \phi_{11} (e_{1a} + e_{2a}) - \phi_{11} A_{12} A_{22}^{-1} e_{1b} - \phi_{12} e_{2c} - \phi_{11} (B_{13} - B_{12} B_{22}^{-1} B_{23}$$

$$+ A_{13} - A_{12} A_{22}^{-1} A_{23}) \hat{d}$$

In the Error Analysis Program, on the other hand, we combine both sets of data at once and find values for $\Delta\hat{a}$, $\Delta\hat{b}$, and $\Delta\hat{c}$. We have,

$$\begin{bmatrix} A_{11} + B_{11} & A_{12} & B_{12} \\ A_{21} & A_{22} & 0 \\ B_{21} & 0 & B_{22} \end{bmatrix} \begin{bmatrix} \Delta\hat{a} \\ \Delta\hat{b} \\ \Delta\hat{c} \end{bmatrix} = \begin{bmatrix} e_{1a} + e_{2a} \\ e_{1b} \\ e_{2c} \end{bmatrix} - \begin{bmatrix} A_{13} + B_{13} \\ A_{23} \\ B_{23} \end{bmatrix} \Delta\hat{d}$$

or, letting

$$\begin{bmatrix} \quad \end{bmatrix}_2 \text{ denote } \begin{bmatrix} A_{11} + B_{11} & A_{12} & B_{12} \\ A_{21} & A_{22} & 0 \\ B_{21} & 0 & B_{22} \end{bmatrix}$$

and denoting the inverse of $\begin{bmatrix} \quad \end{bmatrix}_2$ by

$$\psi = \begin{bmatrix} \psi_{11} & \psi_{12} & \psi_{13} \\ \psi_{21} & \psi_{22} & \psi_{23} \\ \psi_{31} & \psi_{32} & \psi_{33} \end{bmatrix}$$

we have

$$\begin{bmatrix} \Delta\hat{a} \\ \Delta\hat{b} \\ \Delta\hat{c} \end{bmatrix} = \psi \begin{bmatrix} e_{1a} + e_{2a} \\ e_{1b} \\ e_{2c} \end{bmatrix} - \psi \begin{bmatrix} A_{13} + B_{13} \\ A_{23} \\ B_{23} \end{bmatrix} \Delta\hat{d}$$

or

$$\Delta\hat{a} = \begin{bmatrix} \psi_{11} & \psi_{12} & \psi_{13} \end{bmatrix} \begin{bmatrix} e_{1a} + e_{2a} \\ e_{1b} \\ e_{2c} \end{bmatrix} - \begin{bmatrix} \psi_{11} & \psi_{12} & \psi_{13} \end{bmatrix} \begin{bmatrix} A_{13} + B_{13} \\ A_{23} \\ B_{23} \end{bmatrix} \Delta\hat{d}$$

We shall now show that the expressions for $\Delta\hat{a}$ obtained by these two different methods are equivalent.

By matrix partition,

$$\psi_{11} = \left[(A_{11}+B_{11}) - (A_{12}\ B_{12}) \begin{pmatrix} A_{22} & 0 \\ 0 & B_{22} \end{pmatrix}^{-1} \begin{pmatrix} A_{21} \\ B_{21} \end{pmatrix}\right]^{-1}$$

$$= \left[A_{11}+B_{11} - A_{12}\ A_{22}^{-1}\ A_{21} - B_{12}\ B_{22}^{-1}\ B_{21}\right]^{-1}$$

$$= \phi_{11}$$

$$\left[\psi_{12}\ \psi_{13}\right] = -\ \psi_{11} \left[A_{12}\ B_{12}\right] \begin{bmatrix} A_{22} & 0 \\ 0 & B_{22} \end{bmatrix}^{-1}$$

$$= -\ \psi_{11} \left[A_{12}\ A_{22}^{-1},\ B_{12}\ B_{22}^{-1}\right]$$

$$\psi_{12} = -\ \psi_{11}\ A_{12}\ A_{22}^{-1}$$

$$= -\ \phi_{11}\ A_{12}\ A_{22}^{-1}$$

$$\psi_{13} = -\ \psi_{11}\ B_{12}\ B_{22}^{-1}$$

$$= -\ \phi_{11}\ B_{12}\ B_{22}^{-1}$$

so

$$\Delta\hat{a} = \phi_{11}\ (e_{1a}+e_{2a}) - \phi_{11}\ A_{12} A_{22}^{-1}\ e_{1b} - \phi_{11}\ B_{12}\ B_{22}^{-1}\ e_{2c}$$

$$- \left[\phi_{11}\ (A_{13}+B_{13}) - \phi_{11}\ A_{12} A_{22}^{-1}\ A_{23} - \phi_{11}\ B_{12} B_{22}^{-1} B_{23}\right] \Delta\hat{d}$$

$$= \phi_{11}\ (e_{1a}+e_{2a}) - \phi_{11}\ A_{12} A_{22}^{-1}\ e_{1b} - \phi_{12}\ e_{2c}$$

$$- \phi_{11} \left[A_{13}+B_{13} - A_{12} A_{22}^{-1}\ A_{23} - B_{12}\ B_{22}^{-1}\ B_{23}\right] \Delta\hat{d}$$

and this is identically the same as the form obtained in the actual data processing. Hence, both methods lead to the same estimate and the same covariance.

The process of induction may be used to extend this demonstration to more than two batches of data by assuming that it holds for n batches of data and showing that it then holds for $n + 1$ batches of data.

The Bissett-Berman Corporation 2941 Nebraska Avenue, Santa Monica, California EXbrook 4-3270

APOLLO NOTE NO. 384
(Task II - Item II)

J. Holdsworth/
L. Lustick
18 November 1965

OPTIMAL BATCHING OF ESTIMATES

INTRODUCTION

In this note, we shall address a very interesting problem which we may roughly describe in the following way. We assume that from m separate batches of data that m estimators $\hat{\theta}_i$, $i = 1, 2, \ldots m$, of the same parametric vector θ are made. The data vectors corresponding to the various batches contain nuisance parameters of no physical interest for which a priori values are available. In the calculation of the estimates $\hat{\theta}_i$ from the different data sets (hereafter called batches) these a priori nuisance parameters are treated as though they are exact or equivalently, no use is made of the a priori uncertainties in the nuisance parameters in forming the m estimates $\hat{\theta}_i$.

Time marches on, the scene changes, and we now assume that the original data batches have been misplaced or destroyed and that only the m vector estimates $\hat{\theta}_1, \ldots \hat{\theta}_m$ have been preserved for our use. At this late date, we are told that the nuisance parameters whose values we used were not exact, but drawn from a certain population with a specified, known error variance - covariance structure. Since we have thrown our original data sets away we are not able to recompute our $\hat{\theta}_i$ estimates. We are, however, permitted to use this new found information in conjunction with the $\hat{\theta}_i$ estimates which we have retained in order to form a composite vector estimate $\hat{\theta}$ as a linear function of the $\hat{\theta}_i$ according to an optimality criterion to be specified shortly.

BASIC EQUATIONS

To be a bit more precise, we assume that the $\hat{\theta}_i$ are all unbiased estimates of θ. The composite estimate we seek is one of

the form:

$$\hat{\theta} = \sum_{i=1}^{m} W_i \hat{\theta}_i \tag{1}$$

where the weighting matrices W_i are square matrices with the same number of rows as the parametric vector θ.

The optimization problem we consider is the following. We wish to determine m weighting matrices W_i, $i = 1, 2, \ldots m$, such that for any value of the parametric vector θ, the estimate $\hat{\theta}$ given by (1) is unbiased and such that it is a minimum variance estimate. Explicity, we wish to determine the matrices W_i such that

$$E\,\hat{\theta} \equiv \theta \tag{2}$$

for arbitrary θ, and such that for any arbitrary fixed vector a the mean square error given by:

$$E\left[(a^T \hat{\theta} - a^T \theta)^2\right] \tag{3}$$

is minimized.

From (1) and (2) it follows that an equivalent statement of the problem is to minimize (3) for an arbitrary vector (a) subject to the constraint that

$$\sum_{i=1}^{m} W_i = I \tag{4}$$

It is important to note that the estimate $\hat{\theta}$ given by (1) involves the basic data only through the m batch wise estimates $\hat{\theta}_i$.

The analysis and solution of this problem have already been done in Apollo Note No. 268. A timely observation of L. Lustick enables us to write down immediately the solution as well as expressions for the resulting error variance covariance matrix by properly identifying certain features of the present problem with their counterparts in note 268. As has been shown in earlier notes, the optimal weighting matrices W_i do not depend upon the fixed but arbitrary vector a.

We shall now describe the calculation of the optimal weighting matrices. Since each of the estimates $\hat{\theta}_i$ is an unbiased estimate of the parametric vector θ, we may write:

$$\hat{\theta}_i = \theta + \Delta\hat{\theta}_i \tag{5}$$

where

$$E\,\Delta\hat{\theta}_i = 0 \tag{6}$$

The basic data which we have at our disposal consists of the m(6 by 1) estimates $\hat{\theta}_i$ of the 6 by 1 parameter vector θ. Thus, we see that we may write the following equation:

$$X = \phi\theta + n \tag{7}$$

where

$$X = \begin{pmatrix} \hat{\theta}_1 \\ \cdot \\ \cdot \\ \cdot \\ \hat{\theta}_m \end{pmatrix} \tag{8}$$

$$\phi = \begin{pmatrix} I \\ \cdot \\ \cdot \\ \cdot \\ I \end{pmatrix} \tag{9}$$

$$n = \begin{pmatrix} \Delta\hat{\theta}_1 \\ \cdot \\ \cdot \\ \cdot \\ \Delta\hat{\theta}_m \end{pmatrix} \tag{10}$$

The identity matrices in (9) are 6 x 6, since we assume that θ is a 6 x 1 column vector to be estimated, so that ϕ is a 6m x 6 matrix. As noted by Lustick, the optimal method of combining the $\hat{\theta}_i$ batchwise estimates to form a composite estimate follows directly from considerations given in notes 268, 269 and other places so that the optimal batchwise estimate is given by:

$$\hat{\theta} = F_{\hat{\theta}} X \tag{11}$$

where X is given by equation (7).

The interbatch filter $F_{\hat{\theta}}$ is explicitly given by:

$$F_{\hat{\theta}} = \left(\phi^T \operatorname{cov}^{-1}(n)\, \phi\right)^{-1} \phi^T \operatorname{cov}^{-1}(n) \tag{12}$$

where

$$\operatorname{cov}(n) = E(n\, n^T). \tag{13}$$

The covariance matrix in (13) is a 6m x 6m matrix which may be partitioned into 6 x 6 submatrices and written in the following form:

$$\operatorname{cov}(n) = \begin{pmatrix} \operatorname{cov} \Delta\theta_1 & \cdots\cdots & E(\Delta\theta_1\, \Delta\theta_m^T) \\ \vdots & & \\ E(\Delta\theta_m \Delta\theta_1^T) & \cdots\cdots & \operatorname{cov} \Delta\theta_m \end{pmatrix} \tag{14}$$

Since, at this stage of the game, we assume both cross and auto covariance information about the estimator error vectors $\Delta\hat{\theta}_i$ the matrix cov (n) given by (14) may be explicitly computed. Once this is done, direct substitution into equation (12) gives the 6 x 6m

filter matrix $F_{\hat{\theta}}$. The m 6 x 6 weighting matrices W_i may be readily obtained from $F_{\hat{\theta}}$ by writing $F_{\hat{\theta}}$ in the following partitioned form:

$$F_{\hat{\theta}} = (W_1, W_2, \ldots\ldots, W_m) \tag{15}$$

Note that the basic data available to us are the batchwise estimates $\hat{\theta}_i$ so that our optimum $\hat{\theta}$ is only provisionally optimal due to the constraint that we were not allowed to meddle with the internal structure of any one batch of data.

The error covariance matrix of the batchwise optimal estimate $\hat{\theta}$ is easily shown to be given by:

$$\text{cov}\, \Delta\hat{\theta} = E(\Delta\hat{\theta}\, \Delta\hat{\theta}^T) \tag{16}$$

$$= (\phi^T \text{cov}^{-1}(n)\, \phi)^{-1} \tag{17}$$

This result follows easily either by direct calculation or from note 268.

EVALUATION OF Cov(n) FOR THE ORBIT PARAMETER CASE

We conclude by briefly indicating the form that the partitioned submatrices $E(\Delta\hat{\theta}_i\, \Delta\hat{\theta}_j^T)$ assume in the orbit parameter problem. What we shall do is merely to write down the form of the equations with some explanatory comments. The detailed derivations are quite standard and will appear as a separate appendix to this note if there is a sufficient demand.

It is convenient to consider two separate cases. First, when there are a priori estimates available on just the nuisance parameters; and secondly, when a priori estimates exist for both the orbit and nuisance parameters. In what follows b will denote the vector of non-

R. Wagner

updated nuisance parameters and b_o will denote the a priori unbiased vector estimate of b so that we have:

$$b_o = b + \Delta b_o \tag{18}$$

where

$$E\,\Delta b_o = 0 \tag{19}$$

First Case

When there are a priori estimates available for the vector of nuisance parameters only, it may be shown that the estimator error vector for the estimator error in $\hat{\theta}_i$ obtained from the ith batch of data may be written as:

$$\Delta\hat{\theta}_i = M_{b_o}(i)\,\Delta b_o + M_e(i)\,e(i) \tag{20}$$

In equation (20), e(i) is the N_i x 1 column vector of additive noise samples which corrupt the N_i measurements which comprise what we call the ith batch of data.

That is, if the N_i x 1 vector constituting the ith batch of measurements is written in terms of the unperturbed function of the parameters and the additive noise as:

$$d_m(i) = d_a(i, \theta, b) + e(i) \tag{21}$$

then the usual linearized treatment will show that in the case where a priori values are available just for the nuisance parameters, we may write:

$$M_{b_o}(i) = -\left(\frac{\partial d_a^T}{\partial\theta}(i)\ \mathrm{Cov}^{-1}\left[e(i)\right]\ \frac{\partial d_a}{\partial\theta}(i)\right)^{-1}\left(\frac{\partial d_a^T}{\partial\theta}(i)\ \mathrm{Cov}^{-1}\left[e(i)\right]\ \frac{\partial d_a}{\partial b}(i)\right) \tag{22}$$

and

$$M_e(i) = \left(\frac{\partial d_a^T}{\partial \theta}(i)\ \mathrm{Cov}^{-1}\left(e(i)\right)\ \frac{\partial d_a}{\partial \theta}(i)\right)^{-1} \frac{\partial d_a^T}{\partial \theta}(i)\ \mathrm{Cov}^{-1}\left(e(i)\right) \tag{23}$$

where the partial derivatives appearing in the above matrices are calculable from the reference trajectory and where

$$\mathrm{cov}\left(e(i)\right) = E\left[e(i)\ e^T(i)\right] \tag{24}$$

Using the fact that there is no cross-batch correlation between the noise vectors $e(i)$, and that there is no correlation between Δb_o and $e(i)$, it follows from equation (20) that

$$\mathrm{cov}\ (\Delta\hat{\theta}_i) = E\left[\Delta\hat{\theta}_i\ \Delta\hat{\theta}_i^T\right] \tag{25}$$

$$= M_{b_o}(i)\ \mathrm{cov}\ (\Delta b_o)\ M_{b_o}^T(i)$$

$$+\ M_e(i)\ \mathrm{cov}\left(e(i)\right)\ M_e^T(i) \tag{26}$$

and for $i \neq j$:

$$E\left[\Delta\hat{\theta}_i\ \Delta\hat{\theta}_j^T\right] = M_b(i)\ \mathrm{cov}\ (\Delta_{b_o})\ M_b^T(j) \tag{27}$$

where:

$$\mathrm{cov}\ (\Delta b_o) = E\ (\Delta b_o\ \Delta b_o^T) \tag{28}$$

Thus, equations (26) and (27) in conjunction with equations (22) and (23) permit the construction of the optimal weighting matrices W_i as well as the evaluation of the error covariance matrix cov $(\Delta\hat{\theta})$ of the composite interbatch estimate when a priori values are available

just for the non-updated nuisance parameters b. The evaluation is performed by plugging (26) and (27) into (14) and then into (15) and (17).

Second Case

In this case, we assume that we have an unbiased a priori estimate θ_o for the orbit parameters θ as well as the unbiased estimate b_o of the non-updated nuisance parameter vector. That is, we are now given a θ_o such that:

$$\theta_o = \theta + \Delta\theta_o \tag{29}$$

with

$$E(\Delta\theta_o) = 0. \tag{30}$$

Proceeding as before, we may write the following equation for the estimator error $\Delta\hat{\theta}_i$ from the ith batch of data:

$$\Delta\hat{\theta}_i = P_{\theta_o}(i)\,\Delta\theta_o + P_{bo}(i)\,\Delta b_o + P_\epsilon(i)\;\epsilon(i) \tag{31}$$

where

$$P_{\theta_o}(i) = \left(\frac{\partial d_a^T}{\partial\theta}(i)\,\mathrm{cov}^{-1}\left(\epsilon(i)\right)\frac{\partial d_a}{\partial\theta}(i) + \mathrm{cov}^{-1}(\Delta\theta_o)\right)^{-1}\mathrm{cov}^{-1}(\Delta\theta_o) \tag{32}$$

$$P_{b_o}(i) = -\left(\frac{\partial d_a^T}{\partial\theta}(i)\,\mathrm{cov}^{-1}\,\epsilon(i)\,\frac{\partial d_a}{\partial\theta}(i) + \mathrm{cov}^{-1}(\Delta\theta_o)\right)^{-1}\frac{\partial d_a^T}{\partial\theta}(i)\,\mathrm{cov}^{-1}\left(\epsilon(i)\right)\frac{\partial d_a}{\partial b}(i) \tag{33}$$

$$P_e(i) = \left(\frac{\partial d_a^T}{\partial \theta}(i)\ \mathrm{cov}^{-1}\left(\epsilon(i)\right) \frac{\partial d_a}{\partial \theta}(i) + \mathrm{cov}^{-1}(\Delta\theta_o)\right)^{-1} \frac{\partial d_a^T}{\partial \theta}(i)\ \mathrm{cov}^{-1}\left(\epsilon(i)\right) \tag{34}$$

The derivation of these latter equations will be deferred to a separate appendix, but it is worthwhile noting that the matrices P_{θ_o}, P_{b_o}, P_e, contain a priori uncertainty information about the updated orbit parameters θ through the appearance of cov $\Delta\theta_o$. On the other hand, the quantity cov Δb_o does not put in an appearance in these matrices — the reason being, of course, that the nuisance parameter estimates are not updated.

Again, assuming that $\epsilon(i)$ is independent of both $\Delta\theta_o$ and Δb_o, from equation (31), we obtain:

$$\mathrm{cov}\ \Delta\hat{\theta}_i = E\left[\Delta\hat{\theta}_i\ \Delta\hat{\theta}_i^T\right] \tag{35}$$

or

$$\begin{aligned}\mathrm{cov}\ \Delta\hat{\theta}_i = {} & P_{\theta_o}(i)\ \mathrm{cov}\ \Delta\theta_o\ P_{\theta_o}^T(i) + P_{b_o}(i)\ \mathrm{cov}\ \Delta b_o\ \mathrm{cov}\ P_{b_o}^T(i) \\ & + P_e(i)\ \mathrm{cov}\left(\epsilon(i)\right) P_e^T(i) + P_{\theta_o}(i)\ E\left[\Delta\theta_o\ \Delta b_o^T\right] P_{b_o}^T(i) \\ & + P_{b_o}(i)\ E\left[\Delta b_o\ \Delta\theta_o^T\right] P_{\theta_o}^T(i).\end{aligned} \tag{36}$$

It is easy to show that equation (36) is equivalent to similar results derived in Note 233.

For $i \neq j$ we have:

$$\mathrm{cov}\ (\Delta\hat{\theta}_i^T\ \Delta\hat{\theta}_j^T) = E\left[\Delta\hat{\theta}_i\ \Delta\hat{\theta}_j^T\right] \tag{37}$$

or

$$\text{cov}\,(\Delta\hat{\theta}_i\,\Delta\hat{\theta}_j^T) = P_{\theta_o}(i)\,\text{cov}\,\Delta\,\theta_o\,P_{\theta_o}^T(j)$$

$$+\;P_{\theta_o}(i)\;\text{cov}\,(\Delta\theta_o\,\Delta b_o^T)\;P_{b_o}^T(j) + P_{b_o}(i)\,\text{cov}\,(\Delta b_o\,\Delta\,\theta_o^T)\;P_\theta^T(j) \qquad (38)$$

$$+\;P_{b_o}(i)\;\text{cov}\,\Delta b_o\,P_{b_o}^T(j)$$

This winds things up as we may now wander back and substitute these quantities in their appropriate places to evaluate cov (n), $F_{\hat{\theta}}$, etc. for the case where a priori values are available for the orbit parameters as well as the nuisance parameters. Our treatment has been quite general in that no restriction has been imposed that the different batches of data are of the same kind. That is, it is perfectly possible for the ith batch to be range and the jth batch to be angle measurements which lends a useful flexibility of interpretation to our results.

FUTURE BATCHING PROGRAM

The Bissett-Berman Error Analysis Program currently determines the errors in the orbit parameters of interest consistent with the following two filters.

I. THE OPTIMUM FILTER

This filter makes use of the apriori uncertainty values in the nuisance parameters, as well as the orbit parameters; and is consistent with weighting functions for the parameters of interest which result in unbiased minimum mean square estimates of the orbit parameters.

II. SIMPLEST MECHANIZATION FILTER

This filter assumes that the apriori uncertainties in the nuisance parameters is zero and under these conditions defines weighting functions

for the orbit parameters which are unbiased and have minimum mean square errors. If the uncertainties in the nuisance parameters were really zero this is indeed the optimum filter and the same filter defined in I. However, in evaluating the error consistent with II, if we use honest estimates of the uncertainty of the nuisance parameters this filter can, under some circumstances, have very undesirable properties. Its designation, as simplest, comes from the fact that it does not require calculations of the partial derivatives of the measurable with respect to the nuisance parameters, and requires calculations of much smaller inverses for its implementation.

The purpose of the batching study is to define filters which are, in some sense, simpler to implement than the optimum filter, but do not have the undesirable properties observed with Filter II.

The following is a list of filter concepts that we believe are worthy of future study. Since the optimum Filter I only differs from Filter II by taking into account the apriori uncertainties in the nuisance parameters, all the following methods will require either a precanned assessment of the statistics of the nuisance parameter noise or a real-time calculation of it.

1. The filter described in this report treats each batch of data with Filter II and then optimally combines the batches taking into account cross-correlation between the estimates from each batch. If there are many batches and the batches contain common nuisance parameters this method can become unwieldly.

2. A simplification of 1 results if the cross-correlation function between batches is neglected and only the covariance of each estimate is used. The covariance used, of course, must include the effect of the nuisance parameters.

3. Another type of compromise can be made in 1 which only requires treatment of two batches at a time. In particular, two batches are combined into one batch and then this batch is used recursively with the next batch.

4. A total precanned noise is calculated, that is, the white noise plus that due to the nuisance parameters. In defining the filter the cross-correlation between the noise is neglected. This is really the same as 2 for batch size one.

5. The total nuisance parameter noise is calculated as a function of time for a particular phase of the mission and this noise characteristic is fitted with a functional form with as few parameters as possible. Filter I is then used on this set of parameters.

6. A filter can be built which is insensitive to linear errors in the Nuisance Parameters.

7. Can make few measurements (batch the measurables) and use the optimum Filter I to handle the few measurements.

APPENDIX TO APOLLO NOTE NO. 384

J. R. Holdsworth
10 December 1965

DERIVATION OF COEFFICIENT MATRICES

This appendix is being written in response to several requests for the derivation of the expressions for certain of the matrices in Apollo Note 384. We shall begin by considering the case where there are a priori values available only for the nuisance parameters and will first derive equations (22) and (23) in this note which corresponds to this case.

For notational convenience we shall supress the index i denoting the ith data batch since we will be working here with just one batch. From equation (21) the N x 1 vector of observations resulting from the ith batch of data may be written:

$$d_m = d_a(\theta, b) + e \tag{1}$$

where θ is the vector of orbit parameters to be estimated and b is the vector of nuisance parameters for which a priori values are available.

We assume the e is a zero mean gaussian noise vector whose covariance structure is known, and as before we let b_o denote the a priori unbiased estimate of the nuisance parameter vector b. Now the person doing the estimating is under the impression that the a priori estimate b_o is an exact value. Under this erroneous assumption, the orbit parameters are chosen to be those functions of the observed data d_m, and nuisance parameters b_o which minimize the quadratic form shown below.

$$Q = \left(d_m - d_a(\theta, b_o)\right)^T \mathrm{cov}^{-1} e \left(d_m - d_a(\theta, b_o)\right) \tag{2}$$

The functional form $d_a(\theta, b)$ is assumed to be known. Q is, of course, proportional to the log likelihood function of the data as the observer believes it since he is unaware that b_o was taken from a

random population. The orbit parameter estimate $\hat{\theta}$ is obtained by differentiating (2) with respect to θ, equating it to zero, and by solving for $\hat{\theta}$ as a function of b_o and d_m. In other words, $\hat{\theta}$ is that function of d_m and b_o such that:

$$\frac{\partial d_a^T}{\partial \theta} \operatorname{cov}^{-1} \epsilon \; d_m - d_a\left(\hat{\theta}, b_o\right) = 0. \tag{3}$$

We now write:

$$\hat{\theta} = \theta + \Delta\hat{\theta} \tag{4}$$

$$b_o = b + \Delta b_o \tag{5}$$

and assume that the following approximations are valid:

$$\frac{\partial d_a}{\partial \theta} (\hat{\theta}, b_o) \approx \frac{\partial d_a}{\partial \theta} (\theta, b) \tag{6}$$

$$\frac{\partial d_a}{\partial b} (\hat{\theta}, b_o) \approx \frac{\partial d_a}{\partial b} (\theta, b) \tag{7}$$

$$d_a (\hat{\theta}, b_o) = d_a (\theta + \Delta\hat{\theta}, b + \Delta b_o) \tag{8}$$

or approximately:

$$d_a (\hat{\theta}, b_o) \approx d_a (\theta, b) + \frac{\partial d_a}{\partial \theta} \Delta\hat{\theta} + \frac{\partial d_a}{\partial b} \Delta b_o. \tag{9}$$

Substituting equations (6) through (9) into (3) we obtain approximately:

$$\frac{\partial d_a^T}{\partial \theta} \operatorname{cov}^{-1} \epsilon \left(d_m - d_a (\theta, b) - \frac{\partial d_a}{\partial \theta} \Delta\hat{\theta} - \frac{\partial d_a}{\partial b} \Delta b_o\right) \approx 0 \tag{10}$$

Noting from (1) that:

$$d_m - d_a(\theta, b) = \epsilon \tag{11}$$

equation (10) may be re-arranged to yield:

$$\frac{\partial d_a^T}{\partial \theta} \operatorname{cov}^{-1} \epsilon \frac{\partial d_a}{\partial \theta} \Delta\hat{\theta} = - \frac{\partial d_a}{\partial \theta} \operatorname{cov}^{-1} \epsilon \frac{\partial d_a}{\partial b} \Delta b_o + \frac{\partial d_a^T}{\partial \theta} \operatorname{cov}^{-1} \epsilon \, \epsilon \tag{12}$$

Equation (12) may be easily solved for the error in the estimate of the orbit parameter to yield:

$$\begin{aligned} \Delta\theta = & -\left(\frac{\partial d_a^T}{\partial \theta} \operatorname{cov}^{-1} \epsilon \frac{\partial d_a}{\partial \theta}\right)^{-1} \frac{\partial d_a}{\partial \theta} \operatorname{cov}^{-1} \epsilon \frac{\partial d_a}{\partial b} \Delta b_o \\ & + \left(\frac{\partial d_a^T}{\partial \theta} \operatorname{cov}^{-1} \epsilon \frac{\partial d_a}{\partial \theta}\right)^{-1} \frac{\partial d_a^T}{\partial \theta} \operatorname{cov}^{-1} \epsilon \, \epsilon \end{aligned} \tag{13}$$

The matrix coefficients of Δb_o and ϵ in equation (13) are the matrices $M_{bo}(i)$ and $M_\epsilon(i)$ as given in equations (22) and (23) of the main body of the note. Recall that in (13) we have suppressed the index i denoting the ith data batch, but that $\Delta\hat{\theta}$ given above is the expression for the orbit parameter estimator error obtained from one particular batch of data.

When we considered the second case, where there was a priori information on both the orbit and nuisance parameters, the underlying assumptions were as follows. The a priori estimate θ_o of the orbit parameter vector was known to be an unbiased statistical estimate of θ with known covariance, cov $\Delta\theta_o$. The a priori estimate b_o of the nuisance parameter vector was assumed, incorrectly of course, to be exact by the person processing the ith batch of data. Thus, if the data processor assumes that the noise ϵ and the a priori estimate θ_o have independent multivariante gaussian distributions, then since he is unaware of the randomness of the a priori values b_o, he is lead to

estimate θ by choosing the estimator $\hat{\theta}$ to be that function of the known quantities d_m, θ_o and b_o which minimizes the quadratic form shown below:

$$Q = (\theta_o - \theta)^T \operatorname{cov}^{-1} \Delta\theta_o (\theta_o - \theta) + \left(d_m - d_a(\theta, b_o)\right)^T \operatorname{cov}^{-1}_{\epsilon} \left(d_m - d_a(\theta, b_o)\right) \tag{14}$$

Equation (14) is what the person processing the ith batch of data assumes to be the joint log likelihood function of the ith batch of data and the a priori estimates of the orbit parameters.

Differentiating (14) with respect to θ and equating the result to zero reveals that the estimate $\hat{\theta}$ is that function of the known quantities θ_o, b_o, d_m which satisfies the following equation:

$$\operatorname{cov}^{-1} \Delta\theta_o (\theta_o - \hat{\theta}) + \frac{\partial d_a^T}{\partial \theta}(\hat{\theta}, b_o) \operatorname{cov}^{-1}_{\epsilon} \left(d_m - d_a(\hat{\theta}, b_o)\right) = 0 \tag{15}$$

We now write:

$$\theta_o = \theta + \Delta\theta_o \tag{16}$$

$$\hat{\theta} = \theta + \Delta\hat{\theta} \tag{17}$$

$$b_o = b + \Delta b_o \tag{18}$$

Assuming that the partial derivatives along the reference trajectories and actual trajectories are approximately equal, we again write:

$$\frac{\partial d_a}{\partial \theta}(\hat{\theta}, b_o) \approx \frac{\partial d_a}{\partial \theta}(\theta, b) \tag{19}$$

and

$$d_a(\hat{\theta}, b_o) \approx d_a(\theta, b) + \frac{\partial d_a}{\partial \theta} \Delta\hat{\theta} + \frac{\partial d_a}{\partial b} \Delta b_o \tag{20}$$

If equations (16) through (20) are inserted into equation (15), and again recalling that:

$$d_m - d_a(\theta, b) = e \tag{21}$$

we may write:

$$\begin{aligned} &\mathrm{cov}^{-1} \Delta\theta_o \; \Delta\theta_o + \frac{\partial d_a^T}{\partial \theta} \mathrm{cov}^{-1} e\, e - \frac{\partial d_a^T}{\partial \theta} \mathrm{cov}^{-1} e \frac{\partial d_a}{\partial b} \Delta b_o \\ &= \left(\mathrm{cov}^{-1} \Delta\theta_o + \frac{\partial d_a^T}{\partial \theta} \mathrm{cov}^{-1} e \frac{\partial d_a}{\partial \theta} \right) \Delta\hat{\theta} \end{aligned} \tag{22}$$

From equation (22) we obtain:

$$\begin{aligned} \Delta\hat{\theta} = &\left(\mathrm{cov}^{-1} \Delta\theta_o + \frac{\partial d_a^T}{\partial \theta} \mathrm{cov}^{-1} e \frac{\partial d_a}{\partial \theta} \right)^{-1} \mathrm{cov}^{-1} \Delta\theta_o \; \Delta\theta_o \\ &- \left(\mathrm{cov}^{-1} \Delta\theta_o + \frac{\partial d_a^T}{\partial \theta} \mathrm{cov}^{-1} \frac{\partial d_a}{\partial \theta} \right)^{-1} \frac{\partial d_a^T}{\partial \theta} \mathrm{cov}^{-1} e \frac{\partial d_a}{\partial b} \Delta b_o \\ &+ \left(\mathrm{cov}^{-1} \Delta\theta_o + \frac{\partial d_a^T}{\partial \theta} \mathrm{cov}^{-1} e \frac{\partial d_a}{\partial \theta} \right)^{-1} \frac{\partial d_a^T}{\partial \theta} \mathrm{cov}^{-1} e\, e \end{aligned} \tag{23}$$

Now direct comparison of the matrix coefficients of $\Delta\theta_o$, Δb_o and e as given above with equations (32), (33), and (34) in the main body of the note, shows that they are identical.

The Bissett-Berman Corporation 2941 Nebraska Avenue, Santa Monica, California EXbrook 4-3270

APOLLO NOTE NO. 385
(Task 2, Item II)

E. Cortina
H. Dale
19 November 1965

TRACKING AND MONITORING DURING LEM ASCENT

In Apollo Note No. 369 it was indicated that the quantities required to build an information matrix for an Error Analysis Program for thrusting trajectories were the vectors:

$$\overline{R}_s, \ \dot{\overline{R}}_s, \ \frac{\partial \overline{R}_s}{\partial a_j}, \ \frac{\partial \dot{\overline{R}}_s}{\partial a_j}$$

It was also noted that only the vector from the Moon's center to the vehicle is affected by powered rather than Keplerian motion. Therefore, the components and derivatives of $\overline{R}_s$, which involve station and Moon location can be represented as in the non-thrusting Error Analysis Program.

In this note are presented equations for the vehicle motion ($\overline{R}'$, $\dot{\overline{R}}'$) with respect to the Moon for a powered ascent from the lunar surface and the partials thereof with respect to parameters which affect this motion.

The vehicle motion is represented in the prime, Moon-centered, inertial coordinate system with X' directed at the launch point at lift off, Y' directed horizontally in the plane of the LEM orbit, and Z' corresponding to a right hand coordinate system.

Assume a LEM acceleration schedule for ascent:

$$\left.\begin{aligned} \ddot{X}'(t) &= 1.925 \text{ m/sec}^2 \\ \ddot{Y}'(t) &= 0 \end{aligned}\right\} \quad 0 \leq t \leq 8 \text{ sec.}$$

$$\left.\begin{aligned} \ddot{X}'(t) &= 0.500 - .0028\, t \text{ m/sec}^2 \\ \ddot{Y}'(t) &= 2.600 + .0082\, t \text{ m/sec}^2 \end{aligned}\right\} \quad 8 < t \leq 325 \text{ sec.}$$

$$\ddot{X}'(t) = -0.384 \text{ m/sec}^2$$
$$\ddot{Y}'(t) = 2.600 + .0082\, t \text{ m/sec}^2 \qquad 325 < t \leq 397 \text{ sec}$$

Integration of the accelerations yields velocity and position components:

$$\dot{X}'(t) = \dot{X}'_o + 1.925\, t$$
$$\dot{Y}'(t) = \dot{Y}'_o \qquad 0 \leq t \leq 8$$

$$\dot{X}'(t) = \dot{X}'_{(8)} + .5\,(t-8) - .0014\,(t^2-64)$$
$$\dot{Y}'(t) = \dot{Y}'_o + 2.6\,(t-8) + .0041\,(t^2-64) \qquad 8 \leq t \leq 325$$

$$\dot{X}'(t) = \dot{X}'_{(325)} - .384\,(t-325)$$
$$\dot{Y}'(t) = \dot{Y}_o + 2.6\,(t-8) + .0041\,(t^2-64) \qquad 325 \leq t \leq 397$$

$$X'(t) = r_m + \dot{X}'_o\, t + .963\, t^2$$
$$Y'(t) = \dot{Y}'_o\, t \qquad 0 \leq t \leq 8$$

$$X'(t) = X'_{(8)} + \dot{X}'_{(8)}\,(t-8) + .25(t-8)^2 - .0014\left(\frac{t^3}{3} - 64\,t + 341\right)$$
$$Y'(t) = Y'_{(8)} + \dot{Y}'_{(8)}\,(t-8) + 1.3\,(t-8)^2 + .0041\left(\frac{t^3}{3} - 64\,t + 341\right) \qquad 8 < t \leq 325$$

$$X'(t) = X'_{(325)} + \dot{X}'_{(325)}\,(t-325) - .192\,(t-325)^2$$
$$Y'(t) = Y'_{(8)} + \dot{Y}'_{(8)}\,(t-8) + 1.3\,(t-8)^2 + .0041\left(\frac{t^3}{3} - 64\,t + 341\right) \qquad 325 < t \leq 397$$

Let:

$$\overline{R}'(t) = \begin{bmatrix} X'(t) \\ Y'(t) \\ Z'(t) \end{bmatrix}$$

$$\overline{R}'(t) = \begin{bmatrix} \dot{X}'(t) \\ \dot{Y}'(t) \\ \dot{Z}'(t) \end{bmatrix}$$

where:

$$\overline{R}'(o) = \begin{bmatrix} r_m \\ 0 \\ 0 \end{bmatrix}$$

$$\dot{\overline{R}}'(o) = \overline{\omega}_m X \overline{R}'_o = \begin{bmatrix} \dot{X}'_o \\ \dot{Y}'_o \\ \dot{Z}'_o \end{bmatrix}$$

$\overline{\omega}_m$ = Lunar angular velocity

r_m = Lunar radius

The non-zero partials of $\overline{R}$ and $\dot{\overline{R}}$ are those with respect to lunar gravitational constant, biases in initial conditions and IMU-AGC parameters. The latter include accelerometer bias, gyro drift, plat form misalignment, etc.

Uncertainties in the parameters propagate as "errors" in acceleration which means that a set of differential equations must be solved to determine the effect on position and velocity. In a subsequent part of this note the equations are derived and approximate solutions presented. If desired, an exact solution can be obtained with the aid of a computer, however, it is felt that the partial derivatives obtained from the approximate solution are of sufficient accuracy for error analysis purposes. Table 1 lists the parameters and the corresponding partial derivatives.

Parameter	$\partial x/\partial a_j$	$\partial y/\partial a_j$	$\partial z/\partial a_j$	$\partial \dot{x}/\partial a_j$	$\partial \dot{y}/\partial a_j$	$\partial \dot{z}/\partial a_j$
Accel. Bias						
X' axis, a_1	$t^2/2$			t		
Y' axis, a_2		$t^2/2$			t	
X' axis, a_3			$t^2/2$			t
Accel. Scale Factor X' axis, a_4	$X'+g_o t^2/2$			$X'+g_o t$		
Y' axis, a_5		Y'			$\dot{Y}'$	
Z' axis, a_6						
Platform Misalign. X' axis, a_7			Y'			$\dot{Y}'$
Y' axis, a_8			$-X'-g_o t^2/2$			$-\dot{X}'-g_o t$
Z' axis, a_9	$-Y'$	$X'+g_o t^2/2$		$-\dot{Y}'$	$\dot{X}'+g_o t$	
Platform Drift X' axis, a_{10}			$tY'-2\int Y'\,dt$			$t\dot{Y}'-Y'$
Y' axis, a_{11}			$-g_o t^3/6-tX'+2\int X'\,dt$			$-g_o t^2/2-t\dot{X}'+X'$
Z' axis, a_{12}	$-tY'+2\int Y'\,dt$	$g_o t^3/6+tX-2\int X'\,dt$		$-t\dot{Y}'+Y'$	$g_o t^2/2+t\dot{X}'-X'$	
Grav. Const. μ, a_{13}	$-t^2/2r_m^2$			$-t/r_m^2$		
Initial Position Bias X' comp, a_{14}	$1+g_o t^2/r_m$			$2g_o t/r_m$		
Y' comp, a_{15}		$1-g_o t^2/2r_m$			$-g_o t/r_m$	
Z' comp, a_{16}			$1-g_o t^2/2r_m$			$-g_o t/r_m$

TABLE 1

Definitions for Table 1 parameters:

$$g_o \mp \frac{\mu}{r_m^2}$$

$$P(t) \equiv \int X\,dt$$

$$P(t) = r_m t + \dot{X}'_o t^2/2 + .321\,t^3 \qquad 0 \leq t \leq 8 \text{ sec.}$$

$$P_{(t)} = P_{(8)} + X'_{(8)}(t-8) + \dot{X}'_{(8)}\frac{(t-8)^2}{2} + .083\,(t-8)^3 - .0014\left[\frac{t^4}{12} - 32t^2 + 341t - 1021\right] \quad 8 < t \leq 325$$

$$P(t) = P_{(325)} + X'_{(325)}(t-325) + \frac{\dot{X}'_{(325)}}{2}(t-325)^2 - .064(t-325)^3 \quad 325 < t \leq 397 \text{ sec.}$$

$$Q(t) \equiv \int Y' dt$$

$$Q(t) = \dot{Y}'_o t^2/2 \qquad 0 \leq t \leq 8$$

$$Q(t) = Q_{(8)} + Y_{(8)}(t-8) + \frac{\dot{Y}'_{(8)}}{2}(t-8)^2 + .43\,(t-8)^3$$

$$+ .0041\left[\frac{t^4}{12} - 32t^2 + 341t - 1021\right] \quad 8 < t \leq 397 \text{ sec.}$$

DERIVATION OF PERTURBATION EQUATIONS

The plat form accelerometers measure the vector difference of Kinetic and gravitational acceleration:

$$\overline{A} = \ddot{\overline{R}} - \overline{G}$$

then:

$$\overline{A}_c = \ddot{\overline{R}}_c - \overline{G}_c$$

where the subscript c denotes value along the reference trajectory.

The actual acceleration will differ from the reference by an error term caused by plat form and gravity reference errors:

$$\overline{A} = \overline{A}_c + \overline{n}$$

$$\ddot{\overline{R}} - \overline{G} = \ddot{\overline{R}}_c - \overline{G}_c + \overline{n}$$

$$\ddot{\overline{R}} - \ddot{\overline{R}}_c = \overline{G} - \overline{G}_c + \overline{n}$$

let:

$$\Delta\overline{R} = \overline{R} - \overline{R}_c$$

$$\Delta\overline{G} = \overline{G} - \overline{G}_c$$

$$\Delta\ddot{\overline{R}} = \Delta\ddot{\overline{G}} + \overline{n} \qquad (1)$$

$$\overline{G} = -\frac{\mu\overline{R}}{R^3}$$

$$\Delta\overline{G} = -\frac{\overline{R}}{R^3}\ \Delta\mu - \frac{\mu\Delta\overline{R}}{R^3} + 3\,\mu\overline{R}\ \frac{\Delta R}{R^4}$$

Since:

$$R^2 = X^2 + Y^2 + Z^2$$

$$\Delta\overline{R} = \frac{X\Delta X + Y\Delta Y + Z\Delta Z}{R}$$

Expressing $\Delta\overline{G}$ in composed form:

$$\Delta\overline{G} = \begin{bmatrix} \frac{-X\,\Delta\mu}{R^3} - \frac{\mu\Delta X}{R^3} + \frac{3\mu X}{R^5}(X\Delta X + Y\Delta Y + Z\Delta Z) \\ \frac{-Y\Delta\mu}{R^3} - \frac{\mu\Delta Y}{R^3} + \frac{3\mu Y}{R^5}(X\Delta X + Y\Delta Y + Z\Delta Z) \\ \frac{-Z\Delta\mu}{R^3} - \frac{\mu\Delta Z}{R^3} + \frac{3\mu Z}{R^5}(X\Delta X + Y\Delta Y + Z\Delta Z) \end{bmatrix} \tag{2}$$

let:

$$\overline{n} = \sum_{i=1}^{4} \overline{n}_i \tag{3}$$

where n_1---n_4 represent the errors due to accelerometer bias, scale factor, plat form misalignment and drift respectively.

ACCELEROMETER BIAS

These biases propagate directly as acceleration errors. Let a_1, a_2, a_3 be the biases in X, Y, Z accelerometers.

$$\overline{n}_2 = \begin{bmatrix} a_1 \\ a_2 \\ a_3 \end{bmatrix} \tag{4}$$

SCALE FACTOR ERROR

These produce an error proportional to the measured acceleration in the corresponding axis. Let a_4, a_5, a_6 represent scale factor

errors in X, Y, Z accelerometers:

$$\bar{n}_2 = \begin{bmatrix} A_X\, a_4 \\ A_Y\, a_5 \\ A_Z\, a_6 \end{bmatrix} \tag{5}$$

PLAT FORM MISALIGNMENT

Let a_7, a_8, a_9 represent small angular misalignments about the X, Y, Z axis respectively. Assume that the angles are sufficiently small such that:

$$a_7,\ a_8,\ a_9 < e$$

$$\cos e \cong 1;\ \text{sine} \cong e$$

The error in acceleration due to plat form misalignment is therefore:

$$\bar{n}_3 = \left[\, 1 - \mathbb{R} \,\right] A$$

1 = unity matrix

$$\mathbb{R} = \begin{bmatrix} 1 & a_9 & -a_8 \\ -a_9 & 1 & a_7 \\ a_8 & -a_7 & 1 \end{bmatrix}$$

$$\bar{n}_3 = \begin{bmatrix} 0 & -a_9 & a_8 \\ a_9 & 0 & -a_7 \\ -a_8 & a_7 & 0 \end{bmatrix} \begin{bmatrix} A_X \\ A_Y \\ A_Z \end{bmatrix}$$

$$\bar{n}_3 = \begin{bmatrix} (-A_Y a_9 + A_Z a_8) \\ (A_X a_9 - A_Z a_7) \\ (-A_X a_8 + A_Y a_7) \end{bmatrix} \tag{6}$$

PLAT FORM DRIFT

Plat form drift is determined in essentially the same manner as plat form misalignment. Assuming that the drift is constant and designating the rate in the X Y Z axis by a_{10}, a_{11}, a_{12} respectively:

$$\bar{n}_4 = \begin{bmatrix} (-a_{12}\, t\, A_Y + a_{11}\, t\, A_Z) \\ (a_{12}\, t\, A_X - A_{10}\, t\, A_Z) \\ (-a_{11}\, t\, A_X + a_{10}\, t\, A_Y) \end{bmatrix} \tag{7}$$

COMBINED ERROR EQUATIONS

The combined error equations can be formed by substituting equations (2) through (7) into (1).

$$\Delta\ddot{X} + \frac{\mu\Delta X}{R^3} - \frac{3\mu X}{R^5}(X\Delta X + Y\Delta Y + Z\Delta Z) = -\frac{X}{R^3}\Delta\mu + a_1 + A_X a_4$$

$$+ (-A_Y a_9 + A_Z a_8) + (-a_{12}\, t\, A_Y + a_{11}\, t\, A_Z) \tag{8}$$

$$\Delta\ddot{Y} + \frac{\mu\Delta Y}{R^3} - \frac{3\mu Y}{R^5}(X\Delta X + Y\Delta Y + Z\Delta Z) = -\frac{Y}{R^3}\Delta\mu + a_2 + A_Y a_5$$

$$+ (A_X a_9 - A_Z a_7) + (a_{12}\, t\, A_X - a_{10}\, t\, A_Z) \tag{9}$$

$$\Delta \ddot{Z} + \frac{\mu \Delta Z}{R^3} - \frac{3\mu Z}{R^5}(X\Delta X + Y\Delta Y + Z\Delta Z) = -\frac{Z\Delta\mu}{R^3} + a_3 + A_Z a_6$$

$$+ (-A_X a_8 + A_Y a_7) + (-a_{11} t A_X + a_{10} t A_Y) \tag{10}$$

Equations (8) through (10) are linear, second order with time varying coefficients.

The coefficients are evaluated along the reference trajectory and are therefore known.

We have:

$$R = (X^2 + Y^2)^{1/2}$$

$$A_X = \ddot{X} + \frac{\mu X}{R^3}$$

$$A_Y = \ddot{Y} + \frac{\mu Y}{R^3}$$

$$A_Z = 0$$

where X, Y, $\ddot{X}$, $\ddot{Y}$ are known functions of time.

Since the equations are linear, a solution corresponding to each perturbation taken singly can be obtained. The ratio of the perturbed variable to the perturbation corresponds to the respective partial derivative. That is, the partials of X and $\dot{X}$ to parameter a_1 are simply $\Delta X/a_1$, and $\Delta \dot{X}/a_1$.

Equations (8) through (10) as presented must be solved on a digital computer. However, since analytic expressions for the partials are convenient an approximate solution will be obtained.

The distance traversed in the ascent trajectory is small compared to the Moon's dimensions. As a consequence gravity remains nearly constant in direction and magnitude and a flat Moon approximation can be used.

For a flat Moon:

$$\overline{G} = -\frac{\mu}{r^2}\, i = g_o i \qquad i = \text{unit vector in } X' \text{ direction}$$

$$\Delta\overline{G} = -\frac{\Delta\mu}{r^2}\, i$$

r = Moon's radius

$$A_X = \ddot{X} + g_o$$

$$A_Y = \ddot{Y}$$

$$A_Z = 0$$

Substituting into (8), (9) and (10):

$$\Delta\ddot{X} = \frac{\Delta\mu}{r^2} + a_1 + (\ddot{X} + g_o)\, a_4 - \ddot{Y}\, a_9 - t\,\ddot{Y}\, a_{12} \tag{11}$$

$$\Delta\ddot{Y} = a_2 + \ddot{Y}\, a_5 + (\ddot{X} + g_o)\, a_9 + (\ddot{X} + g_o)\, t\, a_{12} \tag{12}$$

$$\Delta\ddot{Z} = a_3 - (\ddot{X} + g_o)\, a_8 + \ddot{Y}\, a_7 - (\ddot{X} + g_o)\, t\, a_{11} + \ddot{Y}\, t\, a_{10} \tag{13}$$

The partial derivatives presented in Table 1 were computed from this set of equations with the exception of the partials with respect to initial position errors.

These were computed as follows.

Assume that:

$$R \cong r$$

$$\Delta Y / r^3 \gg \frac{Y \Delta X}{r^4}$$

$$X\Delta X >> Y\Delta Y$$

Then:

$$\Delta\ddot{X} - \frac{2\mu}{r^3}\ \Delta X = 0$$

$$\Delta\ddot{Y} + \frac{\mu\Delta Y}{r^3} = 0$$

$$\Delta\ddot{Z} + \frac{\mu\Delta Z}{r^3} = 0$$

From which:

$$\Delta X = \Delta X_o \cosh \sqrt{\frac{2\mu}{r^3}}\ t + \frac{\Delta X_o}{\sqrt{\frac{2\mu}{r^3}}} \sin h \sqrt{\frac{2\mu}{r^3}}\ t \tag{14}$$

$$\Delta Y = \Delta Y_o \cos \sqrt{\frac{\mu}{r^3}}\ t + \frac{\Delta\dot{Y}_o}{\sqrt{\frac{\mu}{r^3}}} \sin \sqrt{\frac{\mu}{r^3}}\ t \tag{15}$$

$$\Delta Z = \Delta Z_o \cos \sqrt{\frac{\mu}{r^3}}\ t + \frac{\Delta\dot{Z}_o}{\frac{\mu}{r^3}} \sin \sqrt{\frac{\mu}{r^3}}\ t \tag{16}$$

However,

$$\sqrt{\frac{2\mu}{r^3}}\ t_{max} = .565 \text{ rad.}$$

For this small value of the argument:

$$\cos h\, \theta \cong 1 + \theta^2/2$$

$$\cos \theta \cong 1 - \theta^2/2$$

$$\sin h\, \theta \cong \theta$$

$$\sin \theta \cong \theta$$

$$\Delta X \cong \Delta X_o \left(1 + \frac{\mu}{r^3} t^2\right) + \Delta \dot{X}_o t$$

$$\Delta Y \cong \Delta Y_o \left(1 - \frac{\mu}{2r^3} t^2\right) + \Delta \dot{Y}_o t \qquad (17)$$

$$\Delta Z = \Delta Z_o \left(1 - \frac{\mu}{2r^3} t^2\right) + \Delta \dot{Z}_o t$$

In Equations (17) $\Delta \dot{X}_o$, $\Delta \dot{X}_o$, $\Delta \dot{Z}_o$ represent the errors in initial velocity due to the initial position errors.

$$\Delta \dot{\bar{R}}_o = \bar{\omega}_m X \Delta \bar{R}_o$$

To see if this is significant consider the magnitude of one component:

$$\Delta \dot{Y}_o = \Delta X_o \omega_z - \Delta Z_o \omega_x$$

Maximum occurs for equatorial orbit $|\overline{\omega}_m| = \omega_z = 2.5 \times 10^{-6}$ rad/sec, and say ΔX_o max = 1000 meters.

$$\Delta \dot{Y}_o = 2.5 \times 10^{-3} \text{ m/sec.}$$

and:

$$\Delta \dot{Y} \cong \Delta \dot{Y}_o$$

$$\Delta Y = \Delta \dot{Y}_o \, t \cong 1 \text{ meter.}$$

The quantities $\Delta \dot{Y}$ and ΔY are both quite small in terms of the measurement accuracy and, therefore can be eliminated in Equations (17).

Designating the biases in initial position in X, Y, Z directions by a_{14}, a_{15}, a_{16} respectively:

$$\frac{\partial x}{\partial a_{14}} = \frac{\Delta x}{\Delta X_o} = 1 + \frac{\mu}{r^3} t^2$$

$$\frac{\partial x}{\partial a_{14}} = \frac{\Delta y}{\Delta Y_o} = 1 - \frac{\mu}{2r^3} t^2$$

$$\frac{\partial z}{\partial a_{16}} = \frac{\Delta z}{\Delta Z_o} = 1 - \frac{\mu}{2r^3} t^2$$

The partials of the velocity components are obtained by differentiation of (17) with the assumption that $\Delta \dot{X}_o$, $\Delta \dot{Y}_o$, $\Delta \dot{Z}_o$ are negligible.

$$\frac{\partial \dot{x}}{\partial a_{14}} = \frac{\Delta \dot{z}}{\Delta Z_o} = - \frac{2\mu}{r^3} t$$

$$\frac{\partial \dot{y}}{\partial a_{15}} = \frac{\Delta \dot{y}}{\Delta Y_o} = - \frac{\mu}{r^3} \quad t$$

$$\frac{\partial z}{\partial a_{16}} = \frac{\Delta \dot{z}}{\Delta Z_o} = - \frac{\mu}{r^3} \quad t$$

APOLLO NOTE NO. 386
(Task 2, Item II)

E. Pugh
24 November 1965

EQUIVALENCE OF DATA PROCESSING SCHEMES

INTRODUCTION

The purpose of this note is to give some evidence for the equivalence of two data processing schemes given by the following. In scheme I the measurable m_i is assumed to be of the form:

$$m_i = a + bt_i + \eta_i \tag{1}$$

where a is the parameter to be estimated, b is a nuisance parameter and η_i is a sample from a zero mean gaussian noise process with $\overline{\eta_i^2} = \sigma^2$. An unbiased a priori estimate b_a of b is available with $\overline{(b_a - b)^2} = \sigma_b^2$. The estimation of a is done by the method of maximum likelihood.

In Scheme II the measurable is taken as:

$$\begin{aligned} x_i &= m_i - b_a t_i \\ &= a + [\eta_i + (b - b_a)t_i] \end{aligned} \tag{2}$$

where $\eta_i + (b-b_a)\, t_i = e_i$ is considered as noise. The estimation of a is then done by the optimal filter of note 268.

SCHEME I

The maximum likelihood estimates $\hat{a}$ and $\hat{b}$ of a and b are those functions of the data which minimize:

$$L = -\frac{1}{2}\left\{\sum [m_i - (\hat{a} + \hat{b}t_i)]^2/\sigma^2 + (b_a - \hat{b})^2/\sigma_b^2\right\} \tag{3}$$

The estimates of $\hat{a}$ and $\hat{b}$ thus satisfy:

$$\frac{\partial L}{\partial a} = \sum [\, m_i - (\hat{a} + \hat{b} t_i)] / \sigma^2 = 0 \tag{4}$$

$$\frac{\partial L}{\partial b} = \sum t_i [\, m_i - (\hat{a} + \hat{b} t_i)] / \sigma^2 + (b_a - \hat{b}) / \sigma_b^2 = 0 \tag{5}$$

This gives:

$$N\hat{a} + \hat{b} \sum t_i = \sum m_i \tag{6}$$

$$\hat{a} \sum t_i + \hat{b} \left[\sum t_i^2 + \left(\frac{\sigma}{\sigma_b}\right)^2 \right] = \sum t_i m_i + \left(\frac{\sigma}{\sigma_b}\right)^2 b_a \tag{7}$$

Let $F = \sum t_i$, $G = \sum t_i^2 + \left(\frac{\sigma}{\sigma_b}\right)^2$. Then:

$$N\hat{a} + F\hat{b} = \sum m_i \tag{8}$$

$$F\hat{a} + G\hat{b} = \sum t_i m_i + b_a (\sigma/\sigma_b)^2 \tag{9}$$

Eliminating $\hat{b}$:

$$GN\hat{a} + GF\hat{b} = G \sum m_i \tag{10}$$

$$F^2 \hat{a} + GF\hat{b} = F \sum t_i m_i + F\, b_a\, (\sigma/\sigma_b)^2 \tag{11}$$

$$\hat{a} \left[GN - F^2 \right] = G \sum m_i - F \left[\sum t_i m_i + b_a (\sigma/\sigma_b)^2 \right] \tag{12}$$

$$\hat{a} = \frac{G}{GN - F^2} \left\{ \sum m_i - \frac{F}{G} \left[\sum t_i m_i + b_a\, (\sigma/\sigma_b)^2 \right] \right\} \tag{13}$$

$$\hat{a} = \frac{G}{GN - F^2} \left\{ \sum m_i \left[1 - \frac{F}{G} t_i \right] - \frac{F}{G}\, b_a\, (\sigma/\sigma_b)^2 \right\} \tag{14}$$

SCHEME II

In scheme II, we have:

$$x_i = a + \left[\eta_i + (b - b_a)\, t_i \right] \tag{15}$$

where $e_i = \left[\eta_i + (b - b_a)\, t_i \right]$ is considered as noise. From Note 268 the optimal estimate $\hat{a}$ is given as:

$$\hat{a} = (\phi^T A^{-1} \phi)^{-1} \phi^T A^{-1} X \tag{16}$$

where $\phi^T = \left[1, \cdots, 1 \right]$, $X^T = \left[x_1, \cdots, x_N \right]$ and:

$$A = \begin{bmatrix} \overline{e_1^2}, & \overline{e_1 e_2}, & \cdots, & \overline{e_1 e_N} \\ \overline{e_2 e_1} & \overline{e_2^2}, & \cdots, & \overline{e_2 e_N} \\ \vdots & & & \\ \overline{e_N e_1} & \cdots & \cdots & \overline{e_N^2} \end{bmatrix}$$

We show that $\hat{a}$ given by (16) is identical to $\hat{a}$ given by (14) for $N = 2, 3$. Let $t_i = (i - 1)\, \Delta t$ $i = 1, \cdots, N$. Then we have:

$$E e_i^2 = E\left[\eta_i + (b - b_a)\, t_i \right]^2 = \sigma^2 + \sigma_b^2 (i - 1)\, \Delta t^2 \tag{17}$$

$$E e_i e_j = E\left[\eta_i + (b - b_a) t_i \right] \left[\eta_j + (b - b_a)\, t_j \right] = \sigma_b^2 (i-1)(j-1) \Delta t^2, \quad i \neq j \tag{18}$$

Let $g = (\sigma_b / \sigma)^2 \Delta t^2$. Then $A = \sigma^2 \left[f_{ij} \right]$ where:

$$f_{ij} = \begin{cases} (i-1)(j-1)\,g, & i \neq j \\ 1 + (i-1)(j-1)g, & i = j \end{cases} \tag{19}$$

<u>N = 2</u>

We have:

$$A = \sigma^2 \begin{bmatrix} 1 & 0 \\ 0 & 1+g \end{bmatrix} \qquad A^{-1} = \frac{1}{\sigma^2} \begin{bmatrix} 1 & 0 \\ 0 & \frac{1}{1+g} \end{bmatrix}$$

writing out (16) less the σ^2 term which will cancel gives:

$$\hat{a} = \left[\left[1, 1\right] \begin{bmatrix} 1 & 0 \\ 0 & \frac{1}{1+g} \end{bmatrix} \begin{bmatrix} 1 \\ 1 \end{bmatrix} \right]^{-1} \left[1, 1\right] \begin{bmatrix} 1 & 0 \\ 0 & \frac{1}{1+g} \end{bmatrix} \begin{bmatrix} x_1 \\ x_2 \end{bmatrix} \tag{20}$$

$$= \left[1 + \frac{1}{1+g} \right]^{-1} \left[x_1 + x_2 \left(\frac{1}{1+g} \right) \right]$$

Therefore $\hat{a} = \left(\frac{1+g}{2+g}\right) x_1 + \left(\frac{1}{2+g}\right) x_2$ But $g = (\sigma_b/\sigma)^2 \Delta t^2$

$$\hat{a} = \frac{1 + (\sigma_b/\sigma)^2 \Delta t^2}{2 + (\sigma_b/\sigma)^2 \Delta t^2}\, x_1 + \frac{1}{2 + (\sigma_b/\sigma)^2 \Delta t^2}\, x_2 \tag{21}$$

Now from (14) for N = 2 we have:

$$\hat{a} = \frac{G}{GN - F^2} \left\{ m_1 + m_2 \left[1 - \frac{F}{G} \Delta t \right] - \frac{F}{G}\, b_a \left(\frac{\sigma}{\sigma_b}\right)^2 \right\}$$

But $F = \sum t_i = \Delta t$, $G = \sum t_i^2 + \left(\frac{\sigma}{\sigma_b}\right)^2 = \Delta t^2 + \left(\frac{\sigma}{\sigma_b}\right)^2$, $m_1 = x_1$, $m_2 = x_2 + b_a \Delta t$

$$\hat{a} = \frac{\Delta t^2 + (\sigma/\sigma_b)^2}{2\Delta t^2 + 2(\sigma/\sigma_b)^2 - \Delta t^2} \left\{ x_1 + (x_2 + b_a \Delta t) \left[1 - \frac{\Delta t^2}{\Delta t^2 + (\sigma/\sigma_b)^2} \right] - \frac{\Delta t}{\Delta t^2 + (\sigma/\sigma_b)^2} \, b_a \left(\frac{\sigma}{\sigma_b}\right)^2 \right\}$$

$$= \frac{\Delta t^2 + (\sigma/\sigma_b)^2}{\Delta t^2 + 2(\sigma/\sigma_b)^2} \left\{ x_1 + (x_2 + b_a \Delta t) \left[\frac{(\sigma/\sigma_b)^2}{\Delta t^2 + (\sigma/\sigma_b)^2} \right] - \frac{\Delta t}{\Delta t^2 + (\sigma/\sigma_b)^2} \, b_a \left(\frac{\sigma}{\sigma_b}\right)^2 \right\}$$

$$= \frac{\Delta t^2 + (\sigma/\sigma_b)^2}{\Delta t^2 + 2(\sigma/\sigma_b)^2} \left[x_1 + x_2 \frac{(\sigma/\sigma_b)^2}{\Delta t^2 + (\sigma/\sigma_b)^2} \right]$$

$$= \frac{1 + (\sigma_b/\sigma)^2 \Delta t^2}{2 + (\sigma_b/\sigma)^2 \Delta t^2} x_1 + \frac{1}{2 + (\sigma_b/\sigma)^2 \Delta t^2} x_2$$

This checks with (21) completing the proof.

<u>N = 3</u>

We have:

$$A = \sigma^2 \begin{bmatrix} 1 & 0 & 0 \\ 0 & 1+g & 2g \\ 0 & 2g & 1+4g \end{bmatrix}$$

$$A^{-1} = \frac{1}{\sigma^2} \begin{bmatrix} 1 & 0 & 0 \\ 0 & \frac{1+4g}{1+5g} & \frac{-2g}{1+5g} \\ 0 & \frac{-2g}{1+5g} & \frac{1+g}{1+5g} \end{bmatrix}$$

Writing out (16) again gives:

$$\hat{a} = \left(\frac{1+5g}{3+6g}\right) x_1 + \left(\frac{1+2g}{3+6g}\right) x_2 + \left(\frac{1-g}{3+6g}\right) x_3$$

Now $x_1 = m_1$, $x_2 = m_2 - b_a\Delta t$, $x_3 = m_3 - b_a 2\Delta t$. Thus:

$$\hat{a} = \left(\frac{1+5g}{3+6g}\right) m_1 + \left(\frac{1+2g}{3+6g}\right)(m_2 - b_a\Delta t) + \left(\frac{1-g}{3+6g}\right)(m_3 - b_a 2\Delta t) \tag{22}$$

From scheme I:

$$\hat{a} = \frac{G}{GN - F^2}\left\{ \sum m_i\left[1 - \frac{F}{G}\, t_i\right] - \frac{F}{G}\, b_a \left(\frac{\sigma}{\sigma_b}\right)^2 \right\}$$

$$= \frac{G}{3G - F^2}\left\{ m_1 + m_2\left[1 - \frac{F}{G}\,\Delta t\right] + m_3\left[1 - \frac{F}{G}\, 2\Delta t\right] - \frac{F}{G}\, b_a\left(\frac{\sigma}{\sigma_b}\right)^2 \right\}$$

But $F = \sum t_i = 3\Delta t$, $G = \sum t_i^2 + \left(\frac{\sigma}{\sigma_b}\right)^2 = 5\Delta t^2 + \left(\frac{\sigma}{\sigma_b}\right)^2$

Therefore
$$\hat{a} = \frac{5\Delta t^2 + (\sigma/\sigma_b)^2}{6\Delta t^2 + 3(\sigma/\sigma_b)^2}\left\{ m_1 + m_2\left[1 - \frac{3\Delta t^2}{5\Delta t^2 + (\sigma/\sigma_b)^2}\right] + m_3\left[1 - \frac{6\Delta t^2}{5\Delta t^2 + (\sigma/\sigma_b)^2}\right] - b_a\,\frac{3\Delta t(\sigma/\sigma_b)^2}{5\Delta t^2 + (\sigma/\sigma_b)^2}\right\}$$

To check this with (22) we check the coefficients of m_1, m_2, m_3 and b_a. The coefficient of m_1 is:

$$\frac{1+5g}{3+6g} = \frac{1 + 5(\sigma_b/\sigma)^2\Delta t^2}{3 + 6(\sigma_b/\sigma)^2\Delta t^2} = \frac{(\sigma/\sigma_b)^2 + 5\Delta t^2}{3(\sigma/\sigma_b)^2 + 6\Delta t^2} \qquad \text{check}$$

The coefficient of m_2 is:

$$\frac{1+2g}{3+6g} = \frac{1 + 2(\sigma_b/\sigma)^2\,\Delta t^2}{3 + 6(\sigma_b/\sigma)^2\,\Delta t^2}$$

From scheme I the coefficient is:

$$\left[\frac{5\Delta t^2 + (\sigma/\sigma_b)^2}{6\Delta t^2 + 3(\sigma/\sigma_b)^2}\right]\left[\frac{2\Delta t^2 + (\sigma/\sigma_b)^2}{5\Delta t^2 + (\sigma/\sigma_b)^2}\right] = \frac{2\Delta t^2 + (\sigma/\sigma_b)^2}{6\Delta t^2 + 3(\sigma/\sigma_b)^2}$$

$$= \frac{1 + 2(\sigma_b/\sigma)^2\Delta t^2}{3 + 6(\sigma_b/\sigma)^2\Delta t^2} \qquad \text{check}$$

The coefficient of m_3 is:

$$\frac{1 - g}{3 + 6g} = \frac{1 - (\sigma_b/\sigma)^2\Delta t^2}{3 + 6(\sigma_b/\sigma)^2\Delta t^2}$$

From scheme I this coefficient is:

$$\frac{(\sigma/\sigma_b)^2 - \Delta t^2}{3(\sigma/\sigma_b)^2 + 6\Delta t^2} = \frac{1 - (\sigma_b/\sigma)^2\Delta t^2}{3 + 6(\sigma_b/\sigma)^2\Delta t^2} \qquad \text{check}$$

The coefficient of b_a is:

$$-\left(\frac{1 + 2g}{3 + 6g}\right)\Delta t - \left(\frac{1 - g}{3 + 6g}\right)2\Delta t = \frac{-\Delta t - 2g\Delta t - 2\Delta t + 2g\Delta t}{3 + 6g} = \frac{-3\Delta t}{3 + 6g}$$

$$= \frac{-3\Delta t}{3 + 6(\sigma_b/\sigma)^2\Delta t^2}$$

From scheme I this coefficient is:

$$\frac{-3\Delta t(\sigma/\sigma_b)^2}{3(\sigma/\sigma_b)^2 + 6\Delta t^2} = \frac{-3\Delta t}{3 + 6(\sigma_b/\sigma)^2\Delta t^2} \qquad \text{check}$$

This completes the proof for N = 3.

It was hoped that an induction proof for the equivalence of the two schemes could be devised in the following way. Consider two measurements, the first being $\hat{a}$ computed from scheme I for N pieces of data and the second being the $(N+1)^{st}$ measurement:

$$\hat{a} = x_n = a + \eta_n$$

$$x_{n+1} = a + \left[\eta_{n+1} + (b - b_a) t_{n+1} \right]$$

It can be shown from scheme I that $\overline{\eta}_n = 0$, $\overline{\eta_n^2} = \sigma^2 \dfrac{G}{GN - F^2}$

and

$$E\, \eta_n \left[\eta_{n+1} + (b - b_a)\, t_{n+1} \right] = \frac{\sigma^2 G}{GN - F^2} \frac{F}{G} t_{n+1}$$

Thus the filter of scheme II can be applied to these two measurements and compared with scheme I for N + 1 pieces of data. The fallacy in this approach is that the filter of scheme II applied recursively in this way is not the same as the filter applied to the original N + 1 pieces of data.

Though no induction proof can be supplied, it is believed that the two schemes are equivalent and the cases given for N = 2, 3 lend some evidence to this belief.

The Bissett-Berman Corporation 2941 Nebraska Avenue, Santa Monica, California EXbrook 4-3270

APOLLO NOTE NO. 387
(Task 2, Item II)

P. Gluckman
20 December 1965

USE OF CHOLESKY DECOMPOSITION TO INVERT ILL CONDITIONED MATRICES

INTRODUCTION

In the course of performing an expected error analysis on a set of estimable tracking parameters it is necessary to introduce large numbers as "infinities" in matrices to be inverted. The addition of these large numbers forces a matrix usually to be ill-conditioned and a critical problem from a numerical point of view. Since all of these matrices are from theoretical grounds positive definite, it is possible to decompose the matrix into the product of two triangular matrices. Once this is done it is relatively easy to compute the inverse of the matrix without any troublesome numerical problem The nature of the numerical problems usually is floating point over flow or floating point under flow Both are fatal in most numerical processes

This note consists of three sections The first is a theoretical review of the theory of the Cholesky Decomposition and the algorithm for performing the decomposition Also included is some proofs In the second section is the description of how the method is used to perform matrix inversions and how the subroutines are organized The final section expounds upon some of the virtues of using decomposition instead of a straight inversion, in particular how computer time and memory space can be saved

CHOLESKY DECOMPOSITION

The first result given will be to show the existence and nature of the decomposition Consider a real positive definite symmetric matrix A. From A define a lower triangular matrix T, i e , a matrix with only

zero elements above the main diagonal such that:

$$A = T\,T^t,$$

where super t implies the matrix transpose is first performed. The proof is by induction. Assume it true for matrices of order up to (n - 1). If A is a positive definite symmetric matrix of order n, it may be partitioned, by definition, in the form:

$$A = \left[\begin{array}{c|c} B & a \\ \hline a^t & a_{nn} \end{array}\right]$$

where B is a symmetric positive definites matrix of order (n-1) and a is a vector of order (n-1). By the induction hypothesis there is a T of order (n-1) satisfying:

$$T\,T^t = B.$$

If we choose ℓ so that:

$$T\,\ell = a$$

which is clearly done since T is triangular and non-singular, then:

$$\left[\begin{array}{c|c} T & 0 \\ \hline \ell^t & \ell_{nn} \end{array}\right] \left[\begin{array}{c|c} T^t & \ell \\ \hline 0 & \ell_{nn} \end{array}\right] = \left[\begin{array}{c|c} B & a \\ \hline a^t & a_{nn} \end{array}\right] = A$$

where ℓ_{nn} is chosen such that:

$$\ell^t \ell + (\ell_{nn})^2 = a_{nn}$$

which completes the proof.

The algorithm to compute T is iterative in nature and goes as follows:

$$t_{ij} = (a_{ij} - \sum_{k=1}^{j-1} t_{ik}\, t_{jk})/t_{jj} \qquad i > j$$

$$t_{jj} = (a_{jj} - \sum_{k=1}^{j-1} t_{jk}^2)^{1/2}$$

$$t_{ji} = 0 \qquad i > j$$

where each t_{ij} involves only those t_{ij} that have been previously computed. It remains to show that T does indeed have the required property of being triangular and $A = T\,T^t$. Triangularity is obvious and the other property follows from:

$$a_{ij} \overset{?}{=} \sum_{\ell=1}^{n} t_{i\ell}\, t_{\ell j}^{\,t} = \sum_{\ell=1}^{j} t_{i\ell}\, t_{j\ell} \qquad i > j$$

$$= \sum_{\ell=1}^{j-1} t_{i\ell}\, t_{j\ell} + \frac{(a_{ij} - \sum_{k=1}^{j-1} t_{ik}\, t_{jk})}{t_{jj}}\, t_{jj}$$

$$= a_{ij} \qquad i > j$$

$$a_{jj} \overset{?}{=} \sum_{\ell=1}^{n} t_{j\ell}\, t^{t}_{\ell j} = \sum_{\ell=1}^{j} t_{j\ell}^{\,2}$$

$$= \sum_{\ell=1}^{j-1} t_{j\ell}^{\,2} + (a_{jj} - \sum_{k=1}^{j-1} t_{jk}^2)$$

$$= a_{jj}$$

using the algorithm for calculating T.

The value of the decomposition lies in solving a set of linear equations:

$$Ax = b$$

for the unknown vector x. It is possible by the above to rewrite this as:

$$T\,T^t\,x = b$$

or:

$$Ty = b \tag{1}$$

$$T^t x = y \tag{2}$$

where y is an intermediate unknown vector. To solve (1) and (2) is quite easy since T is a triangular matrix. The algorithm to do it is as follows:

$$y_i = (b_i - \sum_{k=1}^{i-1} t_{ik}\ b_k)/t_{ij}$$

for (1) and:

$$x_i = (y_i - \sum_{k=n}^{n-i+1} t_{ki}\ y_k)/t_{ii}$$

for (2).

Another way in which the decomposition can be used is to find the inverse of A. Let e_i be the cartesian coordinate vector with a one in the ith position and zero elsewhere.

Denote the solution of the equation:

$$Af = e_i$$

as f_i.

This is possible by the above algorithm. Let the columns of a matrix C be formed from f_i $(i = 1 \ldots n)$.

$$(AC)_{ij} = \sum_{\ell=1}^{n} a_{i\ell} \; C_{\ell j}$$

$$= \sum_{\ell=1}^{n} a_{i\ell} \; (f_j)_\ell$$

$$= (e_j)_\ell$$

where $(e_j)_\ell$ is the ℓ, jth position of the identity matrix.

The last result is the one used to find the inverse of the required matrix. In the next section the details of how this is done are given.

DESCRIPTION OF THE MATRIX INVERSION SUB-PROGRAM

Figure 1. is a listing of the Fortran source program of the Matrix Inversion Sub-Program. For ease of description a line count has been added on the right. In the calling sequence the matrix to be inverted is A and its size is N. NERF is an error flag that is zero if the matrix A is positive definite and 100 if it is not. For convenience, temporary storage Array B is used since temporary space is available. If temporary space was not available the program could be changed to do without the Array B. In B will be developed the inverse of A and just before exits (43-45) moved from B to A.

Since A is a symmetric matrix the portion below the main diagonal is redundant and will be used to develop T, except for the main diagonal of T. In the algorithm presented in the previous section the elements of the main diagonal of T are used only as divisions. To save computing time since multiplication takes less time than division

```
*       LABEL
        SUBROUTINE MATINV (A,N,NERF)
D       DIMENSION A(40,40), B(40,40), P(40)
        DIMENSION SP(31)
        COMMON SP,B
        NERF=0
         DO 1 I=1,N
         DO 1 J=I,N
D        X=A(I,J)
         L=I-1
         IF (L) 3,3,4
 4       DO 5 K=1,L
D5       X=X-A(J,K)*A(I,K)
 3       IF (I-J) 6,7,6
D6       A(J,I)=X*P(I)
         GO TO 1
 7       IF (X) 8,8,9
D     9 P(I)=1.0/SQRTF(X)
 1       CONTINUE
         DO 20 I=1,N
         DO 20 J=1,I
D20      B(I,J)=0.0
         DO 12 K=1,N
D        B(K,K)=P(K)
         IF(K-N)     22,21,22
 22      CONTINUE
         L1=K+1
         DO 10 I=L1,N
D        Z=0.0
         L=I-1
 13      DO 14 J=1,L
D14      Z=Z-A(I,J)*B(K,J)
D10      B(K,I)=Z*P(I)
 21      CONTINUE
         DO 12 I1=1,N
         I=N-I1+1
D        Z=B(K,I)
         L=I+1
         IF (N-I) 19,12,19
 19      DO 15 J1=L,N
         J=N-J1+L
D15      Z=Z-A(J,I)*B(K,J)
D12      B(K,I)=Z*P(I)
         DO 16 I=1,N
         DO 16 J=1,N
D16      A(I,J)=B(I,J)
         RETURN
 8       WRITE OUTPUT TAPE 6,17
   17 FORMAT (1H0,//,25X,43HMATRIX TO BE INVERTED NOT POSITIVE DEFINITE
     1 //)
        NERF=100
        RETURN
         END
```

Figure 1.

the reciprocal of the elements are stored (17) and used as multipliers (14, 23, 32, and 42). A guarantee of improved accuracy is possible by putting between (17) and (18) the statement:

$$P(I) = .5*(P(I) + \frac{1}{X*P(I)})$$

which comes from Newton's approximation and improves the accuracy of P(I). The statements (6-18) do the decomposition and statements (22-42) are the backsolving to get the inverse. From (27-33) corresponds to algorithm 1 and (34-42) algorithm 2. The first algorithm starts out with the identification that depending on the column of B being considered, part of the first backsolving vector is always zero and the backsolving can be started at the column position with that value of T on the main diagonal (23). The last thing in understanding the program lies at (10, 24, and 38) which is the way a blank sums must be instrumented in Fortran.

The test for positive definiteness is made during the decomposition at (16). Theory says that all of the main diagonal elements of T must be positive. Since developing the program it has been pointed out that there may be a theoretical reason for the matrix A being not positive definite. An example of where this is the case is when the character of the data is such that two parameters cannot be functionally separated and the matrix inversion routine is telling you this. In this case the value of I at (16) should be saved. The next section addresses this problem when it occurs in real time.

POTPOURRI

In a multivariate statistical estimation program like an orbit determination program the only matrices that have to be inverted are positive definite. Likewise, whenever linear equations have to be solved, the matrix usually is also positive definite. The way in which the technique of decomposition can best be used is to take all positive matrices of order N and store them in an N x N+1 array where the main diagonal and above is the matrix in question, while below the main diagonal is the triangular decomposition matrix corresponding to this

matrix. The augmented column is the reciprocal of the main diagonal of the decomposition matrix. In this form it is easy to solve a set of linear equations or actually compute the inverse. The advantage here is that N (N+1) storage cells effectively store a matrix and its inverse and using the decomposition matrix it is possible to solve a set of linear equations directly, which is faster and more accurate than actually inverting the matrix.

A side benefit of using decomposition is that when the decomposition matrix is being computed a test is made of the condition of the matrix. If the matrix is not positive definite, then under the prevailing conditions two parameters are functionally dependent. The test will tell which is the second parameter of the two. A way to solve this problem in real time is to zero out the particular row corresponding to the dependent parameter in the decomposition matrix and set the reciprocal of the diagonal to one. This has the effect of eliminating that parameter from consideration and can be repeated as the decomposition progresses.

The Bissett-Berman Corporation 2941 Nebraska Avenue, Santa Monica, California EXbrook 4-3270

APOLLO NOTE NO. 388
(Task 1, Item 1B)

J. B. Murphy
16 December 1965

GLOBAL TIME-DEPENDENT SLAB MODEL IONOSPHERE PROGRAM

While it is true that the ionosphere contributes considerably less differential phase length than the troposphere, the ionosphere, which is much less predictable, effects larger variances in the measured radar range (and range rate). For this reason, and that the ionosphere is strongly a function of local time and day of the year, it is desirable to obtain a good global time-dependent model of the ionosphere. Apollo Note No. 377 describes a slab model satisfying these requirements. It should be noted that this model is predicted on the assumptions that the vehicle being tracked is entirely outside the ionosphere, that there is thermal equilibrium between the ionosphere, electrons and neutral atoms, and the conditions are relatively quiescent.

Using essentially the same equations as in Apollo Note No. 377, the model described in that note was mechanized as a computer program described in Appendix A of this note. The differences and additional equations needed are described in Appendix B.

This program was then run for the situation:

R (daily sunspot number) = 300

F (daily diameter flux value) = 160 $\frac{10^{-22}\ \text{watt}}{m^2}$

$\bar{F}$ (monthly average flux value) = 160 $\frac{10^{-22}\ \text{watt}}{m^2}$

a_p (three hour geomagnetic index) = 0

λ_o (station latitude) = 20°

f (transmitter frequency) = $2.28 \cdot 10^9$ cps

with six values of elevation ($\phi_o = 5^o, 10^o, 15^o, 30^o, 60^o, 90^o$), for values of azimuth ($\alpha = 0^o, 90^o, 180^o, 270^o$), five local times (T = 8, 12, 16, 20, 24 hr) and four days of the year (D = 80, 173, 266, 356). For each one of these 480 conditions, $\Delta\ell$, h_m, h_c, h_b, and T_m are printed out. A typical output is shown in Figure 1.

From these outputs it is seen that $\Delta\ell$ through the zenith ($\phi_o = 90^o$) varied from about 1 meter on a summer midnight to about 5 meters at summer noon. For a 5° initial elevation, 16 meter range errors occur under many conditions (e.g. D = 266, T = 12 hr., $\alpha = 90^o$).

At present, the effort is being exerted to incorporate this ionosphere error into the Error Analysis Program in order to determine what effect the uncertainty of the ionosphere parameters has on the orbit parameters of a vehicle.

APPENDIX A

Let:

λ_o = initial (at station) latitude

ϕ_o = initial elevation angle of ray

α = azimuth angle of ray

K, L = iteration limits

with all other terms defined as in Apollo Note No. 377. The program to find the phase length difference of a ray passing through the ionosphere then is much as outlined in Apollo Note No. 377.

Using a sequential programming type of equation writing, the equations are as follows:

$$\theta_1 = \frac{4\pi}{365}(d - 97) \tag{1}$$

$$\theta_2 = \frac{4\pi}{365}(d - 173) \tag{2}$$

$$\theta_3 = \frac{2\pi}{365}(d - 80) \tag{3}$$

$$\theta'_4 = \frac{\pi}{12}(t - 14) \tag{4}$$

$$\theta'_5 = \frac{\pi}{12}(t - 20) \tag{5}$$

$$\delta = \frac{2\pi\,(23.56)}{360} \sin\theta_3 \tag{6}$$

$$\begin{aligned} T_\pi = {} & (635 + 0.3\,\overline{F} + 0.012\,\overline{F}^{\,2}) + 2.5\,(F - \overline{F}) \\ & + 0.5\,\overline{F}\cos\theta_1 + a_p + 125\,\left[1 - \exp(-.08\,a_p)\right] \end{aligned} \tag{7}$$

$$n_\pi = 2 \cdot 10^{10} (1 + .02R) \sqrt{T_\pi} \tag{8}$$

$$\psi'_o = \lambda_o - \delta \tag{9}$$

$$\psi_o = \psi'_o \tag{10}$$

$$\theta_4 = \theta'_4 \tag{11}$$

$$\theta_5 = \theta'_5 \tag{12}$$

$$\lambda = \lambda_o \tag{13}$$

$$X = W = Z = 1 \tag{14}$$

Find ψ (using PSI Subroutine) (15)

$$T = T_\pi \left[1 + 0.4 \cos^4 \left(\frac{\psi}{2} \right) \right] \tag{16}$$

$$h = 270 (1 + .22 \psi_o \sin \theta_3)(1 + \cos^2 \theta_5 \cos^6 1.5\psi_o)$$

$$(1 + .001 R) + \left[10 \sin^6 \left(\frac{\psi}{2} \right) \right] (9 + \psi_o \sin \theta_3) \tag{17}$$

$$(1 + .0026R) \left(\frac{T}{T_\pi} \right)$$

If $\left| 1 - \frac{h}{X} \right| < K$, Go to (25) (18)

continue

$$X = h \tag{19}$$

If $\phi_o = \frac{\pi}{2}$, Set $\phi = \phi_o$ and Go to (25) (20)

continue

$$\phi = \cos^{-1}\left(\frac{R_o}{R_o+h}\cos\phi_o\right) \qquad 0 < \phi \leq \frac{\pi}{2} \tag{21}$$

$$\psi_o = \psi'_o + (\phi - \phi_o)\cos\alpha \tag{22}$$

Find λ, θ_4 and θ_5 (using LATLON subroutine) (23)

Go to (15) (24)

Set $T_m = T \qquad \psi_{om} = \psi_o \qquad h_m = h$

$$\lambda_m = \lambda \qquad \psi_m = \psi \tag{25}$$

$$\theta_{4m} = \theta_4 \qquad \phi_m = \phi$$

$$y_m = .2191\,(1+.003R)\left[180\,\psi_{om}\sin\theta_3 + T_m\left(\frac{R_o + h_m}{R_o}\right)^2\right] \tag{26}$$

$$\left.\begin{aligned} h_{mb} &= h_m \quad (27)\\ h_{mc} &= h_m \quad (28)\\ y_c &= y_m \quad (29)\\ y_b &= y_m \quad (30)\end{aligned}\right\} \text{(First approximations)}$$

$$h_c = h_{mb} + .69\,y_c \tag{31}$$

$$h_b = h_{mb} - .31\,y_b \tag{32}$$

$$\phi_c = \cos^{-1}\left(\frac{R_o}{R_o+h_c}\cos\phi_o\right) \tag{33}$$

$$\phi = \phi_c \tag{34}$$

Find λ_c, θ_{4c}, θ_{5c} (LATLON) (35)

Find ψ_c (using PSI) (36)

$$\theta_b = \cos^{-1}\left(\frac{R_o}{R_o+h_b} \cos\phi_o\right) \tag{37}$$

$$\phi = \phi_b \tag{38}$$

Find λ_b, θ_{4_b}, θ_{5_b} (LATLON) (39)

Find ψ_b (PSI) (40)

$$\psi_{oc} = \psi'_o + (\phi_c - \phi_o) \cos\alpha \tag{41}$$

$$\psi_{ob} = \psi'_o + (\phi_b - \phi_o) \cos\alpha \tag{42}$$

$$T_c = T_\pi \left[1 + .4 \cos^4 \left(\frac{\psi_c}{2} \right) \right] \tag{43}$$

$$T_b = T_\pi \left[1 + .4 \cos^4 \left(\frac{\psi_b}{2} \right) \right] \tag{44}$$

$$h_{mc} = 270\,(1 + .22\,\psi_{oc} \sin\theta_3)\,(1 + \cos^2\theta_{5c} \cos^6 1.5\,\psi_{oc})$$

$$(1 + .001\,R) + \left[10 \sin^6 \left(\frac{\psi_c}{2} \right)\right] (9 + \psi_{oc} \sin\theta_3) \tag{45}$$

$$(1 + .0026\,R) \left(\frac{T_c}{T_\pi} \right)$$

$$h_{mb} = 270\,(1 + .22\psi_{ob} \sin\theta_3)\,(1 + \cos^2\theta_{5b} \cos^6 1.5\psi_{ob})$$

$$(1 + .001\,R) + \left[10 \sin^6 \left(\frac{\psi_b}{2}\right)\right](9 + \psi_{ob} \sin\theta_3) \tag{46}$$

$$(1 + .0026\,R)\left(\frac{T_b}{T_\pi}\right)$$

$$y_c = .2191\,(1 + .003\,R)\left[180\psi_{oc} \sin\theta_3 + T_c \left(\frac{R_o + h_{mc}}{R_o}\right)^2\right] \tag{47}$$

$$y_b = .2191\,(1 + .003\,R)\left[180\psi_{ob} \sin\theta_3 + T_b \left(\frac{R_o + h_{mb}}{R_o}\right)^2\right] \tag{48}$$

$$Q = \left|1 - \frac{h_{mc}}{W}\right| \tag{49}$$

$$P = \left|1 - \frac{h_{mb}}{Z}\right| \tag{50}$$

$$W = h_{mc} \tag{51}$$

$$Z = h_{mb} \tag{52}$$

If $Q > L$ Go to (31)
continue (53)

If $P > L$ Go to (31)
continue (54)

$$n_m = n_\pi \left(1 + \sqrt{\frac{T_m - T_\pi}{T_1}}\right) \tag{55}$$

$$S = \sqrt{(R_o + h_c)^2 - (R_o \cos\phi_o)^2} - \sqrt{(R_o + h_b)^2 - (R_o \cos\phi_o)^2} \tag{56}$$

$$n_{s_1} = \frac{Sn_m}{y_m} \left(.7792 - .0377 \sqrt{\frac{T_b}{T_m}} + .2584 \sqrt{\frac{T_c}{T_m}} \right) \tag{57}$$

$$\Delta \ell_1 = -4.026 \cdot 10^7 \left(\frac{n_{s1}}{f^2} \right) \tag{58}$$

PSI SUBROUTINE

$$\cos\psi = \sin\lambda \sin\delta + \cos\lambda \cos\theta_4 \cos\delta \tag{1}$$

$$\cos^4\left(\frac{\psi}{2}\right) = \frac{1}{4}(1 + \cos\psi)^2 \tag{2}$$

$$\sin^6\left(\frac{\psi}{2}\right) = \frac{1}{8}(1 - \cos\psi)^3 \tag{3}$$

$$\psi = \begin{cases} \cos^{-1}(\cos\psi) & \cos\psi \neq 1 \\ \left.\begin{array}{ll} 0 & \lambda = \delta \text{ and } \theta_4 = 0 \\ \pi & \text{otherwise} \end{array}\right\} & \cos\psi = 1 \end{cases} \tag{4}$$

$$\cos a = \cos(\phi - \phi_o)\cos\lambda_o - \sin(\phi - \phi_o)\left|\sin\lambda_o\right|\cos\alpha \tag{1}$$

$$\sin a = \sqrt{1 - \sin^2 a} \tag{2}$$

$$\sin\mu = \sin(\phi - \phi_o)\ \frac{\left|\sin\alpha\right|}{\sin a} \tag{3}$$

$$\cos\mu = \sqrt{1 - \sin^2\mu} \tag{4}$$

If sign $(\cos\alpha) =$ sign $(\sin\lambda_o)$, Go to (7)
continue (5)

If $\tan(\phi - \phi_o) > -\tan\lambda_o/\cos\alpha$, Go to (9)
continue (6)

$$\lambda = \begin{cases} +\sin^{-1}(\cos\mu\sin a), & \lambda_o \geq 0 \\ -\sin^{-1}(\cos\mu\sin a), & \lambda_o < 0 \end{cases} \tag{7}$$

Go to (10) (8)

$$\lambda = \begin{cases} -\sin^{-1}(\cos\mu\sin a), & \lambda_o \geq 0 \\ +\sin^{-1}(\cos\mu\sin a), & \lambda_o < 0 \end{cases} \tag{9}$$

$$\Delta\theta_4 = \begin{cases} +\tan^{-1}(\tan a\sin\mu), & 0 \leq \alpha \leq \pi \\ -\tan^{-1}(\tan a\sin\mu), & \pi < \alpha < 2\pi \end{cases} \tag{10}$$

$$\theta_4 = \theta'_4 + \Delta\theta_4 \tag{11}$$

$$\theta_5 = \theta'_5 + \Delta\theta_4 \tag{12}$$

APPENDIX B

I Elevation Angle in Ionosphere

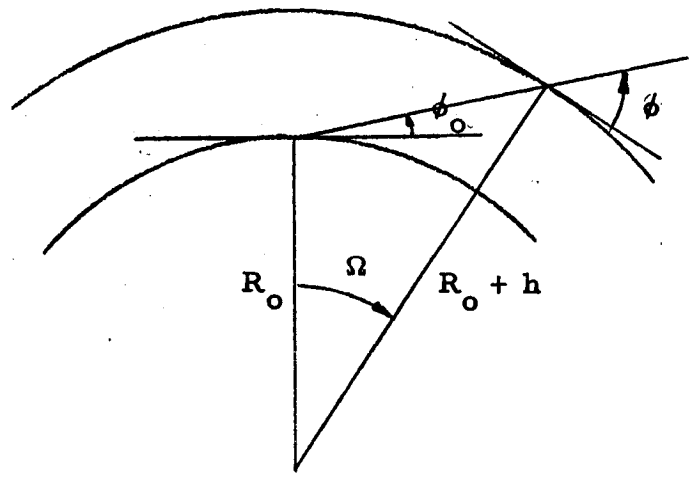

Using law of sine's:

$$\frac{\sin\left(\frac{\pi}{2} - \phi\right)}{\sin\left(\frac{\pi}{2} + \phi_o\right)} = \frac{R_o}{R_o + h}$$

or: (1)

$$\frac{\cos\phi}{\cos\phi_o} = \frac{R_o}{R_o + h}$$

$$\phi = \cos^{-1}\left\{\cos\phi_o \quad \frac{R_o}{R_o + h}\right\}$$

Note that:

$$\Omega + \left(\phi_o + \frac{\pi}{2}\right) + \left(\frac{\pi}{2} - \phi\right) = \pi$$

or:

$$\Omega = (\phi - \phi_o) \qquad (2)$$

Thus central angle changes because of elevation angles less than 90° can be computed by using Equations (1) and (2).

II Path Length Through The Ionosphere

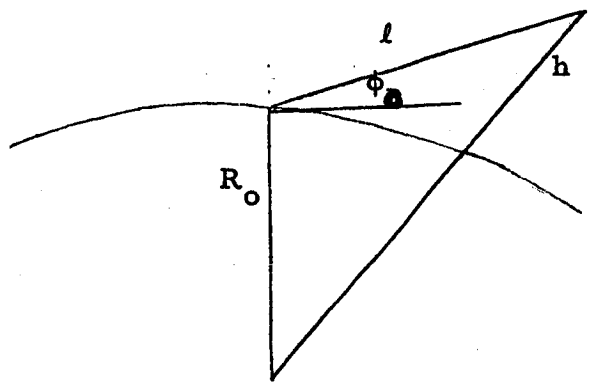

From the law of cosines:

$$\ell^2 + 2R_o \ell \sin \phi_o + R_o^2 - (R_o + h)^2 = 0$$

or:

$$\ell = R_o \sin \phi_o + \sqrt{(R_o \sin \phi_o) + (R_o + h)^2 - R_o^2}$$

or:

$$\ell = R_o \sin \phi_o + \sqrt{(R_o + h)^2 - (R_o \cos \phi_o)^2}$$

Thus, the path length through the ionosphere with the top height of h_c and the bottom height of h_b is:

$$\Delta \ell = \sqrt{(R_o + h_c)^2 - (R_o \cos \phi_o)^2} - \sqrt{(R_o + h_b)^2 - (R_o \cos \phi_o)^2}$$

III Electron Content Along The Ray

By definition:

$$n_s = \int_s N(x)\, dx$$

where N (x) is electron density along the ray. Or similarly.

$$n_s = \overline{N}_s \; S$$

$$\text{where } \overline{N}_s \cong \frac{N_b + N_c}{2} = \frac{N_c}{2} \left(1 + \frac{N_b}{N_c} \right)$$

$$= \frac{n_c}{2y_c} \left(1 + \frac{n_b/y_b}{n_c/y_c}\right) = \frac{n_c}{2y_c} \left(1 + \sqrt{\frac{T_b}{T_c}}\right)$$

However, a better approximation to n_s can be had by assuming N (x) is a second order equation in x with:

$$N(0) = \frac{n_b}{y_b} \; ; \; N(.31S) = \frac{n_m}{y_m} \; ; \; N(S) = \frac{n_c}{y_c}$$

By La Grangian interpolation:

$$N(x) \cong \frac{(x - .31S)(x-S)}{.31\, S^2} \frac{n_b}{y_b} - \frac{x(x-S)}{(.31S)(.69S)} \frac{n_m}{y_n}$$

$$+ \frac{x(x - .31S)}{S(.69S)} \frac{n_c}{y_c}$$

Substituting this equation into the integral:

$$n_s = S\left(-.03764\,\frac{n_b}{y_b} + .77918\,\frac{n_m}{y_m} + .25848\,\frac{n_c}{y_c}\right)$$

$$= S\left(\frac{n_m}{y_m}\right)\left(.77918 - .03764\,\frac{n_b/y_b}{n_m/y_m} + .25848\,\frac{n_c/y_c}{n_m/y_m}\right)$$

$$= S\,\frac{n_m}{y_m}\left(.77918 - .03764\sqrt{\frac{T_b}{T_m}} + .25848\sqrt{\frac{T_c}{T_m}}\right)$$

Latitude and Longitude Along Ray (LATLON)

If a ray is launched at an azimuth α and an elevation ϕ_o from a station located at latitude λ_o and local hour angle θ'_4, the latitude and hour angle of a point on the ray at an altitude h such that the elevation angle at that altitude is ϕ, is found in the following manner:

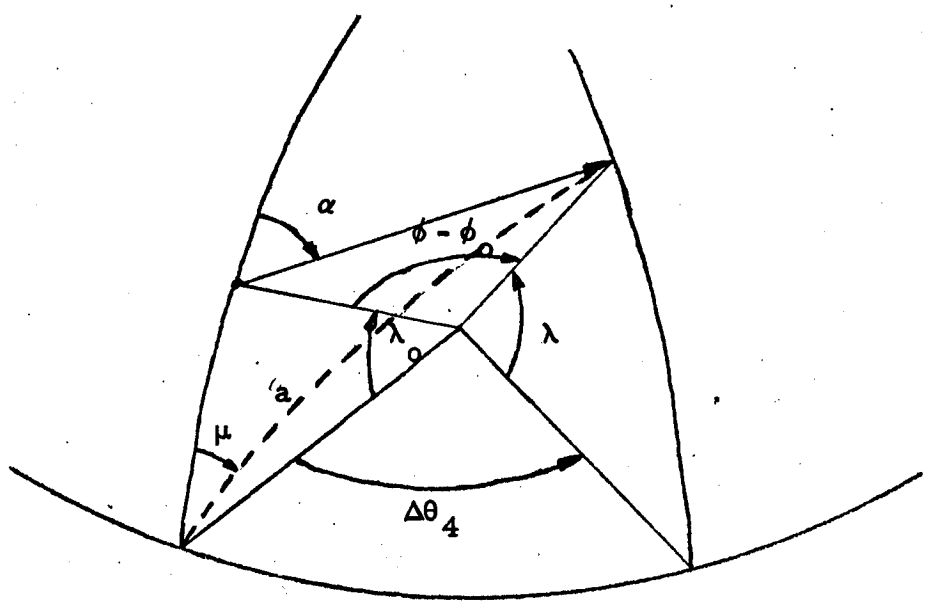

From spherical trigonometry:

$$\cos a = \cos(\phi - \phi_o)\cos\lambda_o - \sin(\phi - \phi_o)\left|\sin\lambda_o\right|\cos\alpha$$

(Note that all calculations are done as if $\lambda_o \geq 0$, $0 \leq \alpha \leq \pi$ and then converted to proper quadrant.

Then:

$$\sin a = + \sqrt{1 - \cos^2 a}$$

Now by law of sines:

$$\sin\mu = \sin\phi - \phi_o) \quad \frac{\left|\sin\alpha\right|}{\sin a}$$

$$\cos\mu = \sqrt{1 - \sin^2\mu}$$

Now if sign $(\cos\alpha)$ = sign $(\sin\lambda_o)$

or if not:

$$-\tan(\phi - \phi_o) > \tan\lambda_o \cos\alpha$$

then using the relationships for spherical right triangles:

$$\lambda = \begin{cases} +\sin^{-1}(\cos\mu \sin a) & \lambda_o \geq 0 \\ -\sin^{-1}(\cos\mu \sin a) & \lambda_o < 0 \end{cases}$$

otherwise:

$$\lambda = \begin{cases} -\sin^{-1}(\cos\mu \sin a) & \lambda_o \geq 0 \\ +\sin^{-1}(\cos\mu \sin a) & \lambda_o < 0 \end{cases}$$

Further:

$$\Delta\theta_4 = \begin{cases} + \tan^{-1} (\tan a \sin \mu & 0 \leq \alpha \leq \pi \\ - \tan^{-1} (\tan a \sin \mu) & \pi < \alpha < 2\pi \end{cases}$$

Then:

$$\theta_4 = \theta'_4 + \Delta\theta_4$$

C. Master

THREE-D IONOSPHERE NO. 2

D= 8.00000000E 01
R= 3.00000000E 02
F= 1.60000000E 02
AP= 0
L= 1.00000000E-04

SMALL F= 2.28000000E 09 CPS
RBAR= 2.00000000E 02
FBAR= 1.60000000E 02
K= 1.00000000E-04

LAMBDA ZERO= 20.0 ALPHA= 0 T= 12.0

PHI ZERO	DELTA L	H SUB M	H SUB C	H SUB B	T SUB M
90.0	-5.53591108E 02	3.85858462E 02	8.39074672E 02	1.82239586E 02	1.40294663E 03
60.0	-6.11988407E 02	3.80058314E 02	8.23753542E 02	1.79790140E 02	1.39901076E 03
30.0	-8.92162644E 02	3.71157147E 02	8.03984305E 02	1.75588499E 02	1.39141704E 03
15.0	-1.20573331E 03	3.62974713E 02	7.90589959E 02	1.70580335E 02	1.38122037E 03
10.0	-1.33179832E 03	3.59480583E 02	7.85753286E 02	1.67717620E 02	1.37475359E 03
5.0	-1.43638886E 03	3.56060165E 02	7.80824303E 02	1.64064231E 02	1.36520503E 03

LAMBDA ZERO= 20.0 ALPHA= 90.0 T= 12.0

PHI ZERO	DELTA L	H SUB M	H SUB C	H SUB B	T SUB M
90.0	-5.53591108E 02	3.85858462E 02	8.39074672E 02	1.82239586E 02	1.40294663E 03
60.0	-6.25518692E 02	3.81693736E 02	8.33650984E 02	1.79896948E 02	1.40911222E 03
30.0	-9.38905261E 02	3.74830854E 02	8.26147742E 02	1.75638526E 02	1.41932490E 03
15.0	-1.29857031E 03	3.67543040E 02	8.20874430E 02	1.70192113E 02	1.43037345E 03
10.0	-1.45147511E 03	3.63840733E 02	8.19292953E 02	1.66794636E 02	1.43616177E 03
5.0	-1.59408196E 03	3.59434139E 02	8.18397607E 02	1.61748420E 02	1.44336852E 03

LAMBDA ZERO= 20.0 ALPHA= 180.0 T= 12.0

PHI ZERO	DELTA L	H SUB M	H SUB C	H SUB B	T SUB M
90.0	-5.53591108E 02	3.85858462E 02	8.39074672E 02	1.82239586E 02	1.40294663E 03
60.0	-6.39067998E 02	3.92245849E 02	8.56400818E 02	1.84859770E 02	1.40668684E 03
30.0	-9.80493386E 02	4.04877375E 02	8.85090534E 02	1.90299263E 02	1.41284009E 03
15.0	-1.33184195E 03	4.20233846E 02	9.03669127E 02	1.98704458E 02	1.41887592E 03
10.0	-1.44840863E 03	4.27775171E 02	9.06342243E 02	2.04619919E 02	1.42144613E 03
5.0	-1.51701886E 03	4.35161397E 02	9.03628762E 02	2.13358089E 02	1.42378003E 03

LAMBDA ZERO= 20.0 ALPHA= 270.0 T= 12.0

PHI ZERO	DELTA L	H SUB M	H SUB C	H SUB B	T SUB M
90.0	-5.53591108E 02	3.85858462E 02	8.39074672E 02	1.82239586E 02	1.40294663E 03
60.0	-6.24005804E 02	3.90297131E 02	8.45007914E 02	1.84761851E 02	1.39637776E 03
30.0	-9.24280095E 02	3.99002356E 02	8.55780380E 02	1.89788521E 02	1.38344739E 03
15.0	-1.23019907E 03	4.10615767E 02	8.66990080E 02	1.97595465E 02	1.36598391E 03
10.0	-1.33120451E 03	4.17688906E 02	8.72361622E 02	2.03317692E 02	1.35516927E 03
5.0	-1.38656935E 03	4.27527782E 02	8.78588411E 02	2.12723090E 02	1.33982641E 03

EXECUTE,,56.

FIGURE 1.

The Bissett-Berman Corporation 2941 Nebraska Avenue, Santa Monica, California EXbrook 4-3270

APOLLO NOTE NO. 389
(Task 2, Item 2)

G. Hempstead
L. Lustick
10 December 1965

MULTIPLE STATION VERSION OF OEA PROGRAM

The "Multiple Station Program" is a variation of the "Orbit Error Analysis Program" which allows calculations of results when not updating nuisance parameters when there are any number of nuisance parameters such as might occur on an Earth parking orbit that is tracked for many orbits with many different stations.

The previous error program was limited in the number of nuisance parameter by the maximum allowable matrix in Program B (40 x 40).

DESCRIPTION AND CONSTRAINTS OF METHOD

Consider a problem where I could assemble the total information matrix in Program B, Let A = a priori covariance matrix.

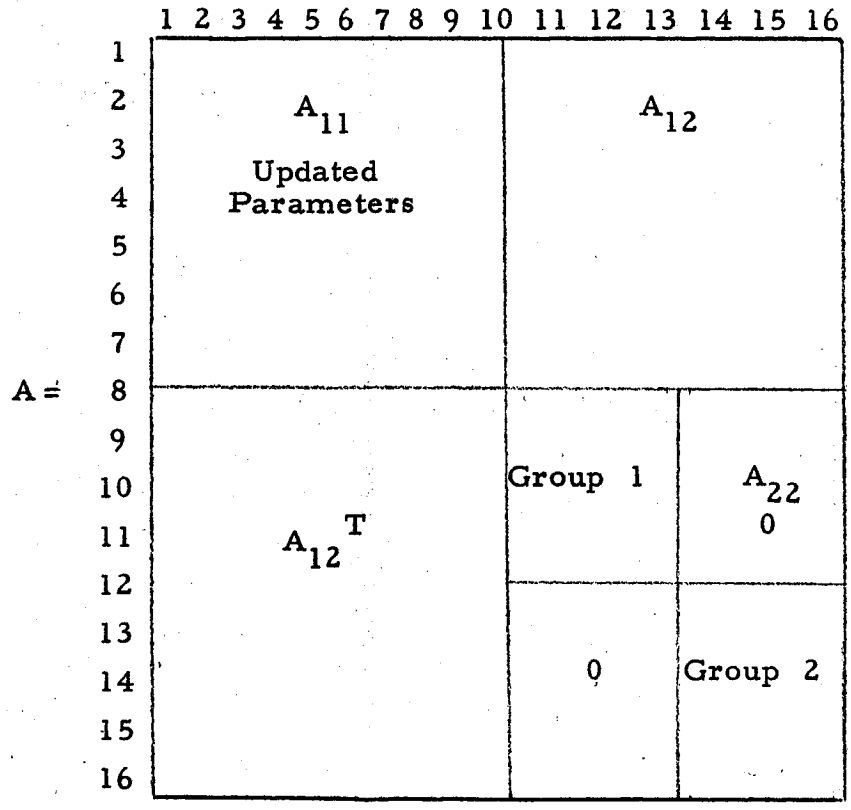

A_{11}-updated parameters

A_{22}-non-updated parameters

The new "Multiple Station Program" finds the error due to each group of nuisance parameters. The only restrictions as to the definitions of the groups is as follows:

1. The cross-correlation between groups of nuisance parameters in the a priori covariance matrix must be zero as illustrated.

2. The sum of the number of updated parameters and the number of nuisance parameters in a group cannot exceed 40.

3. In filling out the Part B sheet for a group if in your problem you are updating a total of say N parameters you must start the allocation of nuisance parameters for the group in Column (N + 1).

PROCEDURE

1. Decide on how you are going to break up the complete set of nuisance parameters for the problem into groups.

2. Fill out a Program B data sheet for each group skipping a line between each group. Each group must contain all information matrices which contain any nuisance parameters considered in that group, a Q matrix for that group if you are projecting your results ahead to some future time, and the a priori matrix for that group.

NOTE:

Restrictions on a priori

1. An a priori data set number should only appear once in any group. That is, do not use the same a priori data set number twice in a group.

2. If you are updating N parameters each a priori data set in the group should have the a priori information for the N updated

parameters properly allocated. The a priori information for the updated parameters must be in every group.

Restrictions on Q Matrix

1. If you are projecting your results to some future time each group must have a Q matrix properly allocated.

2. If the parameters μ or venting do not exist either in the updated or non-updated parameters the Q matrix must be a 6 x 6.

Outputs of Program

1. The errors due to white noise only (no nuisance parameters) considered.

2. The errors solely due to each group of non-updated nuisance parameters.

3. The total error due to white noise and the total nuisance parameters effect.

A number of sample runs showing the input and output from the Multiple Station Program are included for illustrative purposes.

Changes Required on Program B Card

The only addition to the Program B card is that the number of groups must be punched in Columns 13-14. A blank card separates each group, and only one Program B card is required for the entire set of groups.

APOLLO NOTE NO. 390
(Task I, Item IB)

H. R. Wright
14 December 1965

AN EMPIRICAL MODEL OF THE QUIET EQUATORIAL ANOMALY TO DEMONSTRATE ITS WORLD WIDE REFRACTIVE EFFECTS

INTRODUCTION

Although it has been known for many years that in the low latitudes there exists a gross anomaly which has an important influence over much of the world,[1] the phenomena are complex and their description still is not without controversy. Because of this, it is convenient to defer full phenomenological discussions for later sections and present first a brief summary followed by an outline of a model which was derived to account for those anomaly features that are not subject to serious question. While the latter is given in sufficient detail to permit computation, much of its justification first appears in the review discussions that follow.

The chief characteristic of the "equatorial", or "geomagnetic" anomaly, is that the F2 peak electron density, N_m, is a function of I, the magnetic dip angle. Close to the magnetic equator there is a N_m minimum, illustrated in Figure 1, which is known as the "equatorial trough." Magnetic field aligned N_m maxima appear as smooth "crests" in the midlatitudes on both sides of the trough at dip angles ranging between about 20° and 30°. These crests are quite pronounced late at night during magnetically quiet periods near the peak of the solar cycle with the electron density ratio at either crest to that in the trough often reaching 5-10. At such times, h_m, the height of the F2 peak, drops smoothly with magnetic latitude from 700 km in the trough, say, where N_m frequently has the order of 10^6 electron/cc, to a value near the crests of about 350 km where

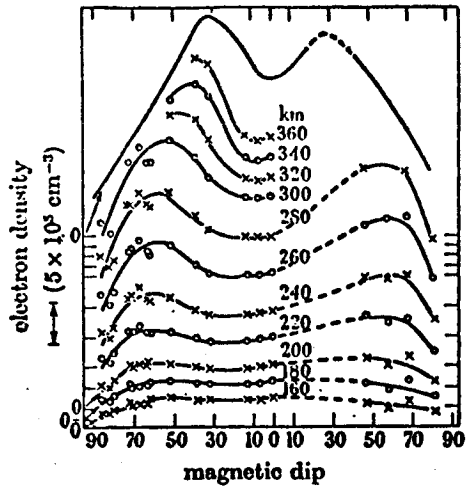

Figure 1. Electron Density Contours at Constant Real Heights Above Ground, as Reported by Croom et. al. (1959) in the Bottom-side of the Ionosphere for Local Noon in September 1957. The top Curve Shows $N_m F_2$. (Ref. 4)

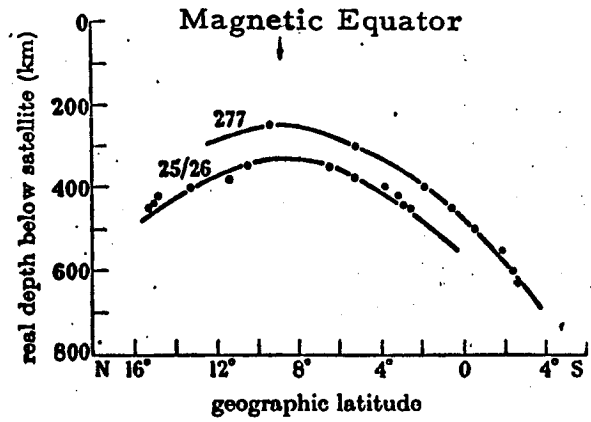

Figure 2. Latitudinal Dependence of the Height at Which the Anomaly Maxima Occurred for Singapore on Alouette, Revolution 277, 19.45 Local Time, and Revolution 25, 10.15 Local Time. The Curves are Field Lines. (Ref. 5)

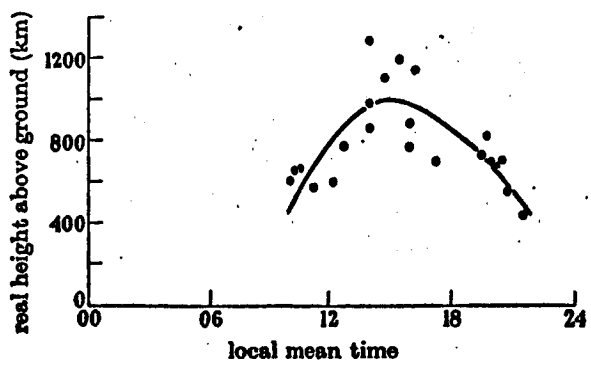

Figure 3. Diurnal Height Variation of the Top of the Equatorial Anomaly at Singapore. During the Period 22.00 to 10.00 Local Time the Anomaly Does Not Exist in the Topside Ionosphere. (Ref. 5)

N_m has increased to about 5×10^6 electrons/cc. The greater ionospheric thickness at the trough is not enough to compensate the reduced N_m, however, and depending on conditions, the equatorial electron content is reduced to perhaps a third of its midlatitude value. For example, taking the anomaly scale height at the crests to be 50 km and the trough scale heights to be 75 km, the one way vertical 3 kmc phase path retardation at about 25° magnetic latitude would be some 4.2 meters and drop to about 1.4 meters at the magnetic equator.

During low solar activity the top of the anomaly reaches its greatest height on the magnetic equator at about 1500 LST as indicated in Figure 2 and Figure 3. It then declines steadily during the afternoon and disappears by 2000 to 2100 LST. On the other hand, during years when the sunspot number is not low, the anomaly persists through the night until about 0300, depending on longitude, with substantial late evening enhancement at the crests, especially on the side toward the geographic equator. Ben'kova and Vasil'yev[2] report, in fact, that ship-based sounding revealed two maxima near the equator at all hours during the active solar years 1956 - 1960.

AN EQUATORIAL ANOMALY REFRACTIVE INDEX MODEL FOR THE EQUINOXIAL PERIODS NEAR THE PEAK OF THE SOLAR CYCLE

When it is recognized that prediction models accounting for day-to-day variability do not appear practical at present and that current theory is capable of little more than qualitative agreement[3], it is difficult to justify the consideration of much more than smoothed out effects to be expected for a given region, time of day, season

and phase of the solar activity cycle. This should not be construed to mean that theory is not useful. Quite the contrary; theory can offer important guidance even if subsequent work proves the only practical procedure is to construct a completely empirical model depending on real time input of ionospheric observables. For instance, while a semi-empirical model would probably be the most practical survey tool, its derivation should not ignore the theory of electron diffusion along magnetic field lines. However, since it has not been established that simple models already derived[18] definitely are inadequate, a more simpleminded approach was adopted. As a first approximation, the drift along the field was not explicitly considered and the model was constructed on a completely empirical basis in which the primary objective was to obtain a simple representation of at least the gross features of the anomaly. In order to accomplish this attention was restricted to rather specialized but representative conditions for a quiet sun but near the peak of the solar cycle. The equinoxial periods were selected on the basis, first of all, that at such times the ionosphere is much more active than at the solstices[12] and the anomaly is quite fully developed. Further, during the equinoxes the anomaly is more symmetric with respect to the dip equator than it is at other seasons. However, before describing the anomaly in more detail at these and other times, the specialized model will be given in outline.

To begin with, at the anomaly onset time, t_o (hours, local time), the peak electron density N(I, t) (electrons/cu meter) is essentially constant as a function of dip angle, I. For about two hours after t_o, N then increases at midlatitudes relative to its value at the magnetic equator. This increase will be assumed to take the form

$$N(I_o, t) = N(0, t)\left[1 + b(t_o + t)/(t_o + 02)\right] \tag{1}$$

$$t_o \leq t \leq t_o + 02$$

in which I_o is the dip angle at the anomaly crest and the notation $N_m = N(I, t)$ will be used with the understanding that t is the local solar time in hours at a point along the ray. Typically t_o is 08 hours and b is about 0.7. Beginning about 2 hours after onset until about 18 h the depth of the anomaly remains essentially constant at

$$N(I_o, t) = N(0, t)(1 + b) \tag{2}$$

$$t_o + 02 \leq t \leq 18$$

After 18 hours, the anomaly is accentuated and this was represented by

$$N(I_o, t) = N(0, t)\left[1 + b + a\,(1 - \cos\theta)\right] \tag{3}$$

$$18 \leq t \leq t_1$$

where

$$\theta = 2\pi(t - 18)/(t_e - 18) \tag{4}$$

in which t_e is anomaly termination time and the time t_1 was chosen to be

$$t_1 = 0.75\, t_e + 04.5 \tag{5}$$

and the anomaly depth is measured by a with values between 1.5 and 4 being representative of fully developed conditions. Now, the crest is assumed to decay according to

$$N(I_o, t) = N(0, t)\left[1 - (a + b)(t - t_e)/(t_e - t_1)\right] \tag{6}$$

$$t_1 \leq t \leq t_e$$

The peak electron density is extrapolated between the crest and trough through

$$N(I, t) = N(0, t)\left\{1 + (I/I_o)\left[N(I_o, t) - N(0, t)\right]/N(0, t)\right\} \tag{7}$$

$$0 \leq I \leq I_o$$

and, on the side of the crest toward the pole, the representation is made by means of

$$N(I, t) = N(I_1, t) + \left[N(I_o, t) - N(I_1, t)\right](I_1 - I)/(I_1 - I_o) \tag{8}$$

$$I_o \leq I \leq I_1$$

where I_1 is the transition dip angle at the poleward extreme of the anomaly. For illustrative purposes, take $I_o = 30^o$ and $I_1 = 60^o$ with hourly N inputs from Huancayo for equatorial data, $N(0, t)$; and inputs from Grand Bahama for transition data, $N(I_1, t)$, respectively. For illustrative calculations, the equatorial diurnal peak electron density variation as given by these inputs may be substituted by an approximation for representative undisturbed days which, at the peak of the solar cycle, has the form

$$N(0,t) = 3 \times 10^{12}\left[1 - 0.18\,(10 - t)\right] \quad \text{el/cu meter} \tag{9}$$

$$05h \leq t \leq 10h$$

$$N(0,t) = 3 \times 10^{12}\left[1 - (9/190)(t - 10)\right] \tag{10}$$

$$10h \leq t \leq 29h$$

$$N(60^{o},t) = 1.5 \times 10^{12}\left[1 - (13 - t)/13.5\right] \tag{11}$$

$$04 \leq t \leq 13h$$

$$N(60^{o},t) = 1.5 \times 10^{12}\left[1 - (t - 13)/22.5\right] \tag{12}$$

$$13 \leq t \leq 28h$$

Take the layer height at the equatorial and midlatitude stations to be at

$$h_p = (15/M_1 - 2) \times 10^5 \text{ (meters)} \tag{13}$$

where M_1 is the (M3000) F2 factor which is given hourly. At points between these stations, take the layer height to be

$$h_p(I,t) = h_p(I_1,t) + \left[h_p(0,t) - h_p(I_1,t)\right]\cos^4(\pi I/2I_o) \tag{14}$$

where $h_p(0,t)$ is h_p evaluated near I = 0 (again Huancayo) and $h_p(I_1,t)$ is h_p as determined by data from a midlatitude station near the same longitude (again Grand Bahama, for example).

The example suggested above is intended to illustrate conditions characteristic of times at which the anomaly width, as measured by the separation of the crests, is extreme. Conditions for small

anomaly widths may be estimated by taking $I_o \cong 20^o$. Here again Huancayo data is suitable for equatorial input. Now, the most convenient transition station is Panama at 39.2°N dip, 79°54' W geographic longitude.

If (M3000) F2 factors are not available as inputs, the choice of h_m values becomes difficult. To illustrate, during the evening h_m near one crest may increase while it is decreasing near the other. At the same time, the layer height at the dip equator may remain at its diurnal minimum for a few hours in the American sector while continuing to rise in the African and Asian sectors. Nonetheless, a reasonable magnitude estimate of the anomaly effects may be made by first assuming that the layer height at I = 0 increases linearly from time t_o until t_s, the time of sunset at the F2 layer peak. Next, assume the sharp h_m decrease for about 3 hours following t_s is linear. From t_s + 3 hours until t_o, the equinoxial layer height remains essentially constant. These assumptions may be expressed by

$$h_m(0,t) = h_m(0,t_s) - \left[h_m(0,t_s) - h_m(0,t_o)\right](t_s - t)/(t_s - t_o) \quad (15)$$

$$t_o \leq t \leq t_s$$

$$h_m(0,t) = h_m(0,t_s) - \left[h_m(0,t_s) - h_m(0,t_o)\right](t - t_s)/3 \quad (16)$$

$$t_s \leq t \leq t_s + 03$$

$$h_m(0,t) = \text{constant} \quad (17)$$

$$t_s + 03 \leq t \leq t_o$$

Illustrative values are: $h_m(0,t_o) = 3 \times 10^5$ meters, $h_m(0,t_s) = 7 \times 10^5$ meters, and t_s depends both on λ, the latitude at the dip equator as well as $h_m(0,t_s)$.

Since the dip equator is always less than 15° from the equator, t_s is well approximated during equinoxial periods by

$$t_s \cong 18 + (12/\pi) \cos^{-1} \left[1 + h_m(0, t_s)/r \cos \lambda\right]^{-1} \tag{18}$$

where r is the earth radius (6.378×10^6 meters). It is presumed here that $h_m(0, t_s)$ is given. There is not much t_s variation because when h_m rises to 700 km, for instance, $t_s = 19.7$ hours at the equator, and at Huancayo ($\lambda = 12^{\circ}$S) $t_s = 19.9$ hours. For the example just given, an adequate representation thus is

$$h(0, t) = \left[7 - (20 - t)/3\right] \times 10^5 \text{ meters} \tag{19}$$

$$08 \leq t \leq 20$$

$$h(0, t) = \left[7 - 4(t - 20)/3\right] \times 10^5 \text{ meters} \tag{20}$$

$$20 \leq t \leq 23$$

$$h(0, t) = 3 \times 10^5 \text{ meters} \tag{21}$$

$$23 \leq t \leq 32$$

When the vehicle is above the ionosphere, assume a slab model in which N(I, t) is constant along the vertical with a thickness given by

$$y(I, t) = 4.133\, H_m(I, t) \tag{22}$$

where H_m is the Chapman scale height. It will be approximated by

$$H_m = 50(1 + 0.002R)\Big\{1.10 + 0.2 \cos \lambda \cos\left[\pi(t - 14)/12\right] + 0.1 \cos^2 \lambda \cos^2\left[\pi(t - 14)/12\right]\Big\}(r + h_m)^2/(r + h_{mo})^2 \tag{23}$$

where $h_m = h_m(I, t)$ and $h_{mo} = h_m(0, t_o)$. The model from which this was derived is described in a later section and is applicable only during the equinoxes.

Assume that 31% of the slab is below h_m and the vertical distance between the slab surfaces where the ray penetrates is

$$Y = 0.31y\,(I_b, t_b) + 0.69y\,(I_c, t_c) \tag{24}$$

where the subscripts b and c identify the bottom and top, respectively. The geocentric distance to the slab base is

$$r_b = r + h(I_b, t_b) - 0.31y\,(I_b, t_b) \tag{25}$$

Let $\phi_b - \phi_c$ ray elevation angle difference between the slab bottom and top and the distance through the slab along the ray becomes

$$S = r_b\left[1 + (1 + Y/r_b)^2 - 2(1 + Y/r_b)\cos(\phi_b - \phi_c)\right]^{1/2} \tag{26}$$

Divide this into j equal parts for which $N_i(I, t)$ is the electron density in the ith segment and take

$$\overline{N} = \sum_{i=1}^{j} N_i(I, t)/j \tag{27}$$

so that the phase path decrease becomes

$$\Delta\ell = 40.26\,\overline{N}S/f^2 \tag{28}$$

with f being the transmitted frequency (cps), and $\overline{N}S$ in mks units, as before.

SOME BASIC CONSIDERATIONS

Corpuscular sources of ionizing radiation make such a minor contribution to the electron density that relatively small effects are attributed to them even during severe magnetic storms. The fact that only charged particle radiation responds to geomagnetic field constraints notwithstanding, the geomagnetic field lines exert a strong ionospheric control. One important reason for this is the fact that, although ionization production is relatively independent of the magnetic field, free electrons tend to diffuse for great distances along magnetic field lines as typified by the Störmer trajectories between the hemispheres.

Since corpuscular energy sources are of secondary importance, maximum energy absorption is in regions where the sun is near the zenith. Both ionization production and thermal atmospheric expansion are greatest there. Significant charge density attains great heights and almost unimpeded diffusion takes place along many field lines which at low latitudes are nearly horizontal and, depending on height over the equator, terminate over wide geographical areas. As a consequence, the equatorial regions exert a strong influence on ionospheric structure over the entire earth through field aligned transport of ionization. These and other physical processes controlling the low-latitude ionosphere are extremely complex with the region being the site of what is probably the most important anomaly influencing precision S-band tracking.

GENERAL CHARACTERISTICS OF THE ANOMALY

When magnetic conditions are undisturbed during periods when solar activity is high, the N(h) profile for a given altitude is flat before sunrise. Later a morning equatorial maximum develops which according to Rao[9] becomes quite strong by 1000 LT. Mid-latitude maxima then develop by 1200 LT as illustrated in Figure 1, leading to a shallow equatorial trough that becomes more pronounced during

the afternoon. A striking feature of the anomaly is that during sunspot maximum conditions it continues to develop throughout the afternoon with a marked enhancement during evening hours. In general, the F2 layer also continues to rise and reaches great altitudes at the trough by late evening. From the trough h_m drops smoothly with magnetic latitude and at the anomaly crests the layer is not much above its daytime level.

Before the topside satellite sounder program was initiated in late 1962 at a time of low solar activity, the latitude dependence of equatorial F2 layer movements was difficult to deduce because the number of observatories in the region is inadequate. Clear evidence now shows that geographical variations of anomaly height are smooth, at least near years of the quiet sun, as illustrated in Figure 2 for November 1962. There the "height of the anomaly maxima" is the altitude at which N peaks as a function of magnetic dip (not of height) and which drops to the F2 peak only at the crests. For a given universal time, these maxima lie along a magnetic field line and the altitude at which that line crosses the magnetic equator is known as the "top of the anomaly." Its diurnal variation is illustrated in Figure 3 for the winter of 1962-1963 where it is seen that even in quiet solar years anomalous electron density crests (not necessarily N_m crests) may be expected late in the afternoon at altitudes as great as 1200 km. The wide scatter of data points is not necessarily an indication of anomaly variability because at least three months are required for the topside sounder orbit to precess enough for the diurnal pattern to become discernible.

Lyon and Thomas[7] have shown that during undisturbed periods of the sunspot cycle maximum the N_m crests approach the equator after 2100 LST and reach 10-13°N and S magnetic latitude by 0000 LST in the American sector and by 0300 in the African sector. They concluded that, in general, the anomaly appears earlier and persists longer in the African and East Asian

sectors than in the American sector. From 1000 to 1500 LST the geographic extent of the anomaly, as measured by the peak separation, increases in the African sector but not in the American sector. In another study that also relates to conditions at the peak of the solar cycle, Rao and Malthotra[10] found that the anomaly occupies the widest belt in the Asian zone and also that there the time of onset is earlier than in either the American or African zones.

Marked asymmetries appear in N_m when the noon sun transits the magnetic equator ("dip equinox") and also during the solstices. For equal magnetic latitudes, higher peak electron densities occur on the winter side of the magnetic equator than on the summer side. Solsticial asymmetries also appear at night but in an opposite sense to those in the day. Then the layer heights are also asymmetric with h_m greater for northern magnetic latitudes in the American sector, but less in the African and East Asian sectors. It appears that, in general, greater layer heights appear on the side near the geographic equator.

Equinoxial f_o F2 and h_m asymmetries are illustrated in Figures 4 and 5. Considering these solsticial and "dip equinox" asymmetries, a rather surprising observation is the fact that during true equinoxial periods, the latitude variations are quite symmetric. This may be related to the circumstance that the ionosphere is much less active during solsticial than equinoxial months.[12]

For several hours after sunrise, the situation is complex but Lyon and Thomas find evidence that the anomaly is shifted 5-10° magnetic latitude northward in the African sector. After 1500 LST, however, the peaks remain fixed at between 16° and 19° magnetic latitude north and south in the African sector, and between 13° to 17° magnetic latitude in the American sector. In fact, from about two hours after onset until about 1800 LST, the latitude variation remains fairly constant between 50° North and South magnetic latitude at which time the trough has an electron density that is about

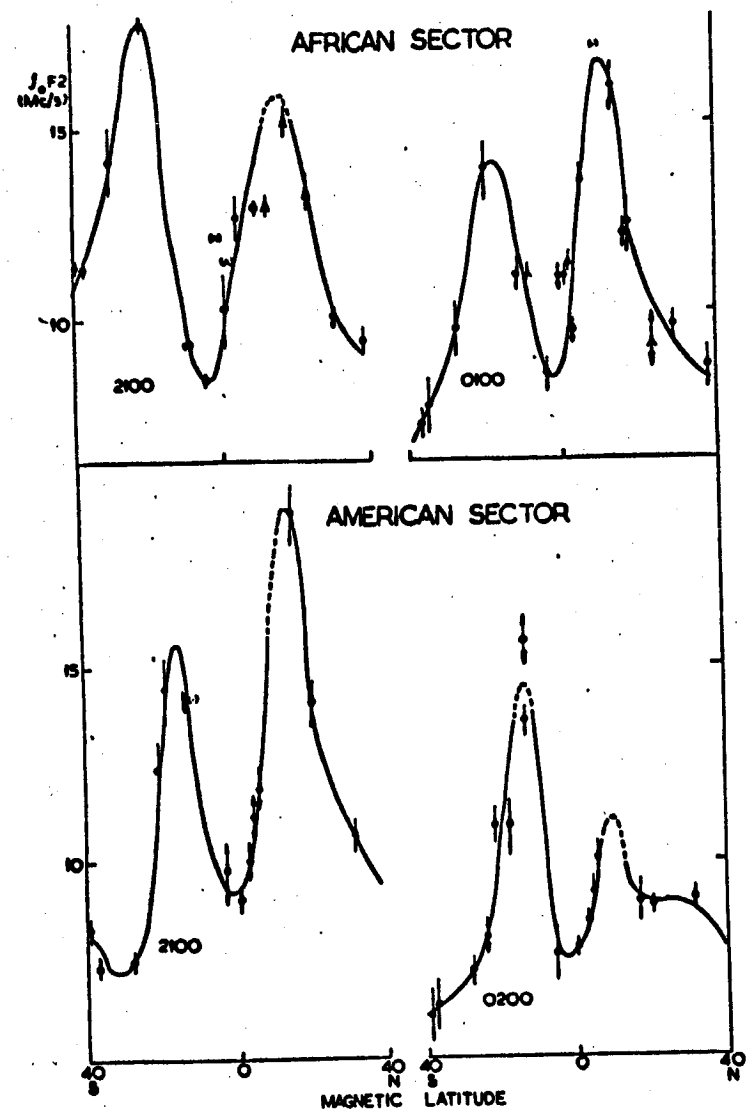

Figure 4. Variations of Median Values of foF2 with Magnetic Latitude for Selected Hours During the Equinox Period, March, 1958. (Ref. 7)

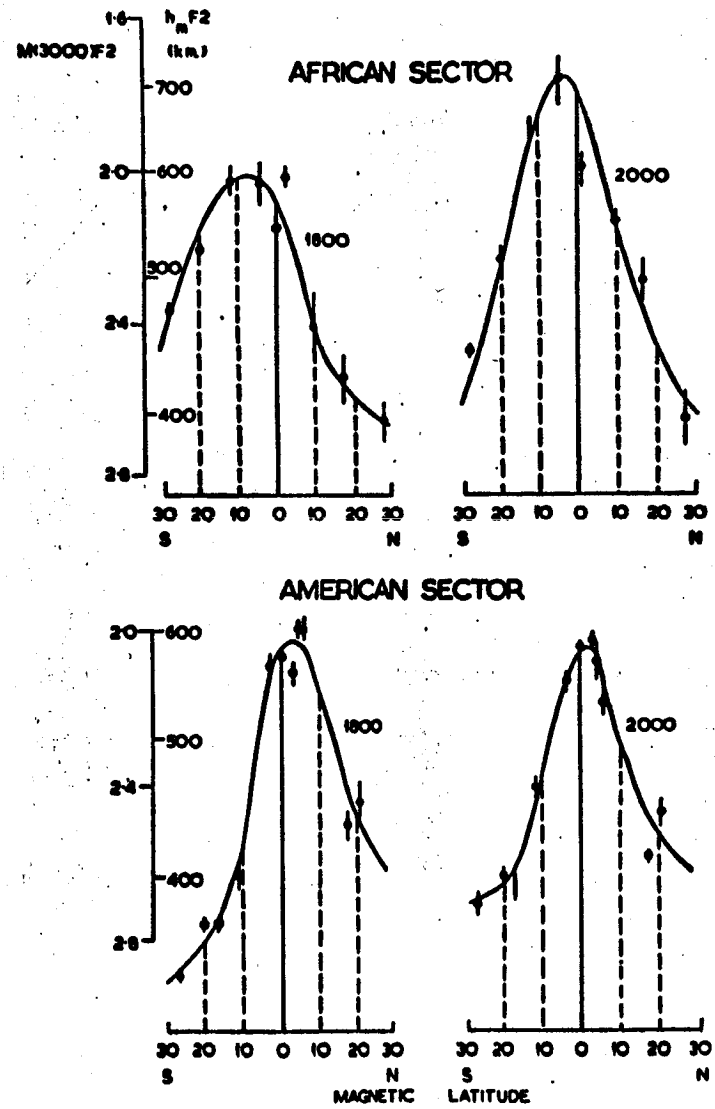

Figure 5. Variation of Median Values of M(3000) F2 With Magnetic Latitude for 1800 and 2000 hours during the Equinox Period, March, 1958. The Scale of M(3000) F2 is Plotted Downwards and That of hmF2, Derived From M(3000) F2 Data For a Parabolic Layer, Is Plotted Upwards. (Ref. 7)

60% of the values at the crests. In the afternoon the African equatorial trough appears to be 1 or 2° south of the magnetic equator while there is a slight displacement to the north in the American sector.

Description of the equatorial anomaly is further complicated by the phenomenon of both a morning and an afternoon peak in the maximum electron density known as "noon bite-out". This effect is almost always observed within 10° of the magnetic equator and has been studied by Rastogi and Sanatani,[11] who have illustrated in Figure 6 how it depends both on solar activity and longitude. It is not entirely absent at higher latitudes as is evident, for example, in the data for Puerto Rico displayed in Apollo Note 370[19] as Figure 4.3.

THE EQUATORIAL IONIZATION "LEDGE"

Topside sounder data show that from sunrise until about 1100 LST electron density contours have a dome shape across the magnetic equator, much like that illustrated by Figure 45 of Apollo Note 303.[17] The dome also is observed bottomside where, for a number of years, it has been known that its profile depends on the season and solar activity. Figures 7 and 8, due to Thomas,[15] illustrate the dependence as deduced from observations made at fixed points on earth. During periods of low solar activity, the morning value of h_m typically increases to 400 km from 250 km at the magnetic equator and the level of the 2 mc plasma frequency (5×10^4 electrons/cc) rises to 750 km from 450 km.

Early in the day, during periods of exceptionally low magnetic activity, the dome becomes an ionization ledge, according to Lockwood and Nelm.[6] This transition also occurs on disturbed days but not until late in the afternoon. As an illustration, from 1100 to 1730 LST the ledge appears when K_p is less than 2^+ while the dome is observed during this interval for greater K_p values. From 1730

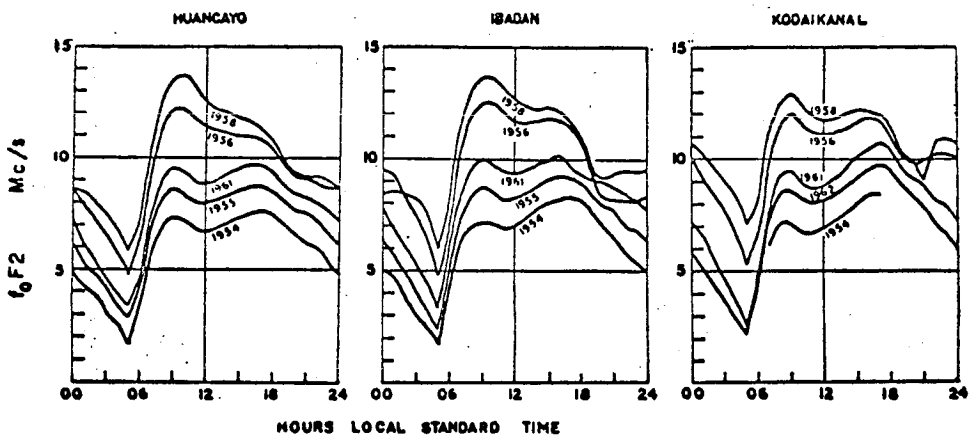

Figure 6. Daily Variations of f_oF2 at Huancayo, Ibadan and Kodaikanal for Years in the Solar Cycle. (Ref. 11)

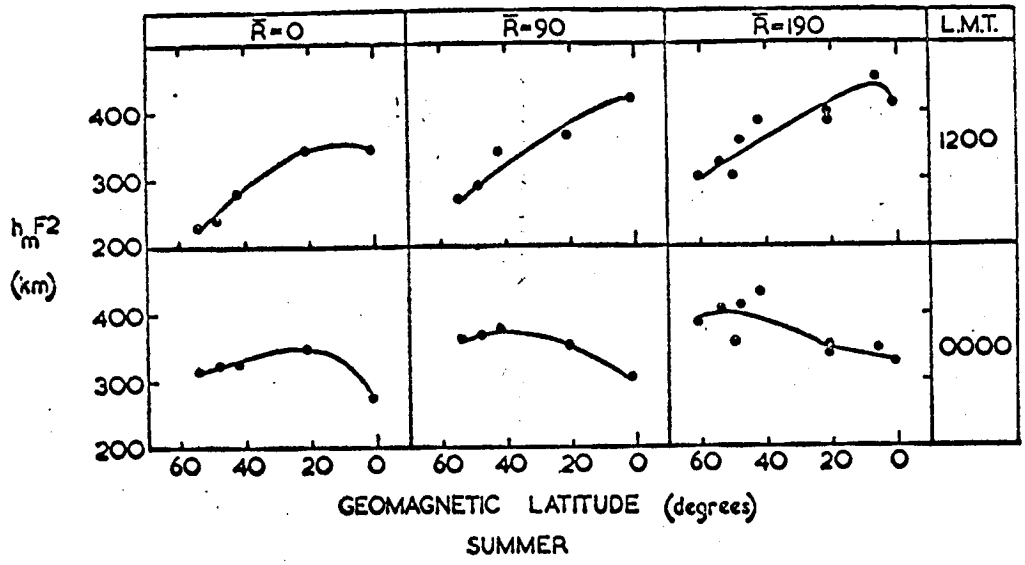

Station Geomagnetic Latitudes

Huancayo	00°36′S
Talara	06°36′N
Panama	20°42′N
Washington	50°18′N
Slough	54°18′N
Inverness	60°48′N
Maui	20°42′N
Watheroo	41°42′S
Christchurch	48°06′S

Figure 7. The Variation With Geomagnetic Latitude of hmF2 Averaged for a Summer Month at Three Epochs of the Solar Cycle. (Ref. 15)

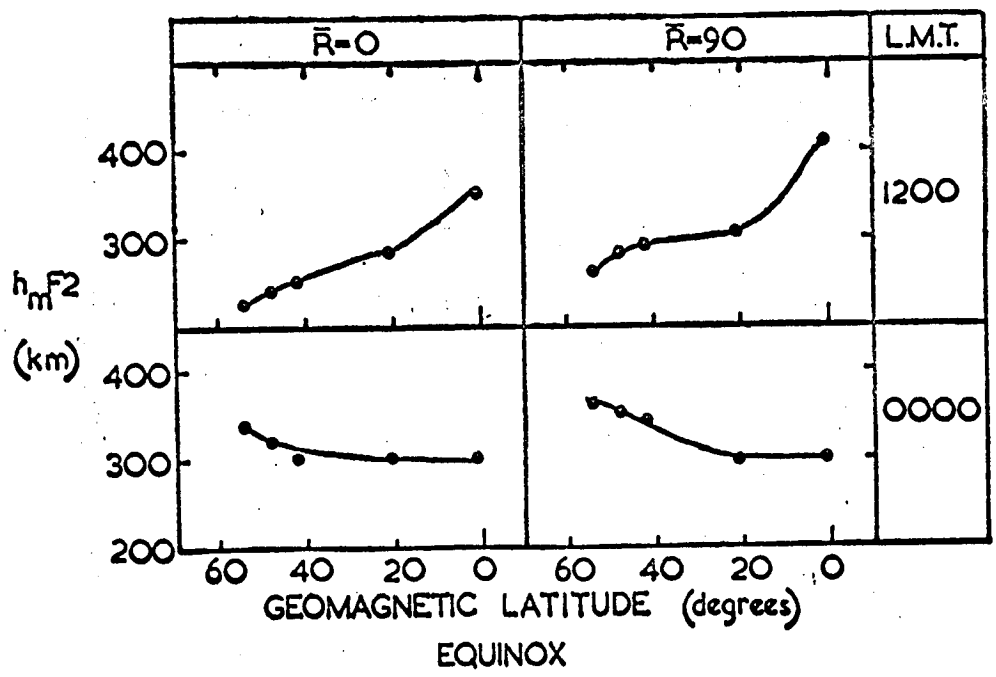

Figure 8. The Variation with Geomagnetic Latitude of hmF2 Averaged for an Equinox Month at Two Epochs of the Solar Cycle. Stations and Geomagnetic Latitudes are given in Figure 7. (Ref. 15)

to 2200 LST, the equatorial ionization ledge exists along successively higher magnetic field lines in the trough of the equatorial anomaly. In effect, the ledge is an ionization sheet with an East-West extent of about 70° that rises to greater heights toward the East. Its North-South limits may be inferred from the fact that the peaks of the equatorial anomaly develop where the ledge merges with h_m. Ledge height at the magnetic equator varies from 500 km at 1200 LMT to 900 km at 2200 LMT. Above the ledge the N contours retain a dome shape while those below tend to be flat and decrease in height toward the equator.

An indication of the influence of this ledge may be obtained from the results published by Sayers, et al,[14] which show the maximum ledge electron density is reached about noon when it is about 6×10^{10}/cu. meter at 700 km. The authors did not cite corresponding N values in the absence of the anomaly but, based on the fact that the relative variations are no greater than those near F2, the effects would be small because N at the ledge is only about 5% of N_m.

FIELD ALIGNED IONIZATION STRATA OR "LEDGES" AT HIGHER ALTITUDES

Analyses of recent topside sounder data indicate it is probable that the "geomagnetic" anomaly is only one of possibly three separate field algined layers of enhanced ionization[13]. A second layer appears to be located on the magnetic shell defined by L = 1.25, that is, the shell located 1.25 earth radii normal to the geomagnetic dipole. This corresponds to a layer altitude of about 1,600 km altitude over the magnetic equator but which drops to ionospheric levels in the direction of the magnetic poles and intersects ground level at about 26° geomagnetic latitude. Both of these strata weaken during the night, but a third, on the L = 1.7 - 1.9 magnetic shell, then becomes more pronounced.

As an indication of magnitudes, the shell at L = 1.8 has been observed with densities as great as 3×10^{4} electrons/cu cm. If it is assumed this layer extends from L = 1.7 to L = 1.9, then 1.0 kmc

phase path defect for the shell at a constant density would be about 15 cm. If further it is assumed the enhancement is only a factor of three, the added phase path retardation is the order of 10 cm. Clearly, this is quite a conservative estimate because it tacitly assumes that the enhancement does not come about through the depletion of other shells. Regions of reduced ionization density have been reported which might, in fact, compensate partially. One is located between the magnetic shells L = 3 and L = 4 but it appears to undergo diurnal variation[13] and the data do not warrant definite assertions regarding possible effects on refractive index models.

Mapping these topside strata is still in progress and much more work will be needed to provide definitive answers to the question of what the overall refractive index effects are; or to the extremely puzzling question of why certain magnetic shells are the recipients of enhanced ionization.

A SCALE HEIGHT MODEL FOR THE GEOMAGNETIC ANOMALY DURING THE EQUINOXIAL PERIODS

It is doubtful if any two workers would concur on all details of an H_m model through the anomaly. There is more or less agreement on at least some of the general features, however, and, on this basis, a model was derived which, it must be admitted, has practically no theoretical support but which is at least credible.

The principal feature on which there is little dispute is that when high latitudes are excluded, as they are here, the scale height by day is usually greater than by night. This is just what would be expected if M, the mean ionizable molecular mass, remained constant. The reason is that by definition H_m is given by

$$H_m = kT/Mg \tag{29}$$

where T is the ionospheric temperature, g is the acceleration of gravity, k is Boltzmann's constant, and H_m is evaluated near the F2 peak. If the subscript o refers to the temperature, T_o, then

$$H_m/H_{mo} = f(M)\, g_o T/gT_o \tag{30}$$

where f(M) = 1 if, as is assumed in simple theory, M actually is constant. Explicit specification of the function f(M) will not be attempted, but it will be assumed that its departures from unity are not serious. It is not presumed here that g is constant because it may drop from, say, 9 meters/sec^2 to less than 8 meters/sec^2 as the F2 layer rises from its diurnal minimum in the equatorial trough.

The assumption will now be made that $H_{mo}f(M)$ may be used to represent a diurnal minimum reference scale height. There is good evidence, which will be described in a later Apollo note, that such a parameter is a function of solar activity. This dependence seems to vary somewhat with geographical location, but this may be ignored here and the numerical relation

$$H_{mo}f(M) = 5 \times 10^4\,(1 + 0.002R) \quad \text{(meters)} \tag{31}$$

taken as representative with R being the daily Zürich sunspot number.

Considering the uncertainties in scale height predictions, there is not much justification for considering more than the diurnal component of the temperature variation. In this case (see Apollo No. 317),

$$T/T_o = 1.10 + 0.2 \cos\lambda \cos\left[\pi(t - 14)/12\right] + 0.1 \cos^2\lambda \cos^2\left[\pi(t - 14)/12\right] \tag{32}$$

where λ is the geographic latitude and this result applies only during equinoxial periods.

Combining these results leads to

$$H_m = 50(1 + 0.002R) \left\{ 1.10 + 0.2 \cos\lambda \cos\left[\pi(t - 14)/12\right] + 0.1 \cos^2\lambda \cos^2\left[\pi(t - 14)/12\right] \right\} (r + h_m)^2/(r + h_{mo})^2 \tag{33}$$

where r is the earth radius (6.378×10^6 meters), h_{mo} is the diurnal minimum F2 layer height at the equator (typically 3×10^4 meters), and h_m is the layer height where H_m is being evaluated.

APPENDIX

a = a constant that scales the evening anomaly depth - $1.5 \leq a \leq 4$ at peak of solar cycle.

b = a constant measuring the depth of the daytime anomaly - typical value is 0.7.

f = transmitted frequency (cps).

g = acceleration of gravity at the height h_m (meters/sec^2).

g_o = acceleration of gravity where h_m is at its diurnal minimum (meters/sec^2).

h_m = height of the F2 peak (meters).

$h_m(I, t)$ = F2 layer height at the dip angle I and time t (meters).

h_{mo} = $h_m(0, t_o)$ (meters)

h_p = the "parabolic approximation" for the F2 layer height based on observed (M3000) F2 factors (meters).

H_m = Chapman scale height (meters).

$H_m(I, t)$ = Chapman scale height at the dip angle I and time t (meters).

H_{mo} = diurnal minimum equatorial scale height (meters).

I = magnetic dip angle at the earth's surface (radians).

I_o = surface magnetic dip at anomaly crest (radians).

I_1 = surface magnetic dip in the anomaly transition region; i. e., the poleward extreme (radians).

I_b = surface magnetic dip where ray penetrates base of slab (radians).

I_c = surface magnetic dip where ray penetrates top of slab (radians).

k = Boltzmann's constant (1.380×10^{-23} joules/deg K).

L = Magnetic shell identification coordinate[8] (earth radii)

M = mean molecular mass of the ionizable constituents (kilograms).

M_1 = (M3000) F2 factor (mc).

$N_m(I, t)$ = F2 peak electron density at the dip angle I and time t (electrons/cu. meter).

$\overline{N}$ = average slab electron density along the ray (electrons/cu. meter).

r = earth radius (6.378×10^6 meters).

r_b = geocentric distance to the slab base (meters).

R = Zürich daily sunspot number.

S = ray path length through the slab (meters).

t = local solar time (hours).

t_o = anomaly onset time (hours).

t_1 = $(0.75\ t_e + 04.5)$ (hours).

t_e = anomaly termination time (hours).

t_s = time of local F2 layer sunset at the F2 peak (hours).

T = temperature of the isothermal ionosphere (^oK).

T_o = diurnal minimum equatorial T (^oK).

$y(I, t)$ = slab thickness through point on ray where the surface dip is I and the local time is t (meters).

Y = $0.31\ y(I_b, t_b) + 0.69\ y(I_c, t_c)$ (meters).

$\Delta\ell$ = phase path length decrease (meters).

θ = $2\pi\ (t - 18)/(t_e - 18)$ (radians).

λ = geographic latitude (radians).

ϕ = elevation angle relative to local horizontal (radians).

ϕ_b = value of ϕ where ray penetrates slab base.

ϕ_c = value of ϕ where ray penetrates top of slab.

BIBLIOGRAPHY

1. E. V. Appleton. "Two Anomalies in the Ionosphere, "Nature, Vol. 157, pp 691-693, 1946.

2. N. P. Ben'kova and K. N. Vasil'yev. "Ionospheric Investigation on the Schooner Zarya: The F2 Layer in the Equatorial Region," Geomag. and Aero. IV, No. 5, 1964.

3. E. N. Bramley and M. Peart. "Diffusion and Electromagnetic Drift in the Equatorial F2 Region, "J. Geophys. Res., 69, No. 21, Nov. 1, 1964, pp 4609-16.

4. S. Croom, A. Robbins and J. O. Thomas. (Reported by King, et al, 1963), Nature, London, 184, p. 2003.

5. J. W. King, P. A. Smith, D. Eccles, G. F. Fooks and H. Helm. "Preliminary Investigation of the Structure of the Upper Ionosphere as Observed by the Topside Sounder Satellite, Alouette, "J. Geophys. Res., 68, pp 464-487, (1963).

6. G. E. K. Lockwood and G. L. Nelms. "Topside Sounder Observations of the Equatorial Anomaly in the 75°W Longitude Zone," Journal of Atmospheric and Terrestrial Physics, Vol. 26, No. 5, pp 569-580, May 1964.

7. A. J. Lyon and L. Thomas, "The F-2 Equatorial Anomaly in the African, American, and East Asian Sectors During Sunspot Maximum," JATP, 25, No. 7, July 1963, pp 373-386.

8. C. E. McIlwain, "Coordinates for Mapping the Distribution of Magnetically Trapped Particles", Journal of Geophysical Research, Vol. 66, No. 11, November 1961, pp 3681-3691.

9. C. S. R. Rao. "Study of the Geomagnetic Anomaly During Sunspot Maximum, " JATP, 24, August 1962, pp 729-737.

10. C. S. R. Rao and P. L. Malthotra. "A Study of Geomagnetic Anomaly During IGY," JATP, 26, pp. 1075-1085 (1964).

11. R. G. Rastogi and S. Sanatani. "Longitudinal Effect in the Equatorial F-2 Region of the Ionosphere," JATP, 25, (1963) pp 739-742.

12. W. T. Roberts. "Proposed Solution to the Geomagnetic Anomalies in the Ionosphere," NASA Technical Memo N-18164, September 24, 1963.

13. J. Sayers, "Field Aligned Strata in the Upper Atmosphere", Space Research V, North Holland Publication Company, pp 161-170.

14. J. Sayers, P. Rothwell and J. H. Wager. "Evidence for a Further Ionospheric Ledge Above the F2 Retion," Nature, 195, No. 4847, pp 1143-1145, September 22, 1962.

15. J. O. Thomas. "The Distribution of Electrons in the Ionosphere," Proc. IRE, 47, p.162 (January 1959).

16. A. P. Willmore and C. L. Henderson. "Magnetic Shell Enhancements During Magnetic Disturbances", Space Research V, North Holland Publishing Company, pp 241-249 (1965).

17. H. R. Wright. "The Quiet Ionosphere as it Relates to Precision Tracking at S Band," Apollo Note No. 303, January 25, 1965.

18. H. R. Wright. "A Simple Time Dependent World-Wide Ionospheric Refractive Index Model," Apollo Note No. 317, April 6, 1965.

19. H. R. Wright. "A Peak Electron Density Model for Refractive Index Predictions in the Anomalous Quiet Ionosphere," Apollo Note No. 370, September 20, 1965.

APOLLO NOTE NO. 391
(Task II, Item II)

H. Engel
20 December 1965

TWO-WAY AND THREE-WAY DATA IN THE OEA PROGRAM

In Figure 1, the ranges from stations 1 and 2 to a vehicle are shown at instants one sampling interval apart. Using change in range as a measurable, the 2-way measurable for station 1 is:

$$M_1 = 2b - 2a = 2(b - a)$$

The 2-way measurable for station 2 is:

$$M_2 = 2d - 2c = 2(d - c)$$

The 3-way measurable for stations 1 and 2 is:

$$\begin{aligned} M_3 &= (b + d) - (a + c) \\ &= (b - a) + (d - c) \\ &= (M_1 + M_2)/2 \end{aligned}$$

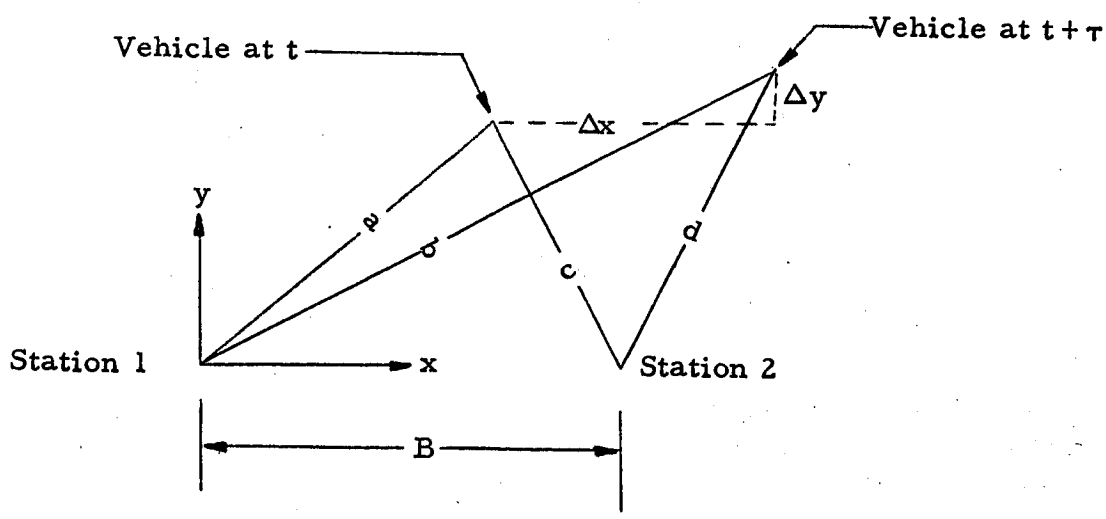

Figure 1.

We can rewrite the expressions for M_1 and M_2 in terms of x, y, Δx, Δy, and B, using approximations based on the assumption that Δx and Δy are small compared to x and y.

$$M_1 = 2\left\{\left[(x+\Delta x)^2 + (y+\Delta y)^2\right]^{1/2} - (x^2+y^2)^{1/2}\right\}$$

$$= 2\,(x^2+y^2)^{1/2}\left\{\left[1 + \frac{2x\Delta x + 2y\Delta y}{x^2+y^2} + \frac{\Delta x^2 + \Delta y^2}{x^2+y^2}\right]^{1/2} - 1\right\}$$

$$\stackrel{\circ}{=} 2\,\frac{x\Delta x + y\Delta y}{(x^2+y^2)^{1/2}}$$

$$M_2 = 2\left\{\left[(x-b+\Delta x)^2 + (y+\Delta y)^2\right]^{1/2} - \left[(x-B)^2 + y^2\right]^{1/2}\right\}$$

$$\stackrel{\circ}{=} 2\,\frac{(x-B)\,\Delta x + \Delta y}{\left[(x-B)^2 + y^2\right]^{1/2}}$$

These two simultaneous equations may be solved for Δx and Δy. We find

$$\Delta x = (x^2+y^2)^{1/2}\,\frac{M_1}{2B} - \left[(x-B)^2 + y^2\right]^{1/2}\,\frac{M_2}{2B}$$

$$= \frac{aM_1}{2B} - \frac{cM_2}{2B}$$

and

$$\Delta y = -\frac{(x-b)}{y}\,(x^2+y^2)^{1/2}\,\frac{M_1}{2B} + \frac{x}{y}\left[(x-B)^2 + y^2\right]^{1/2}\,\frac{M_2}{2B}$$

$$= -\frac{x-B}{y}\,\frac{aM_1}{2B} + \frac{x}{y}\,\frac{cM_2}{2B}$$

Then, the mean square errors in Δx and Δy, using measurables M_1 and M_2, assuming that the errors in M_1 and M_2 are independent and that the mean square errors in M_1 and M_2 are both σ^2, are

$$\sigma^2_{x_{1,2}} = \frac{\sigma^2}{4B^2} (a^2 + c^2)$$

and

$$\sigma^2_{y_{1,2}} = \frac{\sigma^2}{4B^2} \left[a^2 \left(\frac{x-B}{y}\right)^2 + c^2 \left(\frac{x}{y}\right)^2 \right]$$

Introducing measurable M_3 and eliminating measurable M_2 by substitution, we find

$$\Delta x = \frac{aM_1}{2B} - \frac{c\,(2M_3 - M_1)}{2B}$$

$$= \frac{(a+c)\,M_1}{2B} - \frac{cM_3}{B}$$

and

$$\Delta y = -\frac{x-B}{y}\,\frac{aM_1}{2B} + \frac{x}{y}\,\frac{c\,(2M_3 - M_1)}{2B}$$

$$= -\left[\left(\frac{x-B}{y}\right) a + \left(\frac{x}{y}\right) c\right] \frac{M_1}{2B} - \frac{x}{y}\,\frac{cM_3}{B}$$

At present the Orbit Error Analysis Program <u>assumes</u> that the errors in M_1 and M_3 are independent. If we further assume, as before, that the mean square errors in M_1 and M_3 are both σ^2, then

$$\sigma^2_{x_{1,3}} = \frac{\sigma^2}{4B^2} \left[(a+c)^2 + 4c^2\right]$$

and

$$\sigma^2_{y_{1,3}} = \frac{\sigma^2}{4B^2} \left\{ \left[\left(\frac{x-B}{y}\right) a + \left(\frac{x}{y}\right) c \right]^2 + 4 \left(\frac{x}{y}\right)^2 c^2 \right\}$$

Then,

$$\frac{\sigma^2_{x_{1,3}}}{\sigma^2_{x_{1,2}}} = \frac{\left[(a+c)^2 + 4c^2\right]}{a^2 + c^2}$$

$$= 1 + \frac{2c(a+2c)}{a^2 + c^2}$$

$$= 1 + 2\left(\frac{c}{a}\right) \frac{1 + 2\left(\frac{c}{a}\right)}{1 + \left(\frac{c}{a}\right)^2}$$

the minimum value of which is 1, and the maximum value of which is about 5.24.

Also,

$$\frac{\sigma^2_{y_{1,3}}}{\sigma^2_{y_{1,2}}} = \frac{\left[\left(\frac{x-B}{y}\right) a + \left(\frac{x}{y}\right) c\right]^2 + 4\left(\frac{x}{y}\right)^2 c^2}{a^2 \left(\frac{x-B}{y}\right)^2 + \left(\frac{x}{y}\right)^2 c^2}$$

$$= 1 + 2\left(\frac{x}{x-B} \frac{c}{a}\right) \frac{1 + 2\left(\frac{x}{x-B} \frac{c}{a}\right)}{1 + \left(\frac{x}{x-B} \frac{c}{a}\right)^2}$$

the minimum value of which is 1 and the maximum value of which is about 5.24.

Thus, if equipment aboard the vehicle permitted it, the OEAP indicates that it would be preferable to use simultaneous 2-way data from both stations, rather than 2-way data from one and 3-way from the other.

This, however, is not the whole story. Actually, the errors in M_1 and M_3 are <u>not</u> independent. Studies to date indicate that the principal measurement errors are clock errors and troposphere propagation errors. Since the 2-way and 3-way data use the same transmitter clock and share the same path from transmitting station to vehicle, the measurement errors are correlated.

We can describe the errors in M_1, M_2, and M_3 as:

$$\Delta M_1 = n_{T1}(t) - n_{T1}(t+\tau) + 2\, n_{p1}$$

$$\Delta M_2 = n_{T2}(t) - n_{T2}(t+\tau) + 2\, n_{p2}$$

$$\Delta M_3 = n_{T1}(t) - n_{T2}(t+\tau)\, n_{p1} + n_{p2}$$

in which

τ = sample interval

n_{T1} = clock error (phase) of Station 1

n_{T2} = clock error (phase) of Station 2

n_{p1} = error in change in propagation from Station 1 to vehicle over interval τ

n_{p2} = error in change in propagation from Station 2 to vehicle over interval τ

Under these assumptions, and with the further assumptions that

$$\sigma_T^2 = \sigma_{T1}^2 = \sigma_{T2}^2$$

$$\sigma_p^2 = \sigma_{p1}^2 = \sigma_{p2}^2$$

$$\sigma_T^2 \rho^2 = E\left[n_{T1}(t)\, n_{T1}(t+\tau)\right] = E\left[n_{T2}(t)\, n_{T2}(t+\tau)\right]$$

and

$$o = E\left[n_{T1}\, n_{T2}\right] = E\left[n_{p1}\, n_{p2}\right]$$

we find

$$\sigma^2_{x_{1,2}} = \frac{a^2}{4B^2} E(\Delta M_1)^2 - \frac{2ac}{4B^2} E(\Delta M_1 \Delta M_2) + \frac{c^2}{4B^2} E(\Delta M_2)^2$$

$$= \frac{a^2}{4B^2}\left[2\sigma_T^2(1-\rho^2) + 4\sigma_p^2\right] + \frac{c^2}{4B^2}\left[2\sigma_T^2(1-\rho^2) + 4\sigma_p^2\right]$$

$$= \frac{a^2+c^2}{4B^2}\left[2\sigma_T^2(1-\rho^2) + 4\sigma_p^2\right]$$

and

$$\sigma^2_{x_{1,3}} = \frac{(a+c)^2}{4B^2} E(\Delta M_1)^2 - \frac{8(a+c)c}{4B^2} E(\Delta M_1 \Delta M_3) + \frac{4c^2}{4B^2} E(\Delta M_3)^2$$

$$= \frac{(a+c)^2}{4B^2}\left[2\sigma_T^2(1-\rho^2) + 4\sigma_p^2\right]$$

$$- \frac{8(a+c)c}{4B^2}\left[\sigma_T^2(1-\rho^2) + 2\sigma_p^2\right]$$

$$+ \frac{4c^2}{4B^2}\left[2\sigma_T^2 + 2\sigma_p^2\right]$$

Then,

$$\frac{\sigma^2_{x_{1,3}}}{\sigma^2_{x_{1,2}}} = 1 + \frac{2ac}{a^2+c^2} + \frac{-4(a+c)c\left[\sigma_T^2(1-\rho^2)+2\sigma_p^2\right] + 2c^2\left[2\sigma_T^2+\sigma_p^2\right]}{(a^2+c^2)\left[\sigma_T^2(1-\rho^2)+2\sigma_p^2\right]}$$

$$= 1 + \frac{2c(2c-a)}{(a^2+c^2)} + \frac{2c^2\left[2\sigma_T^2+\sigma_p^2\right]}{(a^2+c^2)\left[\sigma_T^2(1-\rho^2)+2\sigma_p^2\right]}$$

$$= 1 + 2\left(\frac{c}{a}\right)\frac{\left[2\left(\frac{c}{a}\right)-1\right]}{1+\left(\frac{c}{a}\right)^2} + 2\,\frac{\left(\frac{c}{a}\right)^2}{1+\left(\frac{c}{a}\right)^2}\cdot\frac{2\sigma_T^2+\sigma_p^2}{\sigma_T^2(1-\rho^2)+2\sigma_p^2}$$

This quantity can be less than unity only if c/a is less than 2/5. For a vehicle at lunar distance, c/a cannot be very different from 1, so for this case $\sigma^2_{x_{1,3}} / \sigma^2_{x_{1,2}}$ is always greater than unity.

Even this is not the whole story. We have discussed only one set of measurements. Successive samples have correlated errors, and these in turn will affect the ratios of accuracies of estimates using 2-way and 3-way data. This subject, however, is left for a later note.

The Bissett-Berman Corporation 2941 Nebraska Avenue, Santa Monica, California EXbrook 4-3270

APOLLO NOTE NO. 392
(Task 2, Item II)

L. Bonin
2 December 1965

EFFECT OF LUNAR EPHEMERIS ERRORS ON THE EXPECTED ORBIT OF A SATELLITE APPROACHING THE MOON

A cursory analysis of the effect of lunar ephemeris errors on the accuracy obtained by tracking a satellite in a circular parking orbit above the Moon is reported in Apollo Note No. 371. This note extends the analysis to the case where the satellite is approaching the Moon in a hyperbolic orbit. Doppler tracking is assumed to initiate as the satellite is entering the lunar sphere of influence (LSOI).

The satellite's orbit is assumed to have an eccentricity of 1.1 with perigee about 80 n. mi. above the Moon. The orbit is inclined 180° to the lunar equator with the satellite located 130° relative to the Earth-Moon line at time zero. This geometry is illustrated in Figure 1. The Moon, at time zero, is located at a latitude of 4° and a longitude of -50°. At this location, the Moon is over the Atlantic Ocean slightly north of South America. The lunar orbit is inclined 18.308° to the Earth's equator.

Range-rate tracking data is obtained from three stations operating in the Doppler mode. The tracking station at Madrid, Spain is considered the master, with the stations at Ascension and Grand Canary considered slaves. The geographic locations of these stations are:

Station	Latitude	Longitude
Madrid (Master)	40.4	- 3.7
Ascension (Slave)	-7.9	-14.3
Grand Canary (Slave)	27.7	-15.6

The relative geometry between the radar sites and the lunar satellite allows at least 5 hours of continual tracking. The tracking data is assumed to have a standard deviation of 0.003 m/sec. for observation intervals of one minute. The a priori standard deviation in station location for the three tracking sites are:

$\sigma_{up} = 66$ m

$\sigma_{east} = 62$ m

$\sigma_{north} = 59$ m.

The a priori standard deviation assumed for the bias in the range-rate measurable is about 0.0021 m/sec. for the master and about 0.0042 m/sec. for the slaves.

The a priori uncertainty in the gravitational potential of the Moon is assumed to be 5.7×10^8 m^3/sec^2. The expected 1-sigma deviations in the lunar ephemeris are:

$\sigma_{\tilde{x}} = 1$ km	$\sigma_{\dot{\tilde{x}}} = 1 \times 10^{-3}$ m/sec.
$\sigma_{\tilde{y}} = 2$ km	$\sigma_{\dot{\tilde{y}}} = 1 \times 10^{-3}$ m/sec.
$\sigma_{\tilde{z}} = 1$ km	$\sigma_{\dot{\tilde{z}}} = 1 \times 10^{-3}$ m/sec.

At time zero, the satellite's velocity is assumed known within a standard deviation of 3 m/sec. in the x', y', and z' directions. The a priori knowledge of the satellite's initial position is assumed to be 1 km along each axis in one case and 10 km along each axis in another case.

These errors provide two cases for solution in The Bissett-Berman Orbit Error Analysis Program. Figures 2 through 5 show the accuracy of initial position and velocity achieved by tracking the vehicle from 30 minutes to 5 hours. The data are presented for three error situations. The lower curve in each figure illustrates the error model in which the nuisance parameters are known perfectly. These errors represent the best accuracy possible for the assumed a priori standard deviation in the satellite's position and velocity.

The All Parameters updated case represents the best accuracy possible when the uncertainties associated with all parameters are considered. This case corresponds to the situation where the tracking data are used to determine all parameters influencing the satellite's motion. The highest curve in each figure illustrates the situation in which only the bias in the measurable is estimated. According to current plans at MSC, this technique will be employed by the MSFN for tracking the Apollo spacecraft during the lunar mission.

Figures 2 and 4 show the variation of RMS uncertainty of initial position with tracking time for a priori position uncertainties of 1 and 10 km, respectively. In both figures, the RMS position uncertainty with the bias in the measurable updated increases after about two hours of tracking. This increase is caused by a cross-correlation between the vehicle position errors and the non-updated station location errors, which cannot be accounted for as a measurable bias over a long time.

Figures 3 and 5 show the effect of tracking time on the RMS uncertainty of initial velocity for a priori position uncertainties of 1 and 10 km, respectively. In these cases, updating only the bias in the measurable is shown to yield highly acceptable results.

Figures 6 through 9 show the RMS position and velocity uncertainties that result when the tracking data are used to predict the satellite's state vector at the end of the observation time. These figures exhibit the same trends observed in Figures 2 through 5.

Figures 10 and 11 show the RMS position and velocity uncertainties when the tracking data are used to predict the satellite's state vector at the end of 5 hours. These figures show that the knowledge of the

satellite's orbit at the end of 5 hours is continually improved as the number of observations increases.

The lunar ephemeris errors studied here produce negligible increases in the satellite's position and velocity uncertainty. When the same cases are rerun without lunar ephemeris errors, the resulting curves are indistinguishable from the data shown in Figures 2 through 11. This conclusion is the same as that reached in Apollo Note No. 371 concerning lunar parking orbits. In addition, updating the bias in the range-rate measurable provides a very satisfactory definition of a lunar orbit.

Figure 1

Schematic of Satellite's Orbit
When Tracking is Initiated

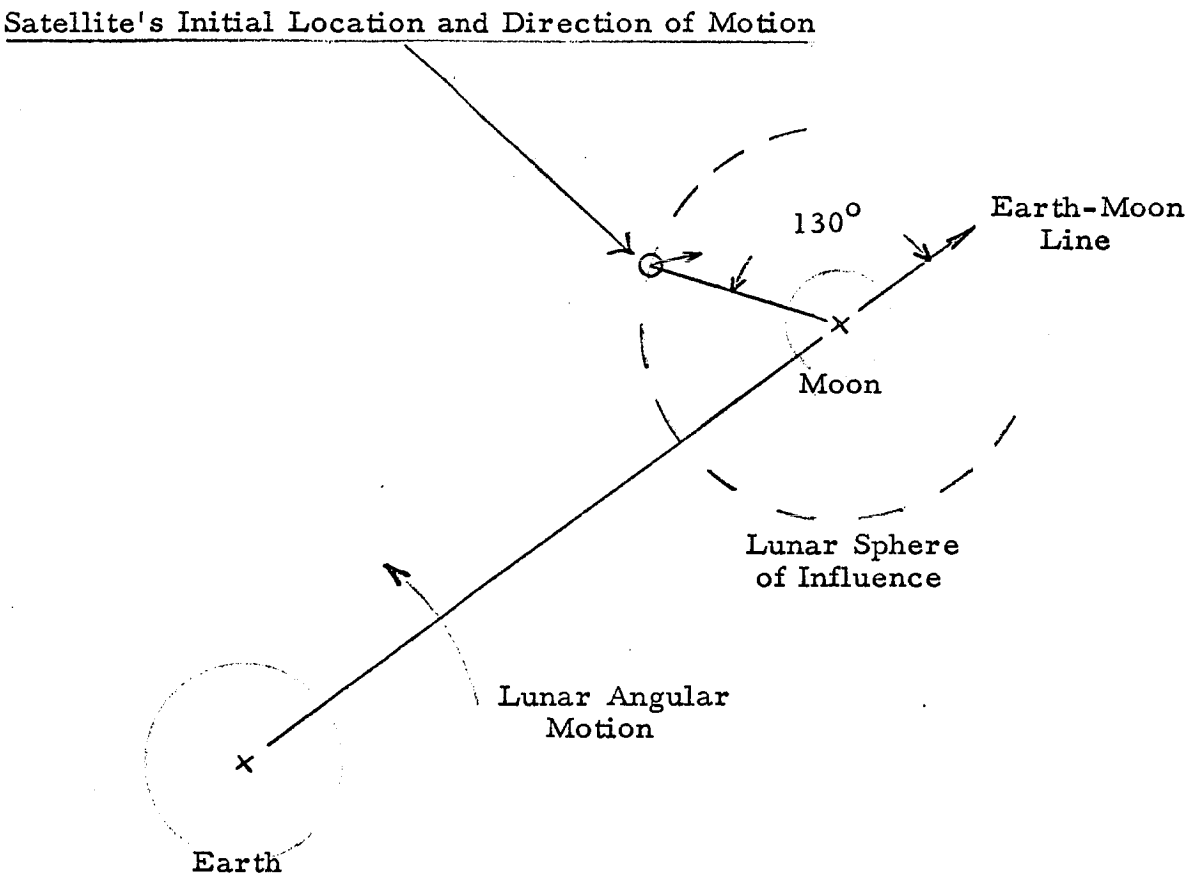

Note: Satellite's orbit plane coincides with lunar orbit plane.

Figure 2

RMS Position Uncertainty For A Satellite Approaching The Moon

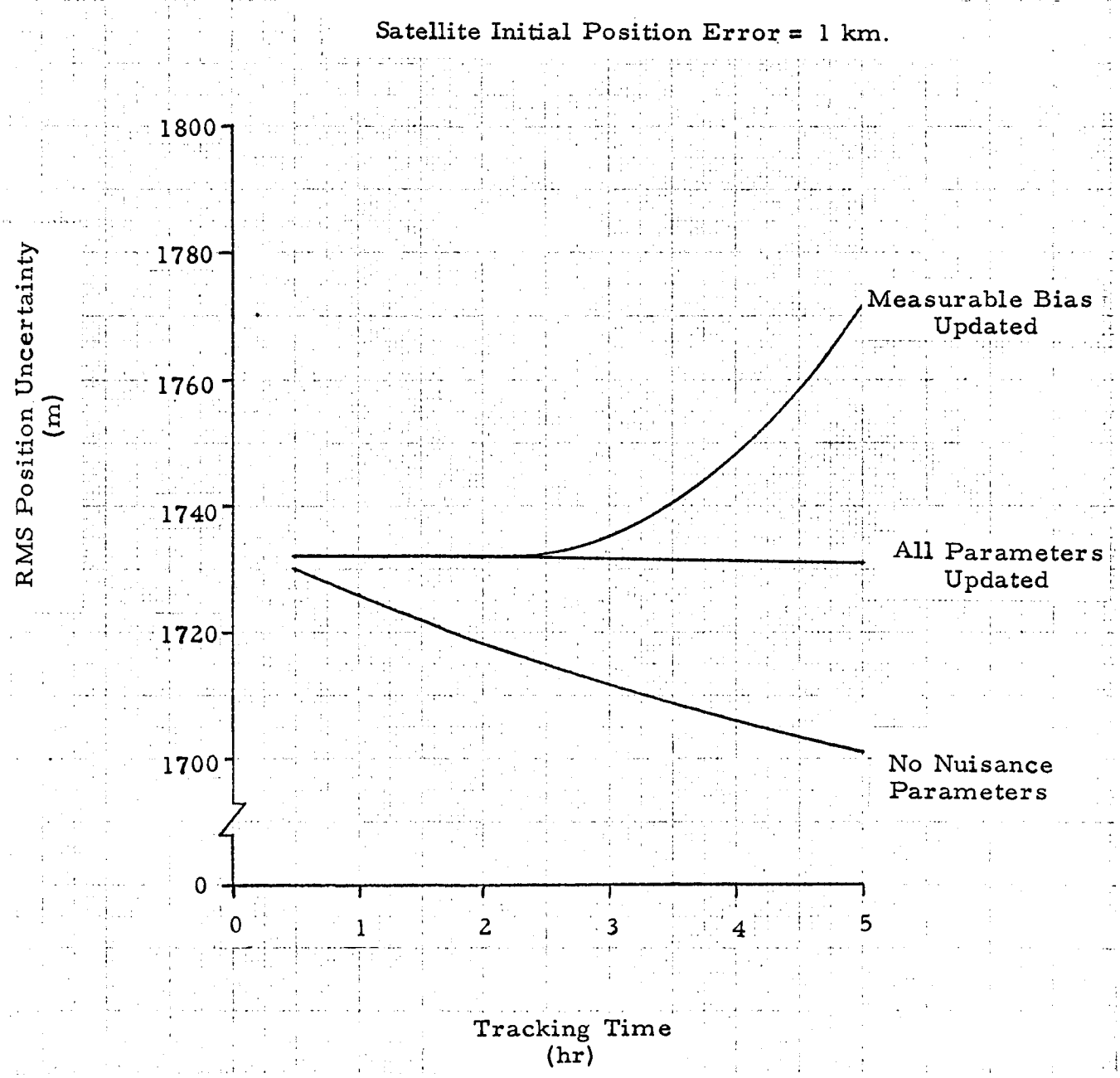

Figure 3

RMS Velocity Uncertainty For A Satellite Approaching The Moon

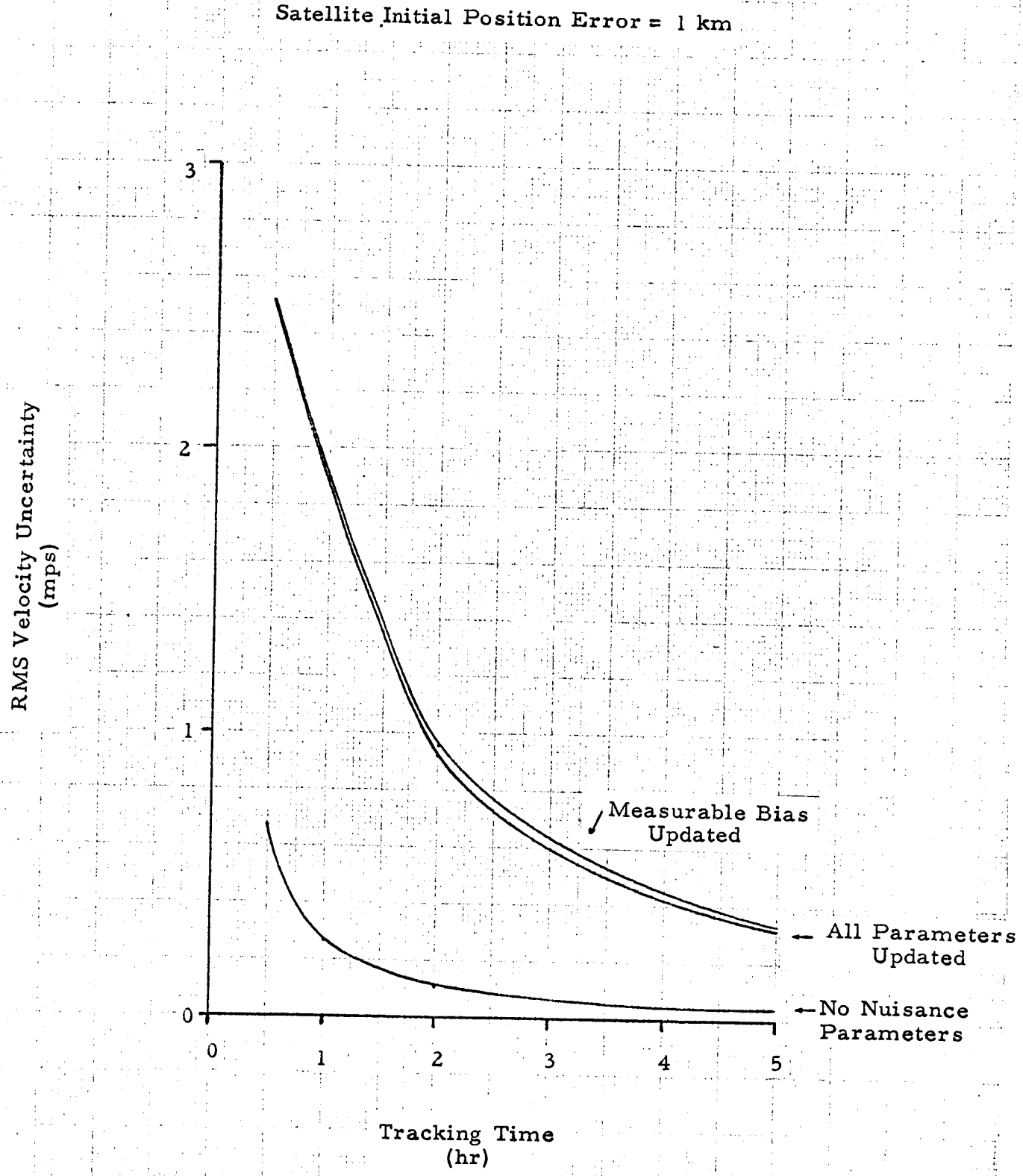

Figure 4

RMS Position Error For A
Satellite Approaching The Moon

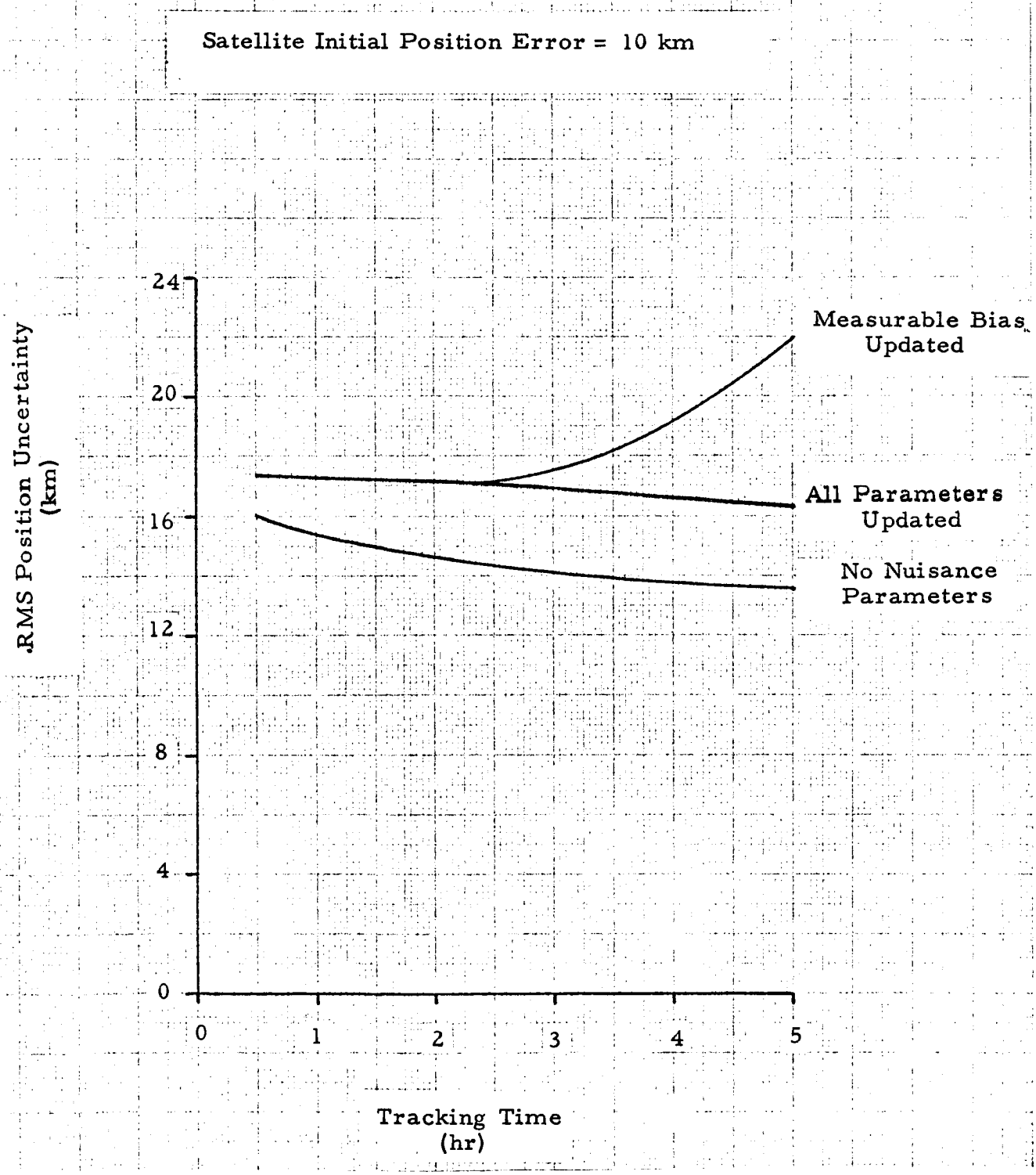

Figure 5

RMS Velocity Uncertainty For A Satellite Approaching The Moon

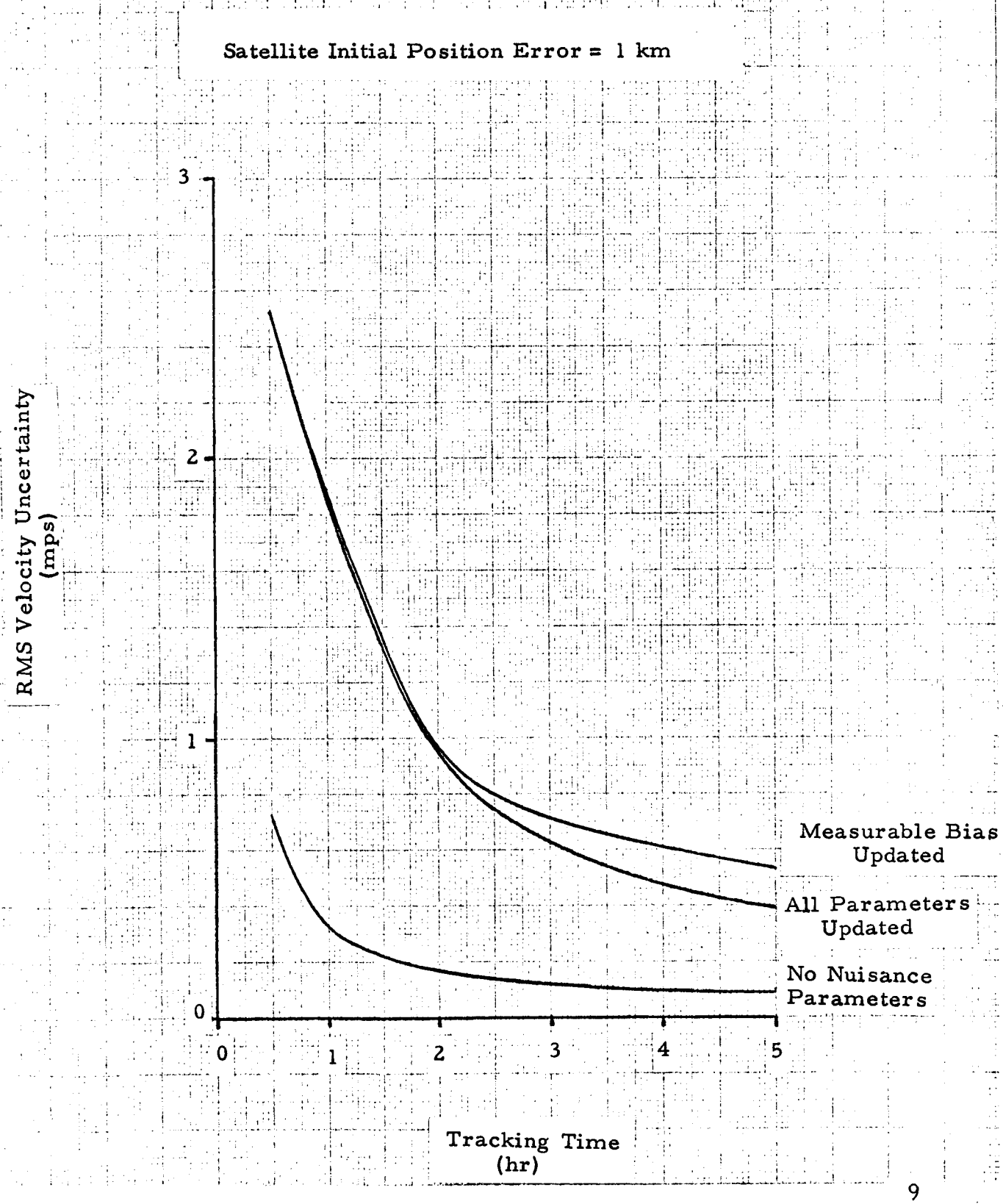

Figure 6

RMS Position Uncertainty At The Completion Of Each Tracking Observation

Satellite Initial Position Error = 1 km

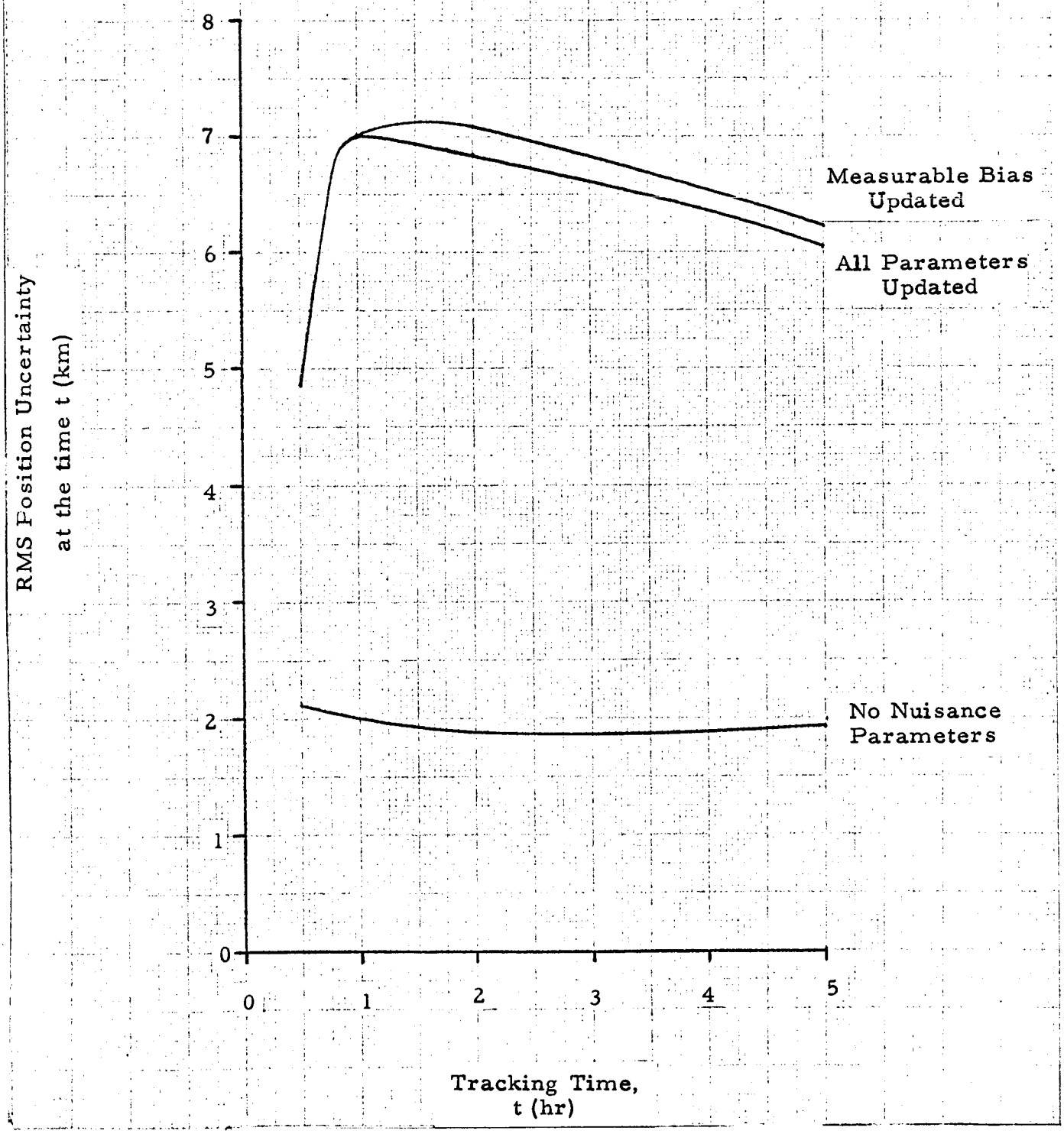

Figure 7

RMS Velocity Uncertainty At The Completion Of Each Tracking Observation

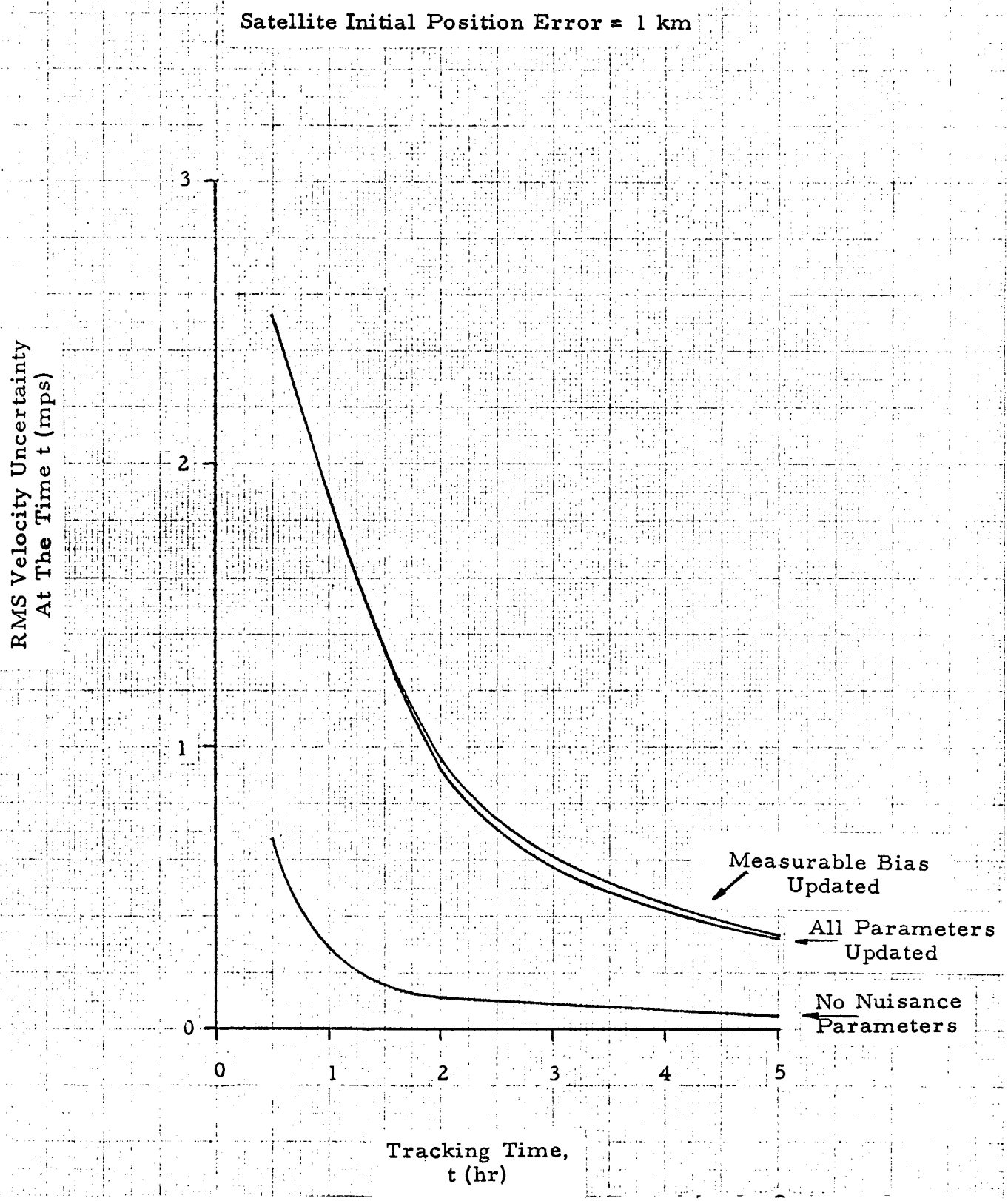

Figure 8

RMS Position Uncertainty At The Completion Of Each Tracking Observation

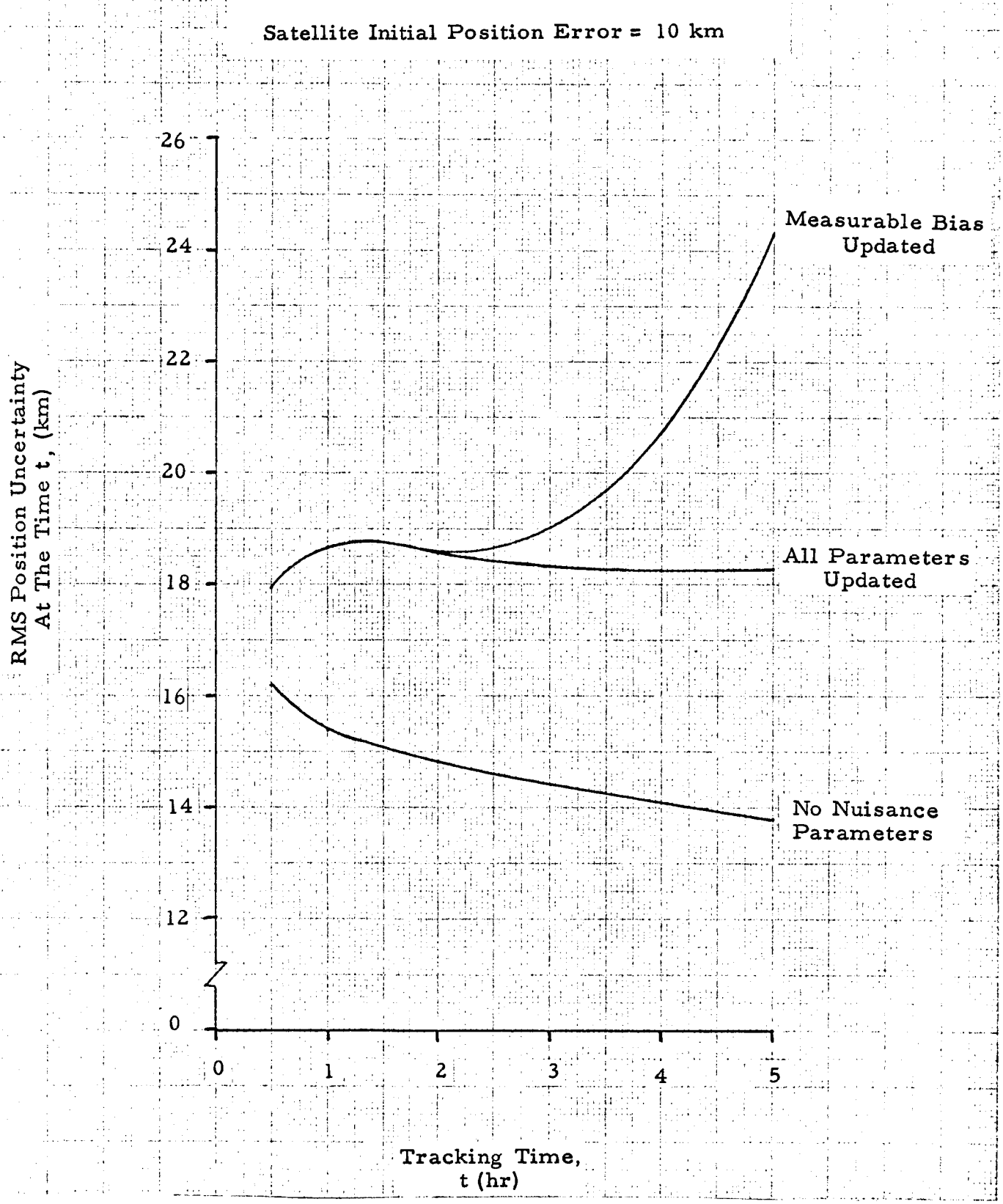

Figure 9

RMS Velocity Uncertainty At The Completion Of Each Tracking Observation

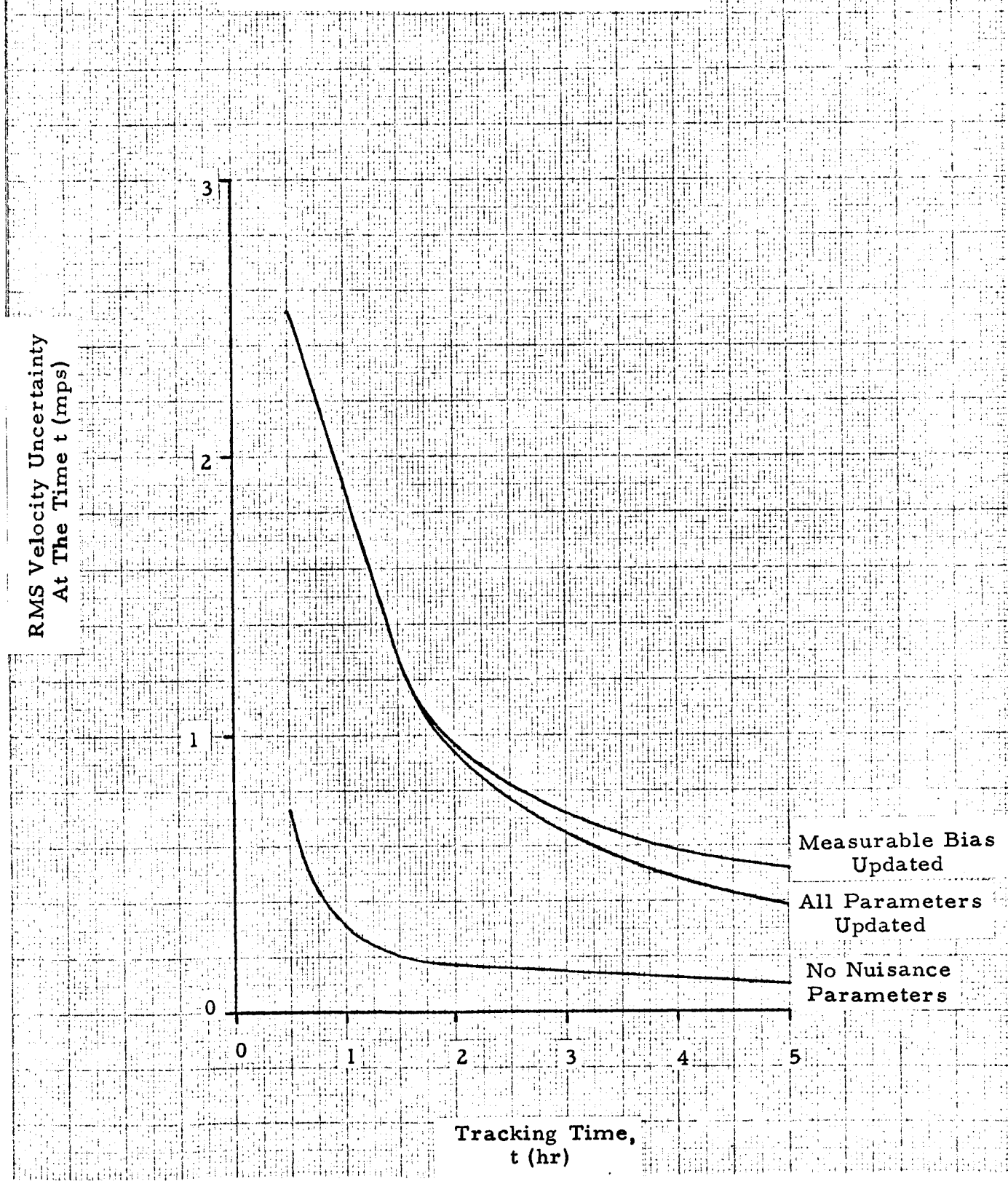

Figure 10

RMS Position Uncertainty 5 Hours After Tracking Initiation

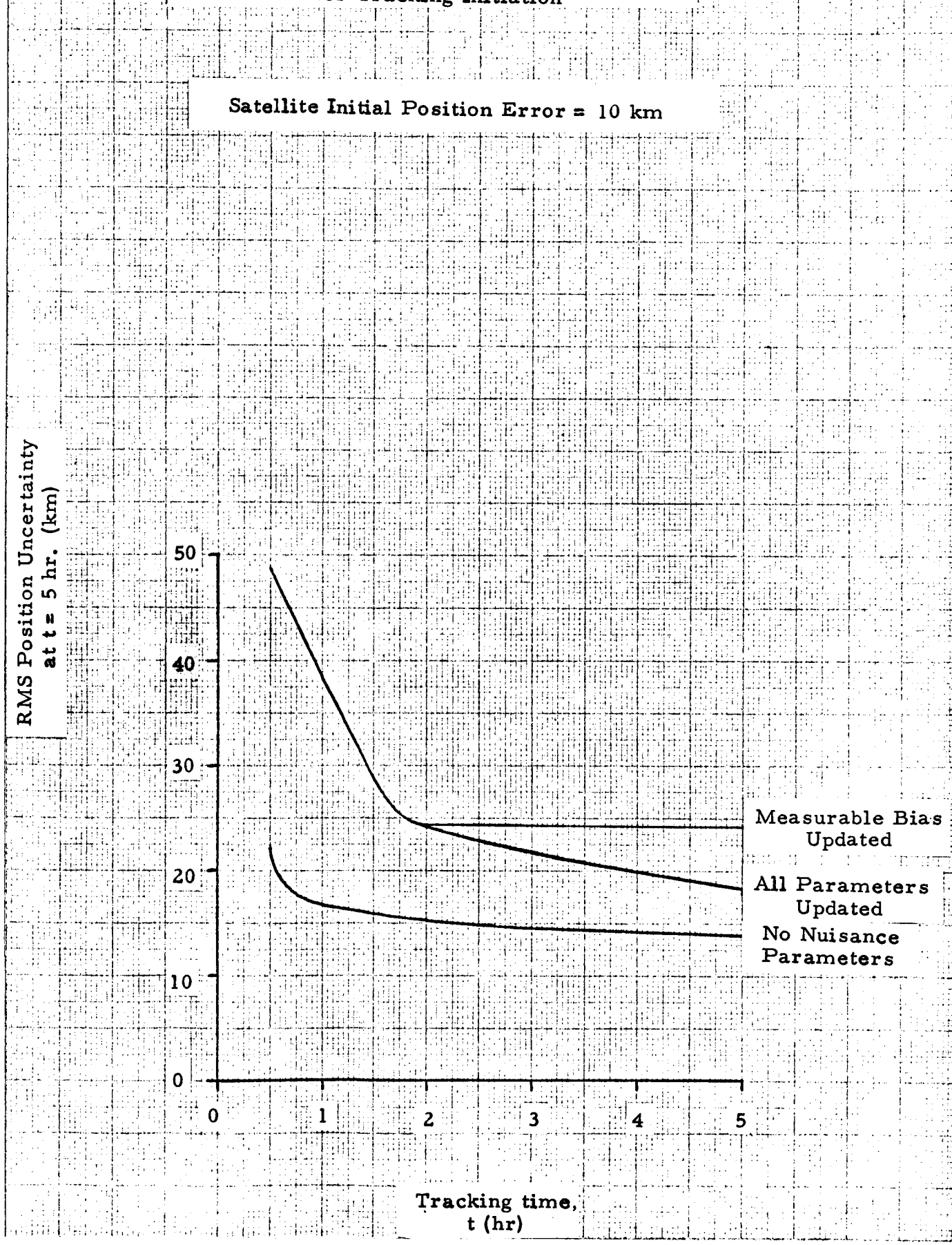

Figure 11

RMS Velocity Uncertainty 5 Hours After Tracking Initiation

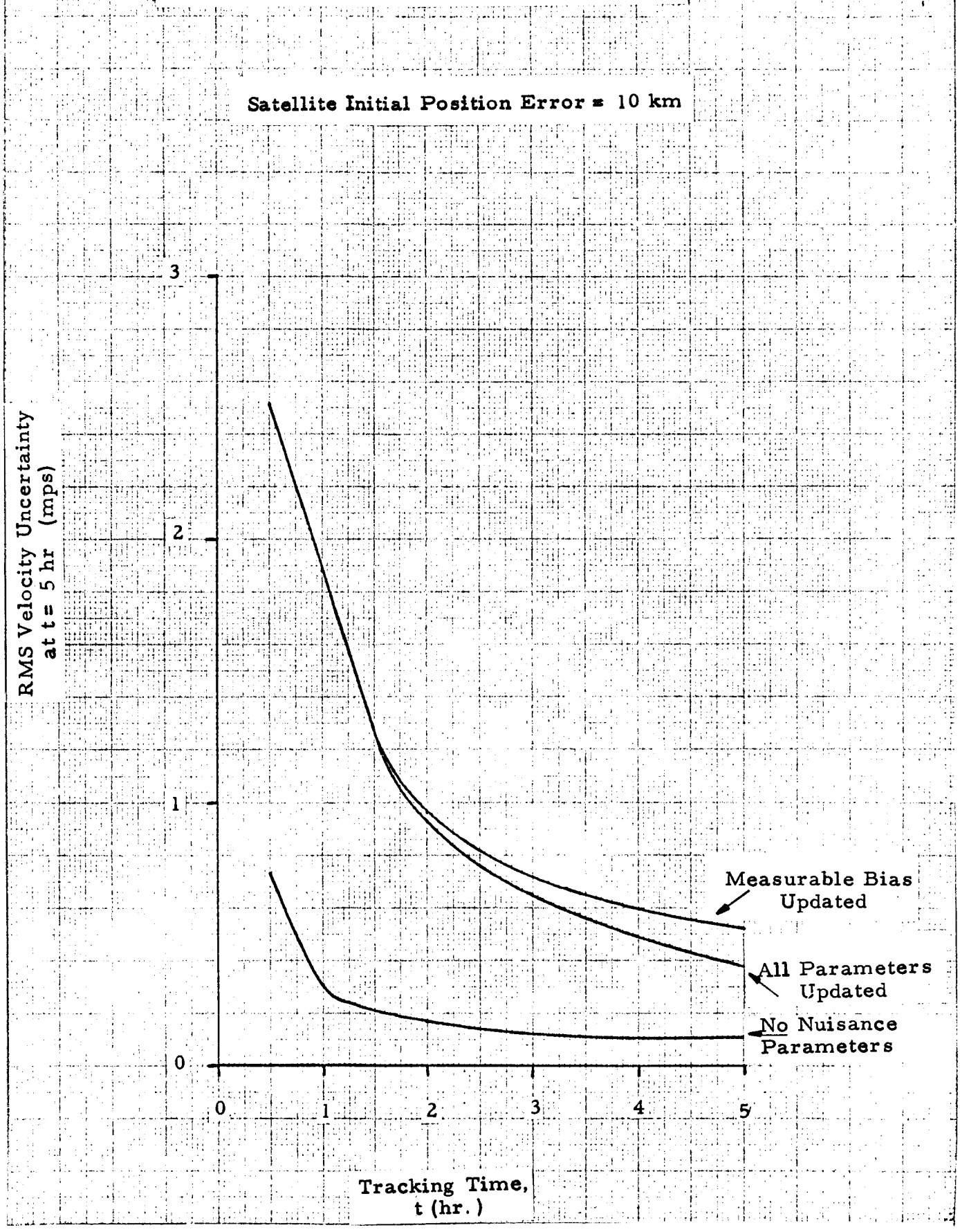

APOLLO NOTE NO. 393
(Task II, Item II)

H. Engel
22 December 1965

THE EFFECTS OF DOPPLER RADAR ERRORS

In the two-way Doppler mode, measurements are made by finding the number of Doppler counts that occur in a fixed time, or else by finding the time it takes to obtain a fixed number of Doppler counts. In actual practice a frequency offset is used, so the time required to obtain a fixed number of Doppler counts does not vary greatly with the velocity of the observed vehicle. Hence, the analysis which we present here for the fixed time mode of operation will apply with very little change to the fixed count mode.

The noise in a Doppler measurement has three parts:

1. A range noise occurring at each end of the measurement interval T, and uncorrelated from one end of the interval to the other. (K_1)
2. A quantization noise occurring at each end of the interval. (K_q)
3. A flat wide-band range rate noise uncorrelated from interval to interval. (K_2)

The variance of the noise on the range change in the sampling interval T is

$$\sigma^2_{\Delta R} = 2K_1^2 + 2K_q^2 + K_2^2 T$$

In our error analysis, we can treat the measurement as though it was a range-rate measurement at the center of the sampling interval, with variance

$$\sigma^2 = \frac{2K_1^2}{T^2} + \frac{2K_q^2}{T^2} + \frac{K_2^2}{T}$$

If the destruct mode of Doppler counting is employed, this is the variance that should be used in the Orbit Error Analysis Program (OEAP) to find the covariance of the resulting estimates of orbit parameters when a least squares ODP is used.

On the other hand, if the non-destruct mode of Doppler counting is employed, the actual covariance of the resulting estimates of orbit parameters when a least squares ODP is used will be <u>far smaller</u> because of the correlation of measurement errors in successive samples. As a consequence, if we wish to use the OEAP to determine the covariance of the estimates of the orbit parameters we must employ a variance smaller than the value σ^2 given above.

Using a least squares filter, we have for the estimate $\Delta\hat{a}$ of the state vector

$$C\Delta\hat{a} = e$$

or

$$\Delta\hat{a} = C^{-1}e$$

in which

$$C = \sum_{i=1}^{N} \left(\frac{\partial M_i}{\partial a}\right)^T \left(\frac{\partial M_i}{\partial a}\right)$$

and

$$e = \sum_{i=1}^{N} \left(\frac{\partial M_i}{\partial a}\right) n_i$$

where M_i is the i-th measurable.

Thus,

$$\begin{aligned} \text{cov}\,(\Delta a, \Delta a) &= E\,(\Delta\hat{a}, \Delta\hat{a}^T) \\ &= C^{-1}\,E(e\,e^T)\,C^{-1} \end{aligned}$$

If the noise is uncorrelated, then

$$E(e\,e^T) = \sigma^2 C$$

and

$$\mathrm{cov}\,(\Delta\hat{a}, \Delta\hat{a}) = \sigma^2 C^{-1}$$

The noise, however, is correlated. We have, then

$$e = \sum_{i=1}^{N} \left(\frac{\partial M_i}{\partial a}\right)^T n_i$$

so

$$E(e\,e^T) = \sum_{i=1}^{N} \sum_{j=1}^{N} \left(\frac{\partial M_i}{\partial a}\right)^T E(n_i n_j) \left(\frac{\partial M_i}{\partial a}\right)$$

Now

$$E(n_i n_j) = \sigma^2 \rho_{i-j}$$

so we can write

$$E(e\,e^T) = \sigma^2 \sum_{i=1}^{N} \left(\frac{\partial M_i}{\partial a}\right)^T \left(\frac{\partial M_i}{\partial a}\right) + 2\,\sigma^2 \rho_1 \sum_{i=1}^{N-1} \left(\frac{\partial M_i}{\partial a}\right)^T \left(\frac{\partial M_{i+1}}{\partial a}\right)$$

$$+ 2\,\sigma^2 \rho_2 \sum_{i=1}^{N-2} \left(\frac{\partial M_i}{\partial a}\right)^T \left(\frac{\partial M_{i+2}}{\partial a}\right) + \ldots + 2\,\sigma^2 \rho_{N-1} \left(\frac{\partial M_1}{\partial a}\right)^T \left(\frac{\partial M_N}{\partial a}\right)$$

Now, if

$$\rho_s = 0 \text{ for } s > s_o \ll N$$

and if

$$\left(\frac{\partial M_i}{\partial a}\right)^T \cong \left(\frac{\partial M_{i+\ell}}{\partial a}\right), \quad \ell \leqslant s_o$$

as is the case for all the kinds of noise with which we are concerned here, then

$$E(e\,e^T) \cong \sigma^2 \sum_{i=1}^{N} \left(\frac{\partial M_i}{\partial a}\right)^T \left(\frac{\partial M_i}{\partial a}\right) + 2\,\sigma^2 \rho_1 \sum_{i=1}^{N-1} \left(\frac{\partial M_i}{\partial a}\right)^T \left(\frac{\partial M_i}{\partial a}\right)$$

$$+ 2\,\sigma^2 \rho_2 \sum_{i=1}^{N-2} \left(\frac{\partial M_i}{\partial a}\right)^T \left(\frac{\partial M_i}{\partial a}\right) + \ldots + 2\,\sigma^2 \rho_{s_o} \sum_{i=1}^{N-s_o} \left(\frac{\partial M_i}{\partial a}\right)^T \left(\frac{\partial M_i}{\partial a}\right)$$

$$= \sigma^2 (1 + 2\rho_1 + 2\rho_2 + \ldots + 2\rho_{s_o}) \sum_{i=1}^{N} \left(\frac{\partial M_i}{\partial a}\right)^T \left(\frac{\partial M_i}{\partial a}\right)$$

$$- 2\,\sigma^2 \left\{ \rho_1 \left(\frac{\partial M_N}{\partial a}\right)^T \left(\frac{\partial M_N}{\partial a}\right) + \rho_2 \sum_{i=0}^{1} \left(\frac{\partial M_{N-i}}{\partial a}\right)^T \left(\frac{\partial M_{N-i}}{\partial a}\right) \right.$$

$$\left. + \ldots + \rho_{s_o} \sum_{i=o}^{N-1-s_o} \left(\frac{\partial M_{N-i}}{\partial a}\right)^T \left(\frac{\partial M_{N-i}}{\partial a}\right) \right\}$$

$$= (1 + 2\rho_1 + 2\rho_2 + \ldots + 2\rho_{s_o})\ \sigma^2\, C$$

$$- 2\,\sigma^2 \sum_{k=1}^{s_o} \rho_k \sum_{i=o}^{k-1} \left(\frac{\partial M_{N-i}}{\partial a}\right)^T \left(\frac{\partial M_{N-i}}{\partial a}\right)$$

Since s_o has been assumed very small compared to N, it follows that

$$E(e\,e^T) \cong (1 + 2\rho_1 + 2\rho_2 + \ldots + 2\rho_{s_o})\ \sigma^2\, C$$

and thus,

$$\operatorname{cov}(\Delta\hat{a}, \Delta\hat{a}) = C^{-1}(1 + 2\rho_1 + 2\rho_2 + \ldots + 2\rho_{s_o})\,\sigma^2\, CC^{-1}$$

$$= (1 + 2\rho_1 + 2\rho_2 + \ldots + 2\rho_{s_o})\,\sigma^2\, C^{-1}$$

Now, the range noise occurring at each end of the interval is correlated from one interval to the next. In terms of range-rate, the error in the p-th measurement is

$$\mathcal{E}_p = \frac{n_p - n_{p-1}}{T}$$

where n_p is the range noise at the end of the p-th interval. Then,

$$\sigma_p^2 = \frac{1}{T^2} E(n_p - n_{p-1})^2$$

$$= \frac{1}{T^2} E(n_p^2 - 2n_p n_{p-1} + n_{p-1}^2)$$

$$= \frac{1}{T^2}(K_1^2 - 0 + K_1^2)$$

$$= \frac{2K_1^2}{T^2}$$

$$\rho_1 \sigma_p^2 = \frac{1}{T^2} E\left[(n_p - n_{p-1})(n_{p+1} - n_p)\right]$$

$$= \frac{1}{T^2} E(n_p n_{p+1} - n_p^2 - n_{p-1} n_{p+1} + n_{p-1} n_p)$$

$$= \frac{1}{T^2} E(0 - K_1^2 - 0 + 0)$$

$$= \frac{K_1^2}{T^2}$$

and

$$\rho_j \sigma^2 = 0 \quad \text{for } j > 1.$$

Thus, within the degree of approximation and the constraints we have employed, we find the contribution of the range noise to cov $(\Delta\hat{a}, \Delta\hat{a})$ is

$$(1 + 2\rho_1 + 2\rho_2 + \ldots + 2\rho_{s_o})\, \sigma^2\, C^{-1}$$

$$= (1 + 2\rho_1)\, K_2^2\, C^{-1}$$

$$= (1 - 1)\, K_2^2\, C^{-1}$$

$$= 0 \quad !!!$$

The quantization noise is correlated in like fashion so within the degree of approximation and the constraints we have employed

$$(1 + 2\rho_1 + 2\rho_2 + \ldots + 2\rho_{s_o})\, \sigma^2\, C^{-1}$$

$$= (1 + 2\rho_1)\, K_q^2\, C^{-1}$$

$$= (1 - 1)\, K_q^2\, C^{-1}$$

$$= 0 \quad !!!$$

The wide band range rate noise results from the clock. The transmitted frequency at any time is $\dot{\phi}$

$$\dot{\phi} = \omega + 2n/c$$

in which n is the frequency noise that leads to the range-rate noise.

The change in transmitted phase during the sampling interval T is

$$\phi(t+T) - \phi(t) = \omega T + \frac{2}{c} \int_t^{t+T} n \, dt$$

The change in received phase in the same interval (for zero range-rate) is

$$\phi\left(t+T-\frac{2r}{c}\right) - \phi\left(t-\frac{2r}{c}\right) = \omega T + \frac{2}{c} \int_{t-\frac{2r}{c}}^{t+T-\frac{2r}{c}} n \, dt$$

in which r is the range to the vehicle and c is the speed of light. The Doppler phase change due to this noise is

$$\Delta\phi = \left[\phi\left(t+T-\frac{2r}{c}\right) - \phi\left(t-\frac{2r}{c}\right)\right] - \left[\phi(t+T) - \phi(t)\right]$$

$$= \frac{2}{c} \int_t^{t+T} \left[n\left(t-\frac{2r}{c}\right) - n(t)\right] dt$$

and the noise on the change in range is

$$N = \frac{c}{2} \Delta\phi$$

$$= \int_t^{t+T} \left[n\left(t-\frac{2r}{c}\right) - n(t)\right] dt$$

Then,

$$\rho_i \sigma_N^2 = E\left\{\int_t^{t+T} \left[n\left(t_1-\frac{2r}{c}\right) - n(t_1)\right] dt_1 \int_{t+iT}^{t+iT+T} \left[n\left(t_2-\frac{2r}{c}\right) - n(t_2)\right] dt_2\right\}$$

$$= E \int_t^{t+T} \int_{t+iT}^{t+iT+T} \left[n\left(t_1-\frac{2r}{c}\right) n\left(t_2-\frac{2r}{c}\right) - n\left(t_1-\frac{2r}{c}\right) n(t_2)\right.$$

$$\left. - n(t_1)\, n\left(t_2-\frac{2r}{c}\right) + n(t_1)\, n(t_2)\right] dt_1 \, dt_2$$

and

$$(1+2\rho_1+2\rho_2+\ldots)\,\sigma_N^2$$

$$= \sum_{i=-\infty}^{\infty} \rho_i\,\sigma_N^2$$

$$= E\int_t^{t+T}\int_{-\infty}^{\infty}\Big[n(t_1-\tfrac{2r}{c})\,n(t_2-\tfrac{2r}{c}) - n(t_1-\tfrac{2r}{c})\,n(t_2)$$

$$- n(t_1)\,n(t_2-\tfrac{2r}{c}) + n(t_1)\,n(t_2)\Big]\,dt_1\,dt_2$$

Since n(t) is considered stationary and t_2 goes from $-\infty$ to ∞, the expected values of the integrals of the four terms above are all the same, so

$$(1+2\rho_1+2\rho_2+\ldots)\,\sigma_N^2 = 0 \quad !!!$$

Thus, we see that, subject to the constraints and approximations we have used, the contribution of each of the three kinds of noise in the Doppler measurements does not contribute to the errors in the estimates of the orbit parameters!

This point requires a more careful examination. In order to simplify the analysis we consider an example and method presented by Dave Curkendall of JPL, the case in which we are estimating a fixed range rate by noisy change in range measurements. The covariance of the estimates of parameters, using a least squares filter, is P,

$$P = (A^T W^{-1} A)^{-1}\; A^T W^{-1} Q\; W^{-1} A\; (A^T W^{-1} A)^{-1}$$

in which

A is the matrix of the partial of the measurables at the sampling instants with respect to the parameters estimated.

W is the covariance matrix of the assumed noise used in designing the filter. In this case W is a diagonal matrix.

Q is the covariance matrix of the actual noise.

In our simple example P is the variance σ_R^2 of the range rate estimate and A is a column vector. We then have that $A^T W^{-1} A$ is simply a number

$$(A^T W^{-1} A) = \frac{M}{T^2 \sigma^2}$$

in which M is the number of measurements, T is the sampling interval, and σ^2 is the variance of the measurements.

Also,

$$A^T = \frac{1}{T} \left[1, 1, \ldots, 1\right]$$

It follows that

$$A^T W^{-1} = \frac{1}{T\sigma^2} \left[1, 1, \ldots, 1\right]$$

Then, by substitution

$$\sigma_R^2 = \left(\frac{M}{T^2\sigma^2}\right)^{-1} \cdot \frac{\left[1, 1, \ldots, 1\right]}{T\sigma^2} \; Q \; \frac{1}{T\sigma^2} \begin{bmatrix} 1 \\ 1 \\ \vdots \\ 1 \end{bmatrix} \left(\frac{M}{T^2\sigma^2}\right)^{-1}$$

$$= \frac{T^2}{M^2} \left[1, 1, \ldots, 1\right] Q \begin{bmatrix} 1 \\ 1 \\ \vdots \\ 1 \end{bmatrix}$$

$$= \frac{T^2}{M^2} S$$

where S is the sum of the elements in the Q matrix. If the measurement noise were uncorrelated, we would have

$$Q = \frac{1}{T^2} \begin{bmatrix} \sigma^2 & & & 0 \\ & \sigma^2 & & \\ & & \ddots & \\ 0 & & & \sigma^2 \end{bmatrix}$$

and

$$\sigma_{\dot{R}}^2 = \frac{T^2}{M^2} \frac{M\sigma^2}{T^2} = \frac{\sigma^2}{M}$$

In the problem in which we are interested, the noise is correlated, so we have

$$Q = \frac{\sigma^2}{T^2} \begin{bmatrix} 1 & \rho_1 & \rho_2 & \cdots & \rho_{M-1} \\ \rho_1 & 1 & \rho_1 & \cdots & \rho_{M-2} \\ \rho_2 & \rho_1 & 1 & \cdots & \rho_{M-3} \\ \vdots & \vdots & \vdots & & \vdots \\ \rho_{M-1} & \rho_{M-2} & \rho_{M-3} & \cdots & \rho_1 \end{bmatrix}$$

so

$$S = \frac{\sigma^2}{T^2} \left[M + 2(M-1)\rho_1 + 2(M-2)\rho_2 + \ldots + 2(1)\rho_{M-1} \right]$$

$$= M\sigma^2 (1 + 2\rho_1 + 2\rho_2 + \ldots + 2\rho_{M-1})/T^2$$

$$- 2\sigma^2 (\rho_1 + 2\rho_2 + 3\rho_3 + \ldots + \left[M-1\right] \rho_{M-1})/T^2$$

Now in the case of range noise or quantization noise S reduces to

$$S = M\sigma^2 (1 + 2\rho_1)/T^2 - 2\sigma^2 \rho_1/T^2$$

$$= 0 - 2\sigma^2 (-\tfrac{1}{2})/T^2$$

$$= \sigma^2/T^2$$

so

$$\sigma_R^2 = \frac{T^2}{M^2} \frac{\sigma^2}{T^2} = \frac{\sigma^2}{M^2}$$

That is, instead of the variance in the estimate of range-rate varying inversely as the number of measurements, it varies inversely as the square of the number of measurements.

In the case of range-rate noise, we have

$$S = 0 - 2\sigma^2 (\rho_1 + 2\rho_2 + \ldots + [M-1]\rho_{M-1})$$

in which

$$\sigma^2 = E \int_t^{t+T} \left[n(t - \frac{2r}{c}) - n(t) \right] dt \quad ^2$$

$$= 2A^2 T$$

where A^2 is the mean square value of n(t), and

$$\rho_i \sigma^2 = C_{1i} - C_{2i} - C_{3i} + C_{4i}$$

where

$$C_{1i} = \int_{o}^{T}\int_{iT}^{iT+T} E\left[n\left(t_1 - \frac{2r}{c}\right) n\left(t_2 - \frac{2r}{c}\right)\right] dt_1\, dt_2$$

$$C_{2i} = \int_{o}^{T}\int_{iT}^{iT+T} E\left[n\left(t_1 - \frac{2r}{c}\right) n\left(t_2\right)\right] dt_1\, dt_2$$

$$C_{3i} = \int_{o}^{T}\int_{iT}^{iT+T} E\left[n\left(t_1\right) n\left(t_2 - \frac{2r}{c}\right)\right] dt_1\, dt_2$$

$$C_{4i} = \int_{o}^{T}\int_{iT}^{iT+T} E\left[n\left(t_1\right) n\left(t_2\right)\right] dt_1\, dt_2$$

Now

$$C_{1i} = C_{4i} \begin{cases} 2A^2T\ , & i = 0 \\ 0\ , & i \neq 0 \end{cases}$$

$$C_{2i} = \begin{cases} \left.\begin{array}{ll} A^2\ \frac{2r}{c}\ , & i = -1 \\ A^2\left(T - \frac{2r}{c}\right), & i = 0 \\ 0\ , & i \neq 0\ ,\ -1 \end{array}\right\} & \frac{2r}{c} \leqslant T \\ \left.\begin{array}{ll} A^2\left(\frac{2r}{c} - jT\right), & i = -j-1 \\ A^2\left(T - \frac{2r}{c} + jT\right), & i = -j \\ 0\ , & i \neq -j, -j-1 \end{array}\right\} & \frac{2r}{c} > T \end{cases}$$

for the integer j such that $0 \leqslant \frac{2r}{c} - jT < T$

$$C_{3i} = \begin{cases} \left.\begin{array}{ll} A^2 (T - \frac{2r}{c}) & , \quad i = 0 \\ A^2 (\frac{2r}{c}) & , \quad i = 1 \\ 0 & , \quad i \neq 0, 1 \end{array}\right\} & \frac{2r}{c} \leqslant T \\ \left.\begin{array}{ll} A^2 (T - \frac{2r}{c} + kT), & i = k \\ A^2 (\frac{2r}{c} kT) & , \quad i = k+1 \\ 0 & , \quad i \neq k, k+1 \end{array}\right\} & \frac{2r}{c} > T \end{cases}$$

for the integer k such that $0 \leqslant \frac{2r}{c} \quad kT < T$

Then,

$$\sigma_{\dot{R}}^2 = \begin{cases} \frac{2}{M^2} \left[A^2 \frac{2r}{c} \right] & , \quad \frac{2r}{c} \leqslant T \\ \frac{2}{M^2} \left[k A^2 (T - \frac{2r}{c} + kT) + (k+1) A^2 (\frac{2r}{c} - kT) \right] & , \quad \frac{2r}{c} > T \end{cases}$$

for the integer k, $0 \leqslant \frac{2r}{c} - kT < T$.

Now,

$$k A^2 (T - \frac{2r}{c} + kT) + (k+1) A^2 (2 \frac{r}{c} - kT)$$

$$= \frac{2r}{c} A^2$$

so

$$\sigma_{\dot{R}}^2 = \frac{\sigma^2}{M^2} (\frac{2r}{cT})$$

Again, instead of the variance of the estimate varying inversely as the number of measurements, it varies inversely as the square of the number of measurements.

For 3-way Doppler, the same arguments can be adduced to show that in the first approximation for non-destruct counting, the contributions of the range noise and quantization noise to the errors in the estimations are zero, but the contribution of range rate noise is not.

In summary, there is a considerable gain in accuracy of orbit parameter estimates through the use of non-destruct counting rather than destruct counting, both for 2-way and 3-way Doppler measurements. Further, if the variance of the measurement noise is used in orbit error analysis programs for least square filters to evaluate the accuracy of orbit determination programs, severely pessimistic estimates of the possible accuracy of orbit determination will be obtained. It is therefore worthwhile to consider employing smaller measurement noise variances as inputs to orbit error analysis programs in estimating the possible accuracy of orbit determination.

The reader is referred also to Apollo Notes 291 and 298 for numerical verification.

APOLLO NOTE NO. 394
(Task II, Item II)

H. Engel
28 December 1965

REMARKS ON COVARIANCE MATRICES

We shall discuss several kinds of covariance matrices P_i.

Let us denote the vector of orbit parameters by a, and the vector of nuisance parameters by b. We let $\mathcal{E}$ be the vector of errors in the vector of measurables M, and let R be $E(\mathcal{E}\mathcal{E}^T)$. We then define C_{aa}, C_{ab}, C_{ba}, C_{bb} by

$$C_{uv} = \frac{\partial M^T}{\partial u} R^{-1} \frac{\partial M}{\partial v}$$

If we assume that all of the nuisance parameters are known perfectly and only the orbit parameters need be estimated, we find

$$P_1 = E(\delta a\, \delta a^T) = C_{aa}^{-1}$$

If we estimate only the orbit parameters, and the non-estimated nuisance parameters have an a priori covariance D_o, then we find P_2, the expected value of $\delta a\, \delta a^T$, as follows

$$\begin{bmatrix} C_{aa} & C_{ab} \\ C_{ab}^T & C_{bb} \end{bmatrix} \begin{bmatrix} \delta a \\ \delta b \end{bmatrix} = \begin{bmatrix} \sum \frac{\partial M^T}{\partial a} \\ \sum \frac{\partial M^T}{\partial b} \end{bmatrix} R^{-1}\, \delta M$$

$$C_{aa}\, \delta a + C_{ab}\, \delta b_o = \sum \frac{\partial M^T}{\partial a} R^{-1}\, \delta M$$

in which δb_o is the a priori estimate of δb. Then,

$$\delta a = C_{aa}^{-1} \left[\sum \frac{\partial M^T}{\partial a} R^{-1}\, \delta M - C_{ab}\, \delta b_o \right]$$

$$P_2 = E(\delta a\, \delta a^T) = C_{aa}^{-1} + (C_{aa}^{-1} C_{ab})\, D_o\, (C_{aa}^{-1} C_{ab})^T$$

If the orbit parameters and all nuisance parameters are estimated we find P_3, the expected value of $\begin{bmatrix}\delta a\\ \delta b\end{bmatrix}\begin{bmatrix}\delta a\\ \delta b\end{bmatrix}^T$ as follows:

$$\left\{\begin{bmatrix} C_{aa} & C_{ab} \\ C_{ab}^T & C_{bb}\end{bmatrix} + \begin{bmatrix} 0 & 0 \\ 0 & D_o^{-1}\end{bmatrix}\right\}\begin{bmatrix}\delta a\\ \delta b\end{bmatrix} = \begin{bmatrix}\sum \frac{\partial M^T}{\partial a} \\ \sum \frac{\partial M^T}{\partial b}\end{bmatrix} R^{-1}\,\delta M + \begin{bmatrix} 0 \\ D_o^{-1}\end{bmatrix}\delta b_o$$

in which δb_o is the a priori estimate of the nuisance parameters.

Then,

$$\begin{bmatrix}\delta a\\ \delta b\end{bmatrix} = \begin{bmatrix} C_{aa} & C_{ab} \\ C_{ab}^T & C_{bb} + D_o^{-1}\end{bmatrix}^{-1}\left\{\begin{bmatrix}\sum \frac{\partial M^T}{\partial a} \\ \sum \frac{\partial M^T}{\partial b}\end{bmatrix} R^{-1}\,\delta M + \begin{bmatrix} 0 \\ D_o^{-1}\end{bmatrix}\delta b_o\right\}$$

and since δb_o is uncorrelated with δM,

$$P_3 = E\left\{\begin{bmatrix}\delta a\\ \delta b\end{bmatrix}\begin{bmatrix}\delta a\\ \delta b\end{bmatrix}^T\right\} = \begin{bmatrix} C_{aa} & C_{ab} \\ C_{ab}^T & C_{bb} + D_o^{-1}\end{bmatrix}^{-1}$$

$$= \begin{bmatrix} P_{3,aa} & P_{3,ab} \\ P_{3,ab}^T & P_{3,bb}\end{bmatrix}$$

in which

$$P_{3,aa} = \left[C_{aa} - C_{ab}\,(C_{bb} + D_o^{-1})^{-1}\, C_{ab}^T\right]^{-1}$$

$$= C_{aa}^{-1} + (C_{aa}^{-1} C_{ab})\,(C_{ab}^T\, C_{aa}^{-1}\, C_{ab} + C_{bb} + D_o^{-1})^{-1}\,(C_{aa}^{-1}\, C_{ab})^T$$

Now, we shall say that one covariance matrix is less than another (where both correspond to the same set of parameters) if the variance of every quantity which is a function of the parameters in the first case is less than the variance of the corresponding quantity in the second. Then, if A and B are two information matrices, it follows that

$$(A+B)^{-1} \quad A^{-1}, \; B^{-1}$$

and for any real matrix α which is commensurate

$$\alpha\,(A+B^{-1})\,\alpha^{T} < \alpha A^{-1}\,\alpha^{T}, \; \alpha B^{-1}\,\alpha^{T}$$

since $(A+B)^{-1}$ is the covariance of the optimum estimate of the parameters based on the information that gave covariance A^{-1} and the information that gave covariance B^{-1}.

It follows that

$$(C_{bb}+D_o^{-1}+C_{ab}^{T}\,C_{aa}^{-1}\,C_{ab})^{-1} < D_o$$

$$(C_{aa}^{-1}\,C_{ab})\,(C_{bb}+D_o^{-1}+C_{ab}^{T}\,C_{aa}^{-1}\,C_{ab})^{-1}\,(C_{aa}^{-1}\,C_{ab})^{T} < D_o$$

and

$$P_{3,aa} < P_2$$

Now, certainly,

$$P_1 < P_{3,aa}$$

so

$$\boxed{P_1 < P_{3,aa} < P_2}$$

In other words, the estimates of the orbit parameters are most accurate if the nuisance parameters are known perfectly, less accurate if the nuisance parameters are unknown but estimated, and least accurate if the nuisance parameters are unknown and not estimated.

Let us now employ a new set of definitions. We let a be the vector of orbit parameters, as before. We denote the vector of nuisance parameters that are always estimated by b, and the vector of remaining nuisance parameters by c. We may define $C_{aa}, \ldots, C_{cc}$ by

$$C_{uv} = \frac{\partial M^T}{\partial u} R^{-1} \frac{\partial M}{\partial v}$$

and we further define C_{dd} and C_{dc} as

$$C_{dd} = \begin{bmatrix} C_{aa} & C_{ab} \\ C_{ab}^T & C_{bb} \end{bmatrix}$$

$$C_{dc} = \begin{bmatrix} C_{ac} \\ C_{bc} \end{bmatrix}$$

Then, if all of the nuisance parameters c are known perfectly and only the orbit parameters need be estimated, we find

$$P_1' = E\left[\begin{pmatrix} \delta a \\ \delta b \end{pmatrix} \begin{pmatrix} \delta a \\ \delta b \end{pmatrix}^T\right] = C_{dd}^{-1}$$

If we estimate only the parameters a and b, and the non-estimated nuisance parameters c have an a priori covariance F_o, then we find P_2' the expected value of

$$\begin{pmatrix} \delta a \\ \delta b \end{pmatrix} \begin{pmatrix} \delta a \\ \delta b \end{pmatrix}^T$$

as follows

$$\begin{bmatrix} C_{dd} & C_{dc} \\ C_{dc}^T & C_{cc} \end{bmatrix} \begin{bmatrix} \begin{pmatrix} \delta a \\ \delta b \end{pmatrix} \\ \delta c \end{bmatrix} = \begin{bmatrix} \begin{pmatrix} \sum \frac{\partial M^T}{\partial a} \\ \sum \frac{\partial M^T}{\partial b} \end{pmatrix} \\ \sum \frac{\partial M^T}{\partial c} \end{bmatrix} R^{-1} \delta M$$

$$C_{dd} \begin{pmatrix} \delta a \\ \delta b \end{pmatrix} + C_{dc}\, \delta c_o = \begin{pmatrix} \sum \frac{\partial M^T}{\partial a} \\ \sum \frac{\partial M^T}{\partial b} \end{pmatrix} R^{-1} \delta M$$

in which δc_o is the a priori estimate of δc. Then,

$$\begin{pmatrix} \delta a \\ \delta b \end{pmatrix} = C_{dd}^{-1} \left[\begin{pmatrix} \sum \frac{\partial M^T}{\partial a} \\ \sum \frac{\partial M^T}{\partial b} \end{pmatrix} R^{-1} \delta M - C_{dc}\, \Delta c_o \right]$$

$$P_2' = E \left[\begin{pmatrix} \delta a \\ \delta b \end{pmatrix} \begin{pmatrix} \delta a \\ \delta b \end{pmatrix}^T \right] = C_{dd}^{-1} + \left(C_{dd}^{-1} C_{dc} \right) F_o \left(C_{dd}^{-1} C_{dc} \right)^T$$

If all the parameters are estimated, we find P_3', the expected value of

$$\begin{pmatrix} \delta a \\ \delta b \\ \delta c \end{pmatrix} \begin{pmatrix} \delta a \\ \delta b \\ \delta c \end{pmatrix}^T$$

as follows

$$\left\{\begin{bmatrix} C_{dd} & C_{dc} \\ C_{dc}^T & C_{cc} \end{bmatrix} + \begin{bmatrix} 0 & 0 \\ 0 & F_o^{-1} \end{bmatrix}\right\} \begin{bmatrix} \begin{pmatrix} \delta a \\ \delta b \end{pmatrix} \\ \delta c \end{bmatrix} = \begin{bmatrix} \begin{pmatrix} \sum \frac{\partial M}{\partial a}^T \\ \sum \frac{\partial M}{\partial b}^T \end{pmatrix} \\ \sum \frac{\partial M}{\partial c}^T \end{bmatrix} R^{-1}\, \delta M + \begin{bmatrix} 0 \\ F_o^{-1} \end{bmatrix} \delta c_o$$

Then,

$$\begin{bmatrix} \delta a \\ \delta b \\ \delta c \end{bmatrix} = \begin{bmatrix} C_{dd} & C_{dc} \\ C_{dc}^T & C_{cc} + F_o^{-1} \end{bmatrix}^{-1} \left\{ \begin{bmatrix} \begin{pmatrix} \sum \frac{\partial M}{\partial a}^T \\ \sum \frac{\partial M}{\partial b}^T \end{pmatrix} \\ \sum \frac{\partial M}{\partial c}^T \end{bmatrix} R^{-1}\, \delta M + \begin{bmatrix} 0 \\ F_o^{-1} \end{bmatrix} \delta c_o \right\}$$

and since δc_o is uncorrelated with δM,

$$P_3' = E \left[\begin{pmatrix} \delta a \\ \delta b \\ \delta c \end{pmatrix} \begin{pmatrix} \delta a \\ \delta b \\ \delta c \end{pmatrix}^T \right] = \begin{bmatrix} C_{dd} & C_{dc} \\ C_{dc}^T & C_{cc} \end{bmatrix}^{-1}$$

$$= \begin{bmatrix} P_{3,dd}' & P_{3,dc}' \\ P_{3,dc}'^T & P_{3,cc}' \end{bmatrix}$$

in which

$$P_{3,dd}' = \left[C_{dd} - C_{dc} (C_{cc} + F_o)^{-1} C_{dc}^T \right]^{-1}$$

$$= C_{dd}^{-1} + (C_{dd}^{-1} C_{dc}) (C_{dc}^T C_{dd}^{-1} C_{dc} + C_{cc} + F_o^{-1})^{-1} (C_{dd}^{-1} C_{dc})^T$$

As before,

$$\boxed{P_1' < P_{3,dd}' < P_2'}$$

In other words, considering a set of orbit parameters and some nuisance parameters, the covariance of the estimates of this set is least if the remaining nuisance parameters are known perfectly, greater if the remaining nuisance parameters are also estimated, and greatest if the remaining nuisance parameters are not known perfectly and are not estimated.

Note that we have not said that the covariance of the estimate of the parameters a and b is decreased by estimating <u>some</u> of the remaining nuisance parameters, only that it is decreased by estimating all of them. Indeed, some now ancient results seemed to indicate that increasing the number of nuisance parameters estimated might increase the covariance.

Now, in the proposed MSC orbit determination program, as we understand it, the only nuisance parameters to be estimated are the biases on the measurables, that μ is to be treated as a non-estimated parameter and that station location, clock errors and the rest are to be treated as known perfectly. Computer results, thus far, indicate that the true covariance of the orbit parameters obtained in this fashion is very nearly the same as the covariance of the orbit parameters obtained when all nuisance parameters are estimated. We do not expect this to be true for very long tracking times, but to be true for short tracking times such as the batch time proposed for use in the orbit determination program. Hence, we expect that the orbit determination program should provide good estimates.

The effects of estimating only measurement biases will be reported more fully in a subsequent note.

The Bissett-Berman Corporation 2941 Nebraska Avenue, Santa Monica, California EXbrook 4-3270

APOLLO NOTE NO. 395
(Task 2, Item II)

E. Pugh
22 December 1965

COMPARISON OF FILTERS

INTRODUCTION

In the interest of obtaining reasonably good sub-optimum filters and avoiding bad ones, a numerical comparison is given in this note of two such filters with the optimum. The mathematical model is as follows. We assume that N values of a measurable, m_i, are taken at times $t_1, \ldots, t_N$ respectively where m_i may be written in the form:

$$m_i = a + bt_i + n_i, \quad i = 1, \ldots, N \tag{1}$$

Here, a plays the role of the orbit parameter to be estimated, b is a nuisance parameter, and the n_i are independent noise samples with zero mean and known variance σ_n^2. Also, we define:

$$\begin{aligned} x_i &= m_i - b_a t_i \\ &= a + (b-b_a)\, t_i + n_i \end{aligned} \tag{2}$$

where b_a is an unbiased a priori estimate of b with known variance σ_b^2.

FILTER 1

In Filter 1 the estimate of a is taken as the value which minimizes the unweighted sum of squares:

$$Q_1 = \sum_{i=1}^{N} (x_i - a)^2 \tag{3}$$

Thus:

$$\frac{\partial Q_1}{\partial a} = -2 \sum_{i=1}^{N} (x_i - \hat{a}_1) = 0 \tag{4}$$

$$\hat{a}_1 = \frac{1}{N} \sum_{i=1}^{N} x_i \tag{5}$$

Note that $\hat{a}_1$ is unbiased since:

$$\hat{a}_1 = \frac{1}{N} \sum_{i=1}^{N} \left[a + (b - b_a)\, t_i + n_i \right] \tag{6}$$

$$E\hat{a}_1 = \frac{1}{N} \sum_{i=1}^{N} a = a \tag{7}$$

The variance of $\hat{a}_1$ is computed as follows:

$$(\hat{a}_1 - a)^2 = \left(\frac{1}{N} \sum_{i=1}^{N} (b - b_a)\, t_i + n_i \right)^2$$

$$= \frac{\left[(b - b_a) \sum_{i=1}^{N} t_i + \sum_{i=1}^{N} n_i \right]^2}{N^2} \tag{8}$$

Squaring and taking the expectation gives:

$$\mathrm{Var}\ \hat{a}_1 = \frac{\sigma_b^2 \left(\sum_{i=1}^{N} t_i\right)^2 + N\,\sigma_n^2}{N^2} \tag{9}$$

Let $t_i = (i-1) = j$, $i = 1, \ldots, N$. Then:

$$\mathrm{Var}\ \hat{a}_1 = \frac{\sigma_b^2 \left(\sum_{j=0}^{N-1} j\right)^2 + N\sigma_n^2}{N^2}$$

$$= \frac{\sigma_b^2 \left(\frac{(N-1)\,N}{2}\right)^2 + N\,\sigma_n^2}{N^2} \tag{10}$$

Let $\delta = \sigma_b^2/\sigma_n^2$. Then:

$$\frac{\mathrm{Var}\ \hat{a}_1}{\sigma_n^2} = (\delta/4)\,(N-1)^2 + (1/N) \tag{11}$$

Note that this variance ratio has the undesirable property of being an increasing function of the number of pieces of data, N, for sufficiently large N.

FILTER 2

In Filter 2 the estimate of a is taken as the value which minimizes the weighted sum of squares:

$$Q_2 = \sum_{i=1}^{N} \frac{(x_i - a)^2}{\sigma_n^2 + \sigma_b^2\, t_i^{\,2}} \tag{12}$$

Thus:

$$\frac{\partial Q_2}{\partial a} = -2 \sum_{i=1}^{N} \frac{(x_i - \hat{a}_2)}{\sigma_n^2 + \sigma_b^2 t_i^2} = 0 \tag{13}$$

$$\hat{a}_2 = \frac{\sum_{i=1}^{N} \frac{x_i}{\sigma_n^2 + \sigma_b^2 t_i^2}}{\sum_{i=1}^{N} \frac{1}{\sigma_n^2 + \sigma_b^2 t_i^2}} \tag{14}$$

Note that $\hat{a}_2$ is also unbiased for:

$$E\hat{a} = E\left\{ \frac{\sum_{i=1}^{N} \frac{a+(b-b_a)t_i+n_i}{\sigma_n^2 + \sigma_b^2 t_i^2}}{\sum_{i=1}^{N} \frac{1}{\sigma_n^2 + \sigma_b^2 t_i^2}} \right\}$$

$$= \frac{a \sum_{i=1}^{N} \frac{1}{\sigma_n^2 + \sigma_b^2 t_i^2}}{\sum_{i=1}^{N} \frac{1}{\sigma_n^2 + \sigma_b^2 t_i^2}} = a \tag{15}$$

The variance of $\hat{a}_2$ is computed as follows:

$$(\hat{a}_2 - a)^2 = \frac{\left(\sum_{i=1}^{N} \frac{(b-b_a)\, t_i + n_i}{\sigma_n^2 + \sigma_b^2 t_i^2} \right)^2}{\left(\sum_{i=1}^{N} \frac{1}{\sigma_n^2 + \sigma_b^2 t_i^2} \right)^2} \tag{16}$$

$$= \frac{\left[(b - b_a) \sum_{i=1}^{N} \frac{t_i}{\sigma_n^2 + \sigma_b^2 t_i^2} + \sum_{i=1}^{N} \frac{n_i}{\sigma_n^2 + \sigma_b^2 t_i^2} \right]^2}{\left(\sum_{i=1}^{N} \frac{1}{\sigma_n^2 + \sigma_b^2 t_i^2} \right)^2} \tag{16}$$

Squaring and taking the expectation gives:

$$\mathrm{Var}\, \hat{a}_2 = \frac{\sigma_b^2 \left(\sum_{i=1}^{N} \frac{t_i}{\sigma_n^2 + \sigma_b^2 t_i^2} \right)^2 + \sigma_n^2 \sum_{i=1}^{N} \left(\frac{1}{\sigma_n^2 + \sigma_b^2 t_i^2} \right)^2}{\left(\sum_{i=1}^{N} \frac{1}{\sigma_n^2 + \sigma_b^2 t_i^2} \right)^2} \tag{17}$$

As before, letting $\delta = \sigma_b^2/\sigma_n^2$ and $t_i = i - 1 = j$, $i = 1, \ldots, N$ we have:

$$\frac{\mathrm{Var}\, \hat{a}_2}{\sigma_n^2} = \frac{\delta \left(\sum_{j=0}^{N-1} \frac{j}{1 + \delta j^2} \right)^2 + \sum_{j=0}^{N-1} \left(\frac{1}{1 + \delta j^2} \right)^2}{\left(\sum_{j=0}^{N-1} \frac{1}{1 + \delta j^2} \right)^2} \tag{18}$$

This variance ratio also has the undesirable property of being an increasing function of N for sufficiently large N since the first series in the numerator is divergent.

FILTER 3

In Filter 3, the optimum filter, the estimate of a is taken as the value which maximizes the joint likelihood of the noise and the a priori estimate b_a of b. Thus, a is chosen to minimize:

$$Q_3 = \sum_{i=1}^{N} \left[m_i - (a + bt_i) \right]^2 / \sigma_n^2 + (b_a - b)^2 / \sigma_b^2 \tag{19}$$

From Note 386 this filter is:

$$\hat{a}_3 = \frac{G}{GN - F^2} \left\{ \sum_{i=1}^{N} m_i \left[1 - \frac{F}{G} t_i \right] - \frac{F}{G} b_a (\sigma_n / \sigma_b)^2 \right\} \tag{20}$$

where:

$$F = \sum_{i=1}^{N} t_i, \quad G = \sum_{i=1}^{N} t_i^2 + (\sigma_n / \sigma_b)^2 \tag{21}$$

Substituting $m_i = a + bt_i + n_i$, we may write:

$$\begin{aligned} \hat{a}_3 = {} & \frac{G}{GN - F^2} \left\{ \sum_{i=1}^{N} (a + bt_i) \left[1 - \frac{F}{G} t_i \right] - b \frac{F}{G} (\sigma_n / \sigma_b)^2 \right\} \\ & + \frac{G}{GN - F^2} \left\{ \sum_{i=1}^{N} n_i \left[1 - \frac{F}{G} t_i \right] - (b_a - b) \frac{F}{G} (\sigma_n / \sigma_b)^2 \right\} \end{aligned} \tag{22}$$

The first term, after simplification, is just a so that Var $\hat{a}_3$ is equal to the expected value of the second term squared. Since the n_i and b_a are mutually independent this reduces to:

$$\mathrm{Var}\, \hat{a}_3 = \left(\frac{G}{GN - F^2} \right)^2 \left\{ \sum_{i=1}^{N} \sigma_n^2 \left[1 - \frac{F}{G} t_i \right]^2 + \sigma_b^2 \left(\frac{F}{G} \right)^2 (\sigma_n / \sigma_b)^4 \right\} \tag{23}$$

which, after simplification, reduces to:

$$\mathrm{Var}\,\hat{a}_3 = \sigma_n^{\,2}\left(\frac{G}{GN - F^2}\right) \tag{24}$$

Thus:

$$\frac{\mathrm{Var}\,\hat{a}_3}{\sigma_n^{\,2}} = \frac{\sum_{i=1}^{N} t_i^2 + \frac{1}{\delta}}{N\left(\sum_{i=1}^{N} t_i^2 + \frac{1}{\delta}\right) - \left(\sum_{i=1}^{N} t_i\right)^2} \tag{25}$$

If we let $t_i = i-1 = j$, $i = 1, \ldots, N$, this reduces to:

$$\frac{\mathrm{Var}\,\hat{a}_3}{\sigma_n^{\,2}} = \frac{1}{N - \frac{(1.5)(N-1)^2 N^2}{(N-1)N(2N-1)+(6/\delta)}} \tag{26}$$

which is a decreasing function of N.

A graphical comparison of the three filters is given in Figures 1, 2, and 3 for $\delta = 1$, .5, and .01 respectively. That the variance is an increasing function of N for sufficiently large N appears to be the penalty paid for not updating the nuisance parameter b as is done in Filter 3. It is noted that for δ as low as .01 no more than 6 pieces of data should be taken when using Filter 1 or Filter 2.

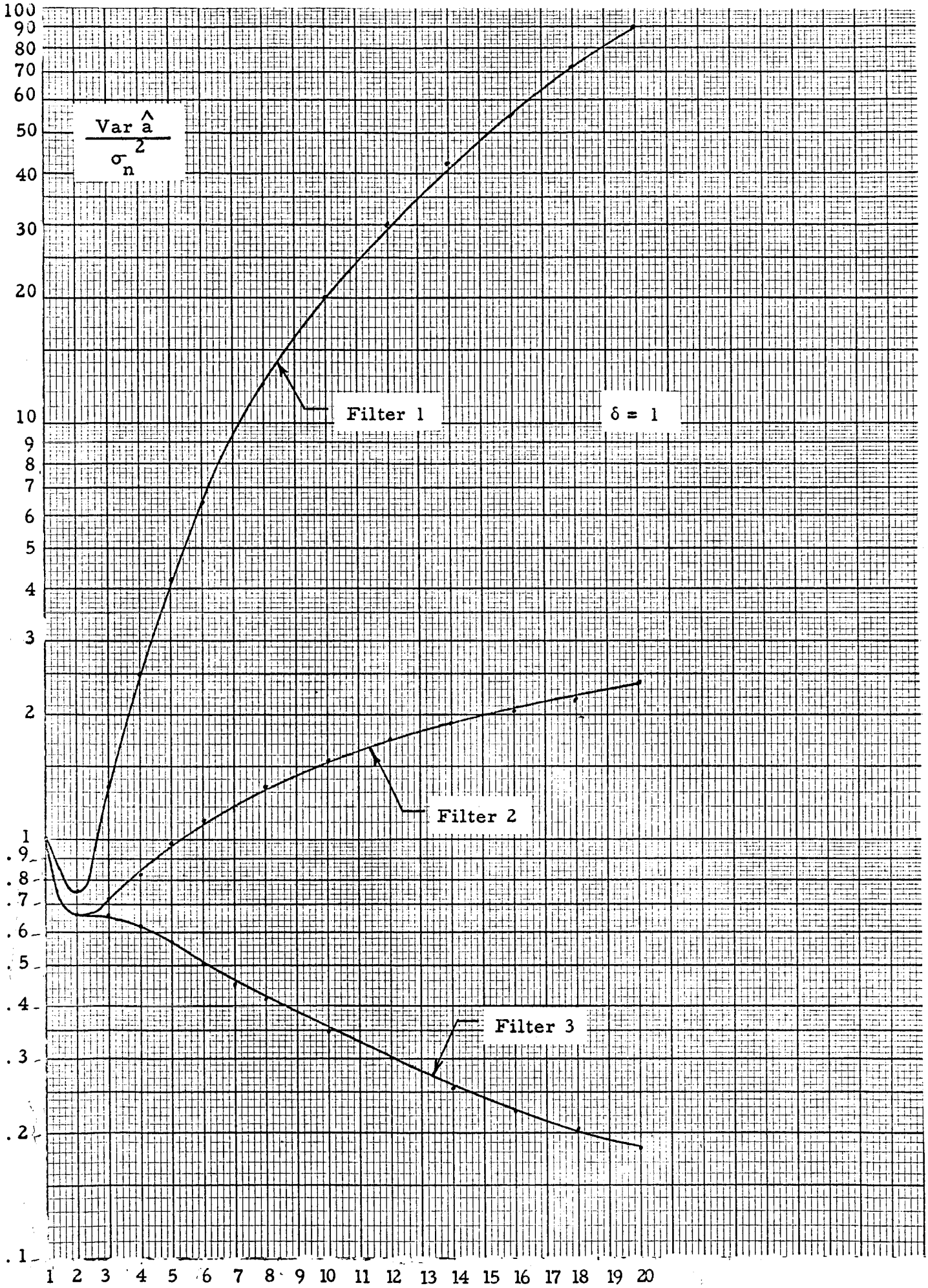
$\frac{\mathrm{Var}\,\hat{a}}{\sigma_n^2}$
Filter 1
δ = 1
Filter 2
Filter 3
100
90
80
70
60
50
40
30
20
10
9
8
7
6
5
4
3
2
1
.9
.8
.7
.6
.5
.4
.3
.2
.1
1 2 3 4 5 6 7 8 9 10 11 12 13 14 15 16 17 18 19 20
N

Figure 1.

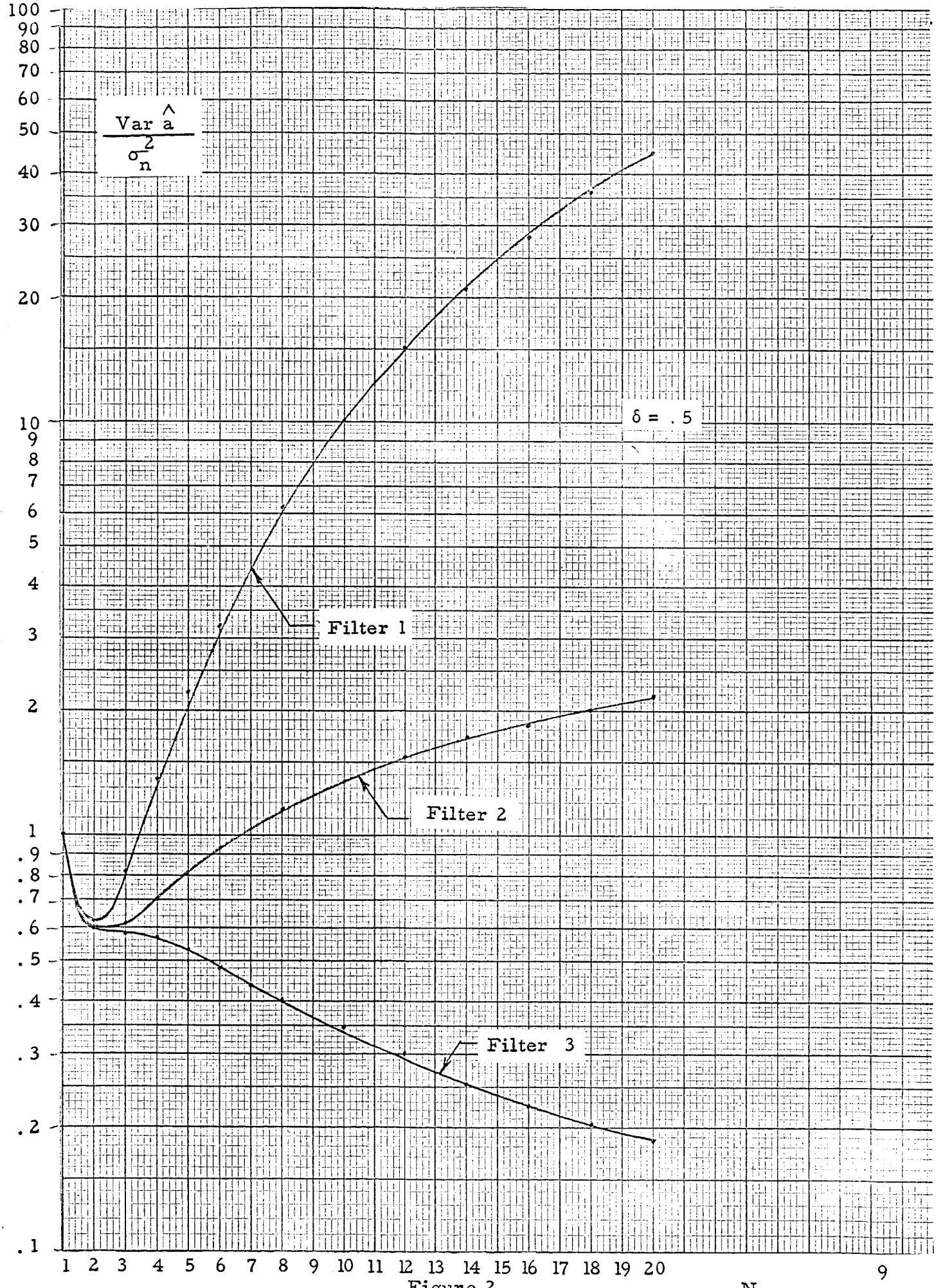
$\frac{\text{Var } \hat{a}}{\sigma_n^2}$
δ = .5
Filter 1
Filter 2
Filter 3
100
90
80
70
60
50
40
30
20
10
9
8
7
6
5
4
3
2
1
.9
.8
.7
.6
.5
.4
.3
.2
.1
1 2 3 4 5 6 7 8 9 10 11 12 13 14 15 16 17 18 19 20
N

Figure 2

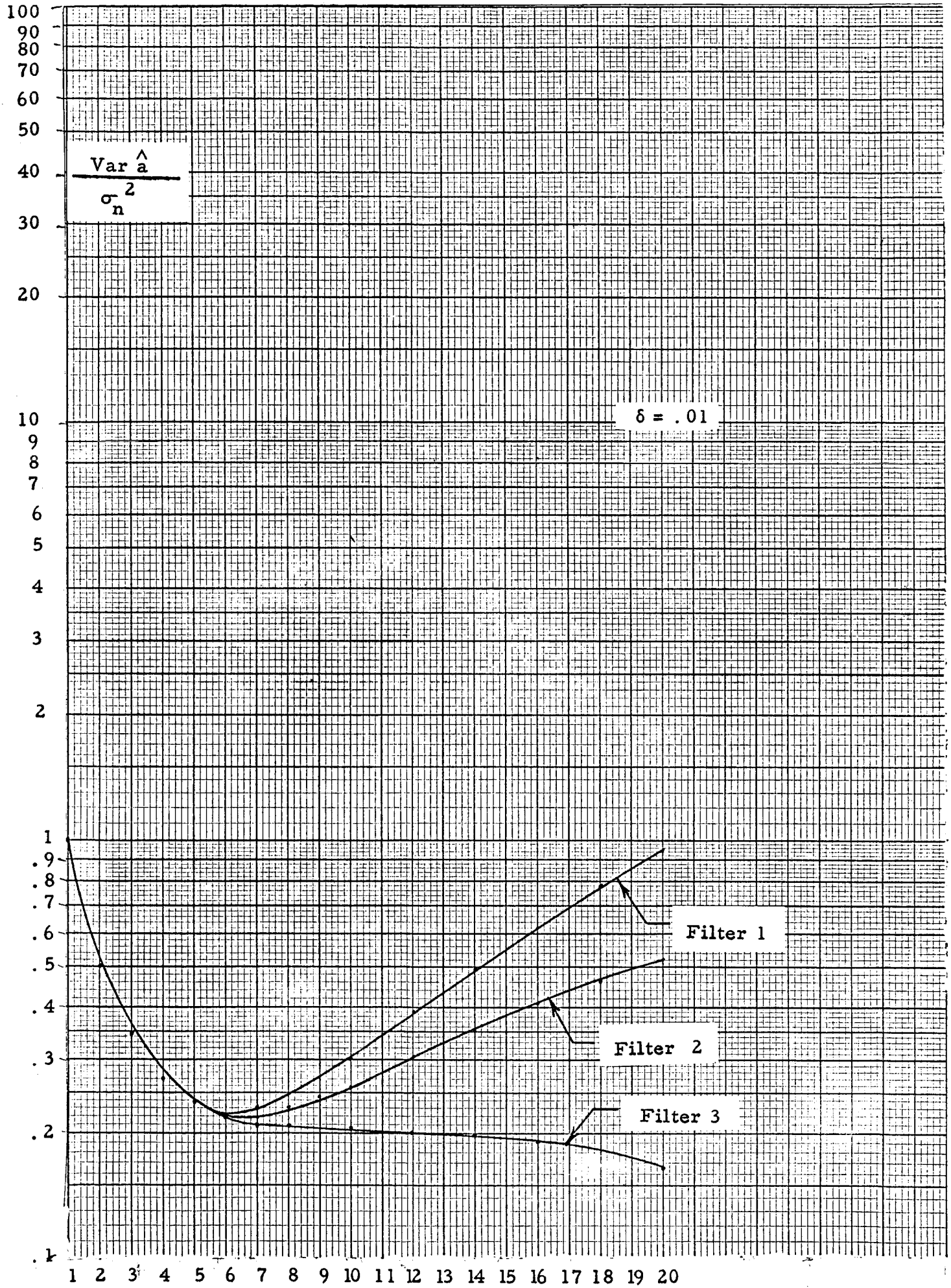
$\frac{\mathrm{Var}\,\hat{a}}{\sigma_n^2}$
δ = .01
Filter 1
Filter 2
Filter 3
100
90
80
70
60
50
40
30
20
10
9
8
7
6
5
4
3
2
1
.9
.8
.7
.6
.5
.4
.3
.2
.1
1 2 3 4 5 6 7 8 9 10 11 12 13 14 15 16 17 18 19 20
N

Figure 3

APOLLO NOTE NO. 396
(Task II, Item II)

H. Engel
29 December 1965

EFFECT OF MODEL ERRORS

The quantity minimized in a least squares filter is R, the weighted sum of the squares of the residuals.

$$R = \sum_i \frac{(y_{mi} - y_{ci})^2}{\sigma_i^2}$$

in which

y_{mi} = measured value of i-th measurement

y_{ci} = computed value of i-th measurement

σ_i^2 = variance of i-th measurement.

Note that this formulation does not restrict us to just one measurable. In order to minimize R, we set its first partial derivatives with respect to each of the estimated parameters to zero. Letting a_j be the j-th estimated parameter, and b_k the k-th non-estimated parameter, we have

$$\frac{\partial R}{\partial a_\ell} = 0 = \sum_i \frac{1}{\sigma_i^2} \left[y_{mi} - y_{ci} - \sum_j \frac{\partial y_i}{\partial a_j} \Delta a_j - \sum_k \frac{\partial y_i}{\partial b_k} \Delta b_k \right] \frac{\partial y_i}{\partial a_\ell}$$

$$= \sum_i \frac{1}{\sigma_i^2} \left[n_i - \sum_j \frac{\partial y_i}{\partial a_j} \Delta a_j - \sum_k \frac{\partial y_i}{\partial b_k} \Delta b_k \right] \frac{\partial y_i}{\partial a_\ell}$$

in which n_i is the noise on the i-th measurement. We now let

$e \triangleq$ column vector with elements e_ℓ

$$e_\ell \triangleq \sum_i \frac{n_i}{\sigma_i^2} \frac{\partial y_i}{\partial a_\ell}$$

$$C_{11} \triangleq \text{matrix with elements } C_{11,\ell j}$$

$$C_{11,\ell j} \triangleq \sum_i \frac{1}{\sigma_i^2} \frac{\partial y_i}{\partial a_\ell} \frac{\partial y_i}{\partial a_j}$$

$$C_{12} \triangleq \text{matrix with elements } C_{12,\ell k}$$

$$C_{12,\ell k} \triangleq \sum_i \frac{1}{\sigma_i^2} \frac{\partial y_i}{\partial a_\ell} \frac{\partial y_i}{\partial b_k}$$

The reason why we are repeating this derivation, which has been presented many times before, is in order to make clear the definitions of e, C_{11} and C_{12} that we are employing; we have sometimes used other definitions and slightly different formulations.

By substitution, we find

$$0 = e - C_{11} \Delta\hat{a} - C_{12} \Delta\hat{b}$$

in which $\Delta\hat{a}$ is the estimated state vector of the estimated parameters and $\Delta\hat{b}$ is the a priori estimated state vector of the non-estimated parameters. Then, by algebraic operations,

$$\Delta\hat{a} = C_{11}^{-1} \left[e - C_{12} \Delta\hat{b} \right]$$

Now,

$$E(e) = 0$$

and

$$E(\Delta\hat{b}) = 0$$

so

$$E(\Delta\hat{a}) = 0$$

Further, for uncorrelated noise,

$$E(ee^T) = C_{11}$$

$$E(e\Delta\hat{b}^T) = 0$$

$$E(\Delta\hat{b}\Delta\hat{b}^T) = \text{cov}(\Delta\hat{b})$$

so

$$\begin{aligned}
\text{cov}(\Delta\hat{a}) &= E(\Delta\hat{a}\Delta\hat{a}^T) \\
&= C_{11}^{-1} E(ee^T) C_{11}^{-1} + (C_{11}^{-1} C_{12}) E(\Delta\hat{b}\Delta\hat{b}^T) (C_{11}^{-1} C_{12})^T \\
&= C_{11}^{-1} + (C_{11}^{-1} C_{12}) \text{cov}(\Delta\hat{b}) (C_{11}^{-1} C_{12})^T
\end{aligned}$$

which is an old, familiar equation. We have now reached the important point.

If σ_i approaches zero, for all i, then the first term in the expression for cov $(\Delta\hat{a})$ also approaches zero — but the second term does not; e.g., if all σ_i 's are alike and equal to σ, cov $(\Delta\hat{a})$ reduces to

$$\begin{aligned}
\text{cov}(\Delta\hat{a}) = {} & \sigma^2 \left\{ \sum_i \left(\frac{\partial y_i}{\partial a}\right)^T \left(\frac{\partial y_i}{\partial a}\right) \right\}^{-1} \\
& + \left[\sigma^2 \left\{ \sum_i \left(\frac{\partial y_i}{\partial a}\right)^T \frac{\partial y_i}{\partial a} \right\}^{-1} \frac{1}{\sigma^2} \sum_i \left(\frac{\partial y_i}{\partial a}\right)^T \frac{\partial y_i}{\partial b} \right] \\
& \text{cov}(\Delta\hat{b}) \left[\sigma^2 \left\{ \sum_i \left(\frac{\partial y_i}{\partial a}\right)^T \left(\frac{\partial y_i}{\partial a}\right) \right\}^{-1} \frac{1}{\sigma^2} \sum_i \left(\frac{\partial y_i}{\partial a}\right)^T \frac{\partial y_i}{\partial a} \right]^T
\end{aligned}$$

$$= \sigma^2 \left\{ \sum_i \left(\frac{\partial y_i}{\partial a} \right)^T \left(\frac{\partial y_i}{\partial a} \right) \right\}^{-1}$$

$$+ \left[\left\{ \sum_i \left(\frac{\partial y_i}{\partial a} \right)^T \left(\frac{\partial y_i}{\partial a} \right) \right\}^{-1} \sum_i \left(\frac{\partial y_i}{\partial a} \right)^T \left(\frac{\partial y_i}{\partial a} \right) \right]$$

$$\mathrm{cov}(\widehat{\Delta b}) \left[\left\{ \sum_i \left(\frac{\partial y_i}{\partial a} \right)^T \cdot \frac{\partial y_i}{\partial a} \right\}^{-1} \sum_i \frac{\partial y_i}{\partial a} \frac{\partial y_i}{\partial b} \right]^T$$

in which the first term goes to zero as σ goes to zero, but the second term is independent of σ.

In other words, the effect of not estimating parameters on the covariance of the estimated parameters can be evaluated separately from the effect of noise on the measurements, in this case, by using the OEA Program and letting σ be arbitrarily small or by subtracting the results in the case where $\mathrm{cov}(\widehat{\Delta b})$ is zero from that in which $\mathrm{cov}(\Delta b)$ is not zero. In the more general case, in which the σ_i's are not all the same the first term in $\mathrm{cov}(\Delta a)$ still approaches zero as the σ_i's approach zero, but the second term is not independent of the σ_i's; instead, it depends on the ratios of the σ_i's. In theory it would be possible to find the ratios of the σ_i's that lead to the worst effect of not estimating parameters. In practice this requires too much effort.

As a practical matter, however, we are often concerned with the case in which all the σ_i's are alike — as when the only data is Dopper radar — and in such a case the effect of not estimating parameters can be determined without question. Again, practically, even where there may be more than one kind of data we can select reasonable values for the σ_i's or their ratios, and so determine separately the effects of not estimating parameters.

Now, not estimating parameters in an ODP is equivalent to having a model error, so the OEA Program provides a means of evaluating such model errors independent of the magnitude of the noise on the measurements. This is especially important, in view of the results in Apollo Note No. 393 which indicate that the effect of the correlated noise in the measurements on the estimates of the parameters will decrease much more rapidly than has been thought in the past, so that the model errors may be the principal source of uncertainties in the estimated parameters. The conclusions derived in the present note are independent of whether or not the noise is correlated, for if the noise is correlated, we have

$$\mathrm{cov}(\Delta\hat{a}) = C_{11}^{-1}\, E\,(ee^T)\, C_{11}^{-1} + (C_{11}^{-1}\, C_{12})\, \mathrm{cov}(\Delta\hat{b})(C_{11}^{-1}\, C_{12})^T$$

about which we can make the same statements as we did the prior form.

The Bissett-Berman Corporation 2941 Nebraska Avenue, Santa Monica, California EXbrook 4-3270

APOLLO NOTE NO. 397 L. Lustick
(Task 2, Item II)

CHECK-OUT OF REFRACTION PARAMETERS

PURPOSE

The purpose of this Note is to indicate the manner in which the refraction parameters were checked-out in the Orbit Error Analysis Program.

INTRODUCTION

The new parameters have been added to the Orbit Error Analysis Program. These parameters are the Zenith Range Error (N_oH) and the surface refractivity (N_o). The analysis for obtaining the approximate partial derivatives of the Orbit Error Analysis Program with respect to these parameters in described in Apollo Note No. 372. The following Table summarizes the expressions for the partial derivatives with respect to the refraction parameters.

Measurable	$\partial M / \partial N_oH$	$\partial M / \partial N_o$
Range	$1 \div \text{SIN EL}$	0
*Azimuth Angle	0	0
*Elevation Angle	0	$\text{ctn } \mathcal{E}\ell$
Range Rate (Two-Way)	$\frac{-\text{ctn } \mathcal{E}\ell}{\text{SIN } \mathcal{E}\ell} \quad \frac{d\mathcal{E}\ell}{dt}$	0
Range Rate (Three-Way)	$\left[\frac{-\text{ctn } \mathcal{E}\ell}{\text{SIN } \mathcal{E}\ell} \quad \frac{d\mathcal{E}\ell}{dt}\right]$ Mas $\left[\frac{-\text{ctn } \mathcal{E}\ell}{\text{SIN } \mathcal{E}\ell} \quad \frac{d\mathcal{E}\ell}{dt}\right]$ Slave	0 0

The partial derivatives for the Azimuth, Elevation Angle measurements are calculated, those fo x/y angles are not.

CHECK-OUT OF REFRACTION PARAMETERS

The following PART A input was used to generate information matrices for the measurables Range, Range Rate, Azimuth and Elevation Angle.

INPUT DATA

01	2.1769418E 07	A1
02	3.2259712E 03	A4
03	2.2552845E 04	A5
04	1.0000000E 00	GAM ID
05	3.1784840E 01	BETA
06	-0	XI
07	-0	ETA
08	-0	ZETA
09	3.2174080E 01	LAMBDA
10	-6.4653640E 01	ALPHA
11	7.2921150E-05	OMEGAE
12	-0	OMEGAM
13	2.0925696E 07	RHOE
14	-0	RHOM
15	1.4076455E 16	MU
16	0	D TIME
16	1.6666600E-02	D TIME
16	3.3333200E-02	D TIME
16	4.9999800E-02	D TIME
17	0	REENTRY RAD
18	2.3567250E 01	BIG L
19	-6.5704000E 01	SMA L
20	1.0000000E 00	RRATE IND
21	1.0000000E 00	RANGE IND
22	1.0000000E 00	Q IND
23	-0	QF IND
24	-1.0000000E 00	ANG 1 IND
25	-1.0000000E 00	ANG 2 IND
26	1.0000000E 00	PVW IND
27	-0	T INIT
28	1.6666600E-02	T INCR
29	3.0000000E 01	DIMENS
30	-0	LAMBDA2
31	-0	ALPHA2
32	-1.0000000E 00	M-S IND
33	1.0000000E 00	F-M IND

The program before the addition of the refraction parameters prints out the Cosine of the Elevation Angle and this portion of the program has been checked out previously. The outputs of the program consistent with the input Data are shown below.

time	Cos $\mathcal{E}\ell$	1 st diff	2 nd diff
0	.9838704		
		-.0000511	
1 sec	.9838193		+.0000028
		-.0000483	
2 sec	.9837710		+.0000027
		-.0000456	
3 sec	.9837254		

Using only this information we can check the expressions for the Partial derviatives with respect to the refraction parameters. The only expression that is not straight forward is the Partial of Range Rate with respect to $(N_o H)$ and its check is described below. As can be seen from the second difference the Cos $\mathcal{E}\ell$ is a 2nd degree function of time.

$$\left(\frac{d\,\text{Cos}\,\mathcal{E}\ell}{dt}\right)_{1\text{ sec}} \cong \frac{\text{Cos}\,\mathcal{E}\ell\,(2\text{ sec}) - \text{Cos}\,\mathcal{E}\ell\,(0\text{ sec})}{2}$$

but $$\frac{d\,(\text{Cos}\,\mathcal{E}\ell)}{dt} = -\text{SIN}\,\mathcal{E}\ell\,\frac{d\,\mathcal{E}\ell}{dt}$$

$$\therefore \quad -\left[\text{SIN}\,\mathcal{E}\ell\,\frac{d\,\mathcal{E}\ell}{dt}\right]_{1\text{ sec}} \cong \frac{\text{Cos}\,\mathcal{E}\ell\,(2\text{ sec}) - \text{Cos}\,\mathcal{E}\ell\,(0\text{ sec})}{2} = Q$$

hence $$\frac{-\text{ctn}\,\mathcal{E}\ell}{\text{SIN}\,\mathcal{E}\ell}\,\frac{d\,\mathcal{E}\ell}{dt} \cong \frac{Q\,\text{ctn}\,\mathcal{E}\ell}{\text{SIN}^2\,\mathcal{E}\ell}$$

Using this formula the $\left.\dfrac{\partial R'}{\partial\,(N_o H)}\right]_{1\text{ sec}} = -8.50207\text{ -}03$

The value the program calculates is

-8. 500218 -03

In view of the fact that there is roundoff in the last significant figure in the Cos $\mathcal{E}\ell$, this agreement is excellent.

The following table compares the check results with the program output at a time of 1 sec.

Measurable	$\partial M/\partial(N_o H)$		$\partial M/\partial N_o$	
	Program	Check	Program	Check
Range	5. 58150	5. 58150	0	0
Azimuth	0	0	0	0
Elevation	0	0	5.491186	5. 491186
Range Rate (Two-Way)	-8.500×10^{-3}	-8.502×10^{-3}	0	0

The three-way doppler mode was checked out by using the same values for slave station location as that for the master and observing that the $\left(\frac{\partial M}{\partial N_o H}\right)_{slave}$ was equal $\left(\frac{\partial M}{\partial N_o H}\right)_{master}$.

INSTRUCTIONS ON REFRACTION PARAMETERS

In order not to extend the sizes of information matrices in PART A, we made use of the Columns 11 and 13 which previously contained parameters which are now obsolete.

Column 11 contains the $\frac{\partial M}{\partial N_o H}$ of receiving station.

Column 13 contains $\frac{\partial M}{\partial N_o}$ for all measurables but three-way doppler and then it contains $\left[\frac{\partial M}{\partial (N_o H)}\right]_{master}$.